



City Research Online

City, University of London Institutional Repository

Citation: Robson, S. (1991). Some influences of the photographic process on the accuracy of close range photogrammetry with a non-metric camera. (Unpublished Doctoral thesis, City, University of London)

This is the accepted version of the paper.

This version of the publication may differ from the final published version.

Permanent repository link: <https://openaccess.city.ac.uk/id/eprint/28548/>

Link to published version:

Copyright: City Research Online aims to make research outputs of City, University of London available to a wider audience. Copyright and Moral Rights remain with the author(s) and/or copyright holders. URLs from City Research Online may be freely distributed and linked to.

Reuse: Copies of full items can be used for personal research or study, educational, or not-for-profit purposes without prior permission or charge. Provided that the authors, title and full bibliographic details are credited, a hyperlink and/or URL is given for the original metadata page and the content is not changed in any way.

City Research Online:

<http://openaccess.city.ac.uk/>

publications@city.ac.uk

Some Influences of the
Photographic Process on the Accuracy of
Close Range Photogrammetry with a Non-Metric Camera.

Author: Stuart Robson BSc.

Qualification: This thesis is submitted for the degree of
Doctor of Philosophy.

Submitted: City University,
Department of Civil Engineering,
February 1991.

Table of Contents

Acknowledgements	15
Abstract.	16
1. Introduction.	C1.1
1.1. Reasons for carrying out research in this area.	C1.1
1.2. Summary of previous work relating to the deformation of photographic materials.	C1.2
1.3. Outline of intentions for the research project.	C1.4
1.4. Thesis structure:	C1.4
2. Photogrammetric applications of photographic theory.	C2.1
2.1. Constituents of photographic materials.	C2.1
2.1.1. Emulsion constituents.	C2.1
2.1.1.1. Silver halides.	C2.1
2.1.1.2. Gelatin.	C2.2
2.1.1.3. Colloidal properties.	C2.2
2.1.2. Film base materials.	C2.4
2.1.2.1. Cellulose.	C2.4
2.1.2.2. Polyester.	C2.5
2.2. Photographic chemistry.	C2.7
2.2.1. Sensitivity to light and the silver halide emulsion.	C2.7
2.2.2. Developers and development.	C2.8
2.2.3. Fixation.	C2.12
2.2.4. Washing and drying.	C2.13
2.3. Image quality factors.	C2.14
2.3.1. Basic sensitometry.	C2.14
2.3.2. Tone reproduction.	C2.15
2.3.3. Information capacity and resolution.	C2.18
2.3.3.1. Granularity.	C2.18
2.3.3.2. Turbidity.	C2.20
2.3.3.3. Modulation Transfer Function.	C2.21
2.4. Factors contributing to in-plane deformation.	C2.24
2.4.1. Humidity changes.	C2.24
2.4.2. Thermal changes	C2.28
2.4.3. Dimensional changes due to processing.	C2.30
2.4.4. Film curl.	C2.33
2.4.5. Aging.	C2.33
2.5. Factors contributing to out-of-plane deformation.	C2.33

2.6.	Chapter summary.	C2.36
3.	Photogrammetric Theory.	C3.1
3.1.	Geometrical optics and considerations leading to the central perspective projection.	C3.1
3.2.	Geometric properties of the compound lens.	C3.3
3.2.1.	Radial lens distortion.	C3.5
3.2.2.	Decentring distortion.	C3.7
3.3.	Film deformation modelling.	C3.8
3.3.1.	Explicit film deformation corrections.	C3.9
3.3.1.1.	Models based on polynomials applied to the deformations at known sites.	C3.10
3.3.1.2.	Linear least squares interpolation.	C3.13
3.3.1.3.	Models based on previous reseau image measurements	C3.15
3.3.2.	Use of additional polynomial terms during photogrammetric adjustment.	C3.16
3.4.	The self calibrating bundle adjustment.	C3.17
3.4.1.	The functional model.	C3.17
3.4.2.	The stochastic model.	C3.19
3.4.3.	Datum definition.	C3.21
3.4.4.	Optimisation of network geometry.	C3.22
3.4.5.	Adjustment quality.	C3.23
3.5.	Chapter summary	C3.24
4.	Initial investigations.	C4.1
4.1.	Investigation of film deformation using a Rollei-Metric 6006.	C4.1
4.1.1.	Methodology.	C4.1
4.1.2.	Analysis of data.	C4.4
4.1.3.	Experimental results.	C4.5
4.1.3.1.	Exposures made on TMAX films during Aerial Survey.	C4.5
4.1.3.2.	Exposures made on Technical Pan 120 and Ektachrome 120 films.	C4.11
4.1.3.3.	Exposures made on FP4 120 and 220 films.	C4.13
4.2.	Reseau plate unflatness tests.	C4.18
4.3.	Correction methods applied to the reseau data.	C4.22
4.3.1.	Globally Applied Transformations.	C4.22
4.3.2.	Local Bilinear Correction.	C4.28
4.3.3.	Linear Least Squares Interpolation.	C4.31
4.4.	Summary of initial investigations.	C4.38

5.	Investigation of in-plane deformation.	C5.1
5.1.	Examination methods.	C5.1
5.1.1.	Master grid preparation.	C5.3
5.2.	Contact reseau experimentation.	C5.5
5.2.1.	Variables contributing to photogrammetric film deformation.	C5.5
5.2.1.1.	Film types.	C5.7
5.2.1.2.	Storage prior to exposure.	C5.7
5.2.1.3.	Exposure.	C5.7
5.2.1.4.	Storage prior to processing.	C5.8
5.2.1.5.	Processing conditions.	C5.8
5.2.1.6.	Storage prior to measurement.	C5.9
5.2.1.7.	Image measurement.	C5.10
5.3.	Experiments conducted and analysis of results.	C5.11
5.3.1.	The relationship between the relative humidity of the measurement environment and scale change for the film types investigated.	C5.15
5.3.1.1.	Homogeneous changes.	C5.15
5.3.1.2.	Inhomogeneous changes.	C5.22
5.3.1.3.	Summary of the measurement relative humidity and scale change relationship.	C5.26
5.3.2.	Storage of film prior to and at exposure.	C5.26
5.3.2.1.	Scale changes.	C5.27
5.3.2.2.	Local residuals.	C5.29
5.3.2.3.	Summary of pre-exposure storage investigation.	C5.31
5.3.3.	Exposure level and uniformity.	C5.31
5.3.3.1.	Homogeneous changes.	C5.32
5.3.3.2.	Inhomogeneous changes.	C5.35
5.3.3.3.	Summary of exposure uniformity experiments.	C5.35
5.3.4.	Processing conditions.	C5.36
5.3.4.1.	Variation of developer formulation.	C5.36
5.3.4.1.1.	Homogeneous deformations.	C5.37
5.3.4.1.2.	Inhomogeneous deformations.	C5.40
5.3.4.2.	Variation of fixing bath formulation.	C5.40
5.3.4.2.1.	Homogenous changes.	C5.42
5.3.4.2.2.	Inhomogeneous deformations.	C5.47
5.3.4.3.	Drying temperature and relative humidity.	C5.50
5.3.4.3.1.	Systematic variations.	C5.50
5.3.4.3.2.	Local deformations.	C5.53
5.3.4.3.	Summary of deformations due to changes in process formulation.	C5.54

5.3.5.	Changes occurring with storage, including hysteresis.	C5.54
5.3.5.1.	Homogeneous variations with storage	C5.55
5.3.5.2.	Changes in local deformations with storage	C5.60
5.3.5.3.	Summary of investigations into the presence of hysteresis.	C5.63
5.4.	Summary of in-plane experimentation.	C5.63
6.	Investigations including out-of-plane deformation.	C6.1
6.1.	In-camera exposure method.	C6.1
6.1.1.	Modification of the Hasselblad SWC camera.	C6.2
6.1.2.	In-camera laboratory exposure method.	C6.5
6.1.3.	Results and analysis of experiments including out-of-plane deformation.	C6.6
6.1.3.1.	Holotest 10E56 film exposed in HS1.. . . .	C6.6
6.1.3.2.	Kodak Technical Pan 120 in HS2.	C6.8
6.1.3.3.	Ilford FP4 120/220.	C6.12
6.1.4.	Summary of in-camera deformations.	C6.15
6.2.	Practical test field evaluation.	C6.16
6.2.1.	Test field design and survey.	C6.16
6.2.1.1.	Zero Order design (Datum).	C6.17
6.2.1.2.	First Order design (Configuration).	C6.17
6.2.1.3.	Second Order design (Measurement).	C6.20
6.2.1.4.	Third Order design (Densification).	C6.22
6.2.2.	Photography of the test field.	C6.22
6.2.3.	Processing of the photogrammetric data.	C6.24
6.3.	The Global Bundle Adjustment.	C6.24
6.3.1.	Analysis of calibration results.	C6.25
6.3.2.1.	Analysis of the UMK and HS1 adjustment results.	C6.27
6.3.2.2.	Analysis of the P32 adjustment results.	C6.31
6.3.2.3.	Modified Hasselblad SWC (HS2) exposures.	C6.34
6.3.2.4.	Hasselblad Non-Metric exposures.	C6.40
6.2.6.	Summary.	C6.43
6.4.	Film/back permutations with HS2.	C6.44
6.4.1.	Image coordinate refinement and datum definition.	C6.44
6.4.2.	Analysis of Results.	C6.45
6.4.2.1.	Changes in estimated parameters.	C6.46
6.4.2.2.	Differences between the photo-coordinate residuals.	C6.50
6.4.2.3.	Differences between the estimated object space coordinates.	C6.53
6.4.3.	Summary of camera back and film type variations.	C6.56

6.5.	The effect of the explicit film deformation correction methods on the precision obtainable during a typical survey.	C6.58
6.5.1.	Photogrammetric processing.	C6.58
6.5.3.	Analysis of results.	C6.58
6.5.3.1.	Analysis of estimated parameters.	C6.58
6.5.3.2.	Analysis of photo-coordinate residuals.	C6.60
6.5.3.3.	Analysis of object coordinate discrepancies.	C6.63
6.5.4.	Summary of results from the pseudo survey.	C6.65
6.6.	Chapter summary.	C6.66
7.	Conclusions.	C7.1
7.1.	In-plane deformations.	C7.1
7.2.	In-camera deformations.	C7.4
7.3.	Test field photography.	C7.5
7.4.	Suggestions for carrying out photography for photogrammetric analysis.	C7.7
7.5.	Suggestions for further work.	C7.8
	Appendix A, a selection of vector plots of film deformation from the in-plane work	AppA.1
	Appendix B, a selection of vector plots of film deformation from the out-of-plane work	AppB.1
	References and bibliography	Bib.1

Tables

Chapter 2

- 2.1. Physical characteristics of base materials. C2.6
- 2.2. Constituents of a typical developer solution. C2.9

Chapter 3. (No Tables)

Chapter 4.

- 4.1. Film types selected for initial investigation. C4.2
- 4.2. Exposures made using the Rollei-Metric 6006 camera. C4.3
- 4.3. Summary of FP4 experimental parameters. C4.14
- 4.4. Correlation coefficients for the estimated parameters of an incomplete third order polynomial after rejection of insignificant parameters. C4.28

Chapter 5.

- 5.1. Film types selected for investigation. C5.7
- 5.2. Processing chemicals. C5.9
- 5.3. Exposures processes and measurements made. C5.13
- 5.4. Regression line gradients for the scale change measurement relative humidity relationship. C5.21
- 5.5. Mean RMS residuals for all film type investigated. C5.23
- 5.6. Pre-exposure conditioning treatments. C5.27
- 5.7. RMS residuals from pre-exposure conditioning treatments. C5.29
- 5.8. Exposure level and uniformity variations. C5.32
- 5.9. RMS residuals from exposure variation treatments. C5.35
- 5.10. Variations of developer formulations. C5.37
- 5.11. RMS residuals from developer variations. C5.40
- 5.12. Variation of fixing bath formulation. C5.42
- 5.13. Mean RMS residual deformations from hardening agent variations. C5.48
- 5.14. Variation of drying environment. C5.50
- 5.15. Drying environment RMS residual deformations. C5.53
- 5.16. Measurement times and environmental conditions. C5.55
- 5.17. RMS residuals for individual grid images. C5.60

Chapter 6.

- 6.1. Reseau specifications. C6.2
- 6.2. Standard deviations of calibrated resseau positions. C6.3

Illustrations

Chapter 2.

2.1.	Generalised cross section through a photographic film.	C2.1
2.2.	Dissociation of silver halide.	C2.2
2.3.	Ionisation and solubility of gelatin.	C2.3
2.4.	Cellulose.	C2.4
2.5.	Schematic diagram of a machine for the solvent casting of film base. . .	C2.5
2.6.	Polyester.	C2.5
2.7.	Schematic diagram of a machine for the melt casting and biaxial orientation of polyester base.	C2.6
2.8.	Schematic diagram of the exposed and developed grain.	C2.8
2.9.	Fine grain development.	C2.11
2.10.	Acutance development.	C2.11
2.11.	Low contrast	C2.11
2.12.	High contrast	C2.12
2.13.	Extreme contrast	C2.12
2.14.	Quadrant tone reproduction diagram	C2.16
2.15.	Quadrant diagram demonstrating changes in the overall tone reproduction curve due to changes in development parameters	C2.17
2.16.	Microdensitometer trace of a uniformly exposed and processed film sample and its frequency distribution	C2.18
2.17.	Granularity as a function of density level for a range of emulsion types	C2.19
2.18.	Line spread and point spread functions	C2.20
2.19.	Microdensitometer trace of knife edge images	C2.20
2.20.	The concept of modulation transfer	C2.22
2.21.	Modulation transfer functions for Kodak TMAX films	C2.22
2.22.	Modulation transfer functions for Ilford FP3 Aerial film and Agfa Aviphot 200 PE films	C2.23
2.23.	Modulation transfer functions for Kodak Technical Pan film, demonstrating the effect of variation of development parameters	C2.23
2.24.	Moisture capacity	C2.24
2.25.	Effect of gel/base ratio on humidity coefficient	C2.24
2.26.	Rate of moisture conditioning for single sheets of film	C2.25
2.27.	Percent size change with relative humidity	C2.25
2.28.	Position of film in magazine, showing present and future frame images	C2.26
2.29.	Leading and trailing edge effects	C2.27
2.30.	Typical hysteresis loop of unprocessed Kodak Plus-X aerial films	C2.28
2.31.	Effect of temperature on moisture loss	C2.28
2.32.	Changes in location of 25 points over a period of 18 hours	C2.29

2.33.	Possible processing dimensional changes	C2.30
2.34.	Hysteresis loop for processed and unprocessed Plus-X film on 102 μ m polyester base	C2.30
2.35.	Average processing dimensional change	C2.30
2.36.	Uniformity of processing dimensional change	C2.30
2.37.	Moiré pattern of a water spot	C2.31
2.38.	Radial distortion effects of unflatness	C2.33
2.39.	Interferogram of film flatness in a Zeiss aerial camera	C2.33
2.40.	Interferogram from a smooth faced pressure pad	C2.33
2.41.	Contour map of film deformation an a 35mm camera system	C2.34
2.42.	Thickness profiles of Kodak Double-X film 2405 (Polyester base)	C2.34
2.43.	Thickness fringes from triacetate film base	C2.35
2.44.	Thickness fringes from polyester film base	C2.35

Chapter 3.

3.1.	The central perspective projection	C3.2
3.2.	Image formation by a lens	C3.4
3.3.	Radial lens distortion curves for two Zeiss lenses at infinity focus	C3.5
3.4.	Variation of principal distance with focus setting	C3.6
3.5.	Observed change of radial distortion with object distance	C3.7
3.6.	GSI's back projected reseau system	C3.9
3.7.	RMS image residuals for 96 image points, obtained with different correction methods applied to the same image marks	C3.12
3.8.	Two reseau deformation patterns from images on 9" square aerial film	C3.12
3.9.	The covariance function and Gaussian equation	C3.14
3.10.	The geometric basis of multi-station convergent photography	C3.18

Chapter 4.

4.1.	Rollei-Metric 6006	C4.1
4.2.	Zeiss (Jena) Stecometer	C4.4
4.3.	Intergraph Intermap Analytic	C4.4
4.4a.	Transformation with origin at centre	C4.5
4.4b.	Transformation with origin at top right	C4.5
4.5.	Affine scale parameters for the two measurement sets of TMY Roll A . .	C4.6
4.6.	Mean residual discrepancies for the two measurement sets of TMY Roll A	C4.6
4.7.	Kodak TMY Roll A, examples from epochs 1 and 2	C4.8
4.8.	Affine scale parameters for frames from TMY Rolls B,C and D	C4.9
4.9.	Mean residual discrepancies for frames from TMY Rolls B,C and D	C4.9
4.10.	Examples of residual vectors from TMY 120 films B,C and D, measured at 58% relative humidity	C4.10

4.11.	Affine scale changes associated with	
4.12.	EPD and TCP, mean discrepancies after scale change.	C4.12
4.13.	Examples of Technical Pan 120 residual vector plots	C4.13
4.14.	Examples of Kodak Ektachrome 120 residual vector plots	C4.13
4.15.	FP4 120 and 220, affine scale change parameters	C4.15
4.16.	FP4 120 and 220, mean residual discrepancies after affine transformation	C4.15
4.17.	Examples of residual vector plots on FP4 120 and 220 film	C4.17
4.18.	Reseau sharpness numbers for FP4 120 film C, frames 1 and 3.	C4.18
4.19.	Schematic diagram of the Zygo Mk III phase measuring interferometer.	C4.19
4.20.	Unflatness of the rear surface of the P32 reseau plate.	C4.19
4.21.	Schematic diagram of the Fizeau interferometer.	C4.20
4.22.	Interferometer pattern for the Rollei-Metric 6006 reseau No.40.	C4.20
4.23.	Unflatness of reseau plate rear surface, Rollei-Metric 6006 camera No. 005298811.	C4.21
4.24.	Residual vectors after global transformations, FP4 120 (3A).	C4.23
4.25.	Residual vectors after global transformations, FP4 220 (3B).	C4.24
4.26.	Mean RMS residuals for transformations applied to frames 01 and 03 of 120 films A and C, and 220 films B and D.	C4.25
4.27.	Results of t-tests to determine the significance of the parameters estimated for FP4 120 frame 03A. (x direction).	C4.27
4.28.	Results of t-tests to determine the significance of the parameters estimated for FP4 120 frame 03A. (y direction).	C4.27
4.29.	Computation of the deformation at pseudo reseau points.	C4.29
4.30.	Residual deformations after local bilinear transformation, applied using circled reseau points.	C4.30
4.31.	Covariance and cross covariance functions for FP4 120 frame N03A. .	C4.33
4.32.	Covariance and cross covariance functions for FP4 220 frame N03B. .	C4.33
4.33.	FP4 03A, Gaussian fit to $C(d)_{xx}$ and $C(d)_{yy}$	C4.35
4.34.	FP4 03B, Gaussian fit to $C(d)_{xx}$ and $C(d)_{yy}$	C4.35
4.35.	Residual deformations for FP4 frames 03A and 03B after linear least squares interpolation based on a variety of site configurations.	C4.37
4.36.	RMS residuals after interpolation using Gaussian function based on a range of site configurations.	C4.36

Chapter 5.

5.1.	Master grid layout.	C5.4
5.2.	The contact exposing situation.	C5.8
5.3.	The NPL modified ZKM measuring microscope.	C5.11

5.4.	Graph of scale change against measurement environment relative humidity for Ilford Pan F 120 roll film.	C5.16
5.5.	The relationship between scale change and measurement environment relative humidity for Kodak Technical Pan 120 roll film.	C5.17
5.6.	The relationship between scale change and measurement environment relative humidity for Ilford FP4 120 roll film.	C5.18
5.7.	The relationship between scale change and measurement environment relative humidity for Kodak TMX, TMY and TRI-X 120 roll films.	C5.19
5.8.	Graph of scale change against measurement environment relative humidity for Ilford FP3 and Agfa 10E75 70mm films.	C5.20
5.9.	Selection of contact grid exposures made onto Ilford Pan F 120 and Kodak Technical Pan 120 films at 5mm and 2.5mm grid spacings. . . .	C5.21
5.10.	Selection of contact grid exposures made onto Kodak TMX 120, TMY 120, TRI-X 120, Ilford FP3 70mm and Agfa Holotest 10E75 70mm films.	C5.22
5.11.	The effect of increasing pre-exposure conditioning time on the relationship between scale change and relative humidity.	C5.28
5.12.	Some contact grid exposures made onto Kodak Technical Pan 120 film with varying pre-exposure conditioning time.	C5.30
5.13.	The effect of variation of exposure level on the scale change at measurement / relative humidity relationship.	C5.33
5.14.	Variation of in-plane deformation with image density variation.	C5.34
5.15.	The effect of variation of developer formulation on the scale change / relative humidity relationship (PAN F).	C5.38
5.16.	The effect of variation of developer formulation on the scale change / relative humidity relationship (TCP).	C5.39
5.17.	Some contact exposures made onto Kodak Technical Pan 120 film with development in Ilford ID11 or perceptol.	C5.41
5.18.	The effect of using hardening and non-hardening fixing baths on the relationship between scale change and relative humidity (FP4 220, TCP 120).	C5.43
5.19.	The effect of using hardening and non-hardening fixing baths on the relationship between scale change and relative humidity (FP4 220). . .	C5.44
5.20.	The effect of using hardening and non-hardening fixing baths on the relationship between scale change and relative humidity (Pan F 120).	C5.45
5.21.	The effect of using hardening and non-hardening fixing baths on the relationship between scale change and relative humidity (TCP 120).	C5.46

5.22.	Selection of contact grid exposures made onto Ilford FP4 120 and Kodak TCP 120 films during the second set of hardening tests.	C5.49
5.23.	Conditioning time after processing, Ilford FP4 220 film, Roll A, Frames 2 and 5.	C5.51
5.24.	Conditioning time after processing, Ilford FP3 70mm film, Roll A, Frames 2 and 5.	C5.52
5.25.	Environmental variation of NPL ZKM measurement room (16th July 1989 to 2nd August 1989).	C5.56
5.26.	Scale change against measurement environment relative humidity for repeated measurements of two grid images (FP4 220).	C5.57
5.27.	Scale change against measurement environment relative humidity for repeated measurements of two grid images (Pan F 120).	C5.58
5.28.	Scale change against measurement environment relative humidity for repeated measurements of two grid images (TCP 120).	C5.59
5.29.	Contact grid exposures made onto Kodak Technical Pan 120 film with measurement in the ZKM over five epochs.	C5.61
5.30.	The effect of measurement environment relative humidity on the mean RMS residuals for two images on Kodak Technical Pan 120 film.	C5.62

Chapter 6.

6.1.	Reseau plate 1, parallelism and unflatness before and after fitting.	C6.3
6.2.	A scanned image of a resolution test target.	C6.4
6.3.	Exposures made using the modified Hasselblad SWC camera (HS1) onto Agfa Holotest 10E56 70mm film	C6.7
6.4.	RMS residuals after affine transformation at reseau image positions for Agfa 10E56 70mm film exposed in HS1	C6.7
6.5.	Exposures made using the modified Hasselblad SWC camera onto Kodak Technical Pan 120 film	C6.9
6.6.	RMS residuals after affine transformation at reseau image positions for all rolls of Kodak Technical Pan 120 film exposed in 120 Back A.	C6.11
6.7.	RMS residuals after affine transformation at reseau image positions for all rolls of Kodak Technical Pan 120 film exposed in 120 Back B.	C6.11
6.8.	Exposures made using the modified Hasselblad SWC camera onto Ilford FP4 120 and 220 films.	C6.13
6.9.	RMS residuals after affine transformation at reseau image positions for all rolls of Ilford FP4 120 film exposed in 120 Back A.	C6.14
6.10.	RMS residuals after affine transformation at reseau image positions for all rolls of Ilford FP4 220 film exposed in the 220 Back.	C6.14
6.11.	Schematic diagram of the network geometry.	C6.19
6.12.	Layout of one of the pinned targets.	C6.21

6.13.	Shoring products survey target 760.	C6.21
6.14.	The concrete tower showing pinned target array.	C6.22
6.15.	Mean RMS photo-coordinate residuals for each camera / back / film permutation.	C6.26
6.16.	Mean RMS photo-coordinate residuals for UMK and HS1 cameras after bundle adjustment.	C6.28
6.17.	Typical photo-coordinate residual vector plots for images produced on Holotest 70mm film in the HS1 camera.	C6.29
6.18.	A typical photo-coordinate residual vector plot from images exposed on Holotest plates in the UMK 10/1318 camera.	C6.30
6.19.	Mean RMS photo-coordinate residuals for the Wild P32 camera after bundle adjustment.	C6.32
6.20.	Typical photo-coordinate residuals for the P32 series of images.	C6.33
6.21.	Graph of radial lens distortion for each of the camera back / film combinations exposed in the modified Hasselblad (HS2).	C6.36
6.22.	Mean RMS photo-coordinate residuals for HS2 images after adjustment.	C6.38
6.23.	Photo-coordinate residuals for different permutations of film and camera back exposed in the HS2 camera.	C6.39
6.24.	Mean RMS photo-coordinate residuals for the non-metric Hasselblad camera after bundle adjustment.	C6.42
6.25.	Photo-coordinate residuals computed during the global adjustment for two images exposed in the Hasselblad 500C camera (HS60).	C6.42
6.26.	Differences between camera calibration parameters from the Global Bundle Adjustment and those estimated during the individual bundle adjustments (TCP 1,B).	C6.46
6.27.	Differences between camera calibration parameters from the Global Bundle Adjustment and those estimated during the individual bundle adjustments (FP4 120/220).	C6.47
6.28.	Graph of radial lens distortion for each of the camera back / film combinations exposed in the modified Hasselblad (HS2).	C6.48
6.29.	Photo-coordinate residuals for Technical Pan 120 film, Back B, Camera station 2.	C6.50
6.30.	Mean RMS photo-coordinate residuals for the camera back and film combinations exposed in the HS2 camera.	C6.51
6.31.	Mean RMS object space coordinate discrepancies for the various camera back / film correction permutations.	C6.53
6.32.	Object space discrepancy vectors for the Technical Pan 120 Back A data set (front view).	C6.54

6.33.	Object space discrepancy vectors for the Technical Pan 120 Back A data set (top view).	C6.54
6.34.	Differences between camera calibration parameters from the Global Bundle and those estimated during the Pseudo Practical Survey.	C6.58
6.35.	Radial lens distortion from Global Adjustment minus radial lens distortion computed during the Pseudo Survey.	C6.58
6.36.	Mean RMS photo-coordinate residuals for the modified Hasselblad camera.	C6.60
6.37.	Photo-coordinate residuals after adjustment using five constrained control points.	C6.61
6.38.	Object space discrepancy vectors for the Pseudo Survey (front view).	C6.63
6.39.	Object space discrepancy vectors for the Pseudo Survey (top view).	C6.64

Acknowledgments

I would like to thank the following people for their contribution made during the production of this research project:

Professor M.A.R. Cooper and **Dr. R.E. Jacobson** my two supervisors for their irreplaceable guidance and constructive criticism made during the course of the research work. Professor Cooper for his advice and logical thought on all things analytical and statistical, and Dr. Jacobson for his knowledge of photographic chemistry. I would like at this point to make especial thanks to Professor Cooper for arranging funding to allow my continued full time work on this project during the last few months.

Dr. C.Forno, Mr S.Oldfield, Mr S.Brown, Dr. R Hunt and **Ms A.Kearney** of the National Physical Laboratory, Teddington, who not only allowed me access to their excellent ZKM measuring microscope, but also contributed advice within a congenial environment on aspects of measurement. Also of importance was their strivance to obtain the ultimate in precision from measurement techniques, which has considerably widened my perspective on the possibilities of optical measurement techniques.

My colleagues at City University:

Mr J.N. Hooker for his help in the construction of and photography of the test field.

Mr J.Clarke who responded rapidly to my requests for additions and modifications to his bundle adjustment program GAP.

Dr. J.H. Chandler, Mr N.E. Lindsey, Mr R Littleworth and **Mr D. Stirling** for their help and advice especially on problems associated with data acquisition and modelling.

Mr S.F. Ray of the Polytechnic of Central London who not only suggested some of the directions for research investigated during this thesis, but also introduced me to the Photogrammetry section at City University.

Professor J Gates of University College who made many useful and constructive comments on the investigative approach and measurement techniques used during this research project.

The Science and Engineering Research Council who provided an Instant award which supported me financially for the first three years of this thesis.

Declaration

"I grant powers of discretion to the University Librarian to allow this thesis to be copied in whole or in part without further reference to me. This permission covers only single copies made for study purposes, subject to normal conditions of acknowledgement".

Abstract

The physical properties of photographic roll film in conjunction with the design of small format cameras are generally optimised for ease of use and reliability during pictorial photography. Such design contributes greatly to the problems associated with the accuracy of camera calibration and analytical data reduction of non and semi metric small format imagery.

The results of experimentation into both in-plane and out-of-plane film deformation, using a variety of commercially available monochrome small format film stocks, are presented. Physical parameters investigated include environmental conditions, image density, processing regime, measurement and film back variations. A standardised photographic process is arrived at, such that in-plane deformations are minimised. The procedure permits modification by variation of emulsion type and development to match the recording characteristics of the photographic material with the subject areas of interest.

In the light of results obtained from the measurement of reseau images produced from an in-house modified Hasselblad SWC camera, film deformations occurring in-camera are found to be an order of magnitude larger than in-plane deformations. In-camera deformations are attributed to unflatness at exposure and tensions during film wind-on, both of which are functions of camera design.

Results from the close range calibration of variety of metric, semi-metric and non-metric cameras are discussed in the light of the above experiments. The accuracies of derived coordinates are examined and show that the small format camera can be considered to be of photogrammetric importance. Transformation methods associated with the use of reseau photography to correct for image deformation are investigated and their suitability compared in terms of their ability to model the specific problems associated with semi-metric photography.

Whilst network geometry is shown to provide the major factor influencing the determination of photogrammetric coordinates, it is shown that given good camera design, analytical photogrammetry using small format images can be limited by the image quality produced by the lens and film combination.

1. Introduction.

Photogrammetry incorporates techniques which are often regarded as two distinct disciplines; applied photography and surveying.

Perhaps the most recent definition of photogrammetry is that due to Karara (1989):

"Photogrammetry is the art, science and technology of obtaining reliable quantitative information about physical objects and the environment through the process of recording, measuring and interpreting photographic images and patterns of radiant imagery derived from sensor systems".

The term "applied photography" covers the use of photography for the production of records of value in the study, understanding and control of basic processes in all branches of science, industry and education (Arnold et al 1971). This second viewpoint places photogrammetry as a specialisation under the general umbrella of applied photography.

Analytical photogrammetry is the simultaneous determination of the camera interior orientation and exterior orientation parameters and the coordinates of object space points of interest. However the photographic viewpoint is pertinent when it is considered that the success of any photogrammetric project (especially one demanding high precision) will depend primarily on the quality, content and dimensions of the images produced.

This thesis sets out to stress the importance of photographic techniques by putting into perspective some of the photographic elements, concentrating especially on film deformation, which contribute to the determination of photogrammetric coordinates in close range photogrammetry.

1.1. Reasons for carrying out research in this area.

Terrestrial photogrammetry was traditionally carried out with cameras which were designed to be distortion free, employed notionally flat glass plate based emulsions as the imaging surface and incorporated an internally defined and stable image coordinate system. Use of such metric cameras meant that the relationship between the object space and its corresponding image could be modelled using simple mathematical assumptions.

Currently there is a trend for smaller semi-metric cameras, which are cameras designed primarily for pictorial photography, but modified for photogrammetric purposes by the inclusion of defined lens focus settings and often a reseau grid plate. These 'pictorial' lenses have significant distortions which must be included in the mathematical model. Additionally the film surface can no longer be assumed to be distortion free. To exploit fully the low cost potential of such cameras

it is necessary to investigate the significance of and devise models for the physical causes of such deformations.

Optical lens qualities demanded by pictorial photography mean that small format lens designs are manufactured to precise tolerances. The stable nature of most designs mean that their significant geometric lens distortions can be stabilised by semi-metric camera modifications and can therefore be modelled mathematically. Consequently the largest potential uncompensated physical factor limiting the photogrammetric application of semi-metric cameras is film deformation.

Considerable work has been carried out to assess physical causes and contributions of film deformation in cameras and photographic films intended for aerial survey. However very little assessment has been made concerning the use of films and cameras intended for pictorial photography.

1.2. Summary of previous work relating to the deformation of photographic materials.

Many evaluations of film deformation have been made, predominantly in the 1960's where the stimulus came from inaccuracies occurring in aerial triangulation using analytical plotters.

Initially work was carried out to determine the extent of film deformations occurring in the 9 inch square images typical of the large format mapping cameras used (Carman 1946; Calhoun et al 1966; Adelstein and Leister 1963). Subsequently simple shrinkage corrections based on the disparity between the calibrated and imaged positions of edge and corner fiducial marks were evolved (Lampton and Umbach 1966; Bender 1972; Ziemann 1971a).

Measurement methods employed to analyze film deformation included pin gauge techniques (Byer 1983), measurement of calibrated contact grid exposures and moiré interference techniques (Calhoun et al 1960; Adelstein et al 1966).

Research continued using both laboratory techniques and cameras equipped with a reseau grid, allowing film deformations over the entire format area to be assessed under both laboratory and practical conditions (Carman and Martin 1969; Ziemann 1971c). The availability of such imagery with known film deformation permitted the emergence of a variety of mathematical correction models, based on the differences between calibrated reseau cross and imaged cross positions (Lampton and Umbach 1966; Ziemann 1971b and 1972a).

Direct measurement of film unflatness within the survey camera was also carried out using interferometric techniques (Clark 1972; Meier 1972). At about the same time Michener (1972) working for Eastman Kodak investigated thickness variations in aerial films. Significantly film unflatness in 35mm cameras was also investigated using interferometric methods (Tsuruta et al

1970).

Photographic film deformation and its physically based correction in analytical photogrammetry has been neatly summarised by Ziemann (1971):

"The geometry of a photographic image changes throughout its life time. These changes can be negligibly small or significant, they can affect the entire format area or only small parts of it. The image deformation can be recognised if reference points are available. The extent of recognition depends not only on the number of reference points but also on their distribution. Examples demonstrate that a dense centrally projected reseau exposed simultaneously with the original negative is the only solution that permits checking of image deformations produced during the recording process. A reseau can also be utilised to correct any deformation of the image to an extent limited only by its density, if analytical procedures are used."

Although made in 1971, these observations are probably still pertinent today, since the basic constituents of photographic film have altered little.

Surprisingly little significant work appears to have been published since the mid 1970's concerning the physical causes of film deformation, although an International Society for Photogrammetry (ISP) working group on image geometry was active during this time. Various film based close range large format camera systems have however evolved (Brown 1984; Dold 1990; Peipe 1990) incorporating various new design and reseau technologies to control film deformation.

Importantly for the restitution of non-metric imagery, the availability of increased computer processing power has directed research towards the production of rigorous photogrammetric models such as the bundle adjustment (Brown 1976; Ebner 1976; Faig 1975; Granshaw 1980). These techniques have been further extended to include both semi-metric and non-metric imagery (Faig 1976; Fraser 1982a 1982b, 1984b; Fryer 1988; Wester-Ebbinghaus 1986), providing methods by which such cameras could be used for high precision photogrammetry.

Film emulsion technology has also advanced with the incorporation of different silver grain morphologies conferring high speed with less granularity than previously possible (Jacobson et al 1989; Kodak 1987a; Ilford 1990b). Also specialist films such as Kodak Technical Pan have been introduced which offer the scientific photographer a wide range of tone and speed flexibility (Kodak 1987b).

Several small format camera systems, modified for photogrammetric purposes, are commercially available (Rollei-Metric 6006 and 3003; Leica Elcovision; Pentax PAMS645-VL ; Hasselblad MK70 and MKW). These cameras use high quality optics and generally incorporate a reseau or vacuum back for the control of film deformation. Several researchers have investigated the use of such non-and semi-metric cameras, producing photogrammetric solutions of generally lower accuracy

than metric cameras made specifically for photogrammetry. (Faig 1976; Fraser 1984; Fryer and Fraser 1986; Fryer 1988).

It should be mentioned that the direction of most current research has again changed, the new direction being provided by the availability of low cost digital imaging systems (Torlegård 1989). These in the long term may replace film as an imaging surface, but at the present time such systems are limited by pixel size and the ability to produce large stable sensor arrays. For example the state of the art in low cost CCD cameras is probably something similar to the Videk Megaplus camera. This camera capable of producing upto seven frames per second incorporates an array of 1340 by 1037 pixels in a 9mm by 7mm area, each pixel of which is $6.8\mu\text{m}$ square (Kodak 1988b). In very approximate terms this array can be compared with the medium format film camera format of 55mm by 55mm, incorporating a mean silver halide grain size of $4\mu\text{m}$. In both cases each array element has the ability to produce 256 grey levels, such that the quantity of data stored on a single film frame is many times greater than that captured by the pixel array (Grun 1988; Arnold et al 1971).

1.3. Outline of intentions for the research project.

The intentions of this research project were to evaluate film deformations occurring in generally available small format film products and to assess some of the factors limiting photogrammetric measurement with small format camera systems.

Experimental work has been carried out to determine the magnitude and significance of film deformation occurring out of camera. Investigations included both reversible dimensional changes, caused for example by environmental fluctuations, and also permanent dimensional changes attributable for example to chemical processing.

Based on the laboratory results, in-camera reseau grid experiments have been conducted. These were directed at assessing the magnitude and deformation patterns occurring when a variety of commercially available 120, 220 and 70mm monochrome film stocks, are exposed in a small format reseau camera.

Finally both metric, semi-metric and non-metric cameras have been used to conduct a photogrammetric survey of a target array. In this way some of the practical photographic and photogrammetric modelling problems associated with the use of small format cameras have been assessed.

1.4. Thesis Structure.

This thesis is composed of seven main chapters, two appendices and a bibliography.

Chapter 2 consists of a brief introduction to basic photographic principles. It also contains a detailed summary of historical experimental work carried out to investigate film deformations.

Chapter 3 is directed primarily at the non-photogrammetrist and contains an outline of the theoretical principles and mathematical models which form the basis of the data processing techniques used during the course of this thesis. It also details the methods which have been applied to model film deformation in small format cameras.

Chapter 4 describes an initial investigation conducted to ascertain the magnitude and correction of film deformation in a small format semi-metric camera.

Chapter 5 gives results from the film deformation investigation conducted in the laboratory, in which individual constituents of the photographic process were varied and their effects on film deformation assessed.

Chapter 6 comprises the in-camera film deformation experiments. It also includes results from the practical study based on the photography of a target array with a variety of cameras.

Chapter 7 evaluates the thesis, and summarises the conclusions and inferences made during the course of the research project.

Appendices A and B are intended for reference and consist of a selection of vector plots showing the film deformations associated with the experimental work detailed in chapters 5 and 6 respectively.

2. Photogrammetric applications of photographic theory.

The aim of this chapter is to present a succinct framework of the physico-chemical theories of the photographic process relevant to the use of photographic materials for photogrammetric work. Throughout the chapter results from other workers and inferences as to their significance to the photogrammetric process are drawn. The significance of the factors are then assessed to provide some directions for the physical analysis of film deformation in small format cameras which constitutes the bulk of the research work described in this thesis. On making such inferences it must be borne in mind that whilst analytical photogrammetric techniques (Chapter 3) can be adapted to model deformations occurring during the photogrammetric process, it is far more preferable to formulate corrections based on the actual physical deformations occurring.

The physical and chemical properties of photographic materials are a function of their individual constituents. A thorough understanding of the nature of dimensional change and the formation and control of the photographic image can only be gained by considering the properties and interaction of the individual photographic film components.

2.1. Constituents of photographic materials.

Conventional photographic film consists of a sandwich of light sensitive, silver halide containing emulsion layers, supported by a base material commonly composed either of cellulose triacetate or polyethylene terephthalate. The properties of the light sensitive layers are selected to confer specific speed, grain and spectral sensitivity characteristics.

2.1.1. Emulsion constituents.

The primary constituents of a conventional photographic emulsion are gelatin and silver halide. Other compounds are added during manufacture, for example sensitising dyes to confer the desired spectral sensitivity.

2.1.1.1. Silver halides.

The silver halides are light sensitive salts, formed by the combination of silver nitrate with ammonium halide. Halides are members of the group

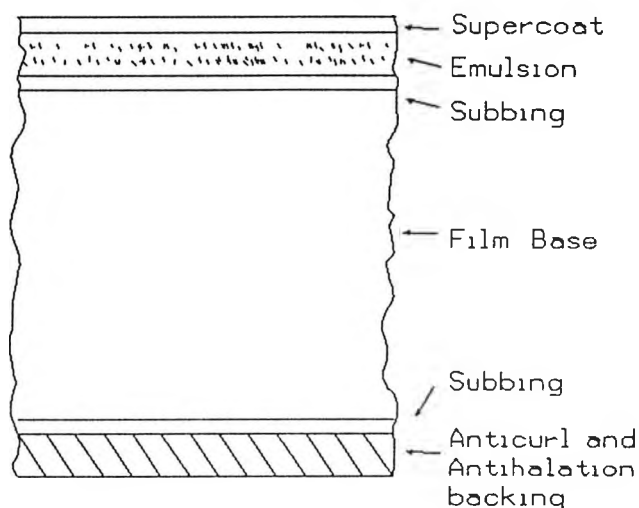


Figure 2.1. Generalised cross section through a photographic film. (Jacobson et al 1983).

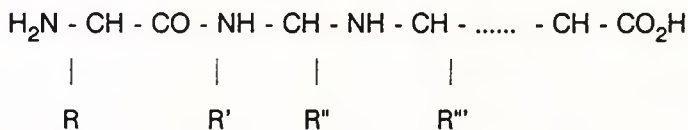
of elements known as the halogens: bromine, chlorine and iodine. They are used in photographic materials in the form of a suspension of minute crystals commonly referred to as grains. Silver halide suspensions are, as described below, inherently unstable and must be combined with a binding agent.

2.1.1.2. Gelatin.

Gelatin provides the binding agent in which the silver halide crystals are suspended. Any movements of the exposed silver halide (or processed silver image) in this suspension will give rise to dimensional differences between the aerial image formed by the camera lens and the photographic image which we actually measure. The position of the image points that we wish to measure will consequently differ from those that are assumed by mathematical functional models based on the lens system alone (Chapter 3.1). The gelatin/silver halide structure accordingly constitutes the physical root of the dimensional properties of the photographic image.

Gelatin is derived from collagen, a polypeptide found in the hides and bones of animals. It is a complex organic macro-molecule having three structural levels each of which contribute to the dimensional and chemical stability of the emulsion layers. The consistency of the gelatin is particularly important, the presence of impurities having a significant effect on the light sensitivity of the photographic emulsion (Duffin 1966).

Primary structure: This constitutes the basic molecular structure of gelatin and is concerned with the order and sequence of the side groups.



R, R', R'', R''' are side groups, approximately 20 of which are known.

Secondary structure: The polypeptide is not linear, but chains are coiled together to form a helical or spring like structure.

Tertiary structure: Gelatin in common with most polypeptides is not helical throughout its length, but the chains are compacted with some short helical regions held together by hydrogen or hydrophobic bonds. It is these weak bonds which furnish gelatin with the colloidal characteristics which provide its basic moisture absorption properties.

2.1.1.3. Colloidal properties.

Gelatin and silver halide both belong to the group of substances called colloids. On combination in a photographic emulsion, the greater stability of the gelatin enhances the stability of the amalgamation as described below. The associated colloidal properties are useful when considering the factors influencing the dimensional stability of photographic materials. For the gelatin/silver halide mixture colloidal characteristics are based on water as the solvent, whilst the components gelatin and silver halide constitute the dispersed matter or sol. Gelatin is lyophilic or solvent loving, whilst silver halide is lyophobic (Sheppard and Sweet 1921; Sheppard and Elliot 1921). These water based properties form the basis of the nature of the dimensional changes which have been demonstrated to occur in practical analysis of photographic materials (Adelstein 1972; Carman and Martin 1969; Colton and Wiegand 1958).

Lyophobic colloids are dispersions of soluble substances with a phase boundary between the small particles and the dispersing medium. Their stability is low and related to the charge carried by the constituent particles, this charge being acquired by adsorption or dissolution.

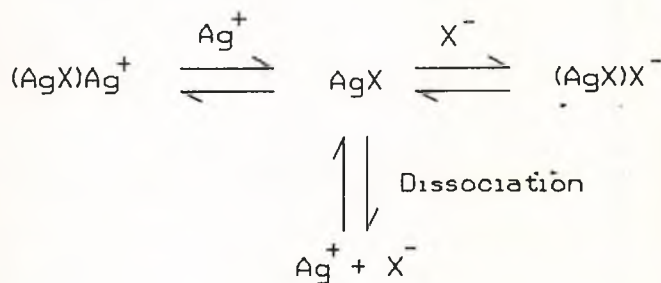


Figure 2.2. Dissociation of silver halide, (Duffin 1966).

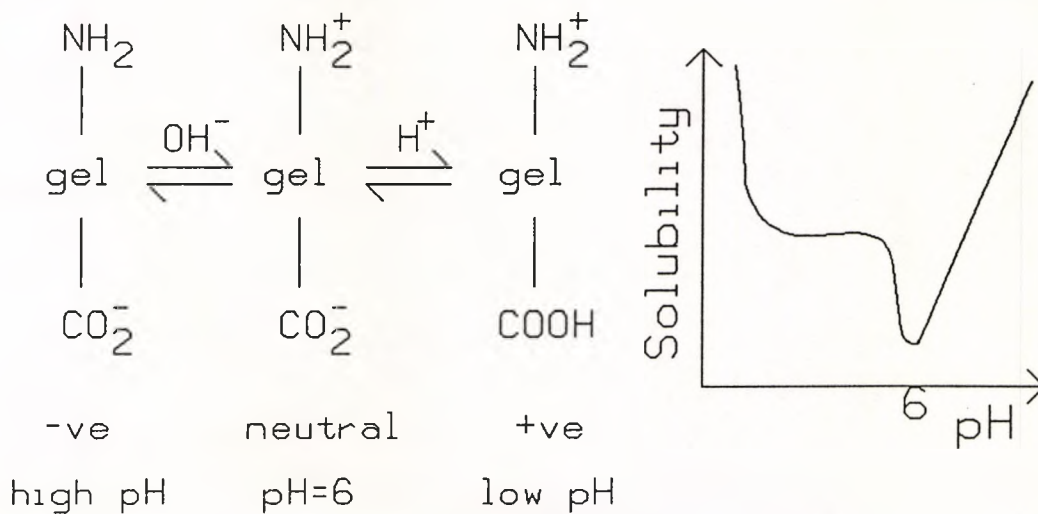


Figure 2.3. Ionisation and solubility of gelatin, (Duffin 1966).

The stability of lyophilic colloids has been attributed to an electrical double layer theory (James 1966). For gelatin the stabilising charge is from ionisation, such that minimum water take-up or swell occurs at the isoionic point, corresponding to a pH of around six (Fig. 2.3). Maintenance of a pH of around 6 during all processing stages, if practical without compromising image quality,

may be important for the minimising of dimensional changes and stresses occurring during processing. Such stresses are thought to be responsible for some of the irregular deformations observed in the thin based Kodak Technical Pan 120 film (Section 5.3.1.2).

The attributes of gelatin have relevance not only to dimensional stability, they also contribute to the processes of manufacture and image formation. For example due to the water based structure coated layers are readily permeated by aqueous solutions facilitating chemical processing, gelatin also acts as a halogen acceptor enhancing and stabilising the latent image during exposure.

Finally following processing, silver images are of archival permanence conferring one of the major advantages of photogrammetry as a measurement technique, images can be stored and measured at a later date. Archival permanence is one of the key advantages offered by images on film as opposed to digital images which are much costly to store, consequently any process developed to minimise dimensional changes should still provide images which are of archival permanence.

2.1.2. Film base materials.

The emulsion layers are soft and must be coated onto a substrate material which for the purposes of small format photography is generally a film base. The film base must provide the structural support necessary to counteract the expansions and contractions of the colloidal emulsion layers (Michener 1972). An assortment of film base materials are available for scientific photography, but since this work is primarily concerned with camera speed products intended for small format roll film cameras we will look in depth only at the two common types. Most films manufactured in volume are coated onto either cellulose tri- (or di-) acetate or polyester (polyethylene terephthalate) which is also known by brand names such as Mylar and Estar. The structural and manufacturing differences between these two film bases contribute to many of the dimensional changes documented later in this chapter.

2.1.2.1. Cellulose.

The cellulose acetates are formed by the acetylation of cellulose, the resultant being based on the ratio between cellulose and acetyl groups.

Cellulose acetate film base is made using the technique of solvent casting, whereby 'dope' a concentrated solution of di- or tri-acetate in solvent (CH_2Cl_2 / CH_3OH) is applied to a heated drum on which the solvent is evaporated to leave 1 to 8% residual (Fig. 2.5). The base is then stripped from the drum. Since the base is not stable, plasticisers may be added to enhance archival permanence. The evaporation of these plasticisers with time has been documented as a possible cause for dimensional changes occurring in triacetate backed materials (Calhoun et al 1960).

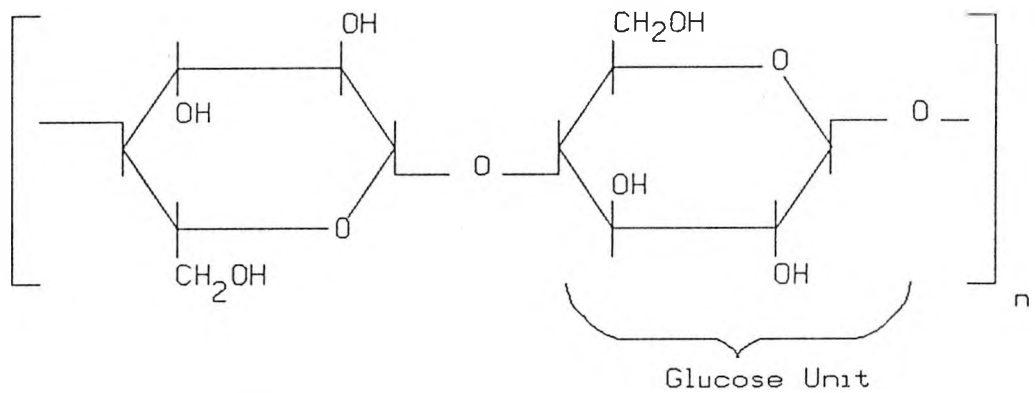


Figure 2.4. Cellulose, (Jacobson 1985).

A thin layer of gelatin is easily attached to the base, in a process known as subbing, facilitating good adhesion between the base and emulsion layers. Regardless of how good the dimensional properties of the base are, without good adhesion, they will not be able to counteract changes in dimension of the emulsion layers.

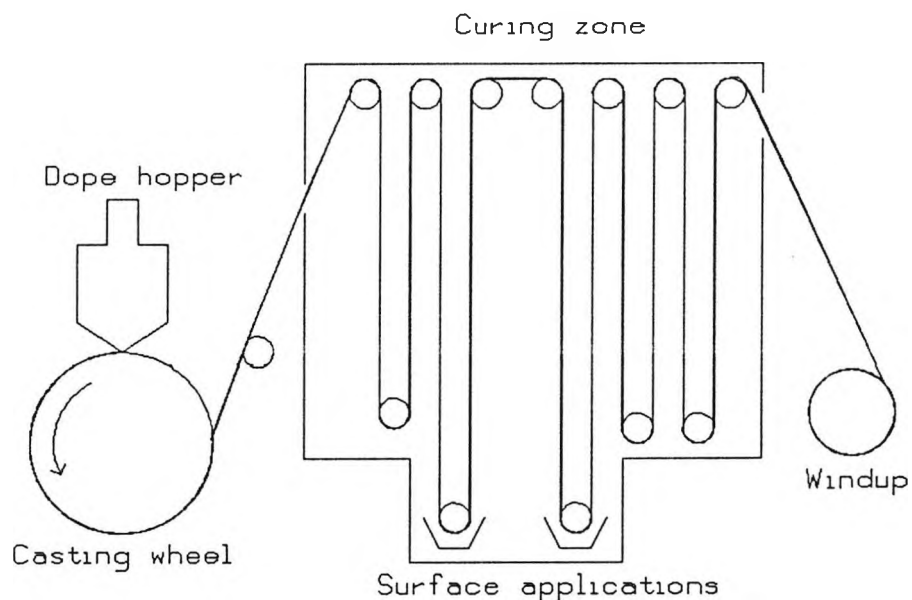


Figure 2.5. Schematic diagram of a machine for the solvent casting of film base, (Jacobson 1985).

2.1.2.2. Polyester.

Polyester is insoluble in most solvents, therefore a manufacturing technique based on melt casting is used (Fig. 2.7). No plasticiser or solvents are used during production conferring higher stability but at the expense of increased cost. For reasons of economics a mass produced film will often be coated onto the cheaper cellulose bases, unless a specific need justifies the increased strength and stability of a polyester base.

In manufacture the material is physically stretched or extruded, this having an important influence

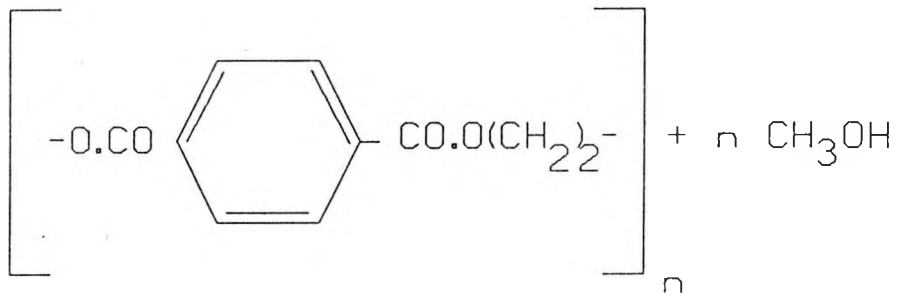


Figure 2.6. Polyester, (Jacobson 1985).

on the final dimensional properties of the material. The degree and rate of stretch is adjusted such that the finished support is manufactured with as high a degree of uniaxialism as possible.

A problem with the material is that it is hydrophobic and hence difficult to subb, a corona discharge must therefore be used to provide a suitably roughened surface for gelatin adhesion.

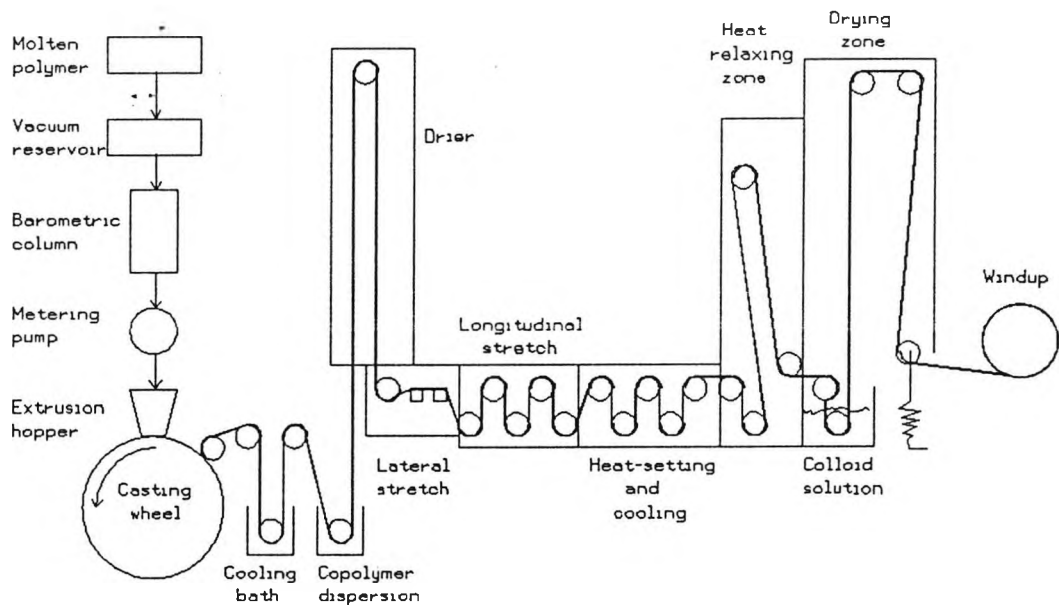


Figure 2.7. Schematic diagram of a machine for the melt casting and biaxial orientation of polyester base. (Jacobson et al 1983)

Whilst table 2.1 demonstrates some dimensional desirability of polyester base over cellulose triacetate, it contains only information on global scale changes as opposed to local changes. Where photogrammetric measurement is concerned it is easy to correct for uniform image scale changes, but assessing localised changes requires a specialised analysis (Section 3.3.1). A literature search has not provided any data concerned with localised changes in film base materials, such that the most advantageous film base for photogrammetric measurement presents a key question to be answered by the practical work conducted for this thesis. This is especially

true when it is considered that a great variety of films intended for small format pictorial photography are readily available on cellulose triacetate base.

Table 2.1. Physical characteristics of base materials

Parameter	Glass	Paper	Tri-acetate	Polyester
Thickness (mm)	0.76 to 6.3	1.0 to 4.0	0.09 to 0.21	0.10
Thermal coefficient of expansion per °C	0.001%	-----	0.0055%	>0.002%
Humidity coefficient of expansion per %RH	0.00%	0.003 to 0.14%	0.005 to 0.010%	0.002% to 0.0004%
Water absorption at 50%RH and 21°C	0.0%	7.0%	1.5%	0.5%
Tensile strength at breaking (kg cm ⁻²)	1400	70	1085	1750
Processing size change	0.00%	0.2 to 0.8%	> -0.1%	0.03%

(Data contained in table obtained from Kodak 1972)

2.2. Photographic chemistry.

The aim of this section is to summarise the elements of photographic chemistry which are at the basis of the control of tone reproduction. Such a knowledge of the physico-chemical controls possible during the photographic process can provide the basis for obtaining optimal images for any given photogrammetric project.

2.2.1. Sensitivity to light and the silver halide emulsion.

To produce photographs we must employ a material which is sensitive to light, that is one that undergoes some chemical or physical change when light acts on it. There are many light sensitive substances, ranging from diazonium salts, through silver halides to silicon charge coupled devices. In this investigation however only conventional materials using silver halide based emulsions have been used, since these constitute the light sensitive material used in most camera speed photographic products intended for small format photography.

There are three silver halides, in descending order of sensitivity; iodide, bromide and chloride. In a primitive emulsion state, as a precipitation in a gelatin medium, they have very low light sensitivity and are of very high contrast, producing essentially a binary image. Also the silver halides are sensitive only to the blue end of the spectrum.

To increase emulsion speed and lower contrast the emulsion must be ripened. Ripening is essentially a heat treatment process, whereby larger grains are formed to produce a mixture of

grain sizes with differing light trapping abilities. The association of crystal size distribution with speed and contrast explains why fast emulsions often give grainy low contrast negatives, whilst fine grained emulsions are slow and of higher contrast.

After washing, a second heat treatment process is used in which sulphur impurities present in the gelatin form sensitivity specks on the crystal surfaces further enhancing speed. To confer extended spectral sensitivity into the green, red and possibly infra-red regions of the spectrum, trace quantities of dye are added (Tamura and Hada 1967).

It is this series of procedures which determine the characteristics (speed/grain/contrast) of the emulsion. Grains of small size but uniform distribution providing slow high contrast emulsions, whilst an emulsion with a distribution of grain sizes will provide higher speed and reduced contrast at the expense of resolution.

On exposure to light, energy in the form of quanta are trapped, resulting in the transfer of electronic charge to the grain sensitivity specks. The metallic silver produced by this mechanism is termed the latent image. The threshold level or minimum quantum requirement to produce a developable image has been shown to be four quanta (Farnell and Chanter 1968).

Recently, differing grain structures have been produced, such as cubic and flattened grains. Flattened grains, known as T grains, are still subject to the same minimum quantum requirement, but because of their larger surface area are able to trap more quanta per sensitivity speck for a given exposure. On controlled development a relatively small clump of silver image, in relation to the grain area, is produced (Jacobson et al 1990). This approach allows increased film speed whilst maintaining image quality, useful for example during aerial survey where exposures are made from a moving platform using ambient light.

2.2.2. Developers and development.

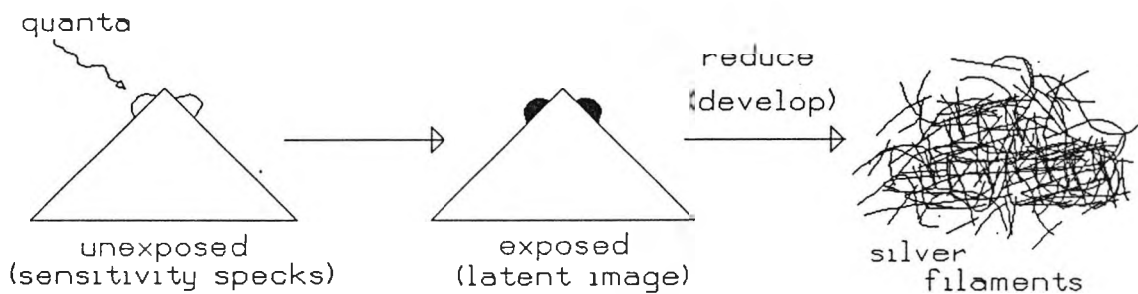


Figure 2.8. Schematic diagram of the exposed and developed grain, (Langford 1982).

To produce a measurable image, the latent image must be developed or amplified using a

reducing agent which is selective in that it only acts on exposed silver halide grains.

Development is a reduction reaction involving electron transfer from the developing agent to the exposed silver halide. It is selective in that it acts faster on exposed grains, probably being catalysed by the metallic silver produced.

Developer formulations are based on variation of three main constituents: developing agent, alkali accelerator and the quantity of solvent (usually water) used.

The general development reaction is shown below:

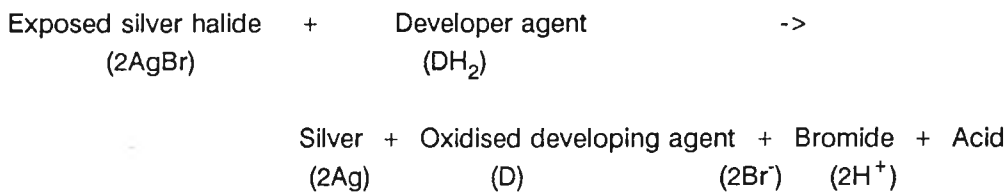


Table 2.2. Constituents of a typical developer solution.

Constituent	Examples
Developing agent	Hydroquinone, 1 phenylpyrazolidone (Phenidone), N-methyl 4-aminophenol (Metol).
Alkali or accelerator	Sodium carbonate, borax, sodium hydroxide.
Preservative	Sodium sulphite.
Restrainer	Potassium bromide and/or organic anti-foggant.

(Data from Jacobson and Jacobson 1980)

Developing agents lose protons (becoming more active reducing agents) as alkalinity of the developing agent is increased. The type of alkali used can therefore have a significant effect on developer activity and the resultant micro-structure of the photographic image. The possible variations applicable to most situations where the concern is to produce a conventional silver image are described in the following section.

Many electrochemical theories have been derived to describe in more detail the way in which the silver image is built up during the development process. The major ones are the charge barrier theory, the catalytic theory and the electrode approach (James 1966; Gurney and Mott, 1938). Of interest to photogrammetrists and consequently this thesis are two recognised methods of metallic silver image growth, which have been derived from these electrochemical theories.

a) Chemical development; in this process the silver ions which form the metallic silver image are obtained from the silver halide crystal. This gives rise to filamentary chains of silver, such that the

resultant developed grain is more light scattering or turbid.

b) Physical development; in this instance the developing agent is slower working, and contains a silver halide solvent. Silver ions from the solution are used to form the image, resulting in a more compact structure.

Obviously if the highest resolution is desired, physical development is preferable, but there is no practical developer which is exclusively of one type. The most useful practical classification of developing solutions is consequently according to functional type, specifically for influences to the contrast / speed / graininess trade-off. It should be mentioned that the influences of the developer solution can only provide a fine tuning of the emulsion, the emulsion grain distribution dominating the final image characteristics.

a) Fine grain; These developing agents employ metol/hydroquinone or phenidone/hydroquinone as the active agent. Borax is used as the alkali to give a pH of 8 to 9. Sodium sulphite at a concentration of about 100 grammes per litre is present as a silver halide solvent to promote physical development (Fig. 2.9). This type of agent is a general purpose developer for most photogrammetric situations. It can provide compact grains without compromising film speed, half a stop loss in emulsion speed being typical.

b) Acutancy: Essentially diluted fine grain developers, where development is influenced by differing exposure levels in adjacent areas. The active developer in less exposed areas carries over to adjacent exposed areas, whilst developer degradation products migrate the other way, causing inhibition of the development reaction. The magnitude of the resultant increased micro-contrast and apparent image contrast, being closely correlated with agitation (Fig. 2.10). Increases in micro-image contrast whilst useful for visual assessment, may not be so useful for photogrammetric measurement because under high magnification the location of the edge or point to be measured may change.

c) Low contrast: To record extreme subject brightness ranges, a low contrast developer such as POTA, can be used. This employs a low concentration of developing agent, usually phenidone or metol, and sodium sulphite as the alkali (Fig. 2.11). Providing some speed loss can be tolerated, this developer can be useful where recording of detail is required over a large range of subject tones. For example to record details in areas of shadow and direct sunlight might be important.

d) **High contrast:** Useful in aerial photography where the subject is generally of low contrast are developers such as D19. Commonly used are a high concentration of hydroquinone/metal developing agent combined with an alkali such as sodium carbonate producing a very active solution. Characteristics are increased emulsion speed and grain (Fig. 2.12).

e) **Extreme contrast:** A process known as infectious development is employed in conjunction with special emulsions, to produce an essentially binary image. Developer formulations incorporate hydroquinone and para-formaldehyde. The para-formaldehyde combines with sulphite to form an aldehyde-bisulphate compound, thereby keeping the sulphite at a low concentration. A low level of sulphite is essential in extreme contrast or lith developers because high levels of sulphite destroy the infectious development effect. Lith developers are used in conjunction with a lithographic emulsion which contains very fine essentially mono-dispersed grains. The grains are of the chloro-bromide type are very slow (Fig. 2.23).

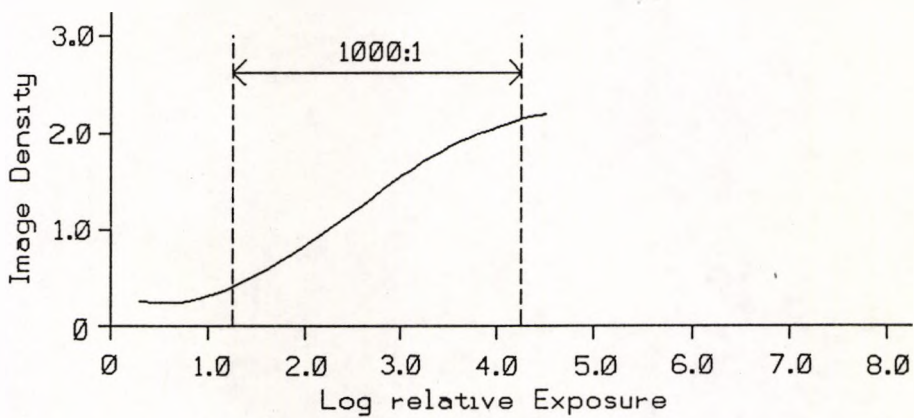


Figure 2.9. Fine grain development.

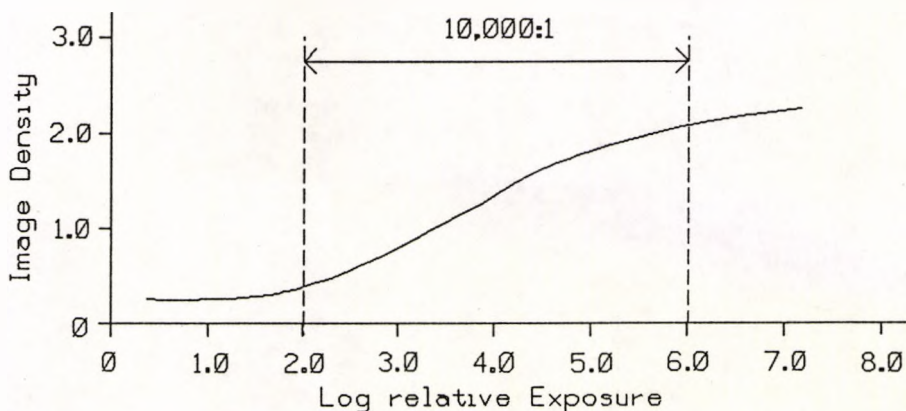


Figure 2.10. Dilute fine grain development.

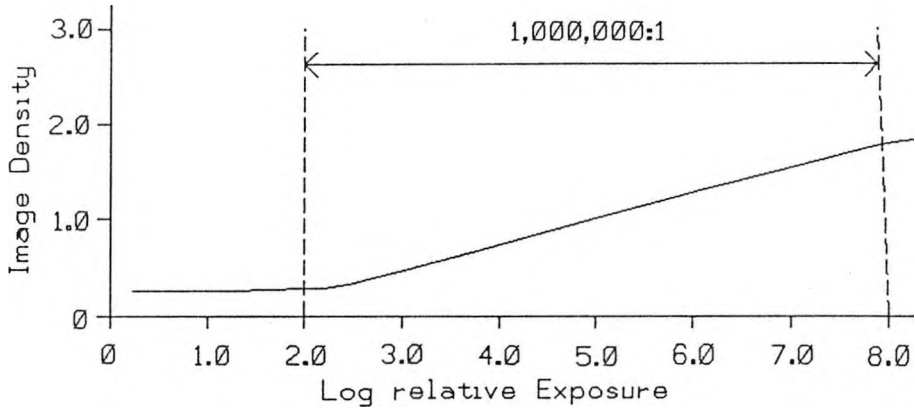


Figure 2.11. Low contrast.

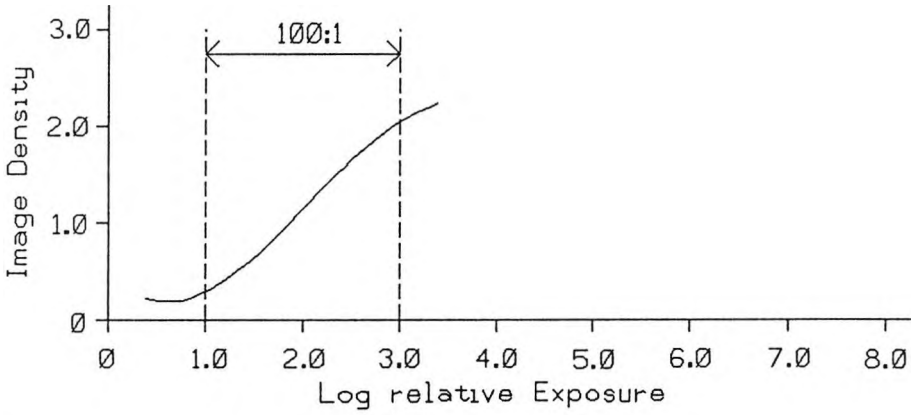


Figure 2.12. High contrast.

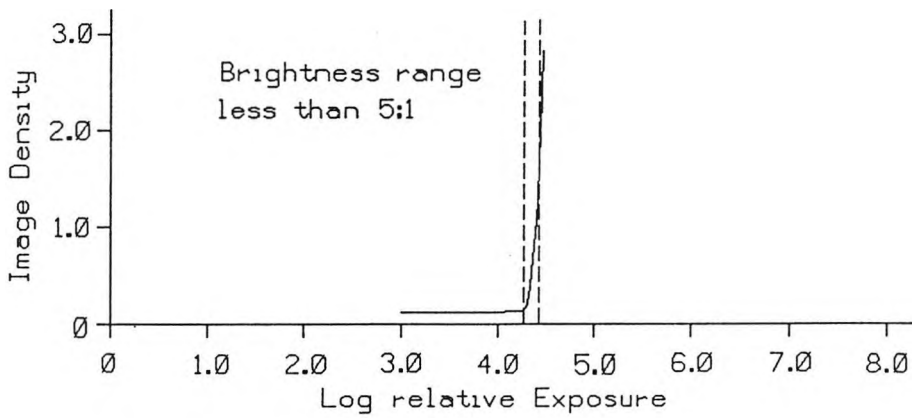


Figure 2.13. Extreme contrast.

(Data from Jacobson and Jacobson 1980).

2.2.3. Fixation.

The main purpose of the fixing bath is to render the photographic image permanent by converting remaining unexposed silver halides to water soluble compounds that can be removed in the fixing bath and the following wash step. The silver halide solvent used is almost exclusively sodium or

ammonium thiosulphate, which reacts with the silver halide in a two stage process to form the water soluble complex monoargento-dithiosulphate.

The rate of fixation is governed by the concentration of thiosulphate ions present in the solution, until these inhibit swelling of the gelatin emulsion and therefore diffusion. The degree of gelatin swell can be controlled by the addition of salts such as ammonium thiocyanate, however the resultant softened gelatin can easily be damaged.

Gelatin has, as described in section 2.1.1.2, a structure not unlike that of a sponge, with water penetration causing the structure to expand. In addition to hardening carried out during manufacture, agents, which promote the cross linking of gelatin chains, and therefore presumably dimensional stability, may be added to the fixing bath. There are two classes of hardening agent:

a) Inorganic; such as aluminium potassium sulphate and chromium potassium sulphate. These are thought to act by the formation of complex ions (Al^{3+} or Cr^{3+}) which link adjacent gelatin polypeptide chains, active ionic groups present in gelatin are also thought to be involved. Such hardeners may also be incorporated during emulsion manufacture to form so called stabilised gel emulsions (Kodak 1970b), conferring decreased dimensional change with humidity variation and improved mechanical resistance. The dimensional effects of such a hardening agent are rigorously investigated during the experimental work (Section 5.3.4.2).

b) Organic hardeners; for example formaldehyde, form covalent bonds between adjacent gelatin chains and the hardener (Itoh et al. 1990). The formation of these bonds has been shown to occur slowly, often taking several weeks to attain maximum strength. This type may be less suitable for photogrammetry since it is often necessary to measure images as soon after processing as practicable when with this agent the hardening process will be incomplete.

2.2.4 Washing and drying.

Washing is carried out to remove residual silver thiosulphate complexes and excess thiosulphate which would otherwise slowly decompose in the emulsion, attack the silver image and cause staining (Kopperl et al. 1988). Since the rate of removal of ions by wash water decreases exponentially with time (Walls 1977), optimum washing requires that the concentration of ions in the water must be as low as possible. The best way of achieving this is by the use of running water. The minimum wash time in running water generally recommended to achieve the archival permanence desirable for photogrammetric images is about thirty minutes at twenty degrees centigrade.

Of primary importance for the control of dimensional change during the wash process is emulsion swell, which as shown in figure 2.3 is linked to pH. As mentioned in section 2.2.3, hardening

agents may be added to increase gelatin cross-linking. Also available are anti-swelling agents, these are usually chemically inert salts such as sodium sulphate, which utilise the principal that water tends to diffuse out of a gel into an adjacent concentrated salt solution.

One of the main factors affecting dimensional change of photographic materials is the drying process, whereby excess water in the gelatin emulsion and to a lesser extent the film base is removed. A discussion of this process and some results obtained by other workers is given in section 2.4.3.

2.3. Image quality factors.

To obtain optimum performance from photographic materials under all conditions, a knowledge of some parameters defining their response are desirable.

Image quality factors cannot be applied rigorously to pictorial photography because the impression given by an image also depends on psychological and physiological considerations. For photogrammetry the recording of image detail for optimum mensuration is of major importance. The measurement process often involves high magnifications so that the microstructure and contrast of small regions of image detail are of primary importance, a situation in which physical image quality factors are most relevant.

2.3.1. Basic sensitometry.

Sensitometry is the objective study of the response of photographic materials to light. There are two forms of sensitometry, **absolute**; where the exposure given to the film is known quantitatively, this being used for absolute film speed determination, and **comparative**; where it is sufficient for the exposure to be constant from test to test.

Sensitometry is primarily concerned with two parameters, the exposure given to the film, measured in lux seconds in the case of absolute sensitometry, and the image density or light stopping power of the resultant image. Absolute exposure is determined using calibrated standard light sources of known luminous intensity and spectral emission, whilst relative exposure may be simply derived from reflectance readings of subject elements.

Image or optical density is defined as the logarithm of the ratio of the light incident on the negative to the light transmitted. The logarithmic unit is used simply because the eye's response to light is approximately logarithmic. Physical measurements of image density are complicated by the reflection and scattering of light, such that different illumination and collection methods give rise to differing densities. In the photogrammetric situation, images on transparent bases are measured with parallel illumination and normal emergence, therefore the specular definition of

density and accordingly specular density measurement are more appropriate.

The standard representation for sensitometric measurement is the characteristic curve, conventionally having common axis scales with density as the ordinate and log exposure (absolute) or log relative exposure (comparative) as the abscissa.

For simple evaluations, the three most important parameters defining the shape of the characteristic curve are; the threshold level (base + fog); the near-linear straight line portion having an average gradient γ and; the maximum density (D_{max}). Some illustrations of characteristic curves corresponding to changes in development are shown in figures 2.9 to 2.13. An example of the use of a characteristic curve is in the determination of emulsion speed according to the ISO standard (ISO 1974). Specified parameters are fitted to the shape of characteristic curve derived from absolute exposure and defined processing.

2.3.2. Tone reproduction.

A subject consists of a range of different luminance due to differing reflection characteristics exhibited by disparate areas. These characteristics are affected by angle of view and by the variation in the illumination that they receive. Tone reproduction is the name given to the relationship between the tonal characteristics of a scene and its photographic reproduction.

The quadrant diagram (Fig. 2.14) demonstrates that the final reproduction, a negative for most photogrammetric purposes, will depend on four factors:

- a) The original subject luminosity range, this is a characteristic of the subject and ambient lighting conditions. Modification by use of artificial light sources and reflectors, generally to reduce the range by increasing luminosity in shadow areas, is a very beneficial technique.
- b) Camera lens flare, caused by light scatter at lens surfaces and other constructional features. This scattered light will generally fall evenly on the film surface, giving rise to a uniform degradation of the image shadow areas.
- c) The negative material characteristic curve shape, governed primarily by choice of emulsion with some modification possible by variation of development parameters as was discussed in sections 2.2.1 and 2.2.2.
- d) Viewing flare, caused by light scatter within the optics of the photogrammetric measuring machine, resulting in a uniform degradation of the image highlight areas. Generally a negative image is viewed for measurement, consequently the subject highlight areas will

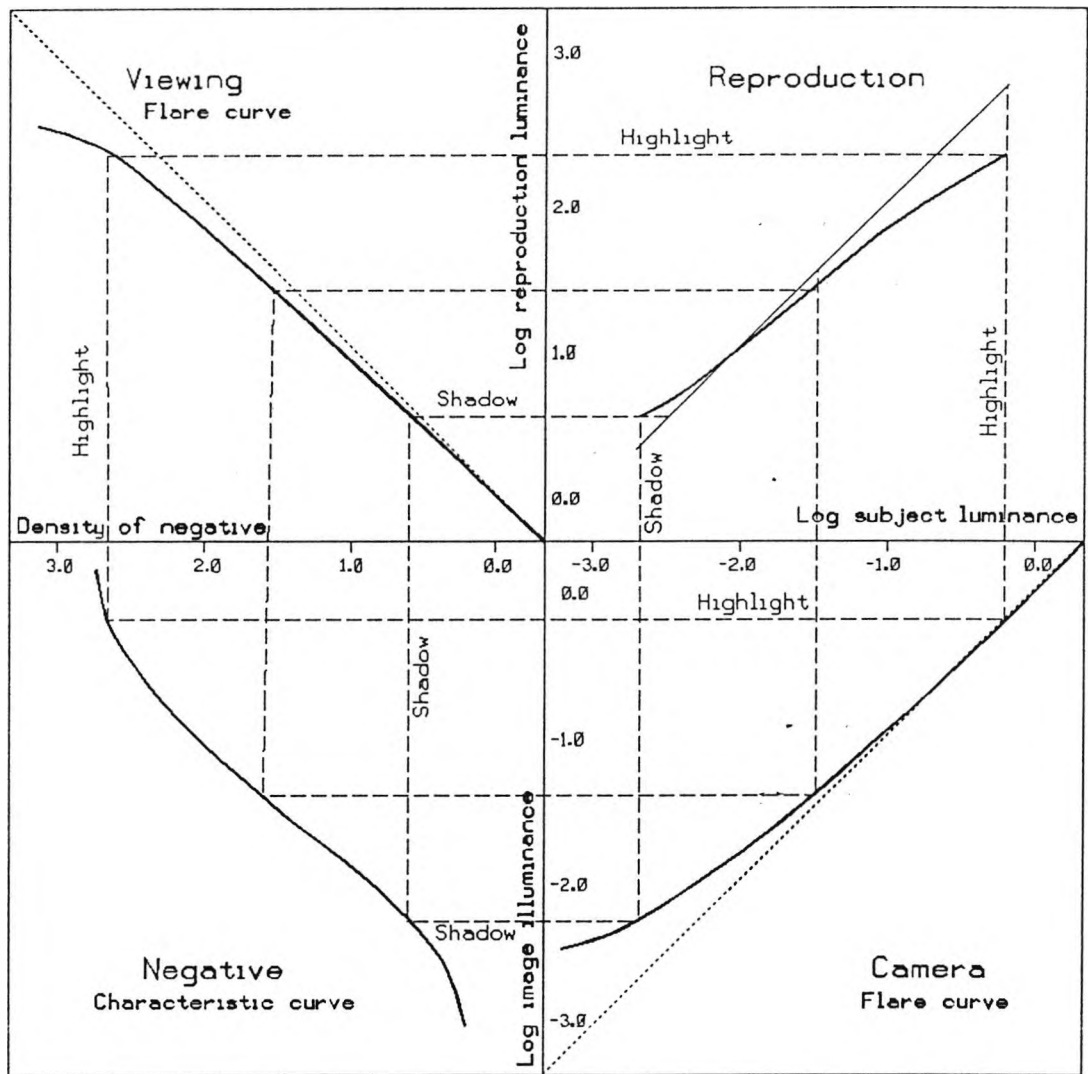


Figure 2.14. Quadrant tone reproduction diagram, (Arnold et al 1971).

be of greatest optical density and therefore the most prone to degradation by scattered light. Cumulatively flare effects result in a decrease in effective density range and a reduction of mid-tone contrast.

The major controllable variable influencing tone reproduction for a given image luminosity range is the characteristic curve of the negative material. Efficient use of this control involves the matching of sensitometrically derived data for film/development combinations to the subject luminance range, or part thereof, that is to be recorded.

An example of the use of this image "design" is described below, where the negative characteristic curve shape is modified by development. The initial situation enabling the recording of a small range of subject tones with high contrast can be useful if the subject areas of interest are for example thin cracks on similarly illuminated grey concrete blocks. The second characteristic curve shape, providing recording of all subject tones with reduced contrast, can be applied to a subject

with a large tonal range, for example where measurement of a structure incorporating both highlight and shadow details is required.

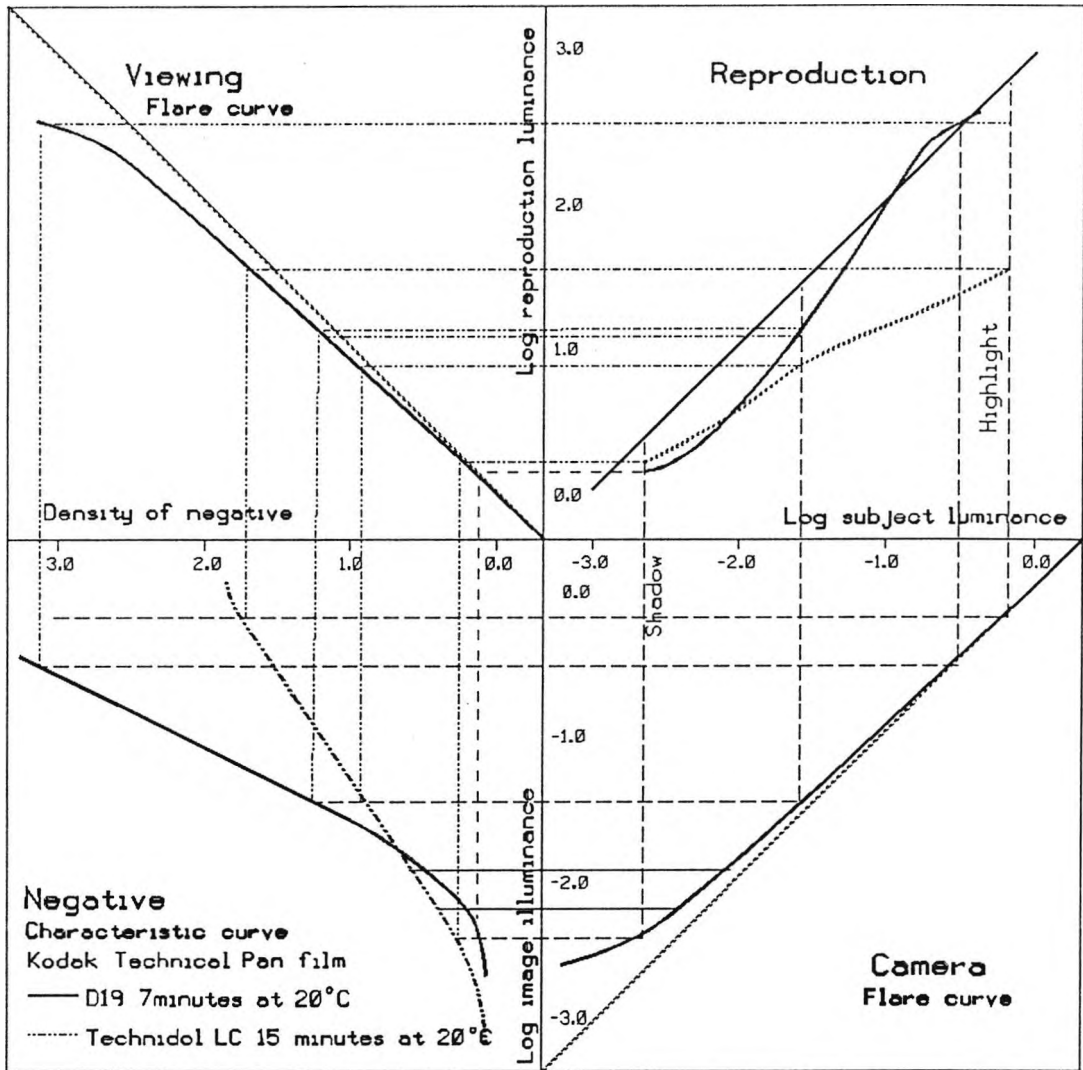


Figure 2.15. Quadrant diagram demonstrating changes in overall tone reproduction curve due to changes in development parameters, (Derived from Kodak 1987b).

Figure 2.15 demonstrates how changing the development parameters and therefore the negative material characteristic curve shape for Kodak Technical Pan film, can alter the overall reproduction curve. Processing in Kodak D19, has produced a characteristic curve with a high gamma, such that the contrast in the overall reproduction in the mid range has increased at the expense of the shadow and highlight regions which have been compressed. In this situation changing the camera exposure given will result in a movement of the curve along the log image illuminance axis, enabling the contrast increase to be produced over any specific region. The use of Technidol LC developer has resulted in a tone reproduction curve of much lower contrast than the original subject, but all subject tones have been recorded without differential compression of tones.

The above example probably represents the maximum degree of control possible by variation of

development. Conventionally, changes in emulsion type would be of more importance. It is clear that if the effects of changes in the photographic process, determined by sensitometric evaluation, are known then the system can be tailored to produce the best reproduction curve for the imaging situation. For example, the location of grey rivets on a grey bridge, or targets positioned both in highlight and shadow areas.

Pictorial photography generally results in a positive image, the negative image being printed onto a second paper based material to produce a print. The printing process is analogous to contact printing the negative onto a diapositive material, to produce a positive image for measurement. This extra step in the photographic process can simply be added to the quadrant diagram and the possible variation in tone reproduction monitored.

2.3.3. Information capacity and resolution.

The quality aspects of photographic images are all related to the non-uniform granular nature of the sensitive layer. The silver grains of the image occupy roughly the same position as the original silver halide grains from which they were formed, but as explained in section 2.2.2 they rarely retain the same shape. This single factor could ultimately provide the limiting factor for photogrammetric measurements made using conventional camera speed photographic products.

The ability of a photographic material to record small details is dependant on two emulsion properties: **granularity** and **turbidity**.

2.3.3.1. Granularity.

Granularity is defined as the objective measure of the inhomogeneity of a uniformly exposed and processed photographic image. Granularity can be evaluated using a microdensitometer, a scanning microscope with which the optical density fluctuations over small regions of film can be measured.

With reference to figure 2.16 (Sturge 1977) , a microdensitometer trace showing the microscopic variations in density about a mean density level, deviations from the mean density can be evaluated and plotted as a density function. This function has been shown to take the form of a normal or Gaussian distribution, such that its standard deviation (σ) may be used as a measure of granularity.

Many models have been derived to relate granularity to the visual perception of graininess. Selwyn (1959) analyzed microdensitometer traces of several samples of photographic materials. Assuming that the spatial distribution of grains in the emulsion was random and that the size of the grains was small in relation to the area of the scanning aperture, he determined that the

Selwyn granularity G for a given film sample was dependent on σ and the area a of the scanning aperture.

$$G = \sigma \sqrt{a} \quad (2.1)$$

Various factors have been identified which affect the magnitude of granularity (Fig. 2.17):

- Most important is the emulsion average grain size, a large average grain size corresponding to high granularity.
- Fine grain developers utilising physical development give rise to images with reduced granularity, however the associated decrease in speed can mean that better results will be obtained by using a slower emulsion.
- Granularity is the result of small area changes in image density therefore increased development producing higher contrast images will also result in greater granularity.
- Finally it has been demonstrated that granularity increases with image density indicating that overexposure should be avoided.

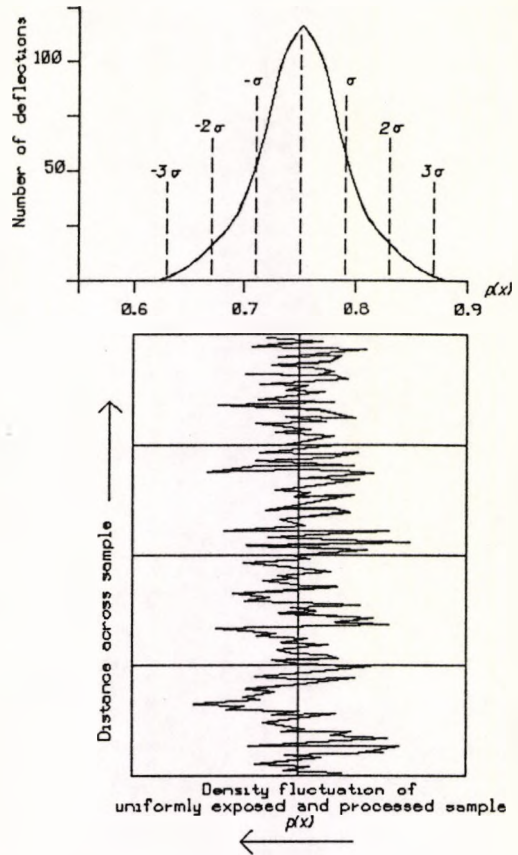


Figure 2.16. Microdensitometer trace of a uniformly exposed and processed film sample and its frequency distribution, (Sturge 1977).

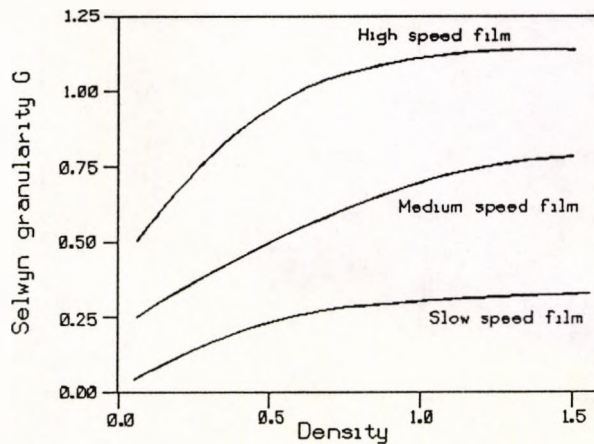


Figure 2.17. Granularity as a function of density level for a range of emulsion types, (Jacobson et al 1983).

2.3.3.2. Turbidity.

Turbidity is the capability of a photographic emulsion to diffuse the exposing light by means of reflection, refraction, diffraction and scattering. It is controlled by three main factors, the size of the silver halide crystals, the emulsion thickness and the opacity of the emulsion to the exposing light.

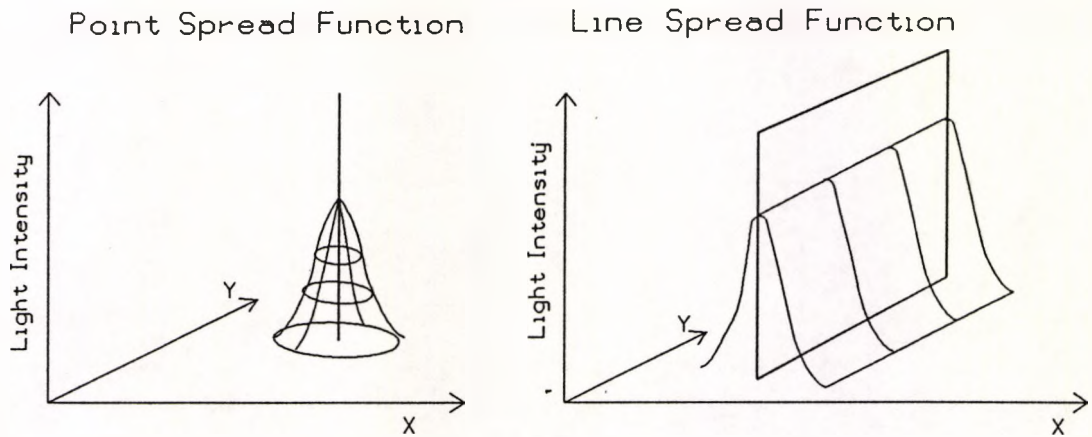


Figure 2.18. Line spread and Point spread functions, (Sturge 1977).

If a very fine pencil of light is incident on the film, as it passes through it will be degraded into a spatial distribution of light, known as the optical point spread function (Fig. 2.18). If a row of such pencils of light are incident on the film, a spread function will be produced, known as the line spread function.

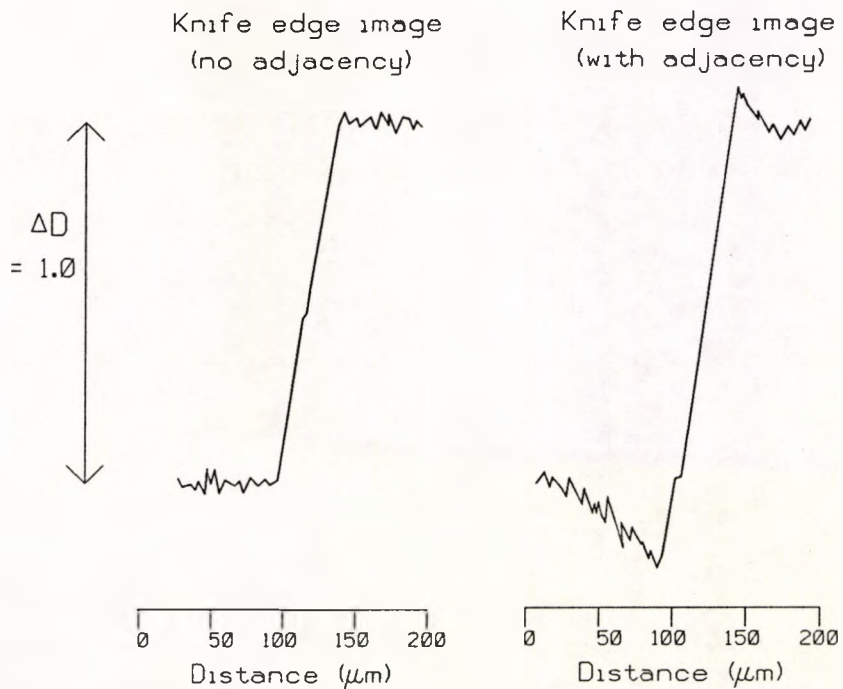


Figure 2.19. Microdensitometer traces of knife edge images, (Jacobson et al 1983).

In practical terms due to the additional effects of granularity, an exposure made of a knife edge with collimated light will produce a density trace as shown in figure 2.19. The presence of any adjacency effects during development, especially if enhanced using acutancy formulations (Section 2.2.2), will give rise to the second trace. Where photogrammetric measurement is concerned this increased edge micro-contrast may not be desirable because the actual location of the line may move.

The point spread function (PSF) of an emulsion shows the size and shape of the smallest image point, it is therefore the fundamental building block of the photographic image. Commonly its magnitude is expressed by the width of the spread function at the ten percent intensity level.

2.3.3.3. Modulation Transfer Function.

The resolution ability of the photographic process can be expressed in a variety of ways. Generally it is thought of in terms of the number of lines resolved per millimetre in the focal plane. A basic assessment can be made by photographing, at specific magnification, sets of bar test targets of standard contrast, then visually assessing the resultant image under high magnification (Section 6.1.1). Such tests are practical as a rule of thumb guide, but without strict standardisation (Brock 1968) provide data useful only for comparing imaging systems evaluated under similar conditions. A major problem with the expression of resolution is that there is no direct way in which known resolution values of system components can be combined to give a reliable total system response. The total system response can be valuable in the design of a photogrammetric survey because it allows the selection of a lens/film combination which will record the appropriate level of subject detail.

A better method of expressing response regards the photographic image as being a summation of an infinite number of point spread functions, each corresponding to a point in the object distribution. This Fourier approach to image formation is founded on the linear combination of sinusoidal exposure distributions of varying spatial frequency (Higgins and Perrin 1959; Lamberts 1958).

The degradation of the original image distribution during its photographic recording occurs solely as a reduction in contrast (Fig. 2.20), the magnitude of this contrast, or modulation drop increasing with spatial frequency. The modulation transfer function is accordingly a curve describing the degree to which the image contrast decreases as spatial frequency is increased.

The MTF for a particular film type is simply the Fourier transform of its line spread function derived from microdensitometer analysis of knife edge exposures (Gerencser 1972). Images of sine wave and possibly square wave targets may also be used (Welch 1971), although the MTF derived will include the contribution from the lens. Since the Fourier definition uses sine waves, analysis of

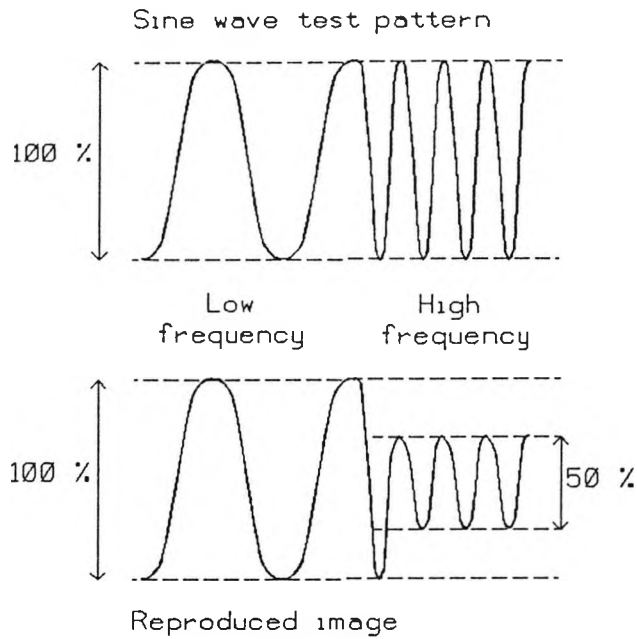


Figure 2.20. The concept of modulation transfer, the low frequency pattern retains the full modulation of the original, but the high frequency pattern is reduced to 50% of the original modulation. (Arnold et al 1971).

a square wave target will give rise to errors, generally resulting in increased modulation due to the added contributions of higher frequency information to lower frequency patterns. Also the apparent increased modulation due to adjacency effects are more obvious from square wave MTFs, such that the modulation may exceed unity at some frequencies.

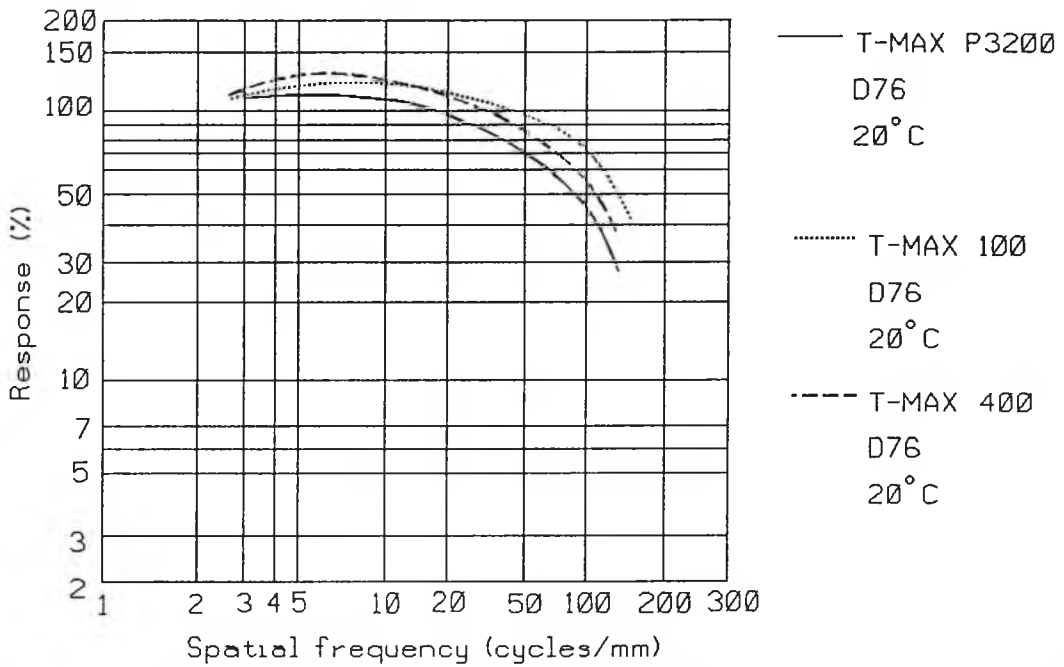


Figure 2.21. Modulation transfer functions for Kodak T-Max films, modulation rises above 100% due to adjacency effects. (Kodak 1987a).

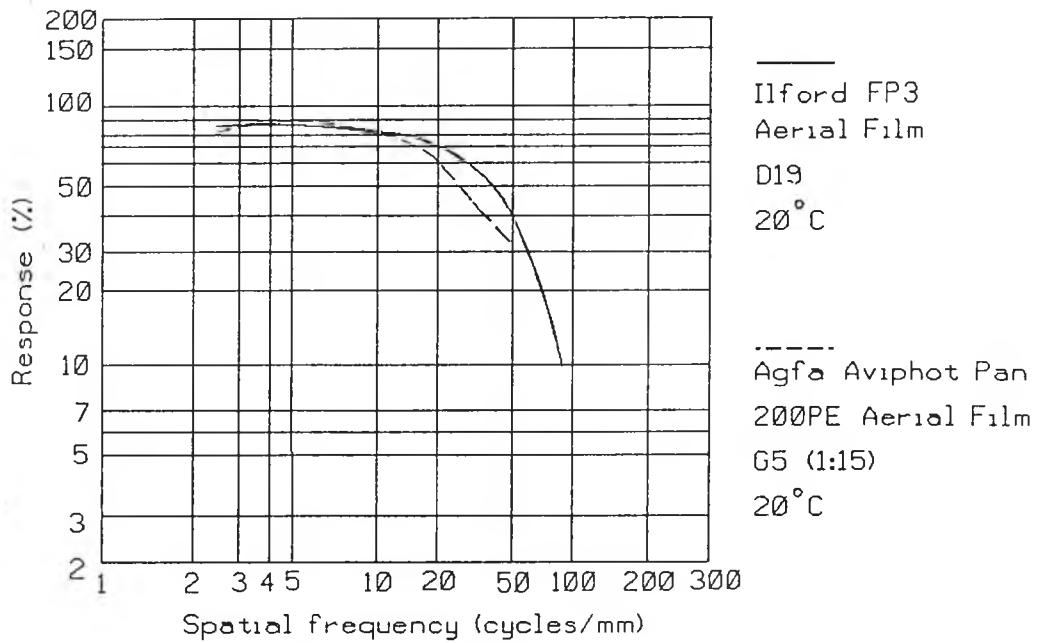


Figure 2.22. Modulation transfer functions for Ilford FP3 aerial and Agfa Aviphot 200PE films, (from Ilford 1982; Agfa 1980).

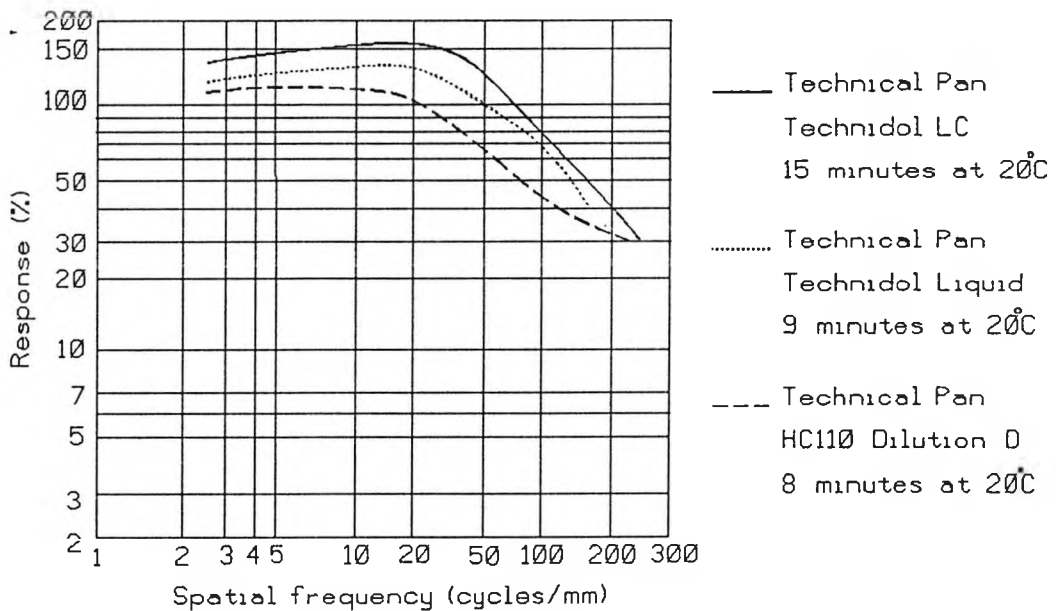


Figure 2.23. MTF curves for Kodak Technical Pan film demonstrating the effect or variation of development parameters, (from Kodak 1987b).

A primary advantage of MTF curves is that the effect of each stage in a system can be simply combined. This is achieved by multiplying the responses of the appropriate lens, film and image motion curves for example, frequency by frequency in a process known as cascading (James 1966) to give a total system response. Alternatively with the above system if the lens, film and system responses are known the MTF associated with image motion can be simply derived. Figures 2.21, 2.22 and 2.23 demonstrate a range of MTF curves, produced from manufacturers data, for a variety of common film types. The use of film and lens MTF data during photogrammetric network design (Section 3.4.4) could enable design to be carried out more rigorously.

2.4. Factors contributing to in-plane deformation.

Film deformations occurring in photographic systems can be conveniently divided into two types; in-plane and out-of-plane. The purpose of this section is to discuss in-plane deformations, those caused by expansion and contraction of the photographic film material. In-plane deformations are based on the fact that the physical characteristics of photographic materials are a function of the emulsion and support combination. The physical characteristics of an emulsion are largely of secondary importance in relation to its sensitometric properties, the base material must provide the required physical properties.

Dimensional change between exposure and measurement for a given photographic image has been shown to depend on the chemical composition and thickness of the base and emulsion, the treatment received in its manufacture, exposure and processing and also on the conditions under which the film is measured and stored.

2.4.1. Humidity changes.

Since water is the dispersing medium for the colloidal emulsion, many of the important physical characteristics of film are related to the high moisture absorption of the emulsion and the low moisture absorption of the support.

The water content of air is expressed in terms of relative humidity. When a gas contains the maximum amount of water vapour it can hold at its present temperature it is described as saturated, the corresponding vapour pressure at this point being the saturated vapour pressure. Relative humidity is defined as the ratio, expressed as a percentage, of the actual vapour pressure to the saturated vapour pressure at the same temperature.

The moisture content of the film as a whole has been shown (Colton and Wiegand 1958) to be a constant for a given environmental condition and is a function of both the relative humidity of the atmosphere with which the film is in equilibrium and of the gelatin to base thickness ratio r .

When the relative humidity of surrounding air is raised the film absorbs water and becomes larger in size and vice versa. Changes of this nature are largely reversible, the size of the film depending on the relative humidity of the surrounding conditions and not on the absolute humidity. Magnitude of change is expressed in terms of a humidity coefficient ($\% \text{ size change} / 1\% \text{RH}$).

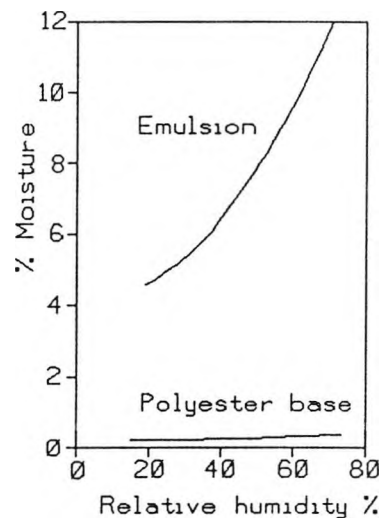


Figure 2.24. Moisture capacity, (Slama 1980).

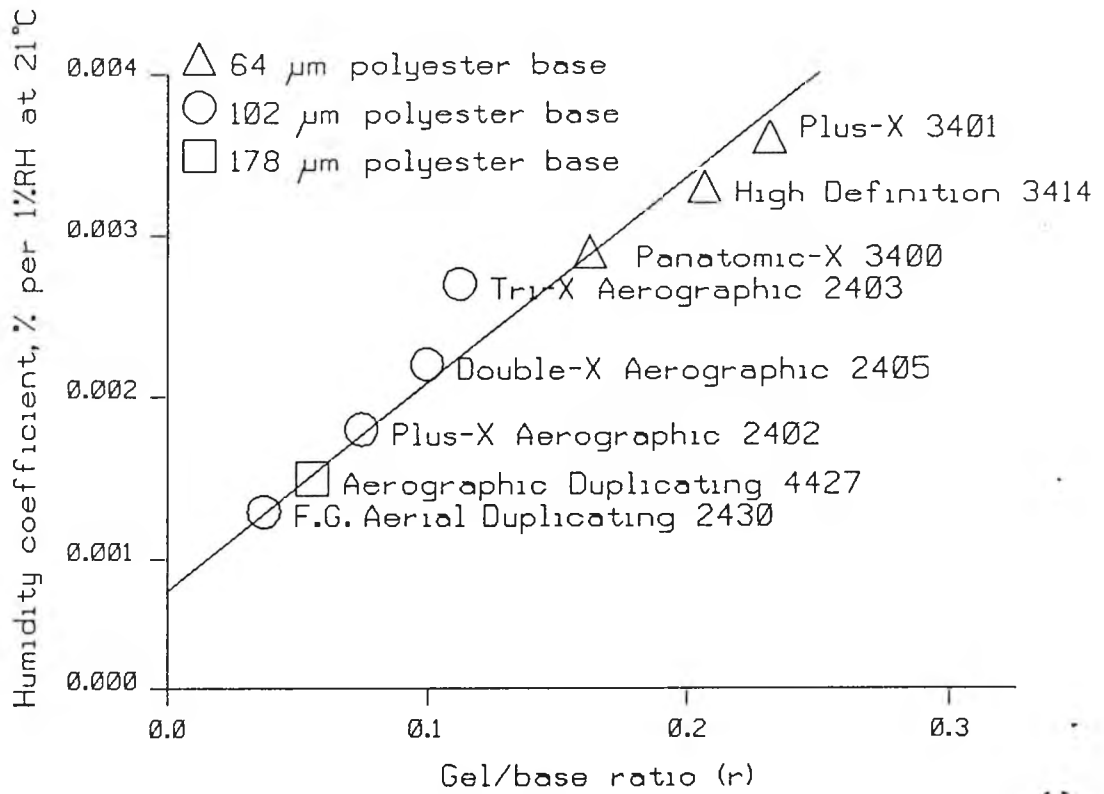


Figure 2.25. Effect of gel/base ratio on humidity coefficient, (Adelstein 1972).

The humidity coefficient has been shown to be dependent on the thickness and type of emulsion and film base used, and on any anti-curl backing present.

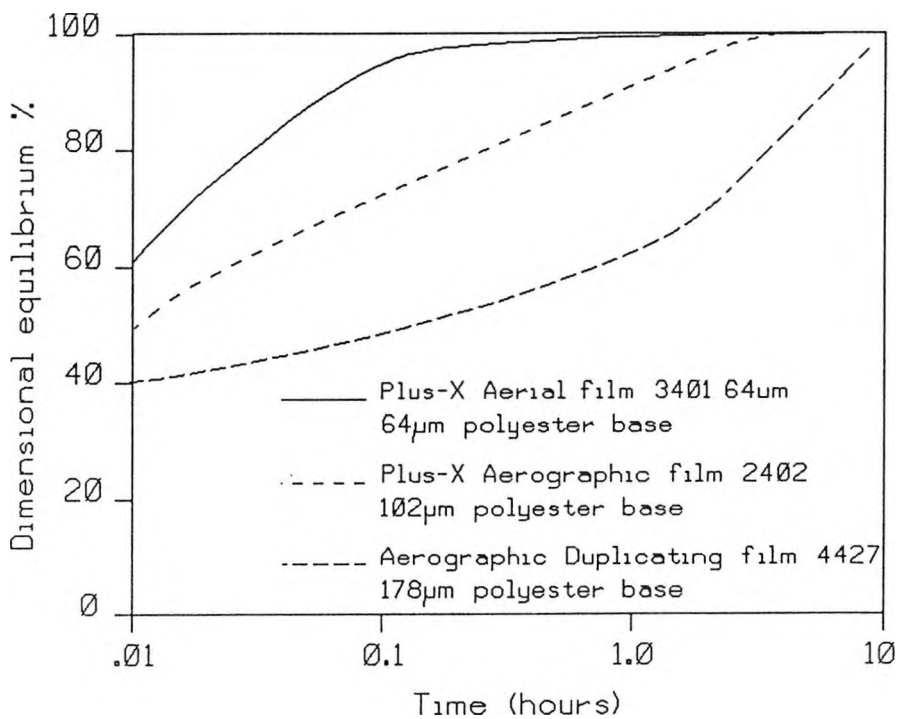


Figure 2.26. Rate of moisture conditioning for a single sheet, (Adelstein 1972).

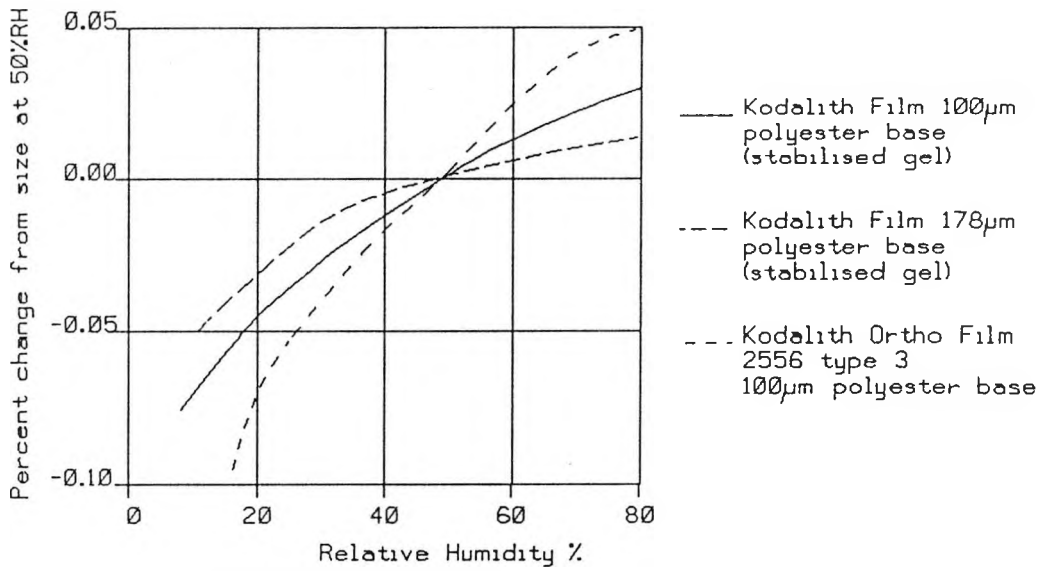


Figure 2.27. Percent size change with relative humidity, (Kodak 1970b).

Moisture interchange between the film and surrounding environment is essentially a diffusion based process, the rate of change is a function of air velocity, relative humidity differential, temperature and the physical form of the film, for example loose single sheets will condition quicker than film stored in roll form (Adelstein 1972).

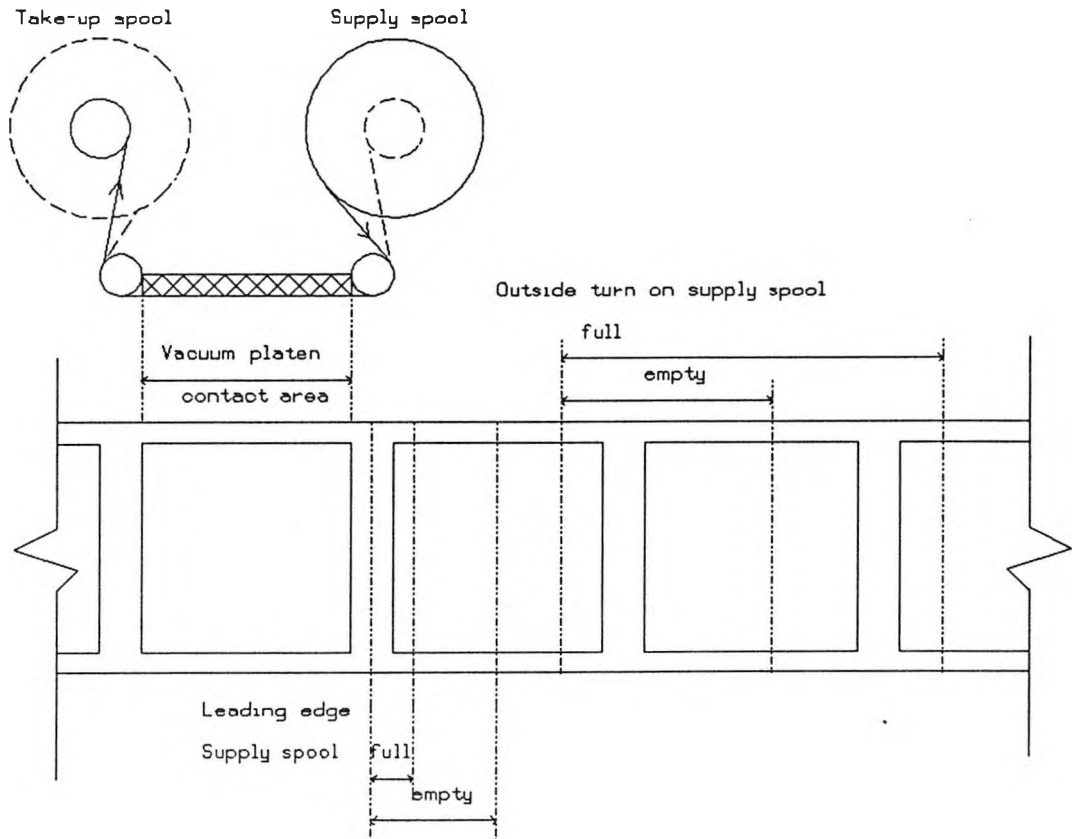


Figure 2.28. Position of film in magazine, showing present and future frame images, (Carman and Martin 1969).

An interesting humidity effect is the change in dimension of film in roll form whilst in the camera. This effect is particularly pronounced in aerial survey cameras, where temperature differential between cabin and external conditions, can result in low relative humidity in the camera compartment.

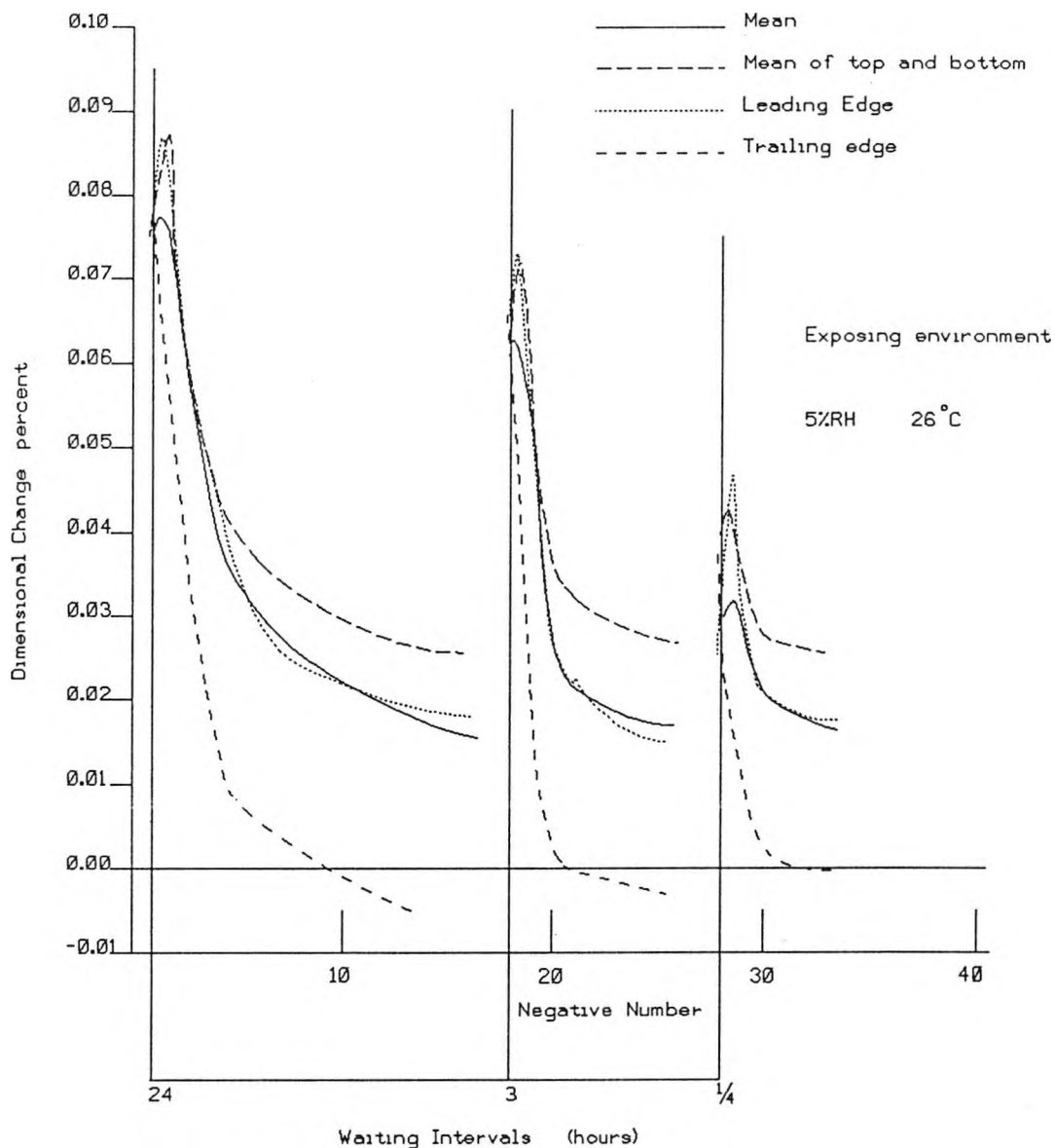


Figure 2.29. Leading and trailing edge effects, (Carman and Martin 1969).

Investigations were carried out (Carman and Martin, 1969) which demonstrated that exposures made after varying waiting periods showed an increase in image size. The effect was attributed to film shrinkage occurring prior to exposure and in proportion to the extent to which the dry air in the magazine reached and dried the film in the position it occupied. In this case the relative humidity differential was between the dry air (5%RH) and the packaged film relative humidity (45 to 55% RH), results are demonstrated in figures 2.28 and 2.29.

As mentioned the time to reach equilibrium is greatly influenced by the exposed film area. In the camera where the area of film directly exposed to the environment varies with the quantity of film on-the-roll, (Fig. 2.29) humidity effects, known as leading and trailing edge effects have been demonstrated. Ideally therefore humidity control should be present in the camera.

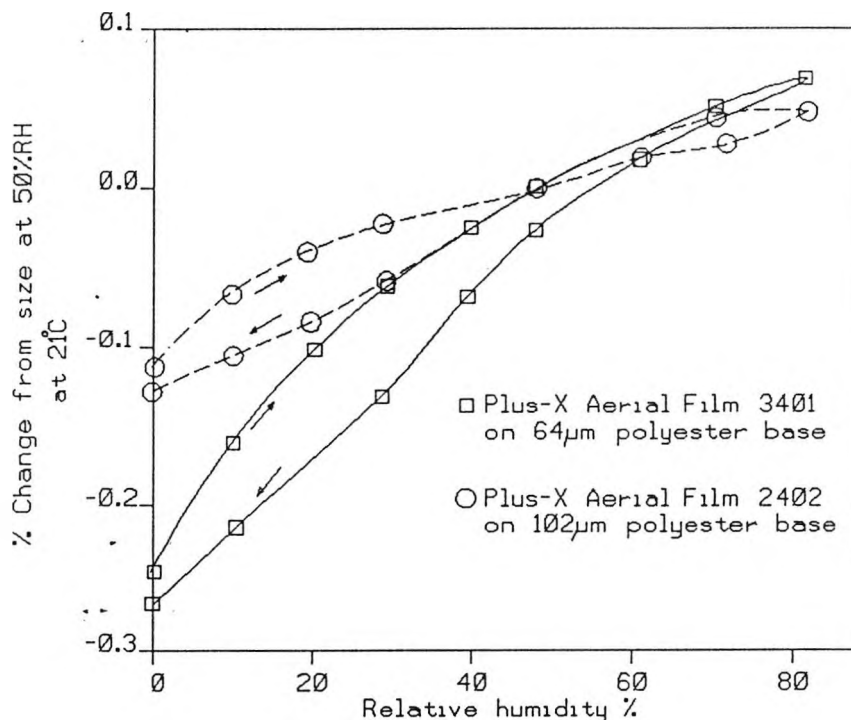


Figure 2.30. Typical hysteresis loop of unprocessed Kodak Plus-X aerial films, (Colton and Wiegand, 1958).

Film dimensions are not only dependent on ambient relative humidity, but also on the direction from which this humidity is approached. At a given relative humidity a polyester based film, for example, will be larger when previously conditioned to a lower humidity than when previously conditioned to a higher humidity. With reference to figure 2.30, film dimension does not necessarily change linearly with relative humidity since the emulsion exerts a much stronger compressive force onto the support at low relative humidity (Colton and Wiegand 1958).

Tension due to the film transport mechanism will also have an effect, although it would appear difficult to attribute causes to a given set of results. (Tension is also produced during processing if transport of any kind is used, section 2.4.3)

2.4.2 Thermal changes

Film size changes with temperature, at higher temperatures the film expands, this being a reversible and non-permanent change. Hence temperature should be the same both for exposure and for mensuration or printing. Change, expressed in terms of a thermal coefficient, is basically a property of the support with base thicknesses and emulsion variations not markedly changing

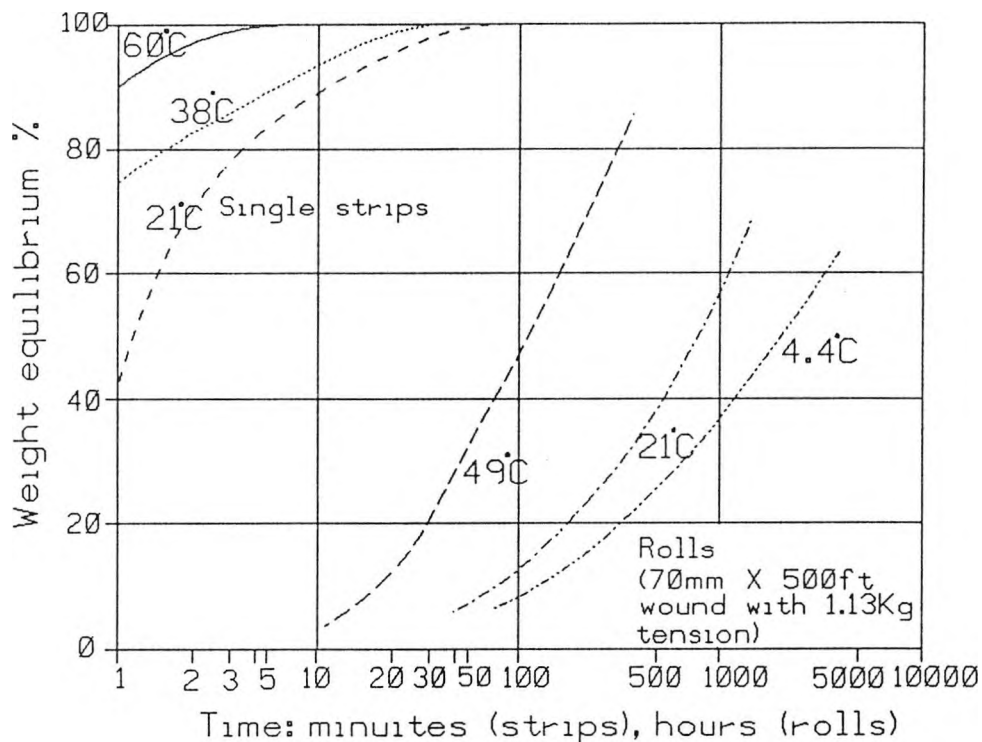


Figure 2.31. Effect of temperature on moisture loss, (Kodak 1972).

the dimensional effect. The coefficient of thermal expansion for cellulose triacetate based films is approximately three times that of polyester based films.

Temperature and humidity are strongly correlated, an increase in temperature often resulting in a decrease in relative humidity. Often the decrease in size due to relative humidity drop can not only compensate for the dimensional increase due to the corresponding temperature increase but can produce a net shrinkage. In fact not only the amount of moisture held, but the rate of moisture loss is also linked to temperature (Fig. 2.31). For these reasons a photogrammetric measurement and storage room in which environmental conditions or at least temperature are controlled would seem to be desirable. Whilst humidity and temperature control have been examined for the case of purpose built aerial cameras (Norton 1980a, 1980b), the bulky equipment required is not suitable for integration into the small format approach.

A laboratory investigation into the effects of temperature and relative humidity (Young and Ziemann, 1972) involved measuring a twenty three centimetre square format at three hourly intervals over an eighteen hour period. The film type investigated was Kodak 4427 aerographic duplicating film on 180 μ m polyester base. With reference to figure 2.32. changes of up to 25 μ m were found to have taken place.

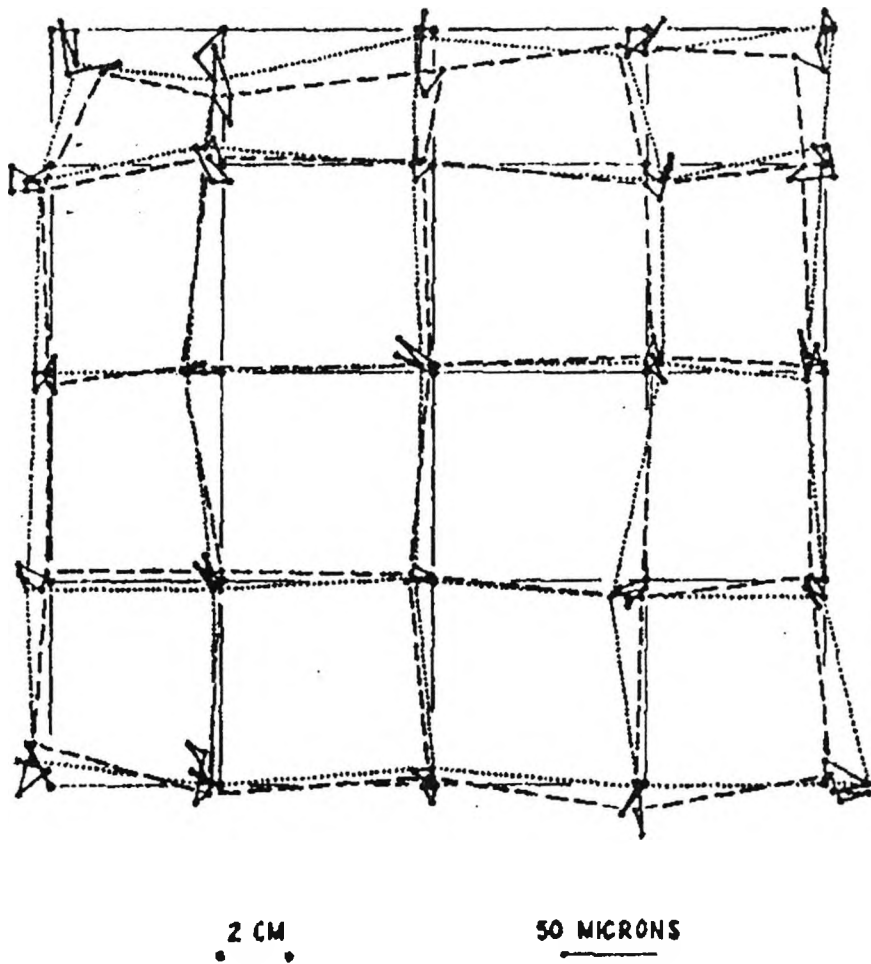
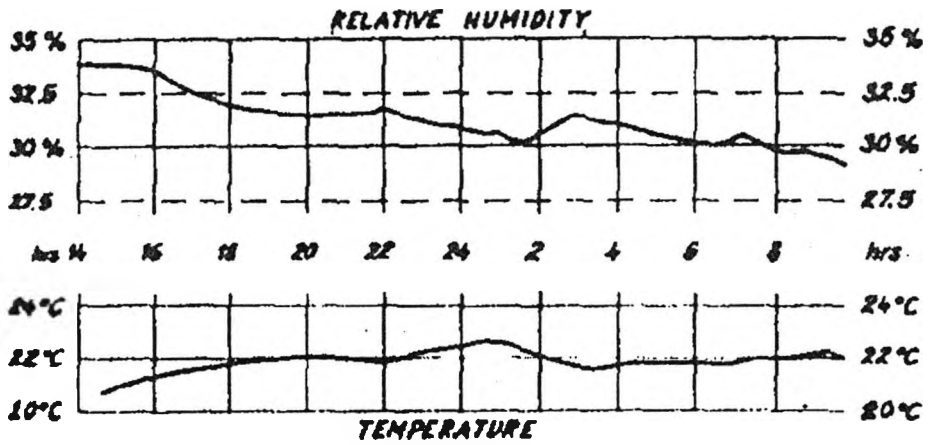


Figure 2.32. Changes in location of 25 points over a period of 18 hours, (Young and Ziemann, 1972).

2.4.3. Dimensional changes due to processing.

Dimensional changes during processing are assumed to be based primarily on the response of the film to changes in moisture.



Figure 1: Graph showing the relationship between Temperature and Time. The temperature decreases as time progresses.

Figure 2: Graph showing the relationship between Temperature and Time. The temperature increases as time progresses.

The following text is extremely faint and illegible, appearing to be a series of lines of text or a list of items.



Figure 3: Graph showing the relationship between Temperature and Time. The temperature remains relatively constant.

Figure 4: Graph showing the relationship between Temperature and Time. The temperature increases and then decreases.

The following text is extremely faint and illegible, appearing to be a series of lines of text or a list of items.

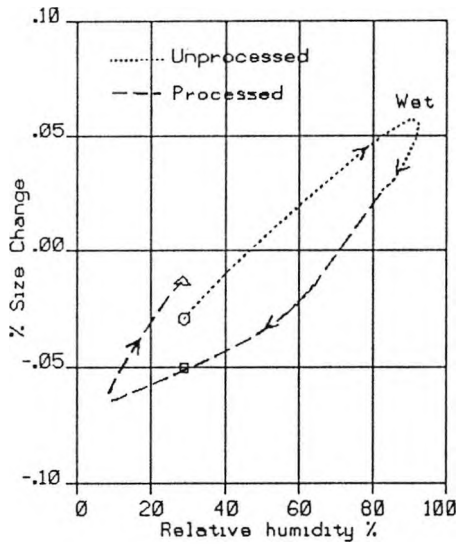


Figure 2.33. Possible processing dimensional changes, (Kodak 1970b).

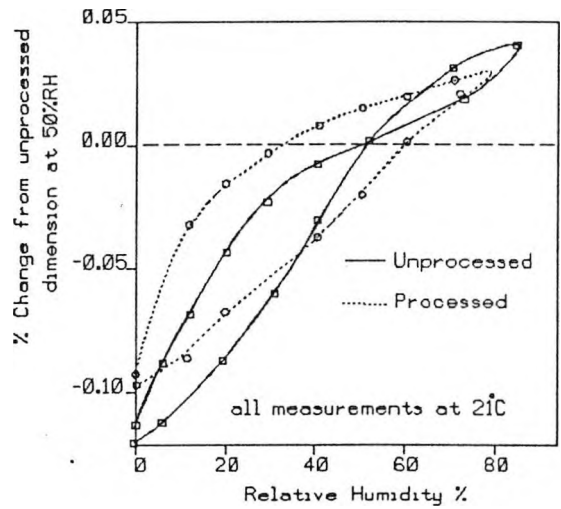


Figure 2.34. Hysteresis loop for processed and unprocessed Plus-X film on 102 μ m polyester base, (Calhoun et al 1960).

Figure 2.33 demonstrates the possible processing dimensional changes which can occur when a film initially exposed at 30%RH is processed. Processing can very simply be regarded as taking the film to 100%RH on the dotted curve. If the film is then dried at 30%RH the film will then equilibrate to the position shown by the square. However if the film was over-dried in a cabinet at elevated temperatures, and therefore at low relative humidity, on conditioning at 30%RH the film would assume the size represented by the triangle.

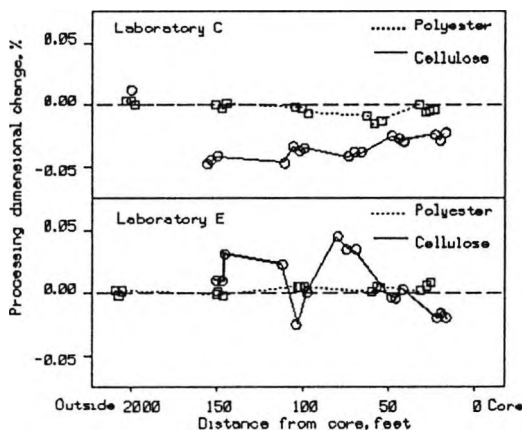


Figure 2.35. Average processing dimensional change, (Adelstein et al, 1966)

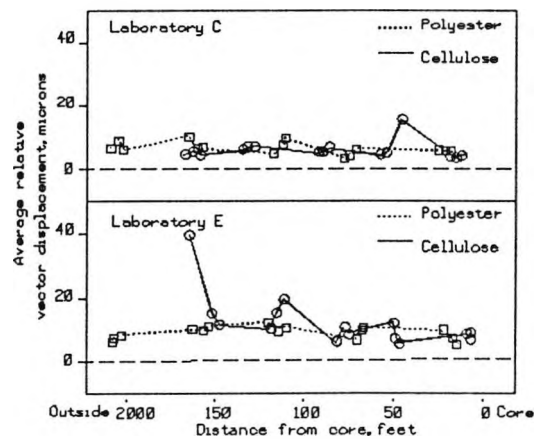


Figure 2.36. Uniformity of processing dimensional change, (Adelstein et al, 1966).

It has been demonstrated (Adelstein et al 1966) that the drying conditions used will determine to a great extent the processing dimensional change. Over-dried film will tend to be oversize on reconditioning, whilst slowly dried film will tend to show shrinkage. Also investigated, by comparison between six different processing laboratories, were variability of processing size

change and uniformity along the length of a roll. Findings (Figs. 2.35 and 2.36) indicated first, that to minimise size variations and non-uniformity, excessive machine tensions had to be avoided. Secondly, drying capacity had to be carefully monitored when drying triacetate based films, because varying moisture retention by the film base caused inconsistencies in the degree of humidity conditioning before measurement. In the experimentation to be carried out during the course of this thesis, manually loaded spiral tanks were used to process the films such that excessive tension could be avoided. The experimentation would also have to include an analysis of the influence of drying conditions.

Other contributory factors include alterations in the gelatin structure caused by wetting and drying, and the removal of unexposed silver halide by the fixing agent, causing the humidity dependence of the processed film to change (Fig 2.34). It is characteristic of films on cellulose-acetate bases to show shrinkage due to the removal of residual solvent during processing.

Most of the changes referred to above are net changes and hence whilst there may be no net change, it does not necessarily follow that there will be no local dimensional change. A good example of a cause of local deformations is water droplets left on the film during drying. These have been found to cause isolated distortions, due to localised swelling and drying of the emulsion. Typical magnitudes, on both film and glass based materials, found by a variety of workers (Burnkam and Josephson 1969, Calhoun, Keller and Newell 1960) are of the order of

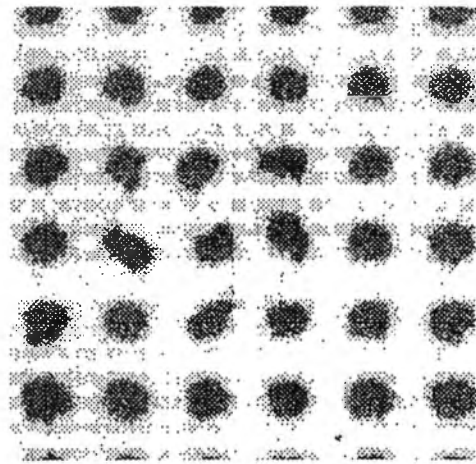


Figure 2.37. Moiré pattern of a water spot, (Adelstein 1972).

10 to 20 μm . Figure 2.37 shows a typical water spot deformation, detected by a moiré technique, where differences in spacing between cancellations relate to changes in dimension between the glass master grid and its exposed and processed image. Distances between cancellations for this particular image are about 50mm.

Local dimensional of the type shown in figure 2.37 can be expected to be difficult to detect in practice, unless a dense reseau grid is exposed onto the film. Fortunately such deformations have been shown to be reduced by decreasing the thickness of the emulsion or by increasing the thickness of the base (Adelstein 1972), such that it may be possible to select film materials to avoid such effects. Another possibility to reduce deformations caused by water spots is to use a mild detergent known as a wetting agent in the final wash (Section 5.2.1.5).

2.4.4. Film curl.

The curl of photographic film is caused by the difference in moisture properties between the emulsion layers and the base. A backing is often used to produce a gelatin/base/gelatin structure, which helps to counteract any unequal forces.

Film curl can also be influenced by flow of the plastic film support when held in roll form, this being known as core set. For this reason there is a difference in the degree of curl between winding film emulsion in and emulsion out. Core set has been shown to increase (Kodak 1972) with storage time on the roll. The effect may provide an important contribution to the degree of irregularity of film unflatness during exposure in camera.

2.4.5. Aging.

A size change will occur from aging of film during storage. In the case of cellulose acetate bases, this is mainly due to solvent loss. Other factors giving rise to change are plastic flow or creep of the base material, generally resulting in shrinkage as a result of the compressive force of the emulsion layer. As expected the magnitude of the change tends to be correlated with gelatin to base ratio and the storage temperature and humidity.

Also of importance during storage is the surface area of the film exposed to the environment, since this will influence the rate at which the film equilibrates with its surroundings (Section 2.4.1). For this reason all exposed films kept in the measurement environment during the course of this project have been stored as cuts of three frames, rather than in roll form. In this way the film would equilibrate with its surroundings in hours rather than the days required by films stored in roll form (Kodak 1972).

In the case of polyethylene terephthalate base, the release of tensions applied during manufacture (Section 2.1.2.2) may be significant (Ziemann 1971d).

2.5. Factors contributing to out-of-plane deformation.

Out-of-plane deformation is the term given to departures of the imaging surface from the ideal plane assumed by the collinearity equations (Brown 1986; Fraser 1982a). Assumptions made by the model for imaging geometry (Chapter 3), mean that out-of-plane deformation is characterised by radial distortions about the intersection between the optical axis and the image plane (principal point). In figure 2.38, the light ray from an object, instead of striking the image plane at I , strikes the film surface at I' , causing a radial deformation K .

Various workers have investigated the physical causes and magnitudes of the departure of imaging surfaces from an assumed plane. Studies undertaken have generally utilising interference fringe methods and have been carried out primarily on 9 inch square aerial survey equipment.

Meier (1972), describes the sources of out-of-plane deformation in aerial survey cameras as being caused by three factors; lack of planeness of the pressure plate, lack of contact between the back of the film and the pressure plate and variations in the thickness of film. It should be noted that these three factors are likely to be significant to the magnitude of out-of-plane film deformation occurring in small format camera designs (Sections 4.2 and 6.1.4).

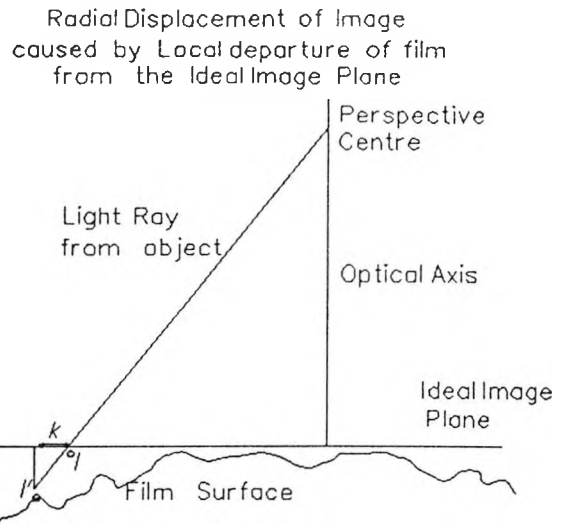


Figure 2.38. Radial distortion effects of unflatness, (Robson 1989).

Figure 2.39 is an interferogram derived from a Zeiss vacuum camera back using Aviphot Pan 30 PE film. In general, large area deviations of $5\mu\text{m}$ to $8\mu\text{m}$ were found, with short period deviations of $6\mu\text{m}$ to $7\mu\text{m}$.

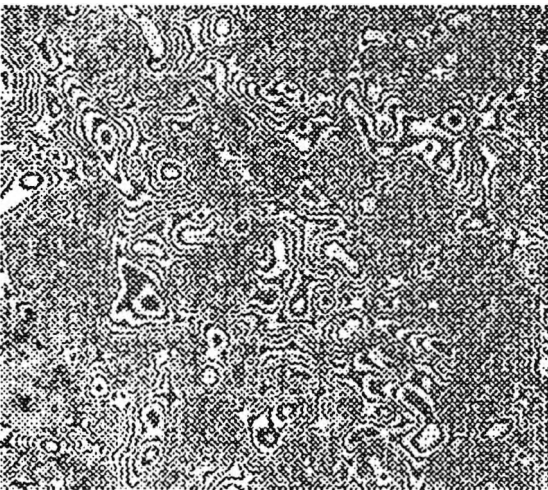


Figure 2.39. Interferogram of film flatness in Zeiss aerial camera, (Meier 1972).

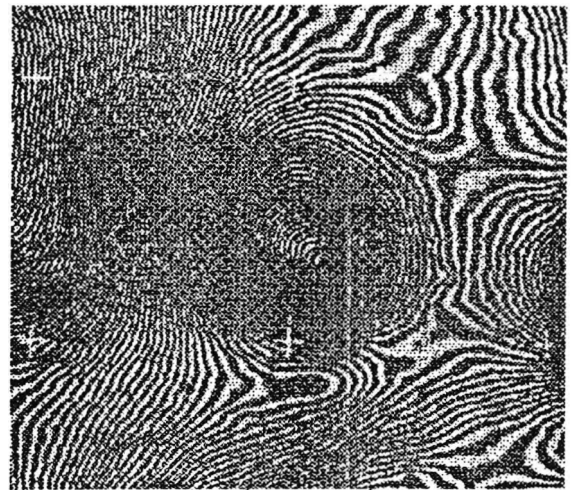


Figure 2.40. Interferogram from a smooth-faced pressure pad, (Clark 1972).

Deviations were found to occur irregularly, there appearing to be no correlation between unflatness and the pattern of holes in the vacuum back. However, Clark (1972) demonstrated that the flattest regions in a vacuum system were in close proximity to the vacuum holes, concluding that film could seal the holes before evacuation of air was complete.

In the same paper Meier also investigated a small format Hasselblad roll film camera, employing a mechanical pressure plate system. In this case large area deviations of up to $25\mu\text{m}$ were found.

Unfortunately no comments concerning the shape and typicality of such deviations were made.

Clark examined the unflatness occurring in survey cameras utilising a register glass / pressure pad system. Findings demonstrated that a well maintained pressure pad could produce more regular flatness patterns although with extremes of the order of 15 to 20 μm . These are shown in figure 2.40 where the contour interval is about 0.25 μm . A major limitation found in the pressure pad system was that it was incapable of rapid flattening due to the slow removal of air trapped between the film and glass register plate. Investigations continued with the development of a roller flattening system, which with modification was able to flatten the film quickly and effectively.

Film deformation in a 35mm camera system, was investigated by Tsuruta, Itoh and Anzai (1970), using a moiré technique whereby interference fringes were produced by combined in-plane and out-of-plane deformations. Figure 2.48. shows a typical contour map obtained from analysis of the fringes produced.

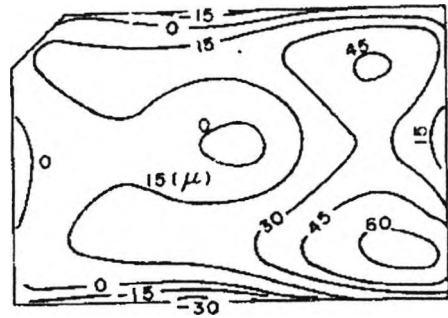


Figure 2.41. Contour map for film deformation in a 35mm camera system, (Tsuruta at al 1970).

A survey of the film unflatness present in 3000 frames from 126 camera cartridges was conducted by Branch, Clark and Milton in 1968. The survey demonstrated that providing the cartridge was seated properly in the camera, the film surface did not deviate more than 200 μm from the assumed plane. The unflatness was satisfactory given that the depth of focus of the camera lens could tolerate out-of-plane deviations of up to 280 μm .

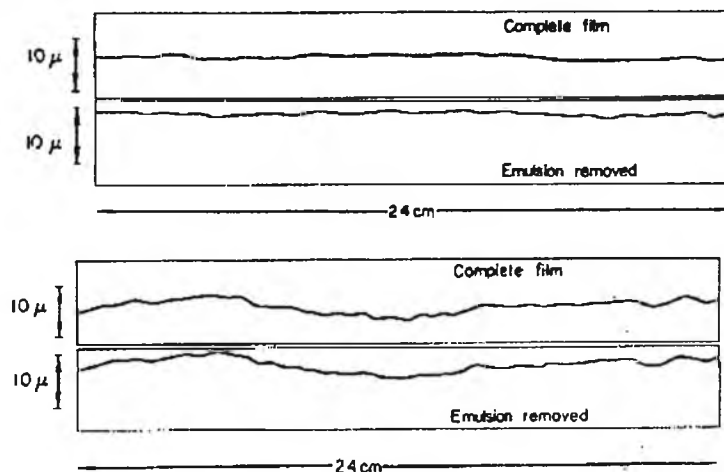


Figure 2.42. Thickness profiles of Kodak Double-X Film 2405 (Polyester base), (Michener 1972).

Variations in the thickness of film were studied by Michener (1972) of Eastman Kodak, who presented results from a series of thickness uniformity evaluations. Tests were carried out on polyester based films using an electro-mechanical gauge having an accuracy of 2.5 μm and a

sensitivity of $0.25\mu\text{m}$. Both film with and then stripped of its emulsion were measured, results indicating that changes in film thickness are primarily due to variations in the film support. Thickness variations ranged from $1.3\mu\text{m}$ to $5\mu\text{m}$ over a 24cm distance. Results (Fig. 2.42) also demonstrated that thickness variations across the width of the film are much greater than for an equal distance along the length, this can be attributed to casting techniques during manufacture.



Figure 2.43. Thickness fringes from triacetate film base, (Clark 1972).



Figure 2.44. Thickness fringes from polyester film base, (Clark 1972).

Clark (1972), also investigated film thickness variation using a transmission interference method. To allow the partial reflection necessary for the technique, film samples were coated on both sides with a thin layer of aluminium. Interference patterns for both polyester and cellulose triacetate based films are shown in figures 2.43 and 2.44. The greatest thickness gradients found among samples of both base types was $1.4\mu\text{m}$ per centimetre.

2.6. Chapter summary.

This chapter has shown that the behaviour of film materials is influenced by many factors. The major influence throughout the photographic process being the differences in moisture dependency between the gelatin and film bases. Such dependency will require that relative humidity and temperature will have to be monitored throughout the experimental work if meaningful results are to be obtained.

A major goal of this project must be the development of a standardised processing regime which will keep any in-plane deformations to a minimum. However such a process must also take into account the tone reproduction and image quality aspects required of images taken for photogrammetric purposes.

Since the largest out-of-plane deformations appear to be closely related to camera design even for metric survey equipment, possibilities for minimising such deformations will be limited by the

camera equipment available. The analytical modelling techniques discussed in chapter 3, allow simple scale changes to be easily removed with few reference marks. Localised deformations, such as those exhibited in figures 2.38, 2.38 and 2.41, and probably typifying film deformation, present a more difficult problem. If localised patterns are found to be, or can be made consistent between frames exposed under the same situation then modelling techniques could be greatly simplified. For example a transformation which represented consistent out-of-plane deformations could be applied (Section 6.4.1.). The identification of similar patterns between frames exposed in different camera backs and on different film types will constitute a major part of the research work undertaken (Sections 4.1 and 6.1.4).

3. Photogrammetric Theory.

The intention of this chapter is to provide the non-photogrammetrist with a brief introduction into the theoretical principles and data handling techniques which constitute analytical photogrammetry. The term analytical is used to denote photogrammetry using analogue (photographic) images allied with digital data handling, as opposed to analogue photogrammetry in which analogue images are processed by opto-mechanical means. It should be noted that photogrammetry is increasingly carried out in a purely digital form where digital or pixel based electronic imagery is allied with digital data handling.

The analytical approach is able to free the photography from the restrictions traditionally placed upon it by analogue methods. These restrictions are mainly in the type of camera which can be used and the geometrical relationships between the camera and object. Importantly for the work described in this thesis, analytical techniques allow cameras designed for pictorial uses to be used photogrammetrically. This chapter initially outlines the mathematical principles of the analytical model and then discusses some of the current extensions which can be included to model some of the physical characteristics of practical cameras.

3.1. Geometrical optics and considerations leading to the central perspective projection.

To relate dimensions on the photographic image to the corresponding object, the photographic image is generally considered as a mathematical model: the central perspective projection of a three dimensional object onto a plane (Fig. 3.1).

In order for this model to be valid, the lens must act as a centre of perspective, and must not deviate the geometrical rays of light as they travel in straight lines from the object (Albertz and Kreiling 1975; Slama 1980).

The main features of the model are: the **principal point (p)**, defined as the base of the perpendicular from the **perspective centre (O)** to the image plane; the **principal distance (f)** being the length of this perpendicular; and the **optical axis (POp)**.

Again considering figure 3.1, for angle i , subtended at **O** by any off-axis object point **A** and an axial object point **P**, whose image coincides with the principal point, the function $r/\tan(i)$ can be written, where r is the distance between the images in the picture plane, will be a constant equal to f .

From the central projection it can be seen that two objects **A** and **B** which result in coincident images at **a**, must necessarily lie on a straight line passing through the perspective centre **ABOa**. This condition is known as collinearity.

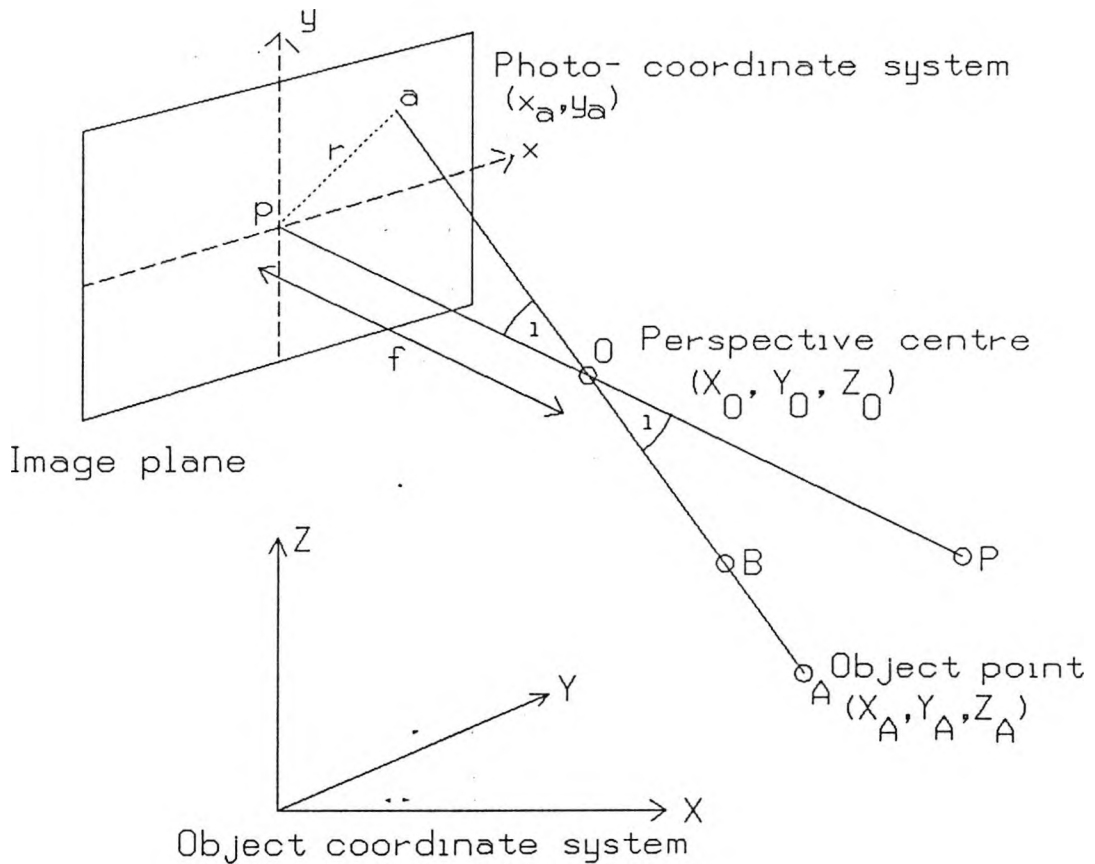


Figure 3.1. The central perspective projection.

Collinearity and the equations expressing this condition form the foundation of analytical photogrammetry in which the geometrical relationships between the three dimensional object, the perspective centre and the image are determined. Many examples of the derivation of the collinearity equations exist in standard texts (Wolf 1985; Slama 1980). So only their form and a working description of their parameters will be given.

$$x_a - x_p - \frac{f [m_{11}(X_A - X_0) + m_{12}(Y_A - Y_0) + m_{13}(Z_A - Z_0)]}{m_{31}(X_A - X_0) + m_{32}(Y_A - Y_0) + m_{33}(Z_A - Z_0)} = 0 \quad (3.1)$$

$$y_a - y_p - \frac{f [m_{21}(X_A - X_0) + m_{22}(Y_A - Y_0) + m_{23}(Z_A - Z_0)]}{m_{31}(X_A - X_0) + m_{32}(Y_A - Y_0) + m_{33}(Z_A - Z_0)} = 0$$

where the m's are functions of the camera axis rotations (ω , ϕ and κ) with respect to the object coordinate system.

$$\begin{aligned} m_{11} &= \cos \phi \cos \kappa \\ m_{12} &= \sin \omega \sin \phi \cos \kappa + \cos \omega \sin \kappa \\ m_{13} &= -\cos \omega \sin \phi \cos \kappa + \sin \omega \sin \kappa \\ m_{21} &= -\cos \phi \sin \kappa \end{aligned}$$

$$\begin{aligned}
m_{22} &= -\sin \omega \sin \phi \sin \kappa + \cos \omega \cos \kappa \\
m_{23} &= \cos \omega \sin \phi \sin \kappa + \sin \omega \cos \kappa \\
m_{31} &= \sin \phi \\
m_{32} &= -\sin \omega \cos \phi \\
m_{33} &= \cos \omega \cos \phi
\end{aligned}
\tag{3.2}$$

x_a is the x coordinate of the image of A in the photo-coordinate system

y_a is the y coordinate of the image of A in the photo-coordinate system

x_p is the x coordinate of the principal point p in the photo-coordinate system.

y_p is the y coordinate of the principal point p in the photo-coordinate system.

X_A, Y_A, Z_A are the coordinates of the object point A in the object space coordinate system.

X_O, Y_O, Z_O are the coordinates of the perspective centre O in the object space coordinate system.

The parameters defining the camera can be regarded in two distinct groups:

- a) **Exterior orientation;** defining the position of the camera perspective centre and optical axis in the object space ($X_O, Y_O, Z_O, \omega, \phi, \kappa$).
- b) **Interior orientation;** comprising the geometric parameters of the camera itself (f, x_p, y_p).

The central perspective model is an ideal case and although approximated by a pinhole is unobtainable when real lenses are used in practice. However expensive metric cameras (such as the UMK 10/1318, Chapter 6) have been designed to approximate the model for all but the highest precision work. The cost and limited application of such cameras is however being questioned, especially with the appearance of the latest generation of both low cost pictorial cameras and new high precision photogrammetric cameras which rely on analytical technique to model their physical departures from the central perspective model.

The most widely accepted extensions to the central perspective model are based on the physical geometry of image formation by practical lenses and camera designs (Karara 1989; Magill 1955). Such principles are also beginning to be evaluated experimentally with the aid of automatic comparators capable of measuring many images positions per second (Fraser and Shortis 1990).

3.2. Geometric properties of the compound lens.

A theoretical thin lens has an optical centre, through which all incident rays pass without deviation. To fit the central perspective projection to a practical or 'thick lens' this point must be conceptually divided into two points: the front and rear perspective centres.

The camera lens generally consists of a front and rear element, with an aperture stop between them. The stop is necessary for light control and maintenance of sharp focus within a required depth of field.

For a lens focused at infinity two cardinal points of unit angular magnification, the front and rear nodal points can be regarded as analogous to the perspective centres. The nodal points are defined by a unique ray (the chief or principal ray), which when produced meets the axis at the front node, passes through the centre of the iris, then emerges along a line parallel to its original direction.

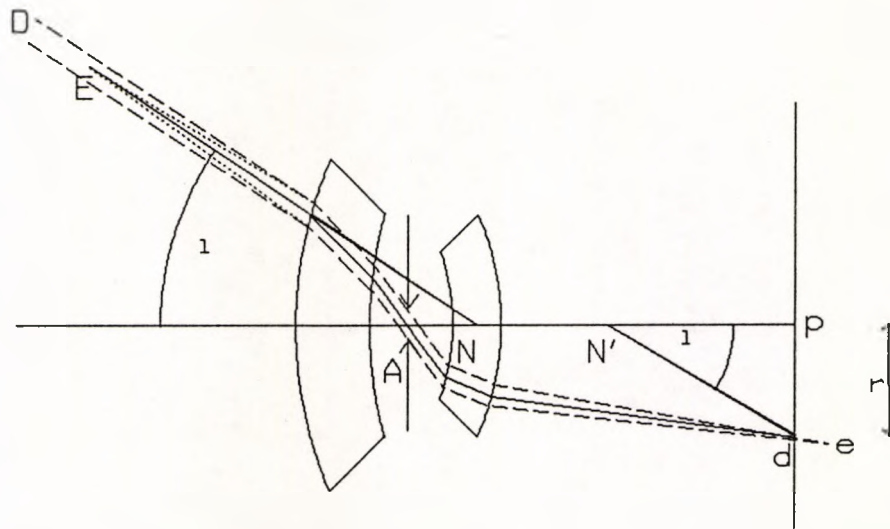


Figure 3.2. Image formation by a lens, (Scott 1977).

Figure 3.2 illustrates this concept, where an object point **D** at infinity creates an image point **d**, with **N** and **N'** representing the front and rear nodes respectively. The actual image forming process is illustrated by the dotted lines, representing the bundle (or pencil) of rays from **D** being limited by the aperture stop **A**, then focused to an image point at **d**, the plane of which in this case coincides with the film plane of the camera and is conjugate to **D**. Rays from a second object point **E** closer to the lens, will undergo a similar procedure, but will be focused behind the film plane at **e**. The resulting image at the picture plane will ideally be an elliptical (out of focus) image of **E** centred on **d**, termed the blur circle, the diameter of which is reduced to the circle of confusion by decreasing the diameter of the aperture stop.

Whilst no unique perspective centre exists, an analogy can be made in this case by using the nodal points **N** and **N'** as the front and rear lens perspective centres. Hence a ray from **D** making an angle i with the axis creates an image **d** at a distance r from the principal point. Where;

$$N'P = r \cot i = f.$$

3.2.1. Radial lens distortion.

If the lens produces an image such that f is a constant for all possible values of angle i , then the resultant image at the film plane will be geometrically the same as that produced by a central projection, this condition being known as orthoscopic. However for practical lenses focused at infinity, the position of the front and rear lens perspective centres vary with angle i . This gives rise to departures from the central

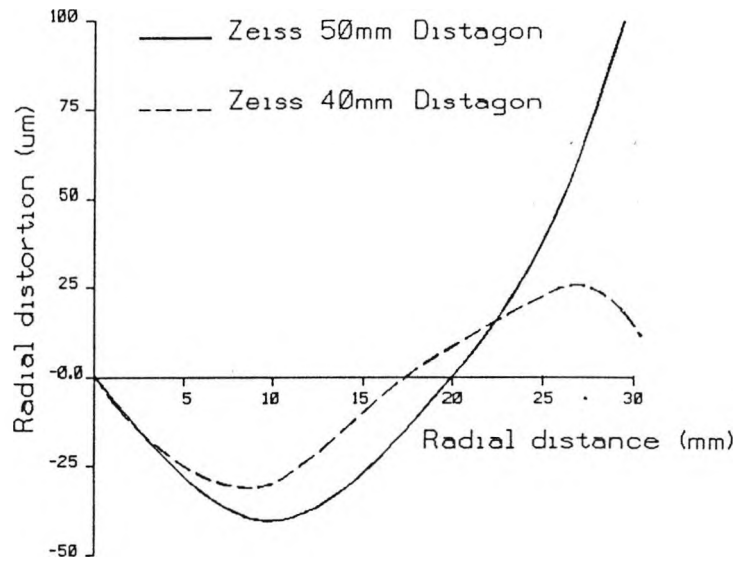


Figure 3.3. Radial lens distortion curves for two Zeiss lenses at infinity focus, (Hasselblad 1989)

perspective projection, known as radial lens distortion since its magnitude Δr is dependent only on radial distance r from the optical axis (Thompson 1957)

An example of radial distortion derived by practical calibration is given in figure 3.3 which shows two radial distortion curves for 40 and 50mm Zeiss lenses focused at infinity. The magnitudes of distortion for these lenses are large when compared with the 5 to 10 μ m values typical of lenses designed for metric cameras, but both these lenses are intended for pictorial use, are mass-produced and consequently considerably cheaper.

The magnitude of radial lens distortion Δr for a lens focused at infinity can be expressed by a polynomial series of even powered terms, (Abdel-Aziz 1980) where k_1, k_2, k_3 are known as the coefficients of radial distortion. This particular radial lens distortion model has been included in the City University general adjustment program (GAP), the features of which are described in chapter 6.

$$\Delta r = k_1 r^2 + k_2 r^4 + k_3 r^6 \quad (3.3)$$

Whilst such formulae have been successfully applied to a range of photogrammetric applications (Chandler and Cooper 1988; Chandler et al 1989b), it is shown below that optical distortions are not independent of object distance.

Scott (1977) demonstrates that at reduced object distances the rear perspective centre coincides not with the static rear node, but with the exit pupil, defined as the image of the aperture stop seen from the image space.

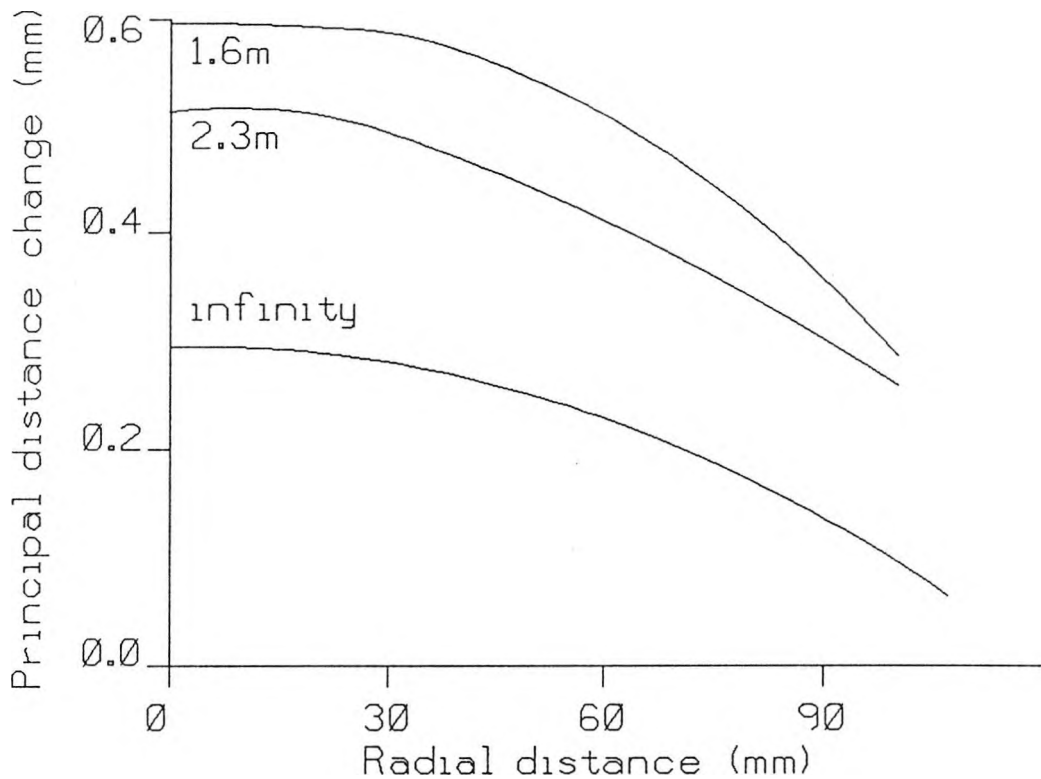


Figure 3.4. Variation of principal distance with focus setting (Scott 1977).

When the camera lens is moved away from the film plane by a physical extension e , to facilitate the focusing of a close object, the principal distance will not only be increased by e , but also by an extra increment which will vary with radial distance, due to disparity between the rear node and exit pupil (Fig. 3.4).

The variation of principal distance with focus setting must be determined through photogrammetric calibration of the camera, since the exit pupil position is very difficult to locate in practice.

When object distances are reduced to within a few tens of focal lengths from the camera, the magnitude of radial distortion correction has been shown to change (Magill 1955). Variation is caused by the position of the outer perspective centre altering with object distance, such that a radial lens distortion curve derived from objects at infinity will change its shape continuously throughout the imaged object distance range (Fig. 3.5).

Magill (1955) and Brown (1971) have derived formulae which consider the variation of radial distortion with object distance, given that the magnitude of the polynomial coefficients, for example that in equation 3.3, at two object distances spanning the range of interest are known. This work has been further extended by application to results from the high precision calibration of a variety of different metric camera systems (Fraser and Shortis 1990).

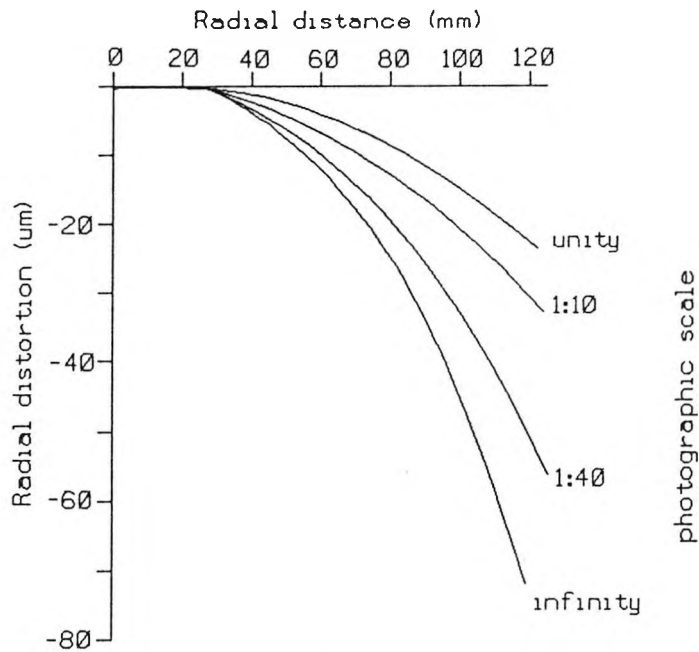


Figure 3.5. Observed change of radial distortion with object distance (Fryer and Brown 1986).

3.2.2. Decentering distortion.

Each element of a lens has its own unique axis which is defined as the line joining the centres of curvature of front and back surfaces. Decentering distortion, misalignment of the unique axes to the optical axis of the compound lens, is caused by manufacturing errors and therefore is a highly individual property. Lens elements can either be aligned with their optical axis displaced, but parallel, to the theoretical axis, or inserted at an inclination to the desired principal axis.

Equations 3.4 have been developed by Conrady (1919) and Magill (1955) to describe the magnitude of decentering distortion at one focused distance.

$$\Delta x_d = [p_1(r^2 + 2(x-x_p)^2) + 2p_2(x-x_p)(y-y_p)] \quad (3.4)$$

$$\Delta y_d = [p_2(r^2 + 2(y-y_p)^2) + 2p_1(x-x_p)(y-y_p)]$$

where: p_1 and p_2 are the parameters of decentering distortion.

Δx_d and Δy_d are the components of decentering distortion at an image point x, y .

It is worth noting that Brown (1972) and Fryer and Brown (1986) have again extended the model to account for variability of object distance within the photographic field.

The high precision surveys at varying object distances used to extend both the radial and tangential distortion models have been made using target arrays consisting of many hundreds of targets. Additionally image scanning techniques (Brown 1982, 1984) have been used for image

measurement. The test field experimental work conducted in the case of this thesis (Chapter 6), has been concerned with semi metric cameras and used slower semi-automated image measurement (Section 5.2.1.7), consequently the work has been limited to a set of photographs produced for nominally one object distance. The network used (Section 6.2) is not capable of estimating the lens distortion object distance extensions, so the basic lens distortion model (Equations 3.3 and 3.4) have been used.

These optical considerations are simply added to the image measurements as additional parameters, thereby modifying the collinearity functional model.

$$\Delta x_{lens} = \Delta r + \Delta x_d \quad (3.5)$$

$$\Delta y_{lens} = \Delta r + \Delta y_d$$

where: Δx_{lens} and Δy_{lens} are the total corrections to be added to the image coordinate measurements.

3.3. Film deformation modelling.

The photogrammetric mathematical model assumes that all image points are co-planar, necessitating that the film in the image plane must be flat during exposure. Also collinearity requires that there should be no change of the in-plane position of the image between exposure and measurement.

From sections 2.4 and 2.5 it is clear that in practical cameras (especially of pictorial design) significant systematic and irregular departures from these assumptions can occur when photographic film is used as the imaging surface. To compensate for these departures a mathematical model must be developed which can be applied to the measured image coordinates. The reliability of suitable algorithms and the estimation of their associated parameters depends on the information available about the magnitudes, patterns and influences of both in-plane and out-of-plane deformations (Torlegård 1989).

There are two classes of technique for the mathematical correction of film deformation:

- a) Explicit corrections in which the film deformation, either at known sites, or derived according to some physical model, are used to correct the measured image coordinates before the computation of the collinearity equations. This process is often referred to as image refinement.

- b) A second approach is the use of additional parameters in the adjustment procedure. This is analogous to the methods used for the correction of radial and tangential lens distortion, but utilising a set of equations which conform to some physical circumstance, or more usually to statistical data (Brown 1974). This approach is however less favourable than explicitly applied corrections since it can increase the instability of the adjustment procedure and could also model other departures from the collinearity condition causing unwanted correlations between additional parameters (Section 3.4). However, in cameras where a reseau is not present this technique applied with care can present a useful approach (Fraser 1982b).

3.3.1. Explicit film deformation corrections.

Traditional photogrammetric cameras designed for use with glass plates, typically use four or eight calibrated register or fiducial marks at the edges of the format to define the image coordinate system. Differences between the imaged positions of these marks and their calibrated positions can be used for image deformation correction. Unfortunately, especially when film is used in these cameras, the peripheral positions of the reference marks can result in the computation of invalid corrections at the centre of the format, especially if out-of-plane deformations are present.

A more rigorous method of determining the physical magnitude of deformations over the format area, is to introduce a calibrated reseau grid into the camera system. The grid is positioned close to the focal plane, enabling either an active or passive projected reseau grid to be recorded sharply onto the film. Measurement and analysis of such a reseau image will provide the overall magnitude of film deformations produced from the instant of exposure to measurement in the comparator. Such grids are often used to modify pictorial cameras for photogrammetric use. Unfortunately for this analysis, differences in location between the calibrated positions of the reseau crosses and their imaged positions can only be attributed to a combination of in-plane, out-of-plane and measurement deformations, not individual physical causes.

An innovative reseau array developed at Geodetic Services Inc for use in their CRC1 and CRC2 cameras enables a distinction to be made between in-plane and out-of-plane deformations. Each reseau image is produced by an annular back projection system (Fig. 3.6), the resultant annular reseau images being intended for automated image measurement, Brown (1984). The centroid of the concentric reseau image is used to locate the position, whilst the diameter of the outside annulus provides a direct measure of the unflatness at exposure.

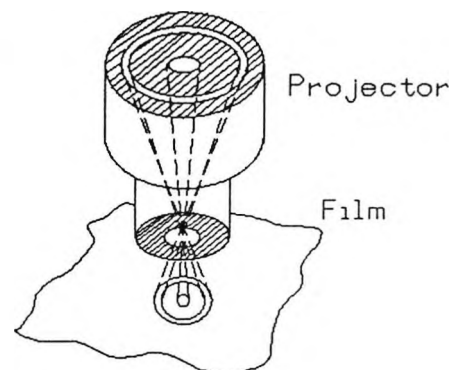


Figure 3.6. GSI's back projected reseau system.

3.3.1.1. Models based on polynomials applied to the deformations at known sites.

The effectiveness of models based on the deformation at known sites have been shown to be related to reseau grid density and to the method of correction applied (Kratky 1971; Ziemann 1971b).

Correction methods can be global in nature such that a single transformation is applied to all image points on the photograph. Alternatively the correction can be localised, using individual transformations based only on sites surrounding the image point of interest.

In each case the parameters of the transformation can be derived by minimising the sum of squares of the residual deformations at all known reseau sites, for displacements in x and subsequently displacements in y . The x and y corrections to be applied to the observed point can then be computed by substituting its x and y coordinates into the transformation.

Ziemann (1971b) used large format imagery to investigate a range of algorithms based on a variety of known site configurations. He concluded that the standard deviations of image coordinates after adjustment could be minimised if local corrections based on the four reseau points surrounding the image point to be corrected were applied. In his work he categorised the methods of correction into two main types:

a) Different mathematical treatment applied to:

- i) all image marks at the same time (a single transformation for all points of a photograph).
- ii) a selected number of different image marks for each point to be corrected.

b) Different locations of reference marks:

- i) only image marks along the frame edge, for example fiducial marks in a traditional metric camera.
- ii) image marks equally distributed over the entire image.

Some possible transformations for the explicit correction of film deformation have also been summarised by Ziemann (1971b);

Linear conformal transformation (C) (3.6)

$$\begin{aligned}x &= a_0 + a_1x - b_1y \\y &= b_0 + b_1x + a_1y\end{aligned}$$

Linear Affine transformation (A) (3.7)

$$\begin{aligned}x &= a_0 + a_1x + a_2y \\y &= b_0 + b_1x + b_2y\end{aligned}$$

Projective transformation (P) (3.8)

$$\begin{aligned}x &= (a_0 + a_1x + a_2y)/(1 + c_1x + c_2y) \\y &= (b_0 + b_1x + b_2y)/(1 + c_1x + c_2y)\end{aligned}$$

Bilinear transformation (B) (3.9)

$$\begin{aligned}x &= a_0 + a_1x + a_2y + a_3xy \\y &= b_0 + b_1x + b_2y + b_3xy\end{aligned}$$

Second order polynomial (S) (3.10)

$$\begin{aligned}x &= a_0 + a_1x + a_2y + a_3xy + a_4x^2 + a_5y^2 \\y &= b_0 + b_1x + b_2y + b_3xy + b_4x^2 + b_5y^2\end{aligned}$$

Incomplete third order polynomial (TI) (3.11)

$$\begin{aligned}x &= a_0 + a_1x + a_2y + a_3xy + a_4x^2 + a_5y^2 + a_6x^2y + a_7xy^2 \\y &= b_0 + b_1x + b_2y + b_3xy + b_4x^2 + b_5y^2 + b_6x^2y + b_7xy^2\end{aligned}$$

Third order polynomial (T) (3.12)

$$\begin{aligned}x &= a_0 + a_1x + a_2y + a_3xy + a_4x^2 + a_5y^2 + a_6x^2y + a_7xy^2 + a_8x^3 + a_9y^3 \\y &= b_0 + b_1x + b_2y + b_3xy + b_4x^2 + b_5y^2 + b_6x^2y + b_7xy^2 + b_8x^3 + b_9y^3\end{aligned}$$

These transformations were applied to a distribution of image points situated within a range of reseau images. Comparisons of results demonstrated that, for a given reseau density, the localised correction to each image point yielded a more effective image deformation reduction than the simultaneous correction of all image points (Fig.3.7). The difference in favour of the local correction was found to increase with the irregularity of the image deformation. With reference to figure 3.8, the margin between the global and localised applications of the transformations would probably be greater in the case of reseau B which exhibits some large localised deformations.

Again as with the additional parameters included within the adjustment, these explicitly applied transformations tend to be derived according to statistical significance of parameters (Section 4.3.1) not physical film deformations. This explains why the local corrections, which by virtue of

being fitted to four reseau crosses at a time with very few degrees of freedom, are fitted to the physically derived reseau data thereby producing smaller image residuals (Fig. 3.7).

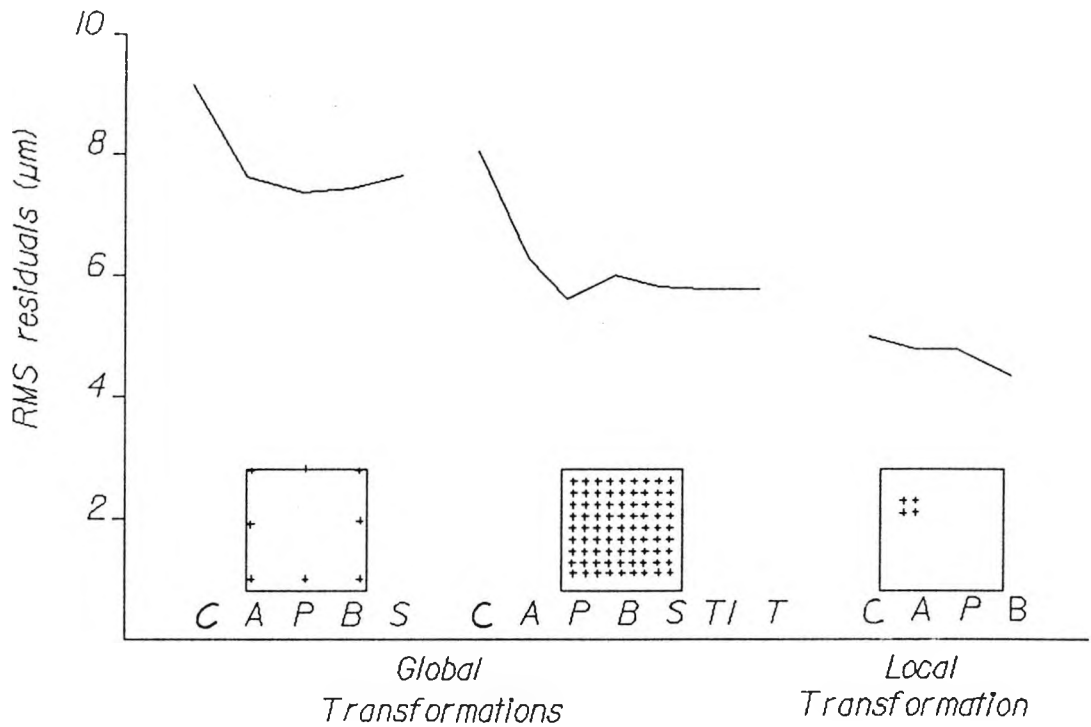


Figure 3.7. RMS image residuals for 96 image points, obtained with different correction methods applied to the same image marks, (Ziemann 1971b).

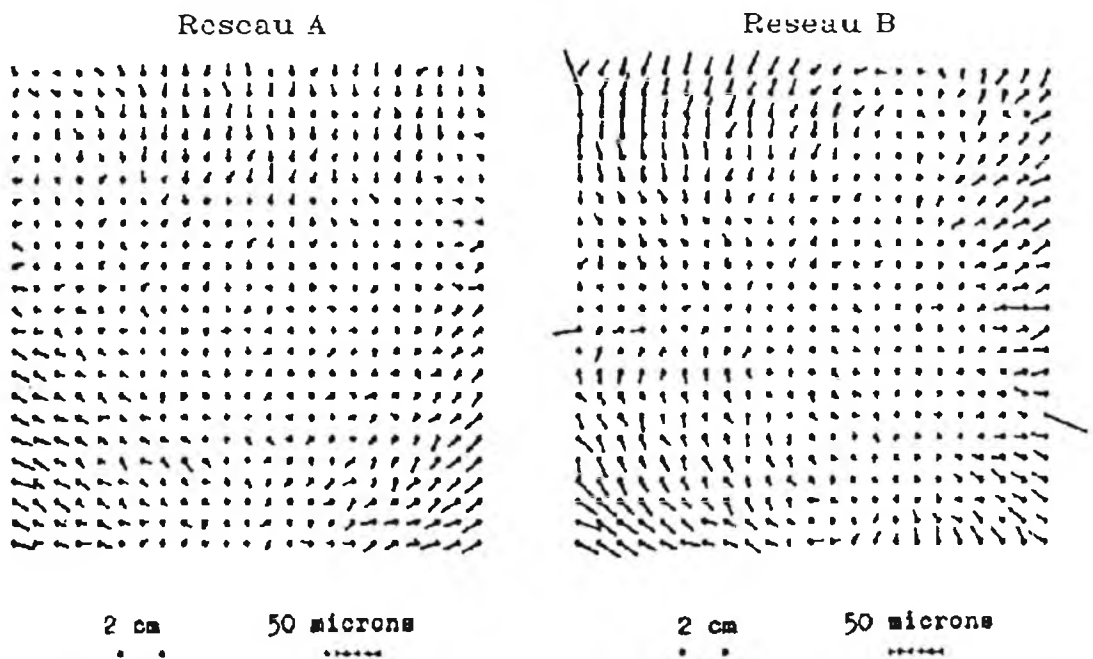


Figure 3.8. Two reseau deformation patterns from images on 9" square aerial film, (Ziemann 1971b).

3.3.1.2. Linear least squares interpolation.

A disadvantage of the transformations applied by Ziemann is their lack of statistical foundation, for example random reseau measurement errors can be directly transferred to the corrected image coordinates. A more recent approach, linear least squares interpolation theoretically incorporates statistical concepts to a much greater degree. The method involves the use of empirically derived covariance functions to model the relationship between the distortion components of pairs of points. This method of interpolation is based on the theory of stationary random functions, devised by Yaglom (1962).

The information at each reseau point is considered to be composed of two classes of random variables, namely, correlated stochastic variables which are described by the covariance function and observational errors. Although the theory has been extended to multi-dimensional cases, an assumption that the deformations in x and y are mutually independent can be made to simplify computation. (Schut 1974; Kubik and Botman 1976; Hardy 1977).

The method involves four main steps: trend removal; computation of covariance functions; modelling of the derived covariance functions; and corrections to the image point coordinates.

a) Initially, to meet theoretical considerations, (Kraus 1972; Kraus and Mikhail 1972), any trends in the data must be removed. For example, the removal of systematic effects due to fluctuations in environmental conditions can be accomplished by conformal or affine transformations.

b) Secondly, the covariance function must be computed. The covariance function is produced, independently for both x and y displacements, from the known displacement error at each reseau point, by computing the covariance between pairs of points at given separations. Statistically the covariance contains only the systematic part of the vector field, the observational errors having been filtered out.

The Variance:
$$\sigma_p^2 = \left(\frac{1}{n}\right) \sum_{i=1}^n l_i^2 \quad (3.13)$$

The covariance:
$$C(d) = \left(\frac{1}{n_{ij}}\right) \sum_{k,j} l_i l_j \quad (3.14)$$

Where: σ_p^2 is the variance at any point i
C(d) is the covariance function between two points i and j separated by distance d.
n is the number of repeated measurements.
 l_i, l_j are the measured magnitudes of the reseau image deformation.

Theoretically the covariance depends only on distance, the value of the covariance function approaching zero as d increases indefinitely, however computations based on analysis carried out during the initial investigations (Section 4.3.3) would appear to show significant practical differences.

c) Each covariance function can be modelled, by for example a Gaussian curve (3.15) (Kraus 1971a). The coefficients $C(0)$ and k can be evaluated by a least squares fit to the covariance function data. $C(0)$ represents the covariance of pairs of infinitely close points. As $C(d)$ is composed entirely of correlated stochastic variables, the difference between $C(0)$ and σ_p^2 represents the operational measurement error.

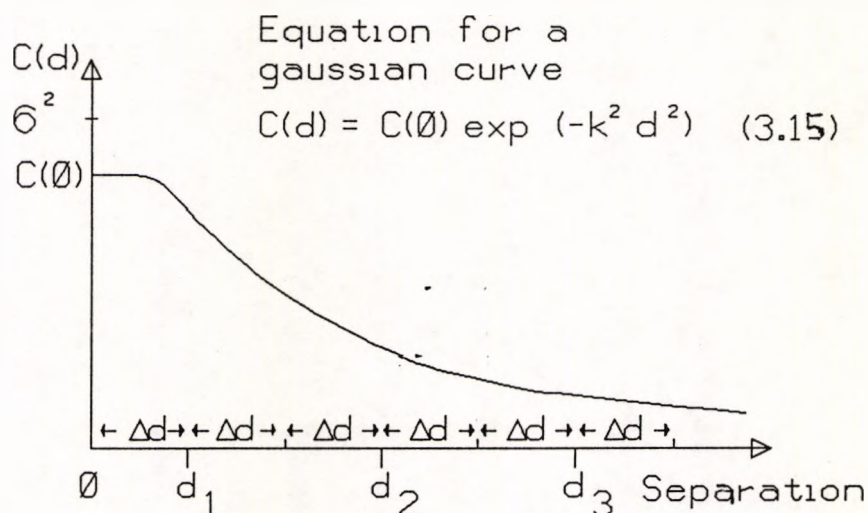


Figure 3.11. The covariance function and gaussian equation, (Kraus 1971a).

d) Corrections to each image point can then be derived by the method of linear least squares interpolation, using the minimum variance estimate for the refined image point coordinates, such that the variances of the corrections are minimised (Cooper and Cross 1990).

The method is best described by considering the vector

$$\begin{bmatrix} u \\ v \end{bmatrix} \quad (3.16)$$

where:

u is a vector of known values at p data points.

v is a vector of values to be estimated at q data points.

and assuming that the associated covariance matrix C of the vector is known.

$$C = \begin{bmatrix} C_{uu} & C_{uv} \\ C_{vu} & C_{vv} \end{bmatrix} \quad (3.17)$$

The requirement is to find G where $\hat{v} = G u$ and \hat{v} is any linear estimate of v from transformation of u through G .

If \hat{e} denotes the error of the linear estimate \hat{v} such that $\hat{e} = \hat{v} - v$, then G must be chosen to give the minimum variance estimate of v , that which minimises the variances of \hat{e} . It can then be shown (Cooper and Cross 1990) that the minimum variance estimate is given by:

$$v = Cuv Cuu^{-1} u \quad (3.18)$$

which in full can be written:

$$\begin{bmatrix} v_1 \\ v_2 \\ \vdots \\ v_q \end{bmatrix} = \begin{bmatrix} C(u_1 v_1) & C(u_2 v_1) & \dots & C(u_p v_1) \\ C(u_1 v_2) & C(u_2 v_2) & \dots & C(u_p v_2) \\ \vdots & \vdots & \ddots & \vdots \\ C(u_1 v_q) & C(u_2 v_q) & \dots & C(u_p v_q) \end{bmatrix} \begin{bmatrix} C(u_1 u_1) & C(u_1 u_2) & \dots & C(u_1 u_p) \\ C(u_2 u_1) & C(u_2 u_2) & \dots & C(u_2 u_p) \\ \vdots & \vdots & \ddots & \vdots \\ C(u_p u_1) & C(u_p u_2) & \dots & C(u_p u_p) \end{bmatrix}^{-1} \begin{bmatrix} u_1 \\ u_2 \\ \vdots \\ u_p \end{bmatrix} \quad (3.19)$$

The estimation procedure therefore utilises the covariance between the image point to be corrected and each reseau point, as computed using the gaussian curve since the separation between points is known. The major advantage of the method is that reseau measurement observational errors are not transferred to the computed corrections.

The application of this method and both the local and global transformations (Section 3.3.1.1.) to real data are evaluated in chapter 4.

3.3.1.3. Models based on previous reseau image measurements.

Another approach, which has been applied to large format photography, is to look at the physical causes of individual deformation factors and to model their deterministic and functional properties. A good theoretical example is that due to Tempfli (1973 and 1974), who analyzed film unflatness and existing reseau photography to derive representative algorithms and their associated parameters.

The developed models were based on deterministic functions describing the known error sources with additional stochastic functions to evaluate random departures. Full development was limited by the data available, this being taken from reseau image measurements of aerial survey camera images produced during operational use. Tempfli concluded that the method appeared applicable for deformations that could be 'reasonably expected'. Interestingly the high degree of consistency of the film deformations found between differing sub areas tended to support the use of simple analytical expressions for the basic distortion patterns.

The basis of Tempfli's technique is used in chapter 6, where a bilinear correction is locally applied using mean reseau image measurements computed from all similarly exposed frames, rather than from the specific image being modelled (Section 6.4).

3.3.2. Use of additional polynomial terms during photogrammetric adjustment.

As explained in section 3.4, provided the system configuration is adequate for their recovery, additional parameter models can be included in the self-calibration adjustment. Such parameters can not only be included to model lens distortions, but by virtue of the bundle adjustment technique will also model film deformations.

A variety of parameter sets have been proposed (Kilpelä 1980; Bauer and Müller 1972). The parameter sets employed are generally selected by statistical techniques, analogous to those used in section 4.3.1, and as such are unlinked to any specific physical process. The nature of the least squares adjustment process means that parameters simply model mathematical departures from the collinearity assumptions, not specific error sources as in section 3.3.1.1, additionally the effectiveness of such treatments will be a function of the photogrammetric network.

For example a parameter set proposed by Brown (1980):

$$\begin{aligned} \delta x = & a_1x + a_2y + a_3xy + a_4y^2 + a_8xy^2 + a_7x^2y^2 \\ & + \frac{x}{f} [a_{13}(x^2 - y^2) + a_{14}x^2y^2 + a_{15}(x^4 - y^4)] \\ & + x [a_{16}(x^2 + y^2) + a_{17}(x^2 + y^2)^2 + a_{18}(x^2 + y^2)^3] \end{aligned} \quad (3.20)$$

$$\begin{aligned} \delta y = & a_8xy + a_9y^2 + a_{10}x^2y + a_{11}xy^2 + a_{12}x^2y^2 \\ & + \frac{y}{f} [a_{13}(x^2 - y^2) + a_{14}x^2y^2 + a_{15}(x^4 - y^4)] \\ & + y [a_{16}(x^2 + y^2) + a_{17}(x^2 + y^2)^2 + a_{18}(x^2 + y^2)^3] \end{aligned}$$

Several additional parameter models have been developed based on physical assumptions concerning the effects of film deformation (Grün 1976; El-Hakim and Faig 1979; Fraser 1982a). A typical example is the modelling of film unflatness where the corrections to the image coordinates are represented by Δx_{flat} and Δy_{flat} such that:

$$\begin{aligned} \Delta x_{flat} &= \left(\frac{x}{f}\right) \Delta Z \\ \Delta y_{flat} &= \left(\frac{y}{f}\right) \Delta Z \end{aligned} \quad \text{where:} \quad \Delta Z = \sum_{i=0}^n \sum_{j=0}^l d_i x^{i-j} y^j \quad (2.21)$$

However since the measurements used to model ΔZ are orthogonal to the image measurements, effective estimation requires a strong network.

Despite these disadvantages, additional parameters can be advantageous because they can be applied individually to each single image (photo-invariant) or to sets of images (block-invariant). For example known optical distortions associated with a given camera lens could be corrected by applying identical parameters to all instances of that optical configuration in a block-invariant approach. Indeed, the technique whereby parameters estimated by calibration and constrained by their estimated standard deviations have been used to advantage in chapter 6. The procedure permits known geometrical distortions to be applied (in this case predominantly lens distortion) to weak photogrammetric networks which are not suitable for estimation of such parameters.

3.4. The self calibrating bundle adjustment.

In analytical photogrammetry, the basic computational unit is the pencil of rays that originate at the object, pass through the exposure station and are produced as an image point. The technique involves simultaneous least squares adjustment of all pencils from all exposure stations to all measured image points. For self calibration the unknown parameters from the extended functional model may be simultaneously estimated during this procedure.

The estimation procedure utilised in the bundle adjustment incorporates both a functional and stochastic model. Mathematical models can be envisaged as simplified descriptions of reality, in this case, the functional or deterministic part being an approximation of image geometry. The more physically appropriate the functional model is made the smaller the magnitude of the errors will be, such that the two models are inter-related.

3.4.1. The functional model.

The functional model has been extended in the above sections by the inclusion of additional parameters chosen to represent physical causes of departures from the ideal collinearity condition in practical cameras. This section summarises the least squares solution to the extended functional model and some aspects of the matrix manipulations involved.

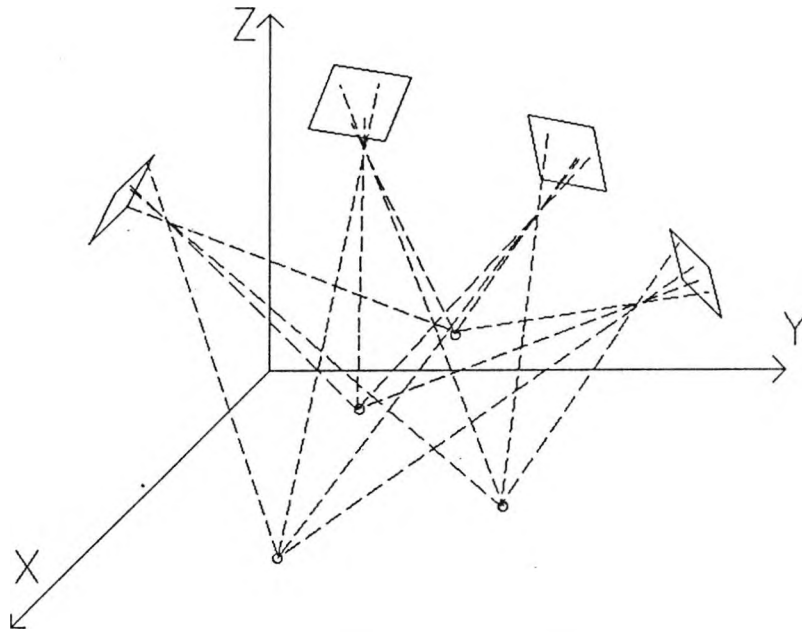


Figure 3.10. The geometric basis of multi-station convergent photography, (Wester-Ebbinghaus 1986).

The non-linear functional model f_x and f_y can be represented:

$$f(x, l, c) = \frac{-f (m_{11}(X_A - X_0) + m_{12}(Y_A - Y_0) + m_{13}(Z_A - Z_0))}{m_{31}(X_A - X_0) + m_{32}(Y_A - Y_0) + m_{33}(Z_A - Z_0)} - x_a - x_p - \Delta x_{lens}$$

$$f(y, l, c) = \frac{-f (m_{21}(X_A - X_0) + m_{22}(Y_A - Y_0) + m_{23}(Z_A - Z_0))}{m_{31}(X_A - X_0) + m_{32}(Y_A - Y_0) + m_{33}(Z_A - Z_0)} - y_a - y_p - \Delta y_{lens}$$
(3.22)

where for self calibration:

\hat{x} is the vector of parameters to be estimated, such as $X_A, Y_A, Z_A, X_0, Y_0, Z_0, \omega, \phi, \kappa$, the three inner orientation parameters if unknown (x_p, y_p, f) and any additional parameters.

l is the vector of elements which have been measured, such as x_a and y_a .

c is the vector of elements whose values are known and are regarded as constant. Generally for self calibration, constant elements are not present, unless the imaging geometry precludes their estimation.

Δx_{lens} and Δy_{lens} are the lens distortion corrections derived from equations 3.5.

These functions must be linearised, using Taylors' expansion, by taking the partial derivatives of

the equations with respect to each of these variables (Brown 1958). In this case, since the function can be written explicitly in each measurement, an observation equation can be written connecting each object point and its corresponding image position. The collected linearised observation equations may then be represented in matrix form.

$$\mathbf{A} \hat{\mathbf{x}} = \mathbf{b} + \mathbf{v}; \text{ with associated weight matrix } \mathbf{W} \quad (3.23)$$

where: \mathbf{A} comprises the partial differentials of the extended collinearity equations with respect to the parameters to be estimated.

\mathbf{v} is the vector of photo-coordinate residuals.

$\hat{\mathbf{x}}$ is the vector of least squares corrections to the approximate parameter values.

\mathbf{b} is the vector of the "observed minus computed" terms.

\mathbf{W} denotes the weight matrix associated with all measurements (Section 3.4.2).

An iterative solution is then used to estimate the unknown parameters by minimising the sums of squares of the residuals for all the equations.

The observation may then be written:

$$(\mathbf{A}^t \mathbf{W} \mathbf{A}) \hat{\mathbf{x}} = (\mathbf{A}^t \mathbf{W} \mathbf{b}) \quad (3.24)$$

and the least squares estimates of the parameters $\hat{\mathbf{x}}$ are:

$$\hat{\mathbf{x}} = (\mathbf{A}^t \mathbf{W} \mathbf{A})^{-1} (\mathbf{A}^t \mathbf{W} \mathbf{b}) \quad (3.25)$$

In order for the solution to exist and be computable certain criteria must be met (Granshaw 1980):

- a) A datum must be defined, since the parameters are not estimable from the measurements alone.
- b) There must be at least as many equations as there are parameters to be estimated.
- c) The geometric configuration of the camera positions in the object must be suitable.

These theoretical criteria are discussed more fully in sections 3.4.3 and 3.4.4, and their practical application to network design is considered in chapter 6.

3.4.2. The stochastic model.

Statistical models are usually based on the assumption that the observations are independent stochastic variables having the same variance, and that the statistical distribution of the variables is assumed to be normal (Hallert 1964). This last condition is however not necessary for Least-Squares.

The stochastic model can take a variety of forms but usually includes the stochastic properties of both the photo-coordinates and the coordinates of object control points. In this basic pattern, the model assumes the form of a diagonal weight matrix \mathbf{W} (Equation 3.23), based on measurement standard errors which are assumed to be normally distributed. As such it is sometimes called the co-factor matrix of the measurements.

The error terms are allowed to propagate through the function to arrive at a second co-factor matrix \mathbf{Q}_x representing the stochastic properties of the estimated parameters.

$$\mathbf{Q}_x = (\mathbf{A}^t \mathbf{Q}_1 \mathbf{A})^{-1} \quad (3.26)$$

where: \mathbf{Q}_x is the cofactor matrix of the estimated parameters, $\hat{\mathbf{x}}$; and
 \mathbf{Q}_1 is the cofactor matrix of the measurements, (if diagonal equivalent to the weight matrix \mathbf{W}).

Also of importance is the associated variance factor, the square of the standard deviation of unit weight. For the work carried out during this thesis the a priori variance factor was defined as being one. Assuming the removal of all gross errors, if the a posteriori variance factor (that estimated by the adjustment) is significantly greater than unity then either the stochastic model assigned a-priori is erroneous or certain systematic errors remain un-compensated.

Taking the assumption that the total photogrammetric error is a sum of elementary errors which are individually independent, Torlegård (1989), among others, has extended the simple diagonal cofactor matrix (weight model). Using the notation portrayed above depicting individual physical departures from the collinearity model, the stochastic model may be described in terms of their corresponding covariance functions to arrive at a "variance component" model.

Important conclusions clearly demonstrated by the variance component model are firstly that observations are not independent, and secondly that the errors of the x,y coordinates of a point are correlated.

A variance-covariance matrix may be derived in which the off-diagonal terms are not equal to zero, but are equal to the covariances of the observations. The cofactor matrix associated with the adjustment is simply the inverse of the variance-covariance matrix.

$$\mathbf{Q} = \begin{matrix} & \sigma_{x_a}^2 & C(x_a y_a) & C(x_a x_b) & C(x_a y_b) \\ C(x_a y_a) & \sigma_{y_a}^2 & C(y_a x_b) & C(y_a y_b) \\ C(x_b x_b) & C(x_b y_a) & \sigma_{x_b}^2 & C(x_b y_b) \\ C(x_a y_b) & C(y_a y_b) & C(x_b y_b) & \sigma_{y_b}^2 \end{matrix} \quad (3.27)$$

where: $\sigma_{x_a}^2$, $\sigma_{y_a}^2$, $\sigma_{x_b}^2$ and $\sigma_{y_b}^2$ are the variances of the individual measurements.
 $C(x_a y_a)$, $C(x_b y_a)$ are the covariances associated with pairs of points.

For inclusion in the adjustment these covariances must either be known a-priori, determined for example from analysis of the individual error sources, or if the adjustment network is suitable they can be estimated as part of the adjustment procedure (Persson 1981). An accurate a priori knowledge of the covariances is difficult to determine in practice (Torlegård 1989), such that a full cofactor matrix is rarely used in photogrammetry. Such is the case for the adjustments described in chapter 6.

The use of a-priori off-diagonal terms instead of a diagonal cofactor matrix influences the estimation of the variance factor. This is reflected in chapter 6, where the photo-coordinate standard deviations computed from the three rounds of comparator measurements need to be multiplied by a factor of three if the a posteriori variance factor is to approach one.

3.4.3. Datum definition.

In section 3.4.1. some of the criteria for the solution of a bundle adjustment were outlined. The definition of a datum arises because the three dimensional object coordinate system, although usually cartesian, is arbitrary and needs to be located in space. This is reflected in the mathematical model (Equation 3.25) by the normal equation coefficient matrix (A^TWA) being singular with a rank defect of seven. Location of the coordinate system in this three dimensional situation is therefore facilitated by the definition of seven datum elements: three rotations; three translations and; a scale factor (Cooper and Cross 1988). The definition of a datum is important for this work, since analysis of the effect of film deformation on object space coordinates (Chapter 6) required that all adjustments were carried out using the same coordinate reference system.

There are various methods of defining a datum. In traditional topographic photogrammetry, fixed coordinates are used, the minimum requirement being two points fixed in X,Y and Z and a third coordinate fixed in one of the coordinate axes (Abdel-Aziz 1984, Cooper 1988).

For the purposes of close range self calibration, this method is inappropriate due to the problems in defining and surveying control point positions to high accuracy (Cooper 1988). In fact errors in control definition will directly lead to distortions of the parameters estimated by the adjustment.

Development of the bundle adjustment (Faig 1975), specifically the use of multi-station convergent photography, has increased the ability to determine the interior and additional camera elements. Importantly for this work, convergent multi-station photography can be used without control points in a so-called "free adjustment". The "free adjustment" applies a minimum number of algorithmic constraints to define the datum and thus to provide a solution (Fraser 1984a). These "minimum constraints" are usually applied to the spatial coordinates of the object points and not to the camera and additional parameters, typically such that the datum is provided by the centroid of the object coordinate starting values. The method is applied in chapter 6 to enable the definition of

a datum which does not introduce shape constraints, since shape of the estimated object coordinates is one of the means chosen to assess film deformation.

3.4.4. Optimisation of network geometry.

Given the extended collinearity equations as a functional model, the major limiting factors are the number and location of camera positions and the precision with which the photo-coordinates are measured. For a strong estimate of the camera calibration parameters (as required for this work) increased redundancy in the form of additional photographs is desirable, as is a convergent geometric configuration between the photographs and the object (Granshaw 1980).

Garafarend (1974) and Fraser (1984a), have summarised the problem of geometric network design in terms of four interconnected stages;

**Zero Order design;
(Datum)** This involves the choice of the datum definition such that specific criteria associated with the project are met. For example, the use of minimum constraints such that the datum introduces no shape distortion of the estimated bundles of rays. In general terms, the concern is to produce an optimum co-factor matrix $(A^TWA)^{-1}$ of the estimated parameters.

**First Order design;
(Configuration)** Concern here is for an optimised network geometry, selected according to some optimised form of the **A** matrix (Equation 3.23), often called the design matrix. In the case of calibration, a multi-station convergent imaging geometry has been shown to be desirable (Granshaw 1980; Fraser 1980).

**Second Order design;
(Measurement)** Here we are interested in maximising the precision of image coordinate measurement, such that the elements of the weight matrix approach the identity matrix. Potential for optimisation apart from the obvious comparator selection, are the use of multiple pointings to each image point and the taking of multiple exposures (Fraser 1982a).

**Third Order design;
(Densification)** Object point precision is largely independent of target array density for multi-convergent imaging geometries. Third order design, concerned with the enhancement of precision by the addition of observations is therefore not as important for optimisation of self-calibration.

The potential for network design has been illustrated by Fraser (1986b) with regard to the high precision monitoring of antennae.

3.4.5. Adjustment quality.

Whilst the bundle adjustment method enables the estimation of object coordinates and camera parameters, it is done in such a way as to be statistically rigorous. In this way the quality of the results can be assessed with respect to gross, random and systematic errors. Cooper and Cross (1988) consider the quality of the least squares estimation procedure in terms of three factors; precision, reliability and accuracy.

Precision; describes the quality of the data set with respect to random errors. Precision may be assessed using the co-factor matrix of the estimated parameters Q_x . Such measures include the variances of the estimated parameters, error ellipses, eigen values and criterion matrices.

Reliability; is concerned with the ease with which gross errors or outliers may be detected. This assessment may be divided into external and internal reliabilities. External reliability is a measure of the effect of an undetected marginally detectable error on the estimated parameters, whilst internal reliability of a measurement is the size of the marginally detectable gross error (Baarda 1976; Föstner 1980). It has been shown (Pelzer 1979) that if internal reliability is high then high external reliability will also result. Parameters for the assessment of reliability are presented in Cross (1983) and Cooper (1988).

Accuracy; describes the quality with respect to systematic errors. The extended collinearity model associated with well calibrated instrumentation is assumed to remove systematic errors. However where film deformations are concerned the mathematical model can be incomplete, such that systematic errors may be significant. Analysis of the accuracy of the adjustment is possible by examination of Q_x (Cooper and Cross 1988).

One important factor concerning adjustment quality, which has been mentioned previously, is the inclusion of additional parameters in the bundle adjustment to model systematic effects. The use of additional parameters not only requires sufficient three dimensional network geometry for estimation, but also their statistical significance and correlation between each other and the interior orientation parameters must be determined (Fraser 1982a; Schroth 1982).

Statistical tests involved in the rejection of unnecessary additional parameters include the correlation coefficient and total correlation, which refer to the interdependence between individual parameters and each parameter and the rest of the set respectively. Also of importance is the t test, a measure of precision, which can be used to compare the value of each estimated parameter with its standard deviation (Jacobsen 1982).

Strong network design, the use of numbered targets and the semi-automatic measurement procedures employed for the adjustments in chapter 6 have reduced the likely-hood of gross measurement errors in the adjustments computed during chapter 6. Consequently adjustment reliability has not been investigated. Adjustment precision has been given a basic assessment, with the application of t-tests to evaluate the significance of the parameters estimated in the various adjustments.

Object coordinates and parameters estimated by the adjustment incorporating all photographs in conjunction with the most complete physical models (Section 6.3) were treated as a reference set. In this way differences between these reference data and object space coordinates and parameters estimated by adjustments incorporating differing film deformation corrections, based on the same datum, could be compared in an assessment of accuracy (Section 6.4).

3.5. Chapter Summary.

In this chapter it has been shown that the bundle adjustment can take full account of the spatial and geometric relationships between the photographs and the ground coordinate system and can therefore be made rigorous. Since the parameters to be estimated and those to be maintained constant can be varied, the analytical bundle adjustment provides one of the most flexible techniques of restitution.

Physically derived corrections for geometric deformations applied explicitly to the measured photo-coordinates provide the most preferable method of modelling departures by the imaging system from the central projection model. However since physical deformations are often unknown or unstable, as is commonly true for the film surface at exposure (Section 2.5), the extended model incorporated in the bundle adjustment can enable the estimation of such deformations. A particularly useful technique is the transfer of parameters estimated from strong networks and representing stable camera specific deformations to weaker networks where the same camera configuration has been used.

4. Initial investigations.

The survey of the current literature (Chapters 2 and 3) has described the problems associated with the use of film based products for photogrammetric surveys. However before any specific directions for research were decided upon, it was necessary to conduct a preliminary study of film deformations occurring under practical small format survey conditions. The main objective of this preliminary study was to gain an impression of the magnitude of film deformation occurring during the complete imaging process, that is from taking the actual photograph to measuring the result. Also to be investigated were some methods of representing and analyzing the derived data.

4.1. Investigation of film deformation using a Rollei-Metric 6006.

Research current at the time (Chandler 1989), involved the use of a Rollei-Metric 6006 camera (Reseau No.40) kindly loaned to the University by Mr M. Kafetz of A.V. Distributors. The camera incorporated a calibrated lens and more importantly for this research, a calibrated reseau grid, on which were etched 121 crosses at intervals of 5mm. Images produced from this system could be used in an assessment of image deformation, by simply comparing the imaged positions of the crosses to their calibrated positions.

4.1.1. Methodology.

Reseau photographs on Kodak TMAX 100 and 400 films, taken by Chandler (Chandler et al 1989b) during a geomorphological survey of a land slip, provided a very useful source of film deformation data obtained under practical conditions. To provide a useful addition to these data, sets of controlled experiments were conducted in the laboratory, using the camera simply as a means of imaging its reseau grid onto 120 and 220 roll films.

The photographs of a landslip near Exeter were taken from a light aircraft on two separate occasions. The frames used for this investigation were selected from both survey flights carried out on 10th of January 1988 and 14th of June 1988. The unsuitability of these photographs for use in this analysis

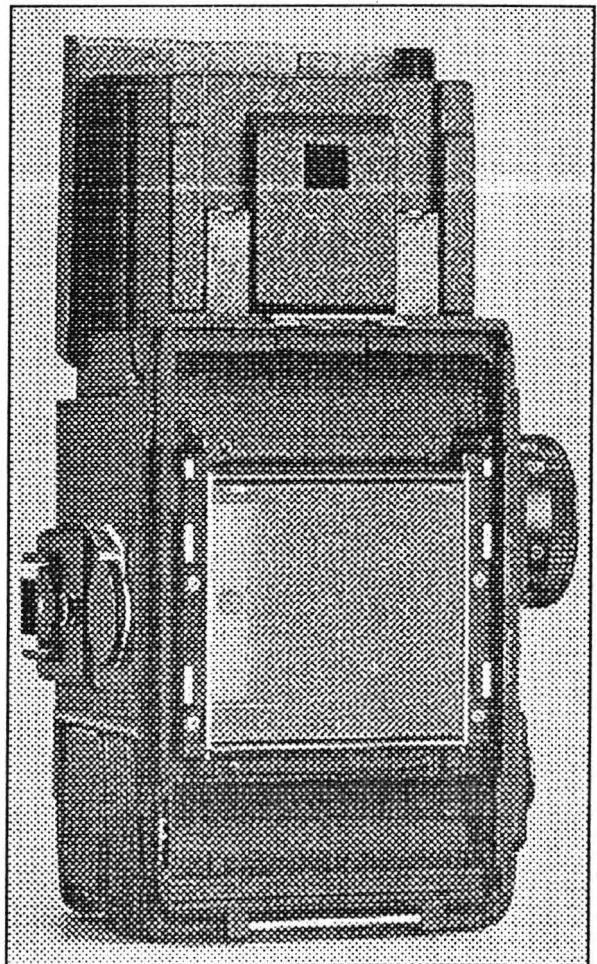


Figure 4.1. Rollei-Metric 6006

was limited to two factors; the environmental conditions were unknown and because of the wide range of tones present in the negatives not all reseau crosses were easily measurable.

These problems could be reduced in the more stable conditions of the laboratory. For this method exposure was made to a uniform tone by placing the camera lens against a light box. This ensured not only that all reseau crosses would be recorded but also that the possible contribution of image density variations to dimensional change would be minimised. Camera handling was standardised, films being loaded immediately prior to exposure into inserts which fitted into the 120 or 220 camera backs. Sequential exposures were then made at the automated film wind-on rate of two frames every three seconds to produce as far as possible consistent treatment within the camera.

Film types selected for experimentation are defined in table 4.1, the criterion for selection being to achieve a range of emulsion types within the limitations of the 120 and 220 roll film backs available (Kodak 1990; Ilford 1991c).

Table 4.1. Film types selected for initial investigation.

Manufacturer	Film	Format	Base Type	Base Thickness	Current Publication
Kodak	TMAX 400 (TMY)	120	Triacetate	0.132mm	Kodak 1987a
Kodak	Technical Pan (TCP)	120	Triacetate	0.091mm	Kodak 1987b
Kodak	Ektachrome 200 (EPD)	120	Triacetate	0.075mm	Kodak 1990
Ilford	FP4	120	Triacetate	Not published	Ilford 1991a
Ilford	FP4	220	Triacetate	Not published	Ilford 1991a

To provide some measure of environmental consistency, ambient conditions for the experiments conducted in the laboratory were measured using a TRACE 323i digital thermo-hygrometer. Table 4.2 summarises not only the processes used, but also gives the average environmental conditions found in each environment on the day of the investigation in question.

All monochrome films were processed in small spiral tanks using the chemical formulations recommended by the manufacturers for pictorial photography, (Kodak 1989a,b,d,e,f; Ilford 1982 and 1985a,b; Agfa 1989). Development was carried out by the time temperature method (Jacobson and Jacobson 1980) using the agents detailed in table 4.2. Subsequent to development a stop bath was used for thirty seconds at 20°C, this in all cases was Kodak Indicator Stop Bath at a dilution of one part concentrate to sixty four parts water (1:64). The fixing bath employed was Ilford Hypam fixer (1:4) for five minutes at 20°C used in conjunction with Ilford Rapid Hardener (1:80). Ilford Rapid Hardener is of the inorganic type as described in section

2.2.3. Subsequent washing was carried out for thirty minutes in running water, the minimum recommended for archival permanence. A wetting agent was used before drying to help prevent the formation of water spots which could have caused localised deformations and drying marks.

Table 4.2. Exposures made using the Rollei-Metric 6006

Film Type	Exposure		Processing			Measurement	
	Date	RH °C	Date	Development	Dry RH °C	Date(s)	RH °C
A TMY 120	10/1/88	Not Known	Jan 88	ID11 1:1 22°C	Cabinet	01/3/88 27/6/88	-- -- 30 18
B TMY 120	10/1/88	Not Known	Jan 88	ID11 1:1 22°C	Cabinet	17/6/88	46 21
C TMY 120	14/6/88	Not Known	15/6/88	TMAX Stock 21°C	Ambient	16/6/88 30/6/88	58 21 60 21
D TMY 120	14/6/88	Not Known	15/6/88	TMAX Stock 21°C	Ambient	16/6/88 30/6/88	58 21 60 21
A TCP 120	7/1/88	Not Known	12/1/88	HC110 Dilution F 20 °C	Ambient	5/7/88 6/7/88	63 19 60 20
A EPD 120	7/1/88	Not Known	Jan 88	PCL E6	Ambient	4/7/88 5/7/88	58 20 52 20
A FP4 120	8/9/88	48 24	8/9/88	ID11 1+1 23.5 °C	28 41	9/9/88 14/9/88	Not Known
B FP4 220	8/9/88	47 24	8/9/88	ID11 1+1 23.5 °C	28 41	9/9/88 14/9/88	Not Known
C FP4 120	8/9/88	48 24	8/9/88	ID11 1+1 23.5 °C	47 23	16/9/88	Not Known
D FP4 220	8/9/88	48 24	8/9/88	ID11 1+1 23.5 °C	47 23	16/9/88	Not Known

All exposed and processed films were cut into strips of four frames and stored in the measuring environment in negative bags. In this way the physical conditions giving rise to the differential roll conditioning effects described in chapter 2 (Carman & Martin, 1969; Kodak, 1972), could largely be avoided.

Initially the reseau grid images produced were measured on a Zeiss Jena Stecometer. This instrument was equipped with digitisers and able to provide a viewing magnification of 14.4 times

in conjunction with a measuring mark diameter of $20\mu\text{m}$. However with no back-driving of the stage plates to approximate image positions it was slow to use, requiring for example about thirty minutes to make two independent rounds of pointings to each of the 121 reseau cross images. This measurement time assumes correct identification of image points, a tedious task since no numbering is present on the reseau grid.

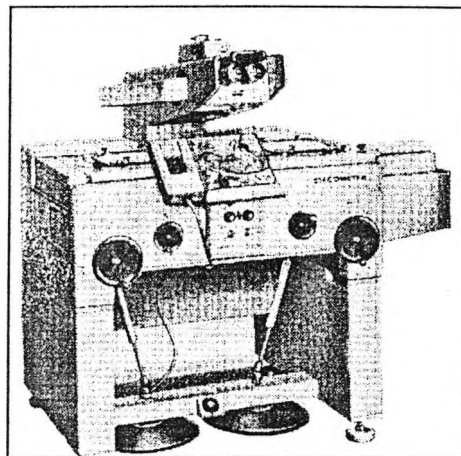


Figure 4.2. Zeiss (Jena) Stecometer

In April 1988 the Department's Intergraph Intermap Analytic (IMA), an analytical stereo-plotter became available for use. This instrument provided back-driving with automatic multiple pointing so that reseau measurement time was halved, resulting in a significant reduction in fatigue. Also important was the ability to vary continuously the diameter of the measuring mark, which in conjunction with a maximum magnification of 40X allowed more precise pointing to reseau cross images. The major advantage however was that the facility provided an air conditioned environment, maintained at 21°C ($\pm 2^{\circ}\text{C}$) and 40%RH ($\pm 4\%\text{RH}$), which was essential for the minimising of environmental factors and the long term storage of film.

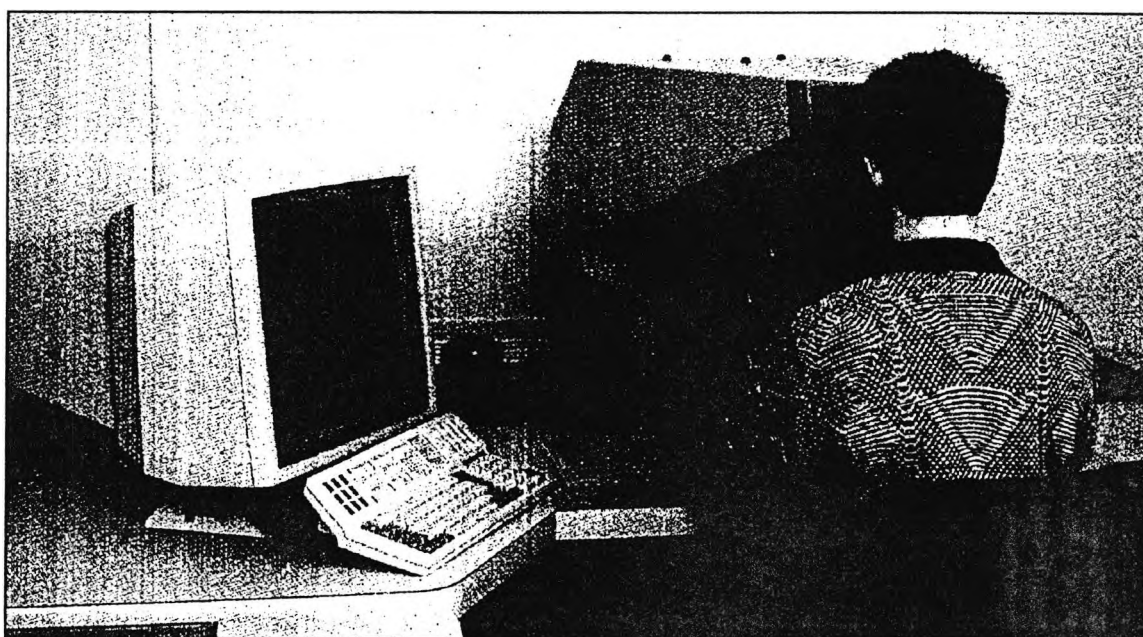


Figure 4.3. Intergraph Intermap Analytic.

4.1.2 Analysis of data.

The basic method chosen to analyze the data was with the use of a vector plot representing the deformations at each of the known sites (Section 3.3.1.1). This type of presentation requires that the image coordinates measured in the comparator coordinate system be transformed to the same coordinate system as the reseau calibration data. A suitable method is provided by the application

of an affine transformation (Equation 3.7), based on minimising the sum of squares of the residual deformations at all reseau points. The affine transformation allows independent correction of any scale changes occurring in x and y due to environmental changes (Ziemann, 1972b).

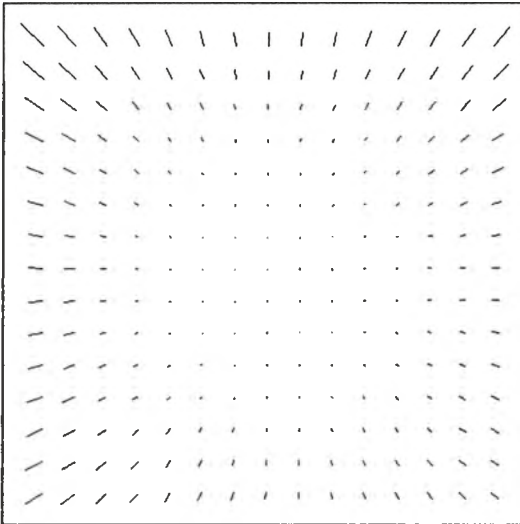


Figure 4.4A. Transformation with origin at centre.

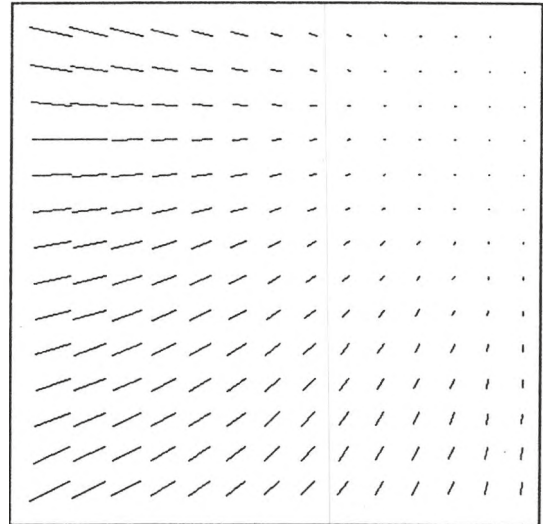


Figure 4.4B. Transformation with origin at top right.

Implicit in computation of the transformation is the assumption of an origin which will have an effect on the appearance of any deformation plot derived from the data. In any instance the contribution of scale changes to the residual vectors will be radial about the chosen origin (Figs. 4.4A and 4.4B). For consistency the origin for all image data processed in conjunction with this work was computed to coincide with the format centre as defined by the calibrated reseau grid.

4.1.3. Experimental results.

A summary of the results of these preliminary studies is best made by considering the investigation in terms of its three main groups: those images produced during the aerial survey; images from the initial uniform exposure tests; and finally the investigation using Ilford FP4 film to compare the 120 and 220 film backs.

4.1.3.1. Exposures made on TMAX films during Aerial Survey.

In this operational case, films (TMY A,B,C,D) exposed in a light aircraft on two separate occasions, were returned to the University for processing using the regimes detailed in table 4.2. A range of frames were measured selected from the rolls according to their geometric contribution to the photogrammetric survey. The first set of measurements was conducted on 1/3/88 using the Zeiss Stecometer, with the second set being made on 27/6/88 using the IMA.

Of importance in figure 4.5 are the dissimilar scale changes between frames over the three month

Kodak TMY 120 Film A, Exposed in Rollei-Metric 6006
 Scale Change Parameters from Affine Transformation.

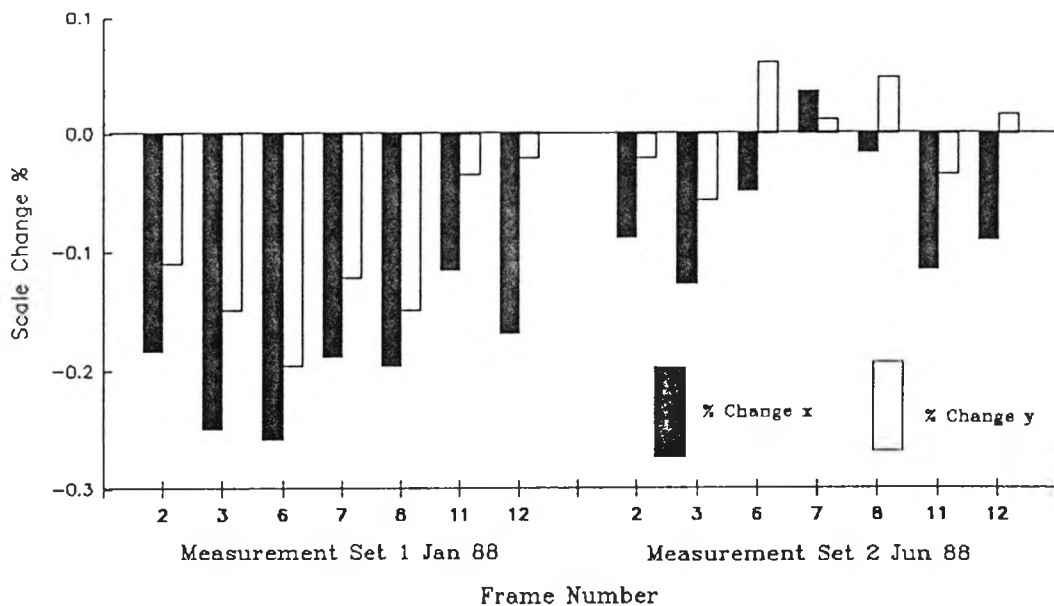


Figure 4.5. Affine Scale change parameters for the two measurement sets

Kodak TMY 120 Film A, Exposed in Rollei-Metric 6006
 Mean residual discrepancies after Affine Transformation.

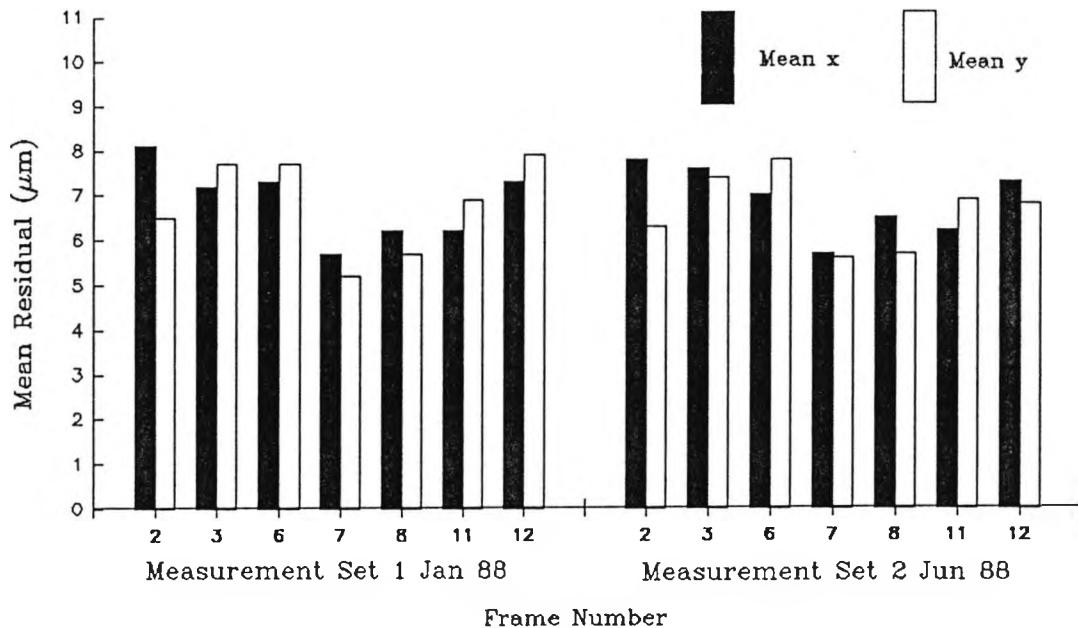


Figure 4.6. Mean residual discrepancies for the two measurement sets.

storage period. During this time the negatives were stored in cuts of four in paper bags with no special attention being paid to environmental conditions. The lack of environmental monitoring in the storage environment makes it difficult to associate any physical processes with the discrepancies seen. However from chapter 2 the most probable causes of the uniform size

changes seen are temperature and humidity fluctuations. The magnitude of the changes seen, a maximum of 25 μ m per 10mm, precludes the scale variations being due to measurement machine differences since both machines have been reliably used for a variety of photogrammetric projects and hold manufacturers calibration certificates.

Analysis of the mean residual discrepancies and the associated vector plots (Figs. 4.6 and 4.7) demonstrate that the overall deformation pattern and its magnitude remained largely consistent over the three month storage period. As such it is reasonable to conclude that these major patterns result from changes occurring between exposure and the end of the photographic processing sequence.

The smaller non-uniform discrepancies between the vector sets associated with the first measurement epoch and those of the second can probably be attributable to three causes;

- a) Variation in the localised physical properties of the film base, such that different areas correspond differently to changes in environmental conditions;
- b) Localised variation of environmental conditions during the three month storage period;
and
- c) Differences between the resolutions of the two measuring instruments used, especially the increased viewing magnification available with the Intergraph instrument.

Due to its greater magnification and ease of use, the IMA was used for the remaining image measurements carried out in this initial investigation.

Further measurements were made of frames from three more Kodak TMY 120 films (**B**, **C**, and **D**) to enable an assessment of the variability between rolls to be made. Roll **B** was exposed during the same survey flight (January 1988) as roll **A** discussed earlier, whilst rolls **C** and **D** were exposed during a second similar survey conducted in June 1988. Scale changes derived from the affine transformations carried out on image measurements from selected frames are in figure 4.8. Frames **1A** and **1B** from each of rolls **C** and **D**, correspond to the two measurement epochs detailed in table 4.2. with the rest of the reseau image measurements from these two films being made with **1A** on 16/06/88.

A comparison of the scale changes required to fit the image measurements to the calibration data for force-dried film **B** measured at 46%RH and the ambiently dried films **C** and **D** measured at 58%RH has been made. From figure 4.8, it can be seen that the differences between scale parameters for the different treatments are not significantly greater than the differences between rolls **C** and **D** which have undergone the same treatment. This result contradicts the results

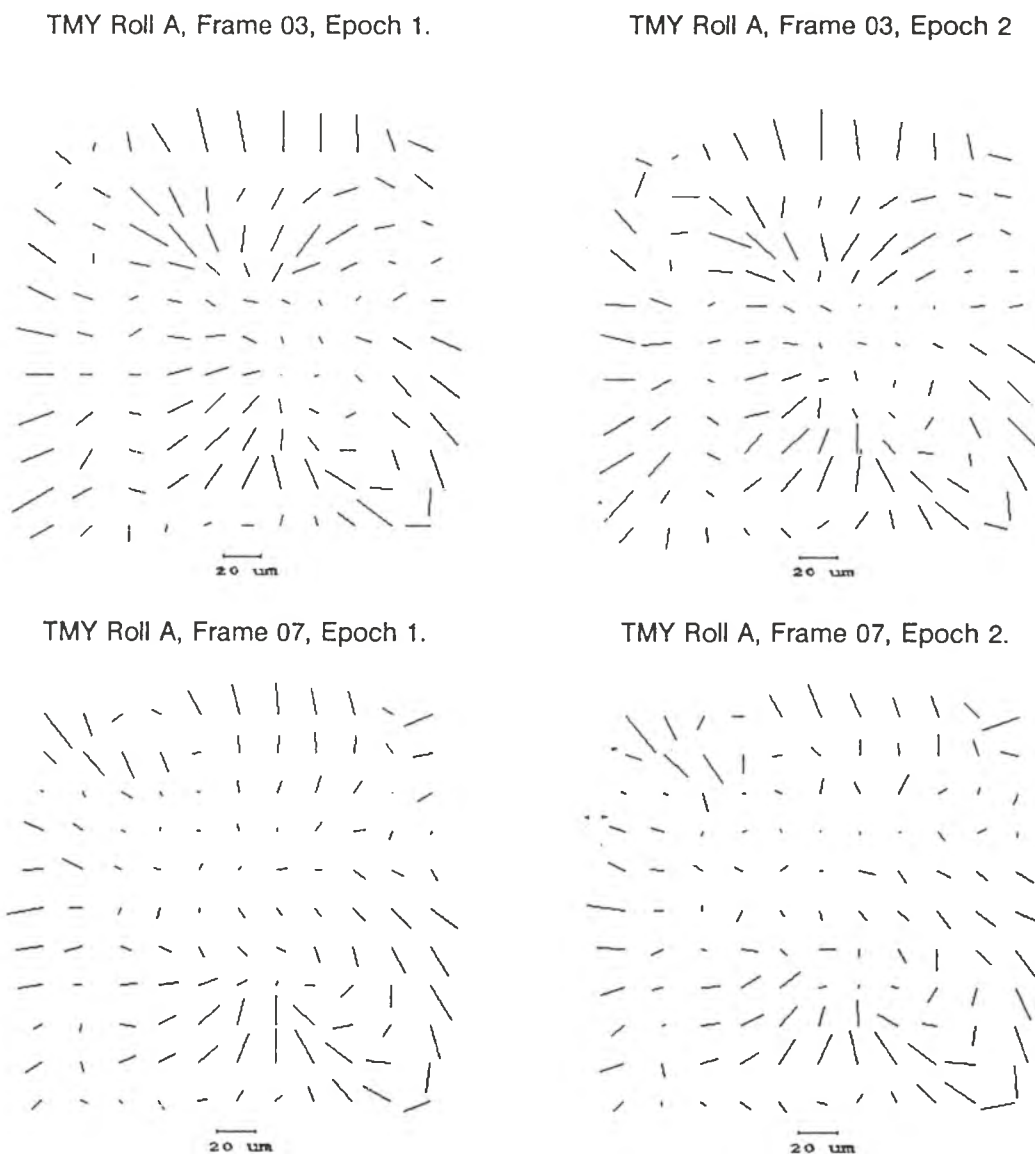


Figure 4.7. Kodak TMY Roll A, examples from epochs one and two.

obtained by Adelstein, Josephson and Leister (1966). However the inconsistency can probably be attributed to the differing exposure, processing and measurement conditions present in this study outweighing the drying effect.

It is worth noting the difference between the mean residual discrepancies in the x direction (across the width of the roll) for the similarly treated films C and D. However the available data allows no firm conclusions as to the cause to be made because too many process variables are in operation.

Finally comparison between the scale parameters produced from the two different measurement epochs for frames 1A and 1B suggests a possible link with the measuring environment ambient relative humidity and temperature (Table 4.2). An increase in relative humidity resulting in a larger scale change due to increased moisture absorption by both the emulsion and base material (Kodak 1970a).

Kodak TMY 120 Films, Exposed in Rollei-Metric 6006
Scale Change Parameters from Affine Transformation.

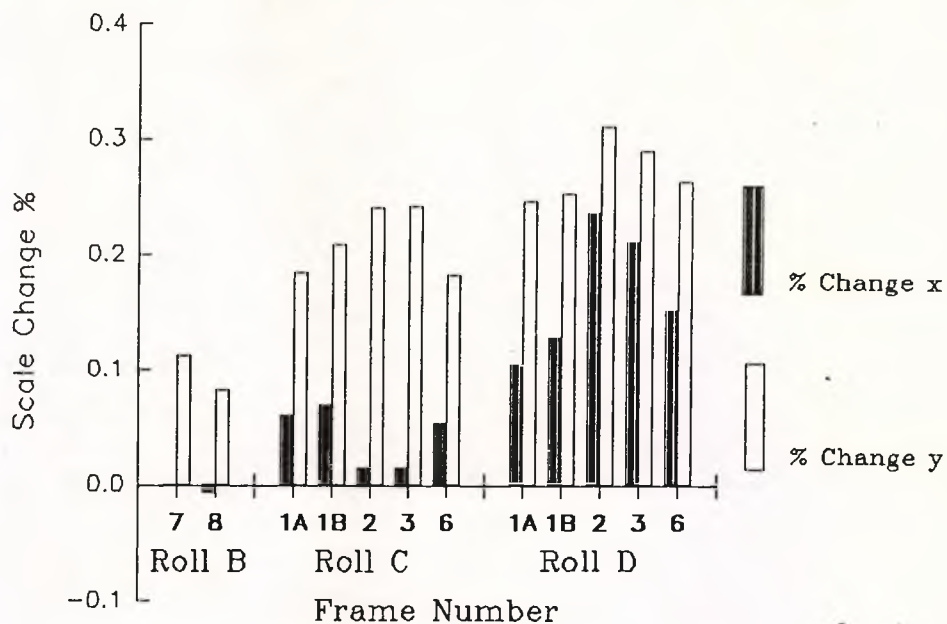


Figure 4.8. Affine scale parameters for frames from TMY rolls B,C and D.

Kodak TMY 120 Films B,C and D, Exposed in Rollei-Metric 6006
Mean residual discrepancies after Affine Transformation.

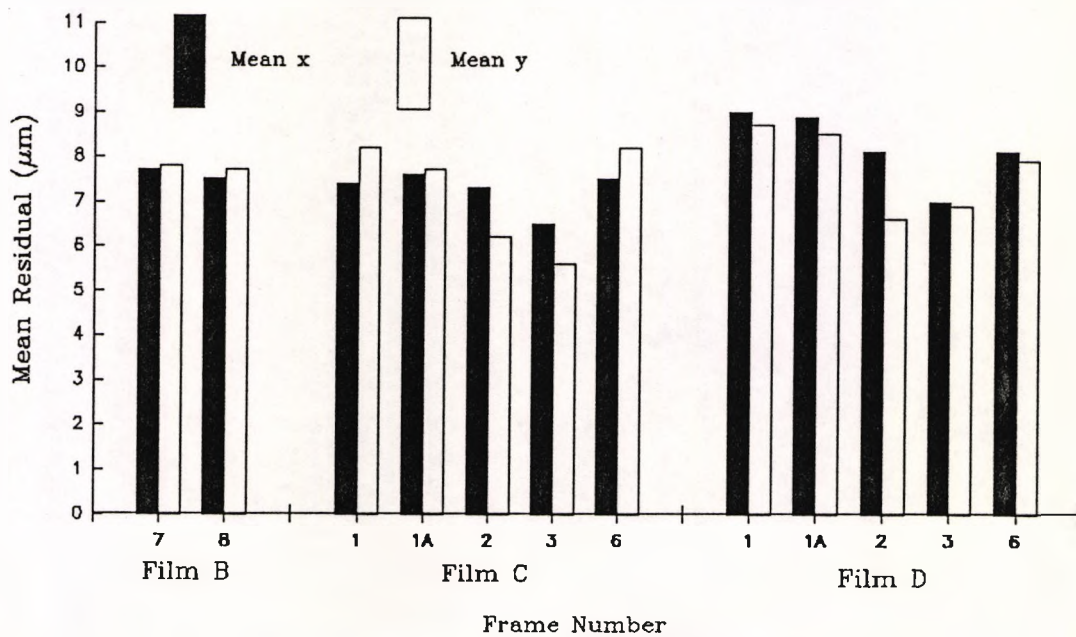
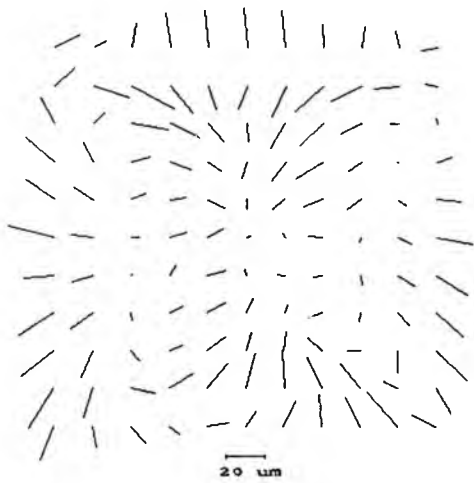


Figure 4.9. Mean residual discrepancies for frames from TMY rolls B,C,D, measured at 58%RH.

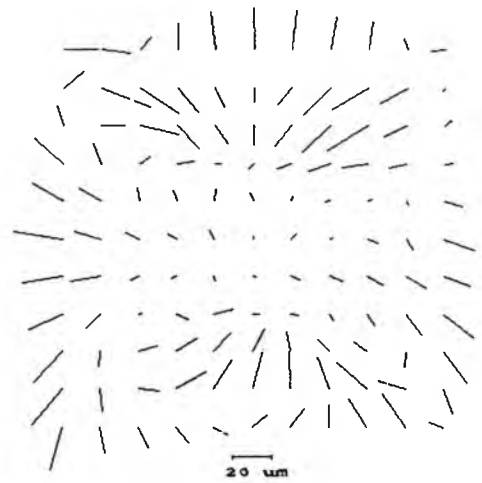
Figures 4.9 and 4.10 show visual correlation of both the magnitude and pattern of the non-uniform deformations between frames from one roll to the next. These similarities are inspite of the differences between the scale change parameters required to fit the images to the reseau calibration data. The predominant deformation pattern seen is therefore likely to be caused by some systematic effect occurring during the image recording process.

Examples of residual vectors from TMY 120 films B,C and D.

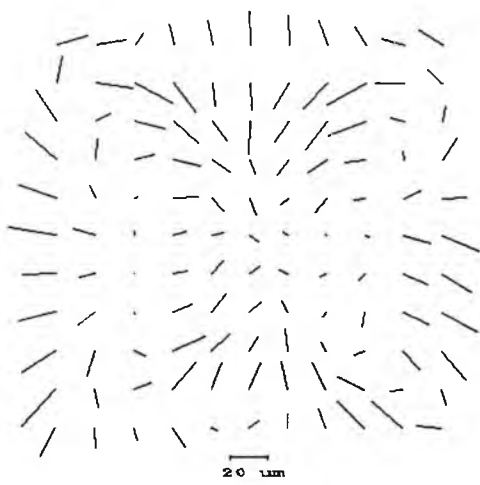
TMY, Roll B, Frame 07.



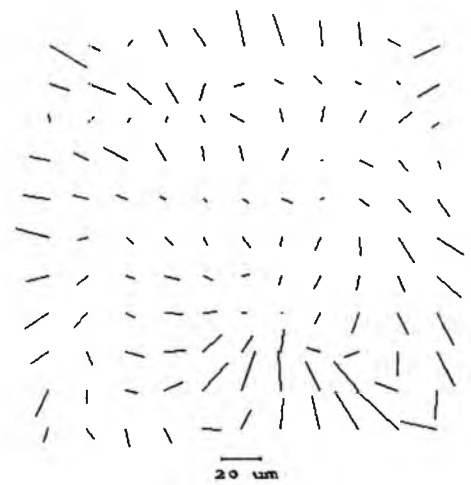
TMY, Roll B, Frame 08.



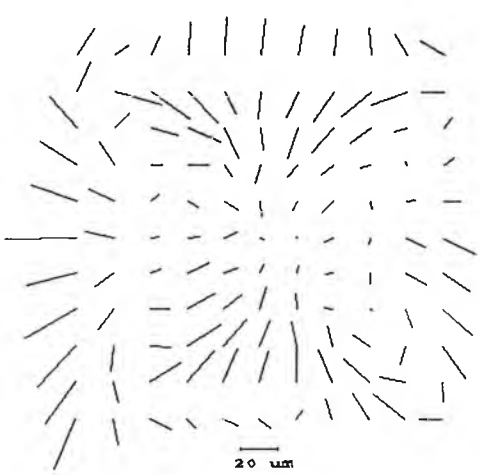
TMY, Roll C, Frame 01.



TMY, Roll C, Frame 03.



TMY, Roll D, Frame 01.



TMY, Roll D, Frame 03.

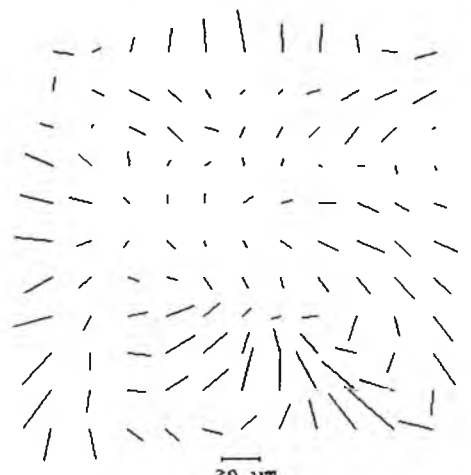


Figure 4.10

The link between the deformation patterns for frames at similar lengths along the roll suggests the presence of an additional minor systematic effect (or effects) occurring along the length of the roll. These effects must have a physical cause and are possibly linked to variation of tension during film wind-on in the camera caused by changes in diameter of the take-up spool as film is wound onto it. A more detailed knowledge of this effect is required such that practical procedures can be modified to minimise the effect on photogrammetrically derived coordinates if necessary.

4.1.3.2. Exposures made on Technical Pan 120 and Ektachrome 120 films.

This set of experiments were conducted using two Kodak 120 Films: Technical Pan, a very fine grain monochrome negative emulsion coated onto a thin (0.091mm) cellulose triacetate base; and Kodak Ektachrome 200 (EPD), a conventional E6 process colour transparency film, coated onto a (0.075mm) cellulose triacetate base (Kodak 1984).

Uniform tone exposures were made as in section 4.1.1, rating the Technical Pan film at 50 ISO, this speed corresponding to its development in Kodak HC110 developer (Dilution F, Kodak 1988). The Technical Pan film was force dried in a drying cabinet. The similarly exposed Ektachrome films, rated at 200 ISO, was processed at The Polytechnic of Central London using an E6 tankline which was maintained within the specified control limits.

Kodak Technical Pan and Ektachrome 200 Daylight 120 Films,

Exposed in Rollei-Metric 6006 on 7/1/88.

Scale Change Parameters from Affine Transformation.

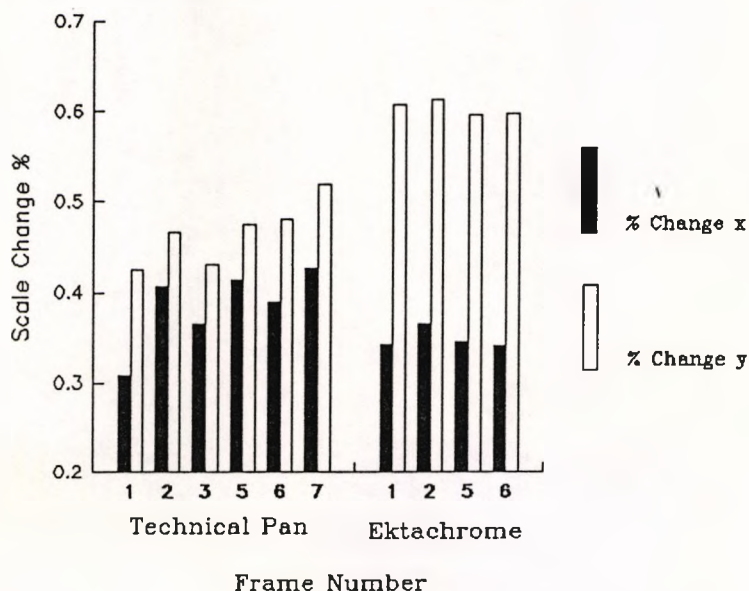


Figure 4.11. TCP 120 and EPD 120, Affine scale change parameters.

The uniform changes associated with these two films are larger than those found from the previous experiments, despite increased control of the photographic process afforded by laboratory exposure. The much greater scale change in y required for the images on Ektachrome film is similar to the x, y differences found for TMY rolls C and D.

The data displayed in figures 4.12 and 4.13 demonstrate that, despite differing physical construction and process requirements, both films types have given rise to similar non-uniform deformations patterns. Given the similarity of the earlier results, the suggestion must be that the majority of the deformations are being produced at a common stage during the photographic process, probably in the Rollei-Metric 6006.

Kodak Technical Pan and Ektachrome 200 Daylight 120 Films
Exposed in Rollei-Metric 6006 on 7/1/88.

Mean residual discrepancies after Affine Transformation.

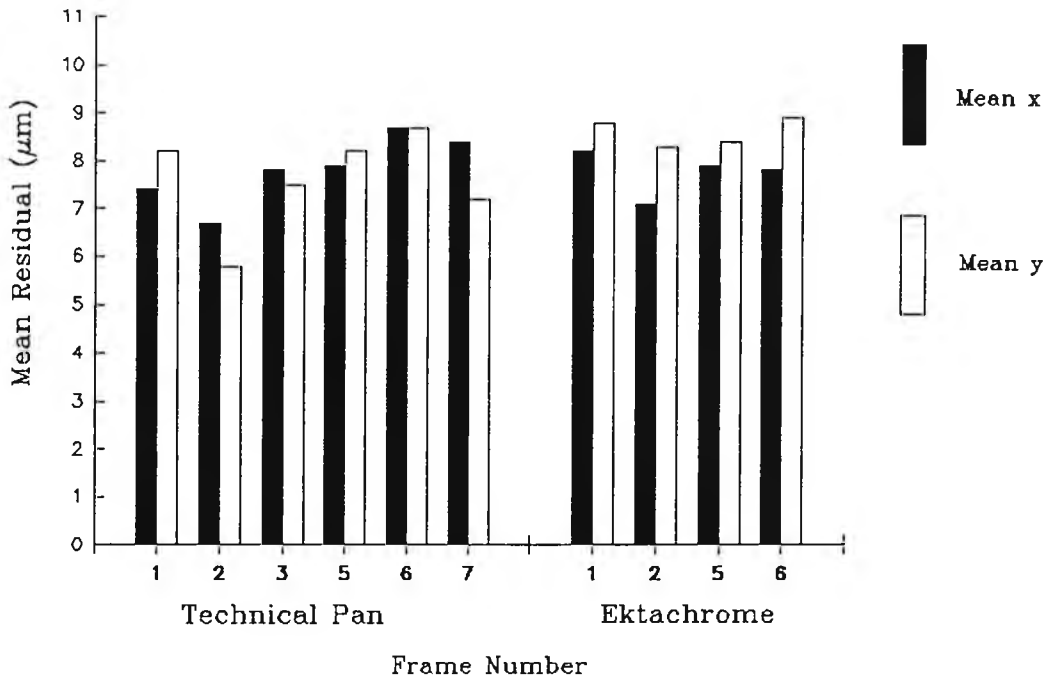
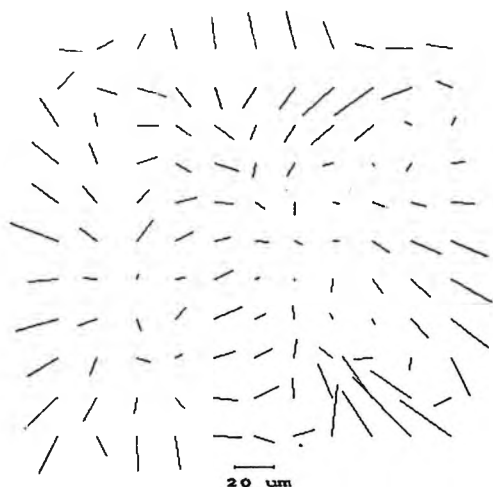


Figure 4.12. TCP 120 and EPD 120, Mean discrepancies after affine transformation.

Technical Pan, Roll A, Frame 01.



Technical Pan, Roll A, Frame 05.

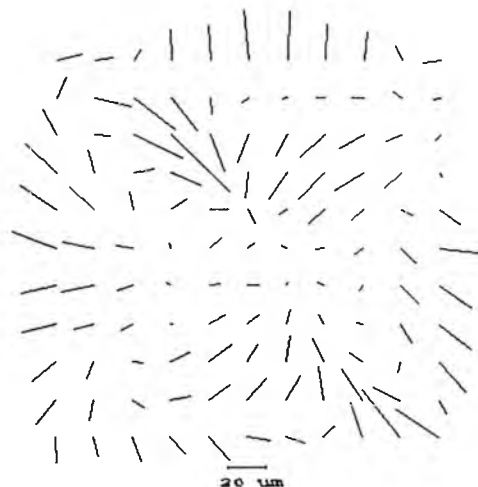
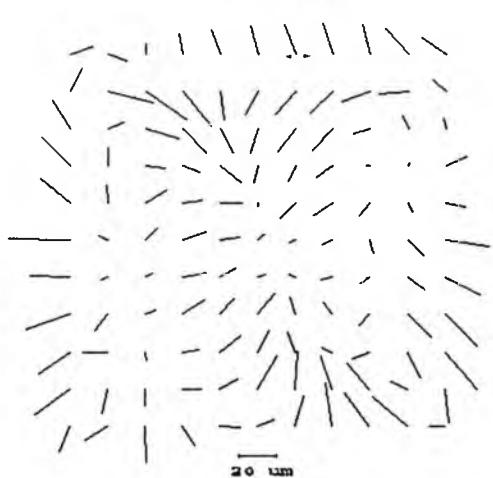


Figure 4.13. Examples of Technical Pan 120 residual vector plots

Ektachrome 200, Roll A, Frame 01.



Ektachrome 200, Roll A, Frame 05.

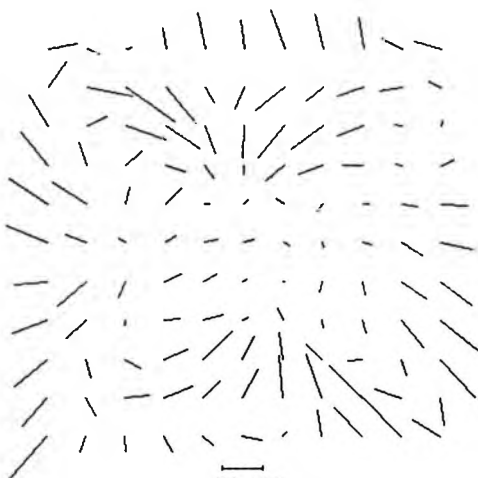


Figure 4.14. Examples of Kodak Ektachrome 120 residual vector plots.

4.1.3.3. Exposures made on FP4 120 and 220 films.

For this series of tests, Ilford FP4 120 and 220 roll films were used in conjunction with 120 and 220 film backs in the Rollei-Metric 6006. In this way an indication would be provided as to the cause of the systematic deformations, since varying the in-camera exposing system would be likely to give an indication of any gross unflatness occurring at the instance of exposure. In addition, to further monitor exposure, the ambient conditions of the exposing environment were measured. The various parameters recorded and the specific processes given are detailed in table 4.3.

Table 4.3. Summary of FP4 experimental parameters.

Camera Back numbers: 120: 206480014 220: 903490017
 Film Batch numbers: FP4 120 02B9X04 | Feb 1993
 FP4 220 98B7X02 | Feb 1992

Exposure conditions 8/09/1988.

Film	Type	%RH	°C	Time	Frame rate
A	120	47.8	24.0	11:10	1 frame / 3 seconds
B	220	47.1	23.9	11:14	1 frame / 3 seconds
C	120	47.6	23.7	11:18	1 frame / 3 seconds
D	220	47.5	23.6	11:25	1 frame / 3 Seconds

Processing conditions 8/09/1988

[Deep tank and spirals].

Film	Development	Stop	Fix	Wash	Drying environment range
A	ID11 1:1 7 minutes at 23.5°C	1 minute at 23.5°C	5 minutes at 23.5°C	30 minutes at 20°C	1 hour at (33°C 30%RH to 49°C 26%RH)
B	ID11 1:1 7 minutes at 23.5°C	1 minute at 23.5°C	5 min. at 23.5°C	30 minutes at 20°C	1 hour at (33°C 30%RH to 49°C 26%RH)
C	ID11 1:1 7 minutes at 23.5°C	1 minute at 23.5°C	5 minutes at 23.5°C	30 minutes at 20°C	12 hours at (26°C 48%RH to 21°C 47%RH)
D	ID11 1:1 7 minutes at 23.5°C	1 minute at 23.5°C	5 minutes at 23.5°C	30 minutes at 20°C	12 hours at (26°C 48%RH to 21°C 47%RH)

All films to be used for this experiment were stored in the freezing compartment of a fridge and removed half an hour before exposure. In all cases the moisture proof wrapping around the film roll was not removed until immediately prior loading the camera back. In this way the system of making the grid exposures could be standardised as far as was practically possible.

Ilford FP4 120 and 220 Films, Exposed in Rollei-Metric 6006

Scale Change Parameters from Affine Transformation.

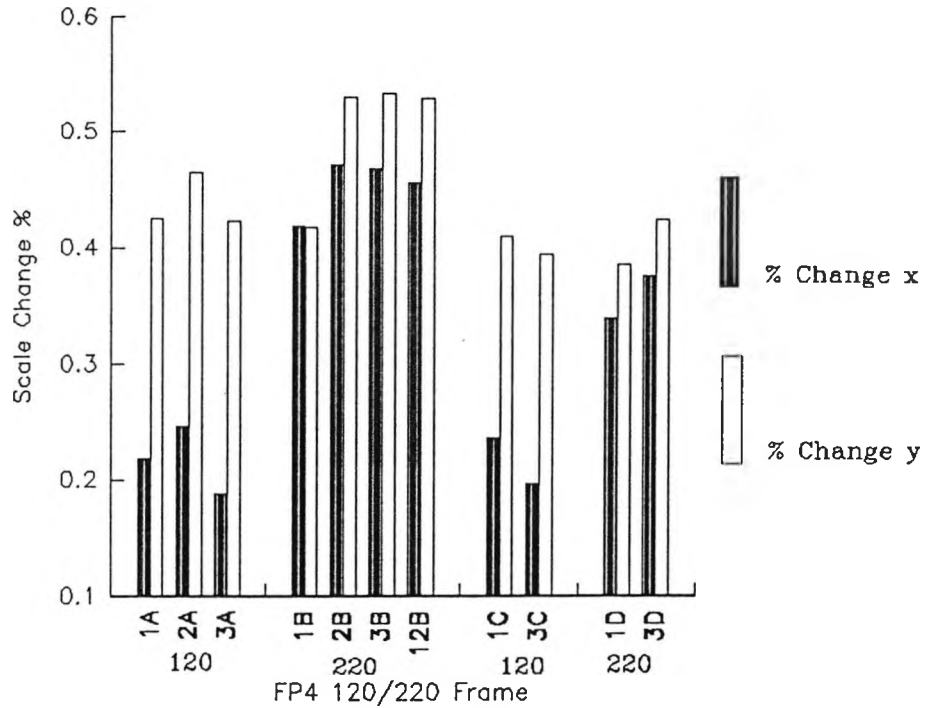


Figure 4.15. FP4 120 and 220, Affine scale change parameters.

Ilford FP4 120 and 220 Films, Exposed in Rollei-Metric 6006

Mean residual discrepancies after Affine Transformation.

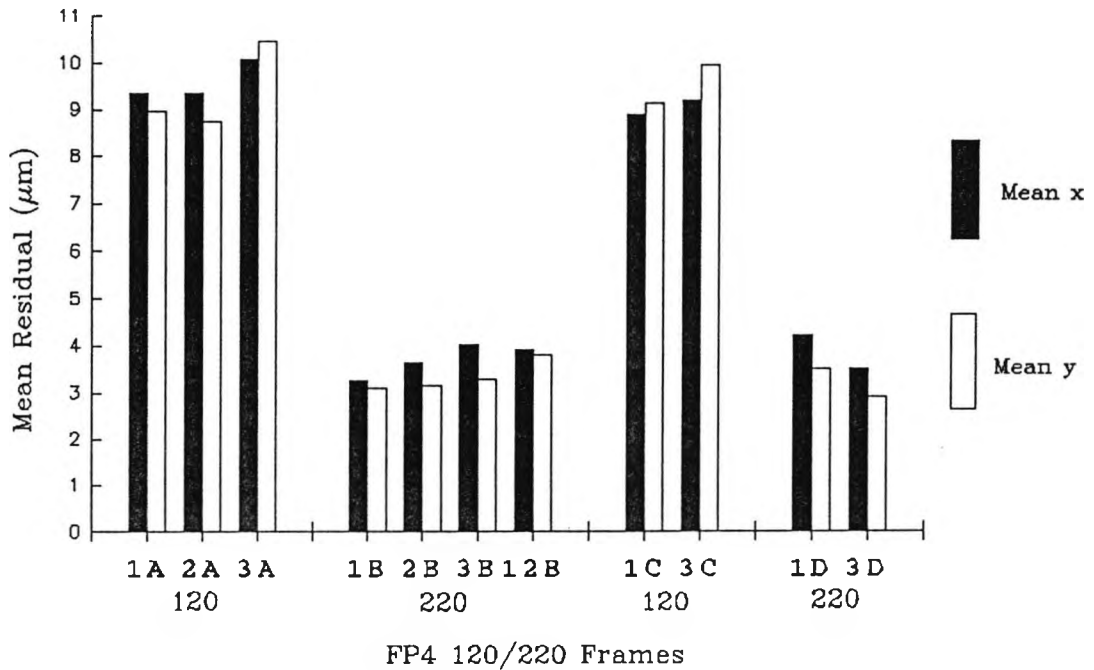


Figure 4.16. FP4 120 and 220, Mean residual discrepancies after affine transformation.

Films were processed simultaneously in a large spiral tank. The rolls were then dried as detailed in table 4.3, prior to their storage in the IMA measurement room.

Image measurements were made on 14/9/88 for the force dried films, **A** and **B**, whilst the ambiently dried films **C** and **D** were measured on 16/9/88.

The affine scale change parameters shown in figure 4.15, demonstrate completely different scale changes in x for the respective 120/220 roll film types. For an understanding of the processes occurring it is necessary to consider these differences jointly with the localised changes occurring, figures 4.16 and 4.17.

The 120 roll films exhibit the largest mean residual discrepancies, and the most non-uniform deformation patterns, as shown by the vector plots (Fig. 4.17). The 220 films however demonstrate the smallest discrepancies yet observed, mean residuals being of the order of $3\mu\text{m}$ in both x and y . However the scale changes required to fit the 220 frames to the calibration data are larger especially in the x direction (across the width of the film).

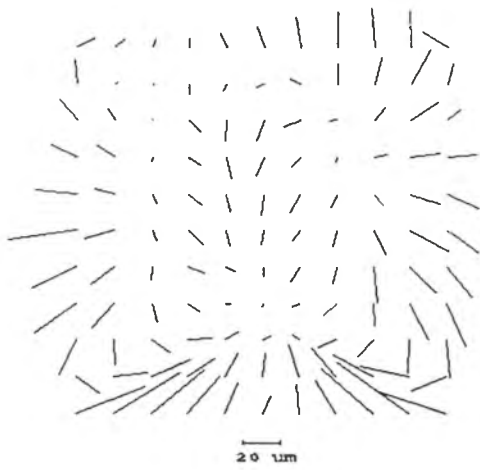
A clue to the cause of these changes is provided by a problem experienced during the measurement of these images. The reseau cross images on the 220 films were all slightly blurred, whilst those on the 120 format varied from very sharp to very blurred. These blurring effects must be associated with a lack of contact between the reseau plate and the film surface at the instant of exposure. This unflatness is further hinted at by the larger scale changes required to fit the 220 frames to the calibration data, since both 120 and 220 films have the same environmental history.

These conclusions were further confirmed by visually grading the sharpness of the reseau cross images on the 120 films. Sharpness was assessed using a visual scale of 1 to 3, where 1 represented a sharp cross, and 3 represented a very blurred cross. The test was conducted using the IMA in reseau measurement mode, with the magnification set at 40X. All assessments were called out to a colleague, such that the operator was not influenced by any patterns which may have been building up in the data.

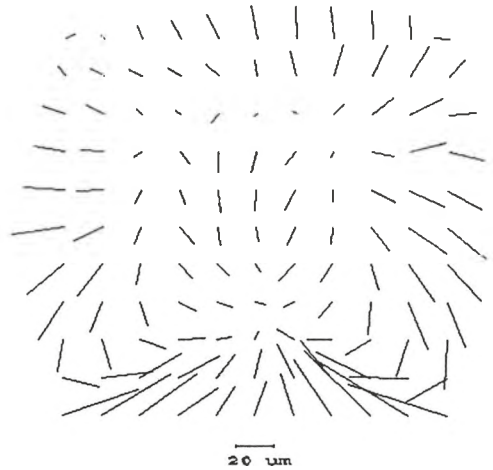
Results of this grading for frames **01C** and **03C** are presented in figure 4.18 in conjunction with their associated residual vector plots. The plots clearly show that the observed deformation pattern is strongly linked to film unflatness in the Rollei-Metric 6006 camera under test.

Examples of residual vector plots on FP4 120 and 220 films.

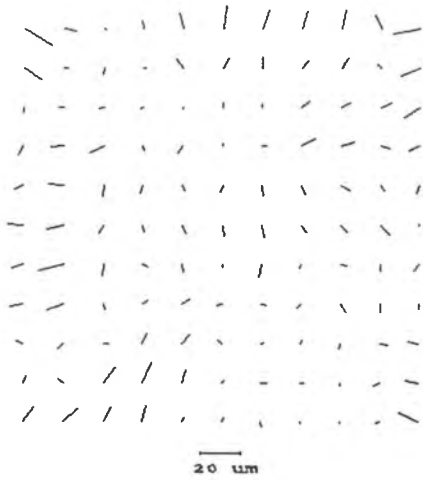
Frame 01, Film A (120)



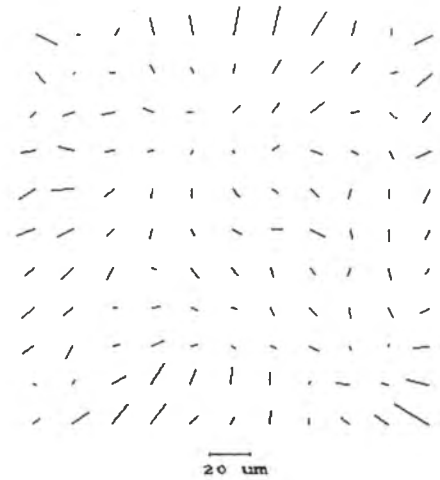
Frame 03, Film A (120)



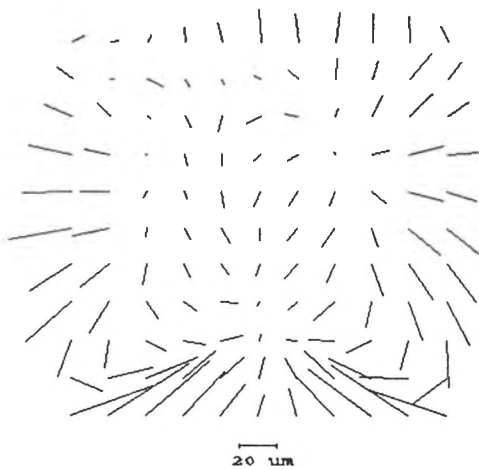
Frame 01, Film B (220)



Frame 12, Film B (220)



Frame 03, Film C (120)



Frame 03, Film D (220)

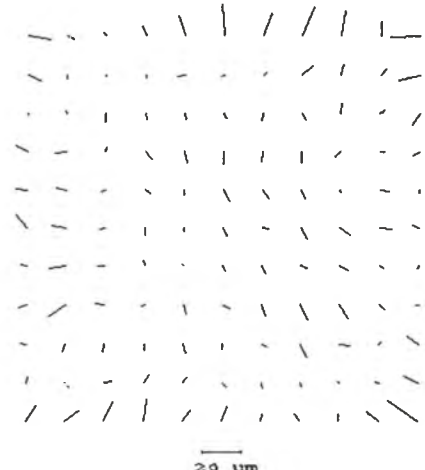


Figure 4.17.

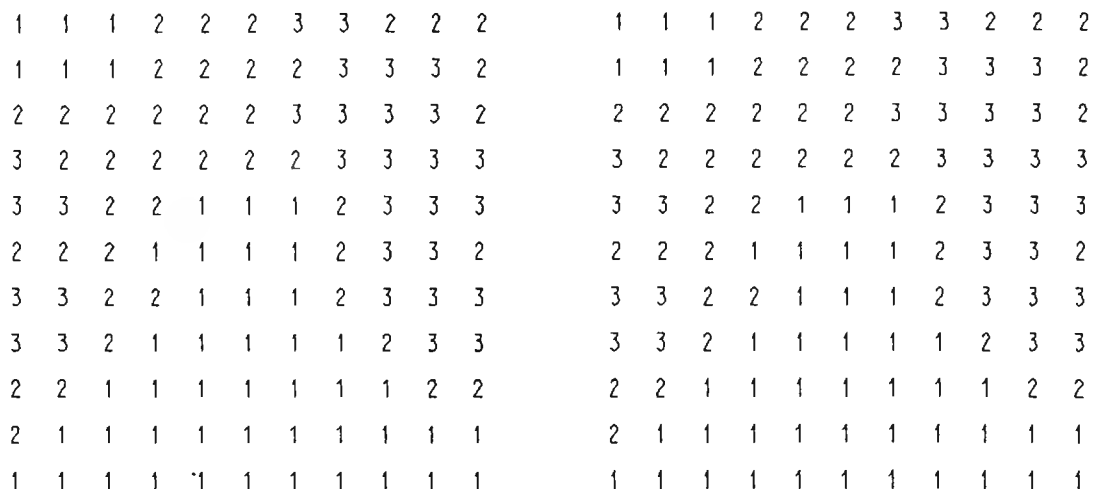


Figure 4.18. Reseau sharpness numbers for FP4 120 Film C, frames 1 and 3.

It is unclear why the 220 frames exhibit little deformation, since the gap between the film surface and the resseau glass means that the film is being held flat purely by the tension caused by film wind-on. There are two obvious factors which could be contributing;

- a) The 220 film unlike the 120 type uses no backing paper, resulting in one less layer in the pressure plate/film/glass sandwich in which air can get trapped causing local deformations (Clark, 1972).
- b) After the experiment AV Distributors informed us that the separation between the pressure plate and film plane in the 220 back was not set up for use with the resseau camera. This would almost certainly have contributed to the larger gap between the resseau glass and film surface found.

The small size of the data sample, coupled with the different measurement environments for the ambient/force dried film treatments has meant that no conclusions can be drawn regarding the effects of force drying the film. However the consistent magnitude and pattern of the non-uniform deformations appears to suggest that any drying effects may be confined to the uniform scale changes required. This is an important possibility especially where rapid measurement access is required from a photogrammetric survey conducted using film based systems.

4.2. Reseau plate unflatness tests.

The results obtained using the 220 and 120 film types exposed in the Rollei-Metric 6006 showed that there were problems associated with the contact between the resseau glass and film surface in this camera. In conjunction with the National Physical Laboratory (NPL), Teddington it was

decided to measure the unflatness of the rear surface of the reseau plate in both this camera and City University's Wild P32 camera. Measurement of the micron accuracy required could be obtained using interferometric techniques (Dyson 1970), specifically using NPL's Zygo MK3 Interferometer.

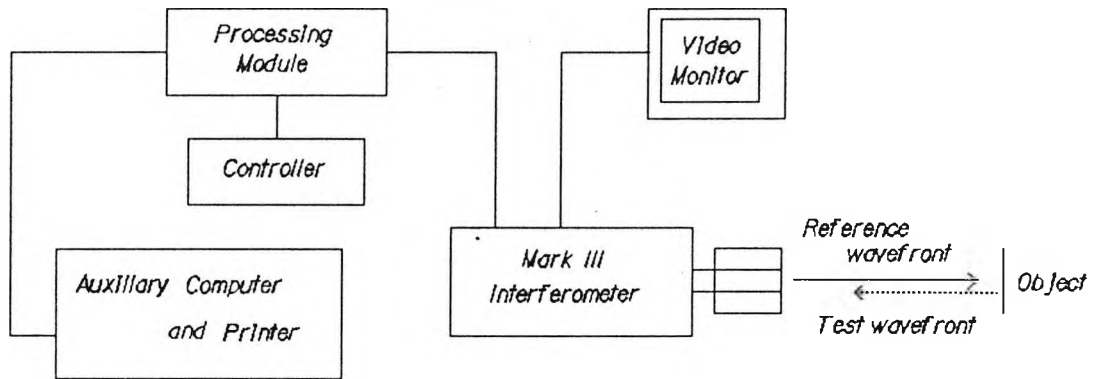


Figure 4.19. Schematic diagram of the Zygo MKIII phase measuring interferometer.

This unit (Fig. 4.19) projects a plane wavefront of coherent laser light which when reflected by a surface produces an interference pattern which is recorded by a camera system for analysis. The wavelength of the laser light used is 633nm such that one interference fringe represents a departure from the plane of $0.3165\mu\text{m}$. Measurements of the rear surface of the P32 reseau plate were made using this system and a contour plot derived from the interference pattern obtained is shown in figure 4.20.

Due to the magnitude of unflatness present in the Rollei-Metric 6006 reseau, it was not possible to produce a recordable interference fringe pattern using the Zygo interferometer (the instrument was too sensitive). Instead a Fizeau interferometer (Fig. 4.21), incorporating a mercury source producing interference fringes representing $2.5\mu\text{m}$ departures was used.

Figure 4.22, is produced from a photograph of the interference pattern produced using the fizeau system. The interference image provides information about the entire reseau plate area, but is

wedge shaped due to the mirror system used to record and view the image. Two sets of fringes

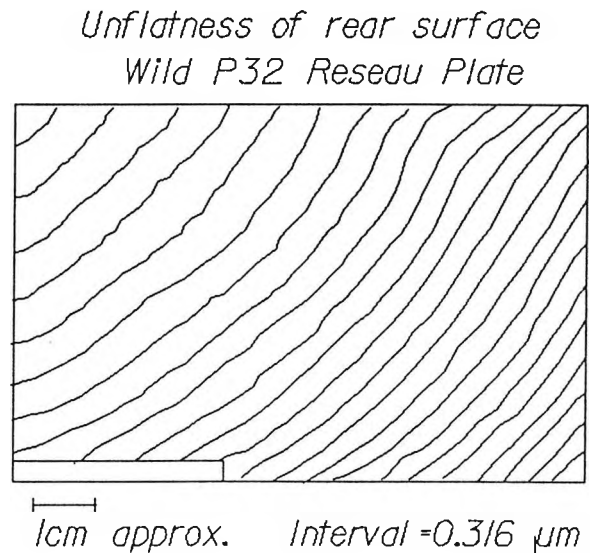


Figure 4.20. Unflatness of the rear surface of the P32 reseau plate.

can be identified; self fringes which are caused by interference between light reflected by the front and rear surfaces of the plate, and surface fringes caused by interference between the light reflected by the rear surface (the film contact side nearest to the mercury source) and the reference beam.

The self fringes show the out of parallel nature of the glass plate, each fringe representing a departure from parallelism of $0.316\mu\text{m}$. The surface fringes provide a measure of the departures from flatness of the rear surface of the reseau plate from

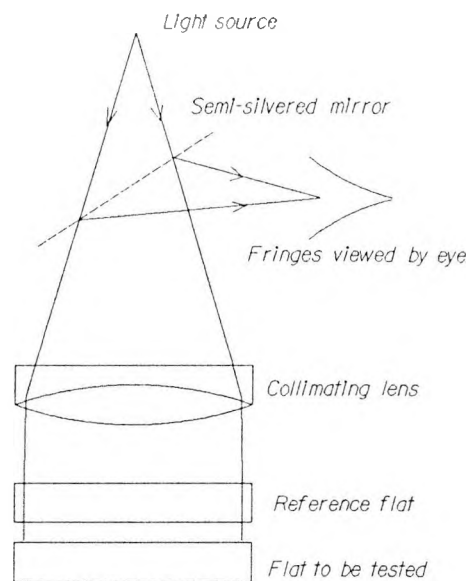


Figure 4.21. Schematic diagram of the Fizeau Interferometer.



Figure 4.22. Interferometer pattern for Rolle-Metric 6006 reseau 40.

the reference plane defined by the plane wavefront, (1 fringe represents a $2.5\mu\text{m}$ departure). A contour plot (Fig. 4.22) derived from the interferogram represents the rear surface unflatness of the reseau plate with its departure from flatness of up to $140\mu\text{m}$.

The 15 to $20\mu\text{m}$ out of parallelism of the Rolle-Metric 6006 reseau glass (as shown by the self fringes in Fig. 4.22) was introduced during its manufacture. This out of parallelism could easily

UNFLATNESS OF RESEAU PLATE REAR SURFACE
ROLLEI/METRIC 6006 CAMERA NO.005298811

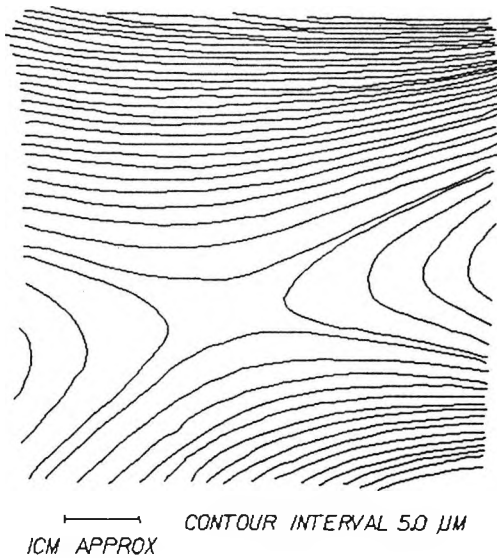


Figure 4.23.

have been minimised by making a selection from a large sample of glass plates before etching the reseau grid. An example of this technique is provided by Eastman Kodak who select glass plates for coating according to various flat and micro-flat physical specifications (Kodak 1982).

Several inferences as to the cause of the saddle shape of the grid plate have been made, the most likely being stresses set up in the glass because of the method used for mounting the plate in the camera.

The Rollei-Metric 6006 under test used a mounting system whereby the reseau plate was gripped tightly at top and bottom by a metal mounting plate. So some of the unflatness may have been caused when the glass plate was clipped onto the camera body. In addition it is probable that this method has not allowed the glass/camera joints to flex according to their differential thermal expansion rates. Rollei now say that the method has been revised and that they are now gluing the plate to the camera body using a flexible epoxy resin (Fahlbusch 1990).

Another way of minimising problems associated with camera mounting is to make the reseau plate thicker. For example, the plate used in the Rollei-Metric 6006 is about 2.5mm thick as opposed to about 9mm for that in the Wild P32. Unfortunately this approach introduces new complexities, the glass plate having to be considered as part of the lens system if reduced image quality is to be avoided. The camera lens used must therefore be re-designed to take account of the optical effects of the reseau glass, resulting in increased camera cost, so reducing the advantages of low cost and lens flexibility conferred by small format camera use. Current manufacturing design appears to assume that with thinner (2mm) glass plates it is possible to select suitable lenses from a standard production batch without compromising image quality, (Linhoff representative ISPRS Zurich, 1990).

In the light of the large unflatness present with the Rollei-Metric 6006 reseau plate, the manufacturer's reseau calibration for this camera gave cause for concern. In all cases measurements of the grid positions corresponded (to the nearest 2µm) to their assumed 5mm separation. This implies that the calibration was carried out before mounting of the plate into the camera and therefore before the stresses had been produced in the glass. The in-plane effect of this calibration may be minimal if the film is in contact with the glass surface. However the grid cannot then correct for any departures of the image surface from a plane.

Despite these unfortunate design and production shortcomings, use of the camera during the landslip analysis produced very encouraging results. The use of local reseau corrections made a significant improvement over the same adjustment carried out using unrefined photo-coordinates (Chandler et al 1989).

4.3. Correction methods applied to the reseau data.

In chapter 3.3, it was described how the photogrammetric mathematical model could be extended to include explicit corrections for both in-plane and out-of-plane departures of the film from the assumed image plane. The aim of this section is to investigate the limitations of the globally and locally applied transformations detailed by Ziemann (Section 3.3.1.1) and the linear least squares interpolation approach described by Schut (Section 3.3.1.1).

Analysis of the methods was made using the FP4 120 and 220 reseau image measurements from section 4.1.3.3, comparing the ability of each method to minimise the RMS residual reseau deformations. In the case of the localised bilinear and interpolation methods, corrections were applied using some of the reseau crosses as image points at which the deformations were to be estimated. A secondary objective of these studies was to test rigorously a suite of image deformation correction software written in Fortran 77.

4.3.1. Globally applied transformations.

Ziemann (1971b) suggested several transformations covering a range of complexity which could be globally applied to the reseau image data. Those listed below were included in the least squares estimation program LSQALG (Robson 1989), written to allow the explicit correction of image deformation before adjustment using City University's adjustment programs (BIF) written by Chandler and later (GAP) written by Clarke. The numbers in brackets are references to the equations detailed in section 3.3.1.1.

Linear Conformal Transformation	C	(3.6)
Linear Affine Transformation	A	(3.7)
Bilinear Transformation	B	(3.9)
Second Order Polynomial	S	(3.10)
Incomplete Third Order Polynomial	I	(3.11)
Third Order Polynomial	T	(3.12)

For this series of tests the transformations were applied using all reseau points. Figure 4.24 demonstrates residual vectors derived by application of the transformations to FP4 120 frame 03 from film A. This image was used as it is highly deformed due to unflatness at exposure (Section 4.1.3.3).

Image Transformations FP4 120

Frame 03A

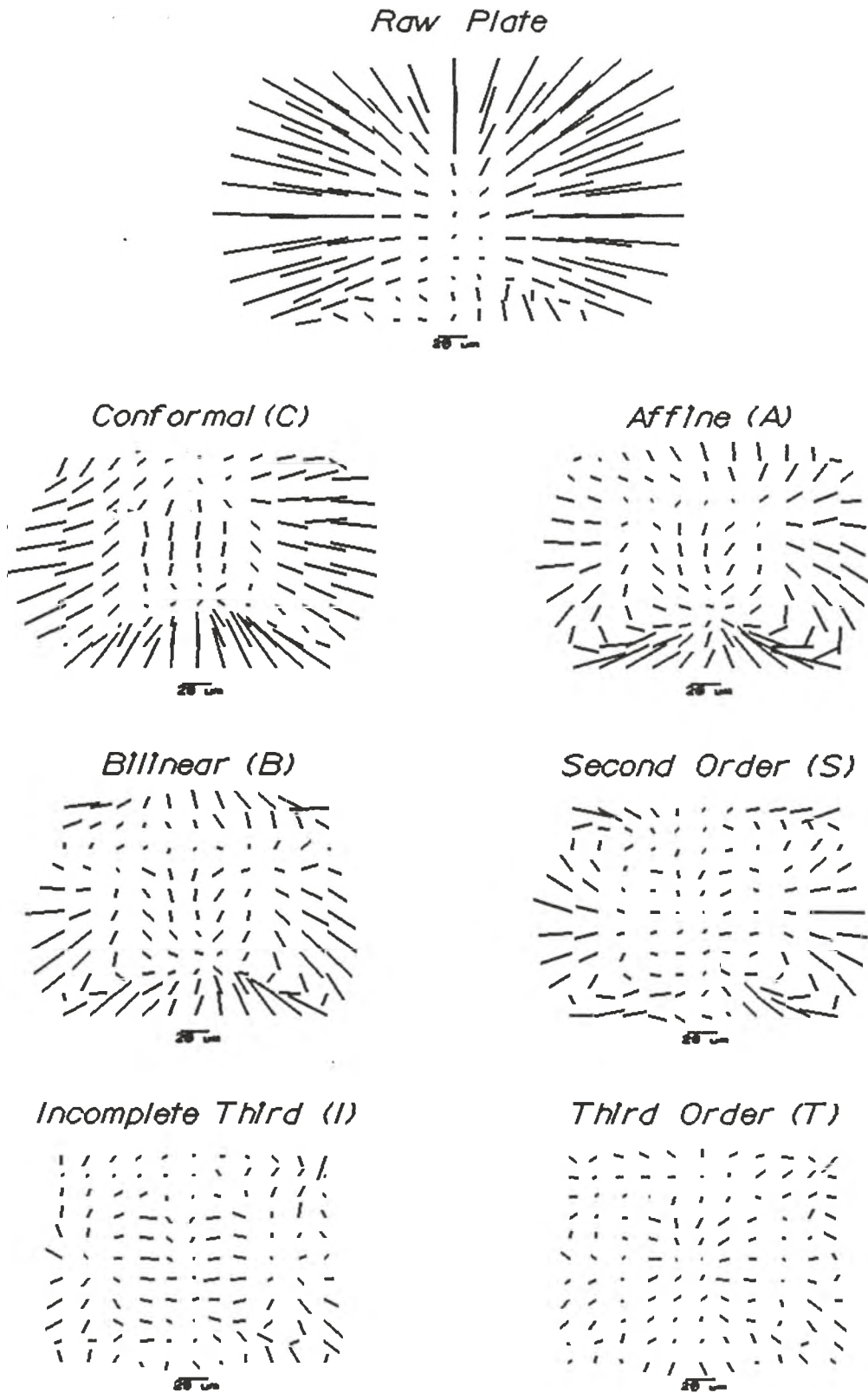


Figure 4.24. Residual vectors after global transformations, FP4 120 (3A).

Image Transformations FP4 220
Frame 03B

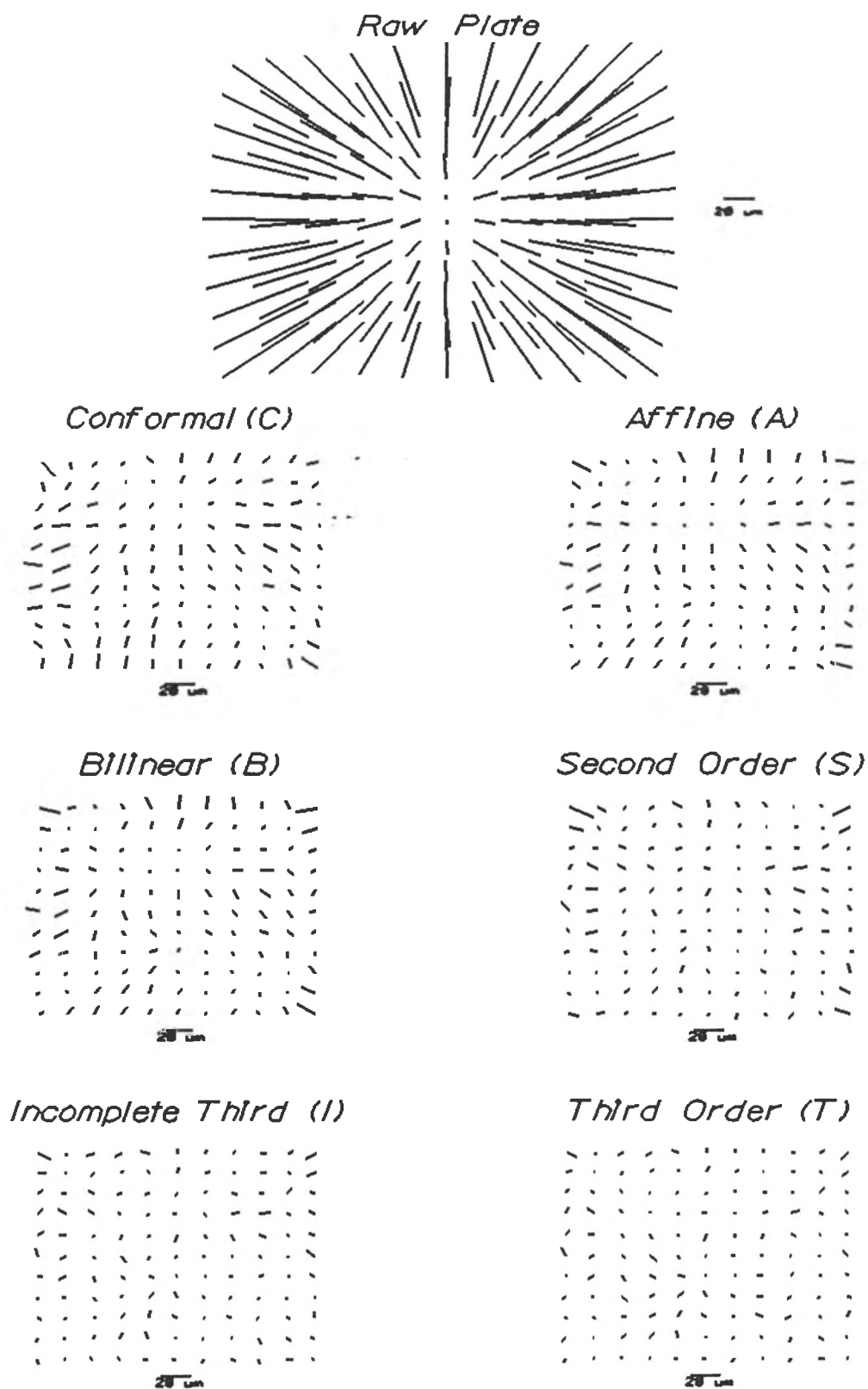


Figure 4.25. Residual vectors after global transformations, FP4 220 (3B).

It is useful at this stage to become familiar with the vector plot representation of deformations. For example from the plots it can be seen that all transformations which include independent x and y corrections are able to remove the differential scale changes. The degree of removal of the residual deformation patterns remaining after the affine transformation is inconsistent over the image area probably because of the harmonious nature of the polynomials used, the degree of the polynomial corresponding to the number of possible inflections.

Figure 4.25. demonstrates the application of the transformations to the more homogeneously deformed frame 03B (FP4 220 roll B). In this case visual assessment of the residual vector plots is less informative since few regions of systematic deformation can be identified.

To provide an global assessment of the transformations, frames 01 and 03 from each of the films A,B,C and D were processed using each of the transformations. Mean RMS residual deformations could then be computed for each film type/transformation combination (Fig. 4.26) by comparing the calibration data with the transformed image data. The data produced clearly demonstrates the minimal improvement obtained by increasing the number of transformation terms for films B and D which exhibit few localised systematic effects.

RMS Residuals for the reseau image measurements
obtained with different correction methods
applied simultaneously to all 121 reseau points.

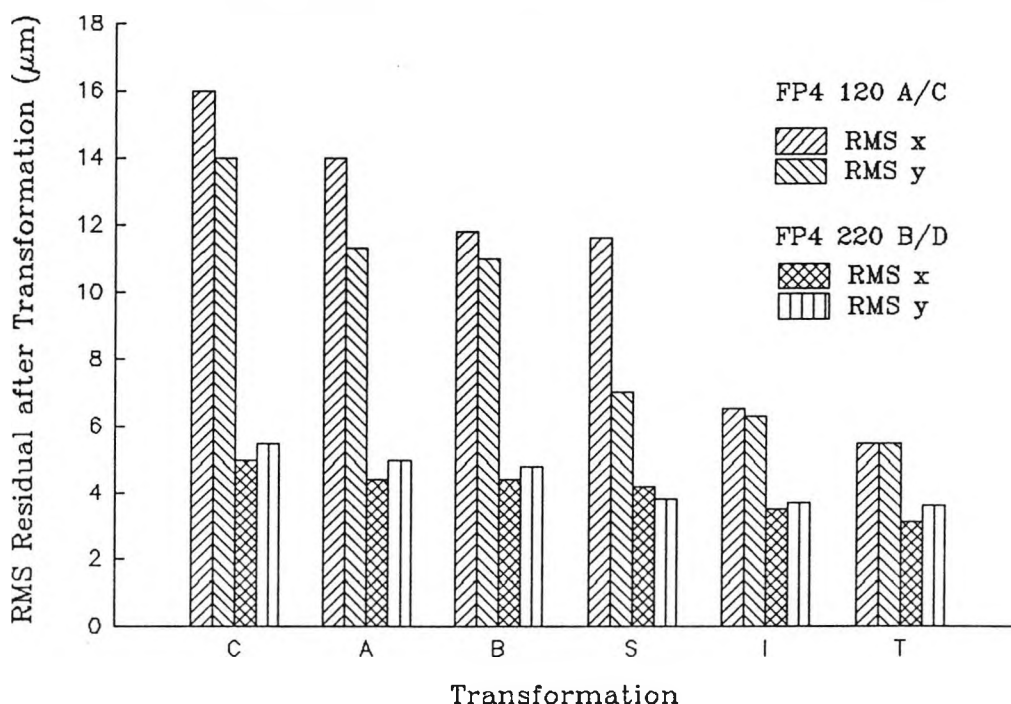


Figure 4.26. Mean RMS residuals for transformations applied to frames 01 and 03 of 120 films A and C, and 220 films B and D.

A more rigorous analysis is required to assess the differences exhibited by the x and y RMS residuals for the images on 120 film. The least squares estimation procedure utilises a cofactor matrix (Section 3.4.2) which on its leading diagonal contains the variances of the estimated parameters. These variances may be incorporated in a statistical test, known as a t-test, to determine if the parameter should be included in the transformation at a given significance level. The t-test makes a statistical examination of the two possible situations;

a) the null hypothesis;

$$H_0: p_0 = 0$$

b) the alternative hypothesis;

$$H_0: p_0 \neq 0$$

In this particular case using a two tailed test, if the value of the computed test statistic, equation 4.1, lies outside the range of its value from statistical tables (assuming a 95% confidence interval) then the null hypothesis is rejected and the value of the estimated parameter is significant (Cooper 1987).

$$t_{calc} = \frac{\text{estimated value of parameter}}{\sqrt{\sigma_p^2}} \quad (4.1)$$

where: t_{calc} is the calculated value of the test statistic;

σ_p^2 is the variance of the estimated parameter, obtained from the covariance matrix.

For this set of tests the t statistic from tables with 95% confidence and 200 degrees of freedom was 1.98. In figures 4.27 and 4.28, some t-test results for the parameters estimated during one of the transformations carried out on frame **03** of roll **A** are presented. Estimated parameters with t_{calc} values below the significance level are rejected and the transformation recomputed using the modified equation. Additionally to enable the test to be valid, the standard error for an observation of unit weight, as estimated by the adjustment, must be unity. If this is not the case σ_p^2 must be multiplied by the variance factor before the test statistic is computed.

The remaining significant parameters demonstrate that for this image the deformations in the x and y directions require different polynomial structures, especially where the lower order terms are concerned. It can also be seen that the square and cubic terms introduced by the higher order polynomials can be very significant in correcting the deformations present.

Results infer that the inclusion of increasingly higher order terms will increasingly minimise the residuals after application of the global transformation. There is however a problem of numerical stability in simply increasing the number of polynomial terms, such that the solution can become over parameterised. Prevention of over-parametisation by rejecting estimated parameters from

Results of t tests to determine the significance of the parameters estimated for FP4 120 Frame 03 A.
(x direction)

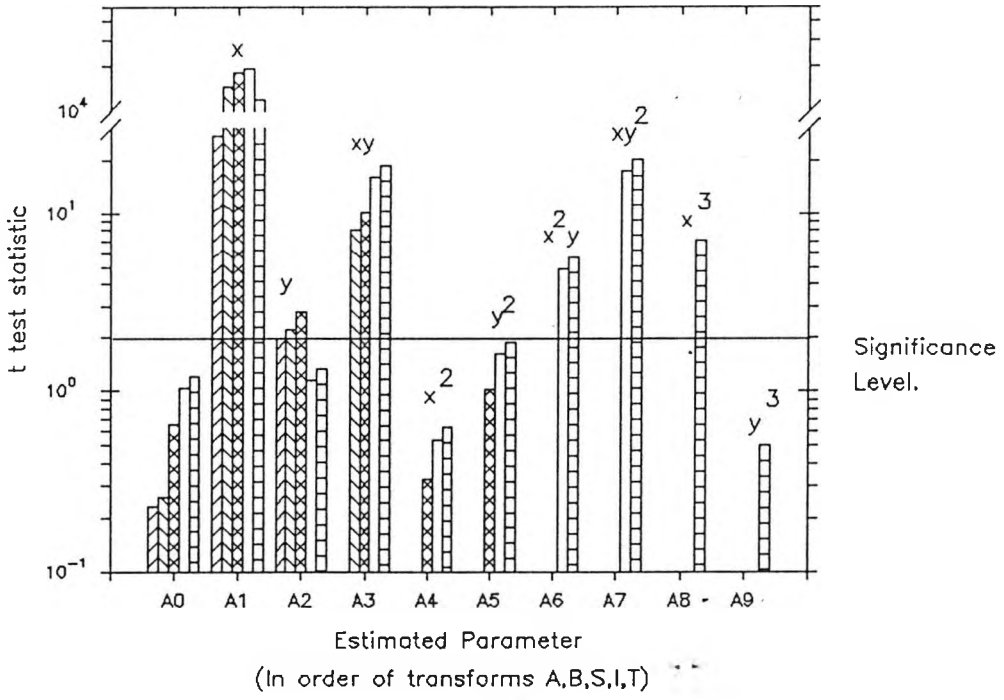


Figure 4.27.

Results of t tests to determine the significance of the parameters estimated for FP4 120 Frame 03 A.
(y direction)

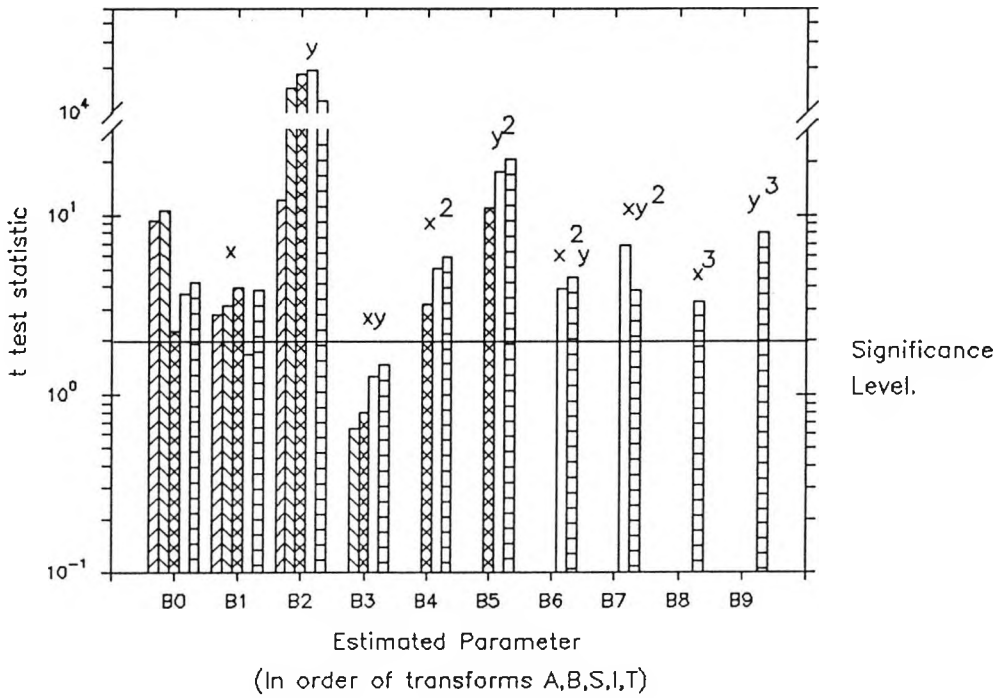


Figure 4.28.

the solution according to results of significance tests based on correlation coefficients was discussed in section 3.4.5. Computation of these coefficients has been included in the LSQALG program. The coefficients for the incomplete third order transformation (after rejection of insignificant parameters) are presented in table 4.4, where a star indicates a strong correlation.

Table 4.4. Correlation coefficients for the estimated parameters of an incomplete third order polynomial, after rejection of insignificant parameters.

x	a ₃	a ₆	a ₇	y	b ₂	b ₄	b ₅	b ₆	b ₇
a ₁	0.002	0.001	-0.7*	b ₀	0.001	-0.6*	-0.6*	0.001	0.000
a ₃	-	0.000	-0.004	b ₂	-	0.001	-0.002	-0.7*	0.000
a ₆	-	-	-0.001	b ₄	-	-	0.001	-0.002	0.000
-	-	-	-	b ₅	-	-	-	-0.001	0.000
-	-	-	-	b ₆	-	-	-	-	-0.001

The starred correlation coefficients demonstrate that even with very few terms the estimated parameters can become highly correlated.

The major conclusion to be drawn from this series of tests is that in the absence of an explicit transformation derived according to physical parameters, the correlation and significance of the estimated parameter sets can be statistically unreliable. The RMS residuals demonstrate that the transformation effectiveness is highly dependent on the deformation patterns present, a disadvantage where a variety of frames must be routinely corrected.

4.3.2. Local Bilinear Correction.

The second transformation suggested by Ziemann (1971b) is a bilinear function applied to each image point in turn based on the known deformations at the four surrounding reseau points. This type of solution although computationally simpler than the preceding global transformations has the disadvantage that any reseau measurement errors are transferred in the correction procedure. A second difficulty is that any image points lying just outside the reseau image area cannot be simply corrected, this problem being especially difficult at the format corners.

Two approaches can be taken to allow for image point positions outside the grid area;

- a) Outlying points can be rejected as unreliable, reasonable since results from research (Adelstein et al 1966; Clark 1972; Ziemann 1971a) have demonstrated the unpredictability of image deformation at the format edges.
- b) The deformations measured at reseau image points near the edge of the format in the

area of interest can be used to extrapolate pseudo reseau points outside the grid area.

In developing software to compute a local bilinear correction it was decided to combine these two approaches by extrapolating pseudo points, but flagging any image points corrected in this way (n and p Fig. 4.29) so that they could be rejected if desired at the photogrammetric adjustment stage.

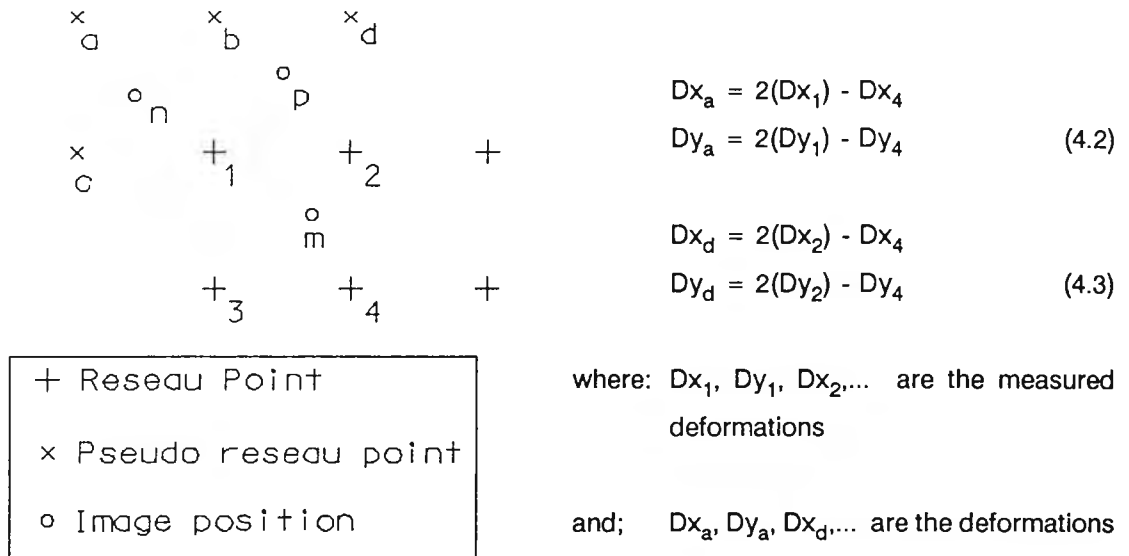


Figure 4.29. Computation of the deformation at pseudo reseau points.

The correction program BILIN (Robson 1989) was written using a sorting routine which searched through the measured reseau data to find the four reseau points surrounding the image point to be corrected. If a pseudo reseau point was required subroutines employing the simple preliminary extrapolations in equations 4.2 and 4.3 were called. The appropriate routine was selected in each case according to the corner or edge nearest to the image point position.

The estimation of the parameters for the bilinear equations used to compute corrections in x and y for image point m in figure 4.29 proceeds as follows. The parameters to be estimated a_0, a_1, a_2 and a_3 are computed using a least squares solution to each of the four sets of simultaneous equations below.

$$\begin{aligned}
 Dx_1 &= a_0 + a_1x_1 + a_2y_1 + a_3x_1y_1 & Dy_1 &= b_0 + b_1x_1 + b_2y_1 + b_3x_1y_1 \\
 Dx_2 &= a_0 + a_1x_2 + a_2y_2 + a_3x_2y_2 & Dy_2 &= b_0 + b_1x_2 + b_2y_2 + b_3x_2y_2 \\
 Dx_3 &= a_0 + a_1x_3 + a_2y_3 + a_3x_3y_3 & Dy_3 &= b_0 + b_1x_3 + b_2y_3 + b_3x_3y_3 \\
 Dx_4 &= a_0 + a_1x_4 + a_2y_4 + a_3x_4y_4 & Dy_4 &= b_0 + b_1x_4 + b_2y_4 + b_3x_4y_4
 \end{aligned}
 \tag{4.4}$$

where: $Dx_1, Dx_2, Dy_1, Dy_2, \dots$ are the measured corrections at each of the four surrounding reseau points (known sites).

$x_1, x_2, y_1, y_2, \dots$ are the measured x and y coordinates of the surrounding known sites.

The estimated parameters (a_0, a_1, a_2 and a_3) are then substituted into a similar pair of bilinear equations to compute the corrections (Dx_m, Dy_m) to the image point position m .

$$\begin{aligned} Dx_m &= a_0 + a_1x_m + a_2y_m + a_3x_my_m \\ Dy_x &= b_0 + b_1x_m + b_2y_m + b_3x_my_m \end{aligned} \quad (4.5)$$

This computational approach requires the inversion of a symmetric 8 by 8 co-factor matrix per image point to be corrected. Computation of the transform for small data sets is accordingly less computer intensive than that required to compute a global third power polynomial where a symmetric 20 by 20 co-factor matrix must be inverted during the least squares estimation.

Tests of the program BILIN were conducted so as to allow comparison between the image measurements made from Ilford FP4 120 and 220 films. To allow corrections to be made on real image data a periodic subset of the 121 point reseau grid image was chosen. 36 points of the regular grid array provided known sites for use in the correction, leaving the remaining 85 points as image points to be estimated. Figure 4.30 demonstrates the residual vectors after bilinear transformation for some of the frames investigated.

Residual deformations after local bilinear transformation, applied using circled reseau points

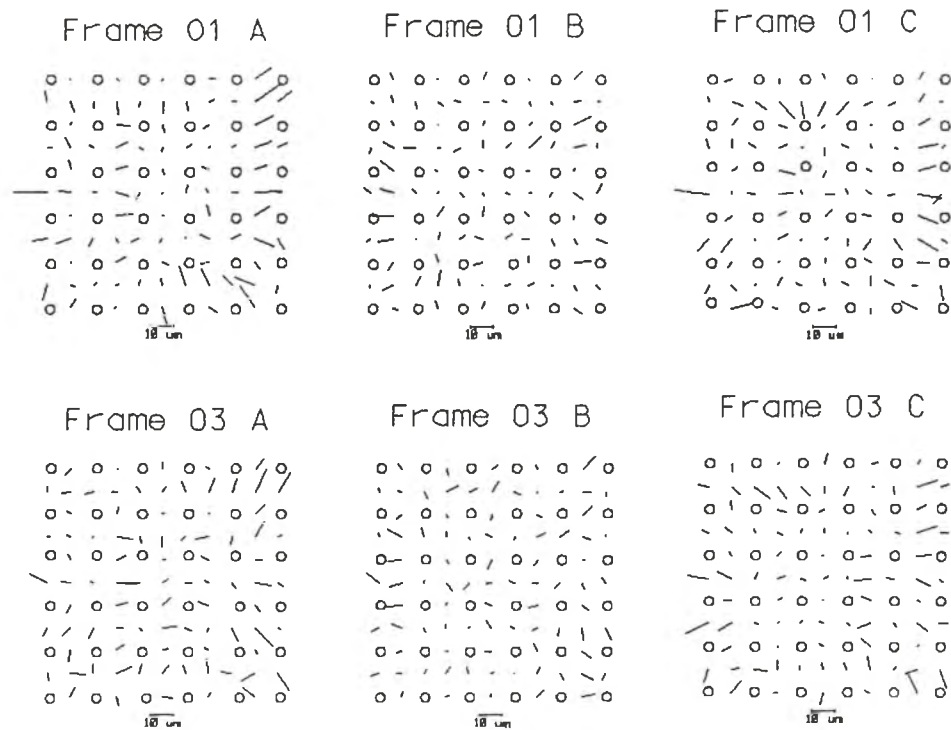


Figure 4.30.

Plotted at twice the vector scale as the plots derived from the global transforms (Figs. 4.24 and

4.25), it can be seen that even with a reduced number of reseau sites the residual deformations are comparable in magnitude to those residuals when using the higher order polynomials.

Table 4.5 presents the RMS residual deformations computed from the differences between the known deformations and those produced by the local bilinear correction. Importantly these are smaller than those derived from any of the previous global solutions.

Table 4.5. RMS residual deformations after bilinear correction.

FP4 Films	RMS residual x(μm)	RMS residual y(μm)
120 N01A,N03A,N01C,N03C	3.72	3.05
220 N01B,N03B,N01D,N03D	2.69	2.62

A further advantage of the local bilinear method is that its ability to correct for localised deformations is determined solely by the reseau spacing, it is therefore independent of the number of reseau points unlike the various global methods. For global transformations the degree of local correction is linked to both the separation and the number of reseau grid crosses, such that more crosses will not provide much improvement to the degree of local correction possible.

To minimise the direct transfer of measurement errors in the correction, it is possible to use for example nine surrounding reseau points and a higher order transformation, but in view of the correction achieved at this stage with the simple local bilinear correction these types of variation have not been investigated. Another simple possibility is to weight the contribution of each reseau measurement in the least squares process according to its measurement standard error.

4.3.3. Linear Least Squares Interpolation.

A method which does consider the surrounding points using a weighted selection procedure is linear least squares interpolation. The theoretical background to the method was discussed in section 3.3.1.2 where the four main steps were detailed: trend removal, computation of the covariance function, modelling of the function and correction of the image point data.

This section applies this theory, using the program INTERPOL (Robson 1989), to the FP4 120/220 (frames **03A,03B**) data set employed earlier. Trend removal has been accomplished in the simple manner recommended by Kraus and Mikhail (1972), by using a globally applied affine transformation to correct all the measurement data. For the one dimensional theory to be valid a second assumption is made, namely that the x and y measurement data are independent, allowing the covariance functions to be treated as one dimensional situations. Independence can be checked since if true the cross covariances, $C(d)_{xy}$ and $C(d)_{yx}$ (obtained according to equations 4.6 and 4.7, which are extensions of equation 3.14) should be zero at all separations.

$$C(d)_{xx} = \left(\frac{1}{n_y}\right) \sum_{k_j} l_{xj} l_{xj} \quad C(d)_{yy} = \left(\frac{1}{n_y}\right) \sum_{k_j} l_{yj} l_{yj} \quad (4.6)$$

$$C(d)_{xy} = \left(\frac{1}{n_y}\right) \sum_{k_j} l_{xj} l_{yj} \quad C(d)_{yx} = \left(\frac{1}{n_y}\right) \sum_{k_j} l_{yj} l_{xj} \quad (4.7)$$

where: l_{ix}, l_{jx}, l_{iy} and l_{jy} are the measured x and y magnitudes of the reseau image deformation.

n is the number of repeated measurements.

$C(d)_{xx}$ and $C(d)_{yy}$ are the covariances in x and y.

$C(d)_{xy}$ and $C(d)_{yx}$ are the cross covariances.

Figures 4.31 and 4.32 show the covariance and cross covariance functions computed from the two frames using a 4mm separation increment d . The magnitude of the covariance functions differ for both frames, easily explained when the differences between their deformation patterns are considered (Figs. 4.24 and 4.25). The computation of the covariance functions is further confirmed by consideration of the variance factors which are simply the squares of the RMS residuals after affine transformation.

The covariance and cross covariance functions appear to conform to theoretical expectations until the separation between points reaches about 15mm. Beyond this point there are two distinct regions for both frames:

- a) A zone beginning at 15mm, where the cross covariance function remains near zero, whilst the covariance functions are negative. The near zero cross covariances imply that the x and y data are independent to the order of measurement accuracy. The negative covariances indicate that there are small periodical effects occurring between reseau point separations of 15 to 25mm in both the x and y directions.
- b) Approaching separations above 45mm both the covariances and to a lesser extent the cross covariances become significant. On considering the vector plots (Figs. 4.24 and 4.25) this is not surprising since there are notable deformation patterns towards the edges of the format. It should be noted that the separation increments with means of 68mm and 72mm have been omitted since these are derived from only 8 and 2 reseau measurements respectively.

FP4 120 Frame 03A, Covariance Functions

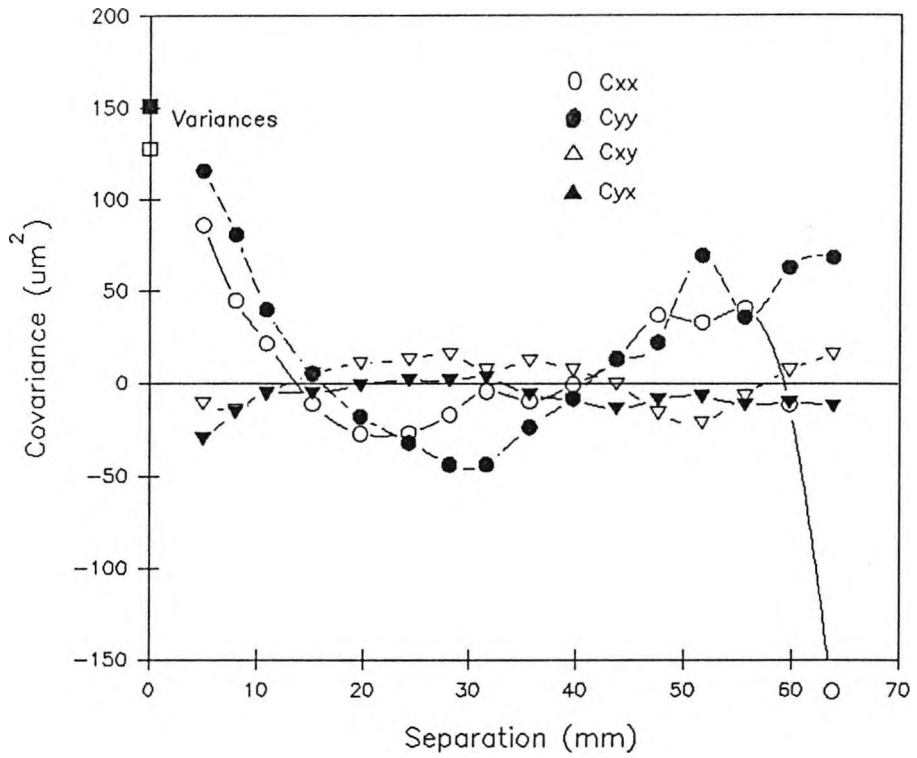


Figure 4.31. Covariance and cross covariance functions for FP4 120 frame N03A.

FP4 120 Frame 03A, Covariance Functions

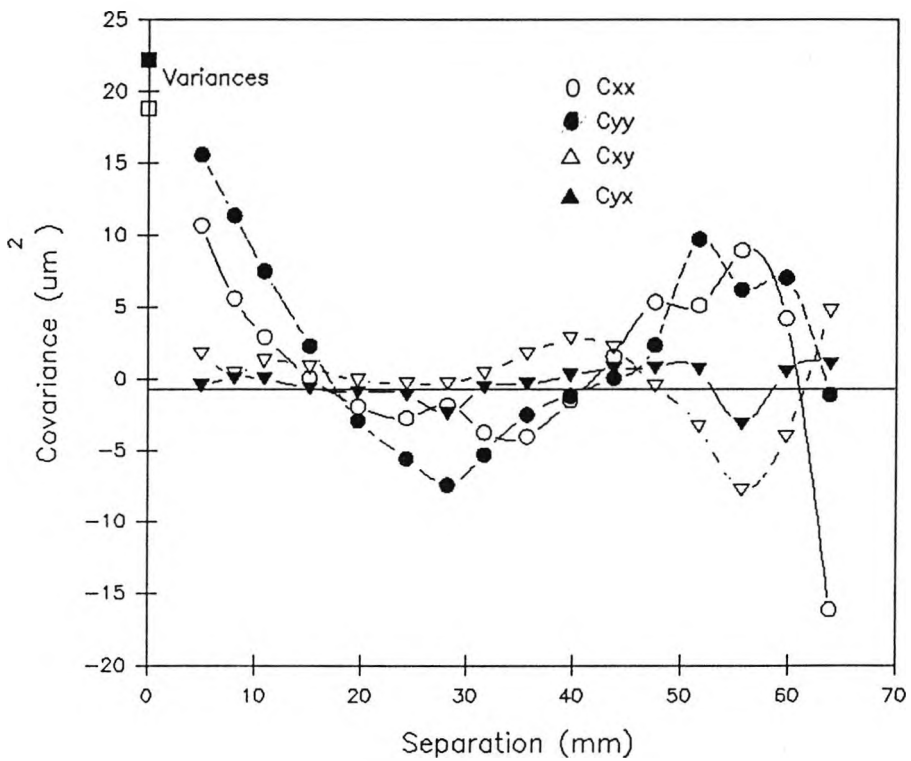


Figure 4.32. Covariance and cross covariance functions for FP4 220 frame N03B.

It would appear that the transformed data has failed to meet the necessary theoretical criterion that any trends should have been removed. Considerations has consequently to be made as to how to remove these trends in the data:

- a) A high degree polynomial could be used, but this negates the statistical merits of the method, since it will impose false constraints on the data.
- b) a physically derived correction representing the trends occurring could be applied to the data. If any physically consistent patterns emerge from this work, then they could possibly be used as a form of trend removal.

Given the preliminary nature of these data the approach decided upon was to reject the covariance function beyond a 25mm separation, where it should theoretically be tending to zero, and to fit Gaussian curves to the remaining data. Using this approach some of the potentials of the method could be evaluated and decisions made as to wether least squares interpolation represented a future direction for this research project.

The Gaussian curves derived from the data using a least squares process are plotted in figures 4.33 and 4.34. The major anomaly in the fitted curves is that the intersection with the covariance (y) axis for both the grossly deformed frame 03A Gaussian curves are all above the variances derived from the data.

The variance is not used in the determination of the gaussian curve parameters because it represents the systematic and irregular components of the vector field whilst the covariance function represents only the systematic part (Kraus 1972). The difference between the variance and covariance for two infinitely close points should consequently represent the irregular components of the measured data, being significantly composed of measurement errors. The discrepancy seen is caused by the steep gradient and lack of data concerning the covariance function in the 1 to 10mm separation region. As before more data and a greater understanding about film deformation trends is required before firm conclusions and corrections can be made.

FP4 120 Frame 03A, Gaussian fit to Cxx and Cyy.

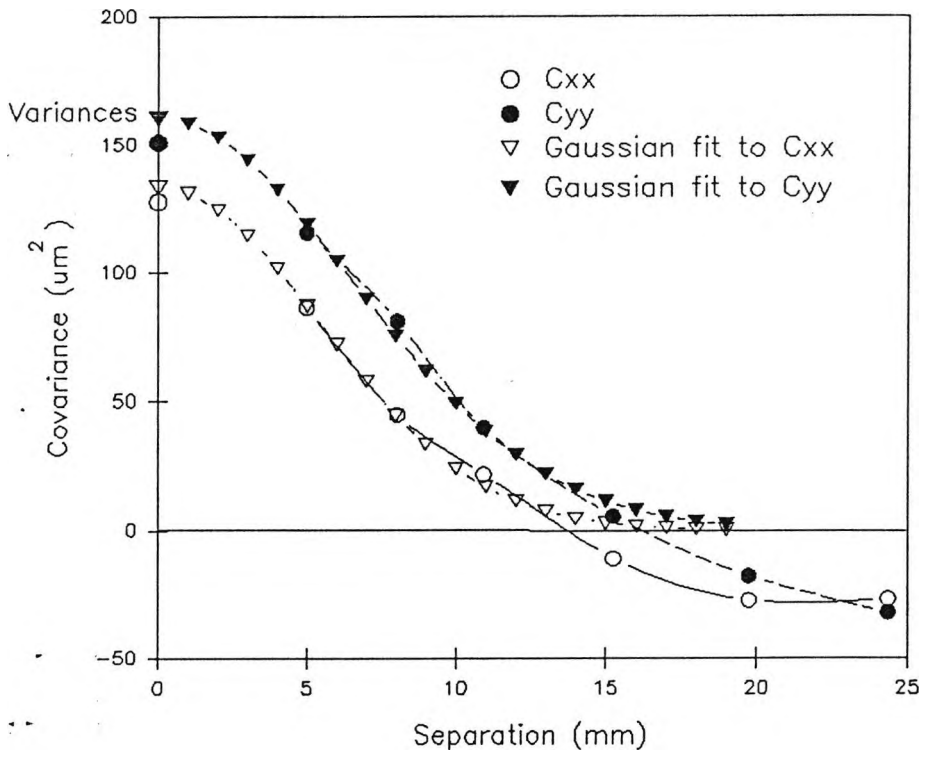


Figure 4.33.

FP4 220 Frame 03B, Gaussian fit to Cxx and Cyy.

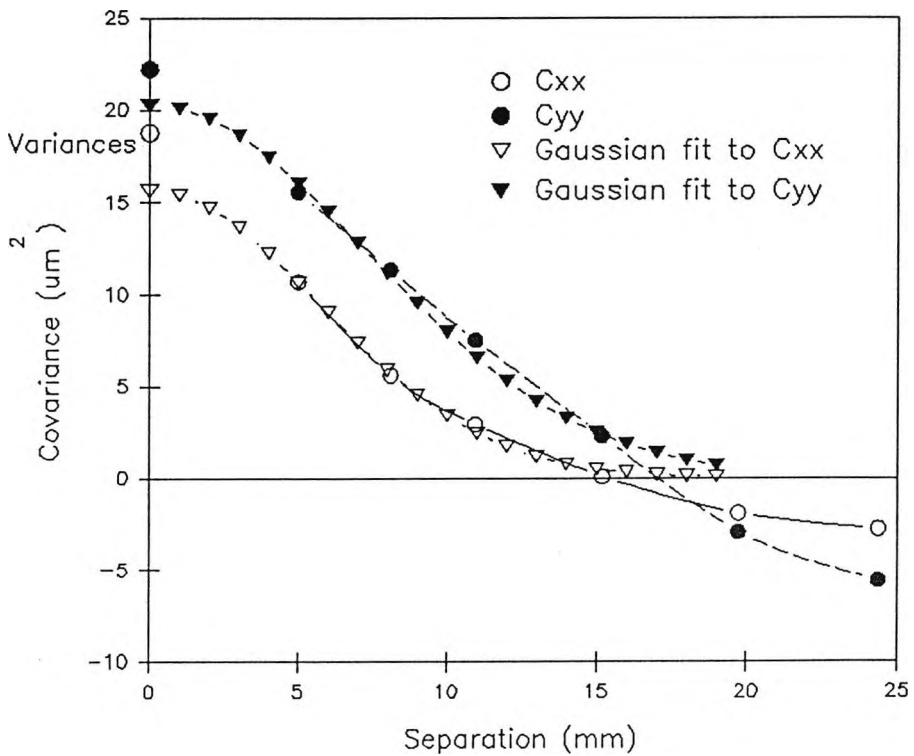


Figure 4.34.

The derived Gaussian curves were then used to produce the C_{uv} matrix (Equation 3.18) necessary for the minimum variance estimate coordinate correction method described in section 3.3.1.2. The 36 by 36 known reseau site configuration employed for the local bilinear correction was also used here enabling a direct comparison of the methods to be made. Also investigated were two other site configurations of 25 by 25 sites and 61 by 61 sites (Fig. 4.35). In all cases the variance rather than the over-large estimated values of $C(0)$ were used for the diagonal matrix terms of C_{uu}^{-1} (Equation 3.19).

The results are encouraging despite the departures from the assumptions made during the derivation of the method. Corrections based on the 61 sites have produced residual deformations which appear random, whilst the correction based on 36 sites has produced RMS discrepancies (Fig. 4.36) of the same order as those from the locally applied bilinear method. The interpolation based on only 25 sites has proved less satisfactory where large edge deformations are present in frame 03A.

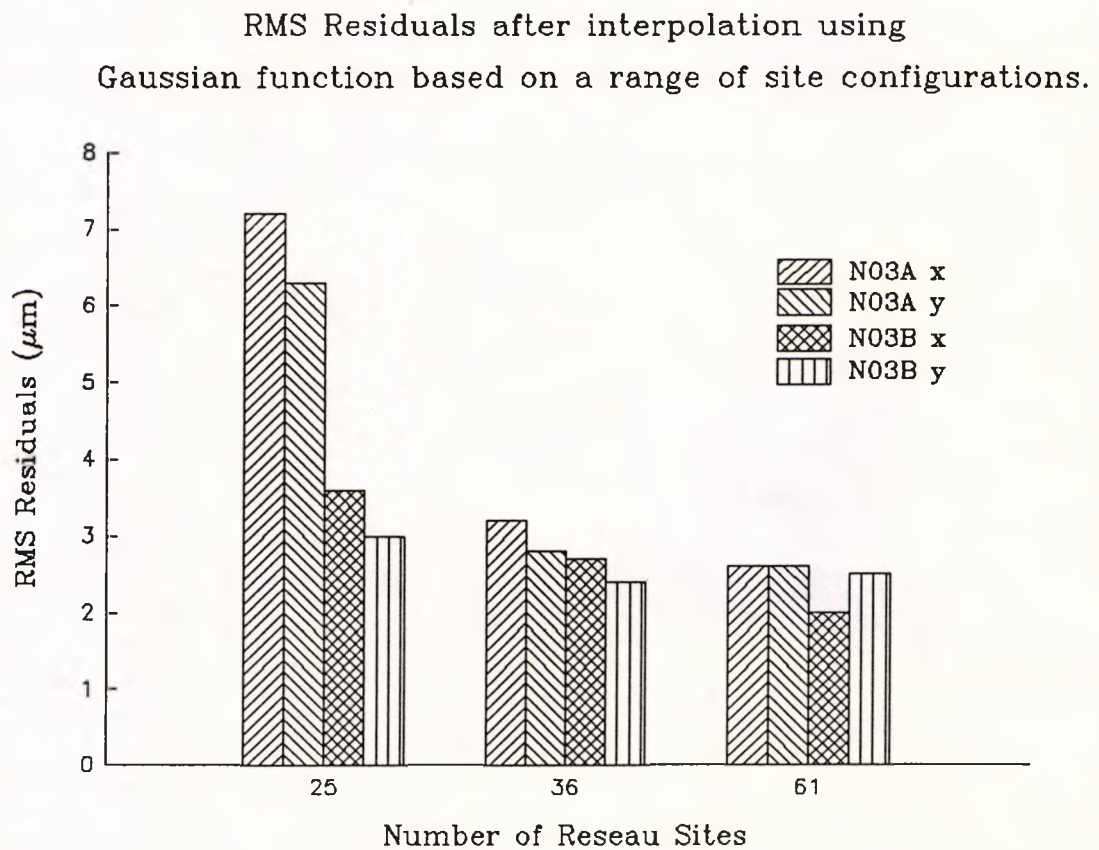
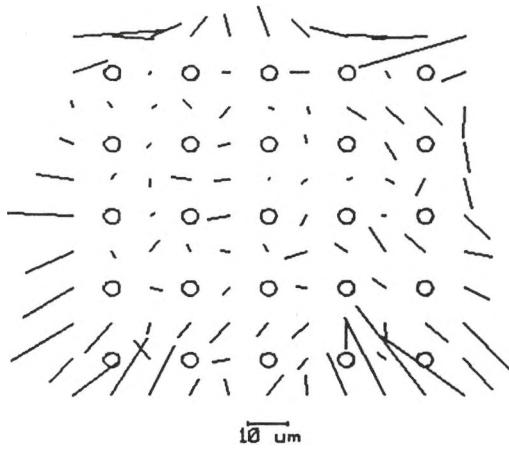


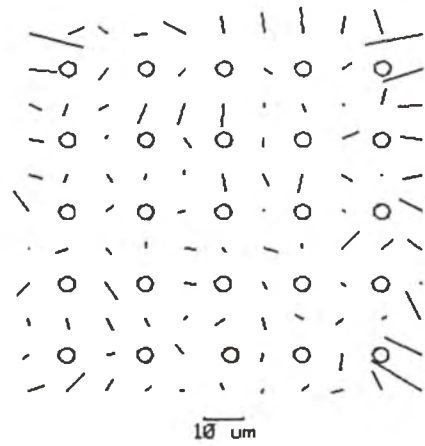
Figure 4.36. RMS residuals after interpolation for the various site configurations.

*Residual deformations for FP4 frames 03A and 03B
after linear least squares Interpolation based
on a variety of site configurations*

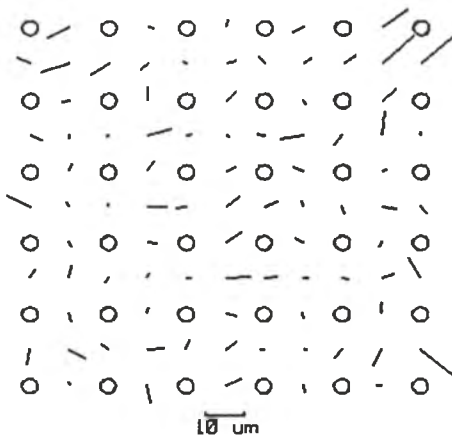
*Frame 03A Interpolation
with 25 known sites.*



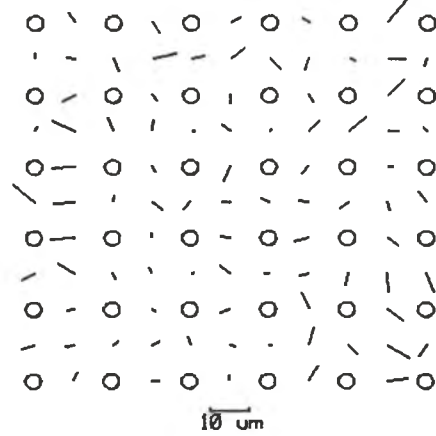
*Frame 03B Interpolation
with 25 known sites.*



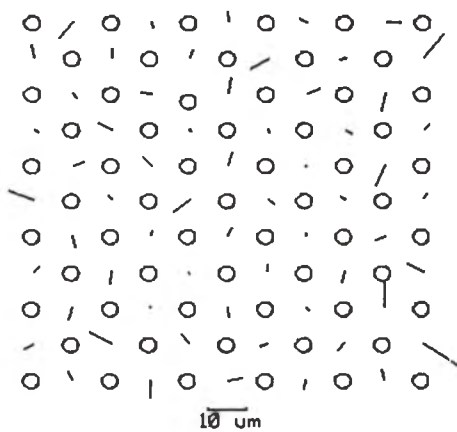
*Frame 03A Interpolation
with 36 known sites.*



*Frame 03B Interpolation
with 36 known sites.*



*Frame 03A Interpolation
with 61 known sites.*



*Frame 03B Interpolation
with 61 known sites.*

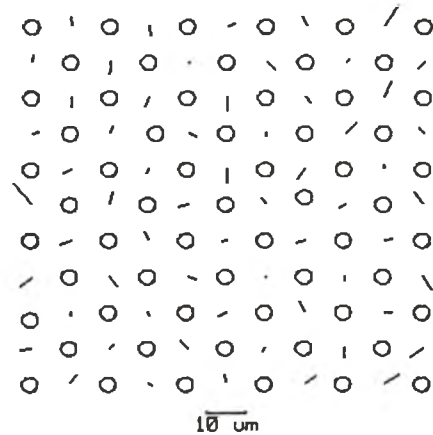


Figure 4.35.

4.4. Summary of initial investigations.

1. Film unflatness has been the major cause of deformations computed from measurements made from grid images exposed in the Rollei-Metric 6006 Camera. For all 120 size film types processed, mean discrepancies after affine refinement of raw photo coordinates have been of the order of $10\mu\text{m}$.

2. The use of 220 roll film in the Rollei-Metric 6006 yielded smaller mean discrepancies of the order of $4\mu\text{m}$ after affine refinement, it can be assumed that the reduction in deformation may be attributed to the lack of a backing sheet with 220 roll film, giving fewer layers between which air may be trapped and thus reducing unflatness, or it could simply be mal-adjustment of the pressure plate. In this situation lack of contact between film and reseau glass yields unsharp cross images which are difficult to measure accurately.

3. Interferometric measurements of the unflatness of different camera reseau plates have shown departures from the assumed image plane of between $3\mu\text{m}$ for a WILD P32 metric camera, to $125\mu\text{m}$ for a Rollei-Metric 6006 Reseau. Departures from parallelism between front and back surfaces of the measured reseau plates have also been seen with magnitudes ranging from between $10\mu\text{m}$ to at least $80\mu\text{m}$.

4. Three explicit film deformation correction methods have been applied to some of the initial reseau data. Global corrections based on the simultaneous least squares fit of a polynomial onto all reseau points have proved the least successful, especially where very localised deformations are present. A better method has been found in the application of a bilinear transformation using the four reseau points surrounding the image point to be corrected. A linear least squares interpolation technique has been investigated, and although giving good results, important departures from its statistical basis are present, specifically with regard to the removal of trends in the data before computation of the covariance function. This method appears to lend itself more as a research tool than a valid correction method for routine work. For example it may be possible to use changes in shape of the derived covariance functions as a sensitive method of analyzing changes in the film deformations present.

5. Investigation of in-plane deformation.

If photographic film is to be reliably used for photogrammetric purposes it is necessary to determine not only the extent and repeatability of any in-plane deformations, but also how they are influenced by variation of the photographic process.

To investigate the processes contributing to in-plane film deformation it is necessary to remove or at least minimise any film unflatness occurring at exposure. During the preliminary investigation the contribution from any in-plane deformation was included in the residual deformations computed at each Rollei-Metric reseau cross, but its magnitude is inseparable from the out-of-plane deformation (Sections 3.3.1 and 4.1.3). A film measurement process which avoids the use of a camera, whilst maintaining the ability to investigate a variety of changes in the photographic process, must consequently be employed.

5.1. Examination methods.

Historically, examinations of in-plane deformation have been limited to looking either at film products intended for aerial survey, or at the changes occurring in graphic arts products where the re-registration of images is important. Documented experiments have been presented not only by the manufacturers (Adelstein et al 1966; Burnham 1969; Michener 1972) to demonstrate the suitability of their products, but also by the end users who were concerned with the errors occurring during the measurement process. Topics investigated (Chapter 2) have included dimensional changes due to processing (Adelstein et al 1966; Byer 1983), changes occurring during storage (Adelstein 1972; Young and Ziemann 1972) and the differences between film base types (Calhoun et al 1960; Jaksic 1972; Kodak 1970b).

Three main methods have been used to measure the film deformations occurring: pin gauge measurements (Byer 1983), grid exposures (Lampton 1966); and moiré interference techniques (Calhoun et al 1960; Burnham 1966). In the research work conducted for this thesis in-plane deformation constituted only one investigative direction, it was therefore decided to concentrate on a single practical method which could be used to investigate any of the photographic process variables. Minimum requirements of the selected method, derived from the initial experiments and literary review, were to measure both homogeneous and non-homogeneous in-plane deformations over a six centimetre square format with a resolution of the order of one to two micrometers.

The mechanical pin register method although quick and applicable to both un-exposed and exposed film samples, has two major short-comings: it is of relatively low accuracy, 1 part in 10,000 ($5\mu\text{m}$ in 50mm) being typical (Byer 1983); and more restricting for the requirements of this work, the method can only provide information concerning two discrete points.

A choice between the grid and moiré methods is more difficult, both are capable of higher accuracy ($3\mu\text{m}$ per 50mm and better), and also give simultaneous information for the whole format area. Two distinct moiré methods have been devised, the first due to Calhoun et al (1960) used a single 250 dot per inch half tone pattern which was contact printed onto the film material and re-registered after processing. This technique, primarily limited by the ability to detect the centre of the half tone cancellations, was able to detect local deviations of the order of $4\mu\text{m}$. The method was consequently not sensitive enough to detect deformations in well handled images on the film stocks of the day, but was well suited to detecting local deformations caused by water spots which could range in diameter from a millimetre to several centimetres (Section 2.4.3).

The second more precise moiré method (Burnham 1966), required the production of at least two precisely ruled glass master images. In Burnham's work the first grid or exposure master used a 40 line per millimetre grid frequency and was exposed in contact with the photographic material under test. The second grid employed a frequency of between 0.18 percent and 0.08 percent lower than that of the exposure master, such that on registration with the exposed and processed film sample a moiré interference pattern was produced. Since the frequencies of the two master grids were precisely known, the metric changes of the photographic image between exposure and registration could be calculated. Burnham's analysis demonstrated that a frequency difference of 0.18% enabled the detection of $1\mu\text{m}$ deformations at the 16 cancellation points digitised over a 50mm square image.

Whilst the moiré cancellation method can yield the high accuracy required, information is confined to the points where cancellations are produced. For the precise method, the number of cancellations per unit area is inversely linked to the accuracy provided. In addition, for the method to be effective the frequencies of the ruled grids must be uniform and precisely known, making their production an expensive process (especially if the UMK 10/1318 camera format of 130 by 180mm size is considered for investigation).

The grid exposure technique utilises a calibrated master grid which is exposed in contact with the film under test. Assuming good contact, which is necessary if in-plane deformations are to be investigated exclusively, the grid method is limited by two factors;

- a) the separation between the calibrated grid positions, which will control the smallest inhomogeneity that the grid array will detect, and
- b) the grid line width which will influence the accuracy of the measurement process, since too thin a line will not be imaged by all film types, and conversely if the line is too thick measurement pointing accuracy will be reduced.

A major production advantage is that the position of the ruled grid intersections can be calibrated after manufacture, and consequently do not need to conform precisely a given frequency over the entire grid area. The method has further advantages concerned with data handling since practical procedures for measurement of the x,y coordinates of a grid image are similar to the measurement of photogrammetric images, and as such include all measurement error sources found in practice. These factors coupled with the simplicity that one dense master grid could be used to cover all circumstances (rather than a variety of contact exposures using different moiré spacings) lead to adoption of the grid method for this investigation.

5.1.1. Master grid preparation.

In determining a useful grid spacing to balance measurement time against the detection of inhomogeneities, the vector plots derived from the Rollei 6006 reseau produced during the initial investigation were reviewed. In the central areas of the format, correlation between the deformation at adjacent reseau points was high, suggesting that in these areas the 5mm spacing used was close enough to detect most inhomogeneities. However at the format edges, correlations were lower, indicating that the period of the film deformation was smaller than the grid spacing. Conclusions as to the optimum grid spacing are not decisive because the images suffered from large out-of-plane deformations, but it is clear that to reliably detect image deformation over the whole format area the grid density should be increased. The trade-off between measurement time and grid density is probably the most important consideration if many process variables are to be investigated.

Determination of an optimum master grid line width was complicated, because light scatter and development effects (Chapter 2) caused the line width of the photographic image of the reseau crosses to vary with image density. Two limiting factors had to be considered to ensure that the same master grid could be used for all tests. Firstly the line width detectable by the higher speed films under test, (TRI-X, FP3, and TMAX 400) needed to be known, and secondly the measuring machine light spot diameter and magnification had to be taken into account. Images of the Rollei reseau on TMAX 400 film demonstrated that its imaged line width of $33\mu\text{m}$ could easily be seen over a range of image densities. Manufacturers' data for the FP3 (Ilford 1982) and TRI-X (Kodak 1987) films quote resolution figures for a high contrast (2.0D) target of 100 lines per millimetre (l mm^{-1}) for both film types. When converted to micrometer line widths (assuming that one reseau line corresponds to one and a half line pairs) a minimum useful reseau line width of $15\mu\text{m}$ is obtained.

The measuring mark on the IMA can be reduced to $10\mu\text{m}$ in diameter, which coupled with the maximum magnification of 40.4X, provides a view of the reseau image crosses in which, despite the graininess being readily apparent, the dot size can still be usefully used. To make optimum use of the $10\mu\text{m}$ measuring mark requires a slightly wider line width, since practice has shown that

the measuring mark can be more easily centred if it is about two thirds of the line width in diameter. This agrees very well with the $15\mu\text{m}$ resolution limit of the fastest films to be tested.

The largest film format which might usefully be investigated was the 130mm X 180mm of the Zeiss (Jena) UMK 10/1318 and 30/1318 cameras. It was accordingly decided that the grid should consist of an overall area of 130mm by 180mm with a separation of 5mm, and an additional central (70mm by 90mm) region containing a grid with a 2.5mm spacing. This central region would cover the 6X6 and 6X9 formats of most 'small format' cameras including that of the University's WILD P32 camera. In this way one single master grid could be used for all potential experiments simply by selecting which grid nodes were to be measured.

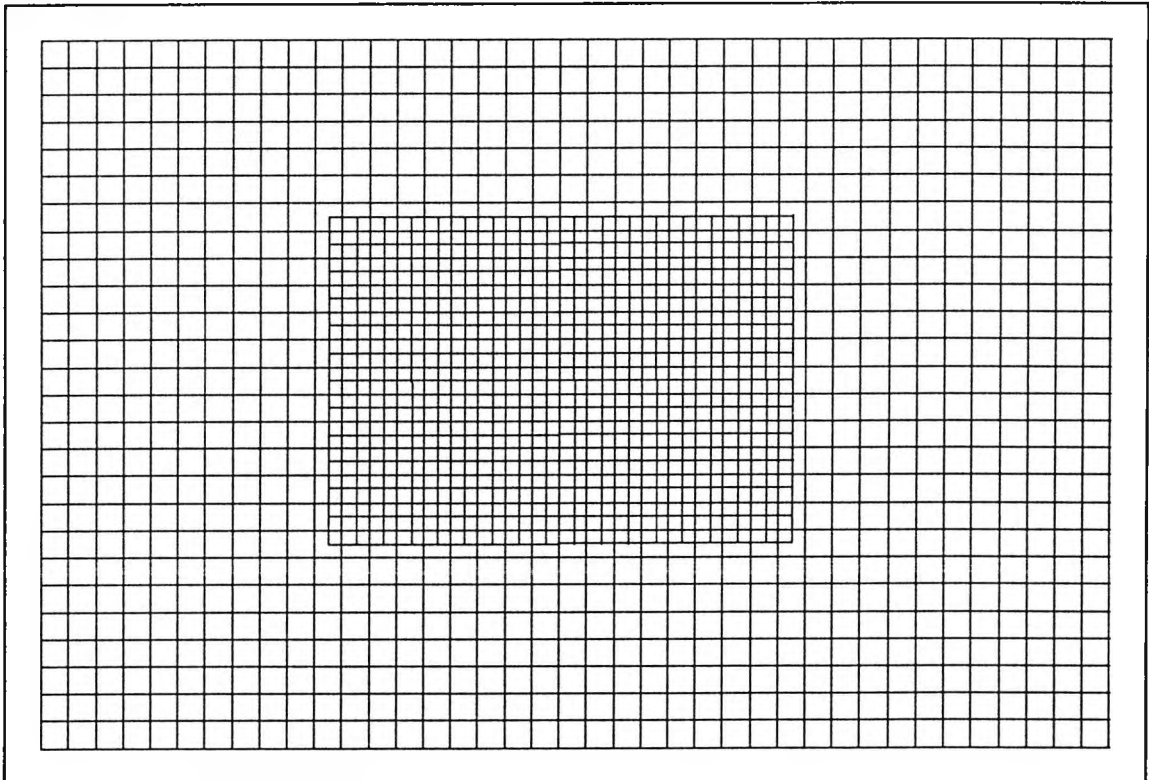


Figure 5.1. Master grid layout

Manufacture of the grid was carried out by Mr Steven Brown at the National Physical Laboratory. Procedures involved the use of a computer driven measuring machine fitted with a microscope objective, scanning a light spot over a sheet of 3mm thick glass coated with Agfa 10E75 Holotest emulsion. The plate was subsequently developed in Kodak D19 developer to produce the final grid image on a clear background. The measuring machine used to scan the plate suffered from a $2\mu\text{m}$ wobble along its axis, necessitating calibration of the grid. The NPL ZKM measuring microscope was employed for this purpose, making three separate rounds of measurement observations at the maximum image magnification of 350X.

5.2. Contact reseau experimentation.

The depth of this investigation depends on the ability to carry out a series of exposures and processes, to measure the resultant images and finally to repeat the procedure, modifying the photographic system according to the conclusions drawn. The limiting factor controlling the ability to investigate many parameters was the measurement time required for a single grid array. Measurement of the 121 point grid array chosen for most experiments required about 20 minutes on the IMA or about 12 minutes on the NPL ZKM measuring microscope.

To arrive at a practical system for the processing of photographic film for photogrammetric use, two main objectives were decided upon:

- a) to determine the magnitude of dimensional change for a range of selected film types, and its variation with measurement environment; and
- b) to minimise the deformation patterns seen, whilst maintaining image quality and archival permanence.

Initial experimentation involved the use of a standard regime which could produce high quality images whilst offering scope for variation of characteristics. Rather than trying to control all environments to which the film was subjected, an almost impossible task, it was decided to use existing facilities. Standardisation of the process could then be used to compensate for environmental fluctuations conferring the advantage that results could be directly implemented in practical applications.

5.2.1. Variables contributing to photogrammetric film deformation.

The factors conceivably influencing the magnitude of in-plane deformation, can be deduced by looking at the sequential steps of the photographic process (Ziemann, 1971b).

- Film types;**
- a) Base type and thickness.
 - b) Number and thickness of emulsion layers.
 - c) Gelatin to base ratio.
 - d) Physical form (roll or sheet).
 - e) Grain size and type.
 - f) Manufacturer.
 - g) Batch to batch variations.
 - h) Usefulness in photogrammetry.

Storage of film prior to exposure;

- a) Relative humidity at which the film has been sealed.
- b) Relative humidity and temperature of the environment.

- c) Rate and non-uniformity of conditioning.
- d) Roll and sheet forms.

- Exposure;**
- a) Relative humidity and temperature at exposure.
 - b) Any un-flatness present.
 - c) Exposure level and uniformity.
 - d) Platen pressure.
 - e) Flatness of register glass.
 - f) Presence of dust.

Storage prior to processing;

- a) Relative humidity and temperature during storage.
- b) Rate and non-uniformity of conditioning.
- c) Sheet or roll form.

Processing conditions; Processor type, tension and agitation.

- i) Development
 - a) Developer type.
 - b) Time and temperature.
 - c) Alkalinity.
 - d) Dilution.
- ii) Stop bath
 - a) Temperature and duration.
 - b) Formulation.
- iii) Fixing bath
 - a) Temperature and duration.
 - b) Formulation.
- iv) Washing
 - a) Temperature.
 - b) Wash rate.
 - c) Duration.
 - d) Form of the film in the wash.
- v) Drying
 - a) Temperature and relative humidity
 - b) Duration
 - c) Use of a drying cabinet.

Storage prior to measurement;

- a) Relative humidity and temperature during storage.
- b) Rate and non-uniformity of conditioning.
- c) Surface area.

Measurement;

- a) Temperature and relative humidity.
- b) Duration.
- c) Machine.
- d) Operator.

5.2.1.1. Film types.

A selection of monochrome film types from the major manufacturers' ranges has been made to include a range of base type, base thickness, emulsion type, emulsion thickness, sensitometry and film size. Some relevant characteristics for each film type investigated are included in Table 5.1. Also of interest are manufacturers' MTF data which, where available are presented in chapter 2, (Figs. 2.21, 2.22 and 2.2.3).

Table 5.1. Film types selected for investigation.

Manufacturer	Film (Code)	Format	Base type	Base thickness	Current publication
Kodak	TMAX 100 (TMX)	120	Triacetate	0.132mm	Kodak 1987a
Kodak	TMAX 400 (TMY)	120	Triacetate	0.132mm	Kodak 1987a
Kodak	TRI-X 120 (TRX)	120	Triacetate	0.091mm	Kodak 1987c
Kodak	Technical Pan (TCP)	120	Triacetate	0.091mm	Kodak 1987b
Ilford	PAN F (PNF)	120	Triacetate	Not published	Ilford 1991c
Ilford	FP4	120	Triacetate	Not published	Ilford 1991a
Ilford	FP4	220	Triacetate	Not published	Ilford 1991a
Ilford	FP3	70mm	Polyester	0.100mm	Ilford 1983
Agfa	Holotest 10E75 (H75)	70mm	Polyester	0.100mm	Agfa 1989
Agfa	Holotest 10E56 (H56)	70mm	Polyester	0.100mm	Agfa 1989

5.2.1.2. Storage prior to exposure.

Storage was standardised using the recommended method for long term storage of most film stocks, namely keeping the films in a freezer with the manufacturers' foil packing intact. Films were removed from the freezer approximately half an hour before exposure, allowing them to warm up sufficiently to prevent the formation of condensation once the packaging was broken immediately before exposure. Exceptions to this procedure were made where pre-exposure conditioning was the variable to be investigated. In this case the film was unpacked and wound onto processing tank spirals for varying periods of storage in the exposing environment. By consistently employing these methods it was assumed that whilst the exposing environment (monitored by a digital probe) varied, experimental batch to batch variations would be minimised using a procedure possible in most practical situations.

5.2.1.3. Exposure.

All films were contact exposed using the NPL glass master grid and an enlarger as the light source. Focal length of the enlarger lens was 80mm and the lens/film distance was 950mm. Although no environmental controls were present in the darkroom, ambient relative humidity and temperature were measured before and after exposure. The large lens-film separation produced a low angle (1.5°) of divergence over the exposure area, which whilst not ideal parallel illumination, minimised the possible contribution from unflatness to a level comparable to the

measurement standard error (an unflatness of $32\mu\text{m}$ producing a $1\mu\text{m}$ distortion in the worst case for a grid point at the edge of the 60mm format).

Exposures were made using 70mm cassettes to receive the exposed film and a 120 Hasselblad insert was used to hold the unexposed roll tight. This enabled three grid exposures to be made on a roll of 120 film whilst minimising the handling of the film. Each exposure involved the positioning of the film over a glass plate, locating the calibrated grid, and then placing three thick glass sheets on top to provide a transparent flattening weight. The exposure required was assessed by making a series of test exposures, and then using ISO speed ratings to derive an exposure duration for each film type.

Where variation of exposure level over the area of a frame was to be assessed, various neutral density filters were taped to the top surface of the glass master grid.

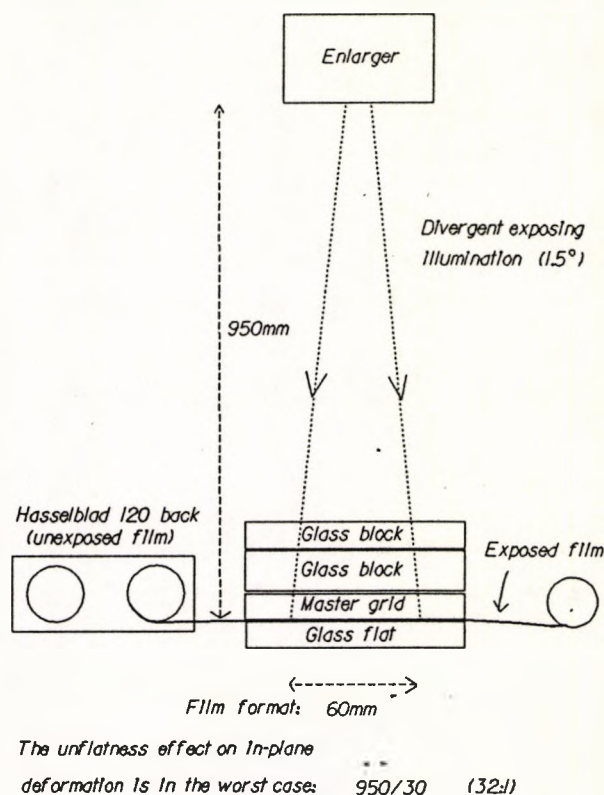


Figure 5.2. The contact grid exposing situation.

5.2.1.4. Storage prior to processing.

The elementary way to minimise this set of variables was to process the film as soon after exposure as practicable. In general the films were undergoing development within ten minutes of being exposed.

5.2.1.5. Processing conditions.

The initial standard regime involved processing the film in small spiral tanks with agitation by inversion every thirty seconds. The developer used was Ilford ID11 1:1, stored as a stock solution for dilution immediately prior to use so that consistent chemical activity was assured. Development time was calculated using manufacturers' data tables, according to the time-temperature method (the formulation of Ilford ID11 1:1 is equivalent to Kodak D76 1:1 for these purposes). In all processes Kodak Indicator stop bath was used, diluted 1:64 with water, films being immersed for thirty seconds. The fixing solution was Ilford Hypam (1:4), allowing the addition of an inorganic hardener to the same fixer solution such that the dimensional effects of

hardening the emulsion layers could be assessed. Washing in every case was carried out for thirty minutes in filtered running water, the minimum generally accepted as necessary to provide archival permanence. During the last few minutes of the wash, Kodak rinse aid was added which, by its detergent action, helped to prevent uneven drying caused by water droplets (Walls and Attridge 1977).

Drying was carried out initially by hanging the films in a drying cabinet. However, over-drying has been shown to produce oversize images on measurement (Adelstein et al 1966; Kodak 1971b). Rather than duplicate these already well documented drying investigations, the films were simply hung up in the measurement environment, drying being regarded simply as part of storage prior to measurement.

Table 5.2 shows the range of processing chemicals used during the course of this work. The developing solutions have been chosen according to manufacturers' recommendations so that as many film types as possible can be directly compared without unnecessary variation of process parameters. The selection allows many modifications of negative characteristic curve shapes to be made enabling any dimensional consequences of tone reproduction variation to be assessed.

Table 5.2. Processing chemicals.

Manufacturer	Type	Dilution	Photographic use
Developing solution			
Ilford	ID11	1:1	Fine grain
Ilford	Perceptol	Stock	Fine grain
Kodak	D19	Stock	High contrast
Stop solution			
Kodak	Indicator stop	1:64	Neutralises developer
Fixing solution			
Ilford	Hypam	1:4	Film fixer
Ilford	Rapid hardener	1:80	In-organic Hardening agent
Rinse aid			
Kodak	Photo-Flo	1:600	Rinse aid

5.2.1.6. Storage prior to measurement.

Films were cut up into strips of three frames and stored in paper negative bags to avoid the well known non-uniform roll conditioning effects documented by Carman & Martin (1969). Initial measurements were made using the Intergraph IMA (Section 4.1.1) which was situated in an air-conditioned environment. The relative humidity of this environment was found to fluctuate quite rapidly, although repeated measurements over the period of its use found that the average conditions were 45%RH ($\sigma=6.9$) and 21.3°C ($\sigma=0.8$).

A major advantage was provided by the measurement environment at NPL in which temperature was controlled to a much tighter tolerance ($\pm 0.1^\circ\text{C}$) using a purpose built refrigeration unit. Environmental conditions of this room were continuously monitored by a chart recorder enabling a more rigorous investigation of hysteresis effects to be made.

5.2.1.7. Image measurement.

The measurement environments have been detailed above (Section 5.2.1.6). The NPL measurement room used for most of the experiments since it provided a much better level of environmental control.

Measurements conducted using the IMA were made using the reseau measurement section of the orientations software package. Although designed to produce look-up image refinement tables based on the global fit of second order polynomials, the package also produced comparator coordinates which had been refined according to stage plate calibration data.

The NPL ZKM measuring microscope consisted of a Zeiss (Jena) ZKM 01-25D modified by the inclusion of linear motors linked to a IBM compatible PC to enable driving to coordinates selected by an input file such as the grid calibration data. The system included a selection of objectives and a vidicon camera which produced magnifications ranging from 35X to 350X onto a television monitor. The measuring mark consisted of a graticule situated in the optical system, the image of which was lined up on the grid centre using a joystick which controlled the x and y movements of the linear motors. Once alignment between the graticule and grid node had been achieved a data button was pressed and the x and y positions of the image crosses (in the comparator coordinate system) were passed to the PC for storage. The whole system was driven using a software package written in BASIC by Oldfield at NPL.

The modified ZKM measuring microscope was capable of achieving accuracies of the order of $1\mu\text{m}$ over a 130mm by 180mm image area (Oldfield 1986). The latest edition of the driving software was able to backdrive the microscope according to a previously defined coordinate data file. This ability coupled with its ease of use enabled a complete 121 point reseau grid to be measured in ten to fifteen minutes. For all grid measurements three rounds of independent pointings were made whilst the position of the image in the stage plate coordinate system was maintained constant. On computing means and standard deviations of the repeated coordinate measurements it was found that standard errors were always in the sub-micrometer range, as opposed to the one to two micrometers typical of the IMA.

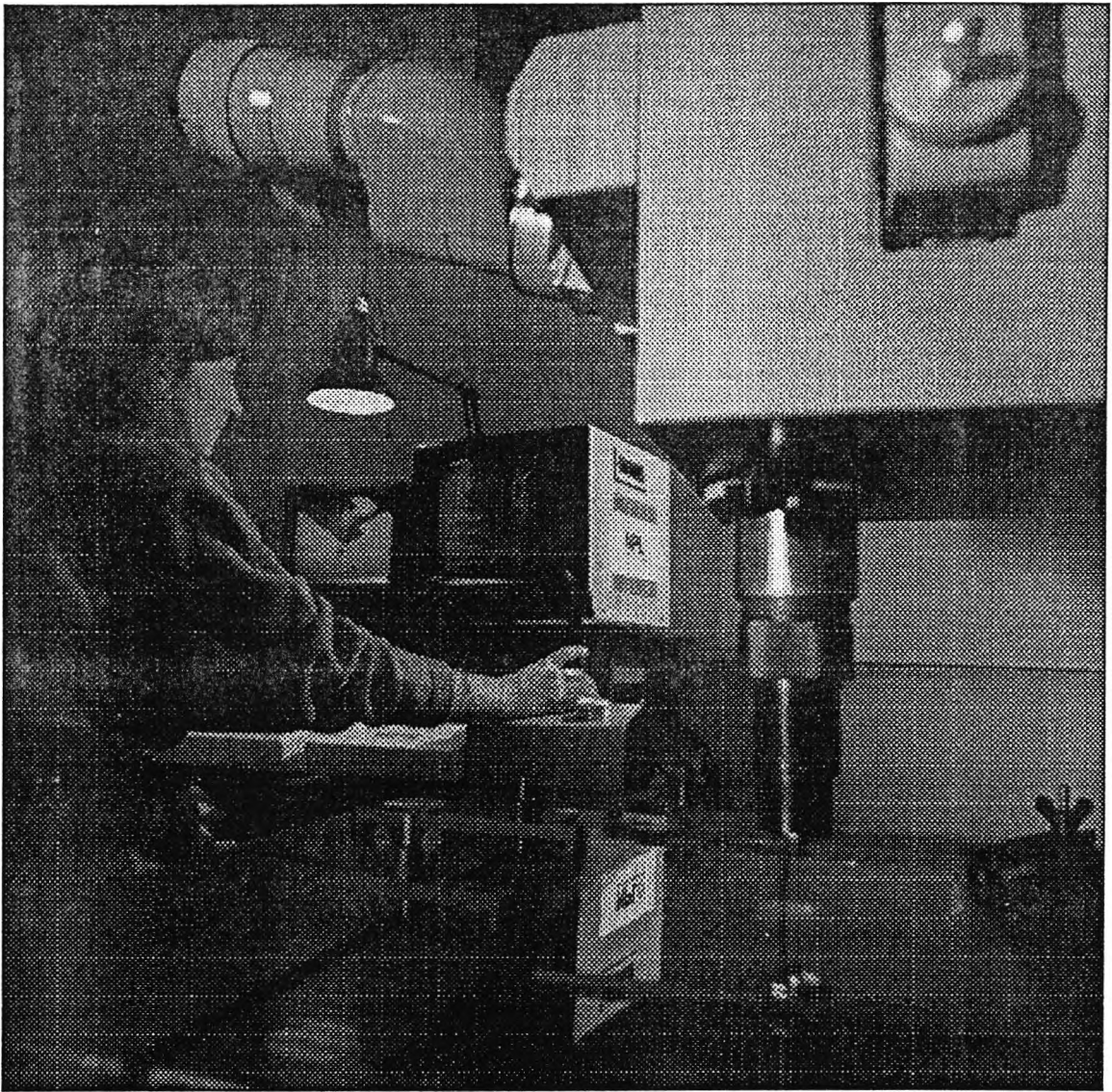


Figure 5.3. The NPL modified ZKM measuring microscope.

5.3. Experiments conducted and analysis of results.

The intention of this section is to assess the contributions of the components of the photographic process to film deformation. Specifically investigated are components which from the review of previous film deformation investigations (Section 2.4) and from imaging considerations (Sections 2.1, 2.2 and 2.3) can be expected to provide the major influences on small format photographic results intended for photogrammetry.

The experiments in this investigation were carried out in twelve batches with the object of achieving distinct goals, based on the conclusions drawn from the previous experiments. The examinations were carried out initially to provide a sample of in-plane deformation data and subsequently to minimise any deformations found. A brief chronological outline of each of the treatments is given below.

Experiment 1, (Rolls 1 and 2) considered contributions from variations in the drying environment. Images were produced on Ilford FP4 220 and FP3 70mm film types and frames were re-measured to analyze dimensional changes caused by conditioning time after processing.

Experiment 2, (Rolls 3 and 4) was carried out in a similar manner to experiment 1, but a non-hardening fixing bath was used.

Experiment 3, (Rolls 5,6 and 7) investigated the dimensional qualities of three different film types (FP4, PAN F and Technical Pan 120 films). The presence of any differences between image deformations on re-measurement were also evaluated.

Experiment 4, (Rolls 8,9,10 and 11). Too many variables (caused by processing in different batches) were present in earlier experiments to determine if there were any dimensional differences caused by different fixer formulations. In this case a reduced grid density (6X6) was used to investigate the contributions from the use of hardening/non-hardening fixing baths. By using Technical Pan 120 and Ilford FP4 220 films, differences between these two films could also be assessed.

Experiment 5, (Rolls 12,13,14,15,16 and 17). The earlier results indicated that the precision achievable with 3 pointings per reseau cross image on the IMA produced an RMS error of similar magnitude to most of the local film deformations occurring. All subsequent measurements were therefore carried out on the NPL ZKM, starting with this set of experiments investigating the effect of hardening fixer on FP4 220, PAN F 120 and Technical Pan 120 films.

Experiment 6, (Rolls 18,19,20,21 and 22). In this sequence any dimensional differences caused by using different developer solutions were investigated. Images were made on Technical Pan 120 and Ilford Pan F 120 films since these provided the best resolution and therefore more reliable pointing to reseau cross images during image measurement.

Experiment 7, (Rolls 23,24,25,26,27). Two sets of parameters were investigated. First, the deformational effect of exposure variation over each frame using Ilford Pan F 120 film, and second the deformations occurring on images made using TMX, TMY and TRI-X films when processed using the standard regime.

Experiment 8, (Rolls 28,29 and 30). Since the results of the exposure variation showed some systematic deformation patterns which did not agree with the different regions of exposure, experiment 7 was repeated. To provide a more comprehensive data set, the exposure pattern was varied and images were made onto both Pan F and Technical Pan 120 films.

Experiment 9, (Rolls 31,32,33,34) provided additional scale change and local deformational data

on several 120 films (FP4, TMX, TMY and TRI-X 120) for which data were lacking. All films were uniformly exposed, then developed in Ilford Perceptol.

Experiment 10, (Rolls 35,36,37,38) analyzed the dimensional contribution made by varying pre-exposure conditioning time. Kodak Technical Pan 120 roll films were transferred from the freezer to the exposing environment at 3 days and at 1 hour before exposure. By treating the films identically at and after exposure the contributions of the pre-exposure differences could be assessed.

Experiment 11, (Rolls 39,40,41,42) was conducted in a similar manner to experiment 10, providing slightly different pre-exposure treatments and the use of a non-hardening fix.

Experiment 12, (Rolls 43, 44 and 45) Investigations were made using Agfa Holotest 10E75 70mm film which, with its thin (7 μ m) emulsion, very high resolution and thick polyester base, could be used to assess both reliability and repeatability of the contact procedure. Two sets of exposures and processes were made and images repeatedly measured to provide a guide to the measurement errors in the experimental procedure.

Table 5.3 details the processes connected with each of the rolls of film processed, in each case the final column in the table describes the primary treatment being investigated.

Table 5.3. Exposures, processes and measurements made.

Roll	Film	ID	Developer	Fixer	Measurement date	Treatment
1	FP4 220	E 6Fr.	ID11 1:1	H.F.	IMA: 5/5 6/5 9/5 13/5 20/5 1/6 22/6	Drying
2	FP3 70mm	A 6Fr.	ID11 1:1	H.F.	IMA: 5/5 6/5 9/5 13/5 20/5 1/6	Drying
3	FP4 220	F 3Fr.	ID11 1:1	N-H.F.	IMA: 6/6 7/6 9/6 22/6	Fixer
4	FP3 70mm	B 3Fr.	ID11 1:1	N-H.F.	IMA: 6/6 7/6 9/6 1/6	Fixer
5	FP4 120	E 2Fr.	ID11 1:1	H.F.	IMA: 13/6 16/6 22/6	Film
6	PNF 120	A 2Fr.	ID11 1:1	H.F.	IMA: 13/6 16/6 22/6	Film
7	TCP 120	B 2Fr.	ID11 1:1	H.F.	IMA: 13/6 16/6 22/6	Film
8	FP4 220	G 3Fr.	ID11 1:1	N-H.F.	IMA: 4/7 5/7 6/7 7/7 10/7 12/7	Fixer
9	FP4 220	H 3Fr.	ID11 1:1	H.F.	IMA: 4/7 5/7 6/7 7/7 10/7 12/7	Fixer
10	TCP 120	C 2Fr.	ID11 1:1	H.F.	IMA: 4/7 5/7 6/7 7/7 10/7 12/7	Fixer
11	TCP 120	D 2Fr.	ID11 1:1	N-H.F.	IMA: 4/7 5/7 6/7 7/7 10/7 12/7	Fixer
12	FP4 220	I 3Fr.	ID11 1:1	N-H.F.	ZKM: 18/7 19/7 20/7 25/7 28/7 2/8	Fixer

Roll	Film	ID	Developer	Fixer	Measurement date	Treatment
13	FP4 220	J 3Fr.	ID11 1:1	H.F.	ZKM: 18/7 19/7 20/7 25/7 28/7 2/8	Fixer
14	PNF 120	B 3Fr.	ID11 1:1	H.F.	ZKM: 18/7 19/7 20/7 25/7 28/7 2/8 10/8	Fixer
15	PNF 120	C 3Fr.	ID11 1:1	N-H.F.	ZKM: 18/7 19/7 20/7 25/7 28/7 2/8	Fixer
16	TCP 120	E 3Fr.	ID11 1:1	H.F.	ZKM: 18/7 19/7 20/7 25/7 28/7 2/8 10/8	Fixer
17	TCP 120	F 3Fr.	ID11 1:1	N-H.F.	ZKM: 18/7 19/7 20/7 25/7 28/7 2/8	Fixer
18	PNF 120	D 3Fr.	D19	N-H.F.	ZKM: 26/7 1/8 8/8	Developer
19	PNF 120	E 3Fr.	ID11 1:1	N-H.F.	ZKM: 26/7 1/8 8/8	Developer
20	PNF 120	F 3Fr.	Perceptol	N-H.F.	ZKM: 26/7 1/8 8/8	Developer
21	TCP 120	H 3Fr.	ID11 1:1	N-H.F.	ZKM: 26/7 1/8 8/8	Developer
22	TCP 120	I 3Fr.	Perceptol	N-H.F.	ZKM: 26/7 1/8 8/8	Developer
23	PNF 120	G 3Fr.	ID11 1:1	N-H.F.	ZKM: 1/8 2/8 8/8 10/8 17/8 18/8	Exposure
24	PNF 120	H 2Fr.	ID11 1:1	N-H.F.	ZKM: 2/8 8/8	Exposure
25	TMX 120	A 2Fr.	ID11 1:1	H.F.	ZKM: 2/8 10/8 16/8	Film
26	TMY 120	E 3Fr.	ID11 1:1	H.F.	ZKM: 2/8 10/8 16/8	Film
27	TRX 120	A 3Fr.	ID11 1:1	H.F.	ZKM: 2/8 10/8 16/8	Film
28	PNF 120	I 3Fr.	ID11 1:1	H.F.	ZKM: 17/8 18/8	Exposure
29	PNF 120	J 3Fr.	ID11 1:1	H.F.	ZKM: 17/8 18/8	Exposure
30	TCP 120	J 3Fr.	ID11 1:1	H.F.	ZKM: 17/8 18/8	Exposure
31	FP4 120	F 3Fr.	Perceptol	H.F.	ZKM: 5/9 7/9	Film/Dev
32	TMX 120	B 3Fr.	Perceptol	H.F.	ZKM: 5/9 7/9	Film/Dev
33	TMY 120	F 3Fr.	Perceptol	H.F.	ZKM: 5/9 7/9	Film/Dev
34	TRX 120	B 3Fr.	Perceptol	H.F.	ZKM: 5/9 7/9	Film/Dev
35	TCP 120	K 3Fr.	D19	H.F.	ZKM: 12/9 14/9	Cond. 1Hr
36	TCP 120	L 3Fr.	D19	H.F.	ZKM: 12/9 14/9	Cond. 1Hr
37	TCP 120	M 3Fr.	D19	H.F.	ZKM: 12/9 14/9	Cond. 3Dy
38	TCP 120	N 3Fr.	D19	H.F.	ZKM: 12/9 14/9	Cond. 3Dy
39	TCP 120	O 3Fr.	D19	N-H.F.	ZKM: 20/9 28/9	Cond. 3Dy
40	TCP 120	P 3Fr.	D19	N-H.F.	ZKM: 20/9 28/9	Cond. 3Dy
41	TCP 120	Q 3Fr.	D19	N-H.F.	ZKM: 20/9 28/9	Cond. 1Hr
42	TCP 120	R 3Fr.	D19	N-H.F.	ZKM: 20/9 28/9	Cond. 1Hr
43	H75 70	X 1Fr.	D19	N-H.F.	ZKM: 20/9 28/9 3/10	Film
44	H75 70	A 6Fr.	D19	H.F.	ZKM: 20/9 28/9 3/10	Film
45	H75 70	B 4Fr.	D19	N-H.F.	ZKM: 3/10 6/10	Film

The results from each of the experimental tests contain significant overlap because of the large number of contributory factors. Consequently the method chosen to provide an efficient discussion was to work systematically through the components of the photographic process. In this way all experimental results could be drawn upon to make conclusions about the dimensional contribution of each step to the process of photogrammetric measurement. Deformations arising from each stage of the photographic process are discussed below, contributions from each stage being logically separated into homogeneous and inhomogeneous components. For these

purposes inhomogeneous changes are understood as those deformations present after removal of the homogeneous changes, as accomplished by the use of a globally applied affine transformation (Equation 3.7).

5.3.1. The relationship between the relative humidity of the measurement environment and scale change for the film types investigated.

During the course of the investigation a relationship between the scale change parameters and the measurement environment was found. Although out of sequence, an early discussion of these trends will simplify explanation of the deformation effects due to individual components of the photographic process. The data used in this section were drawn from all of the in-plane investigations and therefore a generalised assessment concerning the range of possible dimensional change can be made in this section.

5.3.1.1. Homogeneous changes.

The following graphs (Figs. 5.4 to 5.8) show percentage scale changes derived from a least squares fit of the image measurements to the glass master dimensions using an affine transformation. These scale changes are plotted against ambient relative humidity readings made at the time of measurement using the digital thermo-hygrometer. The relative humidity of both the IMA and the more precisely controlled NPL(ZKM) measurement environments were found to fluctuate according to the external weather conditions, producing a range of 30% to 75%. Efforts were made to measure each film type over the entire relative humidity range, however (due to the un-reliability of weather prediction) this was not always possible and is reflected in the differing coverage of the graphs.

Figures 5.4 and 5.5 represent all measurements made using the ZKM measuring microscope on Ilford Pan F and Kodak Technical Pan 120 films. The results demonstrate good linearity despite the range of treatments given. Assuming linearity, departures from this condition may be attributed to two causes: first the individual experimental treatments have given rise to scale changes and secondly the relative humidity as measured by the probe is an ambient reading, not a direct reading of the moisture content of the film material. Relative humidity fluctuations measured by the probe (with its 2% uncertainty) could reflect changes in the environment to which the film (even in single sheets) was not fully conditioned, (Section 2.4.1).

Also of importance with these two film types (TCP and Pan F) is that the scale change in the x direction (across the roll width) is always less than the scale change in y. Whilst the cause of these differences could be a function of the stresses between the cellulose triacetate base and the attached emulsion layers. However experimental work conducted at NPL has shown that the repeatability of the ZKM is better in the x direction than in y, (Oldfield 1990).

Graph of scale change against
measurement environment relative humidity
for Ilford PAN F 120 roll film

Plotted values from repeated measurements
of 28 frames from 10 rolls of film.

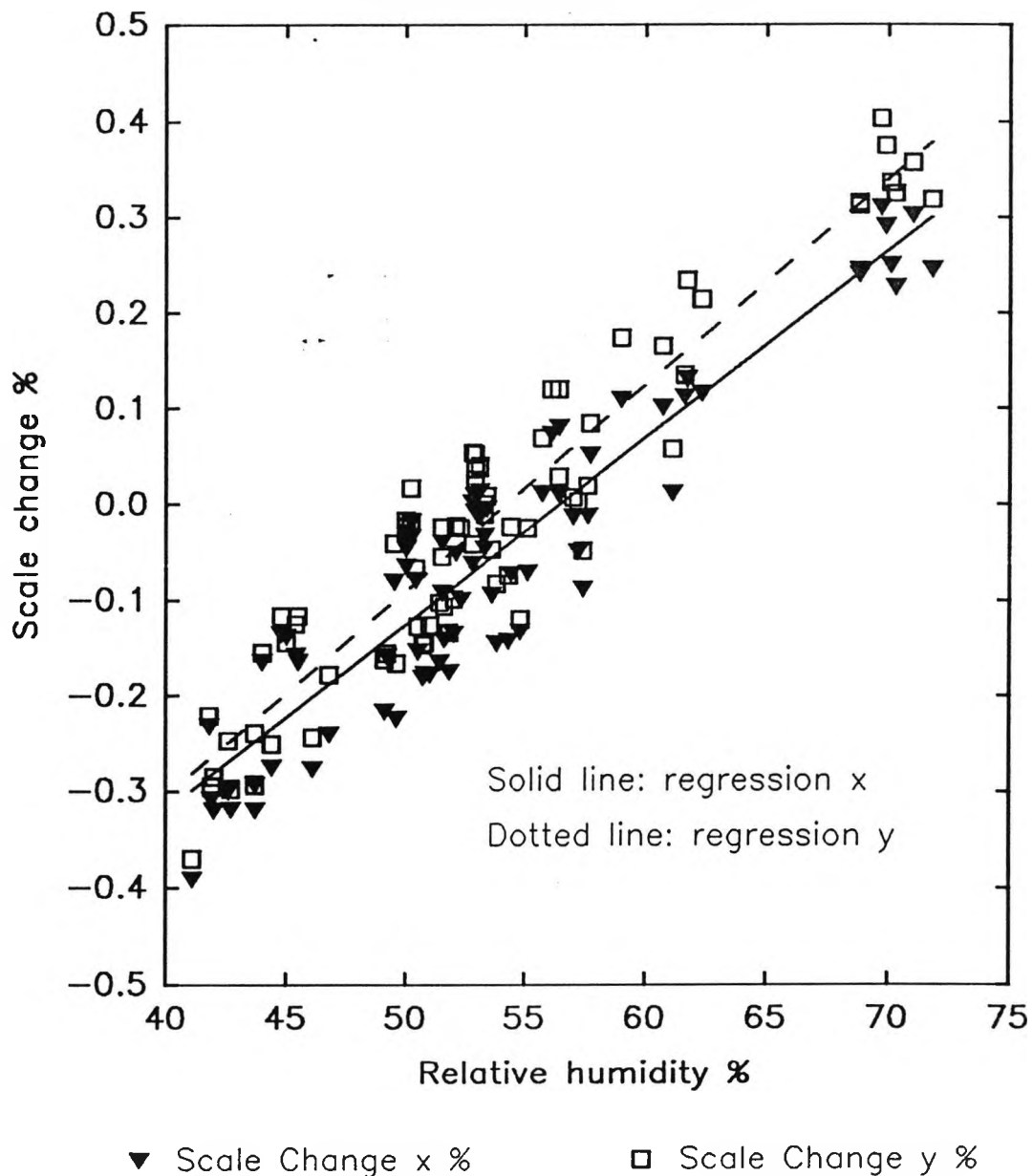


Figure 5.4.

The relationship between
scale change and relative humidity
for Kodak Technical Pan 120 roll film.

Plotted values from repeated measurement
of 48 frames from 17 rolls of film.

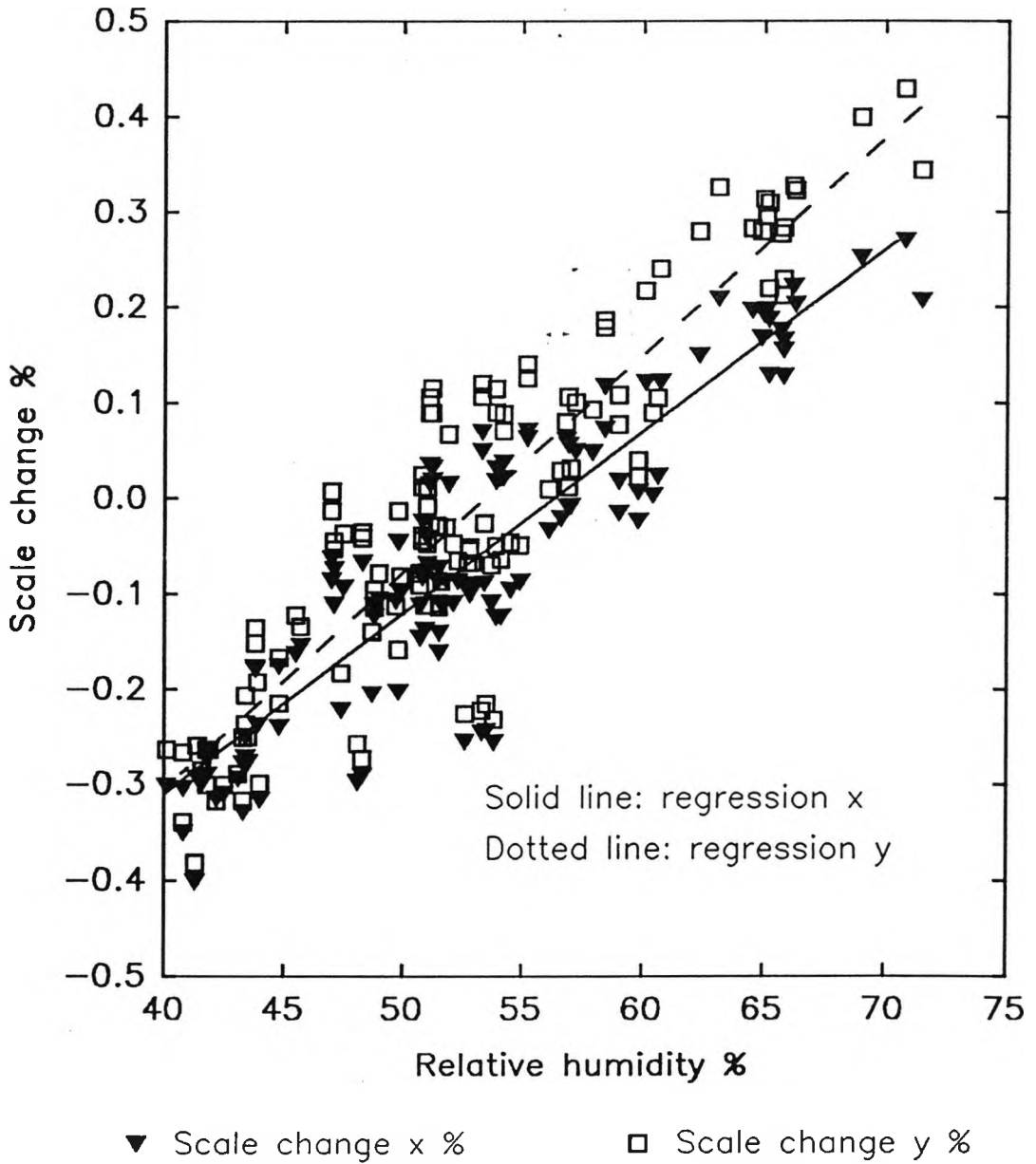
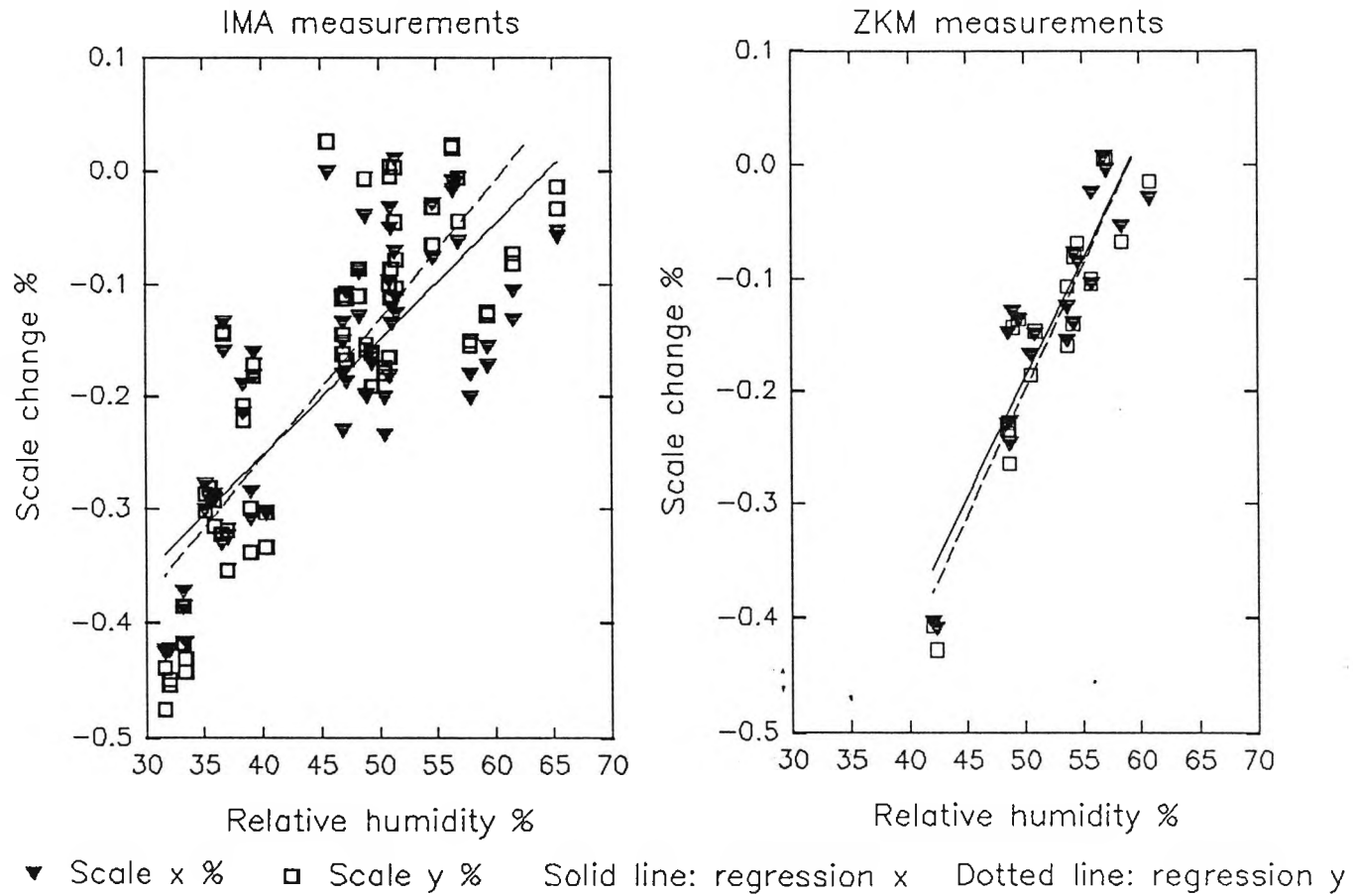


Figure 5.5.

Figure 5.6.

Graph of scale change against measurement environment relative humidity
for Ilford FP4 220 roll film

Plotted values from repeated measurements of 20 frames from 6 rolls of film.



Graph of scale change against
 measurement environment relative humidity
 for Kodak TMX, TMY and TRI-X 120 roll films.

Plotted values from repeated measurement
 of 6 frames from 2 rolls of each film type.

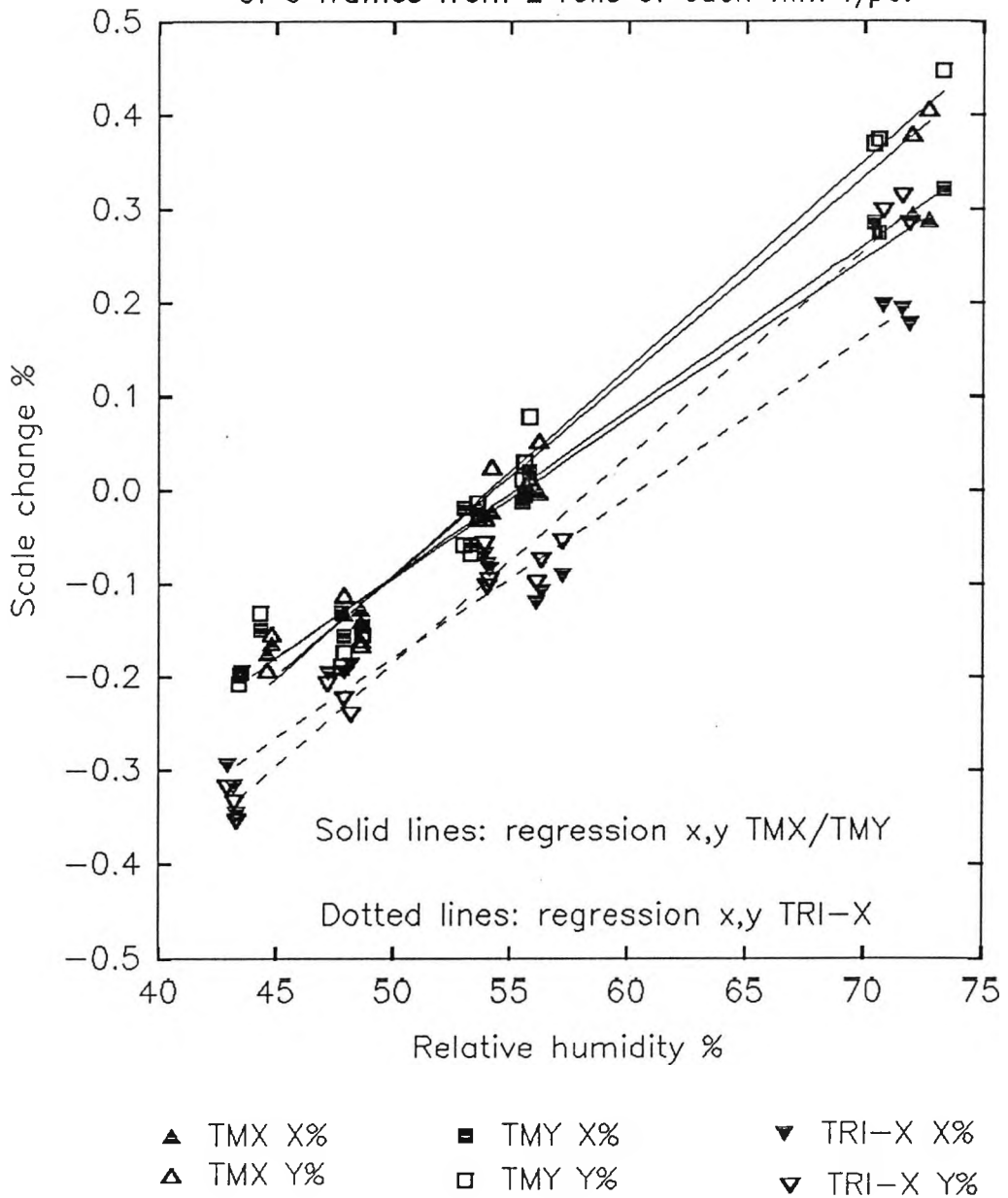


Figure 5.7.

Graph of scale change against measurement environment relative humidity for Ilford FP3 and Agfa 10E75 70mm films
 Plotted values from repeated measurements of frames from 3 rolls of each film type.

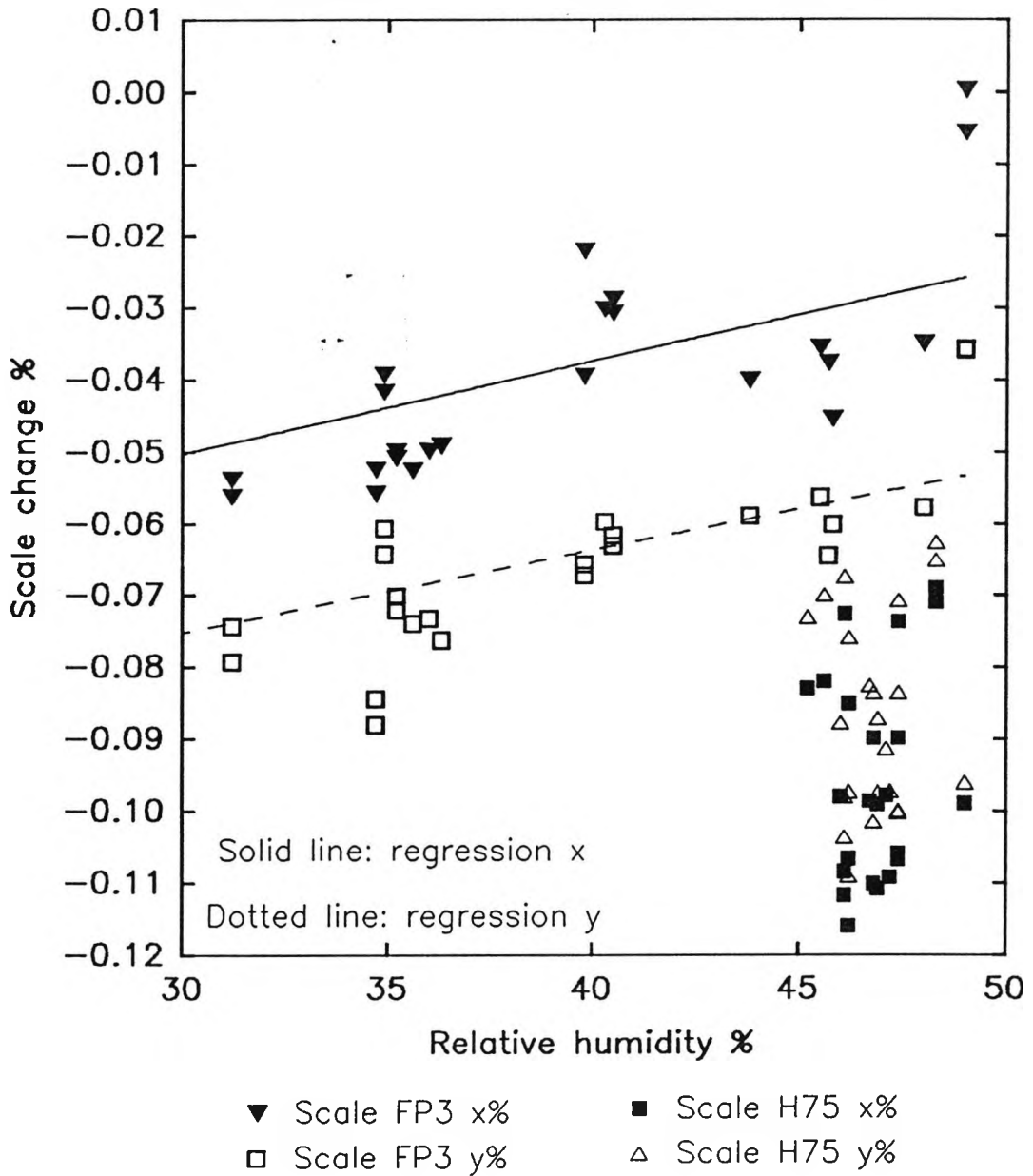


Figure 5.8.

Figure 5.6 demonstrates two similar sets of measurements for grid images on Ilford FP4 220 film. In the case of the measurement set made using the IMA, the linear approximation is less obvious, whilst those produced using the ZKM demonstrate good linearity. The main cause of the variations seen in the IMA data is the presence of both temperature and relative humidity fluctuations in this environment. A significant feature of these data and those from measurements made on Technical Pan and Pan F films, are the non-parallel regression lines, showing that the relative magnitudes of the scale changes in x and y are varying with measurement relative humidity. Table 5.4 shows that the relative scale changes in x are smaller than those in y for all the triacetate based films investigated.

Table 5.4. Regression line gradients for the scale change / relative humidity relationship.

Film	Gradient x (%scale change / 1%RH)	Gradient y (%scale change / 1%RH)
Ilford Pan F 120	0.019 ($\sigma=0.0008$)	0.027 ($\sigma=0.0010$)
Kodak Technical Pan 120	0.019 ($\sigma=0.0008$)	0.022 ($\sigma=0.0010$)
Ilford FP4 220 (IMA)	0.010 ($\sigma=0.0010$)	0.012 ($\sigma=0.0010$)
Ilford FP4 220 (ZKM)	0.021 ($\sigma=0.0021$)	0.022 ($\sigma=0.0019$)
Kodak TMAX 100 120	0.017 ($\sigma=0.0004$)	0.021 ($\sigma=0.0010$)
Kodak TMAX 400 120	0.017 ($\sigma=0.0009$)	0.022 ($\sigma=0.0011$)
Kodak Tri-X 120	0.017 ($\sigma=0.0009$)	0.022 ($\sigma=0.0007$)
Ilford FP3 70mm	0.0012 ($\sigma=0.0004$)	0.0011 ($\sigma=0.0004$)
Agfa Holotest 10E75 70mm	-0.0002 ($\sigma=0.0009$)	0.0001 ($\sigma=0.0005$)

Figure 5.7 demonstrates the range of results obtained from measurement of images on Kodak TMX, TMY and TRI-X 120 films using the ZKM measuring microscope. Again good linearity is present. The measurement epochs are separated along the relative humidity axis due to the small number of measurement sets made in the NPL environment. These three film types are all manufactured on cellulose triacetate bases and interestingly exhibit the x, y scale change differences found previously with the Pan F and Technical Pan films.

The similar gradients (Table 5.4) but dissimilar positioning of the regression lines for the TMX/Y and TRI-X data are possibly indicative of the different base thicknesses of these two types of film material. The gradients computed for each film type compare well with results due to Adelstein (1972). Unfortunately further conclusions concerning the gel/base ratios for these film types cannot be drawn because Kodak do not release gelatin thickness data.

The final graph in this series (Fig. 5.8) describes the variation of scale change against measurement relative humidity for Ilford FP3 and Agfa 10E75 70mm films. Immediately apparent

(when comparing these results with those already presented) is the well documented (Jaksic 1972; Kodak 1972) greater dimensional stability of polyester base. All the scale changes are approximately an order of magnitude smaller than those found for the cellulose triacetate based materials (Polyester: $0.1\mu\text{m}$ per 1%RH change; Triacetate: $2\mu\text{m}$ per 1%RH change).

Whilst the response of the Ilford FP3 film is approximately linear, that of the Agfa film appears almost independent of relative humidity, although the small relative humidity range prevents any definite conclusions from being drawn. The cause of this apparent difference probably lies in the different emulsion thickness used for the two films since both use a $100\mu\text{m}$ thick polyester base. Another interesting point is that for the FP3 film the shrinkage along the length of the roll (y) is significantly greater than that across the width, this may be due to recovery of stretch introduced during manufacture of its polyester film base (Section 2.1.2.2).

5.3.1.2. Inhomogeneous changes.

A selection of typical local changes associated with each film type, from measurements made at NPL, are demonstrated in figures 5.9 and 5.10. Figure 5.9 represents an image on Technical Pan and two images on Pan F measured over a two month period. Two levels of grid density (corresponding to 2.5mm and 5mm separations) have been used. In both pairs of data the deformations are of similar magnitude and pattern, indicating that over the one month storage period (despite changes in environment) little inhomogeneous change has occurred. Furthermore if the sampling of the higher density grid is decreased to the 5mm separation little information as to the systematic trends in the data will be lost. These results justify the decision to conduct all in-plane grid measurements at a 5mm separation (121 points), conferring reduced measurement time and consequently the ability to investigate a greater variety of process variables.

An important point is that the localised deformations appear predominantly independent of relative humidity and temperature changes in the measurement environment. As such these changes must be caused at an earlier stage in the photographic process.

This section must be restricted to generalised comments about the local deformations because the vector plots presented here have been produced from images which have undergone differing treatments.

Both images made on Ilford Pan F 120 film, despite exhibiting some local regions of systematic deformation (up to about $5\mu\text{m}$) are surprisingly homogenous. RMS values for both of these images (1.1(x), 1.4(y) and 1.5(x), 1.6(y) μm) approach the measurement accuracy of the ZKM measuring microscope (approximately $0.5\mu\text{m}$ RMS). The vector plot derived from the image on Technical Pan 120 film exhibits a clear systematic pattern with associated RMS residuals of 1.98(x) and 2.72(y) μm . If the vector plots from images made onto Technical Pan film are evaluated

(Appendix A) in many cases similar configurations can be seen, despite differing photographic treatments. There seem to be two possible causes for this type of deformation: unflatness at exposure; and/or an inability of the 90 μm triacetate base to withstand stresses introduced into the emulsion layers during the photographic process.

Figure 5.10 shows a vector plot from each of the TMAX, TMAX 400 (TMY) and TRI-X (TRX) films investigated. It can be seen that these plots contain residual vectors of similar magnitude to those on FP4 220 and PAN F 120 films. The image on TMY frame E1 (illustrated) contains a large systematic effect. If the vector plots associated with some of the TMY images in appendix A are examined it can be seen that one other image (two out of six) also contains a large systematic vector field. The cause of these effects is not clear, but possible sources are lack of contact with the master grid at exposure, handling during exposure or possibly an uneven base.

The frame on Agfa Holotest 10E75 film has RMS residuals in x and y of 0.77 μm and 0.98 μm respectively. All grid exposures made on to this material have produced similar results which probably represent the noise level of the experimental procedure. The greater deformations seen from exposures made onto FP3 aerial film, also with a 100 μm polyester base, are attributable to its lower resolving power (100 l mm^{-1} as opposed to 3000 l mm^{-1}), and therefore a decreased ability to point accurately to grid image nodes with the measuring graticule.

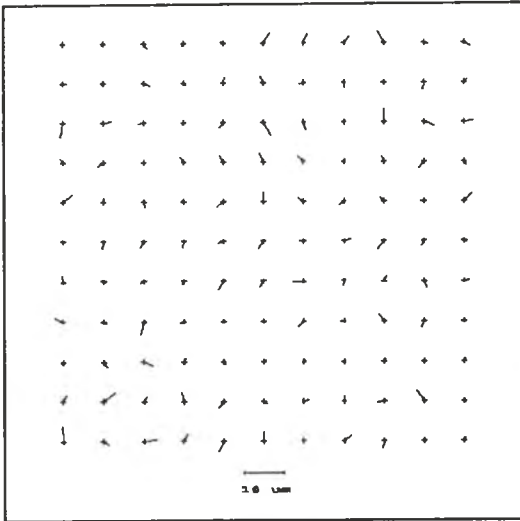
Table 5.5. Mean RMS residuals for all film types investigated.

Film type	RMS residual x(μm)	RMS residual y(μm)
Ilford Pan F 120	1.28 ($\sigma=0.23$)	1.71 ($\sigma=0.31$)
Kodak Technical Pan 120	1.39 ($\sigma=0.44$)	1.51 ($\sigma=0.40$)
Ilford FP4 220	1.69 ($\sigma=0.41$)	1.90 ($\sigma=0.43$)
Kodak TMAX 100 120	1.26 ($\sigma=0.20$)	1.74 ($\sigma=0.18$)
Kodak TMAX 400 120	1.67 ($\sigma=0.50$)	2.05 ($\sigma=0.70$)
Kodak Tri-X 120	1.64 ($\sigma=0.19$)	2.03 ($\sigma=0.24$)
Ilford FP3 70mm	1.36 ($\sigma=0.13$)	1.73 ($\sigma=0.18$)
Agfa Holotest 10E75 70mm	0.84 ($\sigma=0.09$)	1.19 ($\sigma=0.09$)

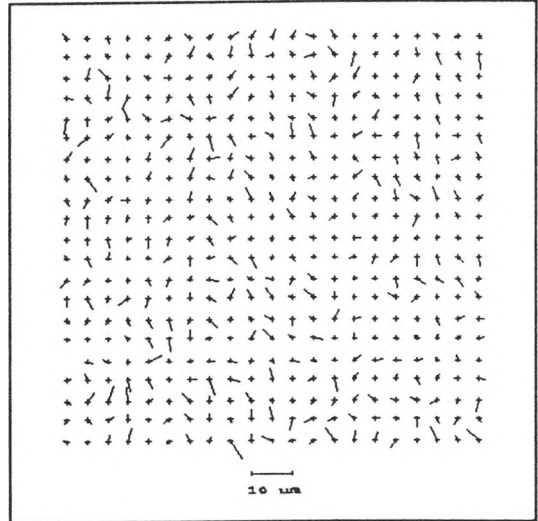
The mean RMS residuals for each film type and their associated standard errors are detailed in table 5.5. There is a broad link with resolving power and RMS mean deformation. Emulsions with high resolving power, such as Technical Pan and Holotest 10E75 have the lowest RMS residuals, whilst those for the fast films (TMY, FP3 and TRI-X) are higher. The standard deviations give an indication as to the variability between the frames in the set. As mentioned above TMY and Technical Pan have the highest variability resulting from physical deformations, whilst the variability of images on FP4 220 film can be linked to the measurements made on the IMA (Fig. 5.6).

Selection of contact grid exposures made onto Ilford Pan F 120
and Kodak Technical Pan 120 films at 5mm and 2.5mm grid spacings.

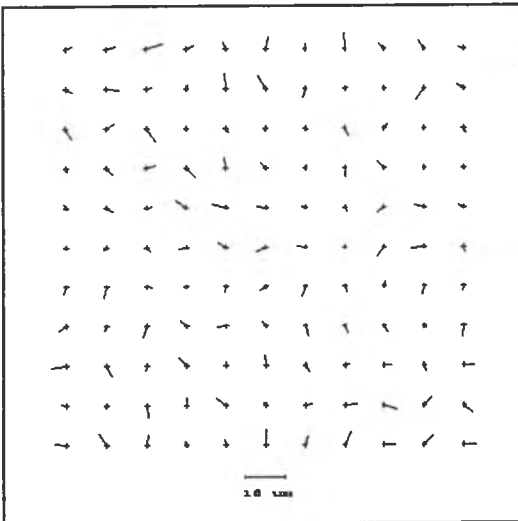
PAN F, Frame B3, Measurement 4.



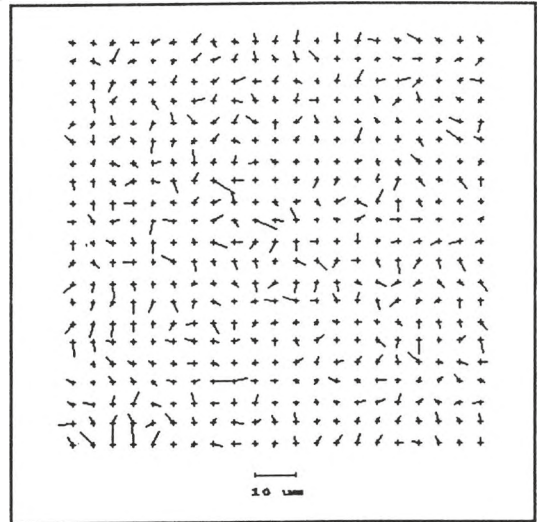
PAN F, Frame B3, Measurement 5.



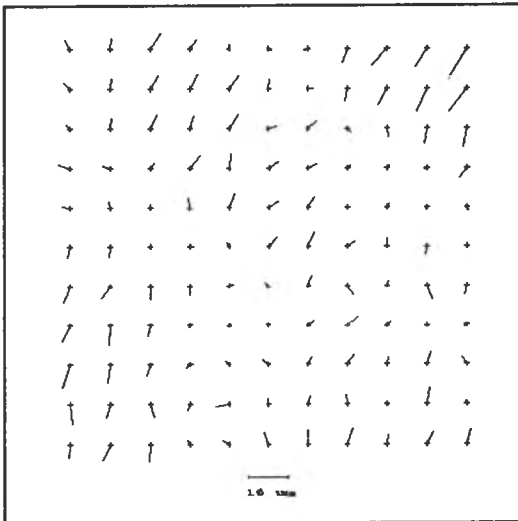
PAN F, Frame I2, Measurement 2.



PAN F, Frame I2, Measurement 3.



TCP, Frame F1, Measurement 4.



TCP, Frame F1, Measurement 5.

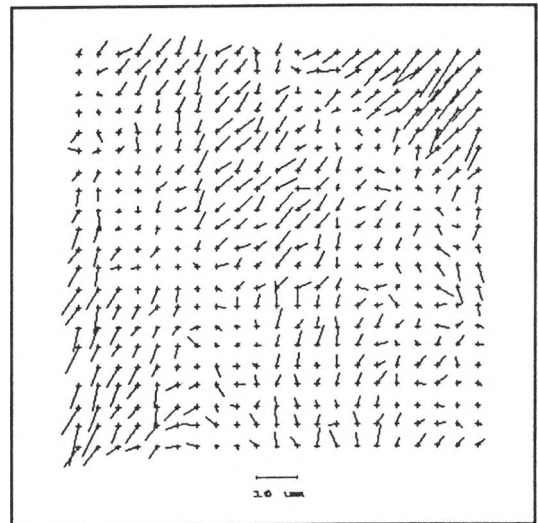
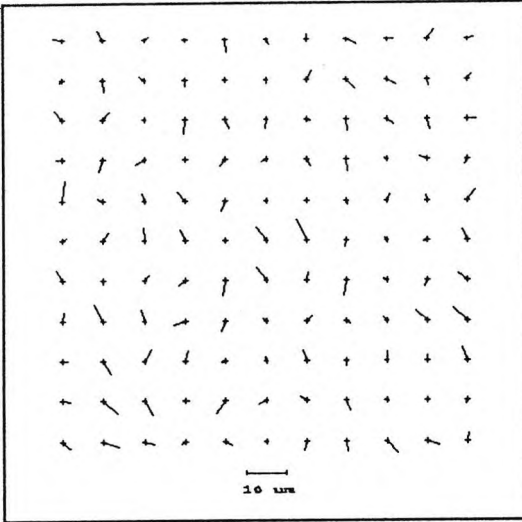


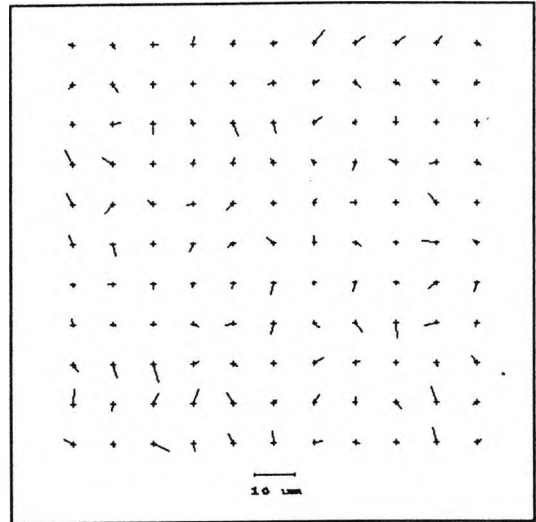
Figure 5.9.

Selection of contact grid exposures made onto Kodak TMX 120, TMY 120,
TRI-X 120, Ilford FP3 70mm and Agfa Holotest 10E75 70mm films.

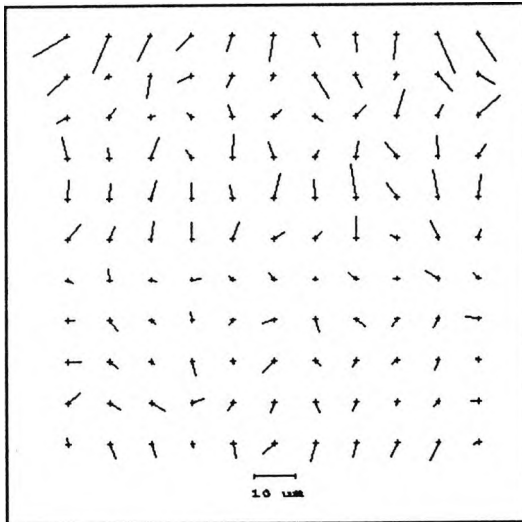
FP4 220, Frame I3, Measurement 2.



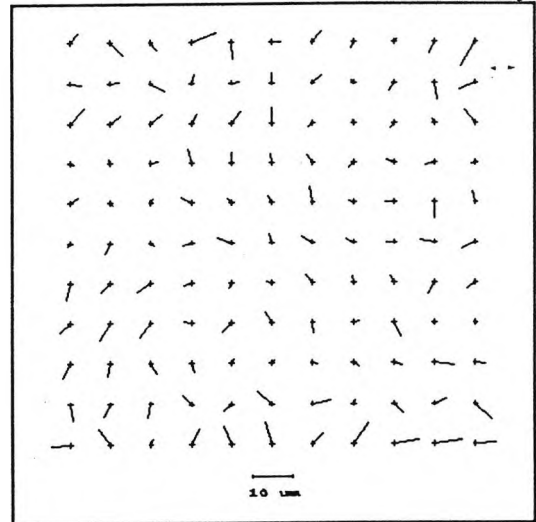
TMX, Frame D2, Measurement 1.



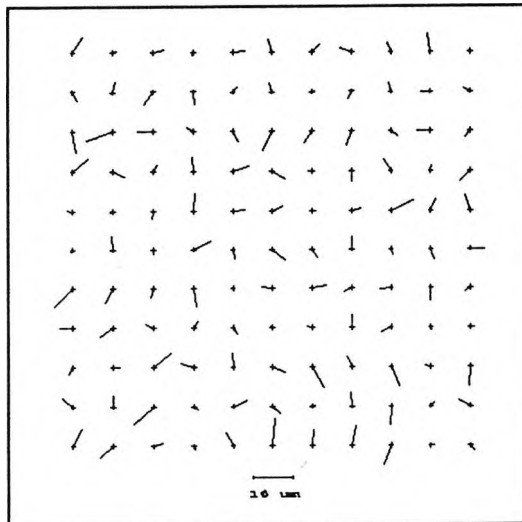
TMY, Frame E1, Measurement 2.



TRX, Frame A3, Measurement 2.



FP3, Frame A1, Measurement 2.



HT75, Frame A1, Measurement 2.

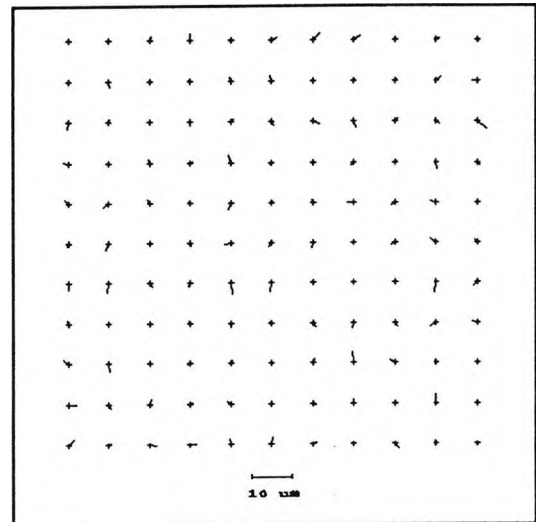


Figure 5.10.

5.3.1.3. Summary of the measurement relative humidity and scale change relationship.

A summary of the variations between film types is difficult to make due to the number of different factors operating. The main points arising are that the global changes appear to follow a linear relationship, albeit with small variations which may be caused by hysteresis (Section 5.3.6). The local deformation patterns for the images discussed appear to be largely independent of measurement environment changes over the 40% to 70%RH range investigated. If true (Section 5.3.5.2) this second factor could be used to advantage for most small format photogrammetric measurement situations, since a reseau image on a given frame need only be measured once and can then be associated with that frame for subsequent measurements as required.

Based on results at two grid densities, measurement of the grid has been standardised at a spacing of 5mm, giving 121 measurement points over the 60mm square image. In this way much of the information from the 2.5mm spacing can still be identified but measurement time is quartered allowing a greater range of factors to be investigated.

The 100 μ m polyester base and thin (7 μ m) emulsion of Agfa Holotest 10E75 has provided the smallest changes with relative humidity. It should be mentioned that Holotest film, although possessing excellent dimensional qualities is confined in its photogrammetric application to a very specific range of tasks. A binary image limited only by the optical properties of the camera lens is produced, but at the expense of emulsion speed. From tests carried out at City University during the course of these investigations, the speed of Agfa Holotest 10E75 has been found to be equivalent to about 3 ISO. Applications are therefore restricted to static cameras and low contrast subjects or flash exposure situations, for example in high precision monitoring using retro-targets, (Cooper and Robson 1990).

Changes with temperature have not been specifically investigated since in both of the measurement environments relative humidity could not be controlled sufficiently well to allow temperature to be the only variable.

5.3.2. Storage of film prior to and at exposure.

Since photographic equipment generally has to be taken to the subject, photogrammetric surveys are conducted under a very wide range of practical conditions. If the results of this analysis are to be applied to practical work, it is necessary to investigate the dimensional effects of changes in the film's pre-exposure environmental history. The following experiments have therefore been conducted with a view to producing a standard procedure which not only minimises local deformations but which can be applied in practical situations.

Historically, Byer among others (Section 2.4.3) has looked at uniform scale change differences, deriving differing hysteresis curves for processed and un-processed films using pin gauge measurement. Obviously un-processed film cannot be examined using a grid exposure technique, instead the effect of differing pre-exposure conditioning on the end result of the whole photographic process was investigated. The specific aim of this experiment was therefore to determine if pre-exposure conditioning influenced the magnitude of inhomogeneous deformations.

In this experiment (10) one pair of Technical Pan 120 films (K&L) was stored in a freezer (in its packaging the standard for all experiments) and a second pair of films (M&N) was stored on processing spirals in the measurement environment for three days prior to exposure. The frozen film was transferred from the freezer to the measurement environment one hour before exposure. After exposure the films were processed in the same batch using the regime detailed in table 5.6. The experiment was repeated one week later under a slightly different measurement environment and with a non-hardening fixing bath.

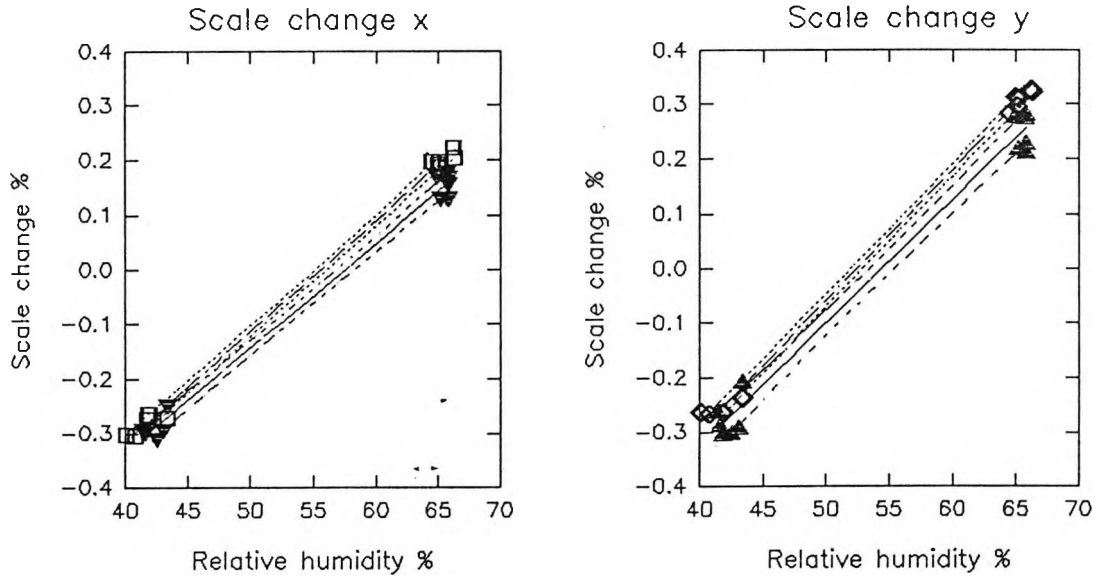
Table 5.6. Pre-exposure conditioning treatments.

Treatment	Experiment 10, Rolls 35,36,37,38.		Experiment 11, Rolls 39,40,41,42.	
Film Type	TCP K&L	TCP M&N	TCP O&P	TCP Q&R
Pre-Exposure	1 Hour	3 Days	1 Hour	3 Days
Exposure	11/9/89 59.6%RH 21.2°C		19/9/89 51.4%RH 21.2°C	
Processing	D19 Small Tank 4.5 min at 21°C		D19 Stock Solution 4.5 min at 21°C	
	Hardening Fix 5 min at 21°C		Non-Hardening Fix 5 min at 21°C	
	Wash in running water for 30 min at 21°C		Wash in running water for 30 min at 21°C	
Drying	IMA 63.3%RH 20.2°C		IMA 50.7%RH 19.7°C	
Measurement	NPL 12/9/89 and 14/9/89		NPL 20/9/89 and 28/9/89	

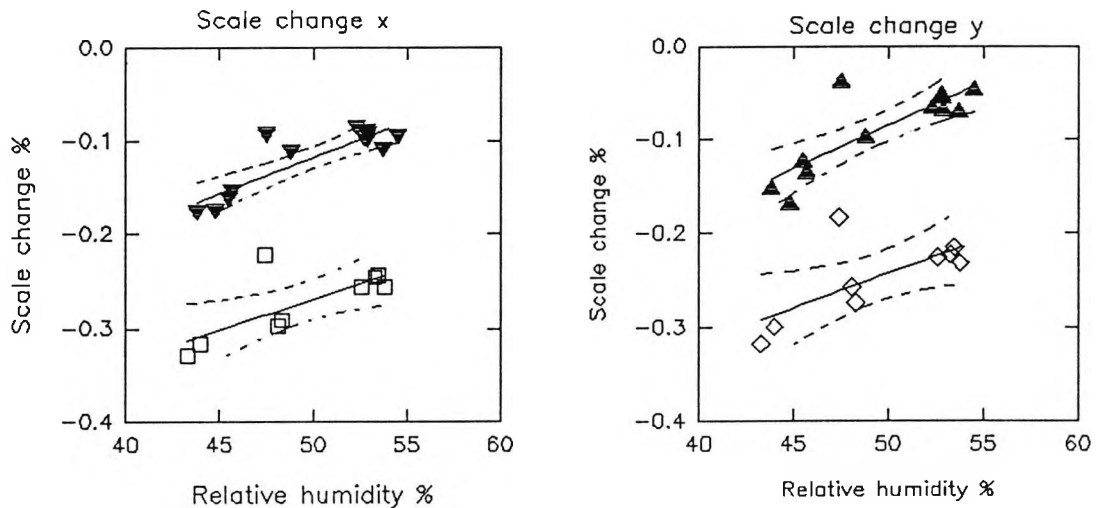
5.3.2.1. Scale changes.

Figure 5.11 details the uniform scale changes associated with the two sets of data. The regression lines with their 95% confidence intervals show that the treatments have given rise to significant differences in image size. Within each data set pre-exposure treatment was the only variable such that these differences (which are similar in both x and y directions) must be due to dissimilarities in film size at exposure. The insignificant variations in gradient are also indicative that the differences in image size are due to the pre-exposure conditioning treatments.

The effect of increasing pre-exposure conditioning time
on the relationship between scale change and relative humidity
Kodak Technical Pan 120 film, rolls K,L,M and N.



Kodak Technical Pan 120 film, rolls O,P,Q and R



(Dotted lines show regression with 95% confidence)

- ▼ Scale change x% 30 min
- ▲ Scale change y% 30 min
- Scale change x% 3 days
- ◇ Scale change y% 3 days

Figure 5.11.

A comparison between the two data sets shows that whilst the results from the one hour conditioned films are similar, (approximately 0.1% at 50%RH) the three day conditioned films demonstrate differing scale changes for a given relative humidity. This difference (about 1.5% at 50%RH) could easily be due to the 10% Relative Humidity disparity at exposure, however there are two further differences in the processes. Firstly data set one used a hardening fixing bath, and secondly there is a 13%RH difference in the post-wash drying environments which could have contributed to the change. The contributions from both of these variables are described in detail in sections 5.3.4.2 and 5.3.4.3 respectively.

5.3.2.2. Local residuals.

The only valid conclusions concerning the effect of pre-exposure conditioning on the magnitude of local deformations are those that can be drawn by comparison between films which have undergone exactly the same process.

Table 5.7. RMS residuals from pre-exposure conditioning treatments.

Treatment	RMS residual x(μm)	RMS residual y(μm)
Set 1 TCP K&L (1 Hour)	1.42 ($\sigma=0.60$)	1.59 ($\sigma=0.33$)
Set 1 TCP M&N (3 Days)	1.46 ($\sigma=0.47$)	1.68 ($\sigma=0.48$)
Set 2 TCP O&P (1 Hour)	1.16 ($\sigma=0.22$)	1.44 ($\sigma=0.24$)
Set 2 TCP Q&R (3 Days)	1.24 ($\sigma=0.20$)	1.30 ($\sigma=0.16$)

Table 5.7 demonstrates RMS residuals after affine transformation (and their associated standard deviations) for both sets of pre-exposure measurement data. Statistical t-tests (Section 4.3.1) carried out on the data to determine whether the means of the samples are equal (null hypothesis) or unequal (alternative hypothesis) have been made. In all cases the null hypothesis was accepted showing that there are no significant difference between RMS residuals within each data set at 95% confidence.

The RMS residuals are a global measure of the local deformations of all grid measurements made for each data set. As such they cannot be used to detect any deformation patterns on individual frames. To investigate such patterns, for example to detect any evidence of differential conditioning, the individual vector plots must be analyzed. Some vector plots associated with these data have been included in appendix A, but four representative plots are included at this point (Fig. 5.12) for specific mention.

The top two plots in the figure are from frames which have undergone the full 3 day conditioning procedure, whilst the lower two have been conditioned for only one hour. The vectors demonstrate that systematic deformations are present, with maximum distortions of the order of

8 μ m. Since both deformed and nominally un-deformed frames are present in both measurement sets, it must be concluded that the major patterns seen are not being caused by the differences in pre-exposure conditioning.

Additionally there are images, (e.g. frame R1) which exhibit regions of systematic deformation of the order of 3 to 5 μ m. Again these images are not confined to one particular treatment set. Since very homogeneous images were obtained on polyester based Agfa 10E75 film (Section 3.5.1.2) verifying the experimental method, the inference is that these small deformations represent the limit of stability which can be expected from films on thin cellulose tri-acetate base.

Some contact grid exposures made onto Kodak Technical Pan 120 film with varying pre-exposure conditioning time.

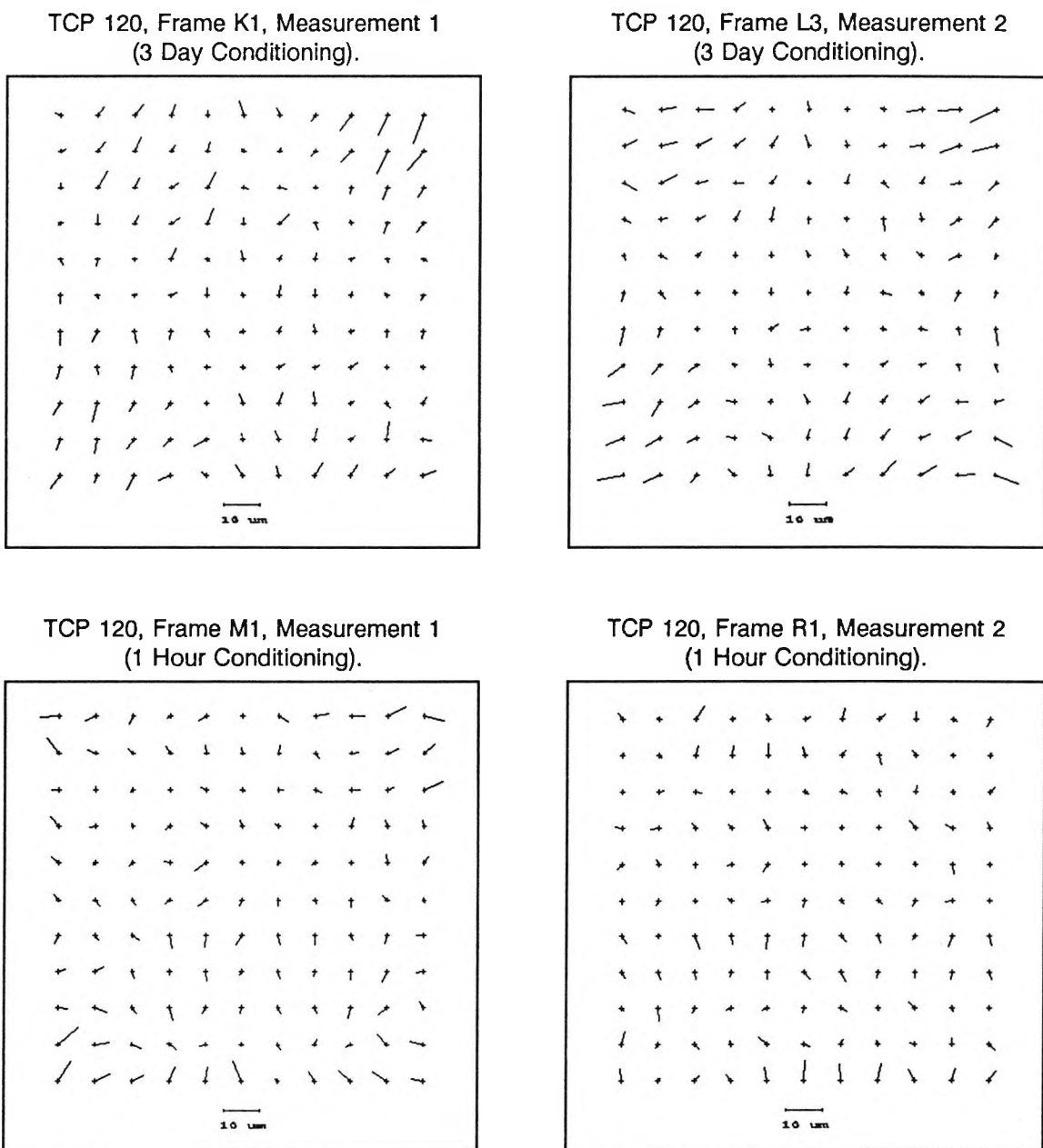


Figure 5.12.

The first part of the book is devoted to a general survey of the history of the United States from the discovery of the continent to the present time. It is written in a clear and concise style, and is well adapted for use in schools and colleges.

The second part of the book is devoted to a detailed account of the political and social conditions of the United States at the present time. It is written in a clear and concise style, and is well adapted for use in schools and colleges.

THE UNIVERSITY OF CHICAGO PRESS

The third part of the book is devoted to a detailed account of the political and social conditions of the United States at the present time. It is written in a clear and concise style, and is well adapted for use in schools and colleges.

The fourth part of the book is devoted to a detailed account of the political and social conditions of the United States at the present time. It is written in a clear and concise style, and is well adapted for use in schools and colleges.

The fifth part of the book is devoted to a detailed account of the political and social conditions of the United States at the present time. It is written in a clear and concise style, and is well adapted for use in schools and colleges.

5.3.2.3. Summary of pre-exposure storage investigation.

Although pre-exposure conditioning controls do not appear (from these limited results) to be strictly necessary for control of local deformations, any conditioning will affect the scale of individual images. These scale changes can be removed by use of a few reference marks, but it is better to ensure that all frames from a survey receive similar pre-exposure treatment. Such pre-exposure treatment would be especially significant if mean corrections or no explicit refinements based on reference mark positions are made to the image coordinate data.

The handling of the roll film packaging seems particularly important for practical survey situations, because the foil packages used provide some measure of control over the film water content (Kodak 1989). A procedure should therefore attempt to preserve the moisture level at which the film was sealed by maintaining the manufacturers' foil packaging intact until immediately prior to exposure. Given the high correlation between the 1 hour pre-conditioned films it is probably advantageous to keep film chilled until shortly before use, to the extent of using a proprietary film chill box on site.

5.3.3. Exposure level and uniformity.

In this section the results from experiments 7 and 8, an investigation into the effects of different image densities on local dimensional changes are presented. Any dimensional changes in areas of differing density could have a significant effect on surveys intended for deformation analysis. For example in most situations the image of the object being deformed is often formed at one density, whilst the static control system outside this area is commonly against an background of different image density.

Literature searches conducted by the author have not turned up any references specifically investigating the dimensional effects of changes in the physico-chemical structure of the emulsion layers caused by the development process. In areas of high density (increased exposure) much filamentary silver is produced (Section 2.2.2) and in regions of low density unexposed silver halide is removed by the fixing solution (Section 2.2.3). If areas of high and low density are included in the image then it is reasonable to conclude that any changes in dimensional properties will be manifest along dividing lines between such regions. This analysis is consequently being conducted to test the assumption that changes in emulsion microstructure give rise to changes in physical properties which alter the local deformation patterns.

Using the grid contact method, changes in exposure can easily be made by taping neutral density (N.D.) filters to the reverse side of the glass master grid. Table 5.8 describes the various exposure configurations made onto Pan F and Technical Pan 120 films.

[Faint Title]

[Faint Header 1]			[Faint Header 2]		[Faint Header 3]
[Faint Cell 1.1]	[Faint Cell 1.2]	[Faint Cell 1.3]	[Faint Cell 2.1]	[Faint Cell 2.2]	[Faint Cell 3.1]
[Faint Cell 1.1]	[Faint Cell 1.2]	[Faint Cell 1.3]	[Faint Cell 2.1]	[Faint Cell 2.2]	[Faint Cell 3.1]
[Faint Cell 1.1]	[Faint Cell 1.2]	[Faint Cell 1.3]	[Faint Cell 2.1]	[Faint Cell 2.2]	[Faint Cell 3.1]
[Faint Cell 1.1]	[Faint Cell 1.2]	[Faint Cell 1.3]	[Faint Cell 2.1]	[Faint Cell 2.2]	[Faint Cell 3.1]
[Faint Cell 1.1]	[Faint Cell 1.2]	[Faint Cell 1.3]	[Faint Cell 2.1]	[Faint Cell 2.2]	[Faint Cell 3.1]
[Faint Cell 1.1]	[Faint Cell 1.2]	[Faint Cell 1.3]	[Faint Cell 2.1]	[Faint Cell 2.2]	[Faint Cell 3.1]
[Faint Cell 1.1]	[Faint Cell 1.2]	[Faint Cell 1.3]	[Faint Cell 2.1]	[Faint Cell 2.2]	[Faint Cell 3.1]
[Faint Cell 1.1]	[Faint Cell 1.2]	[Faint Cell 1.3]	[Faint Cell 2.1]	[Faint Cell 2.2]	[Faint Cell 3.1]
[Faint Cell 1.1]	[Faint Cell 1.2]	[Faint Cell 1.3]	[Faint Cell 2.1]	[Faint Cell 2.2]	[Faint Cell 3.1]
[Faint Cell 1.1]	[Faint Cell 1.2]	[Faint Cell 1.3]	[Faint Cell 2.1]	[Faint Cell 2.2]	[Faint Cell 3.1]

[Faint paragraph of text]

[Faint Section Header]

[Faint paragraph of text]

Table 5.8. Exposure level and uniformity variations

Treatment	Experiment 10, Rolls 23,24.		Experiment 11, Rolls 28,29,30.		
Film	PAN F 120 Roll G	PAN F 120 Roll H	TCP 120 Roll J	PAN F 120 Roll I	PAN F 120 Roll J
Exposure	20/7/89		15/8/89 47.1%RH 24.0°C		
Number of exposure densities	Frame 2:3D	Frame 1:3D Frame 2:3D Frame 3:3D	Frame 1:3D Frame 2:3D Frame 3:3D	Frame 1:2D Frame 2:2D Frame 3:1D	Frame 1:3D Frame 2:3D Frame 3:1D
Processing	ID11 1:1 6 min at 25°C		ID11 1:1 8 min at 22°C		
	Non-Hardening Fixer 5 min at 25°C		Hardening Fixer 5 min at 22°C		
	Wash 30 min at 25°C		Wash 30 min at 22°C		
Drying	IMA		IMA 51.5%RH 20.8°C		
Measurement	NPL 1/8/89, 2/8/89, 8/8/89, 10/8/89		NPL 17/8/89 and 18/8/89		

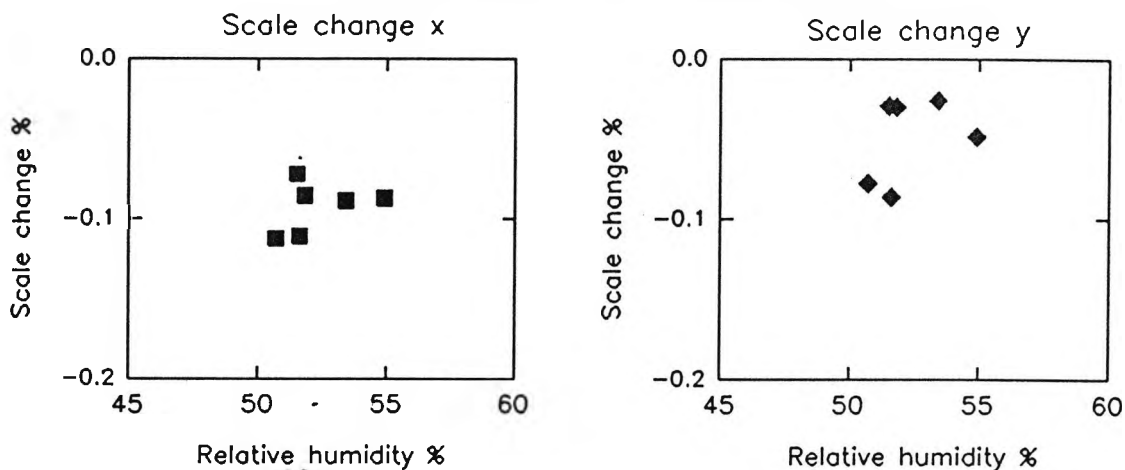
Where a uniform (1D) control exposure was made the standard contact printing procedure was used. In the dual density case (2D) a 0.3 N.D filter (1 stop) was taped diagonally across the back of the glass master. By fixing the filter to the glass master, the exposure gradient coincided with the same grid positions for each exposure enabling direct comparison between frames to be made. To provide three different densities a 0.6 N.D (2 stops) filter was introduced, the filters being taped diagonally so as to divide the format into thirds. To enable direct comparison, tests were conducted so that the same time exposure could be given for all filter permutations. The experiments were repeated to determine whether the results were typical.

5.3.3.1. Homogeneous changes.

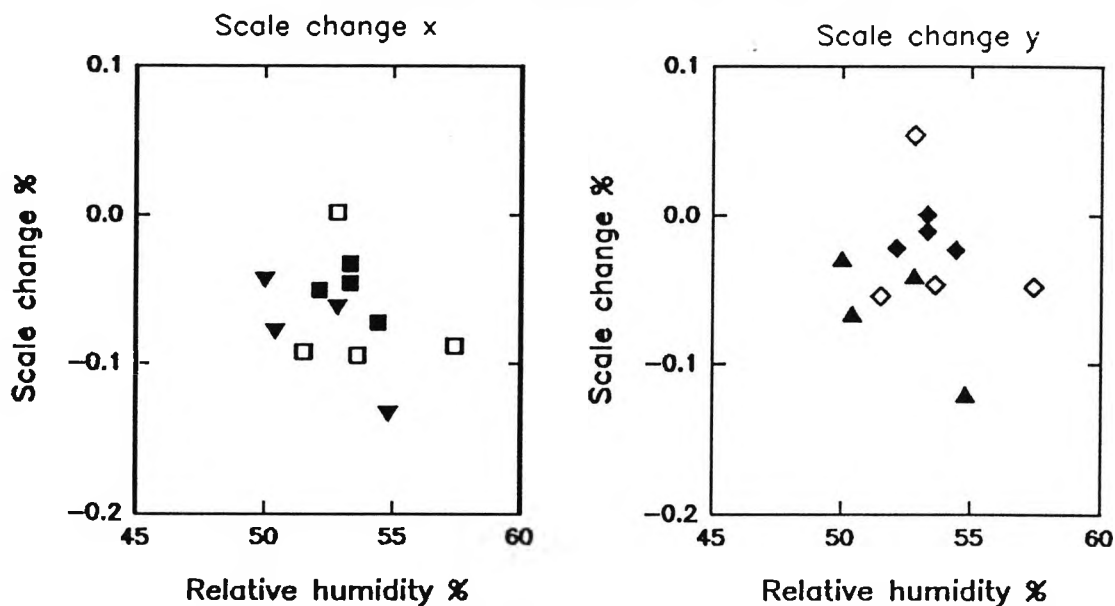
Due to the small number of repeat image measurements made in this experiment, it is difficult to assess the effect of image density on the relationship between scale change and measurement environment relative humidity. Results are illustrated in figure 5.13 where it can be seen that the range of scale change for all treatments is about 0.1%. This scale range is analogous to that found for all measurements made on these film types over the complete range of relative humidity, consequently no atypical scale changes can be identified in this data set.

The effect of variation of exposure level on the scale change at measurement / relative humidity relationship.

Kodak Technical Pan 120 film, roll J.



Ilford PAN F 120 film, rolls G,H,I and J.



- ▼ Scale x% uniform exposure
- Scale x% two exposure levels
- Scale x% three exposure levels.
- ▲ Scale y% uniform exposure
- ◇ Scale y% two exposure levels
- ◆ Scale y% three exposure levels

Figure 5.13.

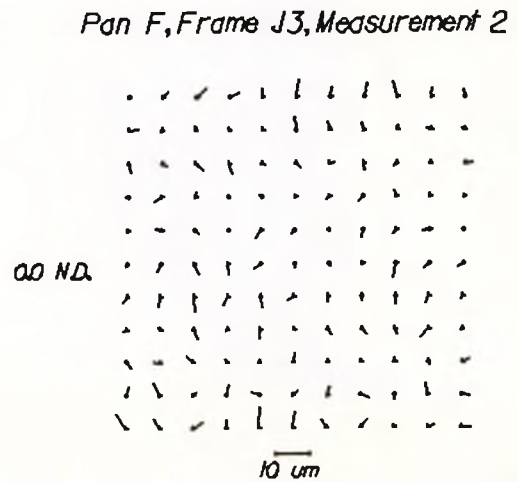
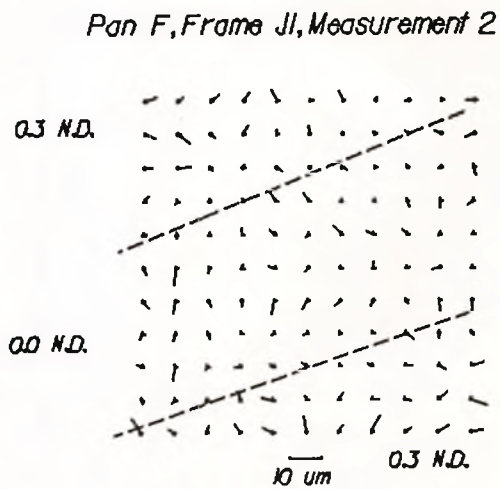
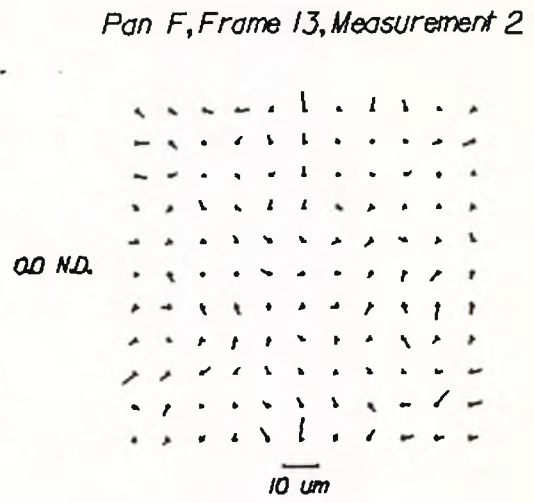
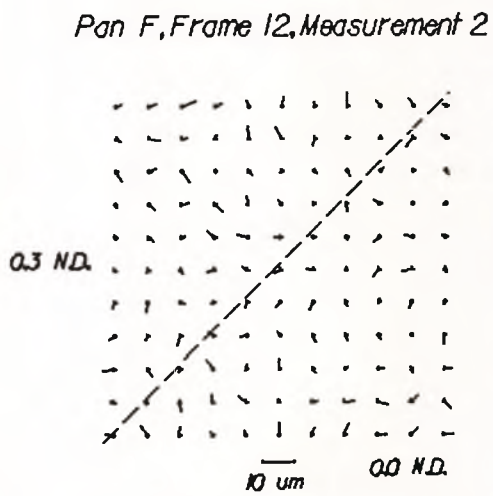
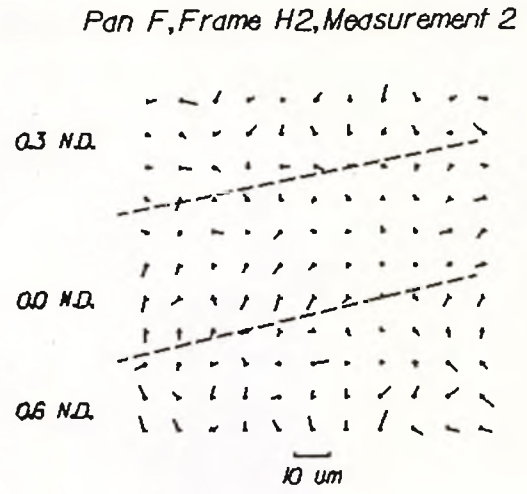
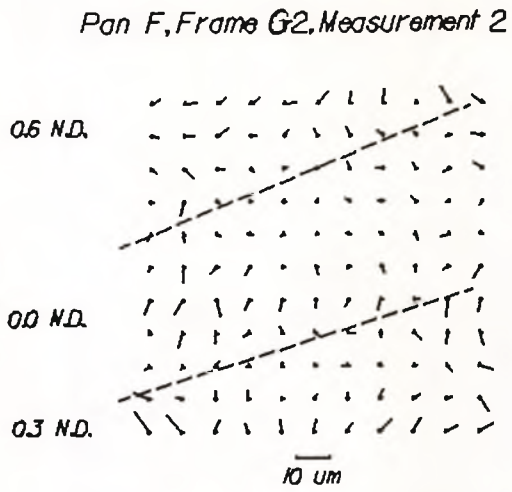


Figure 5.14. Variation of in-plane deformation with image density variation.

5.3.3.2. Inhomogeneous changes.

Figure 5.14 shows some of the vector fields and their associated exposure regions, derived from the tests carried out. Whilst areas of systematic deformation can be identified in all images, there are no clear visual similarities between these patterns and the exposures given. This lack of correlation is especially obvious when the uniformly exposed frames are considered (these were processed in the same batch).

The means of the RMS plate residuals (Table 5.9) were compared by applying t-tests to the data. For all exposure treatment sets the means in x or in y were equal at the 95% confidence interval used, indicating that there were no significant local differences at the grid density used. Similar comparisons conducted between the frames on Technical Pan Film and those on Pan F from the same data set demonstrated that the RMS residuals on Technical Pan film were significantly smaller, possibly due to its increased resolving power (Section 2.3.3.3).

Table 5.9. RMS residuals from exposure variation treatments.

Treatment	RMS residual x(μm)	RMS residual y(μm)
Ex.10 PNF G,H (3D)	1.65 ($\sigma=0.23$)	2.24 ($\sigma=0.20$)
Ex.11 PNF J (3D)	1.52 ($\sigma=0.32$)	1.93 ($\sigma=0.11$)
Ex.11 PNF I (2D)	1.40 ($\sigma=0.25$)	1.88 ($\sigma=0.18$)
Ex.11 PNF I&J (1D)	1.38 ($\sigma=0.20$)	2.01 ($\sigma=0.21$)
Ex.11 TCP J (3D)	1.11 ($\sigma=0.10$)	1.43 ($\sigma=0.22$)

T-tests conducted with the paired x, y data from each treatment generally showed that these means were not equal at 95%. All RMS residuals in the y direction are greater, implying that there are significant differences between the x and y local deformations. The reason for this discrepancy is possibly a physical film deformation effect, but as mentioned in section 5.3.1.1 tests of the ZKM measuring equipment at NPL have shown that its repeatability in the x direction is better than that in the y direction, (Oldfield, 1990).

5.3.3.3. Summary of exposure uniformity experiments.

This series of experiments has shown that for the grid density and exposure variation used, no local deformations caused by changes in exposure level could be detected. The analysis has however pointed to several opportunities for further work, for example increasing grid density to allow a link to be made between micro-image density variations and visual edge detection for target recognition. A localised analysis using moiré methods would enable the effect of the presence of dust to be evaluated, possibly providing a physical explanation for the apparently random deformation vectors seen in some of the vector plots.

5.3.4. Processing conditions.

As mentioned in sections 2.22 and 2.23, the elements of the photographic process were (as far as possible) held constant to provide manufacturers recommended procedures for pictorial photography. The following variations, those expected to provide the major contributions to dimensional change (Chapters 1 and 2), were investigated.

a) Developer variation.

The variation of development for tonal control, enabling the matching of the negative material characteristic curve to the subject luminance range, can only be valid if changes in the developer solution do not cause adverse dimensional change. The dimensional effects of varying developer formulation for Technical Pan and Pan F films were investigated, for a range of developers which might commonly be used for photogrammetric survey photography.

b) Fixer formulation.

Theoretically (Section 2.2.3), the addition of a hardening agent to the fixing solution should increase the stability of the gelatin emulsion layers with respect to changes in environmental parameters. The contribution of an inorganic hardening agent is evaluated in this section using a range of cellulose triacetate based films.

c) Drying temperature.

According to Kodak (1972b) overdrying produces (on reconditioning) oversize negatives. The use of a drying cabinet as opposed to drying the film in the measuring environment is investigated. Conditioning time after washing is also evaluated, since this is an important consideration when measurement turn-around time is of importance.

5.3.4.1. Variation of developer formulation.

In chapter 2 it was described how developer formulations could be varied thereby altering the shape of the negative material characteristic curve to match the subject luminance range for optimised photogrammetric recording. In this section, results from an experiment are presented in which some different developing solutions were used. Table 5.10 details the process parameters applied to uniform grid exposures made onto Pan F and Technical Pan 120 films.

Three developer formulations were chosen for investigation.

- a) Kodak D19; a high contrast developer.
- b) Ilford ID11; a general purpose developer.
- c) Ilford Perceptol; a fine grain developer.

Table 5.10. Variation of developer formulation.

Treatment	Experiment 6, Rolls 18,19,20,21 and 22				
Film	PNF 120 Rolls D,E and F			TCP 120 Rolls H and I	
Exposure	20/7/89 46.7%RH 27.7°C				
Processing 20/7/89	D19 Stock 5 min at 23°C	ID11 1:1 5 min at 23°C	Perceptol Stock 5 min at 23°C	ID11 1:1 5 min at 23°C	Perceptol Stock 5 min at 23°C
	Non-Hardening Fixer 5 min at 23°C				
	Wash 30 min at 23°C				
Drying	IMA 50.3%RH and 22.7°C				
Measurement	NPL 26/7/89 1/8/89 8/8/89				

The rolls of Technical Pan and Pan F films were exposed with the glass master grid as detailed in table 5.10, then processed simultaneously in small tanks according to the time-temperature method. Simultaneous processing enabled process fluctuations to be minimised with development the only variable parameter. The slightly elevated temperature used (23°C) was forced by the temperature of the University cold water supply, development times being correspondingly reduced according to manufacturers' data tables (Ilford 1985a).

5.3.4.1.1. Homogeneous deformations.

The homogeneous scale changes computed from the measurement data are shown in figure 5.15 for Pan F film and figure 5.16 for Technical Pan film. In each figure the dotted lines represent 95% confidence intervals associated with the (solid) linear regression lines drawn. Whilst the ID11/Perceptol and Perceptol/D19 intervals overlap, a small (0.07%) scale difference between the position of the ID11 and D19 regression lines at high relative humidity can be identified. This marginal effect may possibly be attributed to the physical structure of the developed silver, since from section 2.2.2. it could be expected that a greater proportion of chemical development would occur with the D19 formulation. However the effect could simply be a difference between the actual moisture content of the film and the ambient relative humidity as measured by the digital probe.

Figure 5.15.

The effect of variation of developer formulation on the scale change / relative humidity relationship.

Ilford Pan F 120 film, rolls D,E and F.

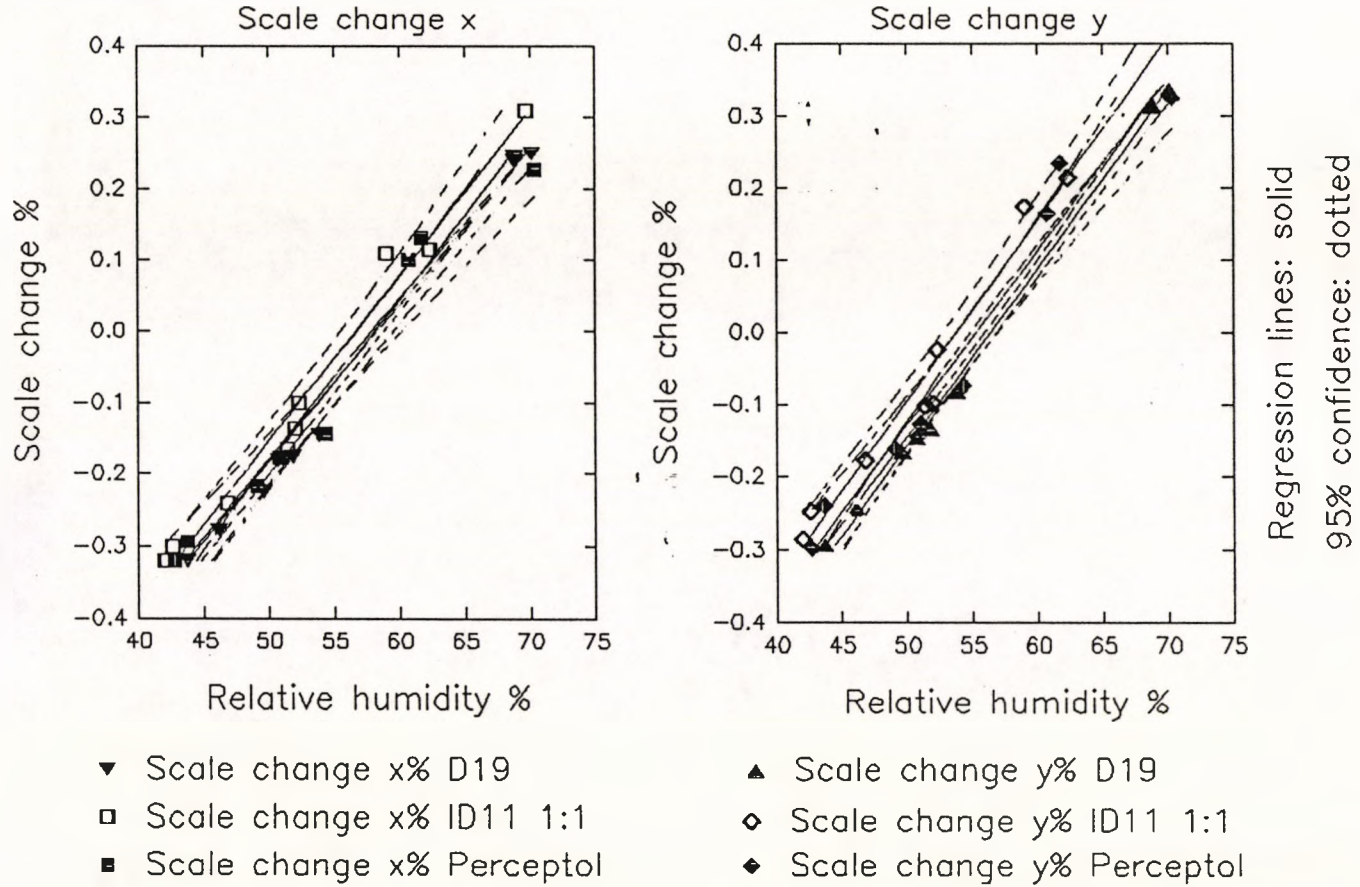
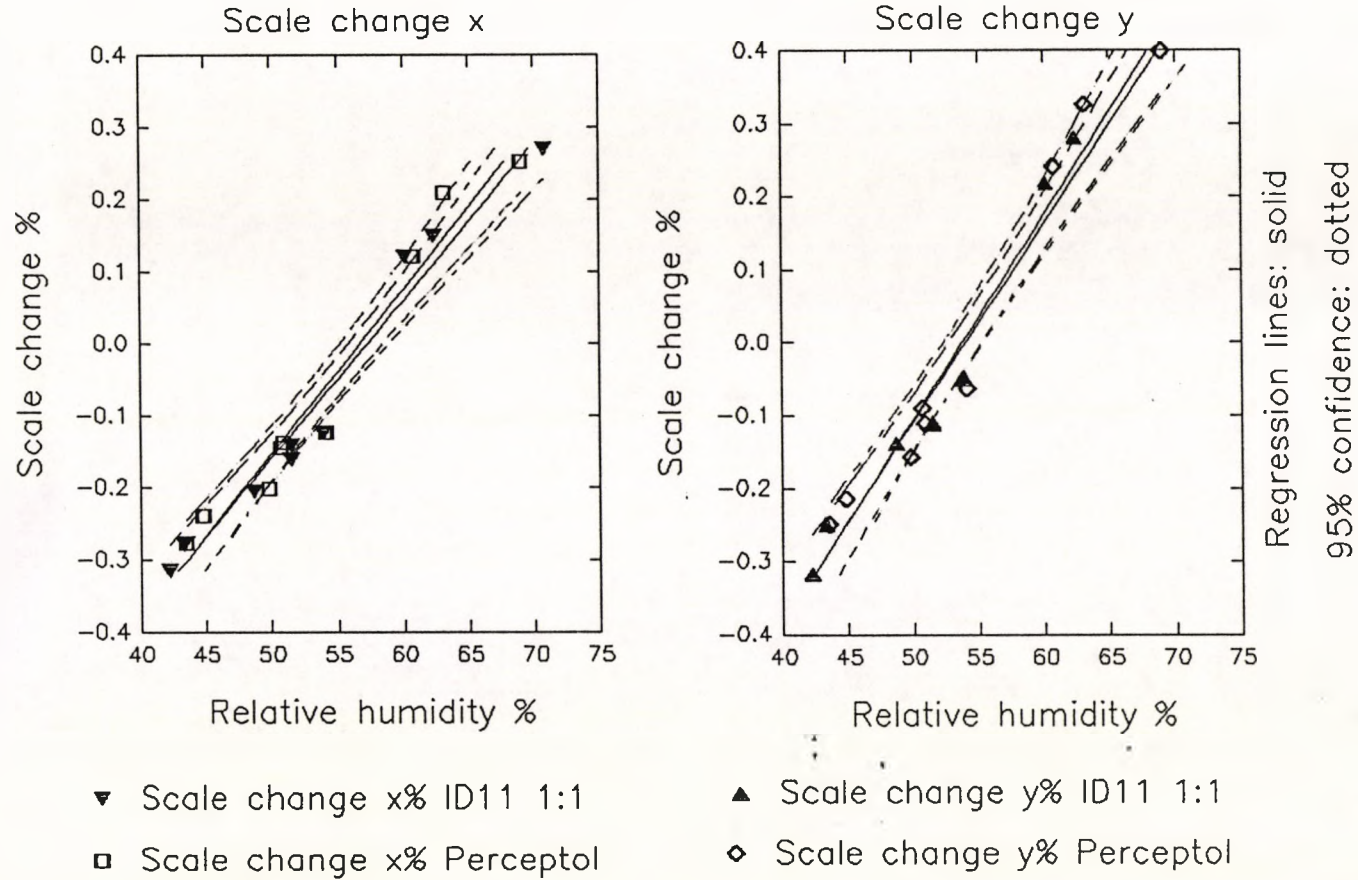


Figure 5.16.

The effect of change of developer formulation
on the relationship between scale change and relative humidity
Kodak Technical Pan 120 film, rolls H and I.



5.3.4.1.2. Inhomogeneous deformations.

Mean RMS residual deformations for the sets of measurement data are detailed in Table 5.11. In agreement with the investigation comparing developer formulations there are no statistical differences between the sample means if the x and y directions are considered separately. Again probably due to the measuring machine axis precision disparity, the deformations in y are greater than those in measured in x.

Table 5.11. RMS residual deformations from developer variations.

Film	Developer	RMS x(μm)	RMS y(μm)
PNF 120	D19	1.18 ($\sigma=0.10$)	1.69 ($\sigma=0.11$)
PNF 120	ID11 1:1	1.20 ($\sigma=0.17$)	1.43 ($\sigma=0.16$)
PNF 120	Perceptol	1.18 ($\sigma=0.11$)	1.55 ($\sigma=0.11$)
TCP 120	ID11 1:1	1.18 ($\sigma=0.12$)	1.28 ($\sigma=0.13$)
TCP 120	Perceptol	1.55 ($\sigma=0.40$)	1.32 ($\sigma=0.18$)

An anomaly (RMS x is greater than RMS y) is present in the RMS results obtained for Technical Pan film processed in Perceptol. This discrepancy can however be explained by considering some of the vector plots derived from contributory images. The sample of vector plot data shown in figure 5.17 exhibits nominally random deformations except for frame I3. Similar systematic deformation patterns were observed and discussed in section 5.3.2.2 and as such cannot be attributed to changes of developing agent.

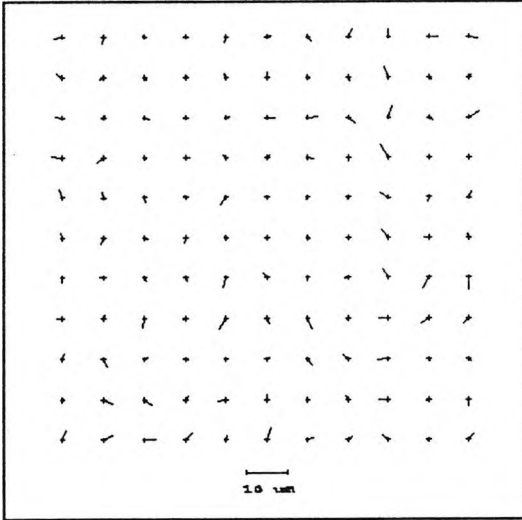
5.3.4.2. Variation of fixing bath formulation.

In common with developer formulation, variation of fixer solution does not appear to have been discussed by photogrammetric workers investigating film deformation. These experiments were conducted on the assumption that enhancement of molecular interlinking within the gelatin should reduce its ability to absorb water and consequently result in a reduction in global scale change (Duffin 1966). Increased stability could also reduce the magnitude of any local deformations if they were caused by localised forces within the emulsion.

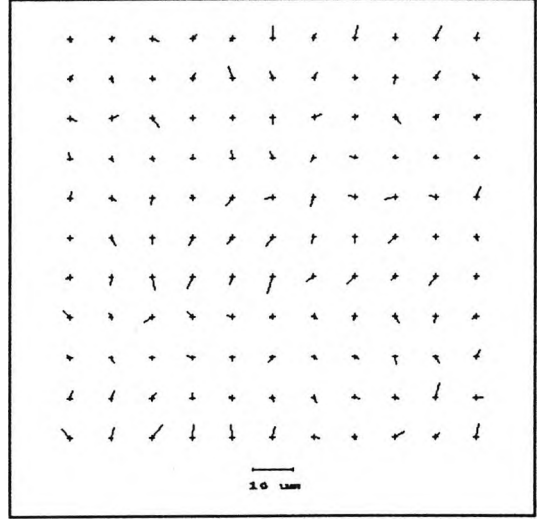
Two sets of experiments were conducted in this investigation. In both cases the consistency of the photographic process was maintained by processing all films simultaneously. Fixing solutions were varied by mixing up two identical solutions based on Ilford Hypam, and adding Ilford Rapid Hardener to one of the baths. In common with all experiments, fresh chemicals were mixed before each test to ensure that solution activity was at its optimum.

Some contact grid exposures made onto Kodak Technical Pan 120 film with development in Ilford ID11 or Perceptol.

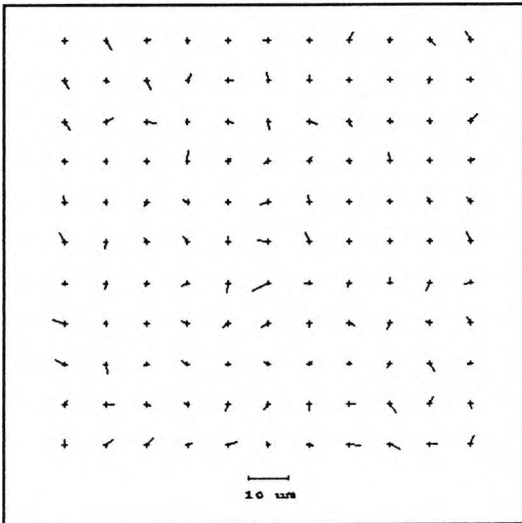
TCP 120, Frame H1, Measurement 2
(ID11 1:1).



TCP 120, Frame H3, Measurement 3
(ID11 1:1).



TCP 120, Frame I1, Measurement 3
(Perceptol).



TCP 120, Frame I3, Measurement 3
(Perceptol).

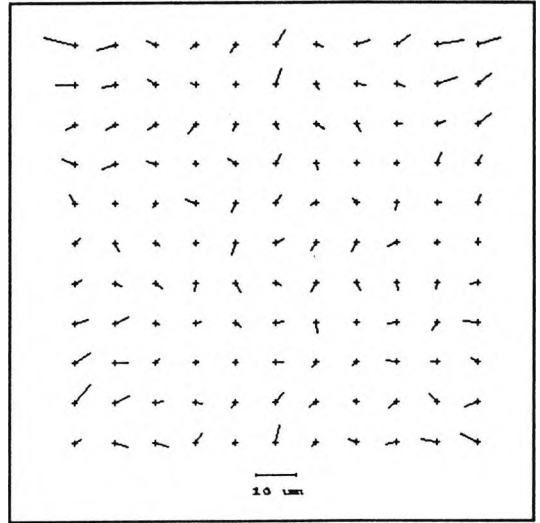


Figure 5.17.

Table 5.12. details the parameters associated with the processes conducted and also the film types used.

Table 5.12. Variation of fixing bath formulation.

Treatment	Experiment 4, Rolls 8,9,10 and 11.		Experiment 5, Rolls 12,13,14,15,16 and 17.	
Film	FP4 220 Roll G and TCP 120 Roll C	FP4 220 Roll H and TCP 120 Roll D	FP4 220 Roll J, TCP 120 Roll F and PNF Roll C	FP4 220 Roll I, TCP 120 Roll E and PNF 120 Roll B
Exposure	2/7/89, 44.5%RH, 22.4°C		14/7/89 42.8%RH 24.7°C	
Processing	ID11 1:1 8 min at 22°C		ID11 1:1 8 min at 22°C	
	Non- Hardening Fix 5 min at 22°C	Hardening Fix 5 min at 22°C	Non-Hardening Fix 5 min at 22°C	Hardening Fix 5 min at 22°C
Drying	IMA 2/7/89 49.9%RH 20.1°C (2 Days)		IMA: 52.3%RH 20.6°C (2 Days)	
Measurement	IMA 4/7/89, 5/7/89, 6/7/89, 7/7/89, 10/7/89, 12/7/89		NPL 18/7/89, 19/7/89, 20/7/89, 25/7/89, 28/7/89, 2/8/89, 10/8/89.	

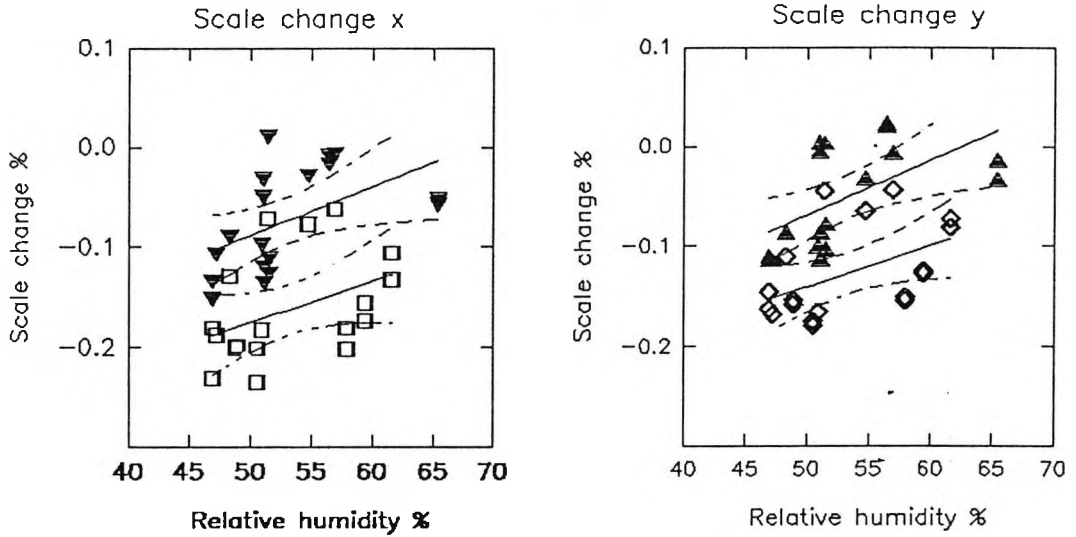
5.3.4.2.1. Homogenous changes.

Homogeneous scale changes derived from repeated measurement of images from the first series of tests are shown in figure 5.18. This series of images on Kodak Technical Pan 120 and Ilford FP4 220 films were measured using the City University IMA, in conjunction with a reduced (6X6) grid array. Evaluating the results it can be seen that whilst they largely follow the linear scale change with relative humidity relationship, there are points which represent significant departures. These departures can be explained by the variations in the measurement environment temperature occurring over the period of measurement (a range of 19.5 to 22.2°C). Whilst there appears to be no direct link with temperature, the measurement environment fluctuated rapidly (11%RH and 2°C over a 2 hour period) such that the film samples may not have been fully conditioned to the environmental conditions as measured by the digital probe. This slow response to environment fluctuations would be enhanced by the moisture absorption properties of the cellulose triacetate film base, which is known to condition much more slowly than the emulsion layers (Slama 1980).

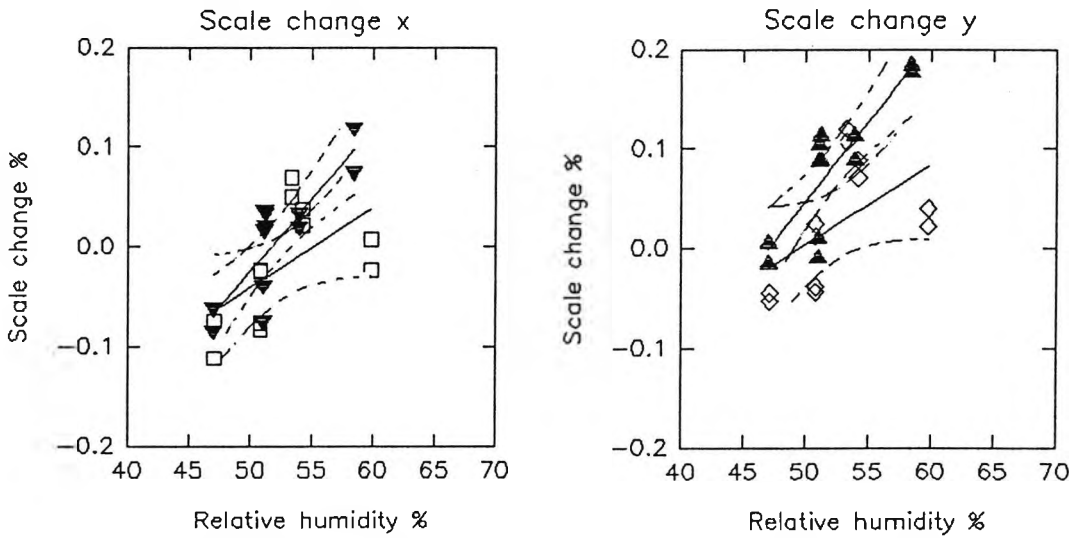
The photographic images constituting the second data set were stored and measured in the more stable NPL measurement environment. Immediately apparent from the graphs of percentage scale change against measurement environment relative humidity (Figs. 5.19, 5.20 and 5.21) is the more linear nature of the data. Departures do exist especially in the Technical Pan measurement data, but in this case the discrepancies are within the 0.1% range which can be attributed to variation between frames along the length of the film roll. Hysteresis effects (Section 2.4.1) may also contribute to this range. Hysteresis is specifically discussed in section 5.3.6, appearing to contribute minor changes to scale parameters derived from re-measurements of the same frame.

The effect of using hardening and non-hardening fixing baths on the relationship between scale change and relative humidity

Ilford FP4 220 hardener roll H, no hardener roll G.



Kodak Technical Pan 120 hardener D, no hardener roll C.



▼ Scale change x% hardener

▲ Scale change y% hardener

□ Scale change x% no hardener

◇ Scale change y% no hardener

Regression lines: solid

95% confidence: dotted.

Figure 5.18.

Figure 5.19.

The effect of using hardening and non-hardening fixing baths on the relationship between scale change and relative humidity Ilford FP4 220, hardener roll J, no hardener roll I.

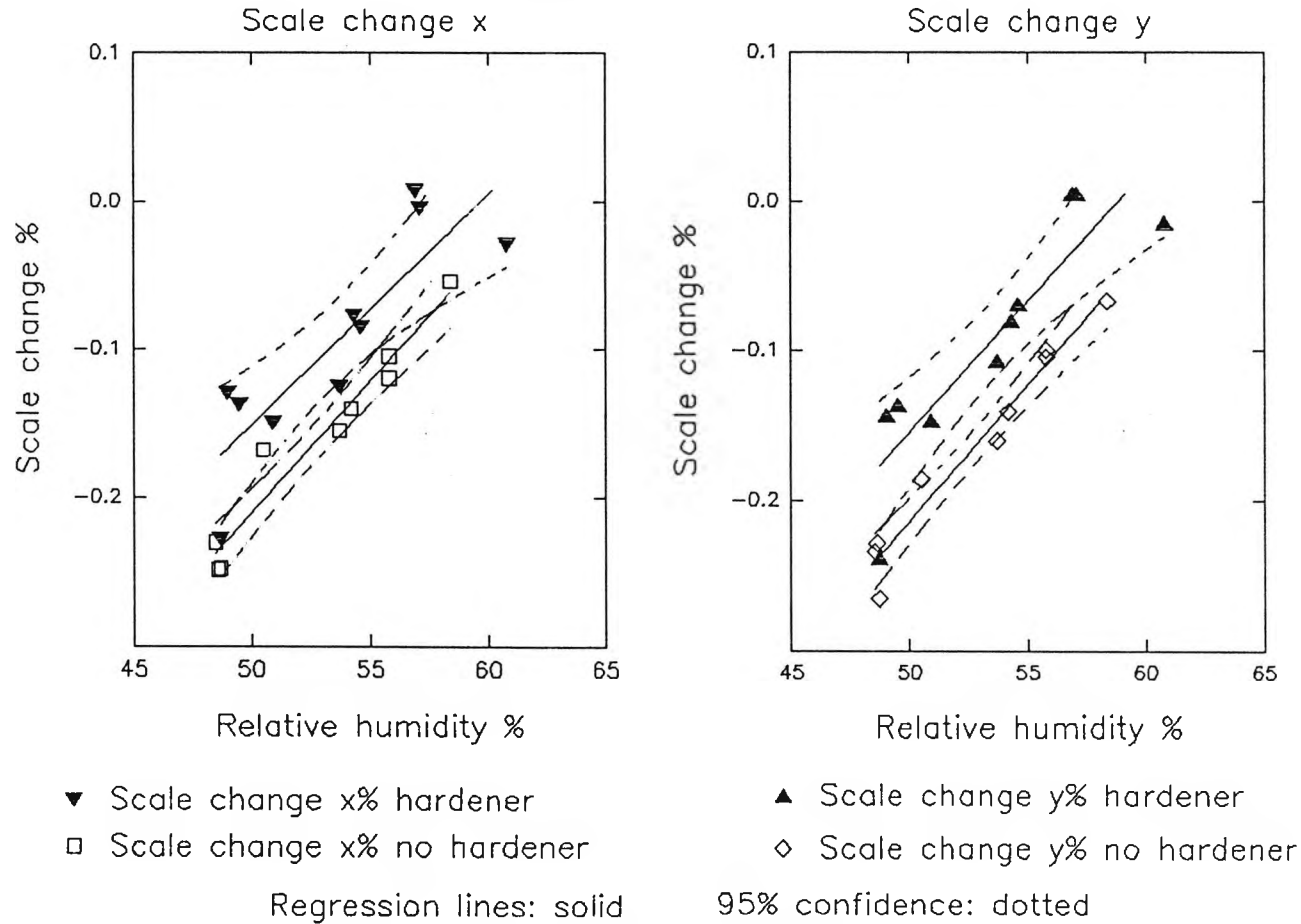


Figure 5.20.

The effect of using hardening and non-hardening fixing baths on the relationship between scale change and relative humidity
Ilford Pan F 120 film, hardener roll B, no hardener roll C.

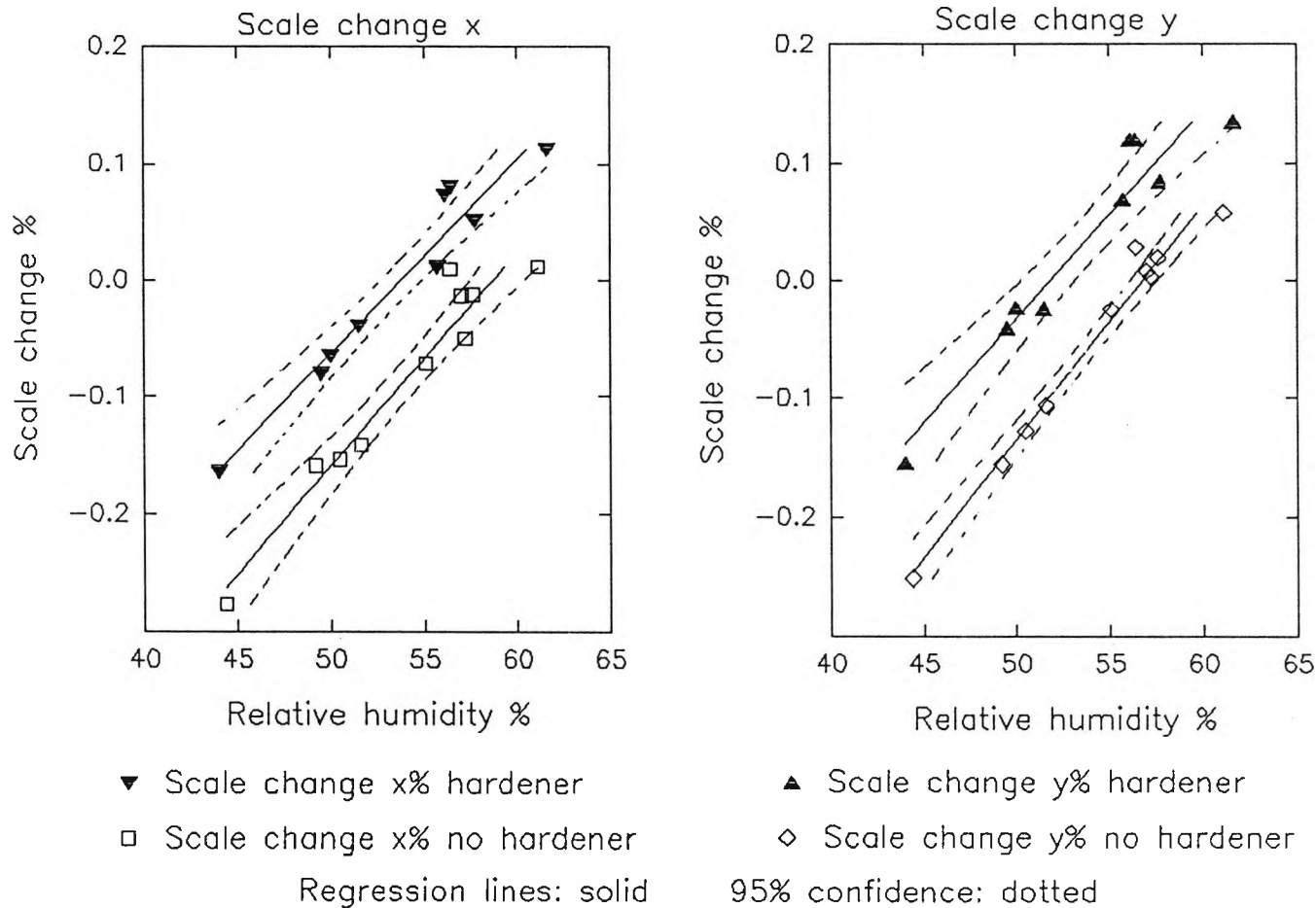
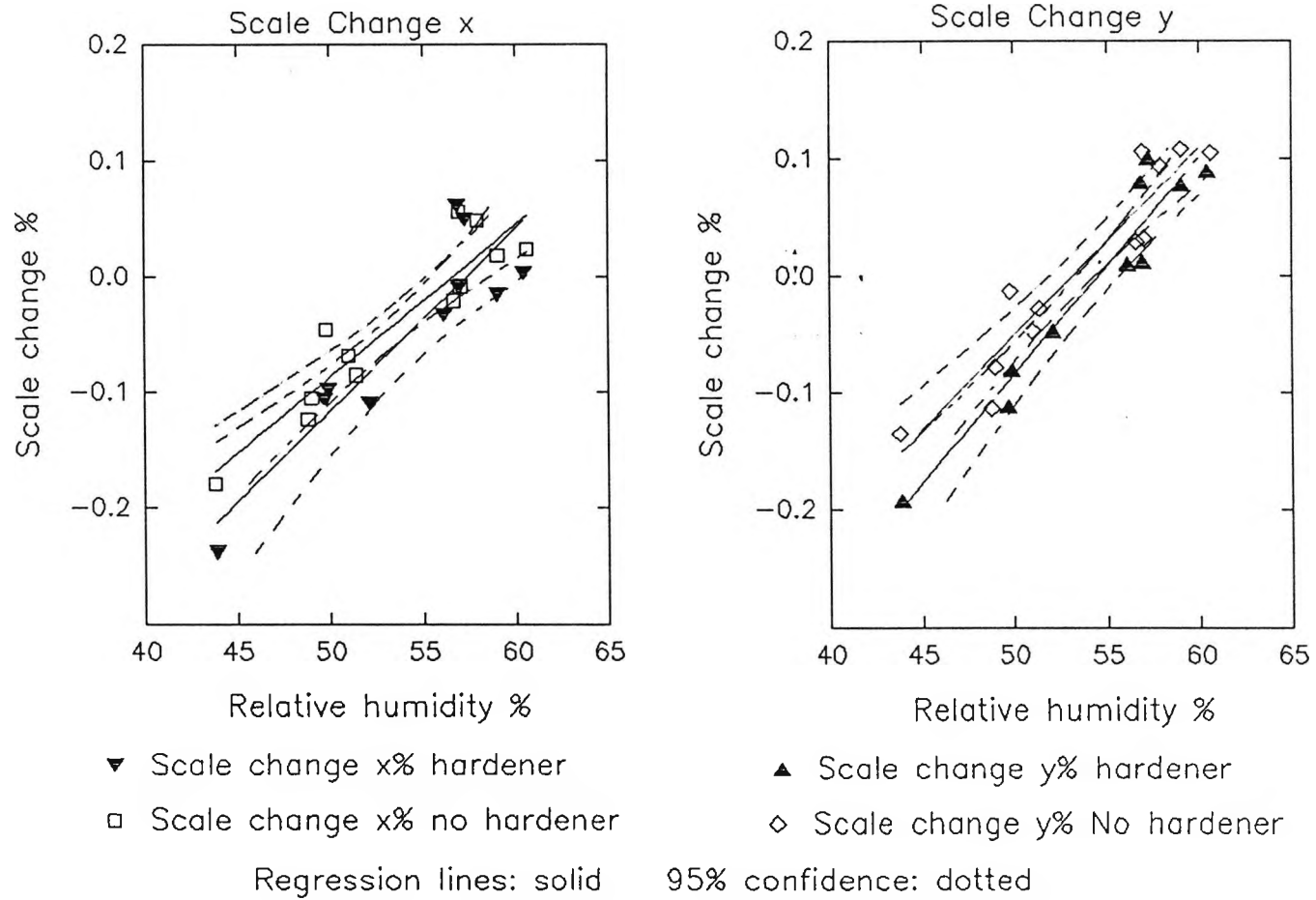


Figure 5.21.

The effect of using hardening and non-hardening fixing baths on the relationship between scale change and measurement relative humidity.

Technical Pan 120 film, hardener roll E, no hardener roll F.



Both Ilford products demonstrate significant differences in regression line position, processing with the hardening fix bath providing the minimum scale change. However within the limits of the 95% confidence interval, there are no significant differences between the gradients of the regression lines. This indicates that the hardening action is influencing the size of the image after processing, but not its subsequent response to changes in the relative humidity of the measuring environment.

Results on Kodak Technical Pan film demonstrate that the use of a hardening fixer does not make a significant difference to the size of images on this film. This must mean that the Kodak emulsion has been hardened during manufacture to a higher degree than the Ilford products. It is possible that it incorporates a stabilised gel emulsion, a term used by Kodak Ltd to describe some of its graphic arts products (Kodak 1971a).

5.3.4.2.2. Inhomogeneous deformations.

The mean RMS residuals (and their associated standard deviations) for all groups of grid images measured during these two experiments are presented in table 5.13. No firm conclusions can be drawn concerning the influence of the hardening agent for the first set of data measured on the IMA, the RMS residuals being of a similar order to the $2\mu\text{m}$ to $3\mu\text{m}$ RMS repeatability of this instrument.

Analysis of the vector plots derived from these images does suggest that some local systematic effects are occurring, especially with the images on Technical Pan film some examples of which are shown in figure 5.22. However the 10mm grid spacing (only 25 points) used for this measurement set, (an attempt to increase the number of grid images that could be measured in a given time) has resulted in a loss of information and is not suitable for the detection of inhomogeneous deformations. It should be mentioned that this was the last set of measurements to be made on the IMA, the machine being rejected in favour of the NPL ZKM monocomparator which for this work was faster, more precise and easier to use.

Paired t-tests were carried out on the mean RMS data from the second set of measurements to determine if the magnitudes of the mean deformations, occurring in each frame, in the x and y directions were significantly different. Whilst the differences between means for the images on FP4 roll I and the Technical Pan films were insignificant, all the other images demonstrated deformations in x which were significantly smaller than those in y. This dissimilarity can be attributed to the differences between the x and y repeatability of the ZKM measuring microscope where the variation between frames is small. In the case of the images on FP4 220 roll I and both the Technical Pan films, the large spread caused by the presence of deformed images is significantly greater than the contribution from the ZKM.

Table 5.13. Mean RMS residual deformations from hardening agent variations.

Film	Fixing bath	RMS x(μm)	RMS y(μm)
FP4 220 G	No Hardener	1.60 ($\sigma=0.23$)	1.88 ($\sigma=0.28$)
FP4 220 H	Hardener	2.18 ($\sigma=0.40$)	1.93 ($\sigma=0.28$)
TCP 120 C	No Hardener	2.71 ($\sigma=1.10$)	2.25 ($\sigma=0.38$)
TCP 120 D	Hardener	2.54 ($\sigma=1.22$)	2.31 ($\sigma=0.27$)
FP4 220 I	No Hardener	1.52 ($\sigma=0.17$)	2.35 ($\sigma=0.73$)
FP4 220 J	Hardener	1.32 ($\sigma=0.14$)	1.46 ($\sigma=0.17$)
PNF 120 C	No Hardener	1.12 ($\sigma=0.15$)	1.55 ($\sigma=0.15$)
PNF 120 B	Hardener	1.15 ($\sigma=0.09$)	1.47 ($\sigma=0.10$)
TCP 120 F	No Hardener	1.81 ($\sigma=0.59$)	1.95 ($\sigma=0.62$)
TCP 120 E	Hardener	1.46 ($\sigma=0.22$)	1.40 ($\sigma=0.27$)

The local deformation patterns seen on some of the Technical Pan images are similar to those mentioned in earlier discussions. The gross image deformation associated with the FP4 film is confined to one frame (I1) which was measured twice (Fig. 5.22). There are also some local deformations on some of the FP4 grid images which are similar in pattern, but smaller in magnitude to those on Technical Pan, examples are I2 and J3 in figure 5.22. It is interesting to note that the majority of images demonstrating local systematic deformations in the second data set are the unhardened frames on FP4 and Technical Pan films.

To provide a larger data set, the data from all image measurements made at NPL were evaluated to see if there was any difference between the instance of local systematic deformations on hardened and non-hardened images. The evaluation was made by visual assessment of the vector plots associated with images on Technical Pan, Pan F and FP4 films. Findings showed that 33% (11 out of 33) of the hardened images exhibited clearly identifiable regions of systematic deformation, whilst in the case of the non-hardened images 31% (12 out of 39) demonstrated deformations. A hardening fixing solution doesn't therefore prevent local systematic deformations.

T-tests comparing the mean RMS deformations between the hardened and un-hardened images in x and subsequently in y show significant differences in both cases. It can therefore be concluded that localised deformations are marginally larger where the film is not hardened during fixation.

Selection of contact grid exposures made onto Ilford FP4 220
and Kodak Technical Pan 120 films during the second set of hardening tests

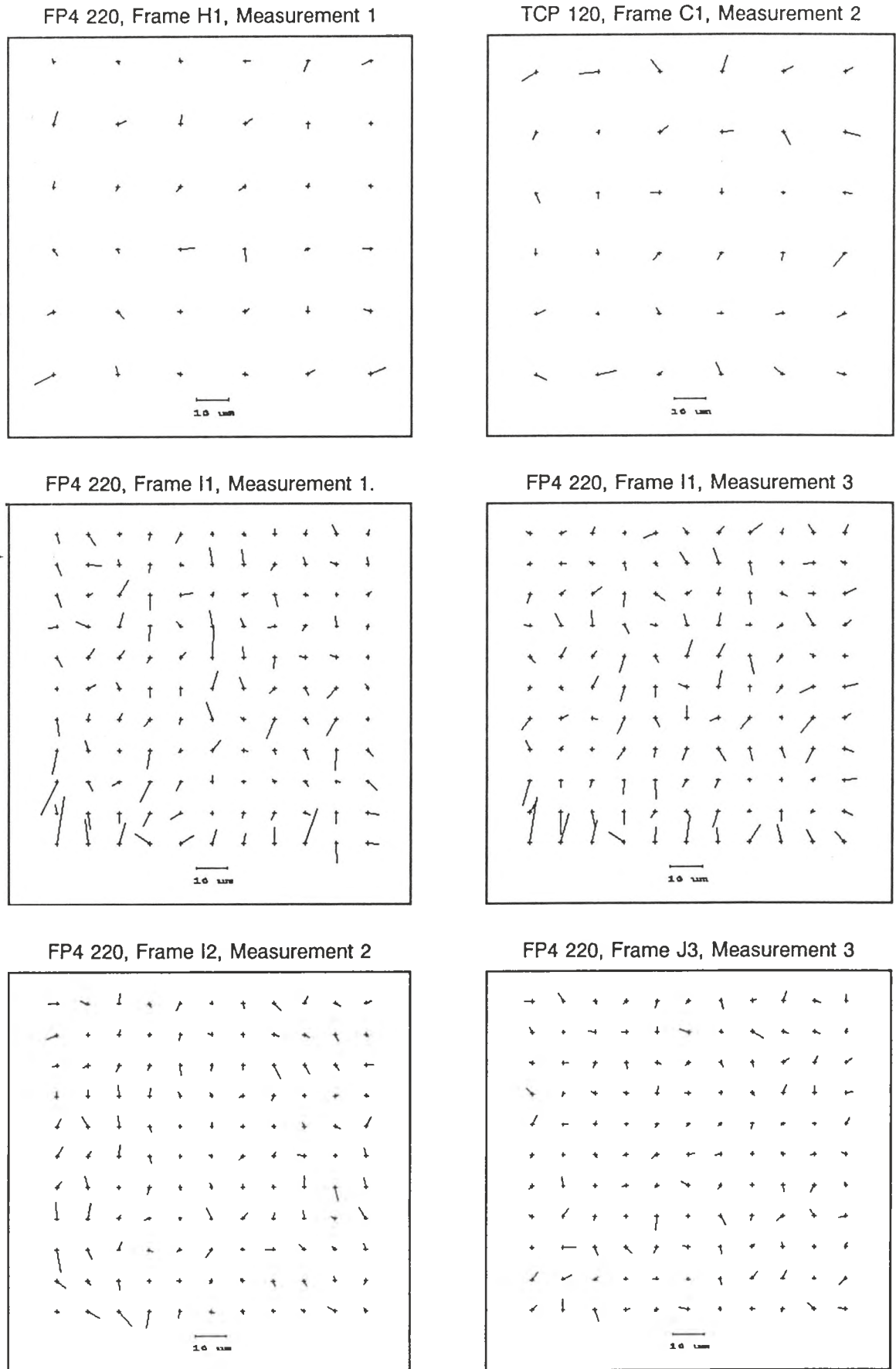


Figure 5.22.

5.3.4.3. Drying temperature and relative humidity.

The oversized nature of negatives caused by overdrying after processing is well documented (Adelstein et al 1965; Kodak 1972b). The purpose of this investigation, (the initial in-plane deformation test conducted) was to evaluate the effect of two different drying environments on scale changes and local deformations. Also investigated was the duration of conditioning time between processing and measurement to determine if there were any problems associated with the acquisition of data immediately after processing.

Two film types were investigated, Ilford FP3 70mm film on polyester base and FP4 220 film on cellulose triacetate film base. Contact grid images were made according to the parameters listed in table 5.14. To allow drying variation and to eliminate variations between process batches, each roll was cut into two strips of three frames after washing. Drying was carried out in the IMA measurement room or in a thermostatically controlled drying cabinet for two hours in each case before measurement was conducted. The ambient conditions recorded in table 5.14 were measured with the digital thermo-hygrometer. The experiment thus compared a small post-process environmental difference of 6.9%RH and 2.2°C.

Table 5.14. Variation of drying environment.

Treatment	Experiment 1, Rolls 1 and 2.			
Film	FP4 220 Roll E		FP3 70mm Roll A	
Exposure	5/5/89 51%RH 21.4°C			
Processing	ID11 1:1 9 min 20°C			
	Hardening Fix 5 min at 20°C			
	Wash 30 min at 20°C			
Drying	Frames 1,2,3: IMA 56.5%RH, 20.4°C (2 hours)	Frames 4,5,6 Drying Cabinet 49.6%RH, 22.6°C	Frames 1,2,3: IMA 56.5%RH, 20.4°C (2 hours)	Frames 4,5,6 Drying Cabinet 49.6%RH, 22.6°C
Measurement	IMA 5/5/89, 6/5/89, 9/5/89, 13/5/89, 20/5/89 and 1/6/89			

5.3.4.3.1. Systematic variations.

The results from the measurement sequences are presented in figure 5.23 for the FP4 film and figure 5.24 for the polyester based FP3 film. In both cases frame 2 has undergone conditioning in the measurement environment, whilst frame 5 has been initially dried in the drying cabinet.

Conditioning time after processing
 Ilford FP4 220 film, roll A, frames 2&5.

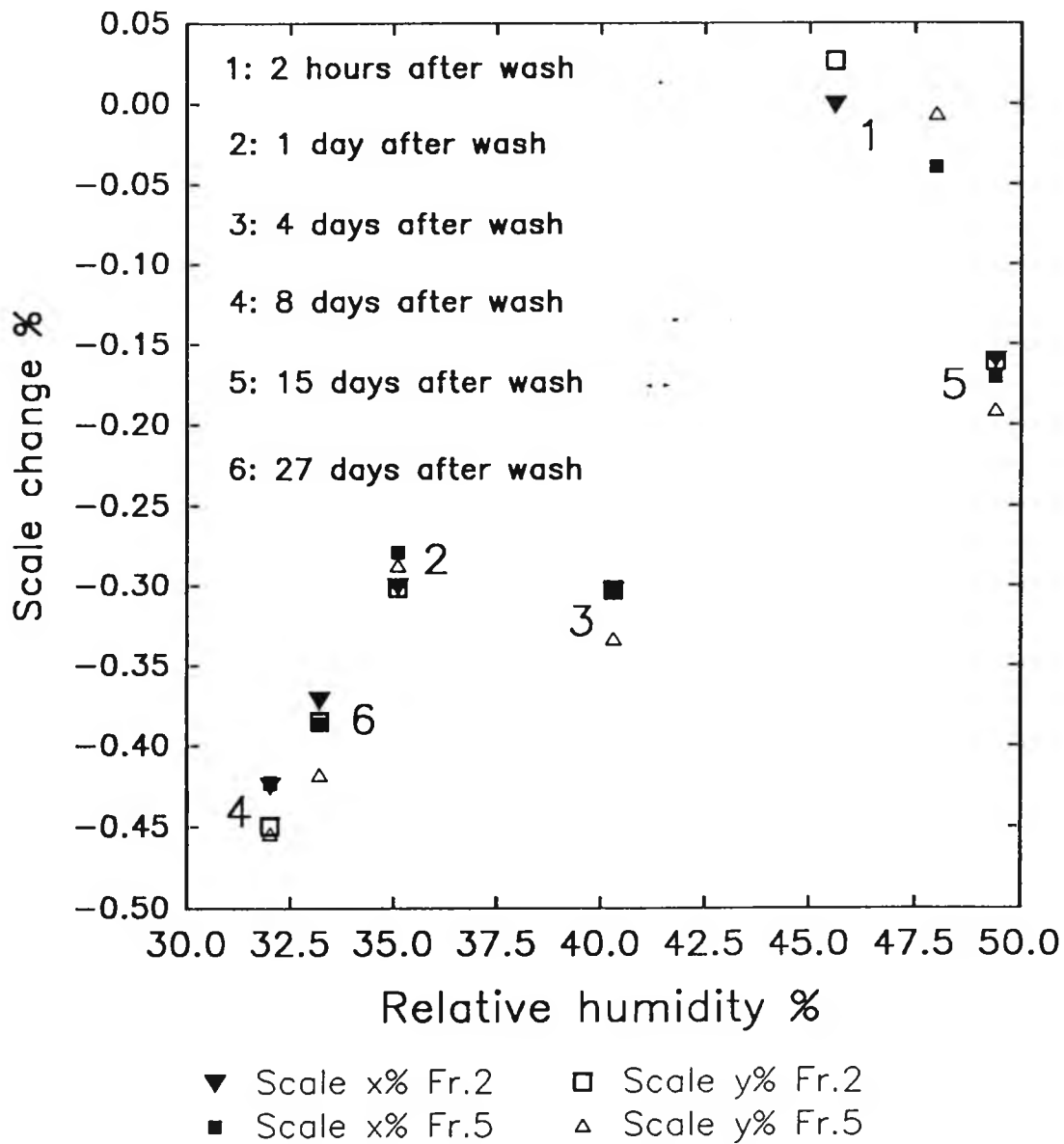


Figure 5.23.

Conditioning time after processing
 Ilford FP3 70mm film, roll A, Frames 2&5

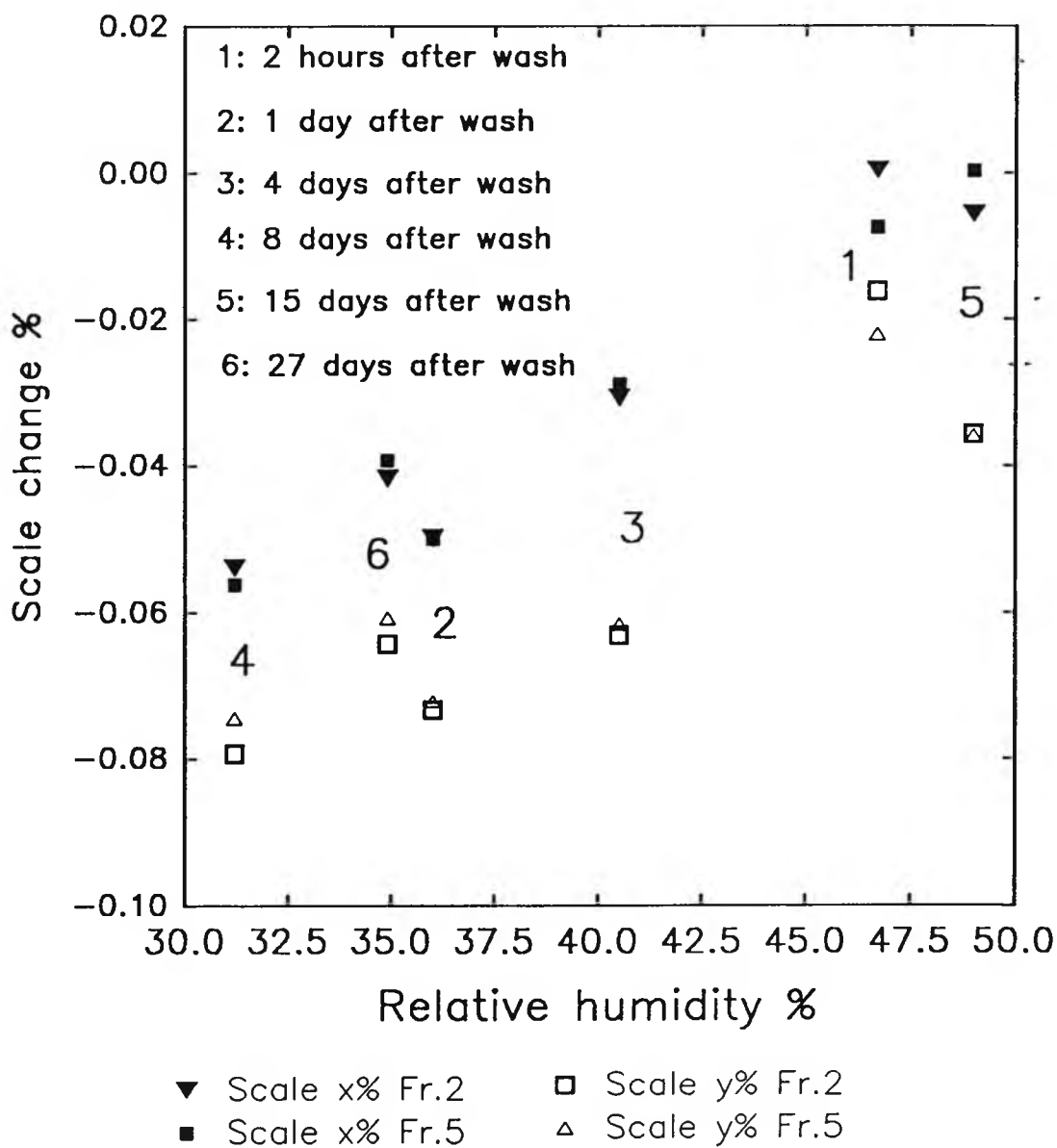


Figure 5.24.

Two hours after washing, frame 2 was found to be larger than frame 5 for both film types, this differential was to be expected because frame 2 has been conditioned to a higher relative humidity and will consequently contain more moisture. The relative sizes of the two images converge as the conditioning time in the measurement environment increases.

If the linearity of previous results made under similar conditions (Section 5.3.4.2) is considered, the maximum frame to frame scale change fluctuations at a given relative humidity and temperature are of the order of 0.1% for triacetate based films. The temperature at measurement in the IMA environment did not fluctuate by more than 0.5°C hence these image measurements on FP4 demonstrate clear departures from linearity at 2 hours after washing and probably one day after washing. The significance of these departures, which it appears can be controlled to some degree by variation of the drying environment, is that cellulose triacetate based film will not have equilibrated with the measurement environment until at least one day after processing.

The effect of changing to a polyester base is seen in figure 5.24, such that scale change parameters and post-process homogeneous dimensional changes are at least an order of magnitude smaller. Again these results are predictable when the respective moisture properties of the two base materials are taken into account (Section 2.1.2).

5.3.4.3.2. Local deformations.

These grid image measurements forming this data set were made using the IMA, consequently any local deformation patterns are likely to be of the order of the 3µm RMS machine error (Sections 5.3.4.2.2 and 5.3.5.).

Table 5.15. Drying environment RMS residual deformations

Film	Drying	RMS x(µm)	RMS y(µm)
FP4 220	IMA	2.31 ($\sigma=0.40$)	2.58 ($\sigma=0.21$)
FP4 220	Cabinet	2.54 ($\sigma=0.32$)	2.57 ($\sigma=0.25$)
FP3 70mm	IMA	2.15 ($\sigma=0.18$)	2.54 ($\sigma=0.18$)
FP3 70mm	Cabinet	2.10 ($\sigma=0.26$)	2.63 ($\sigma=0.20$)

The standard deviations of the mean RMS residuals indicate that no distorted frames (such as those produced in section 5.3.4.2) are present. Given the limitations of the measuring machine, an analysis of the vector plots produced (Appendix A), can make no real judgements as to local changes occurring whilst the film conditions immediately after processing. However because of the magnitude of the global dimensional changes occurring immediately after processing it seems probable that any measurements carried out on cellulose triacetate based film before it has

sufficiently dried will result in increased local dimensional change due to global changes during measurement.

Since exposure and processing of the films used in this analysis were conducted at City University, it was impractical to carry out a more exhaustive post-process conditioning test using the measurement equipment based at NPL.

5.3.4.4. Summary of deformations due to changes in process formulations.

The variation of developer formulation has not given rise to any significant differences in the in-plane deformations produced, therefore development tone reproduction controls can be used to match the negative material characteristic curve to the subject luminance range of interest.

The addition of inorganic hardening agent has resulted in smaller global image scale changes for Ilford FP4 and Pan F films. In the case of Kodak Technical Pan film the effect is insignificant, probably indicating that this film is hardened during manufacture to a greater degree than the Ilford products. A marginal decrease in the magnitude of local deformations was produced in hardened images, but the use of inorganic hardener does not appear to influence the local systematic deformations found in some images on cellulose triacetate base films.

Whilst the benefits of a hardening fixing agent are marginal, its use is not undesirable in any way, so it can be considered as a standard constituent for the processing of images intended for photogrammetry.

Much more significant is the conditioning time between chemical processing and measurement, films on cellulose triacetate base requiring at least one day to equilibrate with the measurement environment. The effect is less pronounced for films on polyester base because of the minimal moisture absorption of the base material (Section 2.1.2.2). These results mean that for all photogrammetric surveys which require measurement of images as soon as possible after photography, polyester based films should be used. It must be mentioned that the limiting factor in the selection of a suitable polyester based film is the availability of emulsions coated on this base material in small format sizes.

5.3.5. Changes occurring with storage, including hysteresis.

The aim of this investigation was to assess the magnitude of film dimensional hysteresis occurring in the NPL measurement environment. This type of analysis was possible since not only was temperature carefully controlled, but the temperature and relative humidity of the environment were continuously monitored by a chart recorder.

The experiment involved continuing to re-measure some of the set of frames produced during the second hardening fix investigation (Section 5.3.4.2) over an extended period of time whilst the relative humidity of the environment fluctuated.

Table 5.14. Measurement times and environmental conditions

Epoch	Date	Mean RH%	Mean °C
1	18.07.89	52	20.5
2	19.07.89	61	20.5
3	20.07.89	44	20.3
4	28.07.89	58	20.6
5	2.08.89	41	22.8

5.3.5.1. Homogeneous variations with storage.

Figure 5.25 is derived from the chart recorder data. Several differences were found between the recorded data and the probe readings made at the time of measurement. The data have been transformed as described below to allow for the various differences.

Relative humidity: The chart recorder response was found to be slightly non-linear at extremes of relative humidity when compared with output from the digital probe. The discrepancy has not been corrected on the graph since all image measurements were made in the 40% to 60%RH range and the chart output will only be used to assess the direction and approximate magnitude of humidity change. The section of the trace situated between the 22nd July at about 12:00 and 24th July at about 6:00 represents relative humidity readings which exceeded the chart recorder range.

Temperature: The ambient temperature trace has been shifted upwards by 0.5°C to correspond with the digital probe readings. Again this does not influence the discussion since only relative changes are involved. The section of trace on 31st July and beyond was caused by a malfunction of the temperature control system and the chart has gone off limits.

All six frames used in this investigation have undergone the same treatment, with the exception of the addition of hardening agent. On each graph (Figs. 5.26, 5.27 and 5.28) a pair of regression lines (dotted for the y axis) have been computed and drawn through the data. It should be noted that in all cases measurement five has been excluded from the computation because it was made whilst the temperature was uncontrolled (a 2.3°C rise).

Environmental variation of NPL ZKM
measurement room
16th July to 2nd August 1989

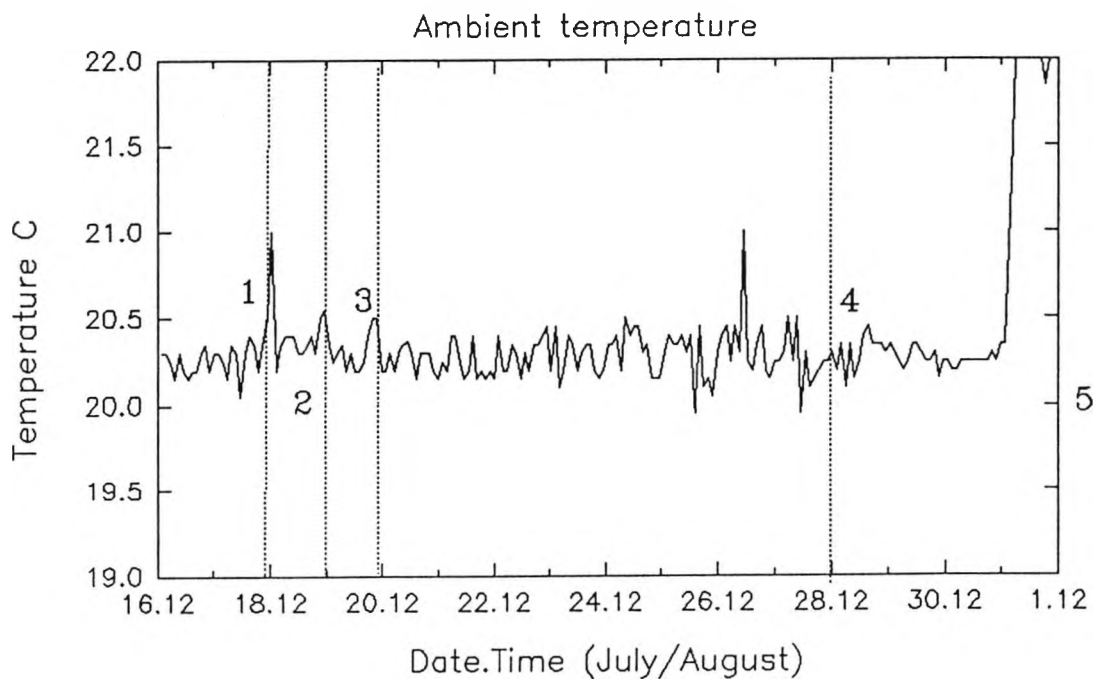
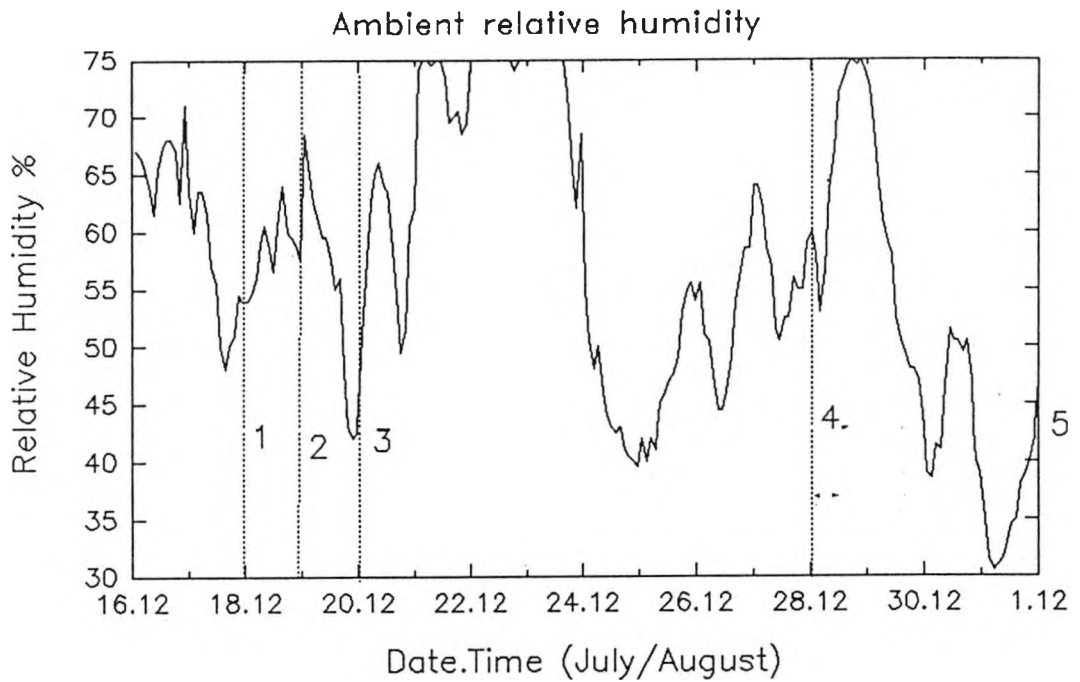
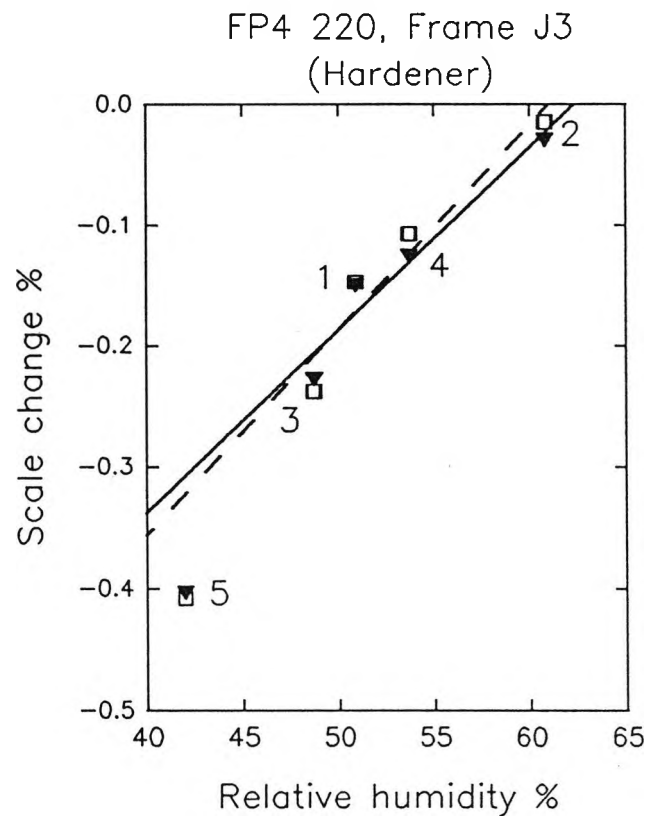
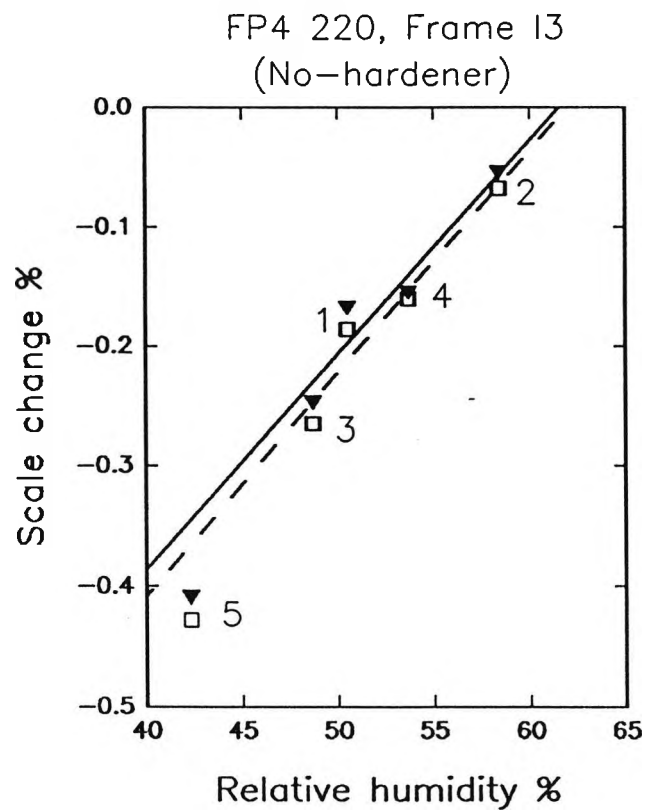


Figure 5.25.

Figure 5.26.

Scale change against measurement environment relative humidity.
for repeated measurements of two grid Images.



▼ Scale change x%
Solid line: regression x

□ Scale change y%
Dotted line: regression y

Figure 5.27.

Scale change against measurement environment relative humidity.
for repeated measurements of two grid images.

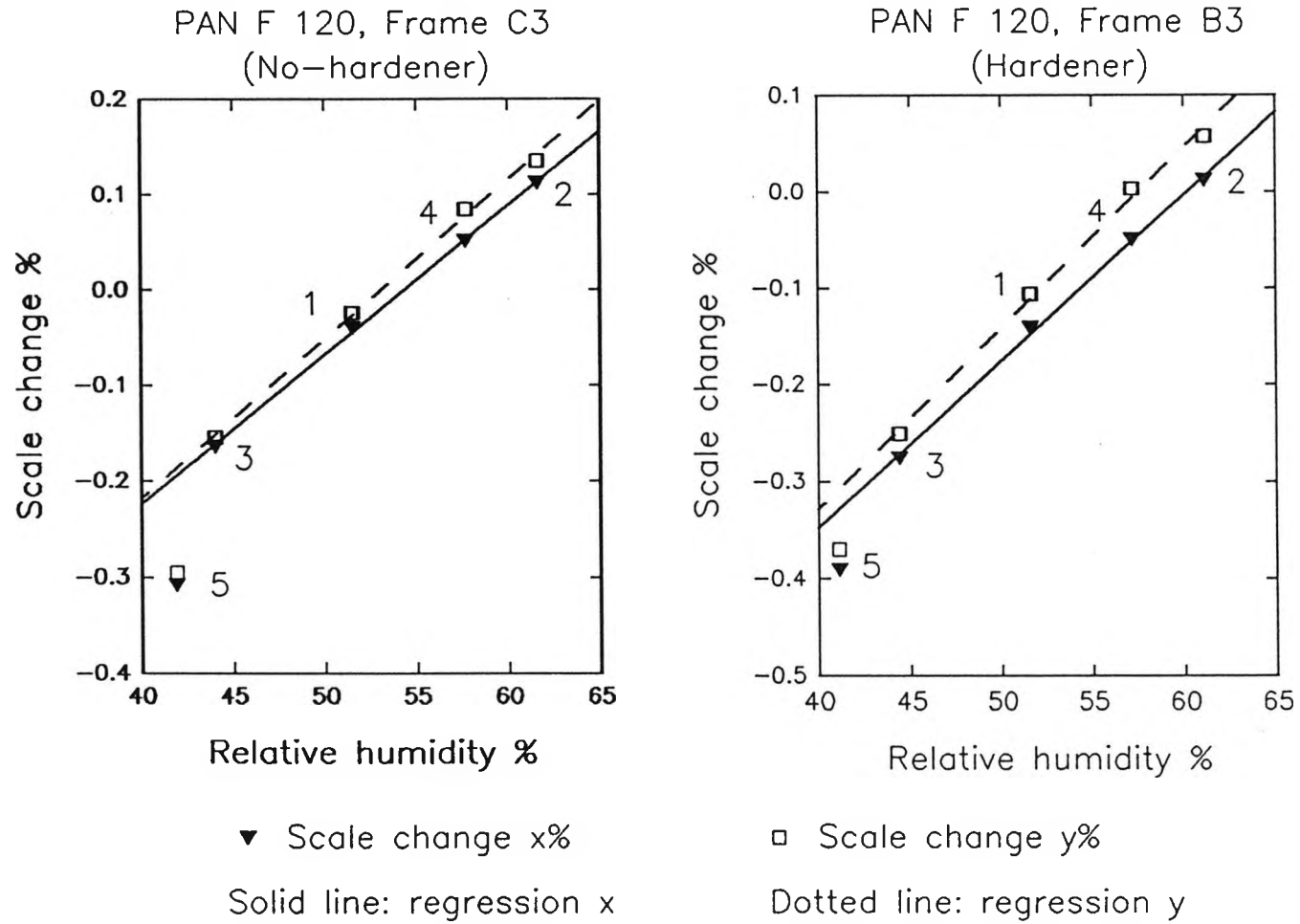
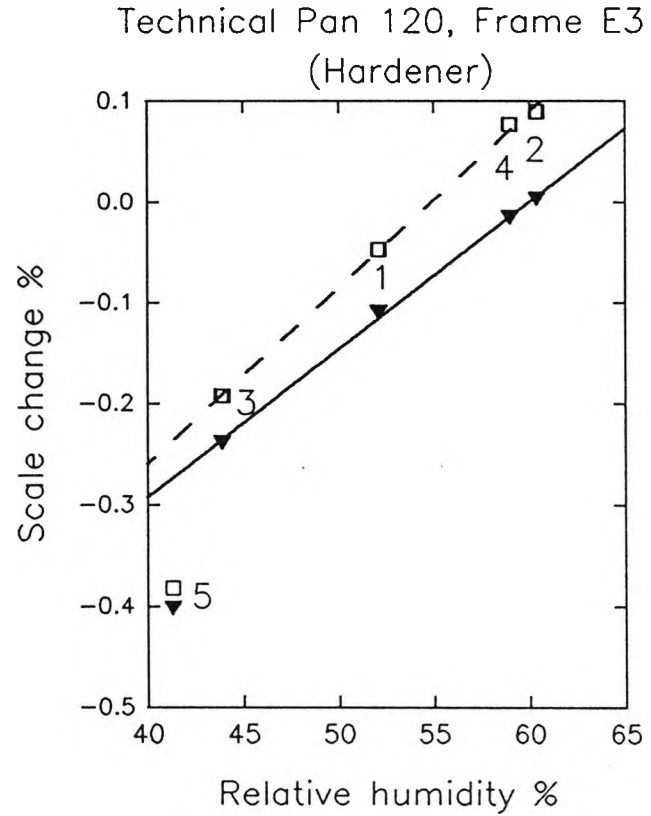
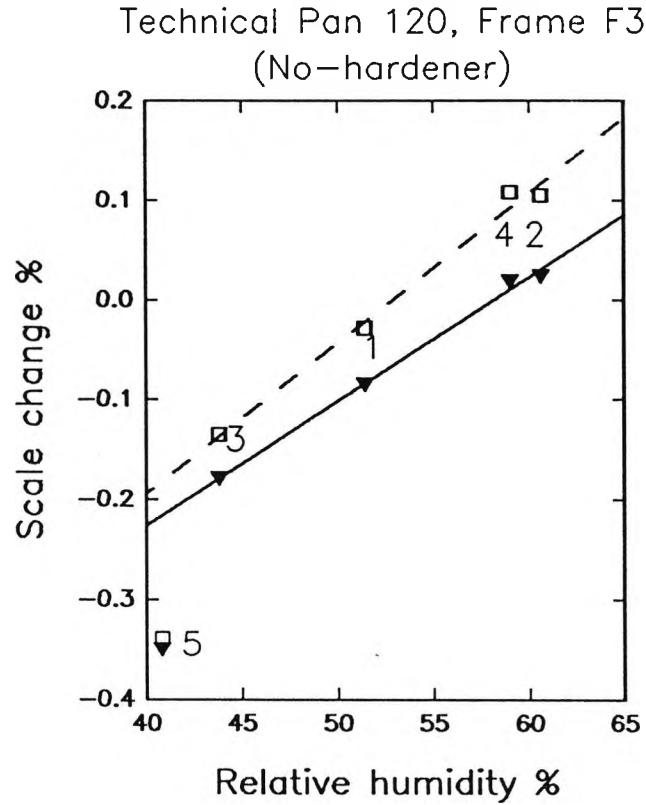


Figure 5.28.

Scale change against measurement environment relative humidity.
for repeated measurements of two grid images.



▼ Scale change x%
Solid line: regression x

□ Scale change y%
Dotted line: regression y

Since the data are very regular it is possible to summarise all the graphical results together. In all cases whilst temperature was controlled, the results exhibit good linearity. The result most indicative of the magnitude of any hysteresis effect is the difference between the image size at epochs 2 and 4. Over this period the relative humidity has gone down to 40%, up above 75%, back down to 40% and then back to around the 60% it was originally (Fig. 5.25). Despite these changes, the differences between scale changes derived from image measurements 4 and 2 are remarkably small in most cases (Figs. 5.27 and 5.28). In fact they are of the same order of magnitude as those produced during experiments conducted by Eastman Kodak on polyester based graphic arts films (Kodak 1972b). Slightly larger discrepancies are present in the FP4 data (Fig 5.26). These differences can probably be attributed to the fact that measurements of these frames were made within half an hour of switching on the ZKM and digital probe. Since it was found that the digital probe appeared to require about thirty minutes to settle after being switched on and therefore was not immediately representative of the moisture content of the film.

More confusing is that measurement 5 made at increased temperature has resulted in a decrease in size far greater than that expected from the drop in relative humidity alone. From table 2.1 an increase in temperature would be expected to contribute to an increase in image size. The most likely cause of these consistent results is that the modified ZKM measuring microscope is temperature sensitive to the order of 0.05% per 1°C.

5.3.5.2. Changes in local deformations with storage.

Table 5.15 details the RMS residual deformation for each frame at each measurement epoch. Also shown is the standard error associated with each set of data, providing a measure of mean RMS residual variability.

Table 5.15. RMS residuals (μm) for individual grid images.

Film	Fixer	RMS	18.07	19.07	20.07	28.07	2.08	σ
FP4 I3	No Hardener	x μm	1.38	1.43	1.41	1.53	1.50	0.06
		y μm	1.97	2.00	2.06	1.84	1.79	0.11
FP4 J3	Hardener	x μm	1.39	1.40	1.34	1.54	1.42	0.07
		y μm	1.37	1.49	1.51	1.47	1.45	0.05
PNF B3	Hardener	x μm	1.15	1.27	1.22	1.11	1.01	0.10
		y μm	1.36	1.52	1.33	1.39	1.44	0.07
PNF C3	No Hardener	x μm	1.02	1.07	1.06	1.44	1.18	0.17
		y μm	1.69	1.66	1.49	1.77	1.58	0.11
TCP E3	Hardener	x μm	1.75	1.38	1.53	1.42	1.81	0.19
		y μm	1.28	1.39	1.24	1.23	1.68	0.19
TCP F3	No Hardener	x μm	2.22	2.69	1.83	2.45	2.31	0.32
		y μm	1.50	1.85	1.63	1.50	1.73	0.32

Contact grid exposures made onto Kodak Technical Pan 120 film with measurement on the ZKM over five epochs.

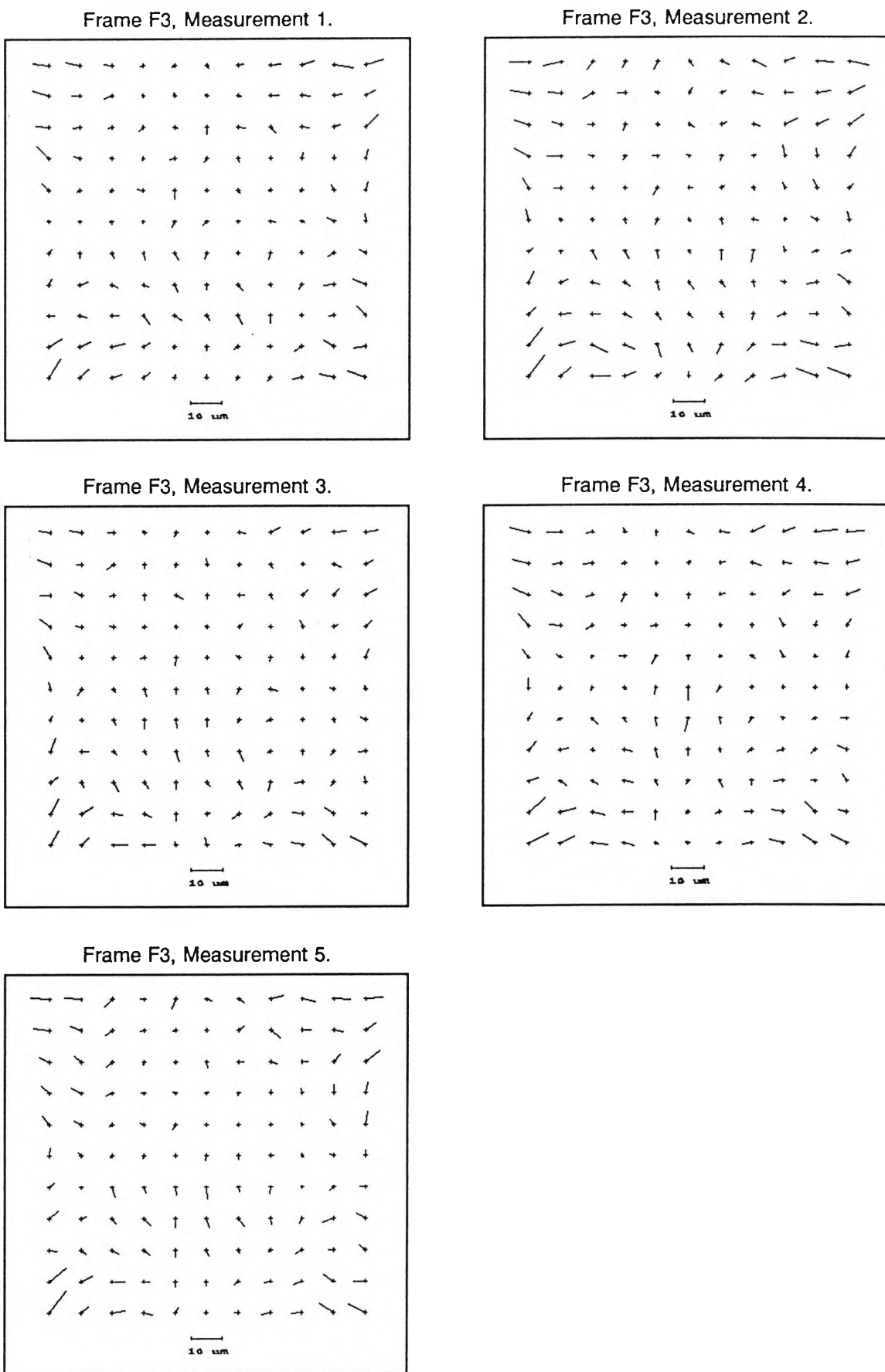


Figure 5.29.

The effect of measurement environment relative humidity on the mean RMS residuals for two Images on Kodak Technical Pan 120 film.

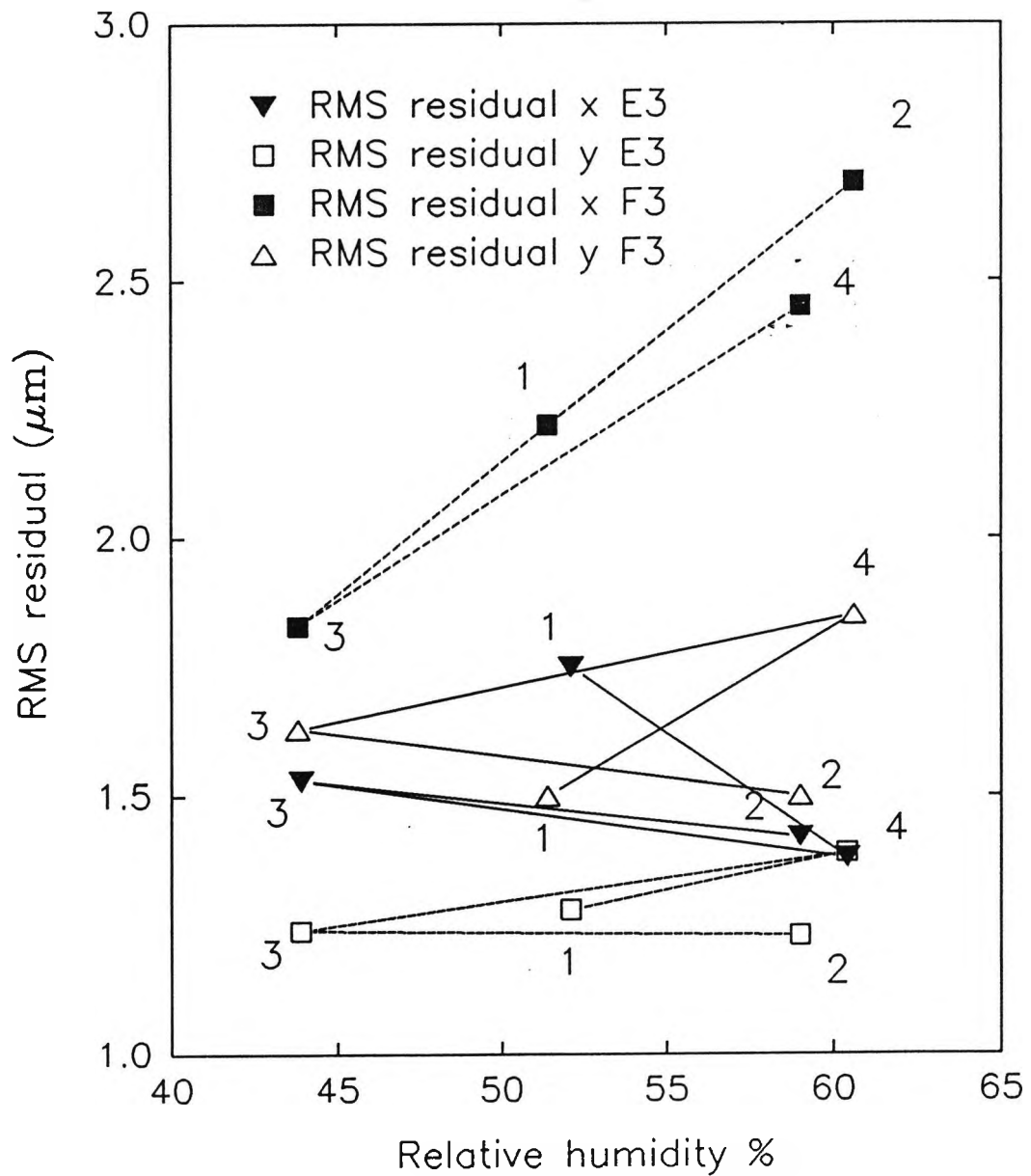


Figure 5.30.

It can be seen that for each frame at all epochs the standard deviation of the RMS residuals is generally of the order of $0.1\ \mu\text{m}$. The exception is Technical Pan frame F3, which shows significant local deformation patterns. Figure 5.29 shows the five vector plots derived from the TCP F3 data set. The plots show that whilst the direction of trends in the data remain the same, small changes occur as the relative humidity of the measurement environment fluctuates.

If the mean RMS residuals from the TCP F3 image data are plotted against relative humidity, a clear trend can be seen in the x direction (Fig. 5.30). The magnitude of the residual deformations in the x direction increases with relative humidity. The effect does not occur significantly in the homogeneously deformed images, probably because in these cases a greater proportion of the differences between residuals are due to measurement errors.

5.3.5.3. Summary of investigations into the presence of hysteresis.

Whilst slight changes do occur with variations in the measurement environment, none of the presented evidence confirms the presence of hysteresis effects. In fact the size of the differences occurring, whilst similar in magnitude to those reported for polyester based films (Byer 1983) are insignificant when the total size change with relative humidity for films on triacetate base are considered.

In the photogrammetric situation it must be remembered that global size changes can easily be corrected (providing deformations are homogeneous) by the use of three or preferably four calibrated camera reference marks. This means that whilst the scale changes occurring are important they can easily be removed.

It appears that for images exhibiting few systematic local deformations (at the approximate $1.5\ \mu\text{m}$ RMS measurement limit imposed by the film image quality) residuals are independent of the measurement environment relative humidity given constant temperature. This result is highly significant because it means that for all but the highest accuracy work a reseau grid need only be measured once and its correction can then be applied (after global correction) to all subsequent measurements made on that image.

5.4. Summary of in-plane experimentation.

The most striking conclusions from this analysis are the remarkably good dimensional qualities of small format film products, especially when it is considered that they are designed primarily for pictorial photography not dimensional stability. Many comments concerning the respective City University (IMA) and NPL (ZKM) measurement machines and environments have been made during the course of this discussion. Analysis of the in-plane measurement data has shown that the IMA and its loosely controlled environment are not stable enough to obtain the highest possible precision out of small format film products. To raise the precision of small format

measurement, especially on cellulose triacetate bases, temperature must be well controlled during measurement.

The in-plane experiments conducted using the ZKM have shown that the limiting process can be the precision with which the measuring mark is placed onto the true grid image position. Given the high magnifications available with the ZKM system, pointing precision is primarily dependant on image quality aspects and in-camera image magnification.

During the evaluation of the operational factors, several important dimensional influences have been distinguished. Foremost is that dimensional stability is largely independent of the chemical processing regime used, as long as manufacturers' guidelines are followed. This means that tone reproduction control can be fully exploited without risk of creating dimensional problems. It is this control which can produce a positive effect on the pointing precision attainable, and therefore on the precision of the photogrammetric survey.

Handling of the film material is probably the major cause of inhomogeneous dimensional change, but this is easier to avoid in practice by a standardisation procedure. For example in the contact grid situation the film had to be handled frame by frame, whereas in camera only the packaging material need be touched when loading the film. Generally maintaining consistent film handling and film and chemical batches throughout the photogrammetric survey procedure is the key to avoiding inconsistent and inhomogeneous dimensional change.

The conditioning interval between processing and measurement should be of the order of one day to ensure deformational consistency for films on cellulose triacetate bases. This is not so necessary for films on polyester base. However the limited range of emulsion types available on this base means that most small format surveys will use cellulose triacetate based products.

6. Investigations including out-of-plane deformation.

This chapter sets out to investigate the magnitudes and effects of film deformation according to three primary aims.

- a) To examine the presence of out-of-plane deformations for a variety of different camera types, taking into account the extent of in-plane deformations obtained from Chapter 5.
- b) To investigate the effectiveness of the reseau correction methods discussed in section 3.3.1 in terms of their effect on the object-space coordinates.
- c) To investigate the effects of film deformation by simulation of a survey situation.

The first aim can be achieved by exposing different films in a reseau equipped camera. The deformations computed by comparing the measurements of the reseau images and the reseau calibration values can then be examined.

The effectiveness of film deformation correction methods can be investigated by conducting a photogrammetric survey of an array of targets with known X,Y,Z object space coordinates. Target positions as estimated by the photogrammetric adjustment can then be compared with their known positions allowing any differences in position introduced by film deformation corrections to be assessed. The key problem associated with this method is to obtain initial X,Y,Z target coordinates at a greater level of precision than those estimated during the photogrammetric adjustment featuring film deformation corrections. This important problem is discussed in detail in section 6.3.1.

Assessment of the contributions made by film deformation corrections in a conventional photogrammetric survey application requires control points derived from conventional survey data, and check points for which the X,Y,Z object space coordinates are known, but not regarded as such in the photogrammetric adjustment. The third objective could therefore be satisfied simply by using a subset of the image measurements made of the target array during the second experiment, but adopting different processing procedures to simulate a survey. In this way an analysis of the potential of the envisaged film deformation methodologies (Section 3.3) to practical surveys could be made.

6.1. In-camera exposure method.

Given minimal in-plane deformation, out-of-plane deformation is more easily investigated, since a good source of data can be provided by reseau images produced during controlled laboratory conditions and processed using the standard regime developed from the in-plane work.

Experiments were carried out using a range of 120 and 220 film products exposed with the same camera lens cone. The investigation aim being to examine the magnitudes and any consistencies in the deformations occurring between individual frames and treatments.

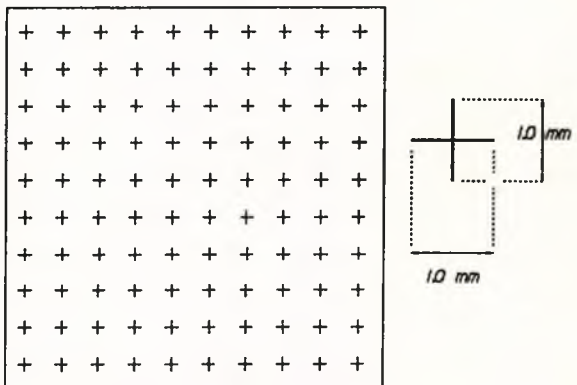
6.1.1. Modification of the Hasselblad SWC camera.

Availability of a suitable reseau equipped camera for these tests was limited. The Rollei-Metric 6006 used in the initial investigation could be hired, but the weaknesses of this particular camera body (Section 4.2) meant that any film unflatness could not be assessed by reseau image measurement. A reseau equipped camera could have been hired from one of the other major manufacturers, but since there was a commercial requirement at City University for a small format survey camera it was decided to modify an existing non-metric 6X6cm camera.

The camera chosen for modification was a Hasselblad SWC, this choice being made because the camera incorporated the excellent Zeiss 38mm Biogon lens rigidly fixed to its body. This lens provided not only excellent optical quality but also the wide angle of view (90° across the format diagonal) necessary for the close range projects envisaged. Modifications carried out by Hooker and Robson included the addition of a 100 point reseau grid plate and pinning the focusing helicoid of the 38mm Biogon lens at a 3 meter focus setting.

Two reseau plates were ordered from Graticules Limited (Tonbridge, Kent) according to a specification based on the conclusions concerning the Rollei-Metric 6006 reseau camera made in chapter 4.

Table 6.1 Reseau specification.

<p>Substrate:</p> <p style="padding-left: 20px;">Glass B270,</p> <p style="padding-left: 20px;">55mm by 55mm by 1.5mm.</p> <p>Pattern:</p> <p style="padding-left: 20px;">Coordinate crosses</p> <p style="padding-left: 20px;">X&Y pitch 5mm +/- 0.005mm,</p> <p style="padding-left: 20px;">Line length 1.0mm,</p> <p style="padding-left: 20px;">Line width 0.012 to 0.015mm.</p>	
--	--

Before calibration using the ZKM, the flatness and parallelism of each of the reseau plates was checked using the Zygo interferometer at NPL. Each reseau plate was then carefully ground at the corners to enable it to be fitted onto a frame which had been rigidly attached to the camera body.

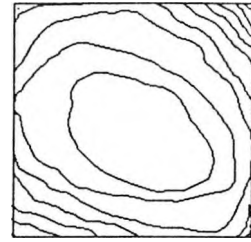
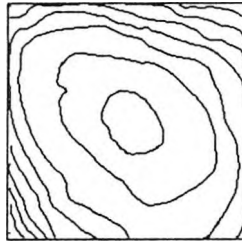
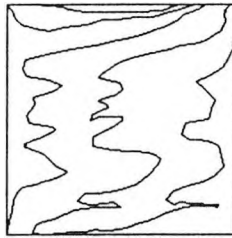
RESEAU GLASS CHARACTERISTICS

UNPARALLEL

UNFLATNESS

BEFORE FITTING

AFTER FITTING



Interval = 0.316 μm

Figure 6.1. Reseau plate 1, parallelism and unflatness before and after fitting.

Calibration measurements were carried out by making three independent rounds of measurements to each of the 100 reseau cross locations at a 350X magnification. The measurements were processed using program STEC a plane coordinate transformation (Chandler 1989) based on the four corner reseau crosses. The standard deviations associated with the grid measurements were also computed at this time. In common with the measurements made using the ZKM measuring microscope throughout chapter 5, the repeatability in x was better than that in the y direction.

Table 6.2. Standard deviations of calibrated reseau positions.

Plate	RMS $\sigma_x \mu\text{m}$	RMS $\sigma_y \mu\text{m}$
Reseau 1	0.36	0.53
Reseau 2	0.27	0.47

Mounting of a plate into the camera was carried out by dabbing epoxy-resin at each of the reseau plate corners, the plate then being fitted into the camera and aligned orthogonal to the optical axis using an autocollimator. Once the resin had set, more resin was teased along the joint between the glass and the metal frame to provide a strong but flexible bond. It was believed that this flexible bond would prevent some of the distortions that had been found in the Rollei-Metric 6006 reseau. The reseau modification was completed by cleaning the glass with acetone and ethanol, then by painting the metal frame attached to the camera matt black to reduce internal flare.

Once fitting was complete the flatness of the rear surface of the reseau glass was again measured using the Zygo interferometer (Fig. 6.1). As can be seen from the figure the differences between the unflatness of reseau plate one before and after mounting are of the order of 0.5 μm .

Adding the reseau glass to the optical system invalidated the manufacturers depth of field tables for the Biogon lens. To select a practical setting for the lens focus distance, before it was pinned,

an array of resolution test targets (Fig. 6.2) were set up and photographed on Kodak Technical Pan 120 film. The target array was arranged such that each resolution target provided a block of line pairs which would be imaged by the 38mm lens at nominal resolution of 50 l mm^{-1} ($20 \mu\text{m}$ per line pair). As such it covered most of the theoretical depth of field range (0.3m to ∞) of the 38mm Biogon lens when focused at 3m and set at its minimum aperture of $f/22$ (based on a circle of confusion $50 \mu\text{m}$ in diameter). Exposures were made at focus settings of 0.9, 1.8, 3.0, and 6.1 meters using each available lens aperture. The processed resolution test chart images could then be visually assessed under the 14.4X magnification available on the Zeiss Stecometer. A visual assessment of the line block corresponding to 50 l mm^{-1} could then be made, the target being defined as distinct if all lines in the block could be seen. A summary of the results, in terms of the usable object distance, is presented in table 6.3.

Table 6.3. Resolution test results.

Focused distance	F/No.	Nearest distinct target	Furthest distinct target
0.9m (3ft)	f/8	<1.0m	1.0m
	f/16	<1.0m	1.2m
	f/22	--	--
1.8m (6ft)	f/8	1.5m	2.3m
	f/16	1.2m	2.9m
	f/22	1.2m	3.5m
3.0m (9ft)	f/8	1.9m	3.0m
	f/16	1.9m	7.6m
	f/22	1.5m	>11.5m
6.1m (20ft)	f/8	3.5m	11.5m
	f/16	2.9m	>11.5m
	f/22	2.3m	>11.5m



Figure 6.2. A scanned image of a resolution test target.

Taking into account that most objects for photogrammetric analysis at City University are photographed within the subject distance range of 1.5m to 30m, the Biogon lens was pinned at a focus setting corresponding to a subject distance of 3m. The results of this analysis could then be used to determine the maximum usable aperture for any particular subject distance.

The design and subsequent modifications to this camera provided a stable optical system on which could be added the variables of film type, film back and exposing environment. At the same time the final calibrated camera would provide a system suitable for use in a wide range of

photogrammetric surveys.

6.1.2. In-camera laboratory exposure method.

In chapter 5 film processing was standardised to minimise in-plane deformations. Taking these results into account, the laboratory method was designed to produce consistently exposed and processed rolls of reseau images, which could then be examined for any deformational trends. Since City University owned only one old 120 Hasselblad camera back, an additional 120 back and a 220 camera back were hired from Leeds Photo Hire. These extra film backs enabled observations to be made concerning not only 120 and 220 film types but also any differences between the two 120 backs.

The use of several different film backs caused problems, because the 120 back used in the initial design of the camera was of an old design, providing an unusually large reseau plate to pressure plate separation. The first set of data captured (Section 6.1.3.1) used the initial modification of the Hasselblad camera (HS1), whilst subsequent tests, included those conducted in the laboratory used the second modification (HS2). The second modification had to be made since a film jam whilst using 120 film back B caused the first reseau plate to crack. This problem was solved by mounting a new reseau plate using less resin between the plate and mounting frame, thereby increasing the separation between the pressure plate and the reseau plate.

According to the standard procedures devised in chapter 5, the Technical Pan 120 and FP4 120 and 220 films to be evaluated were removed from the freezer one hour before loading into the respective camera backs. From this point the ambient laboratory environmental conditions were monitored using the Trace 323i thermo-hygrometer.

The in-plane experiments (Chapter 5) were inconclusive as to the influence of image density on deformation. Standardised exposure was therefore necessary if experiments were to concentrate on deformations caused by out-of-plane deformation. To achieve uniform exposure over the format area and consequently consistent reseau images, exposures were made with the camera objective placed on a light table. Exposure was carried out with one film/camera back combination at a time, using a sequence whereby the film was wound on, five seconds elapsed, an exposure made, the film wound on, and so on until the roll had been completely exposed. It was assumed that this consistent cycle would standardise any differential leading and trailing edge effects occurring between frames (Carman and Martin 1969).

As soon after exposure as practicable, the films were processed in one batch using a pair of small tanks according to the regime developed from the in-plane work (Table 6.4). Image measurements were then made using the ZKM measuring microscope on the dates mentioned in the table.

Table 6.4. Experimental parameters for films exposed in the laboratory

Film	Camera Back	Exposed: 15/1/90		Processed: 15/1/90	Measured	
		RH%, °C	Time		Date	RH%, °C
TCP 1A	120A	41.4, 18.7	8:30	Developer: ID11 1:1 10 min. at 22°C Stop: Kodak Indicator Stop 30 sec. Fixer: Ilford Hypam with Ilford Rapid Hardener 5 min Wash: 30min.	20/2/90	54, 19.5
TCP 2A	120A	44.1, 18.7	8:39		21/2/90	44, 19.7
TCP 1B	120B	43.6, 18.9	8:35		21/2/90	37, 19.4
TCP 2B	120B	44.4, 18.6	8:45		21/2/90	36, 19.5
FP4 120	120A	44.7, 18.5	8:48		21/2/90	42, 19.7
FP4 220	220	44.9, 18.5	8:55		22/2/90	44, 19.8
FP4 220	220	44.9, 18.6	9:00		22/2/90	46, 19.6
				20/2/90	53, 19.8	

6.1.3. Results and analysis of experiments including out-of-plane deformation.

All reseau image measurements were processed using the globally applied affine transformation common to all in-plane experiments. A representative sample of the vector plots of residuals associated with each of the film/camera back combinations are shown in appendix B. For simplicity the results will be discussed in two groups delineated by film type. Also included in the discussion are films exposed in the same camera/film back combinations during the test-field photography (Table 6.10).

6.1.3.1. Holotest 10E56 70mm film exposed in HS1.

The first roll of film exposed in the modified Hasselblad camera was a roll of 70mm Agfa Holotest 10E56 film used during the test field photography (Table 6.10, Set 1). The 10E56 film type had to be used, as opposed to the faster 10E75 used for the in-plane work, because this was the only type available which had the edge perforations required by the Hasselblad 70mm back. The film was exposed in the first modification of the camera (HS1).

Table 6.5 RMS residuals for Agfa Holotest 10E56 70mm Film.

Film	RMS x(μm)	RMS y(μm)
Roll 1	5.22(σ=0.51)	7.01(σ=0.59)

Table 6.5 shows the mean RMS values and their associated standard deviations for all eight frames on the strip of film. Vector plots displaying typical deformation patterns are shown in figure 6.3.

All contact grid images produced on Holotest film exhibited in-plane deformations of the order of $1\mu\text{m}$ RMS, so it must be concluded that most of the deformations found were caused by film deformations present at exposure.

Exposures made using the modified Hasselblad SWC Camera (HS1)
onto Agfa Holotest 10E56 70mm Film

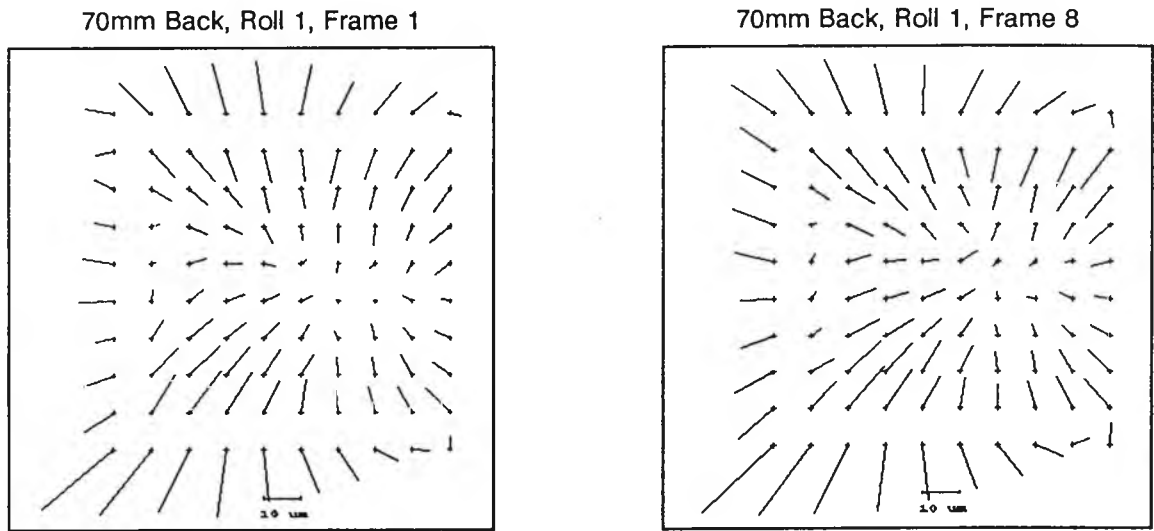
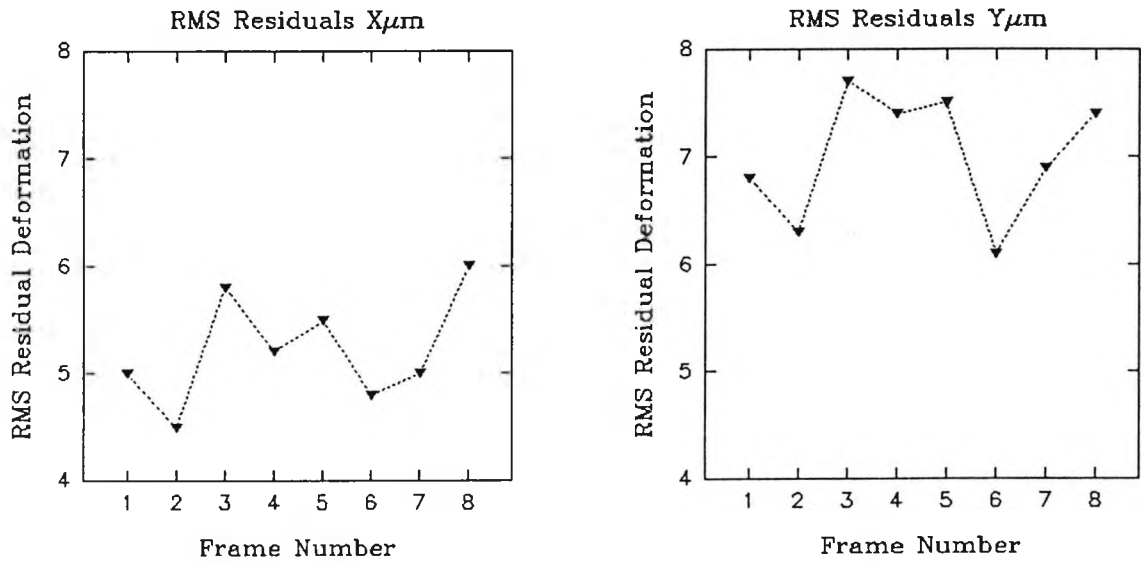


Figure 6.3.

RMS Residuals after Affine Transformation at Reseau Image Positions
for Agfa Holotest 10E56 70mm film exposed in HS1.



▼ AGFA Holotest 70mm film, Exposed at Test Field.

Figure 6.4.

It was mentioned in section 6.1.2. that the reseau glass-pressure plate separation was not consistent over the format area, giving rise to increased film tension during wind-on in the HS1 modification. This physical effect would agree not only with the larger RMS residuals in the y direction (Fig. 6.4) but also with the deformation pattern seen in the vector plots, the large edge vectors, especially those in the bottom left hand corner, being caused by friction between film surfaces and the register glass and pressure plate.

Whilst there are some variations in the RMS residuals between images along the length of the roll, the primary image deformation patterns observed along the length of the film remain consistently typical with the examples presented in figure 6.4. Due to the limited data (eight frames) it is not easy to draw any conclusions concerning the physical cause of such variations, but random local unflatness differences are a possible cause.

6.1.3.2. Kodak Technical Pan 120 in HS2.

This discussion draws upon results from the two rolls of Kodak Technical Pan 120 film exposed in the laboratory in each of the camera backs (Table 6.4) and two rolls of Kodak Technical Pan 120 film exposed during the test field photography (Table 6.10). A summary of the typical deformation patterns (after affine transformation) encountered in each of the 120 camera backs is presented in the upper four vector plots of figure 6.5 (further plots associated with this data set are shown in Appendix B). In addition Table 6.6 shows the RMS residuals and their associated standard deviations, computed from differences between the imaged positions of the reseau crosses after affine transformation and their calibrated positions, for all frames on each roll of film.

Table 6.6 RMS residuals for Technical Pan rolls 1 and 2 in film backs A and B.

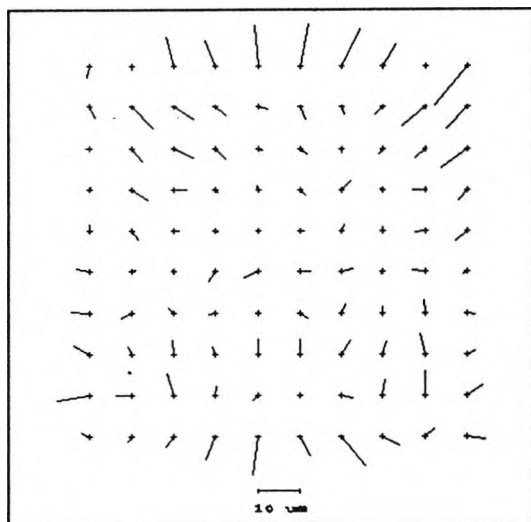
Film	Back A		Back B	
	RMS x(μm)	RMS y(μm)	RMS x(μm)	RMS y(μm)
Roll 1	2.30($\sigma=0.22$)	3.39($\sigma=0.30$)	6.23($\sigma=0.25$)	5.81($\sigma=0.46$)
Roll 2	2.17($\sigma=0.24$)	3.43($\sigma=0.33$)	6.49($\sigma=0.65$)	6.36($\sigma=1.63$)
Roll 3	2.44($\sigma=0.39$)	3.72($\sigma=0.57$)	6.42($\sigma=0.59$)	6.02($\sigma=0.38$)
Roll 3*	3.34($\sigma=3.02$)*	4.98($\sigma=3.95$)*	--	--

* includes roll 3, Back A, frame 6

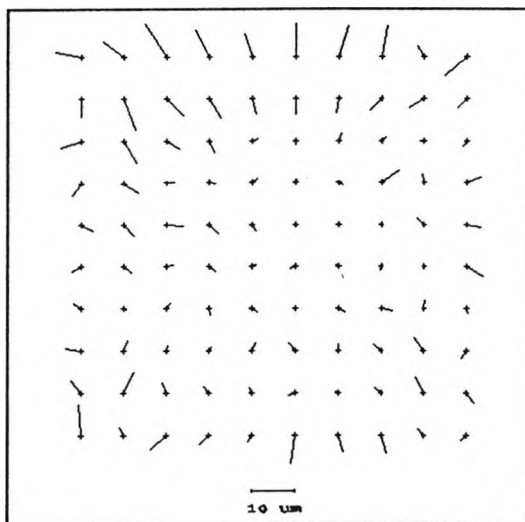
From these data it can be seen that there are distinct differences between both the pattern and magnitude of the deformations associated with each camera back. These effects can be explained by considering the physical differences between the 120 camera backs used. The first back (A) was of an older design, having a thinner pressure plate than the second back (B). It can therefore be concluded that the differences in the deformation patterns seen are due to the differences in separation between the reseau plate and film flattening plate provided by each film back.

Exposures made using the modified Hasselblad SWC camera
onto Kodak Technical Pan 120 Film

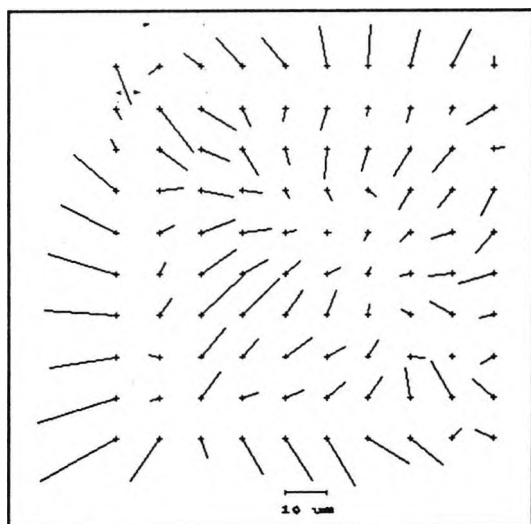
Back A, Roll 1, Frame 1



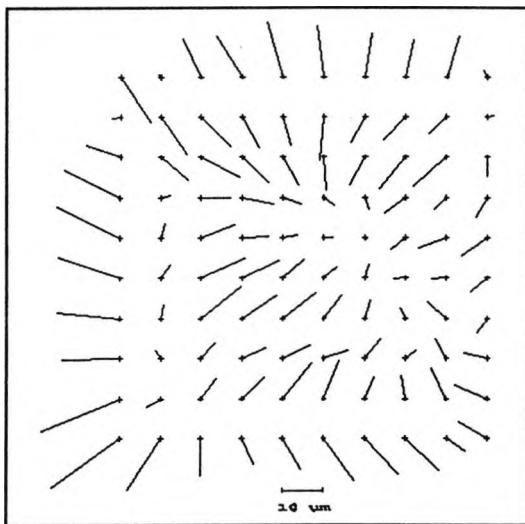
Back A, Roll 3, Frame 2



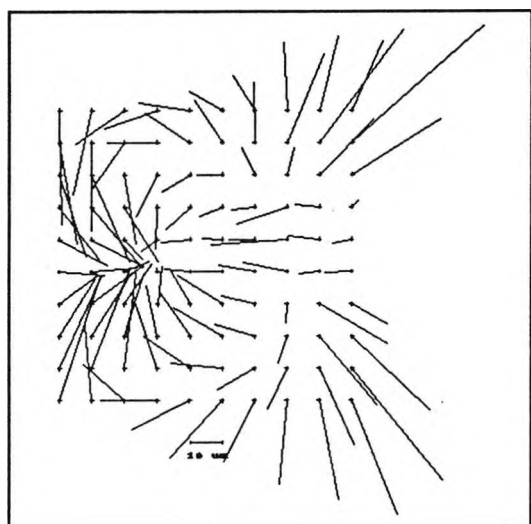
Back B, Roll 1, Frame 4



Back B, Roll 2, Frame 9



Back A, Roll 3, Frame 6



Back B, Roll 2, Frame 7

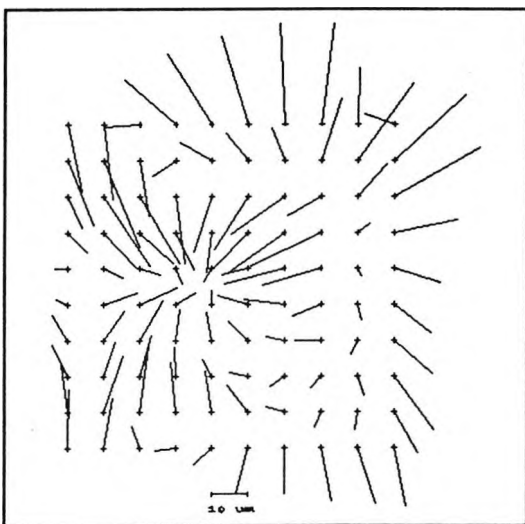


Figure 6.5.

A smaller clearance between pressure plate and reseau provided by back (B) has produced a greater flattening force. Whilst flattening pressure is desirable at exposure, the non-retractive design of the Hasselblad pressure plate means that this force will also be present during film wind-on causing excess friction which may have given rise to the deformations seen at the edges of all frames exposed in camera back B. The problem has been compounded by the reseau plate modification, because although the plate was aligned parallel to the lens filter mount (assumed to be orthogonal to the optical axis) the film did tend to catch on the bottom left corner of the reseau plate, indicating that it was slightly out of alignment with the film plane of the attached film backs.

If similar deformation patterns are found to be present from frame to frame, film deformation corrections could potentially be applied globally to all image measurements from frames in a strip. It has already been shown that visual resemblances exist between frames on similar films exposed in the same camera back, but the standard deviations associated with the RMS residuals for a complete set of frames (Table 6.6) do not provide a comprehensive analysis. To detect any useful trends it is necessary to consider the RMS residuals associated with each individual frame in conjunction with the frames position along the length of the roll (Figs. 6.6 and 6.7).

Considering figures 6.6 and 6.7, two frames exhibit atypical deformations, frame 6 from film 3 exposed in back A and frame 7 from film 2 exposed in back B. Vector plots of residuals associated with these two frames are shown in the bottom two vector plots of figure 6.5. The frame from back A exposed during the test-field photography was noted during the practical work, because the clips attaching the film back to the camera body had come loose during photography. The deformations exhibited by the frame exposed in back B during the laboratory work were however unexpected. The only plausible explanation is again provided by loose catches especially as the vector patterns were similar. Looseness was undetected because it would have been rectified during film wind-on because the camera was held by pushing the camera back down onto the light table during this procedure. This recurring problem must be due to wear of the clips on the camera body, and consequently could be solved by fitting new catches.

Once these anomalous frames are disregarded the RMS residuals associated with each frame on Technical Pan 120 film do not appear to show any major systematic trends with position on the roll. The rolls exposed during the test field photography could be expected to demonstrate systematic trends between groups of frames since they were exposed at varying intervals, providing differing pre-exposure conditioning times. No specific patterns can be seen in the data, although it could be argued that the changes from frame to frame are more irregular along the length of the rolls of film exposed at the test field. Such an effect could be explained by the low temperature and high humidity present during the test field photography, compounded by the fact that exposures were not made at regular intervals.

RMS Residuals After Affine Transformation at Reseau Image Positions
for all Rolls of Kodak Technical Pan 120 Film Exposed in 120 Back A.

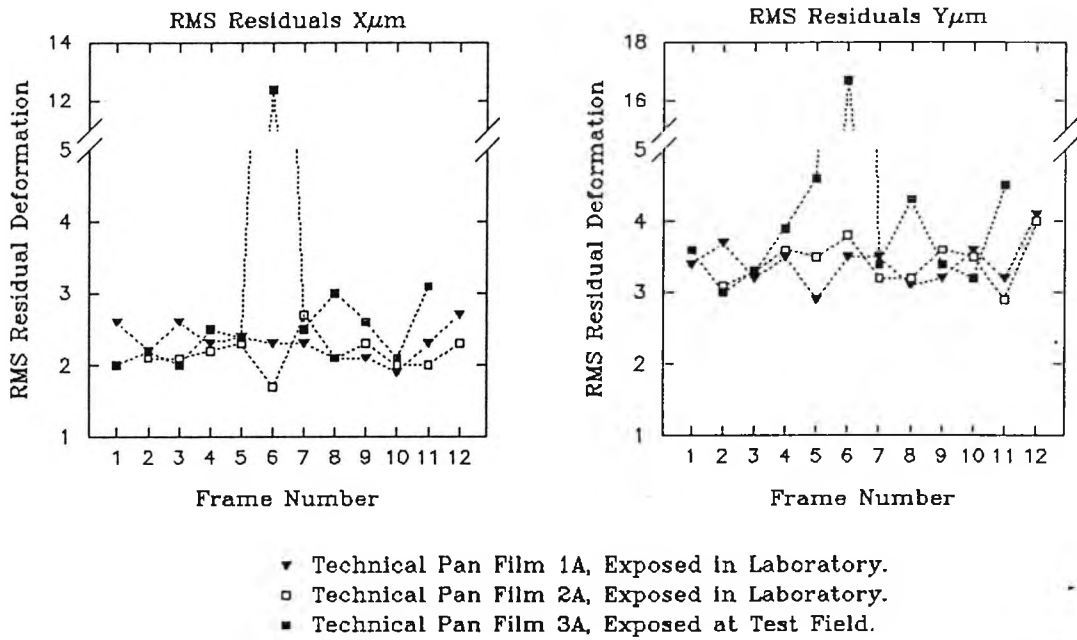


Figure 6.6.

RMS Residuals After Affine Transformation at Reseau Image Positions
for all Rolls of Kodak Technical Pan 120 Film Exposed in 120 Back B.

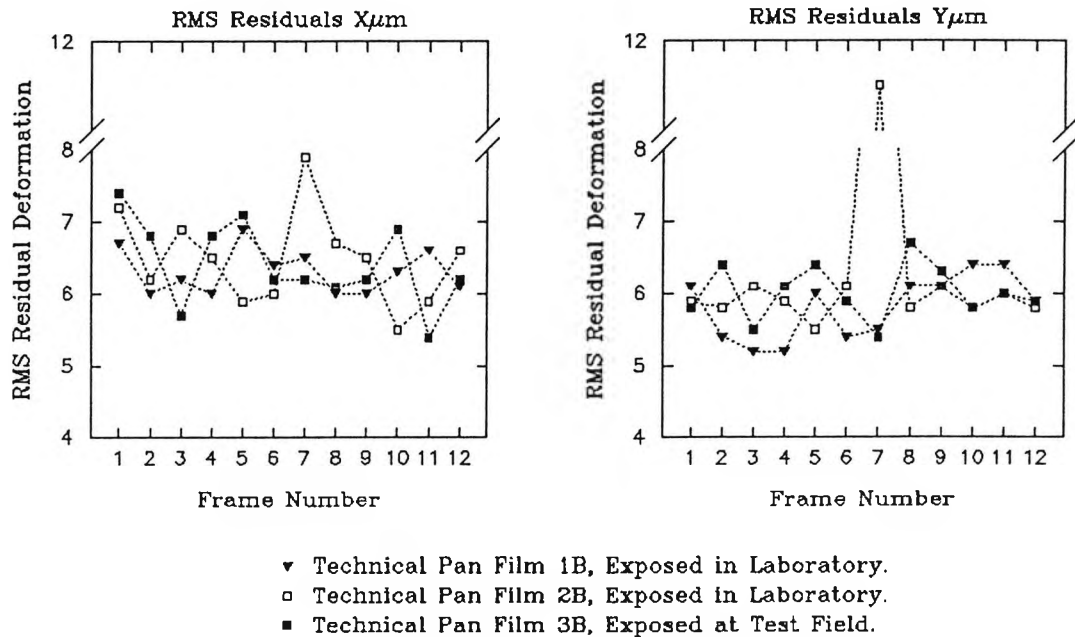


Figure 6.7.

6.1.3.3. Ilford FP4 120/220.

Using back (A) from section 6.1.3.2. and an additional 220 film back, out-of-plane deformations for Ilford FP4 120 and 220 films were compared. With the exception of the top right and bottom left plots, the vector plots in figure 6.8 represent typical deformation patterns produced. Whilst different film backs and thickness of film have been used, their associated deformation vector plots demonstrate significant regions of similar pattern. This suggests that the deformation patterns are dependant on the thickness of the film and backing paper (if present) compared to the separation between each film back pressure plate and the reseau glass.

Table 6.7. RMS residuals for FP4 120 and 220 rolls 1 and 2.

	120 Back A		220 Back	
	RMS x(μm)	RMS y(μm)	RMS x(μm)	RMS y(μm)
Roll 1	2.39($\sigma=0.90$)	3.32($\sigma=0.66$)	2.47($\sigma=0.23$)	3.91($\sigma=0.30$)
Roll 2	--	--	2.70($\sigma=0.23$)	4.25($\sigma=0.36$)
Roll 3	2.03($\sigma=0.25$)	2.86($\sigma=0.18$)	3.32($\sigma=0.90$)	3.86($\sigma=0.71$)

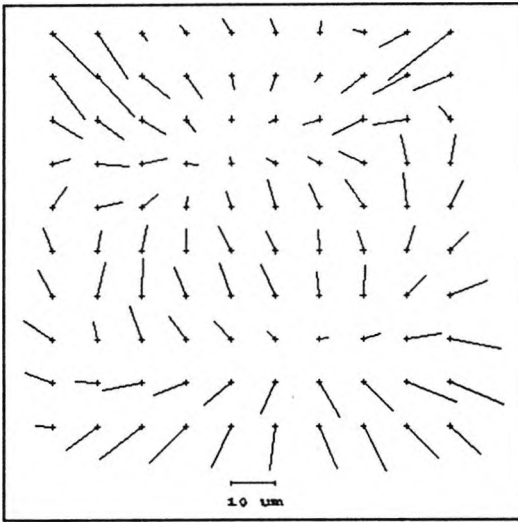
With the exception of frame 1 roll 1, the images on Ilford FP4 120 film demonstrate only small fluctuations between frames along the length of the roll. Again the deformations exhibited by this atypical frame could be due to loose catches, but this link cannot be made conclusively since the deformation pattern is different from those observed earlier and no loosening was noticed during the experiment.

The images on Ilford FP4 220 film produce RMS residuals of a similar order of magnitude to those given by the images on FP4 120 film. However significant trends are present for images along the roll of 220 film exposed during the test field photography. The increasing magnitude of the RMS values from frame 13 onwards, especially in the x direction, cannot be directly linked to any physical process using the available data. Possible causes of the trends seen are likely to be connected to the low temperature and high relative humidity (Table 6.10) at exposure. The absence of a backing paper with 220 film may be a primary factor since: firstly it may have allowed enough conditioning to occur to significantly change the moisture content of the film and; secondly forces produced during film wind-on will be carried by the film base alone.

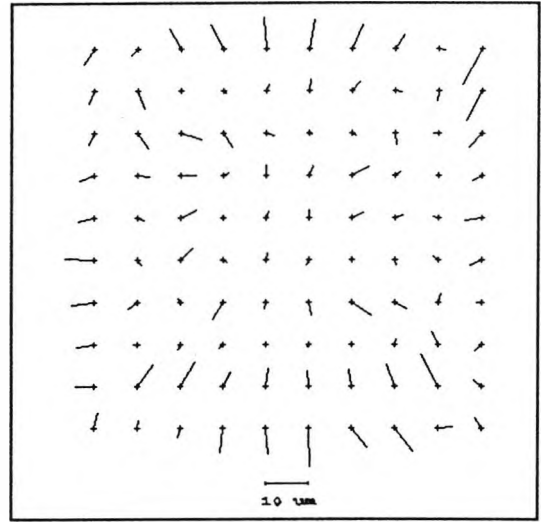
Systematic fluctuations in the RMS data can be identified along the length of the laboratory exposed films. Patterns are predominant in the y direction, corresponding to the length of the film. Again the data do not allow any contributory factors to be identified, especially since the in-plane data could not be analyzed in this way, there only being three frames to a roll. The only clue is that this type of trend is greatest in the FP4 220 and Agfa Holotest films, suggesting that it is either aggravated by these camera backs or that the absence of a film backing paper is significant.

Exposures made using the modified Hasselblad SWC camera
onto Ilford FP4 120 and 220 Films.

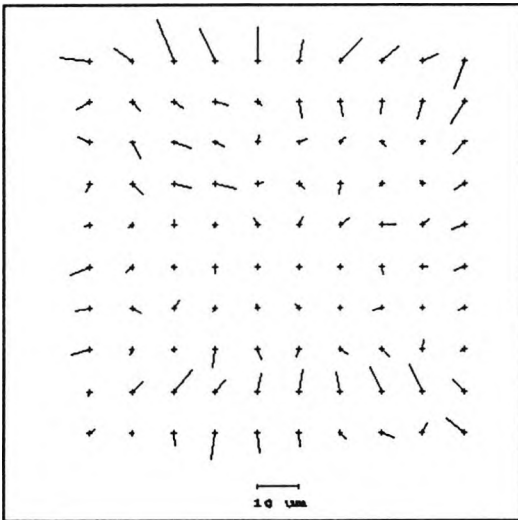
FP4 120 Back A, Roll 1, Frame 1.



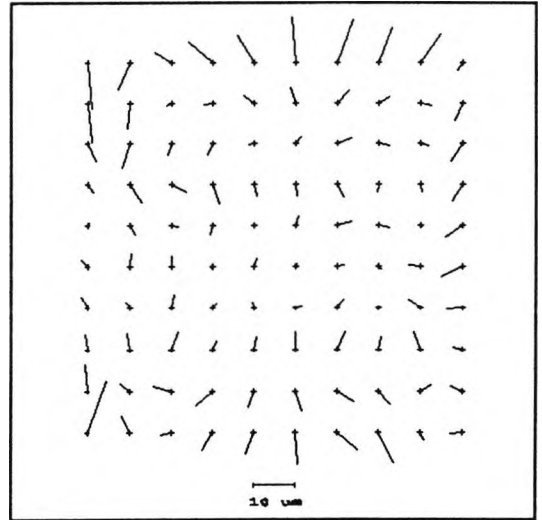
FP4 120, Back A, Roll 1, Frame 8.



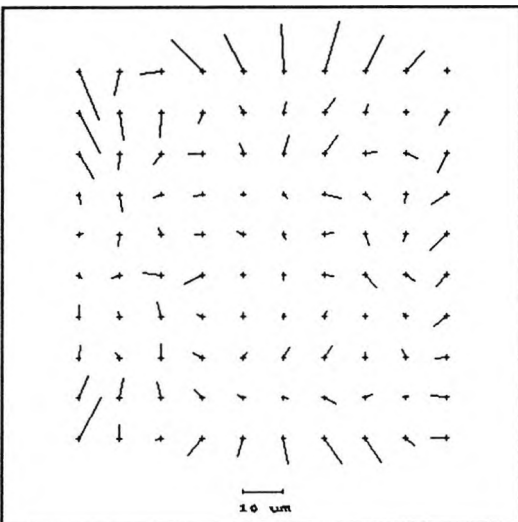
FP4 120 Back A, Roll 3, Frame 10



FP4 220, Roll 1, Frame 10.



FP4 220, Roll 2, Frame 18.



FP4 220, Roll 3, Frame 20.

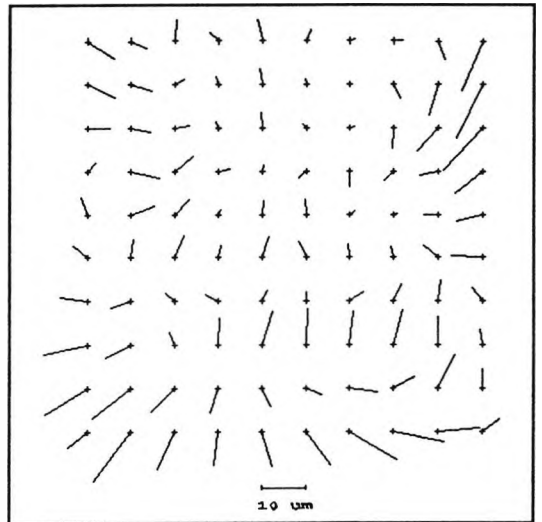


Figure 6.8.

RMS Residuals After Affine Transformation at Reseau Image Positions
for all Rolls of Ilford FP4 120 Film Exposed in 120 Back A.

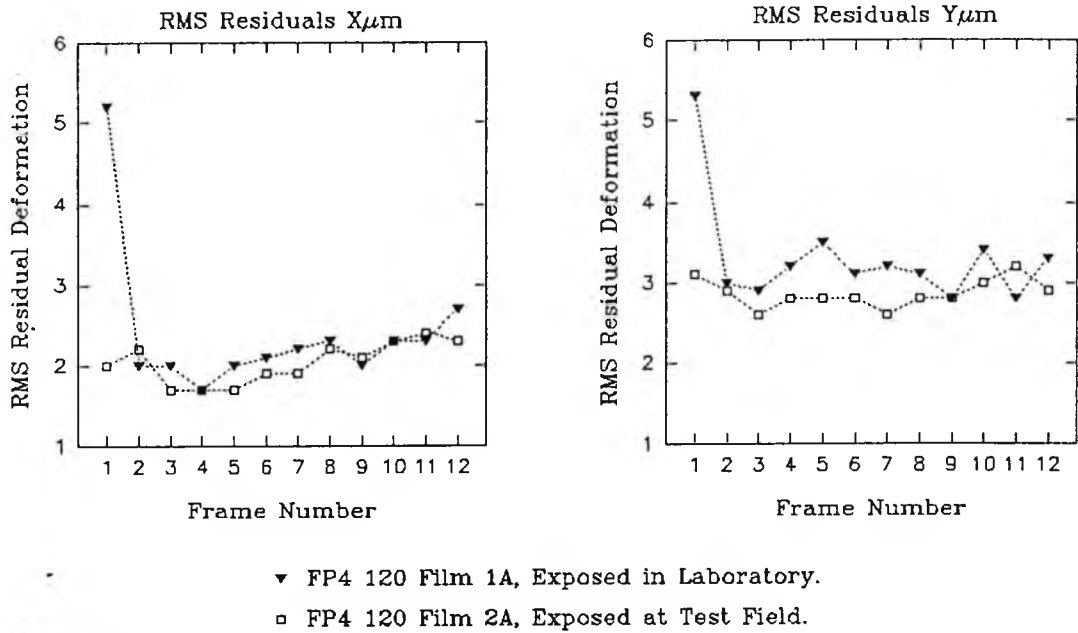


Figure 6.9.

RMS Residuals After Affine Transformation at Reseau Image Positions
for all Rolls of ILford FP4 220 Film Exposed in the 220 Back.

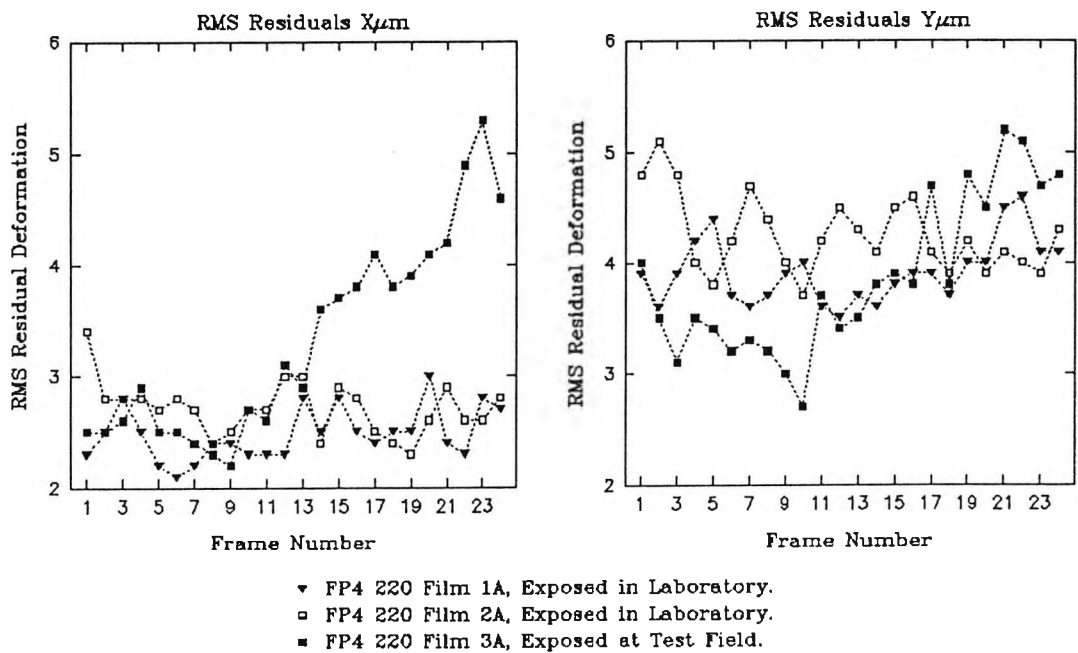


Figure 6.10.

6.1.4. Summary of in-camera deformations.

The main conclusion which can be drawn from this exercise is that deformations occurring in this particular camera are almost an order of magnitude greater than those attributed to in-plane factors.

Distinct differences have been found between different camera backs and film thicknesses, leading to the conclusion that the gap between the pressure plate and the register glass must be critically selected according to the film and backing paper thickness used. This conclusion can of course only be stated for the Hasselblad style of camera back design which uses a fixed sprung pressure plate, as opposed to the retractable plate used in cameras such as the Rollei-Metric 6006.

Since the gap between pressure plate and register glass is critical, it would be expected that a retractable plate would provide significant advantages: it would minimise friction during film wind-on and; it would permit a variety of film thicknesses to be employed in the same camera back. The envisaged improvement is not seen in the Rollei-Metric 6006 camera (Chapter 4) which uses this system, probably because the unflat reseau of the particular camera tested negated any advantages. Another more costly alternative is the vacuum back such as that used in the Pentax PAMS645-VL camera which has been used to produce some excellent results (Fraser 1990).

Further comments concerning in-camera deformations must be confined to the limitations of the Hasselblad camera design and the modifications carried out. The distinct differences between the deformation patterns produced using different film types and camera backs raises the possibility of a film deformation correction procedure based on mean image deformation corrections, specific to each camera and film combination. The effectiveness of such a method will be related to the variation occurring between images measured on any given film. Whilst results have shown that trends in the magnitude of film deformation along the length of the film can occur, data are at present too limited to determine the physical causes and typicality of such trends.

A final comment at this stage concerns the engineering problems associated with the Hasselblad camera modifications, some of which have clearly introduced film deformation. Most problems could be avoided by mounting the reseau plate parallel to the camera back mount rather than in accordance with the front filter mount. In a new camera the camera back mount and the lens filter mount should be parallel, but in this case the difference probably related to the age and well worn condition of the modified camera. However for the price of the system (~£1000) one cannot expect ideal performance, in fact the 2 to 3 μ m RMS deformations produced appear remarkably low.

6.2. Practical test field evaluation.

The objectives of this section are threefold: to look at the effects of film deformation in practice; to evaluate the explicit film deformation modelling methods and; to make a comparison between the photogrammetric possibilities of metric, semi-metric and non-metric cameras.

The basis of the experimental method was to photograph an array of targets, measure the images produced and then to relate the measured image positions to the target positions using a self calibrating bundle adjustment (Section 3.4). Given the image measurement data, the functional model (Section 3.4.1) could be varied to include additional parameters and explicit film deformation corrections, with the object of enhancing the model according to physical effects. Results of the various adjustments could then be assessed by analysis of the associated stochastic model (Section 3.4.2). In this way, employing careful design of the experimental technique, the same data could be used to evaluate not only the above three objectives, but also to calibrate the modified Hasselblad camera for various photogrammetric applications, including architectural surveys, deformation monitoring and engineering projects.

6.2.1. Test field design and survey.

Before designing any photogrammetric network, it is necessary to set some accuracy specifications which describe not only the precision of the object and image space coordinates, but also the precision of the parameters to be estimated. Film deformation effects can give rise to apparent shape changes in the object space, whilst camera calibration requires a good estimation of the parameters describing the geometric properties of the camera system.

An initial working value to be attained by the standard deviations of the estimated object space coordinates was set at 1.0mm, since this represented a realistic practical target centre point and was beyond the 2 to 3mm which could be achieved over a small area by conventional survey. Preliminary standard deviations of some of the interior orientation and additional parameters included in the adjustment to model lens distortion were initially set at the 20 μ m standard deviation quoted by the major manufacturers in their calibration certificates (Zeiss(Jena) 1985; Wild 1984).

Design of the test field array can be logically carried out by giving careful consideration to the requirements of the experiment, grouped according to the four network design orders (Grafarend 1974) discussed in (Section 3.4.4). Although each stage can be described mathematically (Fraser 1984), in this case due to the absence of any integrated network design software, design was evaluated and will be discussed in general terms outlining the important features. These design considerations can then taken into account during the selection of a suitable test field location, before a bundle adjustment using pseudo data based on the physical constraints of the available

object space and camera systems is computed.

6.2.1.1. Zero Order design (Datum).

This design factor is concerned with the way in which the object space coordinates are defined. Changes in shape can be used as a measure of the effects of film deformation (Fraser 1984b; Fryer 1988), consequently the major consideration for this work is that the datum definition should not introduce any shape distortion into the adjustment. In this situation the method of 'free adjustment' (Section 3.4.3) can be used to provide a datum which is independent of object space measurements. The method permits convergent multi-station photography to be used without control points, the datum in this instance being defined by the centroid of the object coordinate starting values used in the iterative least squares process. The method also results in increased parameter estimation precision because the inherently more accurate photogrammetric measurement data are not limited by the precision with which control points can be located in space by conventional survey methods (Section 3.4.3).

6.2.1.2. First Order design (Configuration).

The 'free adjustment' requirement for a multi-station convergent imaging geometry means that the basis of the first order design is already defined (Fig. 3.10). The next step is to refine this imaging geometry to satisfy accuracy and precision requirements (Section 3.4.5), whilst including considerations such as: practical test field location; the precision with which the calibration parameters are to be estimated; and the physical limitations of the camera equipment to be calibrated.

To enable a variety of cameras to be calibrated and different analysis to be carried out, the test field site had to meet several requirements: the array had to be large enough to cover the image format area of all cameras to be evaluated; at least six month's stability and durability were required; additionally there had to be enough room in the object space to permit a range of camera-subject distances.

Dimensional stability and durability were important because an initial calibration was required to check that the estimated parameters were recoverable with the level of precision predicted during the design process. More important for durability, the whereabouts of University apparatus tends to be very unpredictable so that any room although initially clear can soon become unexpectedly obstructed.

An approximate minimum test field size could be determined by computing a limiting magnification. A minimum practical target centre ($\sim 1.0\text{mm } \emptyset$) was decided upon, which when photographed by the Hasselblad SWC camera at the 50 l mm^{-1} possible over the whole field

(Section 6.1.1) would produce a minimum magnification (m) of 0.02. This magnification could then be linked with the focal length (f) of each camera lens, by the equation $u=f(1+1/m)$, to give a maximum subject distance (u) for each camera lens. The angle of view and nearest focus setting of each camera could then be used to determine the minimum test field area required to cover its image format.

Table 6.8 describes the camera systems to be employed together with their computed minimum test field size. From the table it can be seen that the limiting camera (providing the largest test field dimension) is the Wild P32, with its closest focus requirement of 3.5m, (Schlienger 1972).

Table 6.8. Camera equipment selected for test-field photography.

Camera	Lens type, focusing arrangement and minimum distance			Image Format	Angle of View (deg)	Test Field Size at $m=0.02$	Fiducial System	Available Backs
Metric	Zeiss (Jena) UMK 10/1318N	Zeiss Lamegon 100mm f/8	Focus by click stops (1.4m)	130mm by 180mm	79 61	4.3m by 3.1m ($u=2.6m$) ($m=0.04$)	Four illuminated marks	Glass Plates or Film
	Wild P32	64mm f/8	Fixed Focus (3.5m)	65mm by 90mm	64 49	6.7m by 3.7m ($u=3.3m$)	Five reseau crosses	Glass Plates or Film
Semi-Metric	Modified Hasselblad SWC	Zeiss Biogon 38mm f/4.5	Fixed Focus (1.4m)	52mm by 52mm	69	5.0m by 5.0m ($u=1.9m$)	100 reseau crosses	Glass Plates or Film
Non-Metric	Hasselblad 500C	Zeiss Distagon 60mm f/3.5	Free Focus (0.6m)	56mm by 56mm	50	3.6m by 3.6m ($u=3.1m$)	Format edges	Glass Plates or Film

Data in table from manufacturers' data (Zeiss 1983; Wild 1977; Hasselblad 1989)

The most suitable place for a target array was a site on the University roof. This incorporated an 8.4m by 5.7m south facing concrete lift tower and a 21m by 8m area in which camera stations, survey stations and any additional targets could be positioned. Whilst the open air environment conferred the advantage that ambient light could be used to illuminate the targets, it also meant that target design had to take into account not only pointing precision but also the effects of frost.

Although the vertical concrete tower surface only provided a two dimensional target array, the strongly convergent photo-geometry envisaged would simulate a three dimensional array allowing the recovery of focal length (Brown 1972).

The target array had to consist of enough targets to cover the format area, whilst being of a similar density to the reseau array used during the in-plane experimentation so that the effects of film deformation and lens distortion could be assessed. Balanced against the use of a dense array

was the measurement time involved, bearing in mind that multiple camera positions and multiple pointings to each target image would significantly increase the number of measurement time required.

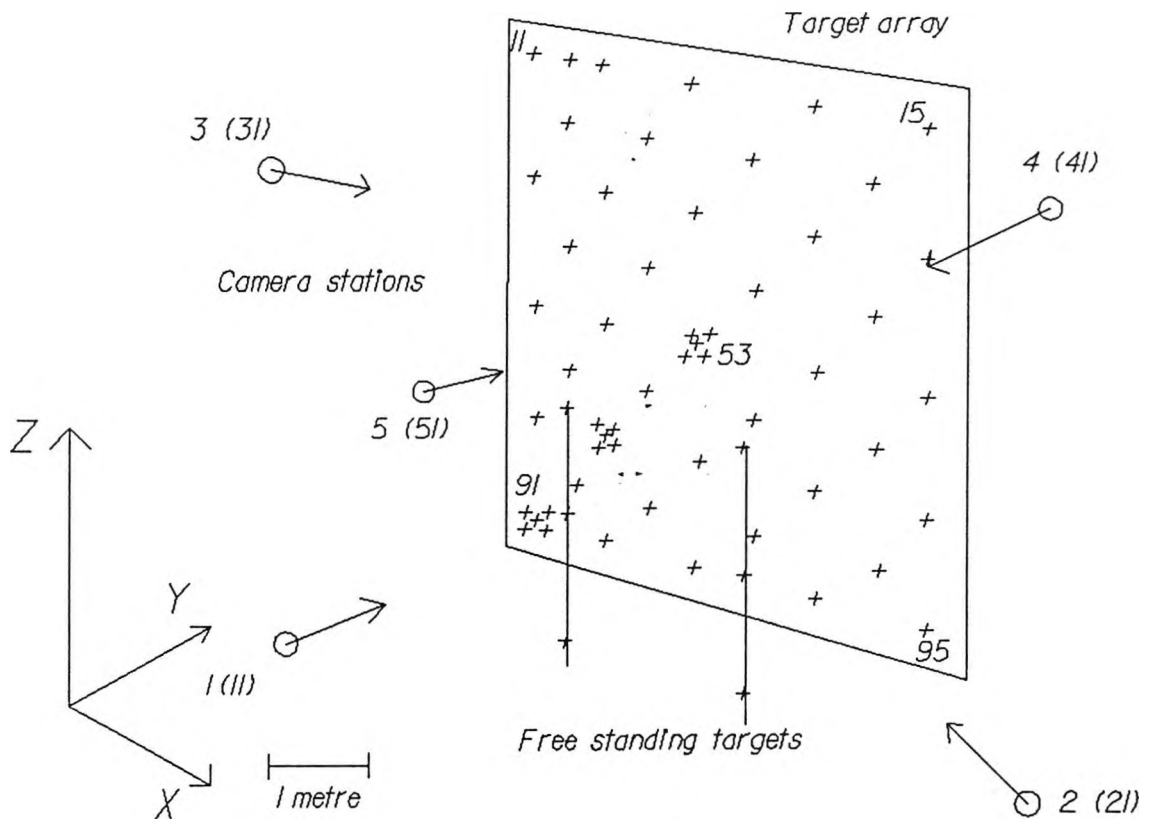


Figure 6.11. Schematic diagram of the network geometry.

As an initial test design, a planar array consisting of 42 targets at 0.75m spacing (Fig. 6.11.), and an additional 6 free standing targets were decided upon. Four pseudo camera stations were then selected to be at the corners of a square-based pyramid situated such that its apex was in the centre of the test field array. The collinearity equations (3.1) could then be employed in a program called NIB (Chandler 1988) to compute appropriate photo-coordinates for each camera. These ideal photo-coordinates were then randomised based on a normal distribution with zero mean and a standard deviation of $5\mu\text{m}$ using a second program RAND (Clarke 1988). The a priori analysis was subsequently extended to include an extra camera in the centre of the base of the pyramid, and then with four extra cameras in identical positions to the first four but with the image format rotated 90° about the optical axis.

Results demonstrate that the envisaged geometry can exceed the initial adjustment objectives. Adding more camera positions has not only strengthened the network but it has provided a larger more representative sample of deformed images. The inclusion of rotated cameras has significantly increased the precision with which the camera calibration parameters and object space coordinates can be estimated. This effect is understandable because not only are there an increased number of photographs, but the camera calibration parameters will be estimated using different test-field attitudes, thereby helping to decrease the reliance of the estimation on geometric camera position.

Table 6.9. A priori standard deviations of the object space coordinates and camera calibration parameters estimated during the network analysis.

Number of Cameras	RMS standard deviations of estimated object space coordinates (mm)			Standard deviations of estimated Inner Orientation parameters (micrometers)			Standard deviations of estimated Additional Parameters				
							Radial distortion			Tangential distortion	
	X	Y	Z	f	px	py	k1	k2	k3	p1	p2
4	0.58	0.65	0.57	21.8	36.6	59.2	3.05	8081	6417729	0.008	0.010
5	0.51	0.60	0.50	20.3	35.5	57.5	2.68	7304	5892752	0.008	0.010
9	0.33	0.46	0.30	11.9	10.6	10.6	1.68	4561	3670791	0.003	0.003

6.2.1.3. Second Order design (Measurement).

The network design carried out so far has assumed random image coordinate errors with a standard deviation of $5\mu\text{m}$. Second order design is concerned with maximising the precision of image coordinate measurement, such that the elements of the weight matrix approach the identity matrix (Fraser 1984a). There are three factors which must be considered if location and measurement of target images positions are to be optimised: target design; measuring machine accuracy and; measurement pointing ability.

a) Target design. The targets had to be designed to record on a wide range of negative materials, and to adhere rigidly to the concrete facing of the lift tower. One of the initial assumptions made concerning the network design was that the target centre should be of the order of 1mm in diameter. A suitable adhesive backed aluminium target was available from Shoring Products, but required some weatherproof method of attachment to the concrete lift tower face to meet all the requirements.

Various glues and resins were used to attach pieces of backing plastic onto similar vertical concrete surfaces on the University roof over the winter of 1989. The major problem appeared to be that the resin glues were initially too liquid such that the target slid down out of position until

the resin dried. This problem was overcome by pinning the targets to the concrete face. A 1mm hole was drilled through the centre of each target and into the concrete tower surface. The hole and surrounding area were then coated with resin so that a 50mm long titanium rod could be inserted through the glued target and into the wall.

To assist identification, each target was numbered with Letraset lettering, the assembly finally being sprayed with matt varnish. The resultant target (Fig. 6.12) was of high contrast facilitating its recording on a wide range of negative materials. However some surface sheen was present which could reduce contrast under very sunny conditions. Figure 6.13 shows another target made by Shoring Products which, being less robust, was simply glued in position at the beginning of each photographic session.

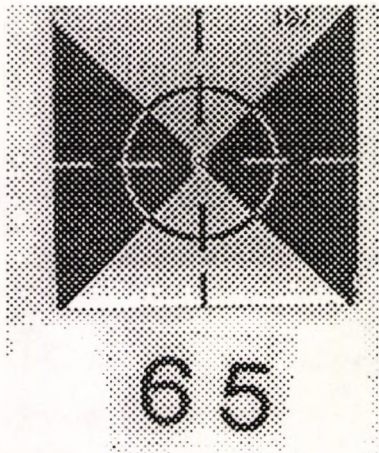


Figure 6.12. Layout of one of the pinned targets.

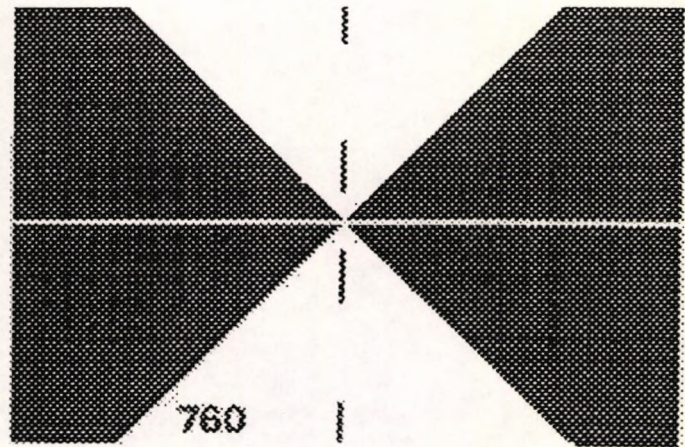


Figure 6.13. Shoring Products Survey Target 760.

b) Measuring machine accuracy. The machine chosen for these studies was the NPL ZKM measuring microscope (Section 5.2.1.7). The features of this machine were well known from the in-plane experimentation and reseau plate calibration. RMS coordinate standard deviations associated with the instrument were of the order of $0.5\mu\text{m}$, very much smaller than the $2\mu\text{m}$ to $3\mu\text{m}$ RMS values quoted but often disputed for most photogrammetric analytical plotters (Laiho and Kilpelä 1988).

c) Measurement pointing ability. The ZKM provided a range of high magnifications and a variety of different measurement graticules, enabling the system to be tailored to the size of the target images to be measured. Another important aspect of this machine was that the gain control of the camera which recorded the microscope image could be altered in conjunction with the TV monitor settings to enhance or reduce the image contrast. Whilst not fully compensating for badly exposed images it did permit optimisation of the system to each particular image. By pointing to all target and fiducial image three times, a mean comparator coordinate position and associated standard deviations could be computed for each image point. The standard deviations could then be included in the weight matrix (Equation 3.23) used in the bundle adjustment.

Using these facilities, image quality and image measurements could theoretically produce a higher level of pointing precision than those conventionally attained during small format photogrammetric surveys. The limitations of small format cameras and film products could be assessed.

6.2.1.4. Third Order design (Densification).

Object point precision is largely independent of target array density for multi-convergent imaging geometries (Fraser 1989), however for the purposes of this exercise a dense target array could enable an assessment of the effectiveness of the envisaged mathematical corrections to compensate for localised film deformations. In designing the basic test field array, a compromise between target density and image measurement time was made. However for the purposes of detecting very localised film deformations it was decided to include several local clusters of targets of the type shown in figure 6.13 which could be simply stuck to the wall immediately prior to photographs being taken.

To summarise, the final array consisted of forty two targets pinned to the concrete wall, six targets supported on poles away from the plane of the wall and three local clusters of targets glued to the wall (Fig. 6.11).

The pinned targets were surveyed as part of a student project (Godfrey 1989), thereby providing X,Y,Z starting values for use in the photogrammetric adjustment. Means and standard deviations of the target coordinates derived from this survey are presented in appendix B.

6.2.2. Photography of the test field.

Photography was carried out on two occasions using the selection of cameras shown in table 6.8. The first set of photographs for calibration were made using the UMK 10/1318 and the modified Hasselblad camera (HS1) both

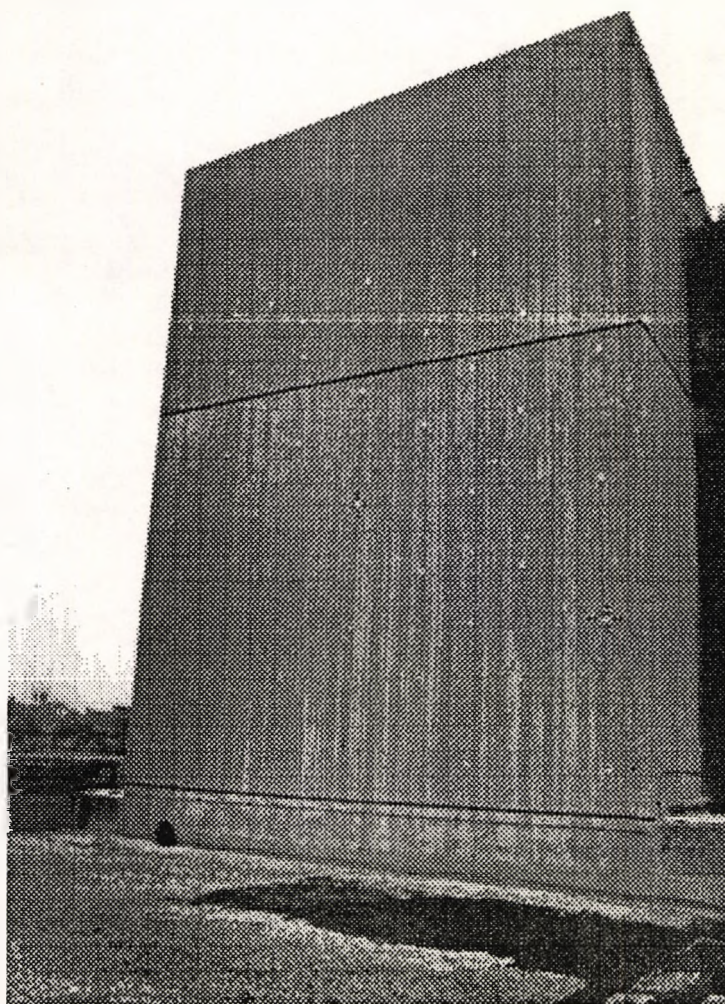


Figure 6.14. The concrete tower showing pinned target array.

with Agfa holotest emulsions. All photographs were made with the camera equipment securely mounted to a tripod, scaffolding being used to provide a stable base for the higher camera positions. By including both metric and semi-metric cameras in this first set, results of the least squares estimation could be used to check that the method was capable of providing suitable precision.

In the second set of photography a Wild P32 provided the metric camera, a variety of different film/camera back combinations were exposed in the modified Hasselblad (HS2), and finally an unmodified Hasselblad 500C camera was used with both FP4 120 film and FP4 glass plates.

The non-metric Hasselblad 500C camera was included so that a comparison could be made between the ability of the mathematical model to correct for distortions occurring in all three classes of camera system. By using the same 120 film and film back on both the Hasselblad cameras it was envisaged that some inferences could be drawn concerning the magnitude and effects of film deformation in the non-metric camera.

The photographic images produced were processed on the day of the photography, according to the regime developed from the in-plane work.

Table 6.10. Exposure, processing and measurement of the test-field photography.

Photo Set	Camera	Film and Back	Exposure	Processing	Measurement (NPL ZKM)
Set 1	UMK	10E75	5/11/89 78.8% 11.0°C	5/11/89 HC110 1:19 9 min at 20°C	15/11/89
	HS1	10E56			16/11/89
Set 2	P32	FP4/120	12/1/90 78.5% 8.9°C	12/1/90 ID11 1:1 12 min at 20.5°C	29/1/90
		FP4/Plate			22/1/90
	HS2	TCP/120A			24/1/90 25/1/90
		TCP/120B			23/1/90 24/1/90
	FP4/120A	29/1/90			
	FP4/220	31/1/90			
	FP4/Plate	22/1/90			
	HS60	FP4/120A			25/1/90
		FP4/Plate			22/1/90

6.2.3. Processing of the photogrammetric data.

All target images were measured three times using the NPL ZKM measuring microscope. For each frame the target array and reseau images were driven around with manual setting of the measuring mark on each point. The comparator coordinates produced could then be processed according to the reference mark system available in each camera.

For the metric cameras, photo-coordinates were computed using an axis best fit (STEC) based on the measured positions of the fiducial coordinates. Calibrated positions of these reference marks were not used since in both cases they were only known to 20 μ m from the manufacturers' calibration certificates.

In the case of the reseau equipped camera, photo-coordinates were derived from the comparator coordinate system, using an affine transformation based on the least squares fit of all measured reseau image positions to their corresponding calibrated values. These data could then be further refined using bilinear corrections based on the deformations at the four reseau crosses surrounding the image position. Corrections in this case were obtained by using the reseau measurements specific to each individual image, this method employing the most physically based correction method for this camera system.

The non-metric camera having no reference marks required another approach, often called inner orientation by edges. Ten image points along each frame edge were measured such that a line could be fitted to the points along each edge by the method of least squares. The intersections of the lines defined in this way for all format edges were then treated as pseudo-fiducial marks, enabling the plane coordinate transformation program (STEC) to be applied. The consistency of this method was enhanced by the ability of the ZKM to drive around an ASCII coordinate file, enabling approximately the same point to be measured from frame to frame.

6.3. The Global Bundle Adjustment.

The first self calibrating bundle adjustment incorporated all the photographs taken from the various camera stations in both photographic epochs. The datum was defined by the method of inner constraints. Only the pinned targets were securely fixed for both epochs of photography, therefore the normal equation coefficient matrix was bordered such that only coordinate starting values corresponding to pinned targets contributed to the datum definition (Program GAP, Clarke 1990). Coordinate starting values were obtained from the survey conducted as a student project (Godfrey 1989). It should be mentioned that none of the survey observations were included with the photogrammetric data in the bundle adjustment since these would have influenced the object space shape (Section 6.2.1.1). Since both sets of photography could be referenced to the same datum, all data could be processed simultaneously and consequently directly compared.

6.3.1. Analysis of calibration results.

Analysis of the camera calibration results was made according to camera type (Metric, Semi-metric and Non-Metric), and the two dates on which the photography was taken. An initial summary of the salient points from table 6.11 will however be made, being possible since all adjustments are based on the same datum.

Whilst target images were consistently pointed to as indicated by the initial 1µm photo-coordinate standard deviations, when a diagonal weight matrix (Section 3.4.2) produced from these values was used in the adjustment the a posteriori variance factor $\hat{\sigma}_0^2$ was found to very significantly greater than one. This indicates, assuming the removal of all gross errors, that either the stochastic model assigned a-priori was erroneous or that certain systematic errors remained un-compensated.

Table 6.11. Some parameters from the Global Bundle Adjustment.

Degrees of Freedom	$\hat{\sigma}_0^2$	RMS photo-coordinate residuals	RMS object space coordinate standard deviations
7736	1.290	x: 2.58µm	X: 57µm
		y: 3.07µm	Y: 68µm
			Z: 45µm

From previous surveys conducted using metric cameras, photo-coordinate standard deviations computed from multiple rounds of image measurements are invariably smaller than those estimated by the bundle adjustment procedure. These discrepancies can probably be attributed to one major source, namely that all photo-coordinates are treated as independent and uncorrelated (Section 3.4.2). Also of significance, especially where a high precision comparator such as the ZKM is in use, the image position being repeatedly visually measured does not necessarily coincide with the physical centre of the target image.

A full treatment of these relationships requires an estimation of the full variance-covariance matrix (Persson 1981; Torlegård 1989). Whilst existing software could be adapted to include the full cofactor matrix, determination of the covariances between measurements are difficult to determine accurately in practice. A similar problem was encountered during the practical derivation of the covariance function for the linear least squares interpolation method of film deformation correction (Section 4.4.3.3). In this particular case the practical covariances derived from known sites, invalidated assumptions made in the theoretical derivation of the method (Section 3.3.1.2).

The incomplete stochastic model meant that the a priori variance factor (set at unity) would not

equal the a posteriori variance factor, consequently an alternative method had to be used if the statistical properties of the parameters estimated from different adjustments were to be compared. An assumption that target design and semi automatic image measurement of the ZKM had prevented any gross errors was made, such that the photo-coordinate standard deviations computed from the three rounds of comparator measurements could be multiplied factor set such the a posteriori variance factor approached one.

The variance factor produced (Table 6.11) was still significantly greater than unity according to a χ^2 test at 95%, consequently all estimated parameter standard errors have been multiplied by $\hat{\sigma}_0$.

Mean RMS Photo-coordinate residuals
for each camera/back/film permutation.

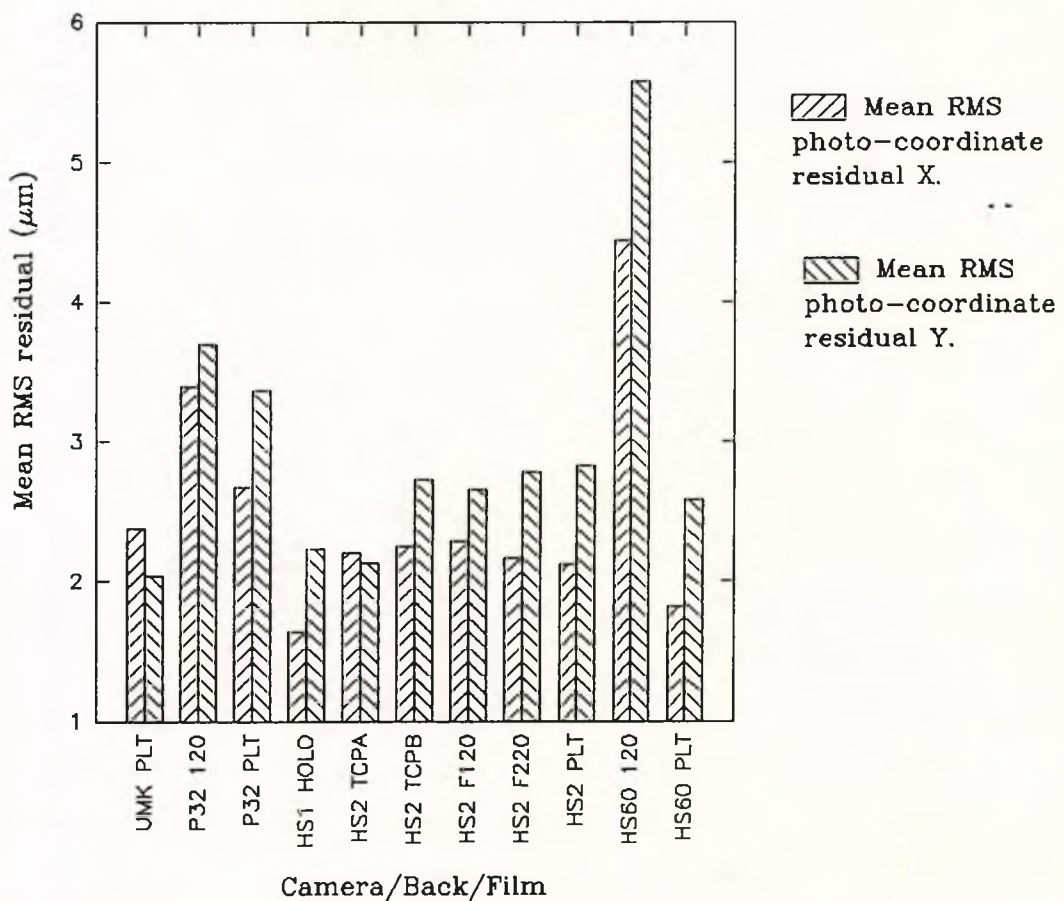


Figure 6.15.

From table 6.11 it can be seen that the mean RMS photo-coordinate residuals for all frames are of the order of $3\mu\text{m}$. Again the greater error in the y direction could be due to the lower precision of the ZKM measuring microscope in this direction, especially as the images were measured monoscopically so that the difficulties of removing y-parallax were avoided.

Figure 6.15 shows the mean RMS residuals for all frames according to camera, film back and film type variations. As expected the non-metric camera permitting no physically based corrections for film deformation has produced the highest RMS photo-coordinate residuals. The similarities between the UMK and HS1 camera results are very encouraging, suggesting that the limiting factor is target pointing precision. However by virtue of its larger format and consequently image magnification the UMK system will, for a given network, still be capable of provide better object coordinate precision. Image residuals for the P32 camera are larger than expected, partly due to lack of correction for film deformation since the residuals on FP4 120 film are larger, but since the results on glass plates are also relatively large the suggestion is that target pointing was less precise with this camera. This important anomaly is discussed further in section 6.3.2.2.

The RMS object coordinate standard deviations are very much smaller than the central target diameter of 1.0mm. These results are due to the strength of the network, primarily because each target has been imaged on almost all of the convergent photographs, and consequently measured many times. The different precision in different object space directions can be explained by the camera station geometry (Granshaw 1980).

Object space precision can be expressed in terms of the longest object space dimensions, a method commonly adopted for high precision photogrammetric surveys (Cooper and Robson 1990).

Table 6.12. Object space precision.

Direction	Longest dimension.	Object space precision
X	4.10m	1:71,940
Y	3.12m	1:45,882
Z	5.47m	1:121,555

Encouragingly object space precision lies between the 1:20,000 reported for similar network geometries incorporating non- and semi-metric cameras (Fraser 1982b; 1984a), and the 1:250,000 for high precision metric CRC1 and CRC2 cameras (Brown 1984; Fraser and Shortis 1990).

These high precision object coordinates can be used as a reference set, allowing the effects of differing cameras and configurations to be evaluated. The principal problem associated with the out-of-plane analysis methodology is consequently solved.

6.3.2.1. Analysis of the UMK and HS1 adjustment results.

Photographs made using the UMK 10/1318 and the modified Hasselblad (HS1) constituted the initial set of test data. In this case a 70mm film back was used with Agfa 10E56 Holotest film in

the Hasselblad camera, whilst Agfa 10E75 Holotest Plates were used in the UMK. The reseau images corresponding to the Hasselblad photographs taken in this set have been discussed in section 6.1.3.1. It should be noted that the geometries between the two sets of photography differ since only one rotated photograph (51) was taken with the UMK.

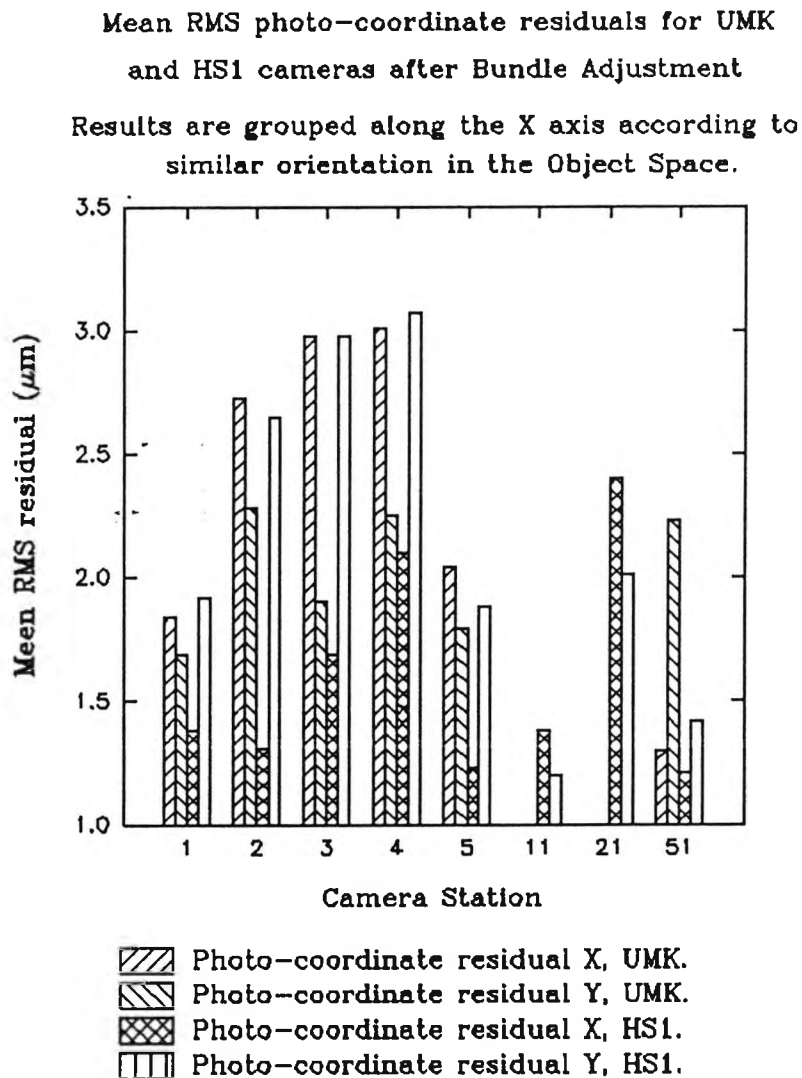


Figure 6.16.

Figure 6.15. demonstrated that the mean RMS photo-coordinate residuals for both cameras were of the order of $2\mu\text{m}$, thereby providing a better fit to the object space coordinates than the images produced in the second photographic epoch. A probable cause of these results is that both Holotest emulsions have resolving powers in excess of 3000 l mm^{-1} , such that the target image quality is limited by the resolving power of the camera lenses, as opposed to a combination of lens and film for the second set of photography.

The RMS photo-coordinate residuals separated according to camera station (Fig. 6.16) show that the Hasselblad images generally exhibit larger residual deformations along the length of the format (y direction). If the vector plots derived from the HS1 camera reseau measurements are considered (Fig. 6.3), it can be seen that there are significant areas of local film deformation, especially at the edges of the format. The lack of systematic patterns (Fig. 6.17) in the photo-coordinate residuals computed for such deformed images demonstrates the ability of the local bilinear correction to model most of the film deformation.

Significantly there are two regions where film deformation is probably not being fully modelled, linked of course to the reseau density. The change in deformation direction present between the last two rows of each reseau image (Fig. 6.3) corresponds to the residuals computed for the bottom two target image positions (Fig. 6.17). The most likely cause of these deformations is the inability of the local bilinear correction to model physical changes occurring in such situations. A second set of systematic patterns are seen at some of the local target clusters. All targets in a cluster fall within the same set of reseau crosses, such that any systematic deformations can be attributed to very localised unflatness. The significance of these results is confirmed by the photo-coordinate residuals computed for the UMK images which don't exhibit such patterns (Fig. 6.18).

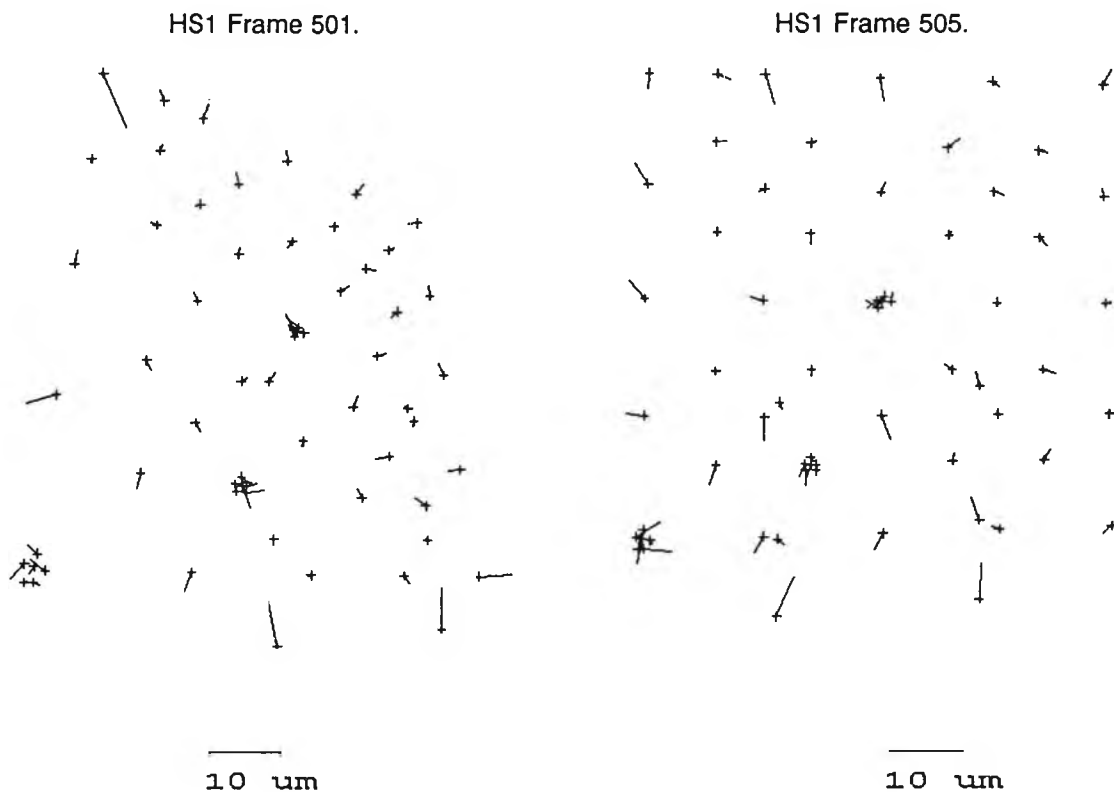


Figure 6.17. Typical photo-coordinate residual vector plots from images exposed on Holotest 70mm film in the HS1 camera.

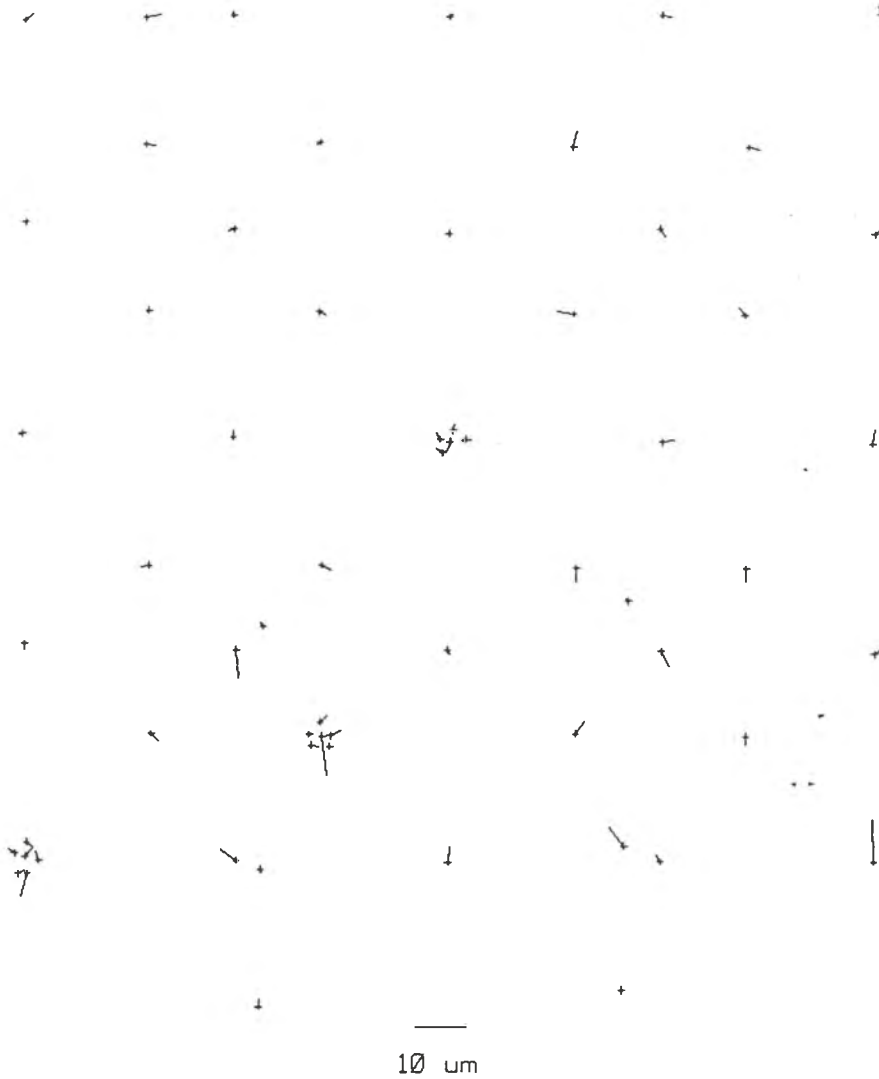


Figure 6.18. A typical photo-coordinate residual vector plot from images exposed on Holotest plates in the UMK 10/1318 camera.

Table 6.13. Camera calibration parameters and their associated standard deviations estimated by the Global Bundle Adjustment.

Camera	Estimated Inner Orientation parameters			Estimated Additional Parameters				
				Radial distortion			Tangential distortion	
	f	p_x	p_y	k_1	k_2	k_3	p_1	p_2
UMK 10/1318	101.277 (0.005)	-0.0354 (0.005)	0.0224 (0.006)	Not Sig.	Not Sig.	Not Sig.	Not Sig.	Not Sig.
HS1 (10E56)	38.604 (0.003)	-0.1389 (0.004)	0.2248 (0.004)	-12.476 (0.513)	11010 (1565)	-3292700 (1438000)	Not Sig.	-0.002 (0.001)

(Numbers in brackets are the standard deviations of the estimated parameters)

Table 6.13 shows that the inner orientation parameters have been estimated with standard deviations which are smaller than those assumed from the network design, and are very much smaller than those presented by camera manufacturers in their calibration certificates. This is due in part to the very large number of degrees of freedom present in the adjustment.

Additional parameters included in the adjustment are insignificantly different from their standard deviations for the UMK camera. This is to be expected because the camera body and Lamegon lens are well known for their metric qualities (Gates et al 1982). The parameters included to model the distortions present in the Biogon lens are much more significant, partly because the Biogon lens has been designed primarily for pictorial use, and also because the additional parameters probably model some of the film deformations still present after the local bilinear correction.

The large principal point offsets (p_x and p_y) present in the modified Hasselblad camera simply reflect the position of the centre of the reseau grid and the optical axis as modelled by the adjustment. Provided these values don't change, inferring that the camera is stable, their magnitude doesn't present any cause for concern.

6.3.2.2. Analysis of the P32 adjustment results.

Both Ilford FP4 glass plates and FP4 120 roll film were exposed in the Wild P32 camera. The theoretical minimum camera to subject distance for this camera was 3.5m at a lens aperture of $f/22$, therefore a less oblique (shorter base) square base pyramid camera station geometry had to be adopted. Further geometrical differences were provided by only four photographs being made per film type, both factors contributing to a less precise estimation of the camera calibration parameters than those derived previously.

Table 6.14 Camera calibration parameters and their associated standard deviations estimated by the Global Bundle Adjustment, P32 with FP4 120 and FP4 glass plate.

Camera	Estimated Inner Orientation parameters			Estimated Additional parameters				
				Radial distortion			Tangential distortion	
	f	p_x	p_y	k_1	k_2	k_3	p_1	p_2
P32 (FP4 120)	64.007 (0.010)	Not Sig.	-0.0368 (0.012)	-0.812 (0.191)	548.5 (247.8)	Not Sig.	-0.005 (0.001)	Not Sig.
P32 (Glass Plate)	64.074 (0.014)	Not Sig.	Not Sig.	Not Sig.	Not Sig.	Not Sig.	Not Sig.	Not Sig.

(Numbers in brackets are the standard deviations of the estimated parameters)

The fact that none of the estimated parameters is significant for glass plate photography is encouraging, since it conforms to the manufacturers' calibration of the P32 camera, providing an

independent check on the adjustment procedure. As the camera lens cone is stable and glass plates and film based images were exposed without resiting the camera at each camera station, it can be concluded that the significant additional parameters and p_y are modelling film deformation, not departures of the optical system from the assumed central perspective projection.

Mean RMS photo-coordinate residuals for the
Wild P32 camera after Bundle Adjustment

Results are grouped along the X axis according to
similar orientation in the Object Space.

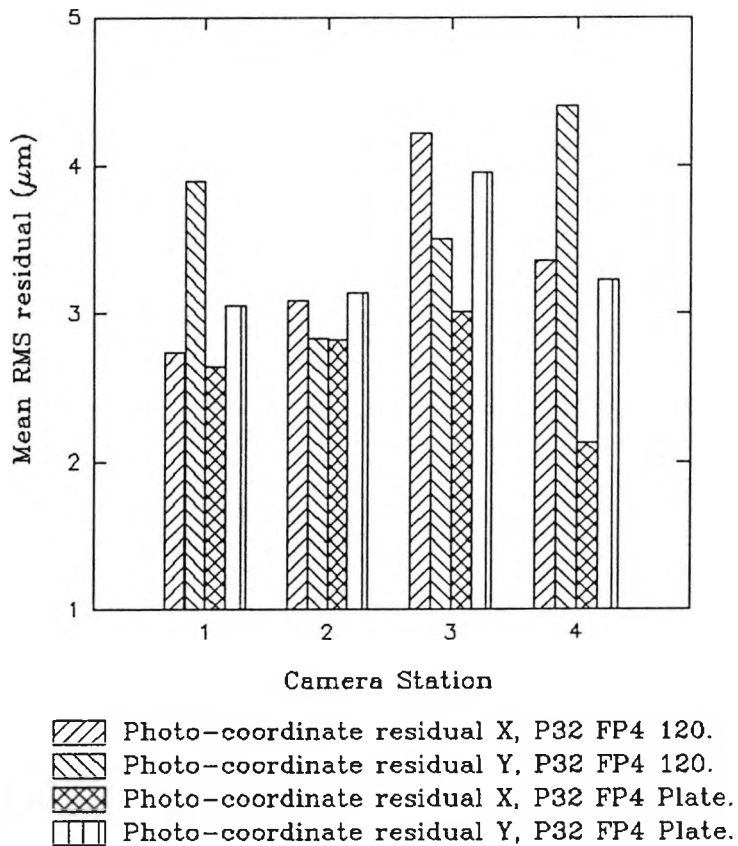
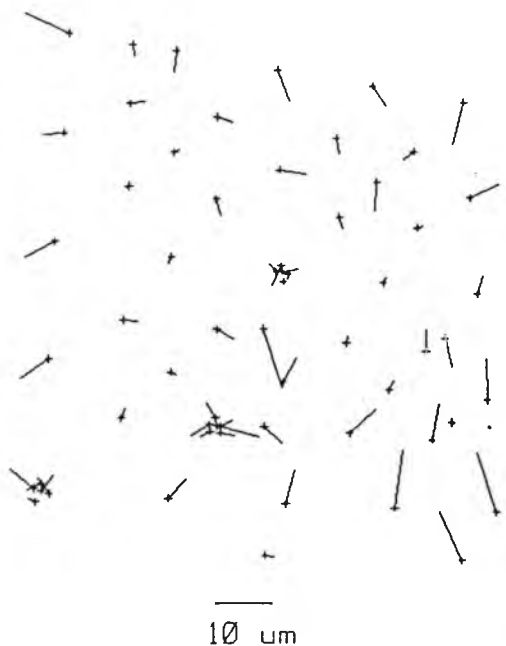


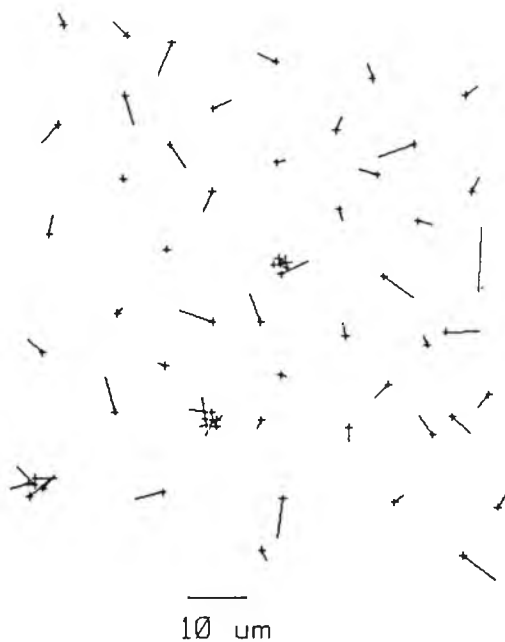
Figure 6.19.

RMS image residuals after adjustment for each of the measured frames are displayed in figure 6.19. As expected when using nominally identical geometries and similar emulsions, the greater stability and flatness of the glass plate based material has generally produced reduced RMS residuals. The differences between the glass and film bases are not as large as might be expected partly because of the ability of the additional parameters to model some of the film deformations. However the major reason for the small difference and also for the significantly larger P32 image residuals in comparison to the other cameras used (Section 6.3.1) are due to target image quality. The depth of field for the P32 camera is given as 3.5m at $f/22$ for a $50\mu\text{m}$ circle of confusion (Schlienger 1972), because of the high magnification used during image measurement this circle diameter is too large resulting in images which are unsharp for these purposes. For a comparison the depth of field tests conducted using the Hasselblad camera were made assuming a diameter of $20\mu\text{m}$.

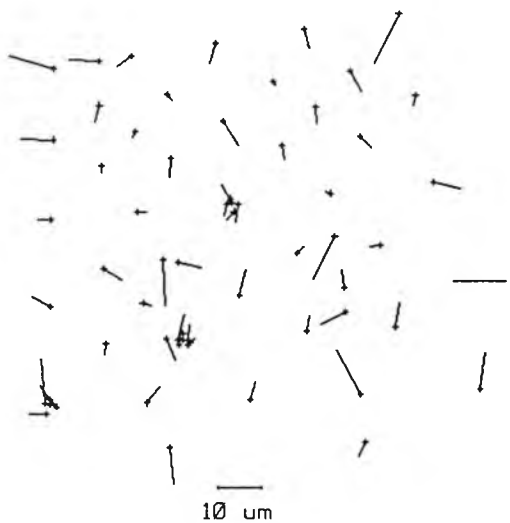
P32, FP4 120, Station 901.



P32, FP4 Plate, Station 901.



P32, FP4 120, Station 904.



P32, FP4 Plate, Station 904.



Figure 6.20. Typical photo-coordinate residuals for the P32 series of images.

From figure 6.20. it can be seen that more systematic patterns can be identified in the photo-coordinate residuals derived from the images made on FP4 120 film as opposed to those on glass plates. In the light of the film deformations seen in the HS1 and HS2 cameras (Section 6.1.2) this is to be expected because rigorous explicit film deformation corrections cannot be carried out on P32 camera images due to the sparseness of the calibration markings on its register glass.

6.3.2.3. Modified Hasselblad SWC (HS2) exposures.

Exposures made in the HS2 camera constituted the major part of this investigation and also provide the data used in the subsequent sections. Detailed in table 6.15 are the five permutations of film back and film type exposed, treating the HS2 camera body as a stable lens cone. All the exposures carried out using the various film backs were made with nominally the same geometry, that described in figure 6.11. An exception was made for the FP4 glass plates, since numbers of these plates were limited.

All the measured image coordinates were transformed using local bilinear corrections based on the calibrated reseau positions, to produce photo-coordinates which had been explicitly refined to take into account the known film deformations. This method meant that any differences between each camera back and film permutation could be expressed in terms of the differences between each associated set of estimated self calibration parameters and the image residuals from each camera station.

Table 6.15. Mean RMS reseau image residuals for exposures made in the HS2 camera and included in the Global Bundle Adjustment.

Film/camera back	RMS x(μm)	RMS y(μm)
TCP BACK A (from Roll 3).	3.52($\sigma=3.34$)	5.09($\sigma=4.39$)
TCP BACK A (from Roll 3)*.	2.41($\sigma=0.32$)	3.64($\sigma=0.56$)
TCP BACK B (from Roll 3).	6.37($\sigma=0.58$)	5.98($\sigma=0.37$)
FP4 120 Back A (from Roll 3).	1.98($\sigma=0.26$)	2.81($\sigma=0.18$)
FP4 220 (from Roll 3).	2.94($\sigma=0.71$)	3.75($\sigma=0.84$)
FP4 Glass Plates.	3.07($\sigma=0.55$)	2.93($\sigma=0.40$)

ignoring grossly deformed frame 6.

For reference the mean RMS image residuals between the calibrated reseau positions and their image positions for the frames used in the adjustment are shown in table 6.15. Of particular note is the inclusion in the data set, of the grossly deformed Technical Pan (Back A, Roll 3, Frame 6) image described in figure 6.5. It should also be noted that one of the rotated frames from the FP4 220 set of exposures was in error not measured, consequently in this particular comparison the FP4 220 data set includes only eight frames instead of nine.

The estimated camera calibration parameters simultaneously computed for each of the camera back and film permutations are shown in table 6.16. Including the information in table 6.13, it is interesting to note that there are significant differences in principal point position (p_x and p_y) between the HS1 and HS2 camera modifications, whilst the magnitudes of the other estimated calibration parameters are of the same magnitude. The difference in principal point location is due

to the fact that the remounted reseau (defining the photo-coordinate system) was not glued in quite the same place with respect to the optical axis. On closer inspection the p_2 tangential parameter is also significantly different inferring either that the reseau plates did not define quite the same film plane or that the 70mm back had different characteristics than any of the other backs used.

Table 6.16. Camera calibration parameters and their associated standard deviations estimated by the Global Bundle Adjustment, HS2 with various film/back permutations.

Camera	Estimated Inner Orientation parameters			Estimated Additional parameters				
				Radial distortion			Tangential distortion	
	f	p_x	p_y	k_1	k_2	k_3	p_1	p_2
HS1 TCP 120 Back A	38.612 (0.003)	0.1119 (0.003)	0.3009 (0.003)	-12.315 (0.316)	10446.4 (805.6)	-2349393 (606965)	-0.004 (0.001)	-0.005 (0.001)
HS1 TCP 120 Back B	38.608 (0.003)	0.1034 (0.004)	0.3047 (0.003)	-11.977 (0.438)	9675.6 (1354.5)	-2189514 (1262367)	-0.002 (0.001)	-0.005 (0.001)
HS1 FP4 120 Back A	38.605 (0.003)	0.1118 (0.003)	0.3066 (0.004)	-11.686 (0.440)	10094.5 (1357.4)	-2357509 (1244721)	-0.004 (0.001)	-0.006 (0.001)
HS1 FP4 220	38.612 (0.003)	0.0945 (0.003)	0.3092 (0.004)	-13.002 (0.312)	13369.6 (779.1)	-4779591 (568902)	-0.002 (0.001)	-0.007 (0.001)
HS1 FP4 Glass Plate	38.607 (0.006)	0.1040 (0.006)	0.3361 (0.008)	-11.695 (0.679)	9697.9 (2006.1)	-1444949 (1705424)	-0.002 (0.001)	-0.011 (0.002)

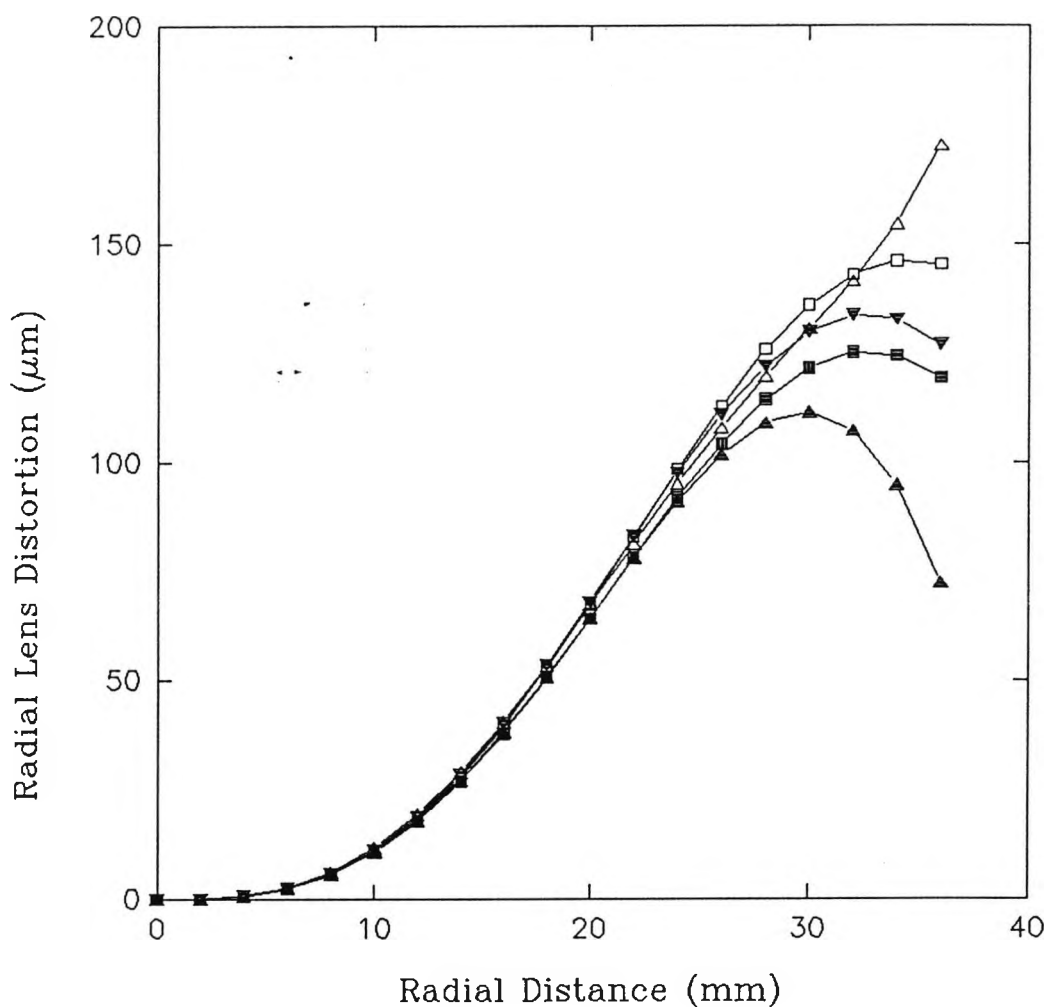
(numbers in brackets are the standard deviations of the estimated parameters)

Whilst the estimated inner orientation and additional parameters appear broadly similar in magnitude for the different film and camera back combinations assessed (Table 6.16), if a statistically based comparison is to be made it is necessary to consider their associated standard deviations. The standard deviations of the estimated parameters are similar for all the exposures made on film based products despite only eight frames contributing to the FP4 220 data set. However the limited geometry (three stations) used for the glass plate based FP4 emulsion has given rise to significantly larger standard deviations in this case.

The results of t-tests between the means of each of the permutations of parameters are presented in table 6.17. The paired t-tests were conducted using a 95% confidence interval, the test statistic being calculated employing the number of degrees of freedom from table 6.11.

Combinations of the p_x , p_y , p_1 and p_2 parameters are different for most of the data sets, indicating that these are modelling any small differences in film deformation remaining after local bilinear correction. The main anomaly is provided by the estimated parameters from the FP4 220 data set. A possible cause being that the camera geometry was deficient by one camera station, however the FP4 glass plate based exposures used an entirely different geometry, but still produced

Graph of Radial Lens Distortion
for each of the camera back/film combinations
exposed in the modified Hasselblad (HS2)



Camera back/film combinations:

- ▼ Technical Pan, 120 Back A
- Technical Pan, 120 Back B.
- FP4, 120 Back A.
- △ FP4, 220 Back.
- ▲ FP4, Glass Plates.

Figure 6.21.

estimated parameters which were insignificantly different from the parameters estimated by the FP4 120 and Technical Pan 120 data.

From figure 6.21 it can be seen how the plots of radial lens distortion computed from the estimated polynomial coefficients differ. Since the camera lens cone was stable throughout the tests, any physical causes of such differences must lie with the film and camera back used. Only the curve derived from the FP4 220 images has been shown (Table 6.17) to be significantly different from the other derivations. Figure 6.21 has been included primarily to enable a comparison of these globally estimated lens parameters with those estimated from the film deformation tests (Section 6.4.2). It could be argued that since the differences between the four curves lie at the extremes of the format, and are therefore derived from few target images and therefore that the differences between polynomials are marginal for most practical purposes.

Table 6.17. Statistically different estimated camera calibration parameters for the different camera and film back permutations.

Film / Camera back	Camera back and film permutations.			
	TCP 120 A	TCP 120 B	FP4 120 A	FP4 220
TCP 120 B	P_x, P_1			
FP4 120 A	f	P_x, P_1		
FP4 220	$P_x, P_y, k_1, k_2, k_3, P_1, P_2$	$P_x, k_1, k_2, k_3, P_x, P_2$	$f, P_x, k_1, k_2, k_3, P_1$	
FP4 Plate	P_y, P_1, P_2	P_y, P_2	P_y, P_1, P_2	P_y, k_1, P_2

In section 6.3.2.1 it was concluded that localised film deformation can produce distortions which cannot be modelled by the local bilinear correction at this reseau density. If the vector plots of deformation derived from reseau image measurements of the FP4 220 frames (Appendix B) are considered it can be seen that not only are they much more homogeneous than those produced in the HS1 Holotest exposures, but they exhibit less deformation than those from the Technical Pan 120 exposures in Back B. However from section 6.1.3 it will be remembered that this particular roll of FP4 220 film (Roll 3) exhibited largely unexplained systematic trends along its length (Fig.6.10). The presence of local effects are also supported by figure 6.23, where it can be seen that some trends in the photo-coordinate residuals do exist. Whilst inconclusive these results do suggest that some physical film deformation effect is responsible for the differences seen in the FP4 220 results.

Comparing the RMS photo-coordinate residuals for the various films (Fig. 6.22) it can be seen that the residuals from the image on the Technical Pan films are generally smaller than those for the frames on both Ilford FP4 films. A probable cause of this difference is that the greater resolution of the Technical Pan films made pointing to target centres more precise. Also significant from this figure is that the bilinear correction carried out on the grossly deformed Technical Pan back A

frame 6 (camera station 2) has been corrected to produce RMS photo-coordinate residuals of the same order as those from the other frames on this roll. This fact is further confirmed by the top left plot in figure 6.23. However it should also be mentioned at this stage that it is surprising that the photo-coordinate residuals from images on Technical Pan film exposed in 120 Back B do not appear to exhibit many local systematic effects despite the nature of their film deformation vector plots.

Mean RMS Photo-coordinate residuals for HS2 images after adjustment

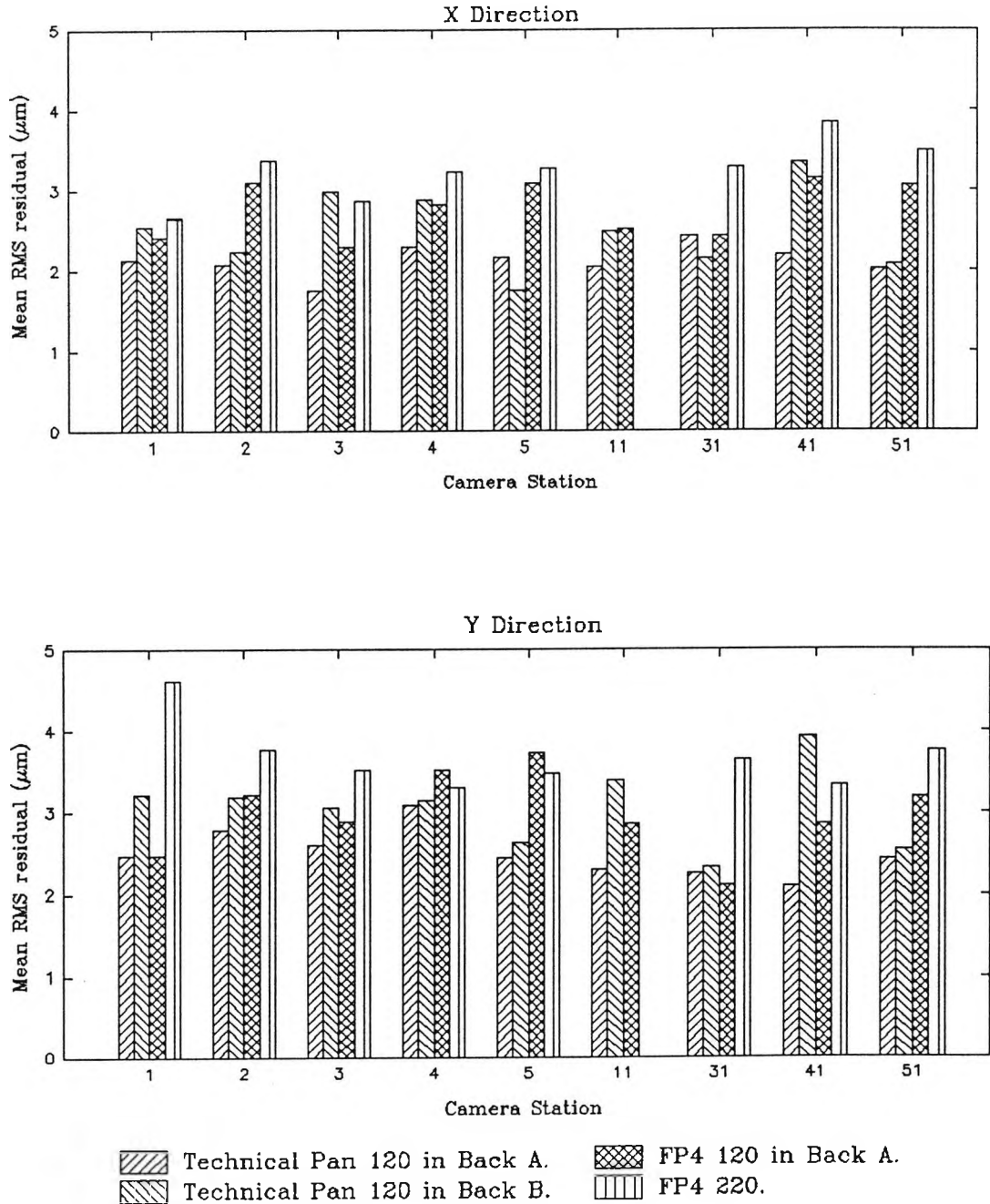


Figure 6.22.

Photo-coordinate residuals for different permutations
of film and camera back exposed in the HS2 camera.

TCP 120 A, Station 2.



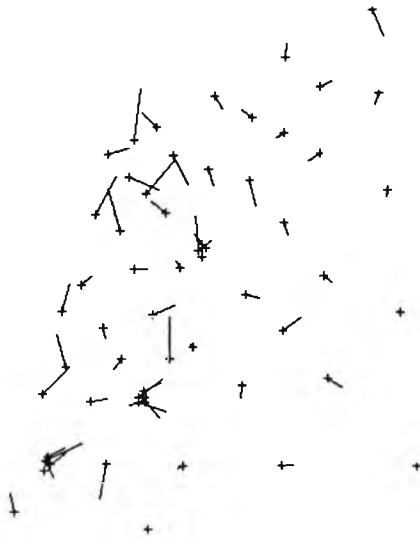
10 μ m

TCP 120 B, Station 2.



10 μ m

FP4 120, Station 2.



10 μ m

FP4 220, Station 2.



10 μ m

Figure 6.23.

6.3.2.4. Hasselblad Non-Metric exposures.

The non-metric Hasselblad 500C camera was included so that a comparison could be made between the ability of the mathematical model to correct for distortions occurring in a camera in which there was no stable interior orientation. As mentioned in section 6.2.3 a photo-coordinate reference system was devised by measuring points along the edges of the frame, then using these to compute pseudo fiducial measurements which could be used to define the coordinate system. It is the repeatability of this axis definition which will provide a major influence on the photogrammetric potential of this non-metric system whenever the bundle adjustment procedure is adopted (Faig 1989). Table 6.18 shows the mean and standard deviations of all seven sets of independently computed pseudo fiducial coordinates for images exposed on Ilford FP4 120 film in the HS60 camera.

Table 6.18. Mean pseudo fiducial coordinates and their associated standard errors.

Point number	Fiducial coordinates		Standard deviations	
	x(mm)	y(mm)	x(μ m)	y(μ m)
1	-27.590	-27.732	8.9	8.3
2	27.610	27.752	8.9	8.7
3	-27.544	27.686	6.5	6.0
4	27.557	-27.698	11.6	15.2

On initial computation of the global bundle adjustment large photo-coordinate residuals were found to be present on many of the HS60 film images. Subsequent analysis showed that the lens focusing helicoid had moved during the test field photography, consequently each frame had to be treated as an individual camera for the purposes of the adjustment.

Table 6.19. shows the significant parameters estimated by the adjustment. From these it is clear that the inner orientation has varied between exposures because the principal point position has varied far more than the standard deviations of the fiducial coordinates would suggest. The variations of the principal point position are consistent with a change in focus of the lens because as the helicoid is rotated the lens will move not only longitudinally along its axis but also laterally.

The estimated parameters are difficult to analyze for the singly treated cameras, since differences in test field image coverage will stress certain areas of the image format. Investigating the mean RMS photo-coordinate residuals derived from the FP4 120 film exposures (Fig. 6.24), it can be seen that despite individual additional parameters being applied to each frame, they are about twice the size of any computed for HS2 camera images. The cause of these large residuals becomes clear when the glass plate images exposed in the same camera are analyzed. The RMS residuals for these frames are very similar to those computed from the HS2 camera images,

indicating that film unflatness is the major source of error occurring in this non-metric camera.

Table 6.19. Camera calibration parameters and their associated standard deviations estimated by the Global Bundle Adjustment, HS60 FP4 120 treated as individual cameras and HS60 with FP4 glass plates.

Camera	Estimated Inner Orientation parameters			Estimated Additional parameters				
				Radial distortion			Tangential distortion	
	f	P _x	P _y	k ₁	k ₂	k ₃	P ₁	P ₂
HS60 FP4 120 1	60.074 (0.121)	0.0791 (0.0633)	0.1216 (0.0123)	-23.336 (3.119)	11589.4 (7581.1)	Not Sig.	Not Sig.	-0.010 (0.007)
HS60 FP4 120 2	60.393 (0.038)	-0.0489 (0.0389)	0.2501 (0.0334)	-19.992 (1.705)	4436.8 (3883.8)	Not Sig.	Not Sig.	Not Sig.
HS60 FP4 120 4	60.603 (0.062)	Not Sig.	0.2822 (0.0890)	-19.252 (3.644)	Not Sig.	Not Sig.	Not Sig.	Not Sig.
HS60 FP4 120 5	60.654 (0.130)	0.1614 (0.0708)	0.2327 (0.0804)	-19.364 (3.375)	Not Sig.	Not Sig.	Not Sig.	Not Sig.
HS60 FP4 120 11	60.598 (0.076)	Not Sig.	0.1702 (0.0633)	-20.857 (3.342)	Not Sig.	Not Sig.	Not Sig.	Not Sig.
HS60 FP4 120 21	60.454 (0.072)	Not Sig.	0.2105 (0.0809)	-19.740 (4.289)	Not Sig.	Not Sig.	Not Sig.	Not Sig.
HS60 FP4 120 41	60.426 (0.075)	0.2529 (0.0887)	Not Sig.	-23.150 (3.973)	Not Sig.	Not Sig.	Not Sig.	Not Sig.
HS60 FP4 Glass Plate	60.648 (0.022)	0.0802 (0.0233)	-0.1017 (0.0273)	-20.561 (1.276)	6295.1 (3179.2)	Not Sig.	-0.007 (0.002)	-0.003 (0.002)

(Numbers in brackets are standard deviations of the estimated parameters)

This conclusion is further confirmed by considering direct measurements of film unflatness in non-metric cameras (Tsuruta et al 1970; Kämmerer 1979) which show the film forming a single convex surface or two convex surfaces towards the lens. Photogrammetrically derived film surfaces (Fraser 1984b; Fryer 1988) describe similar trends. Although these results cannot be taken as typical for all cameras or even for frames exposed in a given camera, they would appear to agree with the predominantly radial photo-coordinate residuals computed for the HS60 film based imagery (Fig. 6.25.). Significantly, the photo-coordinate residuals computed for the glass plate based FP4 images are more random in nature.

Mean RMS photo-coordinate residuals for Non-Metric Hassleblad camera after bundle adjustment

Results are grouped along the X axis according to similar orientation in the Object Space.

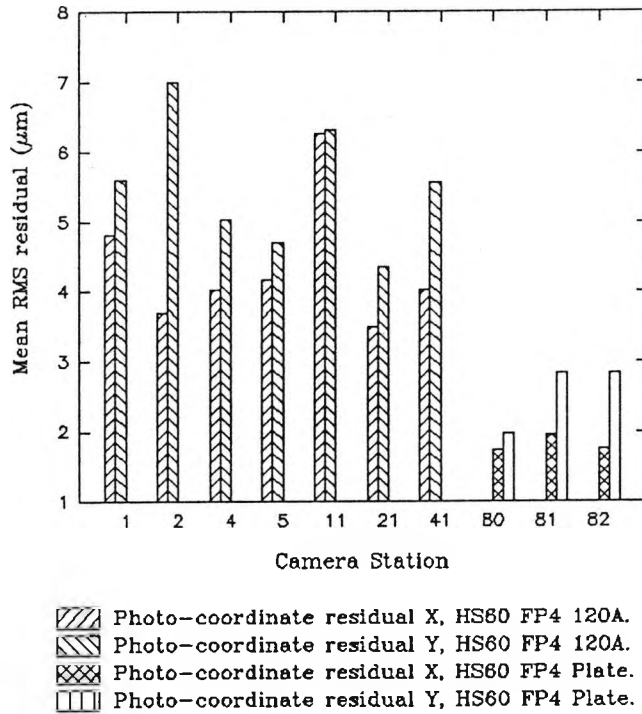


Figure 6.24.

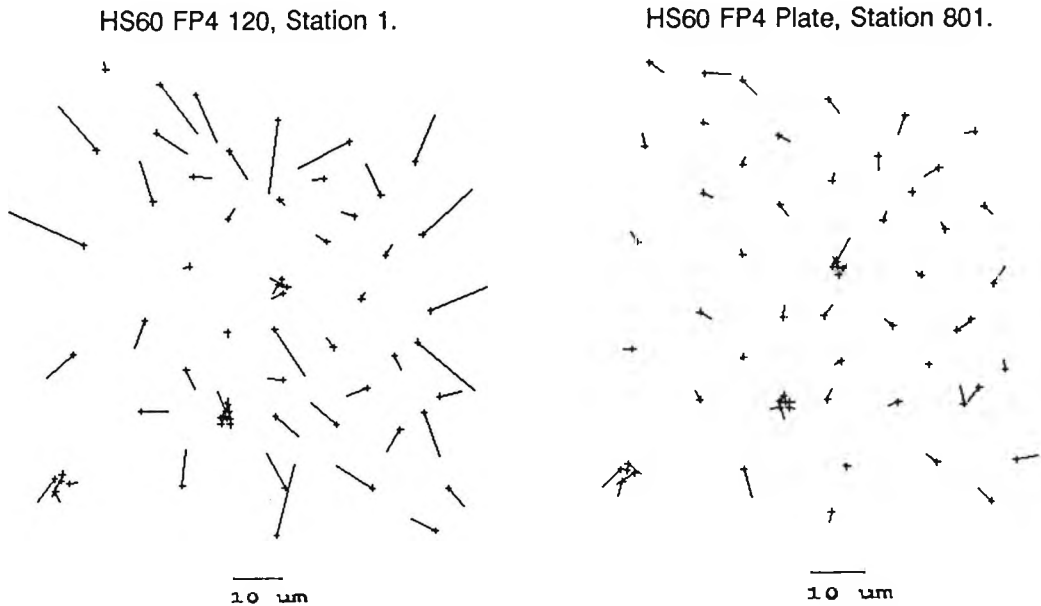


Figure 6.25. Photo-coordinate residuals computed during the global adjustment for two images exposed in the Hasselblad 500C camera (HS60).

6.2.6. Summary.

The global adjustment has enabled the successful production of directly comparable photo-coordinates and estimated parameters for all camera types investigated. Additionally the object space coordinates produced exhibit a precision which is high enough to enable their use as a reference set for the experiments to follow.

The UMK and P32 metric cameras generally performed well when used with glass plates, but are limited in application by for example the large size of the UMK and by the fixed focus lens design of the P32. It is interesting that both cameras only have four or five reference marks which are possibly inadequate both in terms of number and location where film deformation corrections are concerned. Consequently unless film flattening is well controlled by camera design, their metrical qualities are seriously impaired if images are made on film based products. Various manufacturers have now designed high precision film cameras, which try to solve this problem by rigorous film back design. Examples include vacuum flattening, which is available for the UMK, and the latest generation of cameras incorporating various combinations of reseau array and vacuum back, (Brown 1982; Piepe 1990; Dold 1990).

The HS1/HS2 results give an idea of the photogrammetric quality of a very simply modified non-metric camera, which despite its shortcomings is able to approach a limiting factor based on the image quality attainable by its lens/film combinations used, not it appears on film unflatness although localised unflatness could be improved. The estimated calibration parameters for each camera back/film combination used represent departures from the mathematical model which were stable (lens distortion) and also residual film deformations which could be modelled for the frames measured. Consequently these parameters and their estimated standard deviations can be treated as calibration data during subsequent practical surveys carried out with this camera.

The non-metric Hasselblad camera (HS60) shows a potential which would be significantly enhanced if the lens was fixed by focusing click stops. The repeatability of the interior orientation by edges method in defining a photo-coordinate reference system questions the advantages which could be provided by fitting edge reference marks. In conclusion results from this camera will always be limited by un-flatness and the ability of the network geometry to enable its modelling. Possible mathematical treatments (Fraser 1982c, Fraser 1984a, Fryer 1988) include the estimation of camera invariant parameters and image variant additional parameters in the bundle adjustment. However care has to be taken to ensure that the parameters used are statistically significant and not highly correlated to avoid an over parametrised solution, (Section 3.3.2).

6.4. Film and camera back permutations with the HS2 camera.

The initial outline for this chapter proposed an investigation of the effectiveness of the different reseau correction methods discussed in section 3.3.1. Analysis of the photogrammetric effects of the various film deformation correction methods requires some form of measure to determine the success of the transformation. Since the X,Y,Z object space coordinates of the test field targets had been determined with high precision by the dense network used for the global bundle adjustment, these could provide a reference set of 'correct' data. Providing all bundle adjustments incorporating photo-coordinate refinements were based on the same datum, differences in position and shape of the estimated object space coordinate fields could be linked to film deformation.

The images to be used in this analysis were simply taken from the sets of exposures made onto film in the HS2 camera during the second set of test field photography (Table 6.10). Eight images from each set were employed to provide nominally the same geometry for each adjustment. Explicit film deformation transformations could then be applied to each of the camera back/film permutations from section 6.3.2.3.

6.4.1. Image coordinate refinement and datum definition.

For this series of adjustments photo-coordinates were re-computed from the ZKM comparator measurements using the best axis fit program (STEC) treating the four corner reseau crosses as fiducial marks. These raw plate coordinates could then be refined according the transformations outlined below:

a) **Global Affine transformation:** based on the least squares fit of all measured reseau image positions to their corresponding calibrated values.

b) **Mean Bilinear correction:** On the basis that film type and camera back could be identified by visual analysis of the deformation patterns derived from most of the frames produced, it was decided to adopt a method of correction which reflected these similarities. A mean deformation pattern was computed for each set of reseau images produced in each of the camera back/film permutations used. A local bilinear correction could then be applied based on the mean deformations at the four reseau crosses surrounding the image position computed using the mean deformation pattern for the appropriate camera back/film combination. This method potentially offered a camera/film specific correction with all the advantages of the use of a reseau but without the need to measure every reseau grid.

c) **Local Bilinear correction:** This method was identical to that used for all reseau images incorporated in the global bundle adjustment.

It must be mentioned that the least squares linear interpolation method was rejected for the purposes of this analysis as being too computationally intensive for an on-line image refinement technique.

The resultant raw and refined photo-coordinates were processed using the self calibrating (inner constrained) bundle adjustment. To prevent shape distortions due to the choice of datum, the datum was again defined by bordering the design matrix such that only coordinate starting values corresponding to pinned targets contributed to the datum definition. The datum definition was therefore identical to that used during the global adjustment. Since all network geometries were the same for each camera back/film set, and nominally the same for all data sets, any differences between the results produced would be due to camera back, film type and film deformation correction method.

Results from the global adjustment showed that the parameters included in the adjustment with the intention of modelling lens distortion also modelled some of the departures from the collinearity condition caused by film deformation. However in the case of the HS2 camera adjustments, the estimated parameters only modelled systematic deformations which were similar for each frame, often known as block invariant. These values, constrained by their standard deviations, could be used as starting values for the parameters to be estimated in each of the individual adjustments conducted in this section. This method conferred further refinement of the photogrammetric analysis since physically derived constraints were placed on the solution.

6.4.2. Analysis of Results.

Generally when consistent photo geometry is used, comparison between adjustments can be made using the a posteriori variance factor as a crude indicator of the presence of uncompensated systematic errors (Chandler et al 1989b). However interior orientation and additional parameters included in the self calibrating bundle adjustment to model optical distortions also modelled some of the film deformation. The variance factor therefore represents not only the effectiveness of the explicit film deformation correction, but also the ability of the interior orientation and additional parameters included in the adjustment to model departures from the assumptions made by the collinearity equations.

From Table 6.20. it can be seen that the variance factors associated with each treatment don't necessarily decrease with increasing image deformation correction complexity. The only method which consistently provides the lowest variance factor is the local bilinear correction, this being explained simply by the fact that it uses more of the available film deformation information than the other methods. The inconsistency of the mean bilinear correction is at this stage disappointing, but to draw any reliable conclusions it is necessary to evaluate the effects of the corrections on the object coordinates, photo-coordinate residuals and estimated camera

parameters.

Table 6.20. Variance factors derived from each adjustment.

Film / Camera back	Variance factor $\hat{\sigma}_0^2$			
	Raw Plate	Global Affine	Mean Bilinear	Local Bilinear
TCP 120 Back A	2.54	2.86	2.65	1.17
TCP 120 Back B	1.63	2.45	1.73	1.22
FP4 120 Back A	3.06	1.66	1.69	1.44
FP4 220 220 Back	2.56	2.00	1.85	1.44

6.4.2.1. Changes in estimated parameters.

For this set of adjustments calibration parameters were assigned starting values from the results of the global adjustment, according to the camera back/film combination used. Consequently it is possible to assess changes by comparing the differences between the parameter starting values and the values of the parameters estimated during each individual adjustment.

Figures 6.26 and 6.27 show the differences between the camera calibration parameters estimated by the global adjustment and those estimated by each individual adjustment. The largest differences are seen in the parameters estimated for Technical Pan 120 film exposed in 120 Back A. The main reason for these variations are that the group of images constituting this data set included the highly deformed frame 6 from roll 3 (Fig. 6.5). As could be expected any useful correction for this set of frames requires a specific knowledge of the deformations present in this image. In fact the deformations are so large that in the absence of a reseau this frame would probably have been rejected. The degree to which this frame contributes to the adjustment residuals is clearly seen in the variance factors (Table 6.20) associated with this set of corrections. Clearly the correction methods are ineffectual until the local bilinear correction is applied, based on information specific to this frame.

For the other three camera back/film combinations several features can be identified, notably the insignificance of the changes in the tangential distortion parameters (p_1, p_2), implying that these contribute very little to the modelling of film deformation. Whilst the mean bilinear correction has not contributed much to the reduction of the variance factor, it has reduced differences in the estimated parameters to less than or of the same order as the parameter standard deviation as estimated by the global adjustment.

Differences between camera calibration parameters from the global bundle adjustment and those estimated during the individual adjustments.

Standard deviations from the global calibration, used to constrain the estimation in this case are shown as a measure of significance.

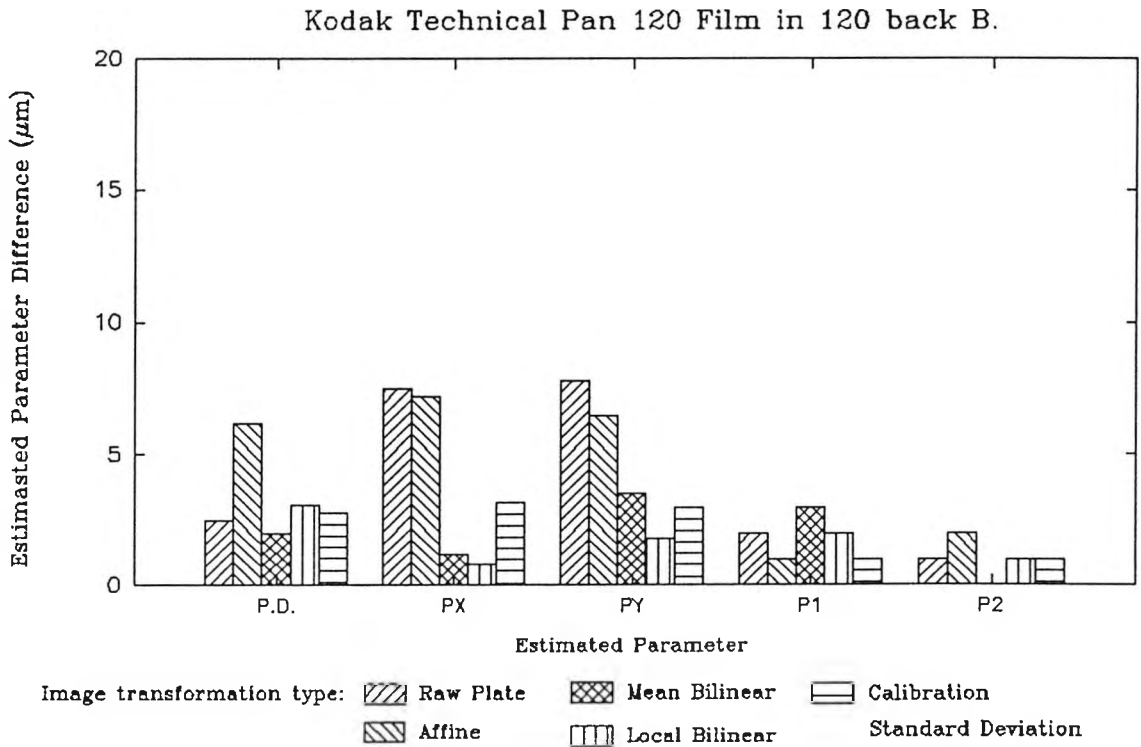
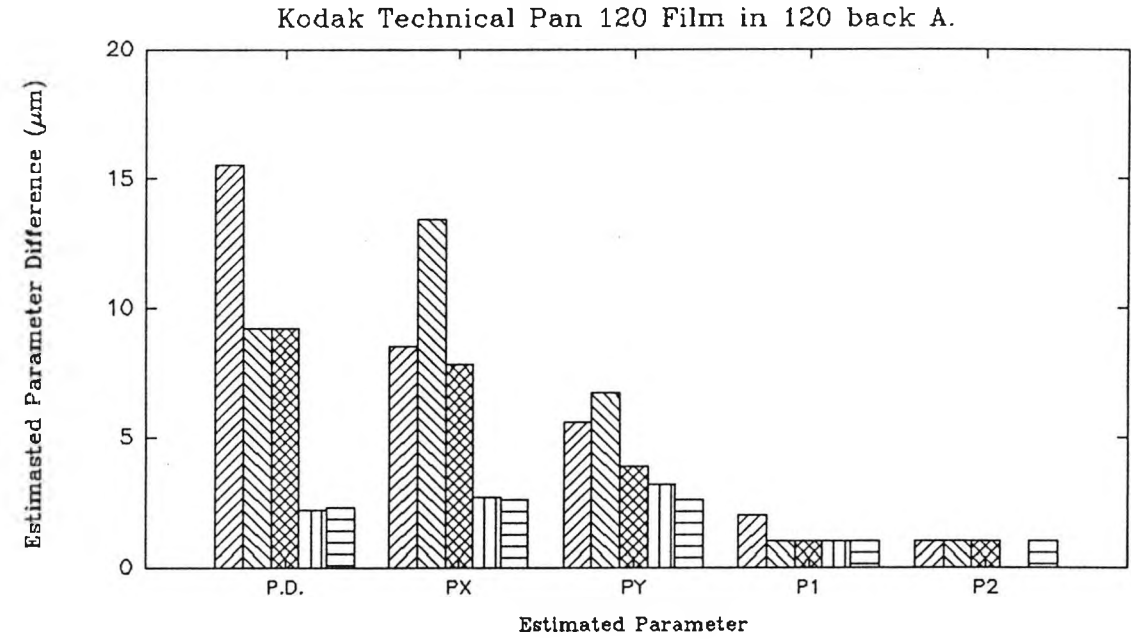


Figure 6.26.

Differences between camera calibration parameters from the global bundle adjustment and those estimated during the individual adjustments.

Standard deviations from the global calibration, used to constrain the estimation in this case are shown as a measure of significance.

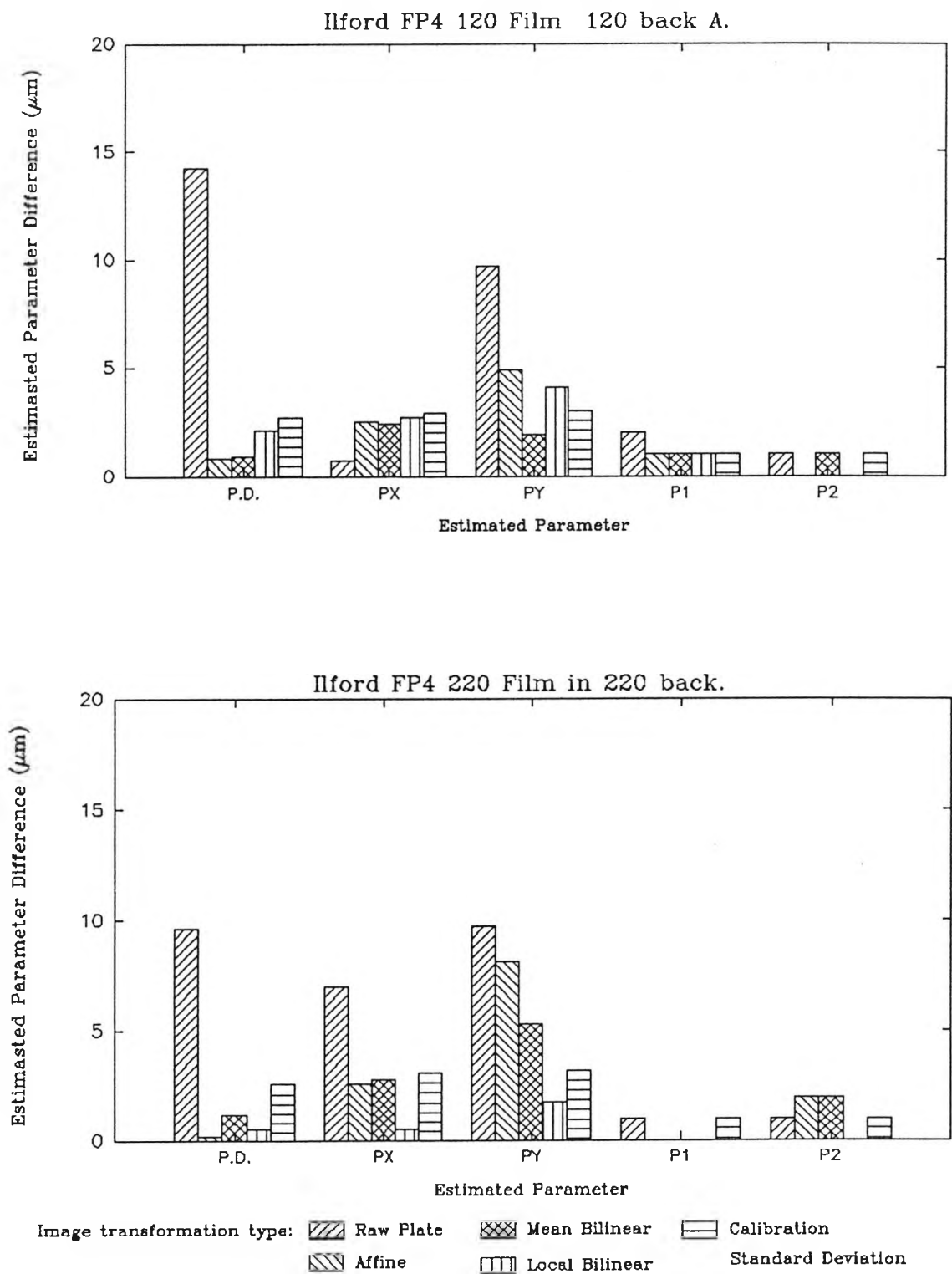


Figure 6.27.

Graph of Radial Lens Distortion
for each of the camera back/film combinations
exposed in the modified Hasselblad (HS2)

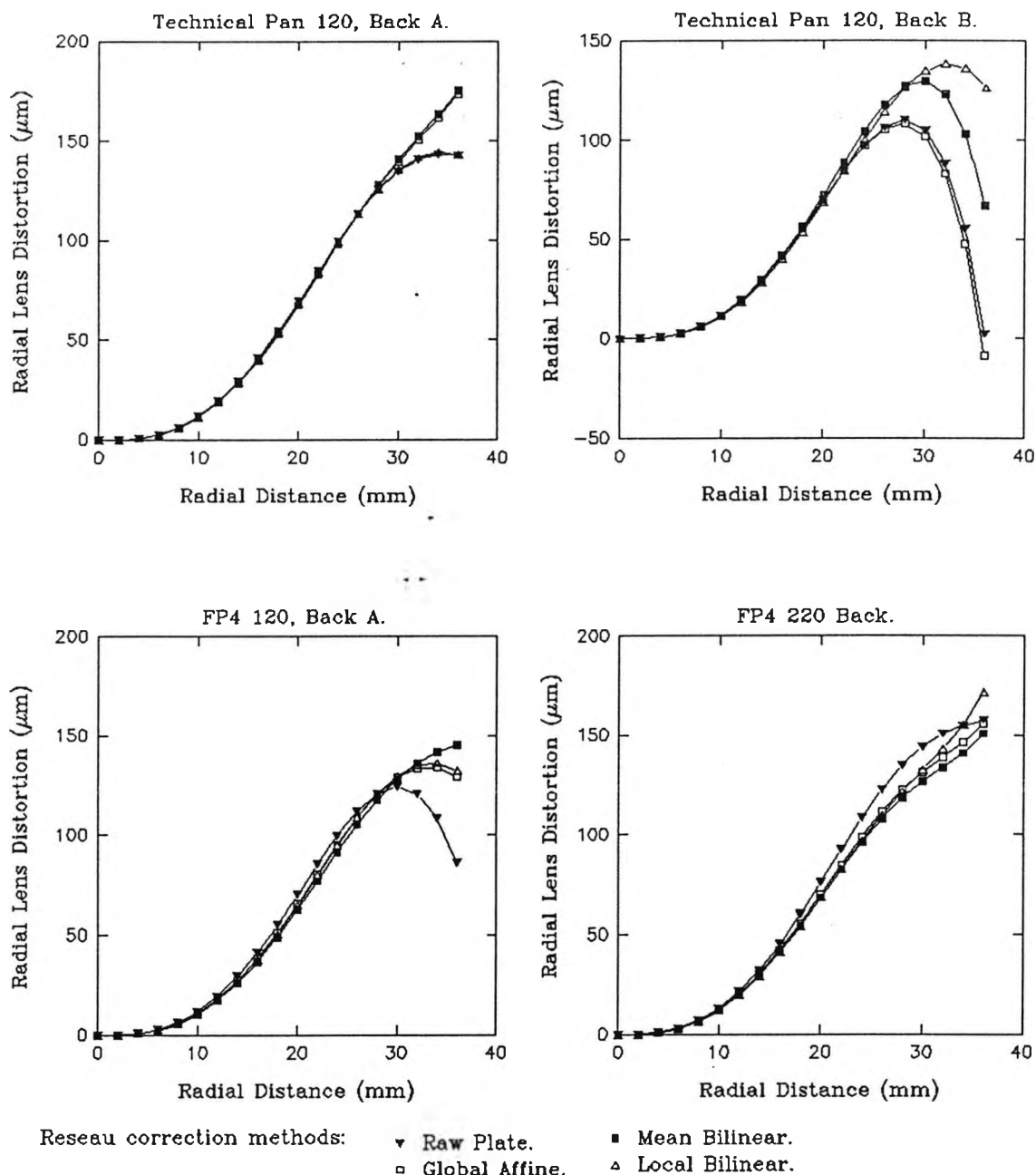


Figure 6.28.

Focal length appears to be acting very significantly to change the photo-scale for the raw photo-coordinate measurements on both FP4 120 and 220 films. The physical cause of such a change must be correlated with measurement environment relative humidity because application of the global affine transformation restores the focal length difference to within the standard deviation derived from the global adjustment. It is unclear why an affine correction to the Kodak Technical Pan images exposed in Back B actually increases the focal length difference, although a link between film deformation at the format edges and target image geometry is suspected.

Changes in the radial lens parameters can be evaluated by considering the graphs in figure 6.28 and those representing the parameters estimated during the global adjustment (Fig. 6.21). It is immediately apparent that the local bilinear correction has given rise to very small differences for all the camera back/film combinations.

The shape and magnitude of the radial lens distortion curves are very comparable up to a radial distance of 25mm, suggesting that radial lens distortion dominates film deformation up to this radial distance. From this point on, uncorrected film deformation, which tends to be larger at the edges of the format, becomes increasingly modelled by the radial lens parameters. The only exception to these trends are seen in the raw photo based adjustments for both FP4 films, which demonstrate small departures before the 25mm radial distance. This means that the lens polynomial has some mathematical relevance to the distortion patterns exhibited by the images on FP4 film.

A brief analysis of some of the changes to the estimated camera exterior orientation parameters defining each camera station perspective centre were made. The standard deviations of the object space coordinates were of the order of 0.4mm in all object directions, whilst most of the estimated coordinates agreed to within 0.7mm. The only exception to these discrepancies coincided with significant focal length changes in adjustments employing raw photo-coordinates, where for example differences might increase up to 3.1mm. This indicates not only that a dynamic system is operating whereby image scale variations are reflected not only by changes in the estimated focal length but also by translations and rotations of the camera with respect to the test field.

6.4.2.2. Differences between the photo-coordinate residuals.

The most obvious reduction of photo-coordinate residuals by an explicit film refinement is provided by the deformed frame on Technical Pan film (Fig. 6.29). For all correction methods other than the local bilinear the data are clearly influenced by the deformed nature of this frame as shown in the deformation plot derived from the reseau image measurements (Fig. 6.5). Plots of photo-coordinate residuals computed from the first three transformations exhibit large systematic vectors. The local bilinear correction is able to remove most of these trends, but systematic residuals can still be identified at one of the local target clusters confirming the limitations imposed by the reseau grid density.

Changes in magnitude of the photo-coordinate residuals with film deformation correction method are presented in figure 6.30. Results again demonstrate that only the local bilinear correction will consistently reduce the magnitude of the photo-coordinate residuals. It is interesting that the images on Technical Pan film have produced the smallest photo-coordinate residuals after local bilinear correction inferring that the greater resolving power of this emulsion is responsible.

Photo-coordinate residuals for Technical Pan 120 film,
Back B camera station 2.

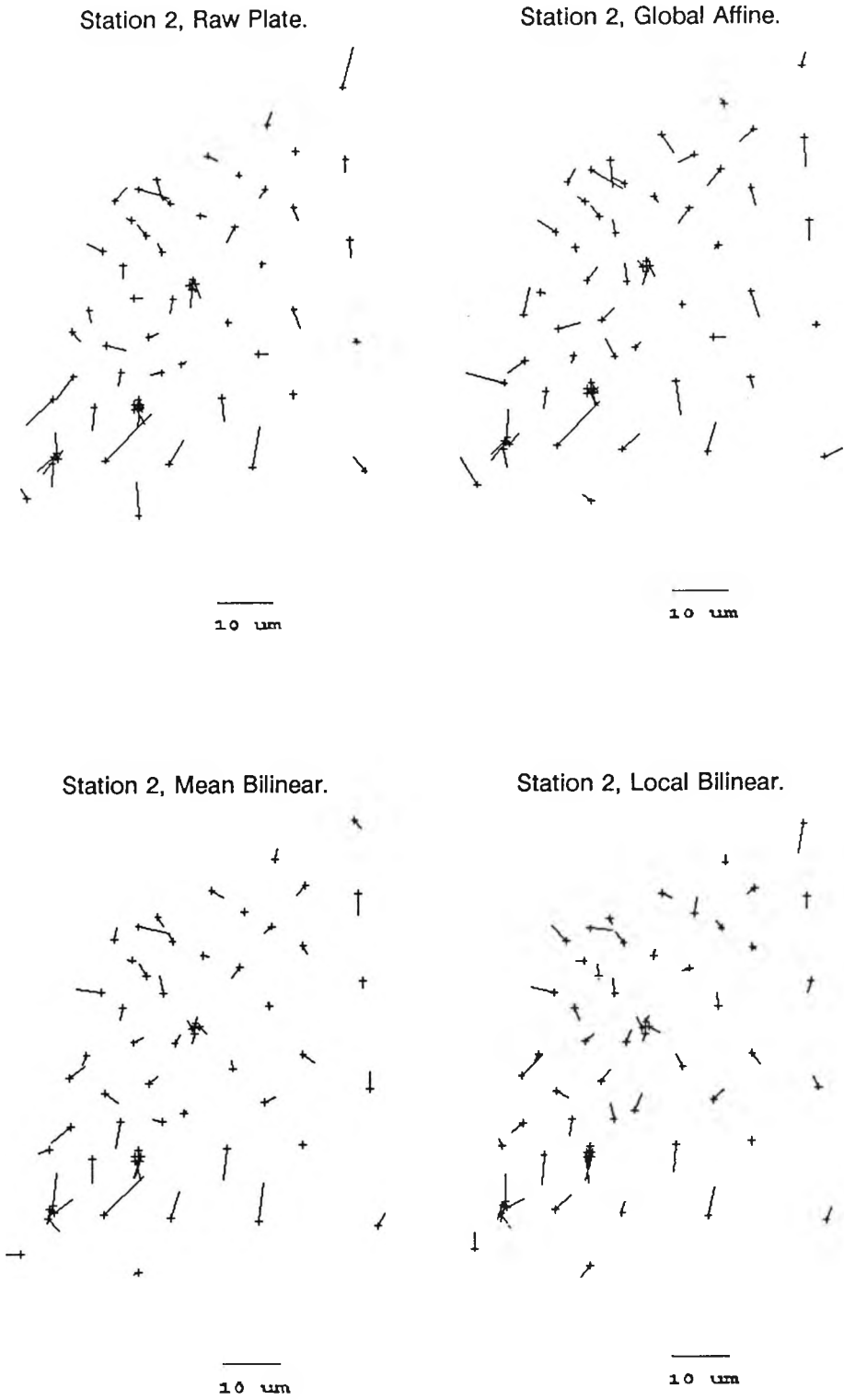


Figure 6.29.

Mean RMS photo-coordinate residuals
for the camera back and film combinations
exposed in the HS1 camera.

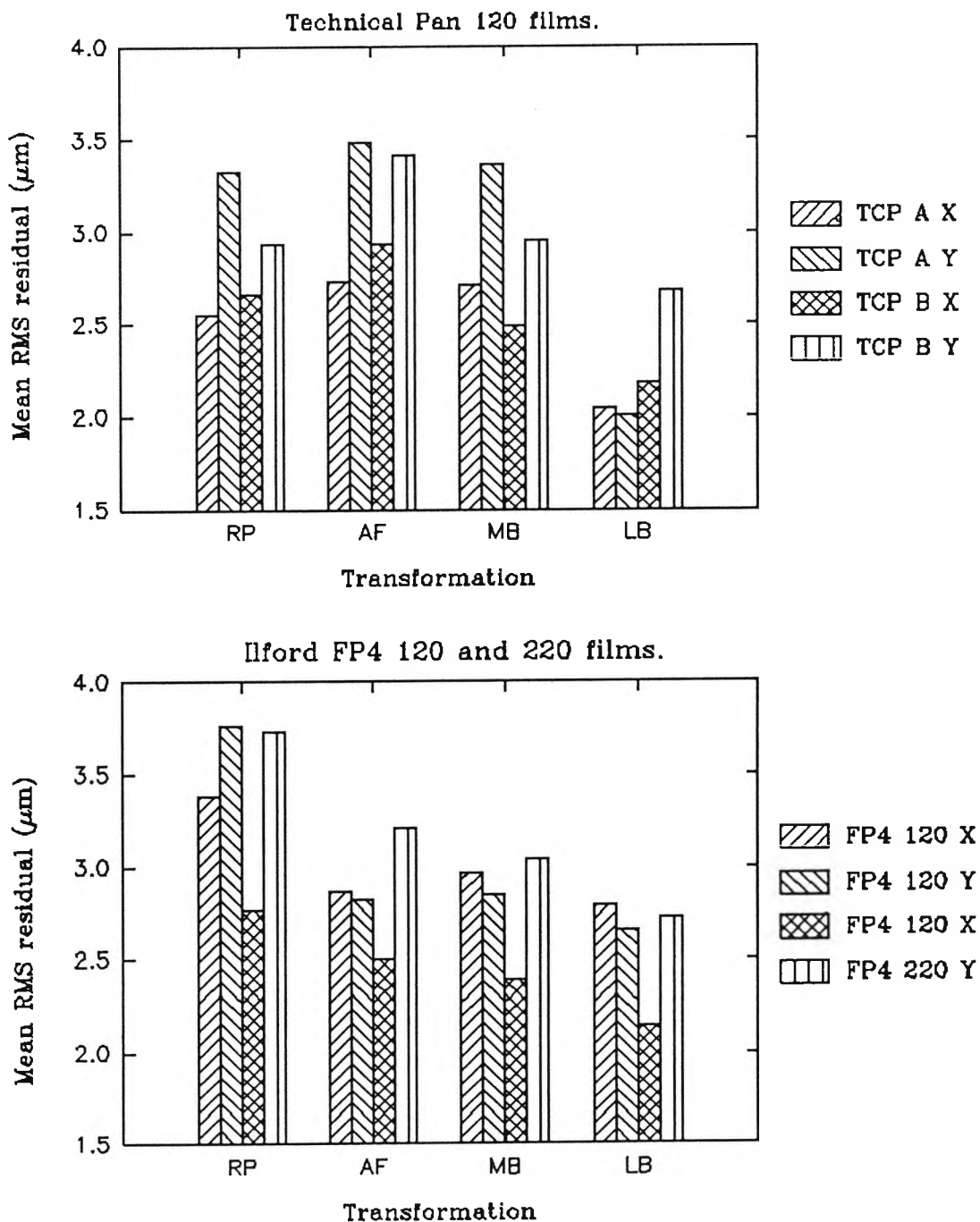


Figure 6.30.

6.4.2.3. Differences between the estimated object space coordinates.

Photogrammetry sets out to measure dimensions and positions of objects according to some reference system or datum. Therefore of primary importance for this analysis is the influence of film deformation and its correction on object space coordinates. As discussed earlier (Section 6.4.1) the global bundle adjustment provided an object space coordinate reference set, against which the coordinates derived from this series of adjustments could be directly compared.

Figure 6.31. shows the RMS object space coordinate discrepancies, computed simply by subtracting each computed coordinate from its corresponding reference coordinate set. It should be noted that the coordinate axis directions defined during the conventional survey (Section 6.2.1) were not orientated with respect to the target array surface (Fig. 6.11). Consequently whilst the Z axis represents the height of the test field, depth and width are represented by a combination of X and Y directions.

The adjustments made using the Ilford FP4 films generally show a reduction in RMS object coordinate discrepancy as the complexity of the image deformation correction is increased. However all the reductions in coordinate discrepancy are of the same order or smaller than the estimated coordinate standard deviations ($150\mu\text{m}$ X, $200\mu\text{m}$ Y, $160\mu\text{m}$ Z), raising the question of the applicability of these corrections for all but the highest accuracy survey work.

Differences between the discrepancies derived from the image sets on Kodak Technical Pan 120 film at first glance show no gradual decrease in discrepancy with transform complexity. The deformed frame in the Technical Pan 120 Back A data set has meant that discrepancies are actually worsened by using the affine and mean bilinear corrections. The only likely reason for this anomaly is that both corrections are spreading the gross image deformations (especially those of frame 6) over the format area and are consequently deforming rather than correcting the central regions where most of the targets are situated.

Technical Pan film exposed in back B produced reseau deformation plots (Fig.6.3) which appeared very radial in nature. Consequently parameters such as focal length and radial lens distortion coefficients included in the adjustment are highly correlated with and have been able to model most of the film deformations (Figs 6.26 and 6.28).

Comments concerning object coordinate discrepancies made so far have only been concerned with RMS object coordinate discrepancies, disregarding any patterns which might be occurring over the test field area. Figures 6.32 and 6.33 are plots of coordinate discrepancy for the adjustments made using the Technical Pan 120 A data set, viewed from the front and top of the test field respectively. With the exception of systematic vectors at the target clusters, the discrepancies appear remarkably random.

Mean RMS object space coordinate discrepancies
for the various camera back/film correction permutations

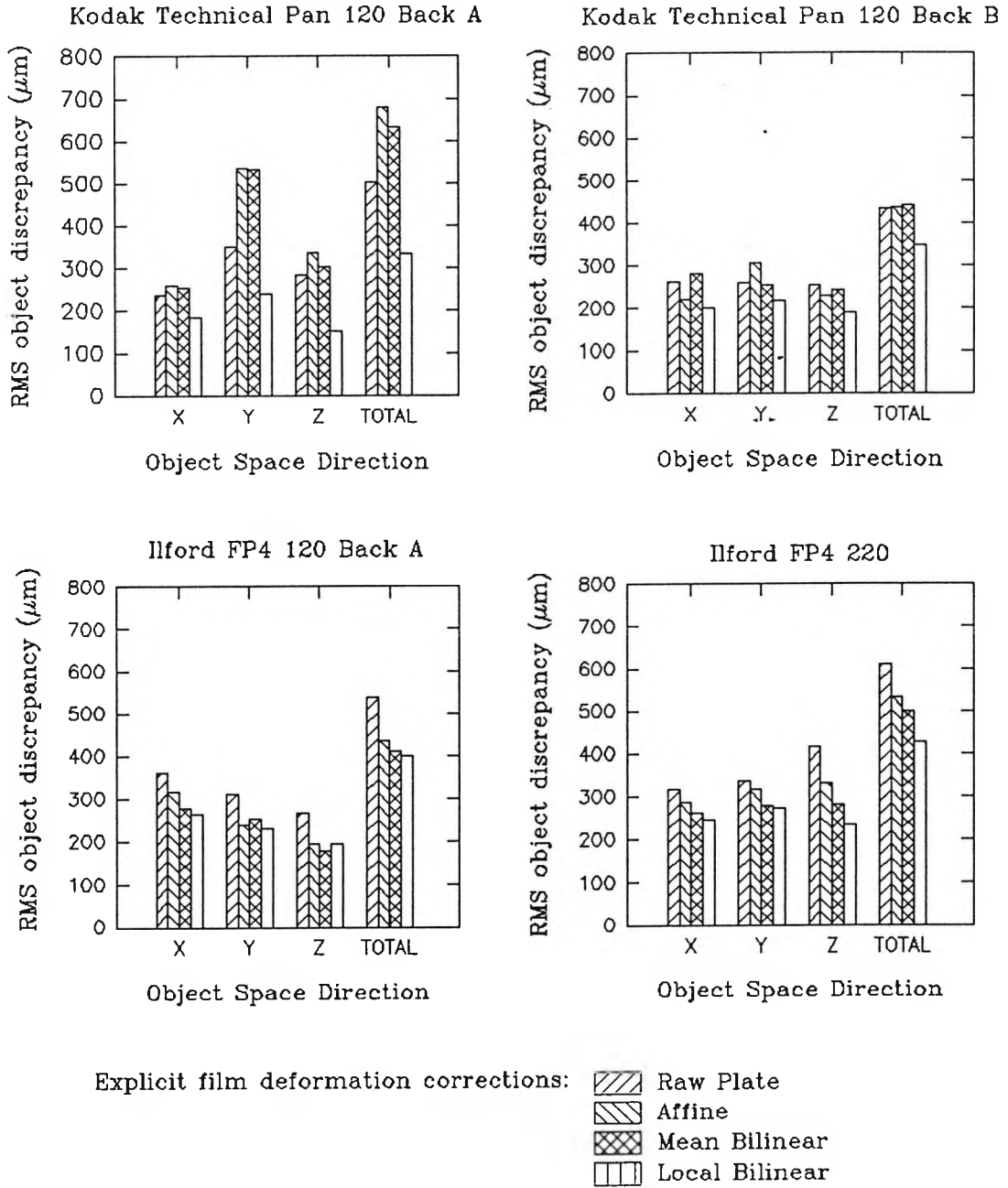


Figure 6.31.

Technical Pan 120 back A

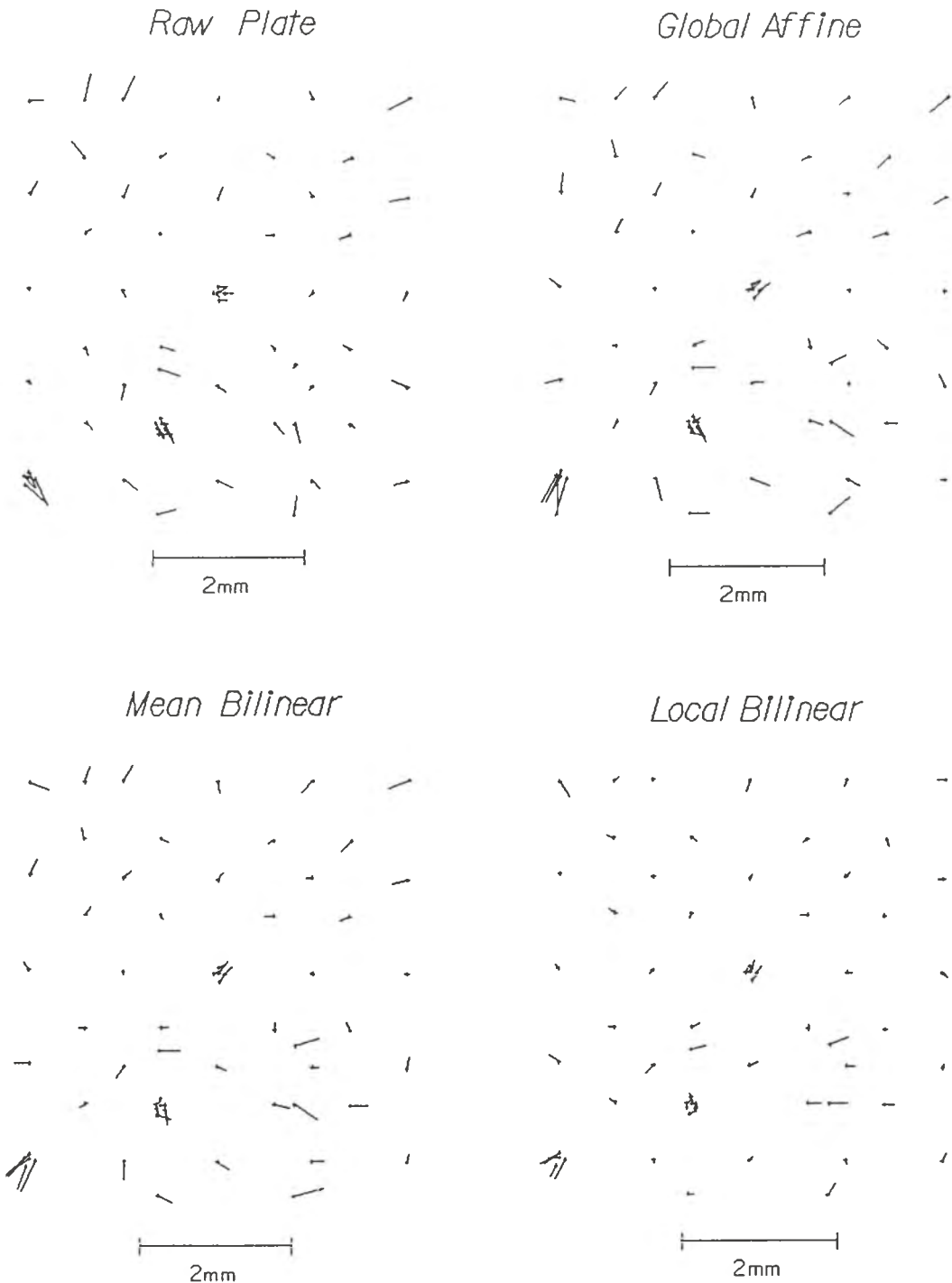


Figure 6.32. Object space discrepancy vectors for the Technical Pan 120 Back A data set (Front View).

This random nature can probably be attributed to the strong network geometry in conjunction with the rotated cameras having the effect of averaging the film deformation. The discrepancies at the local target clusters will of course be largely independent of this effect leading to the high correlations seen between their associated discrepancies. Additionally the reseau grid density limit

mentioned earlier can probably be attributed as the cause of the systematic cluster vectors still present after local bilinear correction.

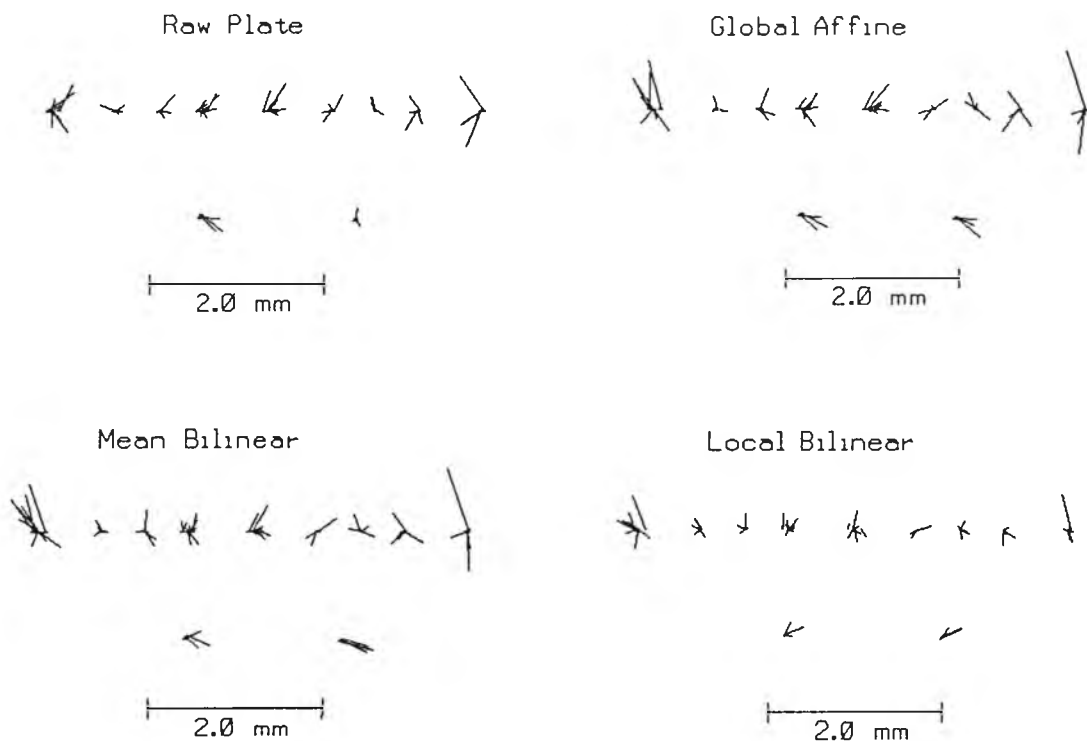


Figure 6.33. Object space discrepancy vectors from the Technical Pan 120 Back A data set (Top View).

Finally object space precision can be computed, for example for the Technical Pan 120 Back A data using the test field dimensions in table 6.12.

Table 6.21. Precision in the object space for the Technical Pan 120 Back A adjustment.

Direction	Mean RMS object coordinate standard deviation	Maximum object space dimension	Precision
X	180 μ m	4.10m	1:22,777
Y	240 μ m	3.12m	1:13,000
Z	160 μ m	5.47m	1:34,187

6.4.3. Summary of camera back and film type variations.

Perhaps the most obvious conclusion which can be drawn from these results is that due to the nature of the least squares process, the mathematical model is acting as one interconnected dynamic system. Uncorrected film deformations are spread around the system, according to the mathematical applicability of the various estimated parameters. The strong nominally symmetric

network has meant that any consistent deformations have either cancelled out or modelled to some degree before being expressed in both the object coordinate estimates and the photo-coordinate residuals. This has resulted in an apparently random object discrepancy vector field.

An exception to this principle occurs where clusters of targets are concerned, since they are extremely localised within the format area they are not averaged over the format area by the small number of photographs involved in each adjustment. The presence of image deformation at these local clusters even after the bilinear correction implied that the reseau density is not small enough to enable all the in-camera deformations to be explicitly modelled.

Adjustments using the local bilinear correction can be regarded as providing the optimum explicit correction available for this reseau camera system. Encouragingly the variance factors associated with each set of photo-coordinates refined using the local bilinear correction (Table 6.19) infer that the target pointing ability associated with the image quality attainable from the lens/film combination begin to limit the solution.

Results confirm the conclusions derived from the global adjustments (Table 6.16) that once an effective localised correction has been applied, unless lens parameters are able to model residual film deformations, the camera parameters included in the adjustment are for most purposes independent of the film back and film used.

Given a strongly convergent network geometry it is arguable whether any film deformation corrections need to be applied for this type of camera, if coordinates in the object space are the only area of interest.

For increased object space accuracy the advantage between the raw plate, global affine and mean bilinear corrections can probably be regarded as insignificant, for high precision work the only worthwhile physically based refinement is the local bilinear. It is worthwhile mentioning that Fraser (1984) for example has had some success by including arbitrarily selected additional parameter sets in the adjustment to model the film surface. However since a strong network is often not the case where practical surveys are concerned, the effectiveness and statistical significance of such additional parameters can often be inappropriate.

From these data there appears to be no reason to assume that the mean bilinear correction will provide a more accurate bundle solution to that provided by the use of affine or raw plate derived photo-coordinates.

6.5. The effect of the explicit film deformation correction methods on the precision obtainable during a typical survey.

In the previous analysis, an unusually strong network in comparison to those commonly adopted for photogrammetry using small format cameras was employed. The intention of this analysis is to determine the effect of the three explicit film deformation corrections on the shape of the object coordinate field when surveyed by a more conventional two camera station network.

For this analysis a subset of the global data could again be adopted, providing the advantage of the precise target coordinate array. New estimates of the target field coordinates could then be computed for the new network again using a self calibrating bundle adjustment.

6.5.1. Photogrammetric processing.

The datum for this adjustment was defined along more conventional lines. Five targets at the four corners and centre of the target array were selected for use as control points. Their coordinates were constrained according to their standard deviations estimated by the global adjustment. Two frames, station numbers 3 and 4, were selected from the Technical Pan Back B data set, providing a pair of camera stations with convergent optical axis. The three sets of refined photo-coordinates and the raw plate coordinates associated with these camera positions were processed in individual self calibrating bundle adjustments. As in section 6.4, the camera calibration parameters estimated during the global adjustment were included as starting values constrained by their standard deviations.

In this way an adjustment was carried out which although keeping to commercial close range photogrammetric survey lines, facilitated the analysis of film deformation corrections.

6.5.3. Analysis of results.

Again this analysis can be split up into three sections: estimated parameters; photo-coordinate residuals and; object space coordinate discrepancies.

6.5.3.1. Analysis of estimated parameters.

Differences between the estimated camera calibration parameters computed during this series of adjustments and those from the global adjustment are shown in figures 6.34 and 6.35. It can be seen at once that in most cases the standard deviations of the parameters estimated during these adjustments are larger than the parameter differences. The only exception is the difference between the p_2 parameter connected with the mean bilinear film deformation correction. The general insignificance of the differences are due entirely to the weak network geometry and the

Differences between camera calibration parameters from the global bundle and those estimated during the pseudo practical survey

Standard deviations of the estimated parameters computed during the adjustment are shown as a measure of significance.

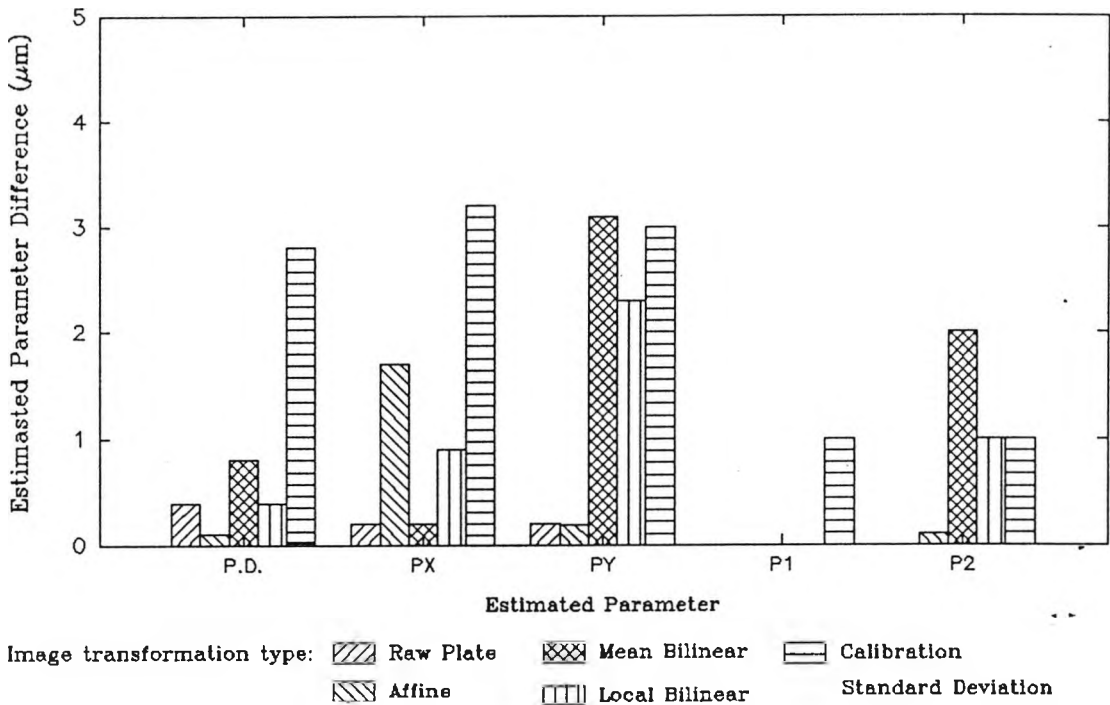
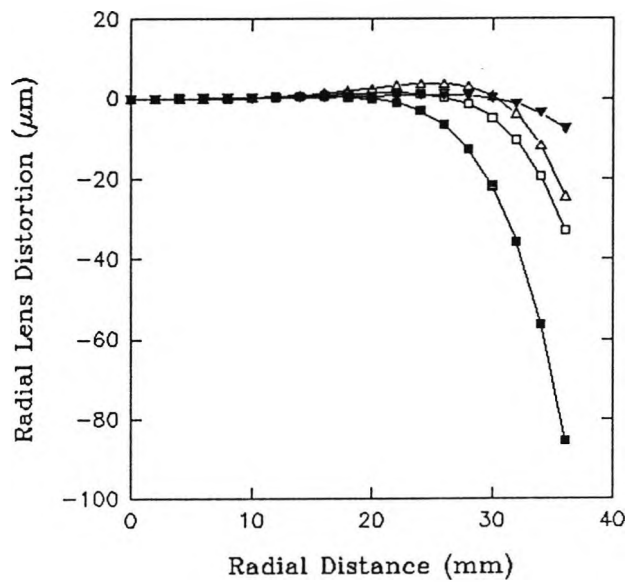


Figure 6.34.

Radial lens distortion from global adjustment minus radial lens distortion computed during the pseudo survey.



Reseau correction methods:

- ▼ Raw Plate.
- Mean Bilinear.
- Global Affine.
- △ Local Bilinear.

Figure 6.35.

fact that constrained starting values were used.

The radial distortion curves from this series of adjustments agree with the global adjustment best estimates, until the edge of the format with its corresponding sparsity of target images is approached.

In agreement with the adjustments carried out to assess the film deformation corrections using a dense network, the camera exterior orientation parameters have significantly changed in compensation for some of the film deformations present. These changes are particularly apparent in the raw-plate, global affine and mean bilinear correction results.

Table 6.22. Rotation and translation discrepancies between camera stations estimated in the Global Adjustment and those estimated during the Pseudo Survey.

Treatment (Station)	Translations (m)			Rotations (°)			$(\hat{\sigma}_0^2)$
	X	Y	Z	ω	ϕ	κ	
Raw Photo (3)	Not Sig.	Not Sig.	-0.0030	0.0422	Not Sig.	0.0352	1.438
Raw Photo (4)	-0.0049	0.0058	0.0014	-0.0116	-0.0476	Not Sig.	
Global Affine (3)	Not Sig.	Not Sig.	-0.0038	0.0701	-0.0260	0.0553	1.716
Global Affine (4)	-0.0045	Not Sig.	0.0015	Not Sig.	-0.0457	0.0160	
Mean Bilinear (3)	-0.0014	0.0010	-0.0024	0.0458	-0.0195	0.0335	1.357
Mean Bilinear (4)	Not Sig.	-0.0016	Not Sig.	Not Sig.	Not Sig.	0.0074	
Local Bilinear (3)	Not Sig.	Not Sig.	Not Sig.	Not Sig.	Not Sig.	Not Sig.	1.038
Local Bilinear (4)	Not Sig.	Not Sig.	0.0014	Not Sig.	Not Sig.	Not Sig.	
St.Dev. (3)	0.0010	0.0008	0.0013	0.0212	0.0113	0.0144	
St.Dev. (4)	0.0013	0.0008	0.0009	0.0092	0.0115	0.0056	

Standard deviations were computed with an a-priori variance factor of 1, they must therefore be multiplied by the square root of the appropriate variance factor in the last column.

6.5.3.2. Analysis of photo-coordinate residuals.

Figure 6.36 shows the mean RMS photo-coordinate residuals for each frame and treatment combination. Whilst little change with treatment type is seen for residuals in the x direction, those in the y direction show some improvement for frame 3.

Mean RMS Photo-coordinate residuals
for the modified Hasselblad camera
Results are grouped along the X axis according to
Frame number and Image Refinement

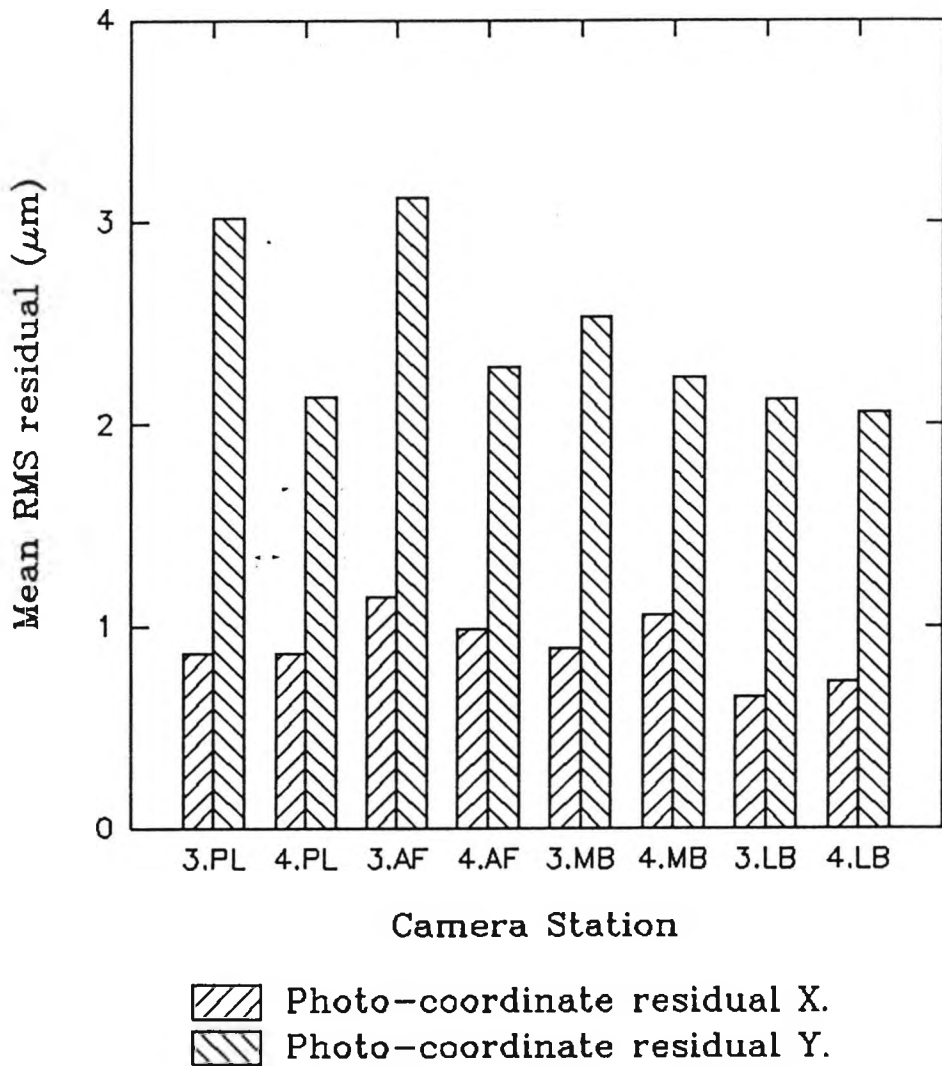


Figure 6.36.

Figure 6.37 demonstrates these improvements, and the presence of any systematic effects in terms of a vector field. It can be seen that the local bilinear correction has removed some of the systematic effects at which occur at the top left and bottom right corners of frame 3.

It can only be assumed that the remaining photo-coordinate residuals and those residuals present in frame 4, are due to localised unflatness and target pointing inaccuracies. The fact that most of the larger vectors are at the bottom of the images would confirm this, since the camera orientations meant that the targets at the bottom of the test field were further away from the camera.

Photo-coordinate residuals after
adjustment using five constrained control points.

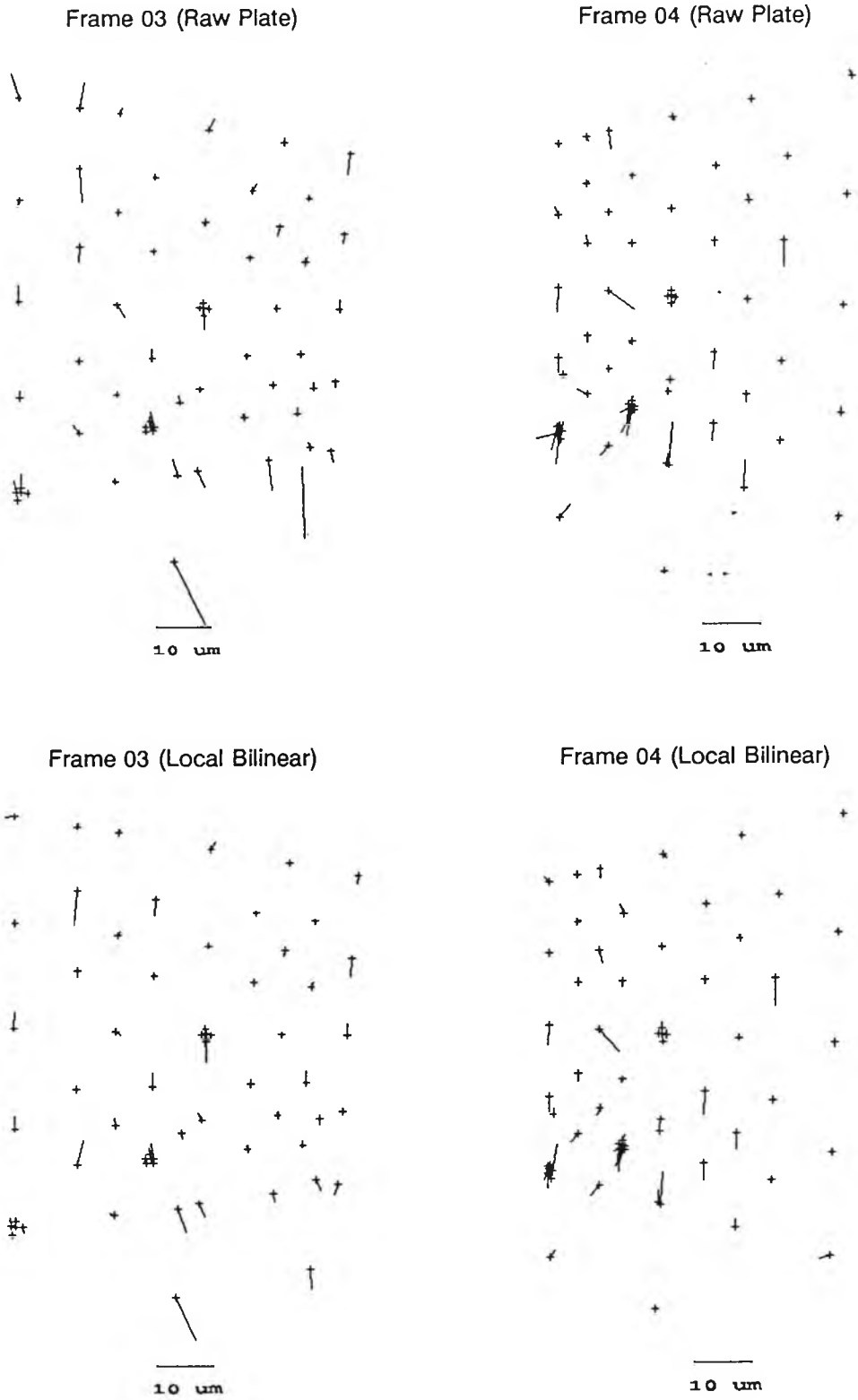


Figure 6.37.

6.5.3.3. Analysis of object coordinate discrepancies.

Discrepancies in the object space are the main concern for this type of survey operation, they may be computed simply by subtracting the set of coordinates estimated during this adjustment from the global adjustment reference set.

From figure 6.38 it can be seen that there are large systematic trends in the estimated object coordinate data. Also a distinct rotation is introduced into the estimated coordinates unless the local bilinear correction is applied (Fig. 6.39).

Despite the large (2mm) discrepancy in one of the left hand targets (Fig. 6.39), the local bilinear correction appears to have removed most of the systematicity from the plan view. However a significant pattern is identifiable in the Z direction at the top right hand corner of the target array (Fig 6.38). The cause of this is unclear, but a clue is provided by the fact that the photo-coordinate residuals are very small in the corresponding image areas. It must be assumed that the least squares process in minimising the sum of squares of the residuals has spread any remaining image deformations, for example the target cluster image measurements, over the test field area. This analysis is confirmed when it is considered that there are effectively only two radial lines defining any given target coordinate.

The systematic patterns seen in the target field are therefore due to uncorrected film deformation and also due to the pointing inaccuracy to target images, especially those at the bottom of the test field furthest from the cameras.

A statement as to the accuracy of attained during this survey is provided by table 6.23, which includes the RMS object discrepancies as opposed to the RMS object coordinate standard deviations.

Table 6.23. Mean RMS object coordinate discrepancies and computed accuracy.

Correction method	RMS object coordinate discrepancies (mm) and computed accuracy.		
	X	Y	Z
Raw Plate	0.969 (1:4,231)	0.693 (1:4,502)	0.698 (1:7,840)
Global Affine	0.886 (1:4,627)	1.064 (1:2,932)	0.901 (1:6,080)
Mean Bilinear	0.516 (1:7,946)	0.703 (1:4,438)	0.498 (1:10,984)
Local Bilinear	0.432 (1:9,491)	0.531 (1:5,875)	0.572 (1:9,563)

Technical Pan 120 back A

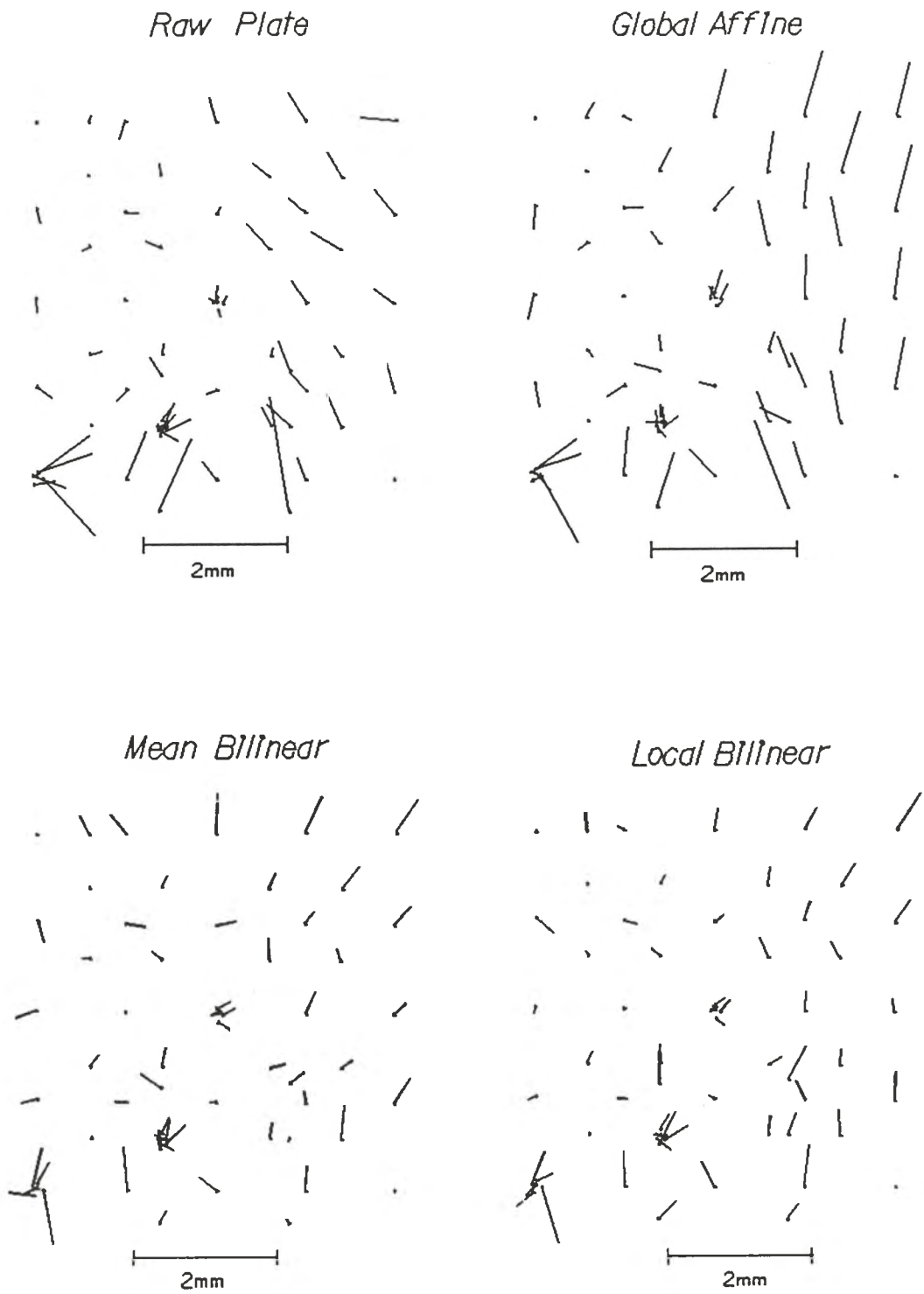


Figure 6.38. Object space discrepancy vectors from the pseudo survey (front view).

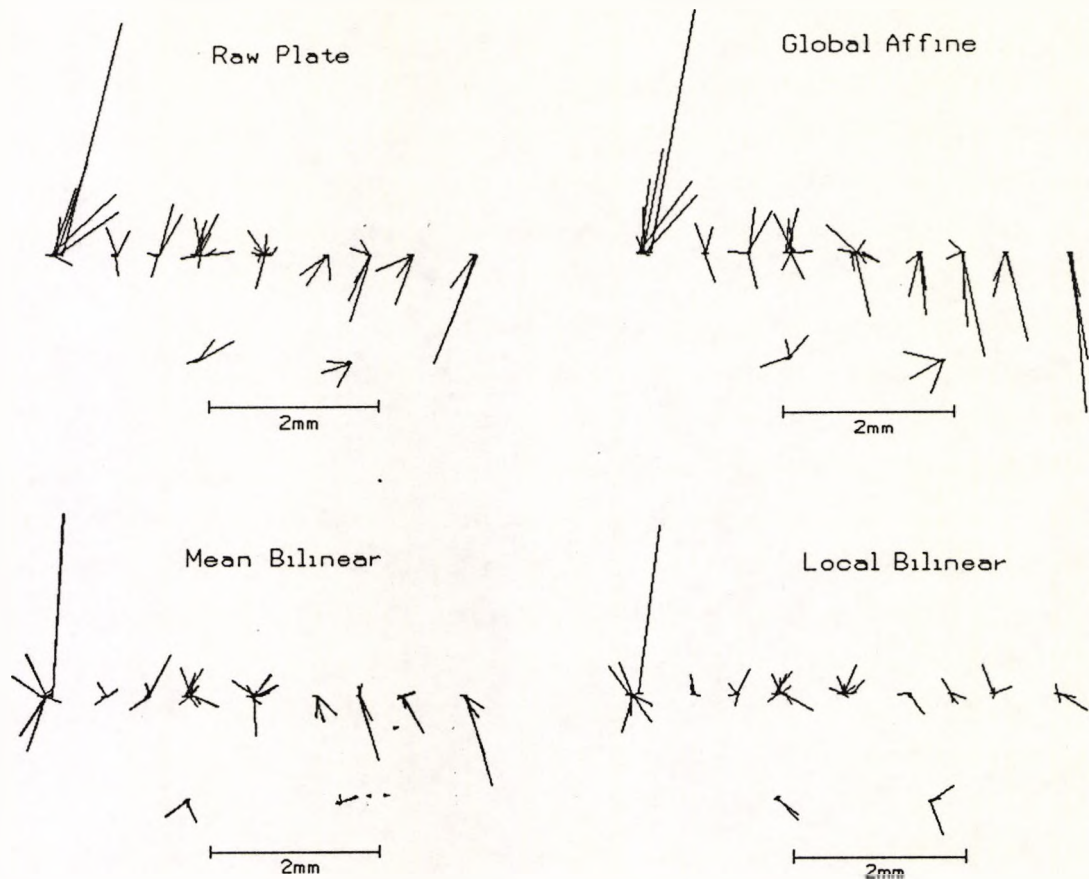


Figure 6.39. Object space discrepancy vectors from the pseudo survey (Top View).

6.5.4. Summary of results from the pseudo survey.

The pseudo photogrammetric survey was limited as intended by weak network geometry. However as shown by the table of RMS object coordinate discrepancies, the camera system is still capable of a respectable 1 part in 6,000 to 10,000 of the object space if film deformation is taken explicitly into account.

The RMS object coordinate discrepancies also show that the mean bilinear correction can provide increased object coordinate precision, but will not necessarily remove systematic effects, such as the rotation seen in the estimated object space coordinates (Fig. 6.39). For precision requirements below 1 part in 5,000 it can be concluded that the extra computational effort involved in carrying out image refinement is unjustified.

The use of constrained inner orientation and additional parameters in this type of adjustment has allowed well defined camera calibration parameters to be used, avoiding the inaccuracies associated with self calibration and weak network geometry.

6.6. Chapter summary.

Whilst the deformations occurring in the modified Hasselblad camera are an order of magnitude greater than the in-plane deformations summarised in chapter 5, these deformations are being caused by physical problems within the camera which could be solved by careful camera design. The main areas for re-evaluation are designing the gap between the reseau plate and the pressure plate to suit the film thickness, and a method of removing the pressure between these two surfaces during film advance. If such re-design were carried out, then it could be expected that the magnitude of in-camera film deformation would approach that of the in-plane deformations.

Adjustment results made with the UMK and P32 metric cameras have shown that when used with glass plate based emulsions these cameras are capable of photogrammetric surveys which are limited by network design and the ability to point accurately to the images of target points. In the P32 camera, which was tested with a film based product, the limitation appeared to be linked to the depth of field offered by the fixed lens and the inability of the adjustment to model local film deformation. This effect is borne out by the non-metric Hasselblad adjustment results, which demonstrated considerably smaller image residuals when glass plate based emulsions were used.

All the adjustments carried out using the modified Hasselblad camera demonstrated the surprisingly good results which could be obtained from modest modification of a conventional production camera. Only the local bilinear correction appeared to be worthwhile out of the three methods investigated, this method proving to be limited by the reseau density. Again stringent camera design may alleviate this problem, since the deformational differences between film backs suggest that it should be possible to remove most of the local deformations seen, potentially to the order of the $2\mu\text{m}$ to $3\mu\text{m}$ RMS target image photo-coordinate measurement error. Given such camera designs, network design can usefully incorporate photographic image quality considerations such as those discussed theoretically in chapter 2.

This work was primarily concerned with reseau photography, consequently the inclusion of additional parameters, either in block or photo-invariant form, to model film deformations within the adjustment have not been investigated. However it should be mentioned that the use of additional parameter sets requires a strong network geometry for reliable estimation (Grün 1978; Fraser 1984). Specifically high correlations can exist between estimated parameters and camera orientation elements if over parametrisation occurs.

An interesting alternative approach which was found too late for experimental evaluation was the application of the finite element method to bundle adjustment (Raidh and Munjy 1986a, 1986b). The finite element technique of processing the image in small elements avoids the geometric assumptions made about deformations when fitting additional parameter sets globally to the whole format area.

7. Conclusions.

This thesis has been primarily directed at evaluating the magnitude and physical causes of film deformation which can be expected when using commercially available small format photographic products. Also investigated are some physically derived analytical possibilities for the correction of photo-coordinate measurements made from images produced on small format equipment.

Observations and conclusions can be summarised under the three section headings used to describe some of the results from chapters 4,5 and 6, namely in-plane deformations, in-camera deformations and modelling of deformed images.

7.1. In-plane deformations.

The small format film products examined generally demonstrated good predictability with respect to in-plane dimensional stability. However several correlations and anomalies have been identified during the course of this investigation.

The approximately linear dependence of x,y image scales on measurement environment relative humidity, shows the desirability for a controlled measurement environment of the standard available at NPL (Oldfield 1988) if the ultimate is to be obtained from small format imagery. However it was shown in section 5.3.1 that global scale changes arising from variations in measurement environment can be routinely corrected by conventional fiducial mark based transformation techniques, allowing image measurement to be carried out in less costly conditions. From a photogrammetric viewpoint, it is the inhomogeneous film deformations occurring within the format area which constitute the major in-plane problem. These deformations not only appear to be uncorrelated with the measurement environment relative humidity at NPL (Section 5.3.1.2), but are also difficult to describe mathematically (Sections 4.4 and 6.4.1).

During the carefully controlled conditions of the in-plane experiments, inhomogeneous film deformations, represented by RMS image reseau coordinate differences after affine transformation, were kept to at or below $2\mu\text{m}$. Bearing in mind that the design of most analytical plotters can provide $\sim 3\mu\text{m}$ RMS, according to manufacturers' data, in-plane film deformation appears to be at the traditional photogrammetric "error budget" level (Laiho and Kilpelä 1988).

Inhomogeneous in-plane deformations were experimentally shown to occur between exposure and drying of the film. No direct physical causes have been identified during experimental variation of photographic process parameters, but the largest systematic localised patterns were identified on Technical Pan 120 film which used the thinnest cellulose triacetate base of all products investigated. Two possible causes of the deformations can therefore be identified: localised moisture changes during handling of the photographic materials, especially during the contact

exposure procedure; and stresses between the emulsion layers and base material, introduced into the film during the processing procedure.

Practical procedures to reduce such deformations must be based on using thicker and more stable (especially polyester) based film products and on taking great care to minimise handling of film materials during all stages in the photogrammetric process. Unfortunately the first suggestion greatly limits the choice of emulsion types available, given manufacturers' current product ranges. However if the significance of target pointing from the in-camera experimental results (Sections 6.3.2.1 and 6.5.3.2) are considered, selection of a suitable film should be made according to sensitometric abilities with a preference for thicker based materials if available.

Since no film handling is required at exposure during conventional small format photography it could be expected that a reduction of inhomogeneous in-plane deformation will be obtained under practical conditions, providing the same practical procedures based on manufacturers guidelines are followed (Kodak 1989a). However forces exerted on the film during film wind-on may act to increase in-plane deformations (Section 6.1.4).

The use of an inorganic hardening agent in the fixing solution resulted in a marginal reduction of inhomogeneous film deformation, and a slight change in image scale for the film products investigated (Sections 5.3.4.2 and 5.3.4.4). This result can be attributed to the physico-chemical basis of in-plane deformation, namely the different moisture absorption properties and thicknesses of the film base and emulsion layers (Section 2.2.3). The hardening agent promotes the formation of chemical crosslinks within the gelatin and therefore reduces moisture dependency. Consequently differences between the moisture absorption properties of the base and emulsion layers will be reduced.

Whilst some modern emulsions are stabilised during manufacture (Kodak 1971a), it still appears worthwhile to use an inorganic hardening agent during the processing of all films intended for photogrammetric purposes. Differences will probably be marginal for most modern emulsions (Section 5.3.4.4), but certainly no detriment will result from the use of such hardening agents.

In common with research conducted on aerial film products (Adelstein and McCrea 1981; Carman and Martin 1969; Ziemann 1972b), homogeneous in-plane film deformations were found to be much reduced for products on polyester base. However due to the limited availability of different emulsion types on such bases, their selection for photogrammetric purposes is not unequivocal. Indeed the target pointing ability conferred by high resolution emulsions can outweigh base type, especially when it is considered that most of the deformational differences between bases were found to be of a uniform nature, and therefore easily corrected for. For example in chapter 6 it was concluded that the image qualities of Kodak Technical Pan emulsion outweighed the fact that this product in 120 form is coated on cellulose triacetate base.

The effectiveness of a photogrammetric survey can be the duration between image acquisition and measurement. For digital images the limitations are primarily those of computation speed, with target recognition and measurement potentially occurring in at video frame rates (Grün 1989).

Whilst results are sometimes required quickly, if image resolution and the potential for an archive are important, given current technologies, photogrammetric images on film may have to be measured as soon as possible after processing. Results from section 5.4.3.3 demonstrated that a one to two day minimum time delay can be required before cellulose triacetate based photographic film will have suitably equilibrated with the measurement environment. The importance of such changes will depend on the purpose of the photographs and the duration of image measurement, but for critical applications it is recommended that polyester or glass plate based emulsions are used.

Differences between the in-plane deformations obtained from this survey of small format (120, 220 and 70mm) products suggest that most dimensional properties are of the same order as those of the large format film products investigated in the late 1960's to early 1970's. There is however one important difference in that any atypical deformations commonly found towards the edges of the format have a greater influence simply because of the smaller format area.

To summarise this section, these observations coupled with recent advances made in terms of the emulsion speed / graininess trade off (Jacobson et al 1990), mean that film products intended for pictorial purposes can provide a recording system which is very adaptable to photogrammetric needs.

Most importantly, variation of film type and subsequent fine tuning of sensitometric properties by variation of development parameters, is possible without the risk of causing adverse dimensional effects. Consequently film sensitometry, speed and resolution can be selected to suit any specific end use that a project may require.

For example when using retro-target methods for high precision surveys, emulsion resolution is of paramount importance whilst flash output can be increased to compensate for reduced emulsion speed (Gates 1984; Cooper and Robson 1990). Additionally, development formulation can be chosen to promote the formation of the binary image useful for automated target recognition. A contrary example is provided by hand held small format aerial photography, where image motion and camera vibration must be minimised to achieve a sharp image (Trinder 1984; Chandler et al 1989). In this case high emulsion resolving power has to be sacrificed for emulsion speed. Again development can be fine tuned within the limits of the emulsion selected to achieve image contrast levels necessary for photogrammetric plotting purposes (Carman 1982a; Horn and Tugwood 1984).

7.2. In-camera deformations.

The similar patterns seen between vector plots of residual deformation along complete film lengths exposed using a variety of 120 film and camera back combinations in the HS2 camera are encouraging. In fact it can be concluded that the reseau plot deformation patterns arising in the HS2 camera are directly linked to the camera back and film type used. These results therefore confirm that it is camera design allied with the thickness of the film product to be used which contributes the major influence on film deformations occurring in small format photography.

Inhomogeneous deformations exist within the generalised patterns, but since the reseau can only identify deformations, not their cause, it is not possible to comment on the physical reasons for the differences occurring between frames. The most interesting anomaly occurred in the FP4 220 film exposed during the practical survey (Section 6.1.3.3). The systematic changes between frames along its length (Fig.6.10) must be linked to the absence of backing paper with this roll type possibly combined with the features of the FP4 220 back used.

The addition of a backing paper in the reseau/film/pressure plate sandwich could have three effects: first the paper could limit the film's response to environmental change; it could reduce some of the stresses exerted on the film during wind-on; and it will definitely influence the pressure and evenness with which the film is pressed against the register glass.

It is interesting to note that differences between the image deformations produced when using 120 and 220 films were also found during the initial work with the Rollei-Metric 6006 (Section 4.4). In this case unflatness of the pressure plate prevented any specific conclusions being drawn, although 220 film produced much reduced deformation.

All in-camera reseau exposures have shown that in-camera deformation, predominantly film unflatness is responsible for deformations of at least an order of magnitude greater than in-plane deformation. Results appear to demonstrate that when the separation between the pressure plate and reseau is matched to the thickness of the film type to be used, minimum out-of-plane deformation is produced. In-camera deformation is consequently a function of camera and film transport design.

Unfortunately photogrammetric techniques are not suitable for the reliable detection of film unflatness, principally because unflatness is occurring orthogonally to the notional image measurement plane. Direct in-camera measurement of film unflatness can be carried out using a variety of interferometric techniques (Clark 1972; Meier 1972), but any measurement necessitates removal of the lens, consequently this type of approach was not possible for the modified Hasselblad camera.

Analysis of the design of both the Rollei-Metric 6006 and HS1/HS2 camera lead to several conclusions concerning camera design. An advantage may be provided by a camera back using a pressure plate that retracts during film advance, since this would minimise separation without friction causing problems during film wind on. Although such a method is used in the Rollei-Metric camera back design, reseau plate unflatness in the particular camera under test (No.005298811) negated any advantages provided by such a system.

Since the completion of the practical work, two new small format cameras incorporating vacuum backs rather than the conventional pressure plate system have come onto the market. The Pentax PAMS645-VL employing a 6cm by 4.5cm format has proven ability (Fraser and Shortis 1990), whilst the Contax RTS III presented at Photokina (1990) although designed primarily for the pictorial photography market has potential for simple modification such as the incorporation of a photo-coordinate reference system. Such innovative small format camera designs present new opportunities by virtue of higher accuracy/cost ratios.

7.3. Test field photography.

The test field photography exercise was conducted in order to compare some of the photogrammetric characteristics of different camera systems and to calibrate a target array to enable the photogrammetric consequences of film deformation and the developed explicit correction techniques to be evaluated.

The UMK and P32 cameras, representing the traditional close range option, were found to be capable of producing results limited only by network design and target image pointing ability. In the case of the UMK camera used with Holotest 10E75 emulsion, image quality was excellent even given the fact that conventional targets rather than retro targets were used. The P32 camera was severely limited by the depth of field of its fixed lens at minimum aperture. Target image pointing errors explain why little difference was found between exposures made using notionally flat glass plates and film products with no deformation corrections. This constitutes a significant disadvantage, such that the metric qualities of the camera are only useful for photography of objects within its design range. This limitation in conjunction with cumbersome operation constitute the major limitations of metric cameras as opposed to pictorial cameras which are designed to combine ease and flexibility of use.

Both metric cameras depend on design to minimise in-camera deformations, such that only four fiducial marks and an additional central mark in the case of the P32 are included. Unfortunately because of a history of practical failure, the UMK vacuum film backs owned by City University were not tested to check whether the film flattening design of this system corresponded with the excellent optical qualities of the UMK camera (Gates et al 1982).

A useful comparison can be made between the parameters estimated in the global adjustment from images made onto FP4 glass plates and FP4 120 film in the P32 camera. The interior orientation and additional parameters included in the adjustment to model lens distortion, whilst insignificant where glass plates are concerned must have modelled some of the systematic film deformations present in the FP4 120 imagery.

Results from the adjustments carried out using the modified Hasselblad camera (HS1/HS2) show that if estimated parameters are to represent the physical properties of a camera lens cone, then film deformation should be removed explicitly, as is the case for the local bilinear correction.

Without explicit film deformation corrections, if network geometry is not such that image coordinate errors are confined to the photo-coordinate residuals (Wester-Ebbinghaus 1989) then film deformations can be transferred to the estimated object space coordinates (Section 6.5). It is especially interesting to note that the physically based mean bilinear correction whilst producing reduced RMS object discrepancies did not remove systematic deformations in the estimated object coordinates (Section 6.5.3.2).

It can be seen from the results of all three types of adjustment carried out with the HS1/HS2 camera that only the local bilinear correction provides a valid film deformation correction for all the image deformation patterns. This effect is especially true where gross unflatness is present in individual images.

Localised deformations of higher frequency than those detectable by the reseau density can be clearly identified by the high correlation between photo-coordinate residuals which correspond to local target clusters. Such localised effects clearly show the limitation of reseau photography and the local bilinear correction, but with current camera designs the few micrometers systematic error which these deformations represent are probably insignificant for most small format survey applications.

The use of additional parameter sets (Section 3.3.2) often included in adjustments to model factors such as film deformation have not been investigated during this work. Primarily sets used are based on statistical significance of parameters (Fraser 1982b; Jacobsen 1982) not on actual physical deformations. Consequently their effectiveness is a function of network geometry which is not necessarily strong in small format photography. Explicit corrections are independent of geometry being applied prior to adjustment, consequently they are more favourable providing physical characteristics are known.

The use of the non-metric Hasselblad camera has shown encouraging results given the lack of any coordinate reference system and the absence of any constraints on film flattening. Adjustments incorporating the non-metric Hasselblad camera have been confined to the Global Adjustment

which included metric cameras. As a consequence results can only demonstrate the ability of the estimated parameters to model distortions occurring in camera, not the photogrammetric ability of the camera. From the results however, it is clear that as with semi-metric cameras it is camera design allied to film flattening which will control the extent to which this type of camera can be routinely employed for photogrammetric purposes.

As an aside it is interesting to note that two factors have been historically significant in directing research into the photogrammetric potential of the non-metric camera. Firstly lower cost in contrast with metric cameras, although this factor is now perhaps less valid given the availability of relatively cheap (~£4000) semi-metric cameras produced by manufacturers' modification of non-metric cameras. The second factor is the desirability to reconstitute existing photographs produced using pictorial cameras. For example survey projects which seek to determine changes of form with time using archival photography which had been taken for other purposes (Chandler 1989).

With the increasing potential and consequently research directed at low cost digital image acquisition, small format film camera design must be refined, if the current resolution and storage advantages offered by film products over the latest generation of digital cameras such as the Kodak Megaplus system (Kodak 1988b) are to be maintained.

7.4. Suggestions for carrying out photography for photogrammetric analysis.

Whilst network design provides the major contribution to the accuracy attainable from photogrammetry, results have shown that the potential indicated by this theoretical approach can be realised in practice only by following strict photographic procedures. It therefore seems appropriate to summarise the findings of this thesis relating to photography with well designed metric and semi-metric cameras by the following:

Photographic technique can significantly affect the dimensional qualities of images produced. The results of this thesis have shown that providing the photographic process is standardised according to manufacturers' product guidelines, but still allowing flexibility of tone reproduction control by variation of development, images which are dimensionally consistent can be produced. For photogrammetric purposes it is the design of the small format camera in relation to controlling film flatness at exposure which provides the major cause of image deformation. Currently the film flattening ability of pictorial camera designs is being re-evaluated, such that a variety of new models, some of which have been modified for photogrammetric purposes, are becoming available from various manufacturers.

For a given network design, the limiting factor influencing photogrammetry with metric and semi-metric reseau cameras can be the ability to be able to identify and measure accurately target

images produced. The quality of the photographic images produced is therefore of primary importance. This thesis has consequently proven that selection of a camera and film type combination for a particular survey should be based on its ability to record, sharply and with maximum contrast, all the subject details of interest. Whilst not new, practical techniques aimed at optimising image sharpness assume an even greater level of importance. For example as shown by the results from the P32 camera, unsharp images can significantly reduce the advantages offered even by metric-camera designs.

Finally, tuning of the photographic process by variation of emulsion type with a preference for thicker based films, and more subtly by development based on manufacturer's data can produce optimal image quality without increasing the magnitude of film deformation.

7.5. Suggestions for further work.

An obvious direction for further research is to integrate photographic image quality considerations with photogrammetric network design. Whilst this has been applied to the limited case of retro-target imagery by for example Brown (1982), the author can find no references to methods incorporating conventional photographic imagery with photogrammetric design. A probable reason for this is the diversity of subjects which can be surveyed by photogrammetric techniques, however certain basic considerations such as lens and film MTF, depth of field and target contrast could be included by means of look up tables relating to different products. The influence on target pointing precision due to the morphology of the developed silver image could also constitute part of this work.

A second direction is to analyze film unflatness in camera using interferometric techniques. This would be especially useful for the latest generation of products, since these are likely to provide more reproducible film surfaces. Such physically derived surfaces could then be modelled explicitly, in a similar way to measurements of plate unflatness from pneumatic gauging which have been used in metric glass plate cameras (Brown 1986; Forno and Kearney 1987).

Third, localised in-camera film deformations require further analysis if small format reseau densities are to remain at the 5mm spacing used throughout this work. The local bilinear correction whilst simple computationally cannot correct for localised deformations occurring within each reseau grid square. A possible solution could be provided by explicitly applying a localised interpolation technique based on a statistical analysis of physical film unflatness measurements. Although such a treatment would currently be computationally prohibitive for most applications, the rapidly reducing cost/performance ratio of computer systems may soon render such methods viable. An alternative method is a bundle adjustment which incorporates finite element techniques to divide the format into individual regions (Raidh and Munjy 1986a, 1986b). Such a method has the advantage of being able to model deformations without making assumptions concerning shape

as is the case when additional parameters are used.

Finally with the advent of many cheap small format based photogrammetric measurement packages (Luhmann and Peipe 1988; Leitz 1989), joint research between the film manufacturers and camera manufacturers could produce some viable camera designs and film types suited to this rapidly expanding measurement field. Especially promising for object measurement would be a network design package based on an alliance between analytical photogrammetric principles and photographic imaging limitations corresponding to a small format camera system incorporating a target scanning measurement package such as the Rollei RS1.

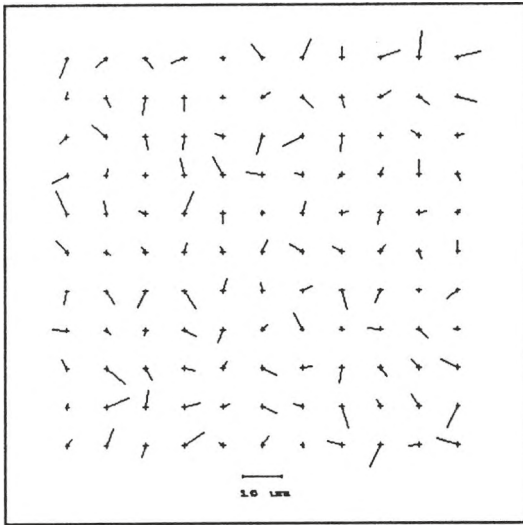
Appendix A.

A selection of film deformation vector plots from the in-plane experimentation.

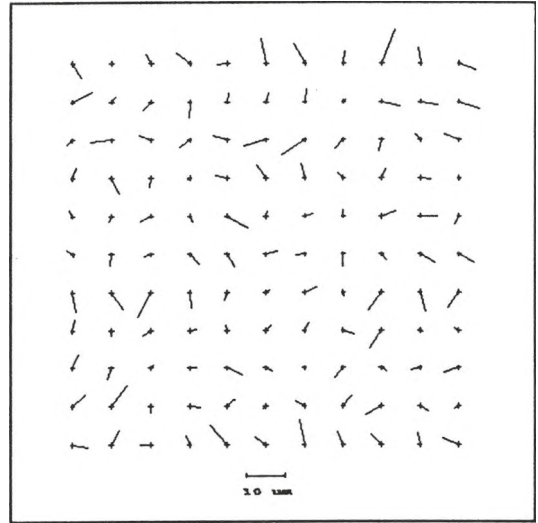
A selection of in-plane deformation plots from Experiments 1 and 2.

Variation of drying environment.

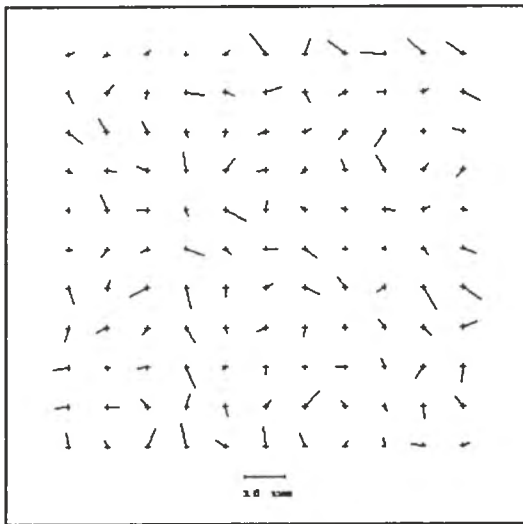
FP4 220, Roll 1, Frame E2, No.2.



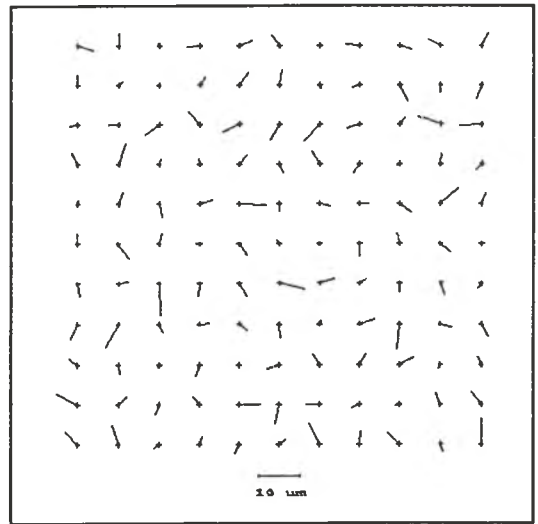
FP4 220, Roll 1, Frame E2, No.3.



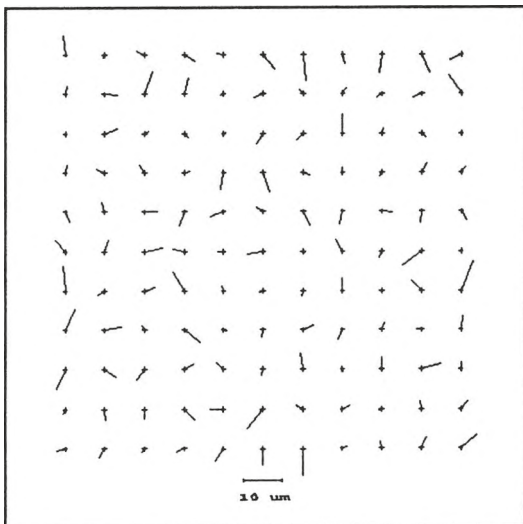
FP4 220, Roll 1, Frame E5, No.3.



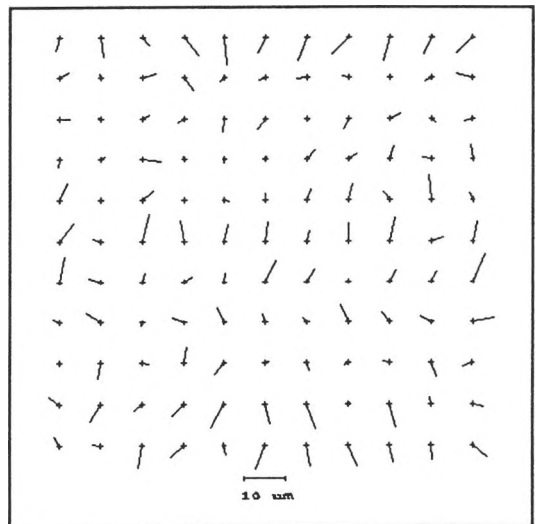
FP3 70mm, Roll 2, Frame A3, No.2.



FP4 220, Roll 4, Frame F2, No.1.



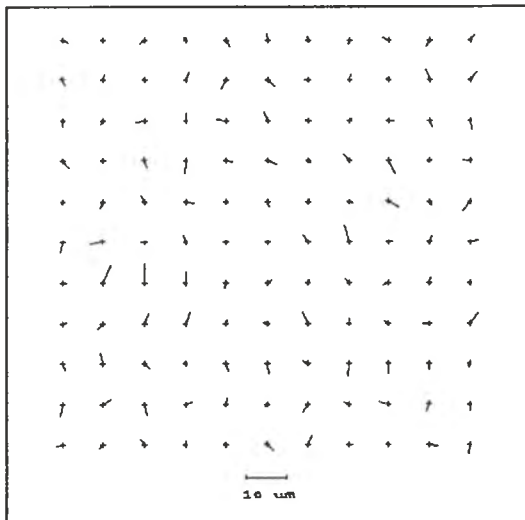
FP3 70mm, Roll 4, Frame B2, No.2.



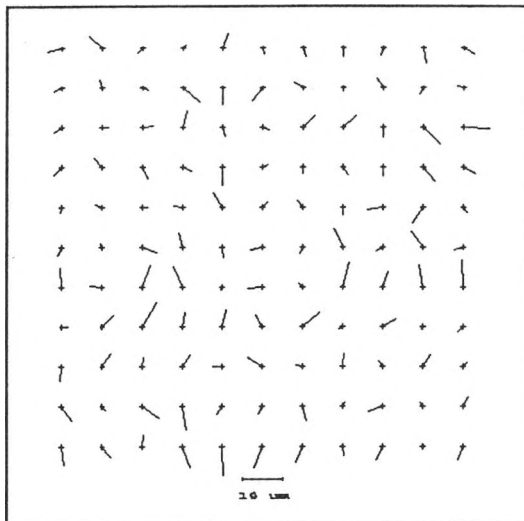
A selection of in-plane deformation plots from Experiment 3.

Variation of film type.

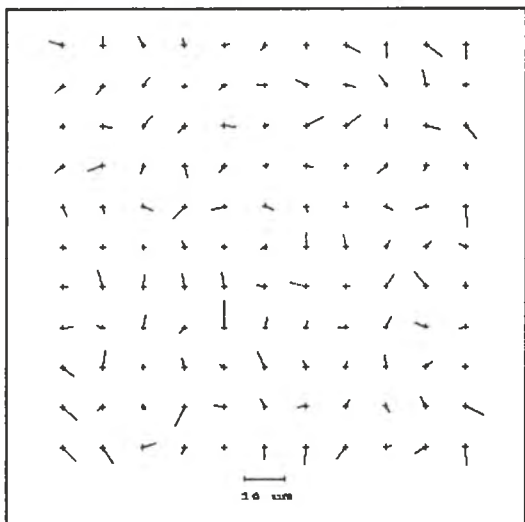
FP4 120, Roll 5, Frame E1, No.4.



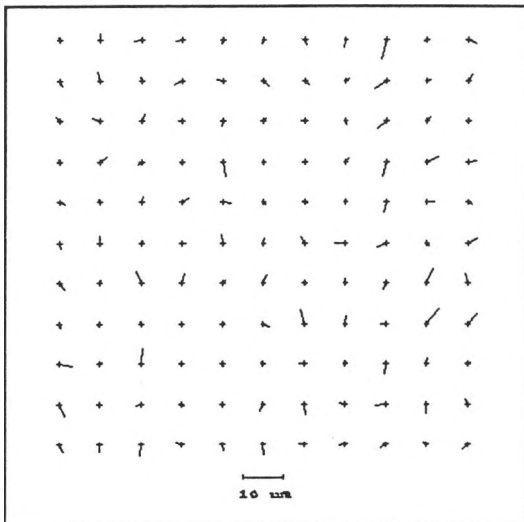
FP4 120, Roll 5, Frame E2, No.1.



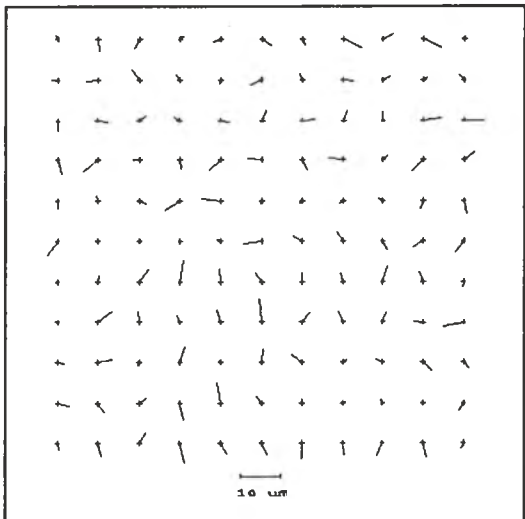
PAN F 120, Roll 6, Frame A1, No.3.



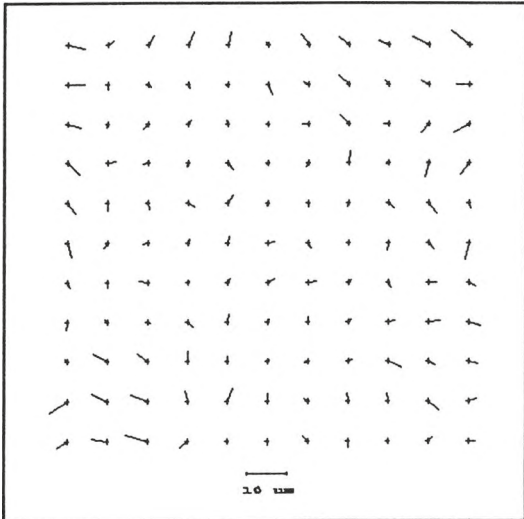
Pan F 120, Roll 6, Frame A2, No.5.



TCP 120, Roll 7, Frame B1, No.1.



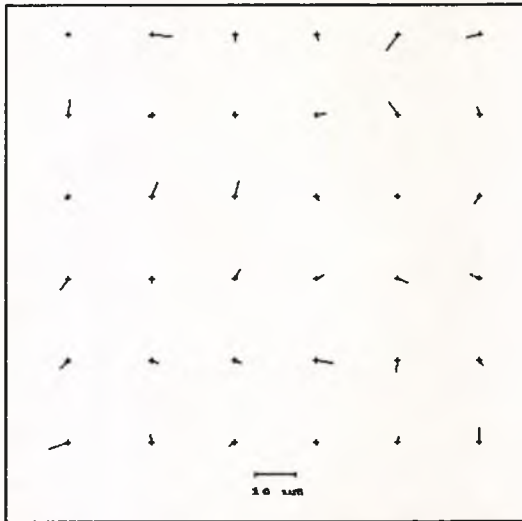
TCP 120, Roll 7, Frame B2, No.4.



A selection of in-plane deformation plots from Experiment 4.

Addition of inorganic hardener to the fixing bath.

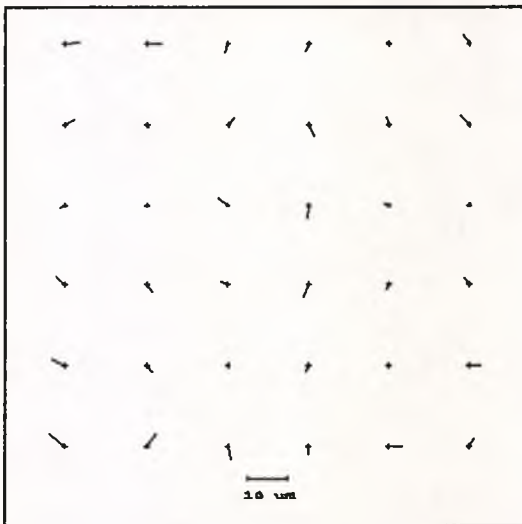
FP4 220, Roll 8, Frame G1, No.1.



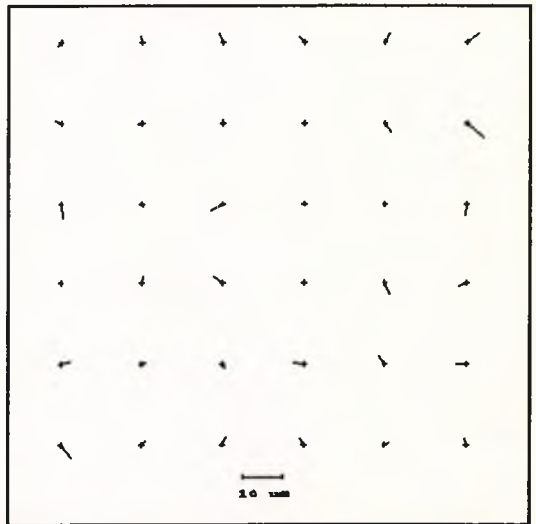
FP4 220, Roll 8, Frame G1, No.4.



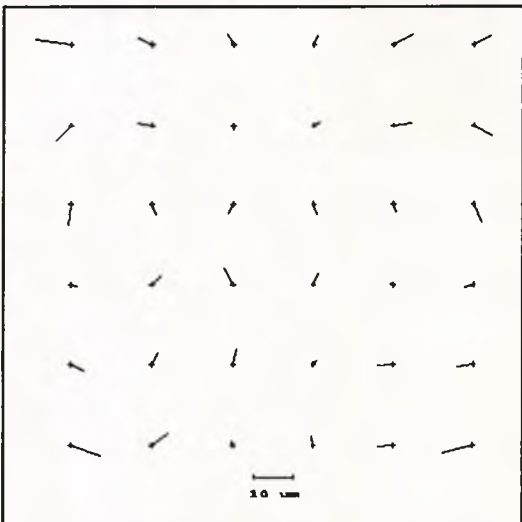
FP4 220, Roll 9, Frame H2, No.4.



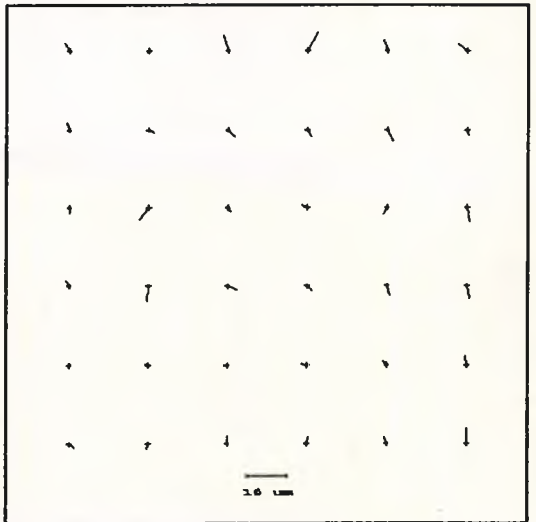
TCP 120, Roll 10, Frame C1, No.5.



TCP 120, Roll 10, Frame C2, No.4.



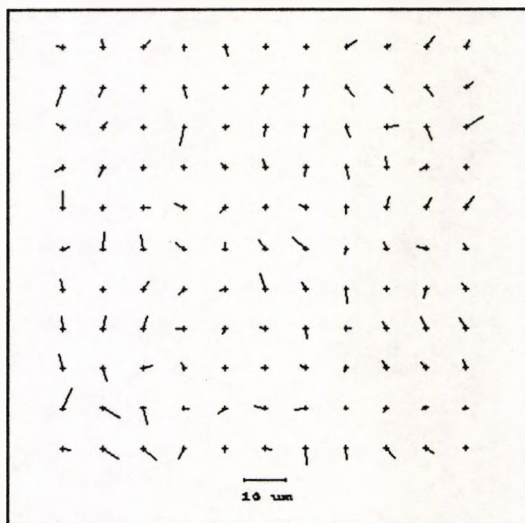
TCP 120, Roll 11, Frame D1, No.6.



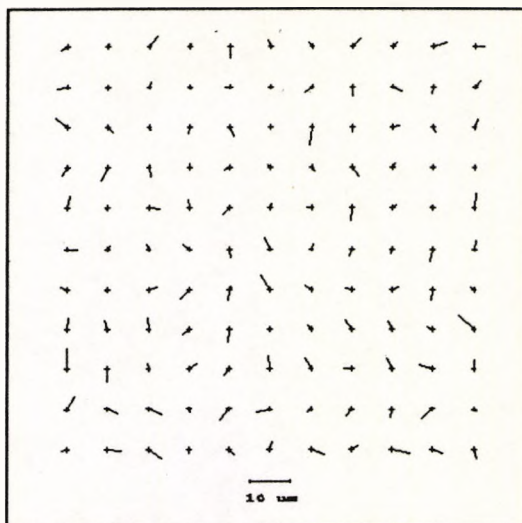
A selection of in-plane deformation plots from Experiment 5.

Addition of inorganic hardener to the fixing bath.

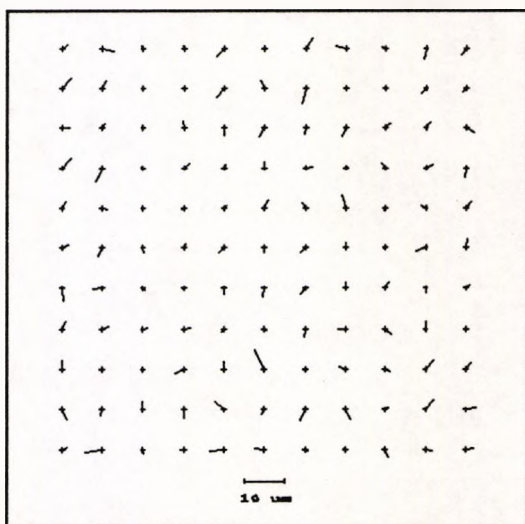
FP4 220, Roll 12, Frame I3, No.3.



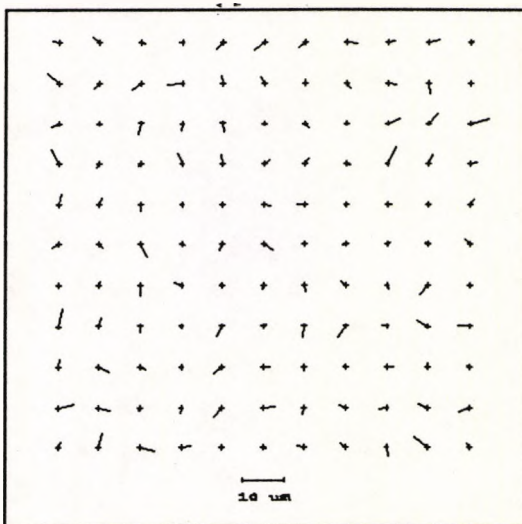
FP4 220, Roll 12, Frame I3, No.4.



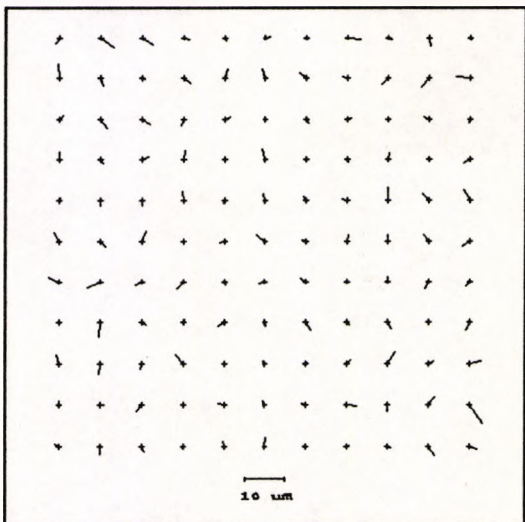
FP4 220, Roll 13, Frame J1, No.2.



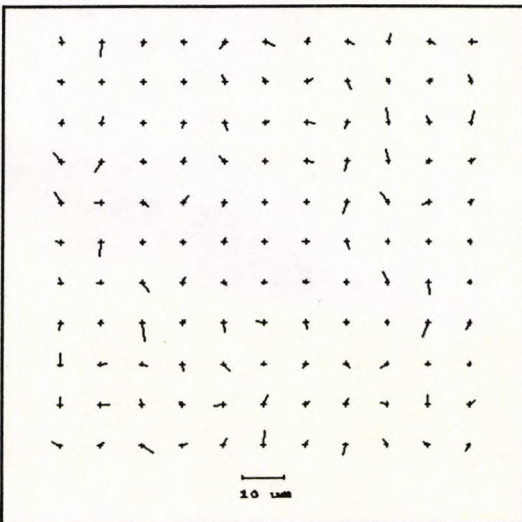
FP4 220, Roll 13, Frame J3, No.4.



PNF 120, Roll 14, Frame B1, No.2.



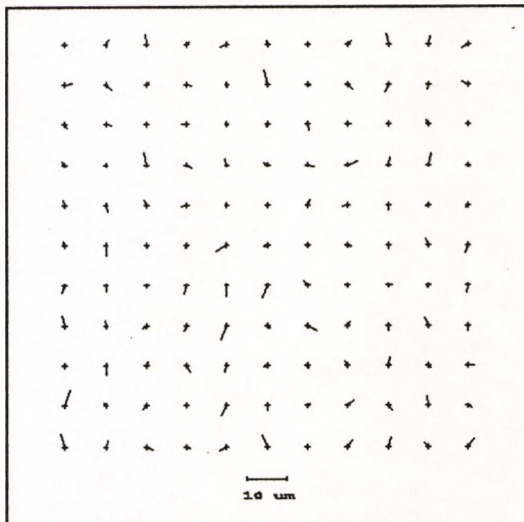
PNF 120, Roll 14, Frame B2, No.2.



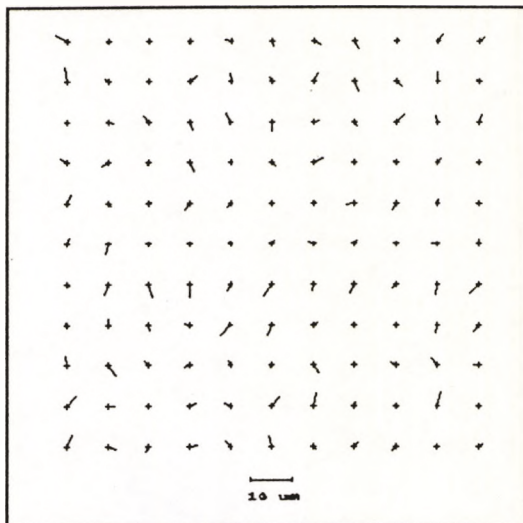
A selection of in-plane deformation plots from Experiment 5, (cont'd)

Addition of inorganic hardener to the fixing bath.

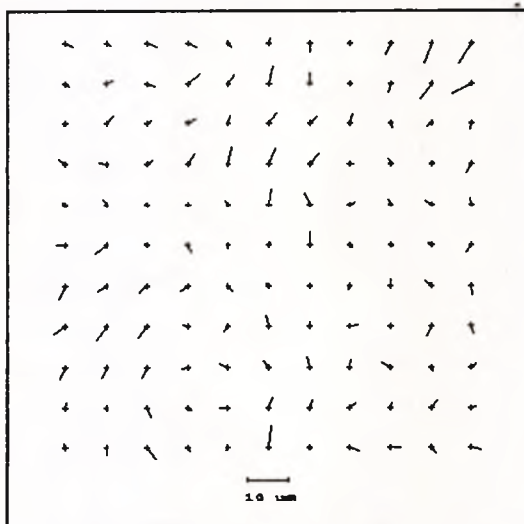
PNF 120, Roll 15, Frame C2, No.2.



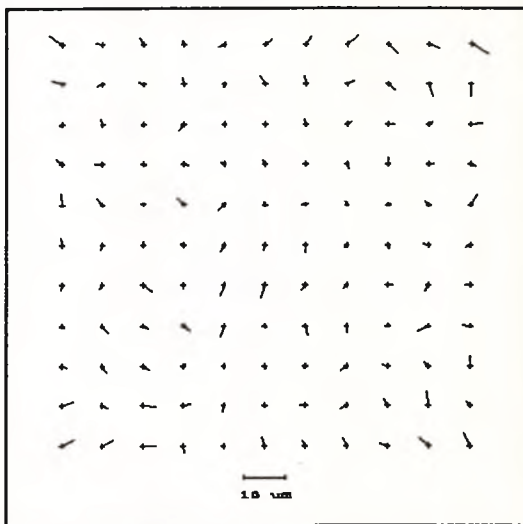
PNF 120, Roll 15, Frame C3, No.3.



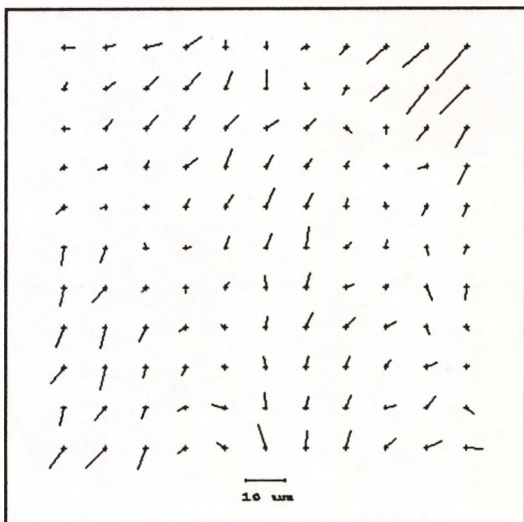
TCP 120, Roll 16, Frame E1, No.2.



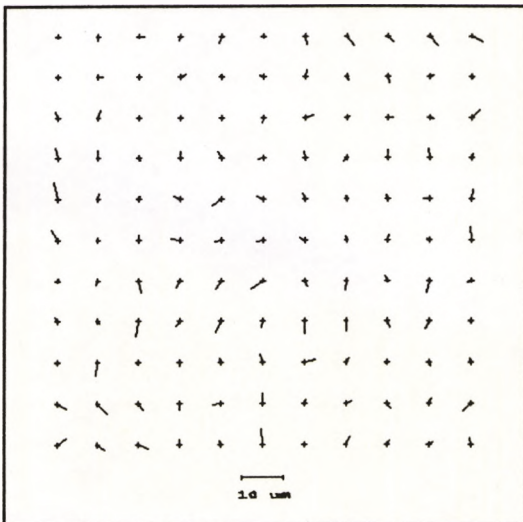
TCP 120, Roll 16, Frame E3, No.2.



TCP 120, Roll 17, Frame F1, No.2.



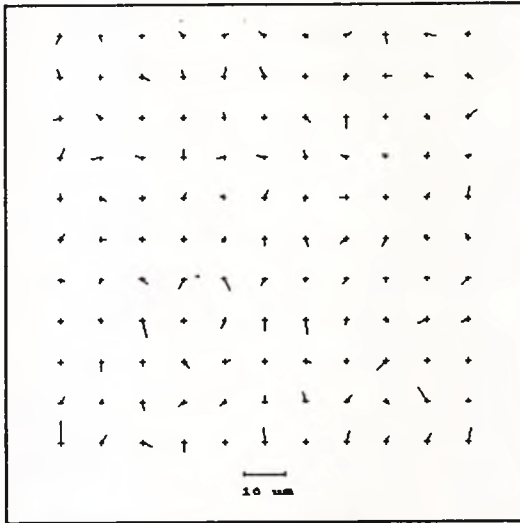
TCP 120, Roll 17, Frame F2, No.4.



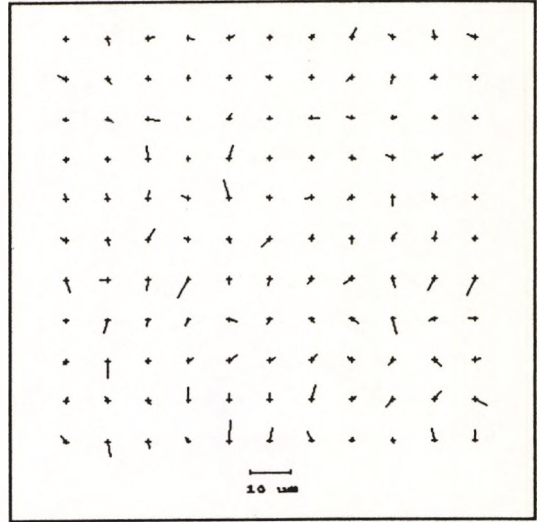
A selection of in-plane deformation plots from Experiment 6.

Variation of developer.

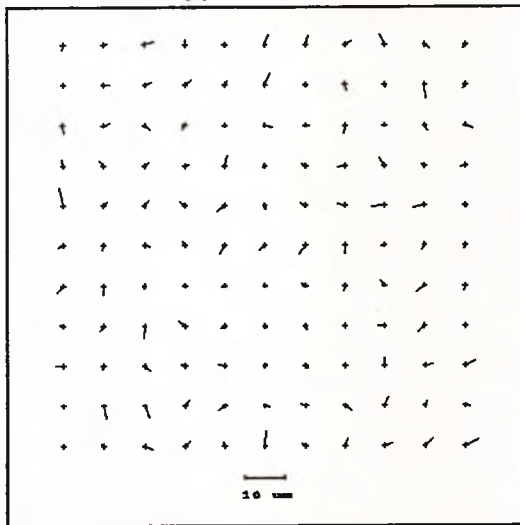
PNF 120, Roll 18, Frame D1, No.1.



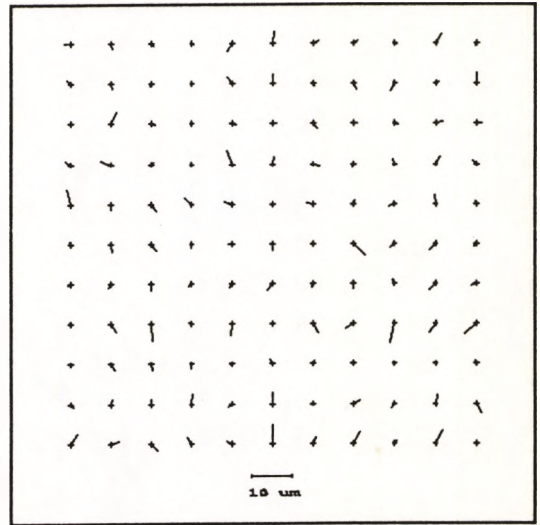
PNF 120, Roll 18, Frame D2, No.1.



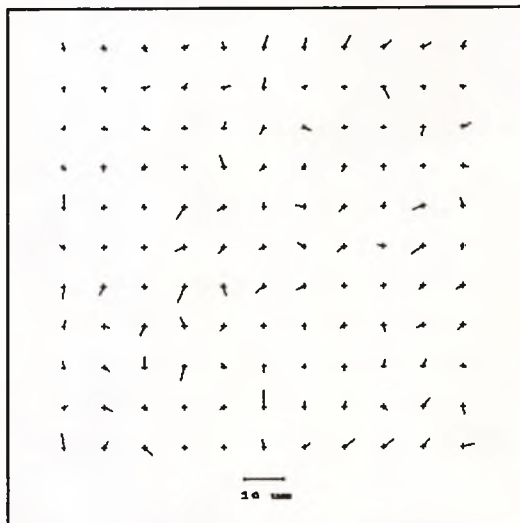
PNF 120, Roll 19, Frame E1, No.2.



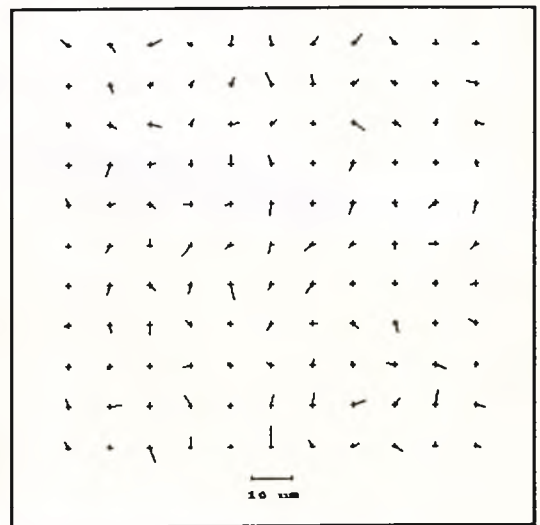
PNF 120, Roll 19, Frame E3, No.3.



PNF 120, Roll 20, Frame F1, No.3.



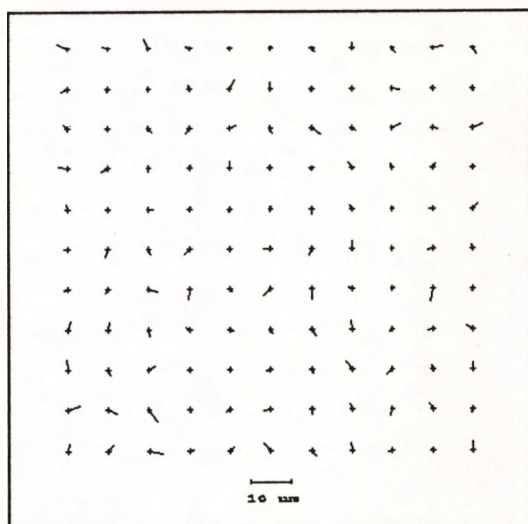
PNF 120, Roll 20, Frame F3, No.1.



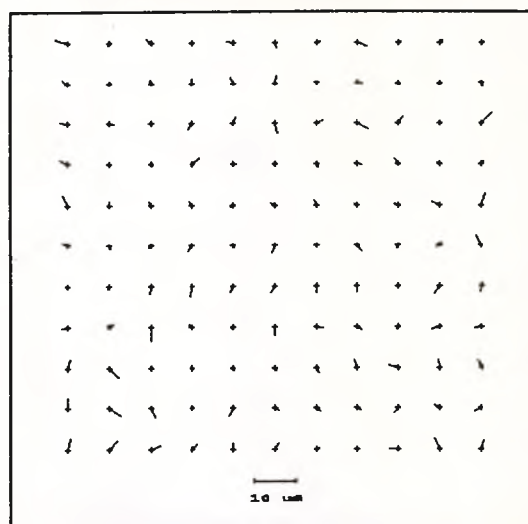
A selection of in-plane deformation plots from Experiment 6, (cont'd).

Variation of developer.

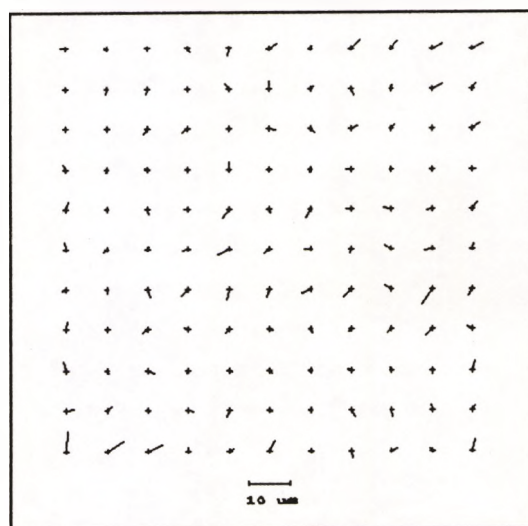
TCP 120, Roll 21, Frame H1, No.1.



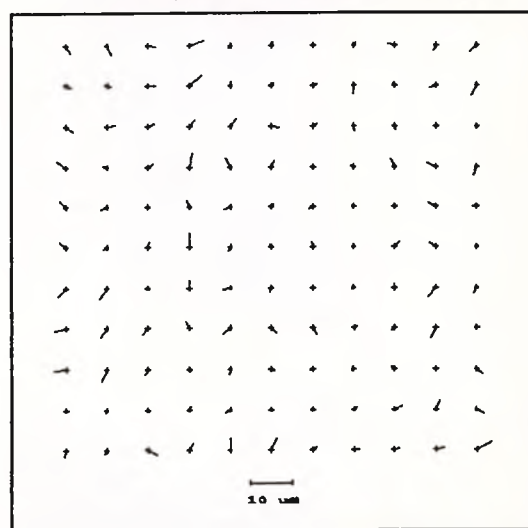
TCP 120, Roll 21, Frame H1, No.3.



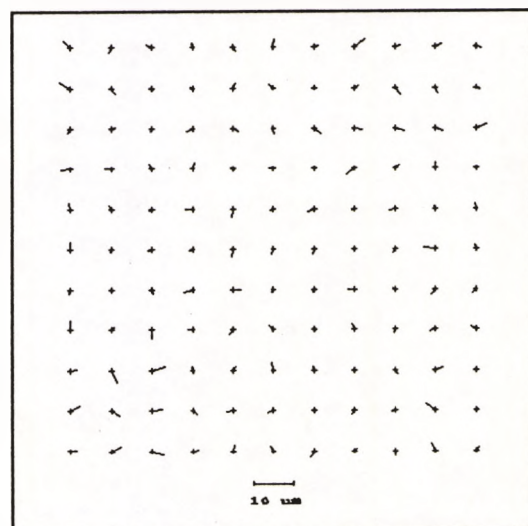
TCP 120, Roll 21, Frame H3, No.2.



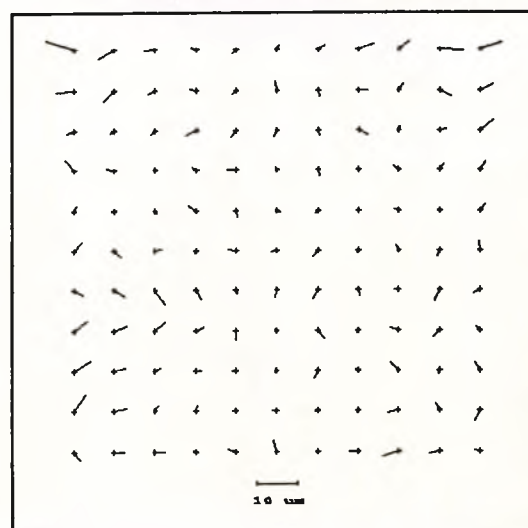
TCP 120, Roll 22, Frame I1, No.2.



TCP 120, Roll 22, Frame I2, No.1.

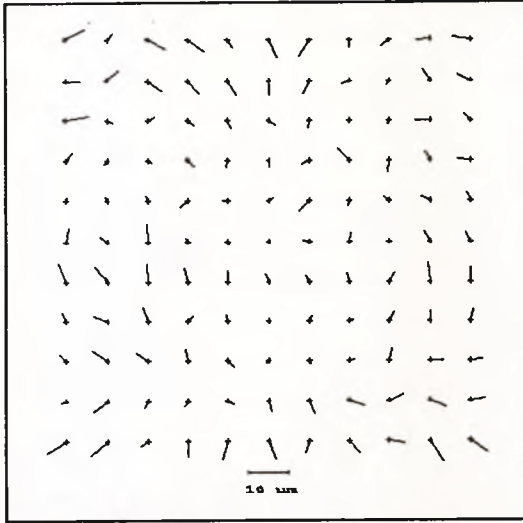


TCP 120, Roll 22, Frame I3, No.2.

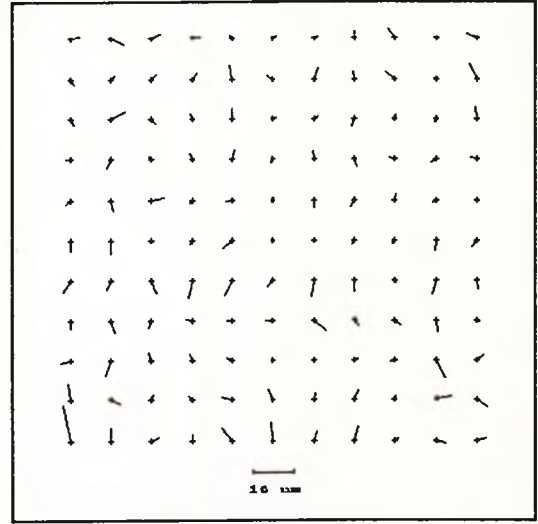


A selection of in-plane deformation plots from Experiment 7.
Variation of exposure over the format area and variation of film type.

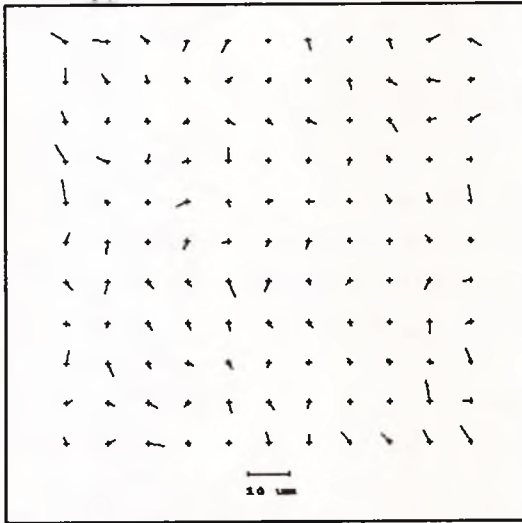
PNF 120, Roll 23, Frame G1, No.4.



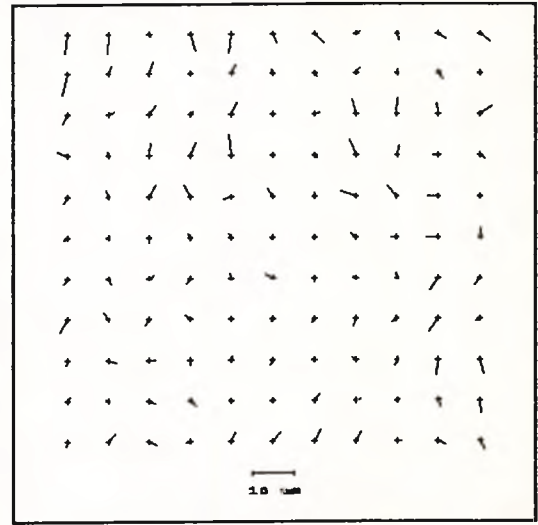
PNF 120, Roll 24, Frame H2, No.3.



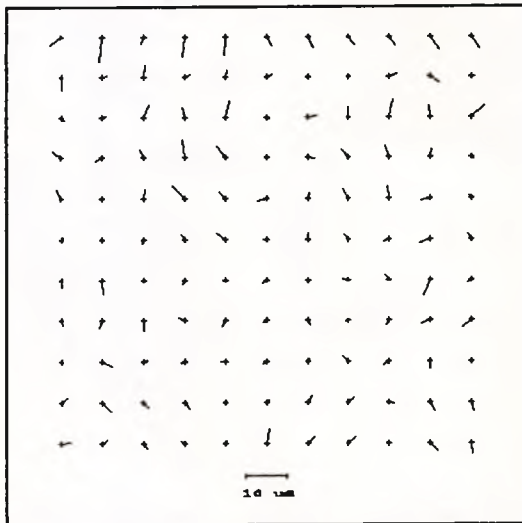
TMX 120, Roll 25, Frame A1, No.1.



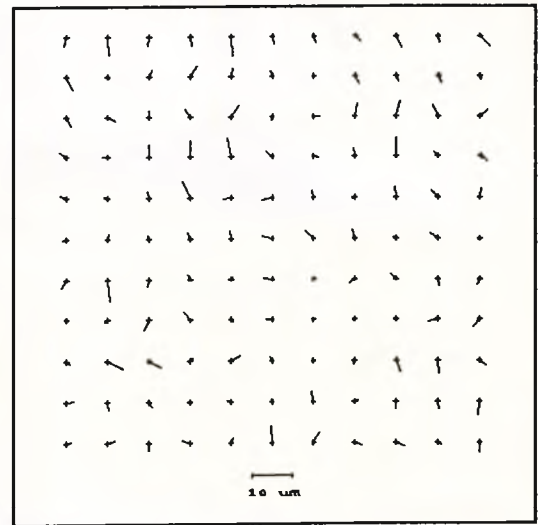
TMX 120, Roll 25, Frame A3, No.1.



TMX 120, Roll 25, Frame A3, No.2.



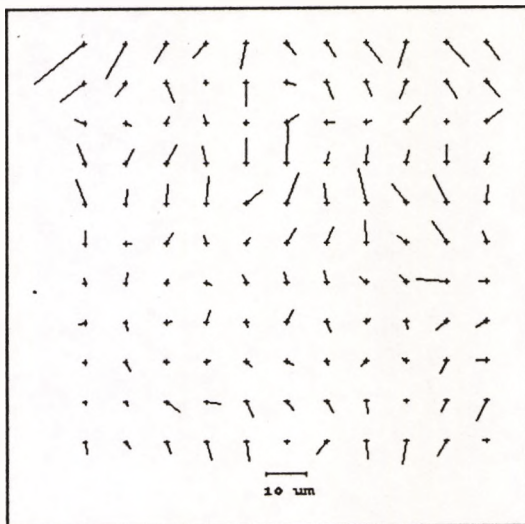
TMX 120, Roll 25, Frame A3, No.3.



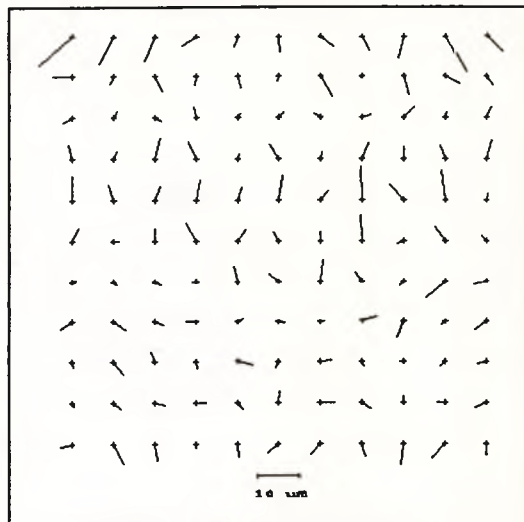
A selection of in-plane deformation plots from Experiment 7, (cont'd).

Variation of exposure over the format area and variation of film type.

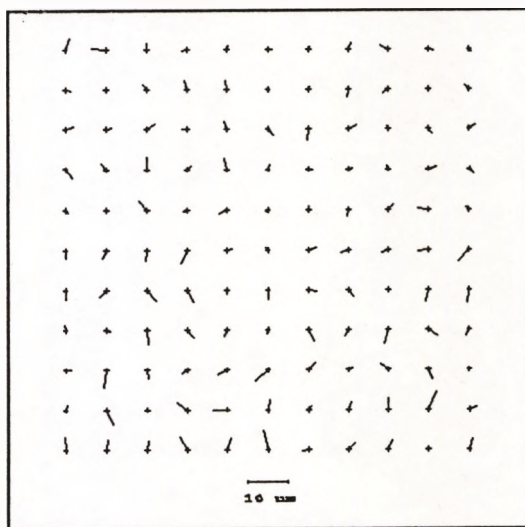
TMY 120, Roll 26, Frame E1, No.1.



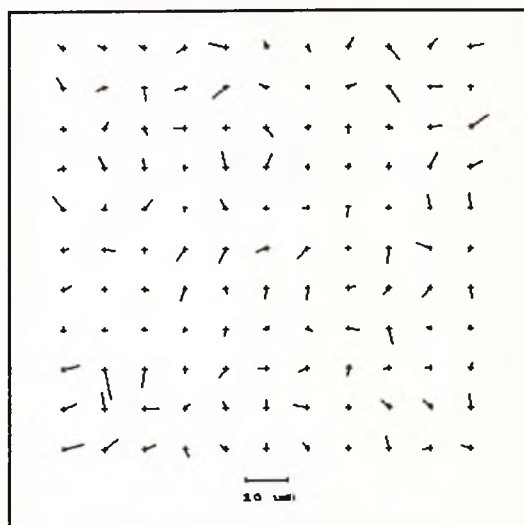
TMY 120, Roll 26, Frame E1, No.3.



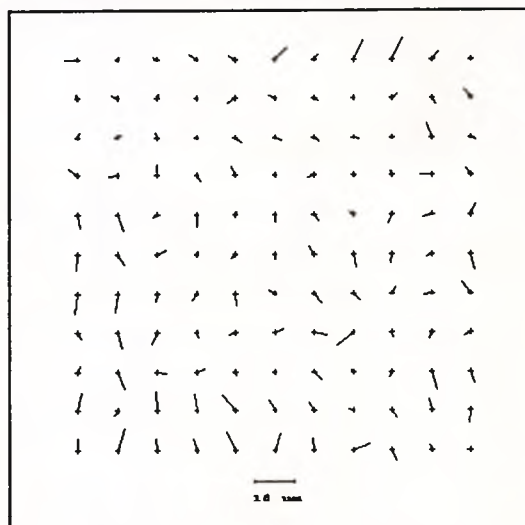
TMY 120, Roll 26, Frame E2, No.2.



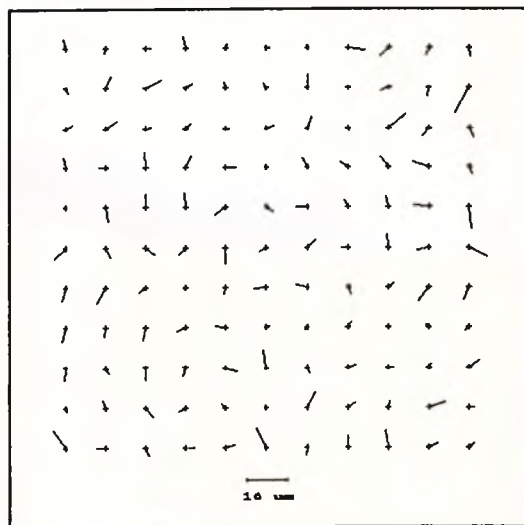
TMY 120, Roll 26, Frame E3, No.1.



TRX 120, Roll 27, Frame A1, No.3.



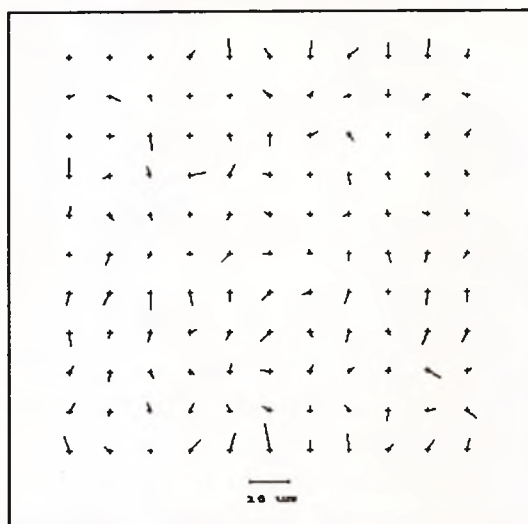
TRX 120, Roll 27, Frame A2, No.3.



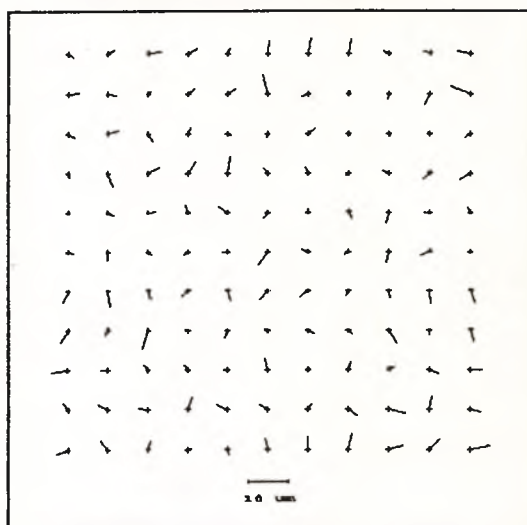
A selection of in-plane deformation plots from Experiment 8.

Variation of exposure level over the format area.

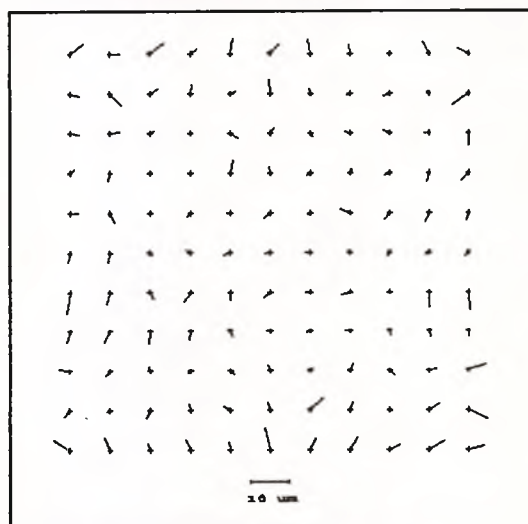
PNF 120, Roll 28, Frame I1, No.2.



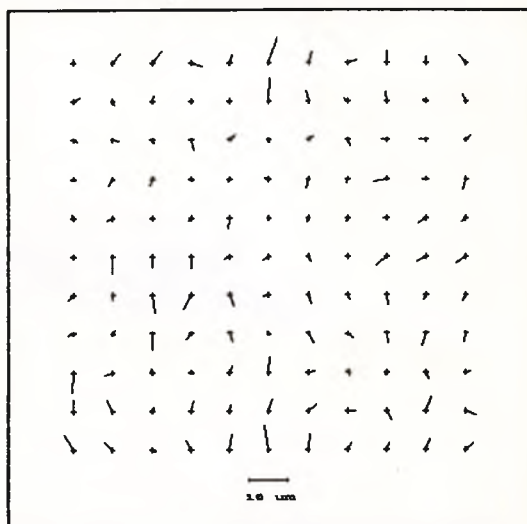
PNF 120, Roll 28, Frame I2, No.1.



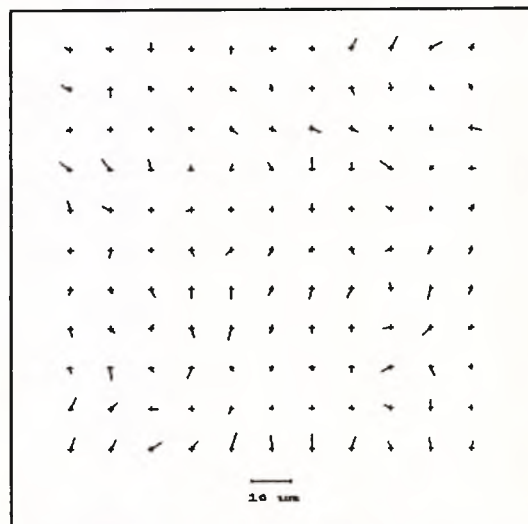
PNF 120, Roll 29, Frame J1, No.1.



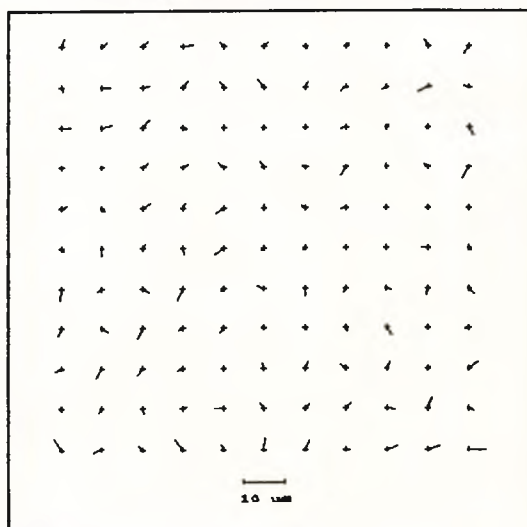
PNF 120, Roll 29, Frame J3, No.1.



TCP 120, Roll 30, Frame J1, No.1.



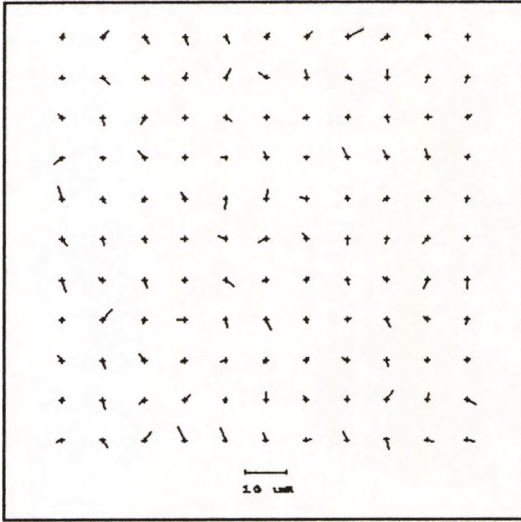
TCP 120, Roll 30, Frame J3, No.2.



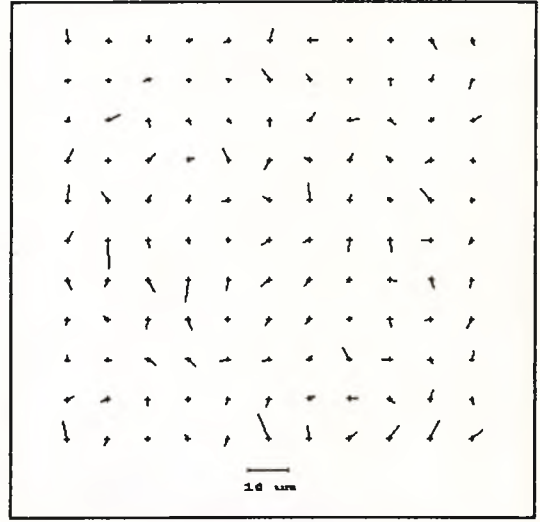
A selection of in-plane deformation plots from Experiment 9.

Variation of film type.

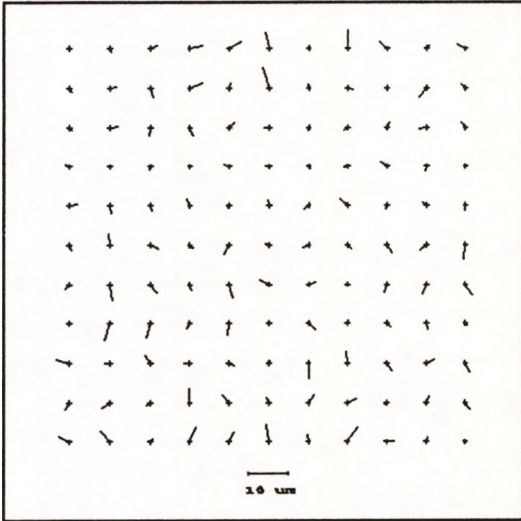
FP4 120, Roll 31, Frame F1, No.1.



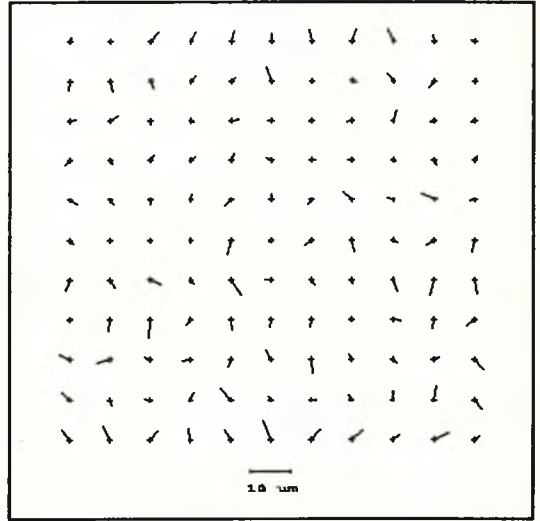
FP4 120, Roll 31, Frame F2, No.2.



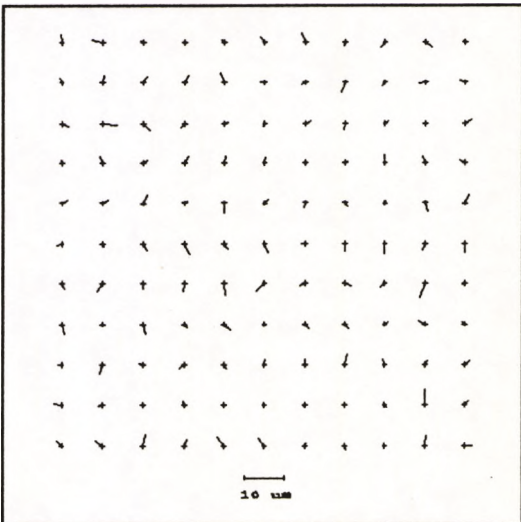
FP4 120, Roll 31, Frame F3, No.1.



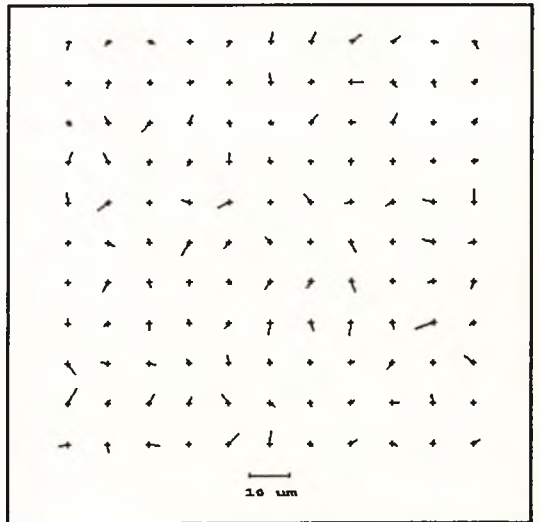
FP4 120, Roll 31, Frame F3, No.2.



TMX 120, Roll 32, Frame B1, No.1.



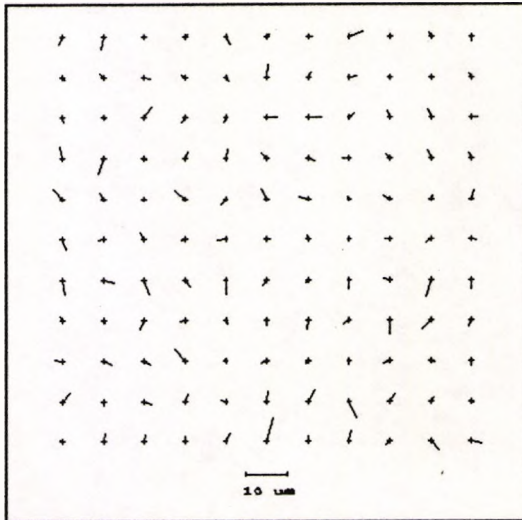
TMX 120, Roll 32, Frame B2, No.2.



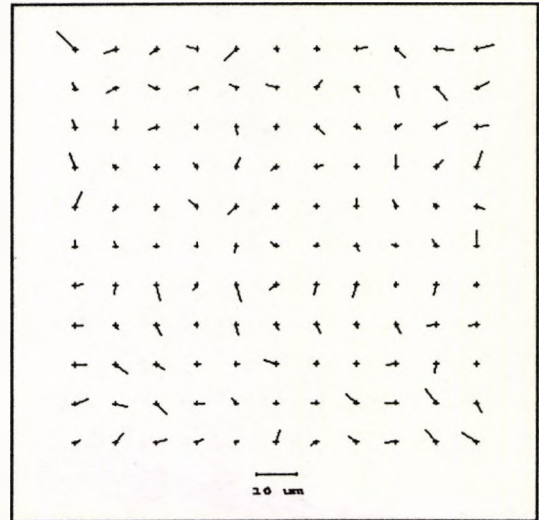
A selection of in-plane deformation plots from Experiment 9.

Variation of film type.

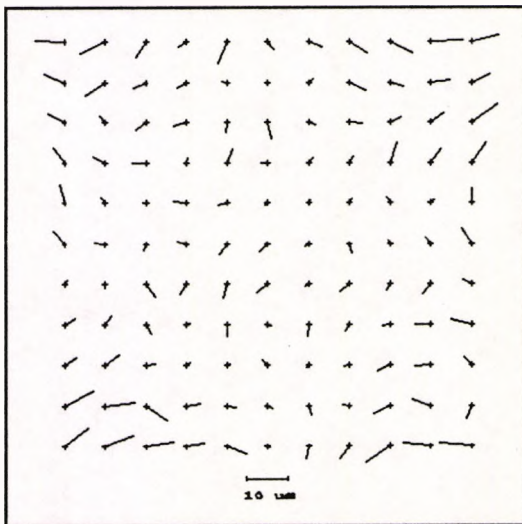
TMY 120, Roll 33, Frame F1, No.1.



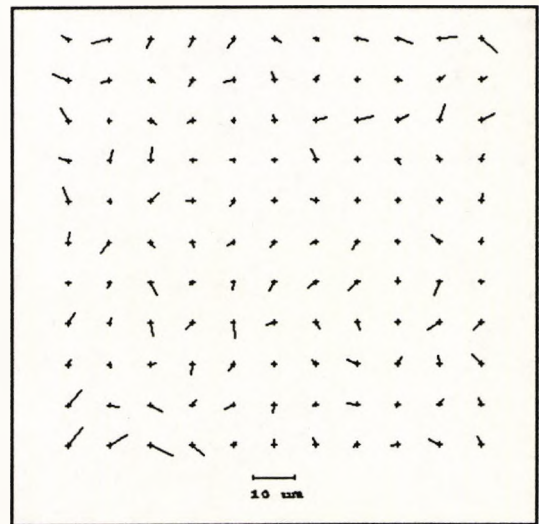
TMY 120, Roll 33, Frame F2, No.1.



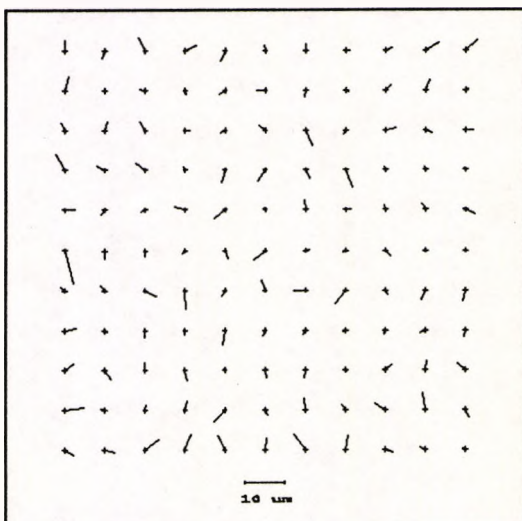
TMY 120, Roll 33, Frame F2, No.2.



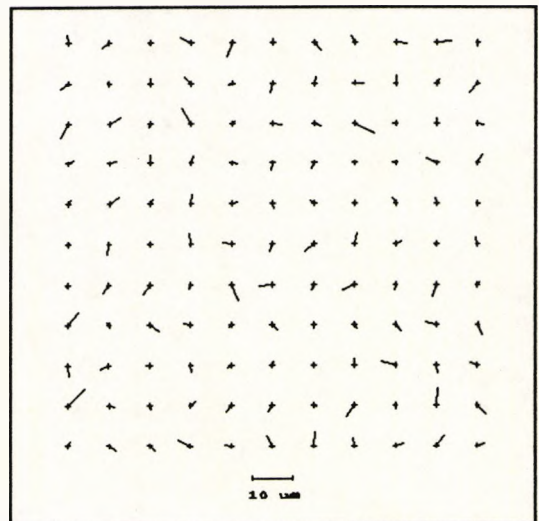
TMY 120, Roll 33, Frame F3, No.2.



TRX 120, Roll 34, Frame B1, No.1.



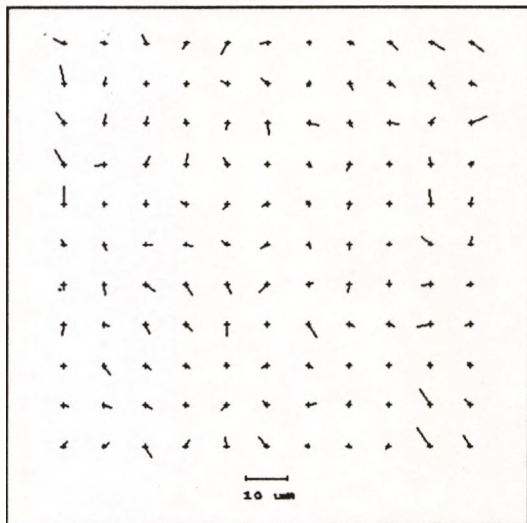
TRX 120, Roll 34, Frame B3, No.2.



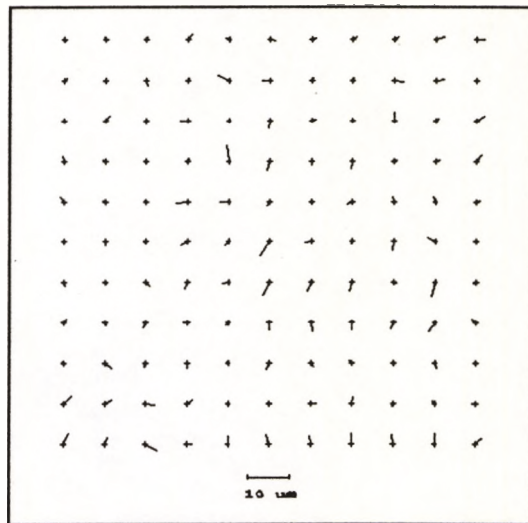
A selection of in-plane deformation plots from Experiment 10.

Variation of pre-exposure conditioning.

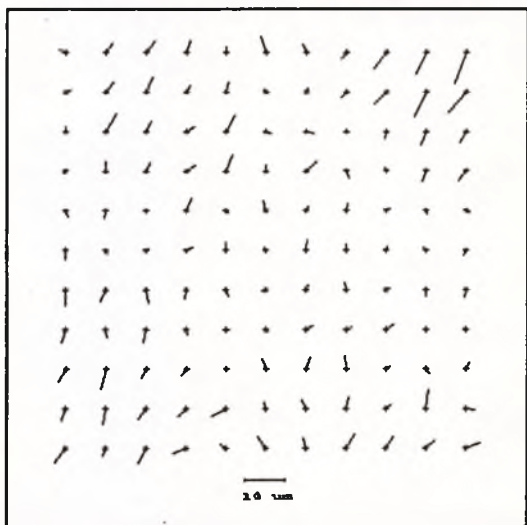
TCP 120, Roll 35, Frame K1, No.2.



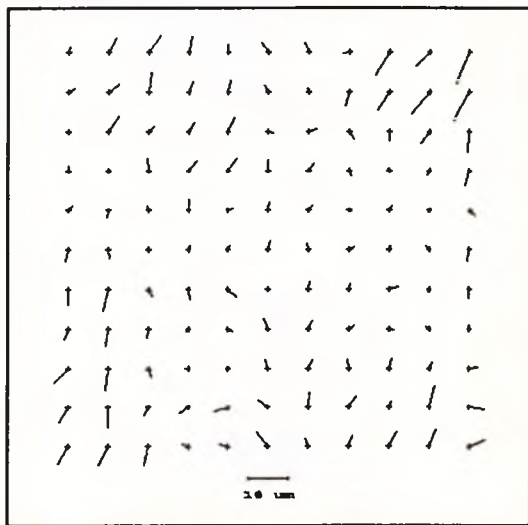
TCP 120, Roll 35, Frame K2, No.2.



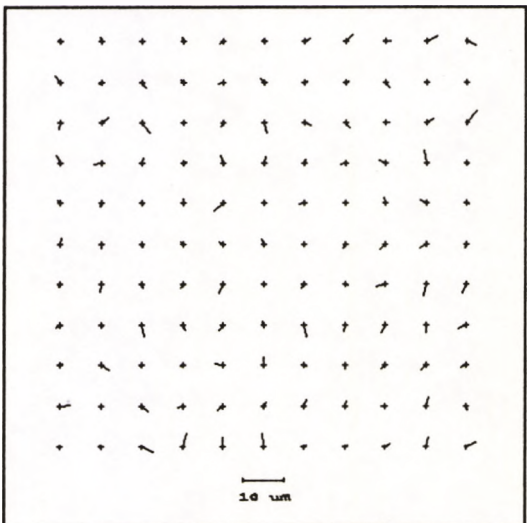
TCP 120, Roll 35, Frame K3, No.1.



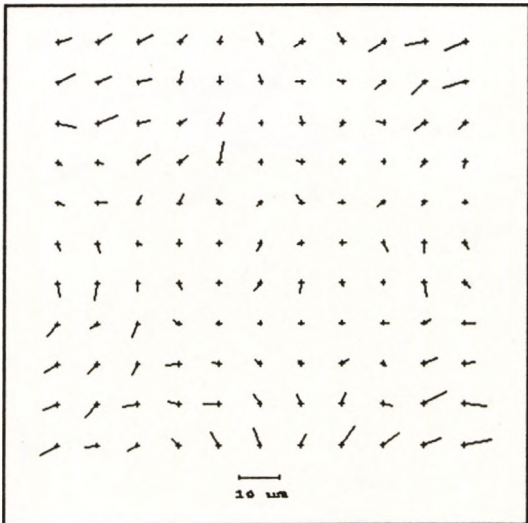
TCP 120, Roll 35, Frame K3, No.2.



TCP 120, Roll 36, Frame L2, No.1.



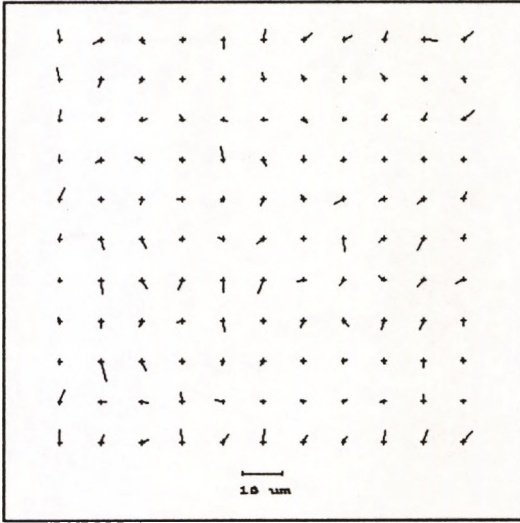
TCP 120, Roll 36, Frame L3, No.1.



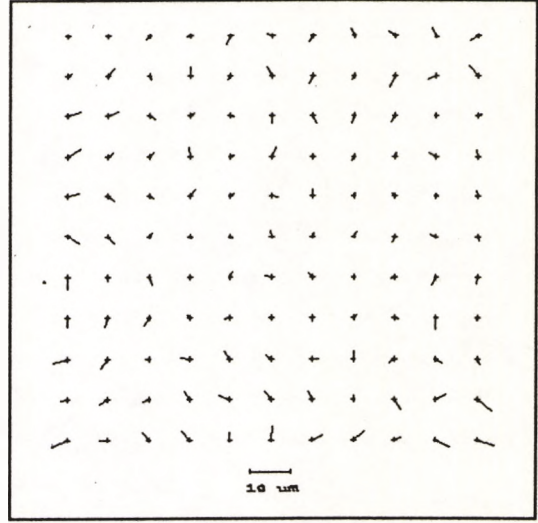
A selection of in-plane deformation plots from Experiment 10, (cont'd).

Variation of pre-exposure conditioning.

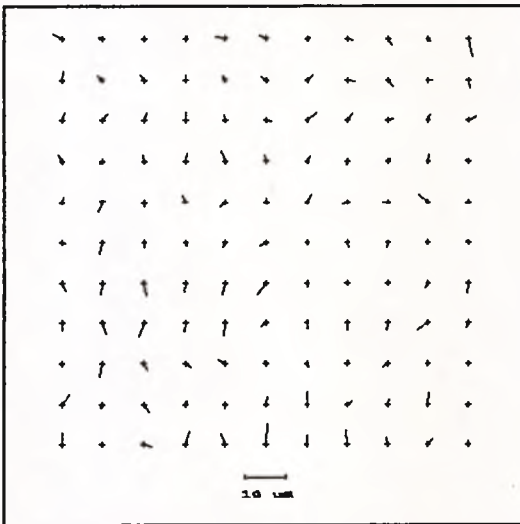
TCP 120, Roll 37, Frame M2, No.1.



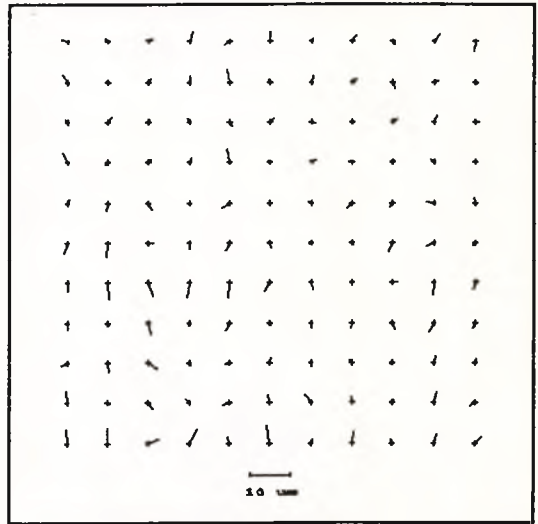
TCP 120, Roll 37, Frame M3, No.1.



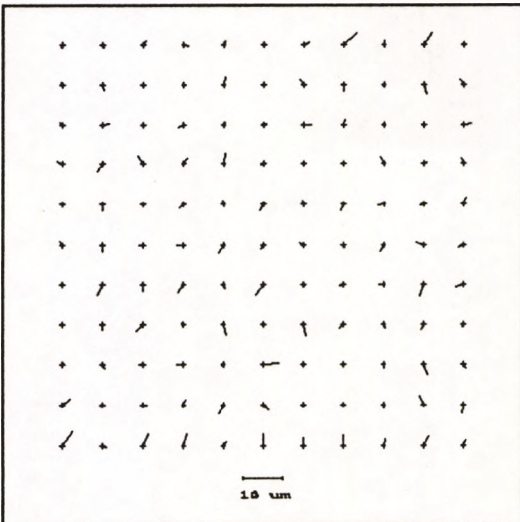
TCP 120, Roll 38, Frame N1, No.1.



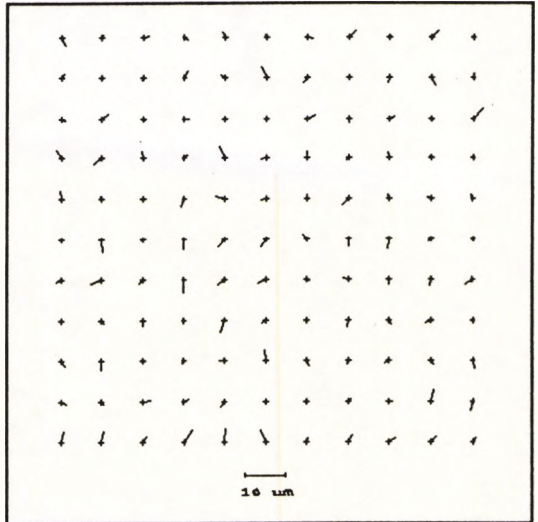
TCP 120, Roll 38, Frame N1, No.2.



TCP 120, Roll 38, Frame N2, No.1.



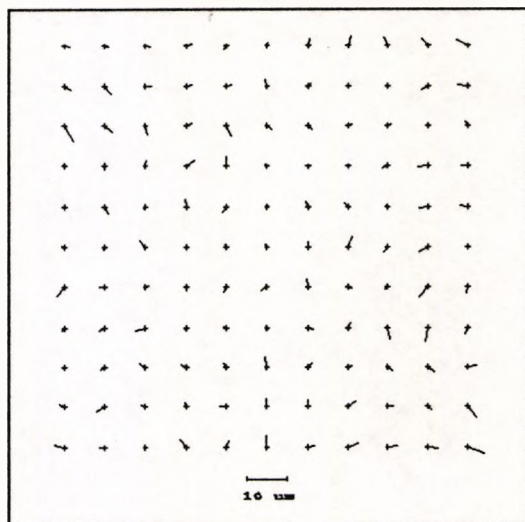
TCP 120, Roll 38, Frame N2, No.2.



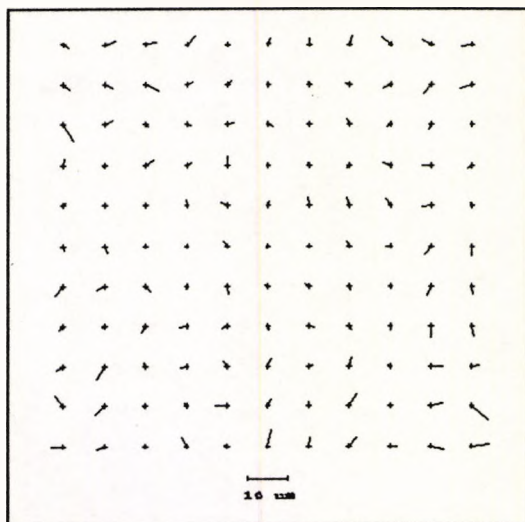
A selection of in-plane deformation plots from Experiment 11.

Repeat of pre-exposure conditioning variation.

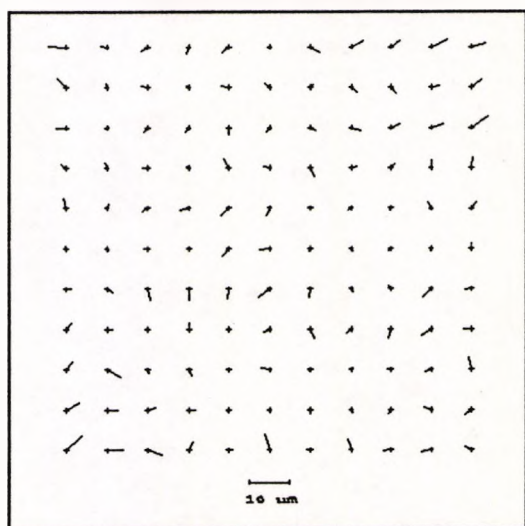
TCP 120, Roll 39, Frame O2, No.1.



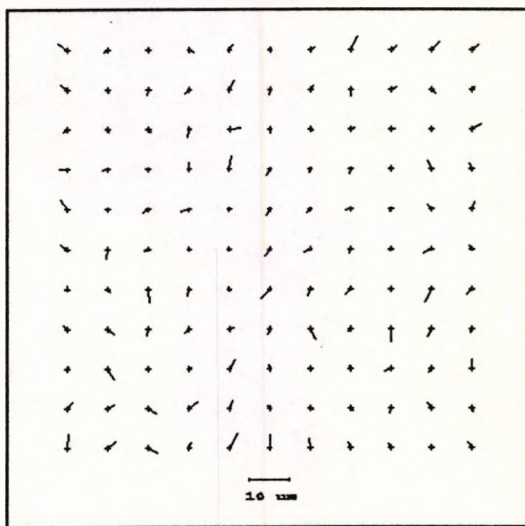
TCP 120, Roll 39, Frame O2, No.2.



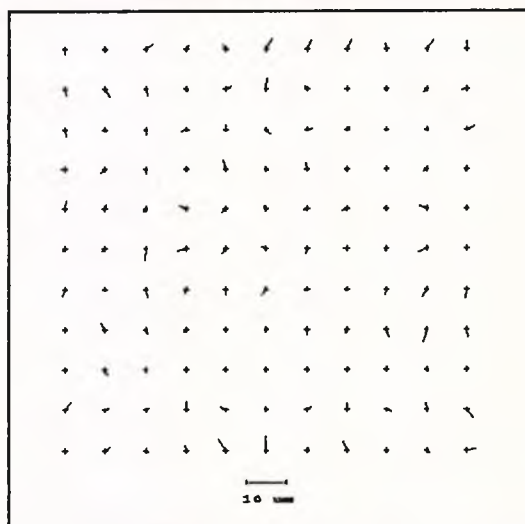
TCP 120, Roll 40, Frame P1, No.1.



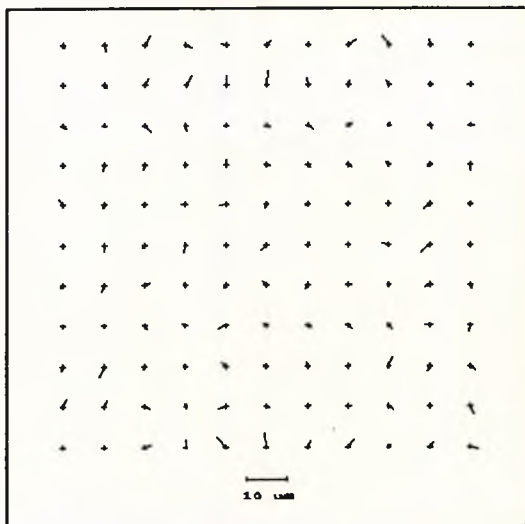
TCP 120, Roll 40, Frame P1, No.2.



TCP 120, Roll 40, Frame P3, No.1.



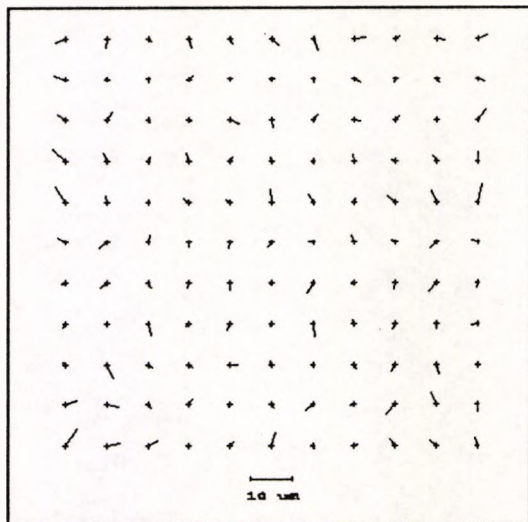
TCP 120, Roll 40, Frame P3, No.2.



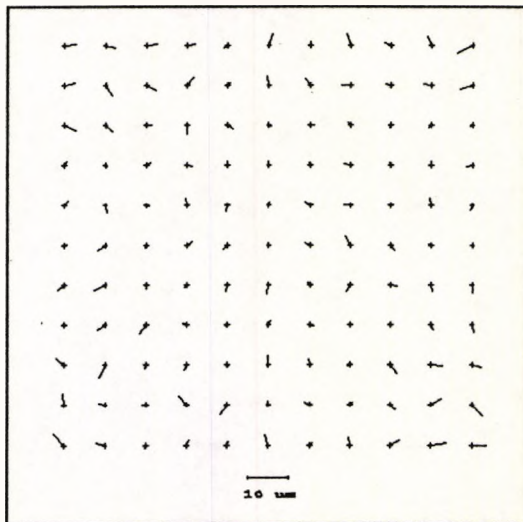
A selection of in-plane deformation plots from Experiment 11, (cont'd).

Repeat of pre-exposure conditioning variation.

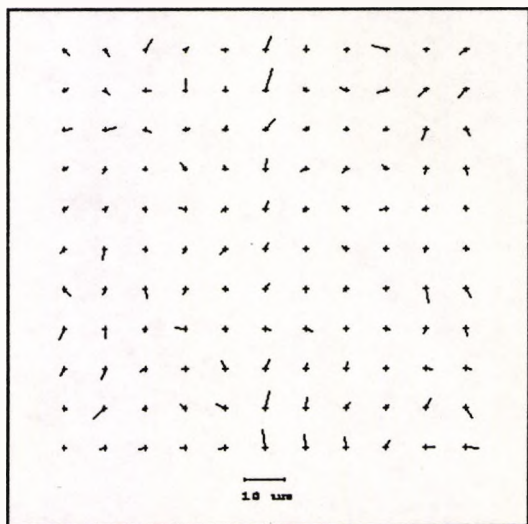
TCP 120, Roll 41, Frame Q1, No.1.



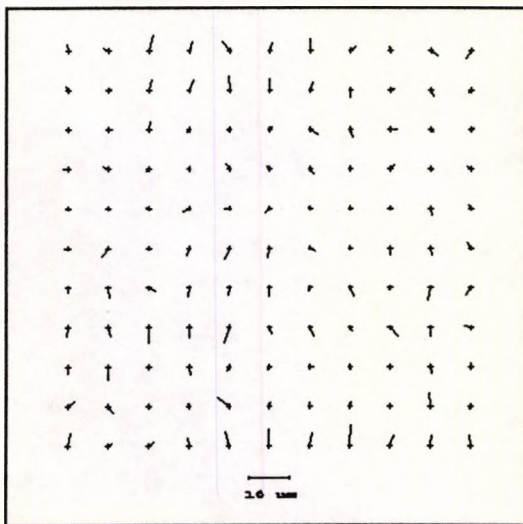
TCP 120, Roll 41, Frame Q2, No.1.



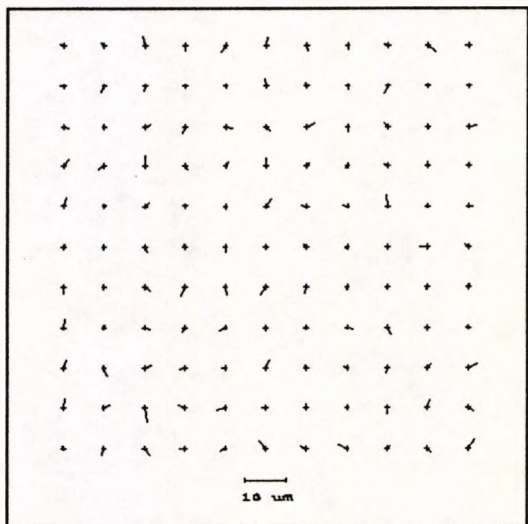
TCP 120, Roll 41, Frame Q3, No.1.



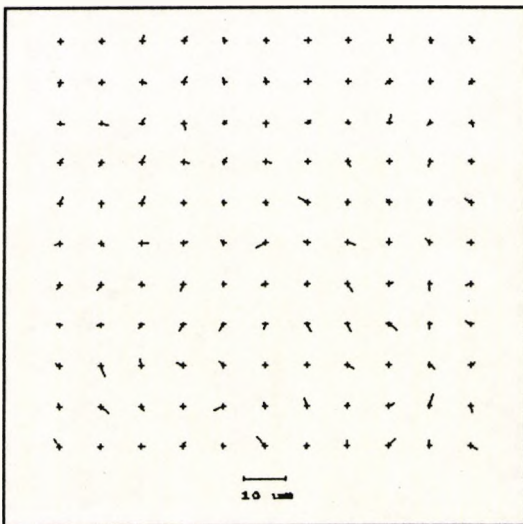
TCP 120, Roll 42, Frame R1, No.1.



TCP 120, Roll 42, Frame R3, No.1.



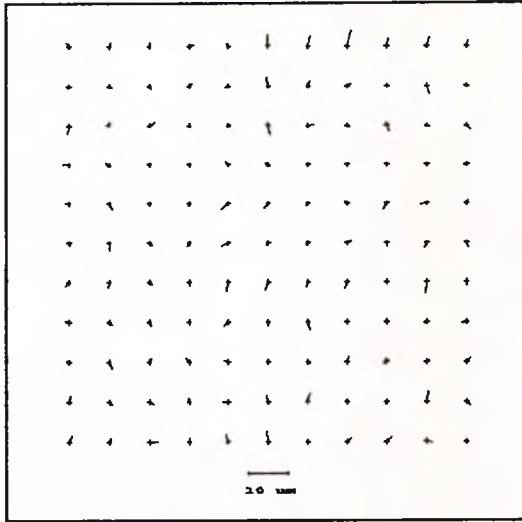
TCP 120, Roll 42, Frame R3, No.2.



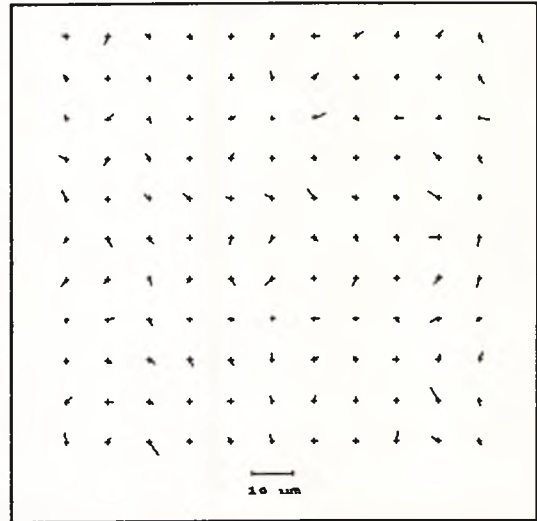
A selection of in-plane deformation plots from Experiment 12.

Exposures made onto Agfa 10E75 Holotest film.

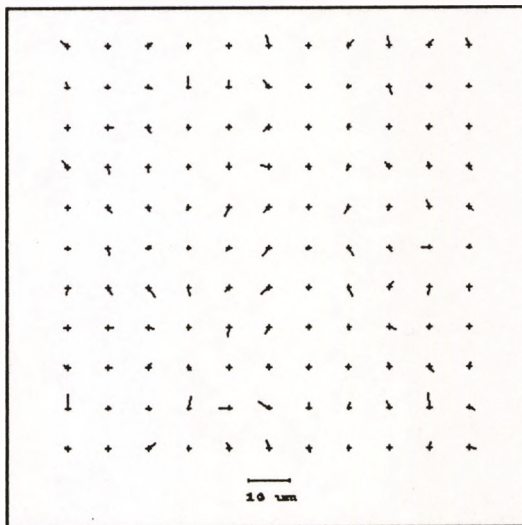
H75 70mm, Roll 44, Frame A2, No.2.



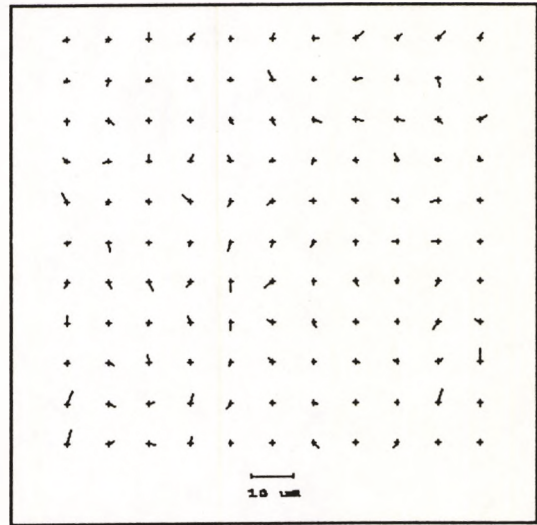
H75 70mm, Roll 44, Frame A3, No.2.



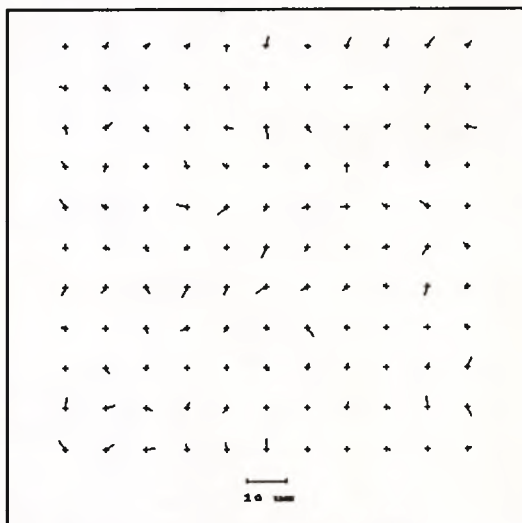
H75 70mm, Roll 44, Frame A4, No.3.



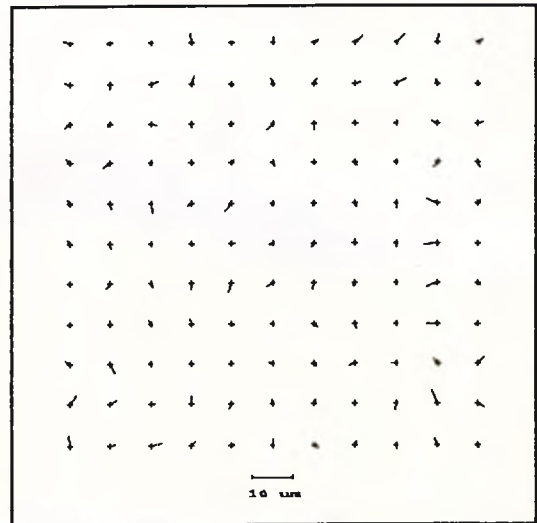
H75 70mm, Roll 44, Frame A6, No.1.



H75 70mm, Roll 45, Frame B1, No.1.



H75 70mm, Roll 45, Frame B4, No.1.

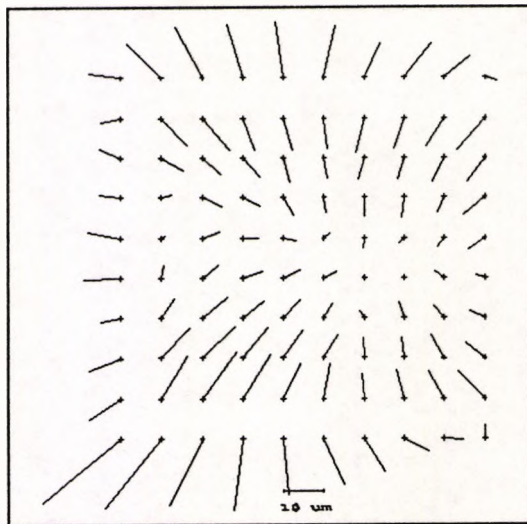


Appendix B

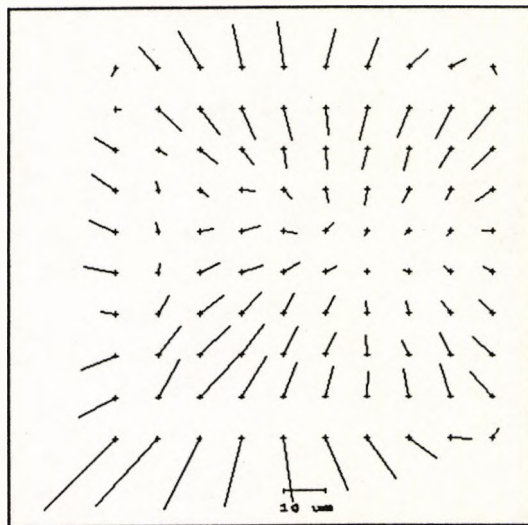
A selection of film deformation vector plots from the in-camera experimentation.

Exposures made using Modified Hasselblad SWC Camera (HS1)
onto Agfa Holotest 10E56 70mm Film.

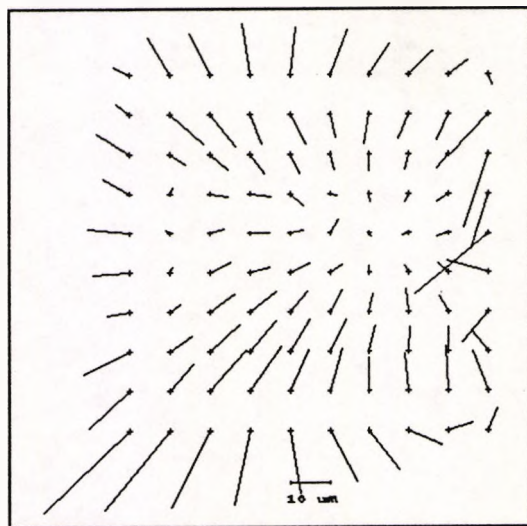
Frame 1



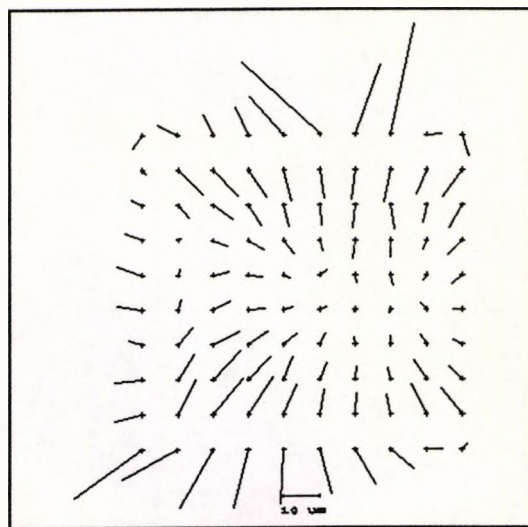
Frame 2



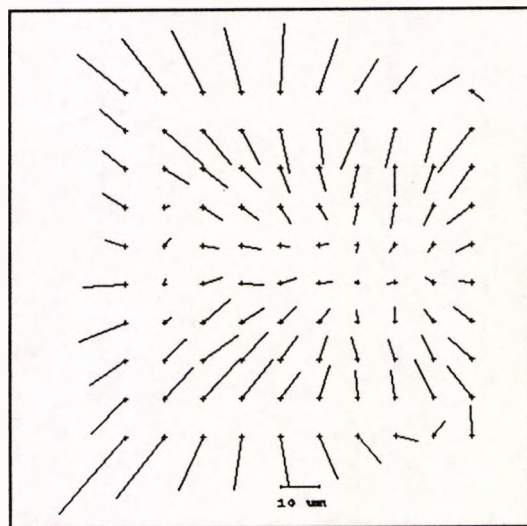
Frame 3



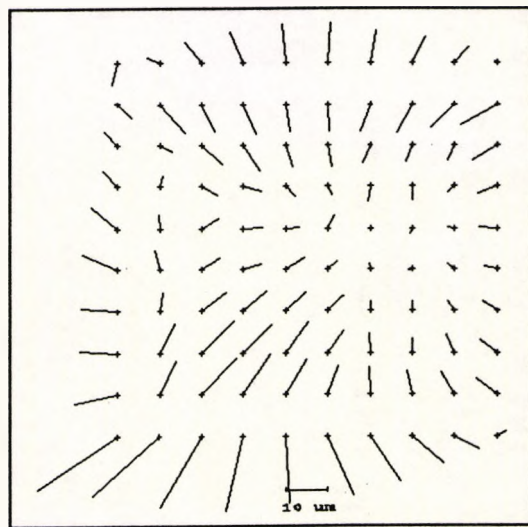
Frame 4



Frame 5

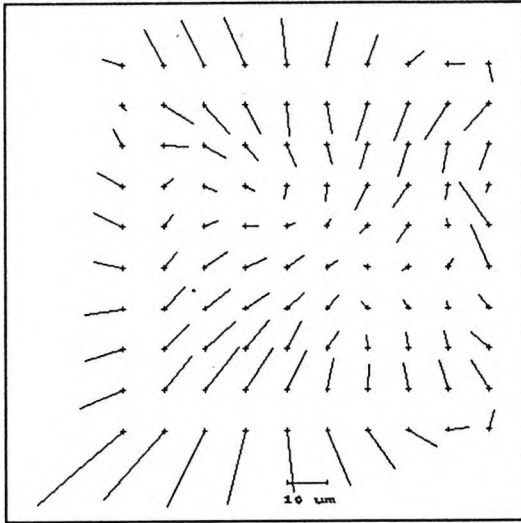


Frame 6

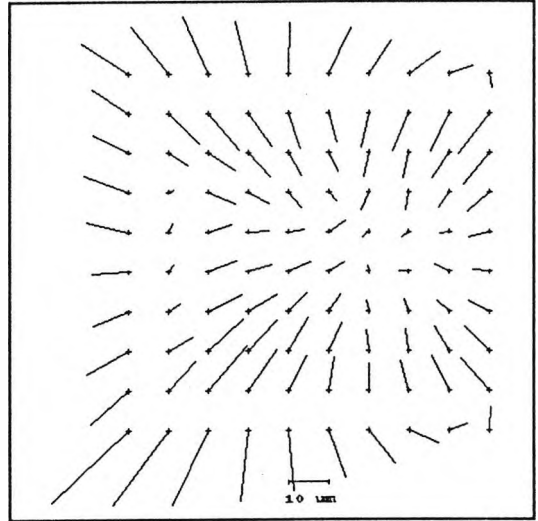


Exposures made using the modified Hasselblad SWC Camera,
onto Agfa Holotest 10E56 70mm film (HS1) and onto Ilford FP4 glass plates (HS2).

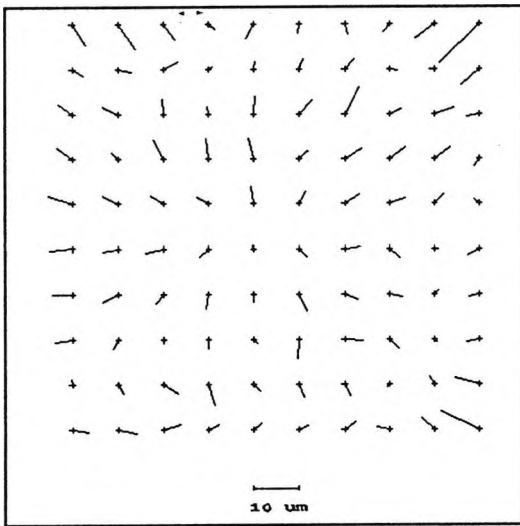
Frame 7



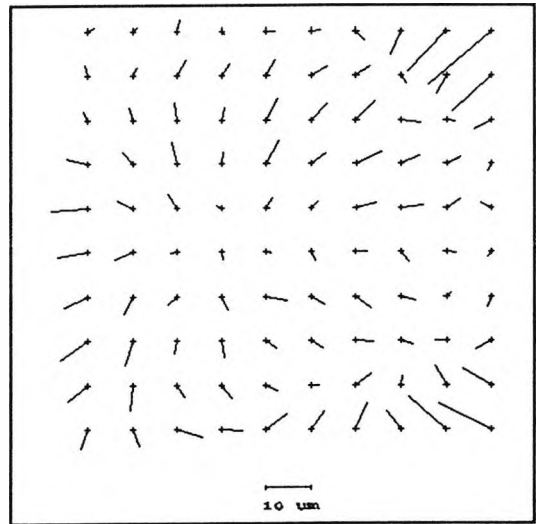
Frame 8



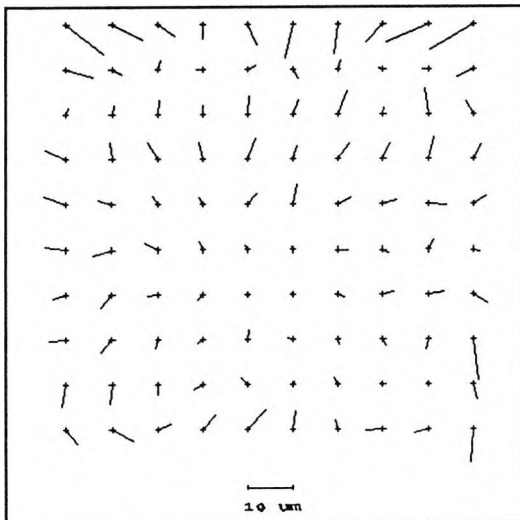
FP4 Plate 1.



FP4 Plate 2.

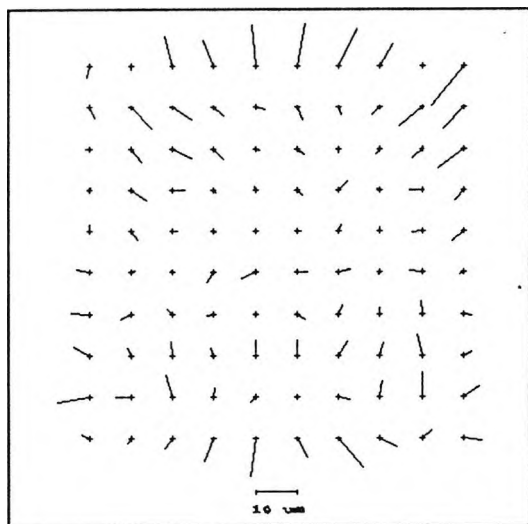


FP4 Plate 3.

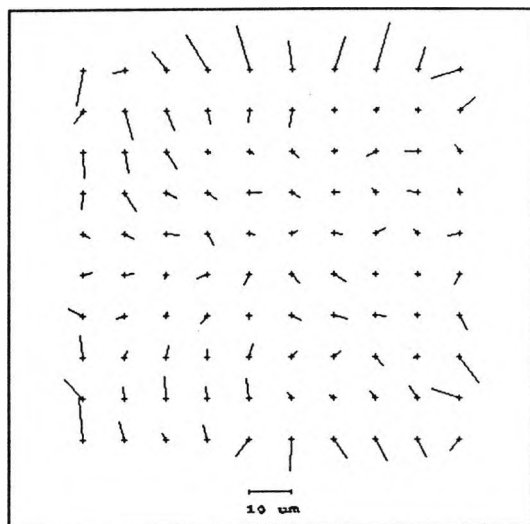


Exposures made using Modified Hasselblad SWC Camera (HS2)
onto Kodak Technical Pan 120 Film (Roll A, Camera Back A).

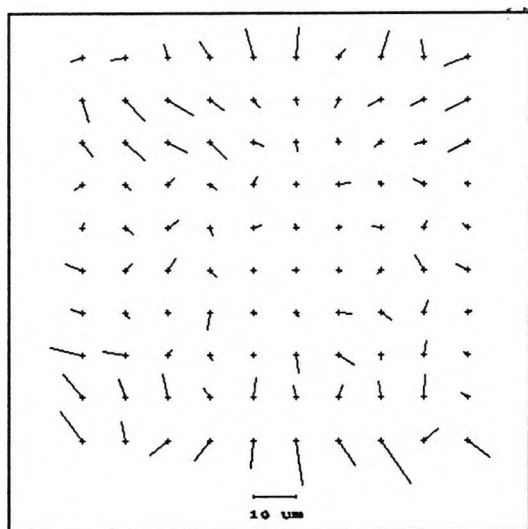
Frame 1



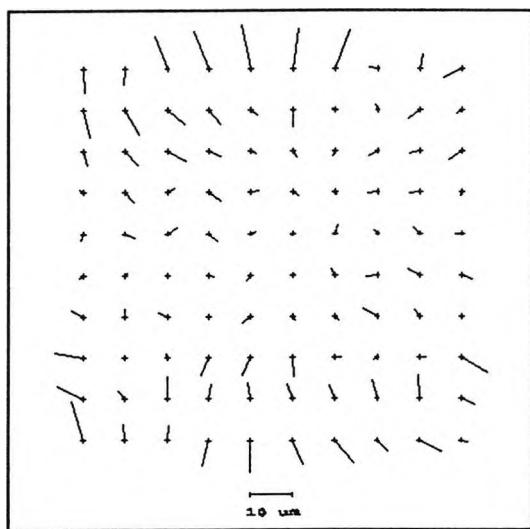
Frame 2



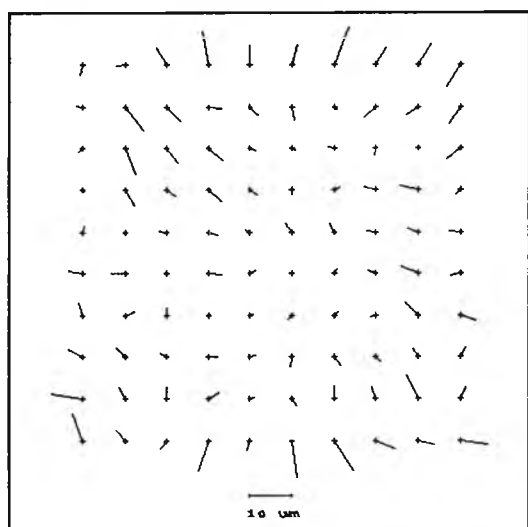
Frame 3



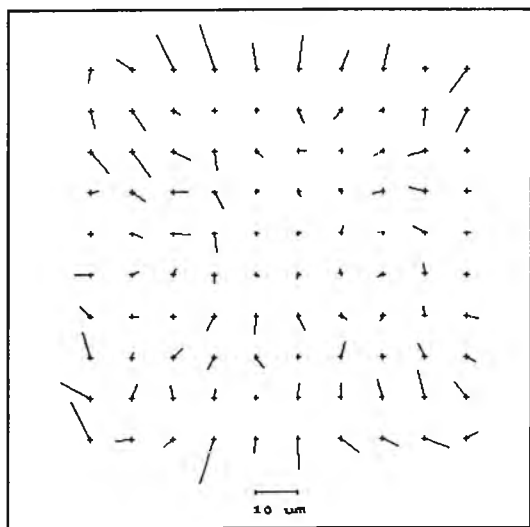
Frame 4



Frame 5

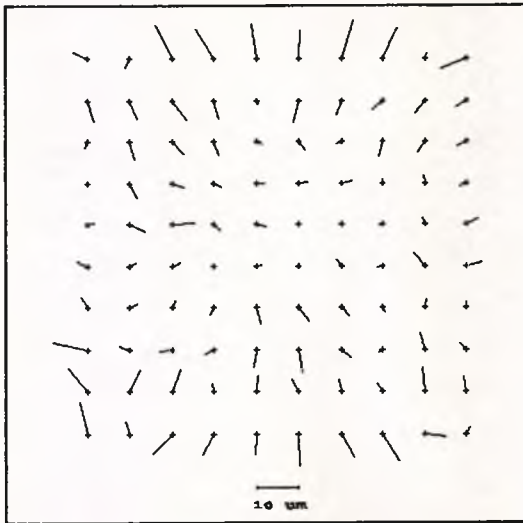


Frame 6

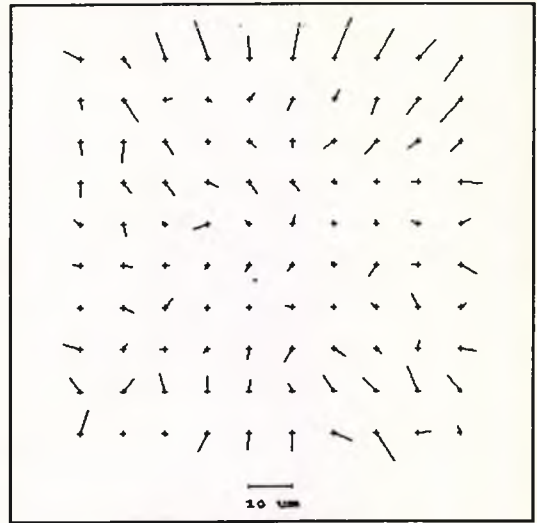


Exposures made using Modified Hasselblad SWC Camera (HS2)
onto Kodak Technical Pan 120 Film (Roll A, Camera Back A).

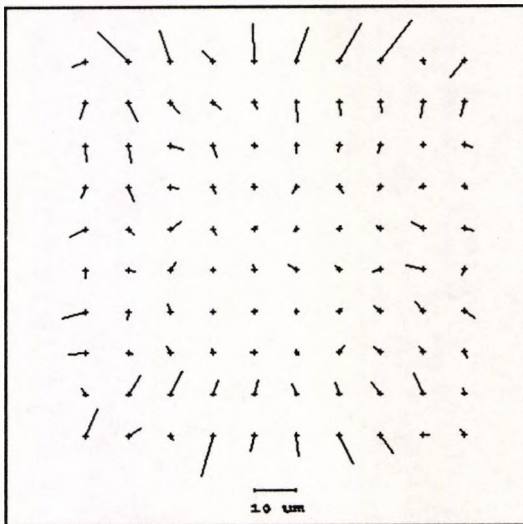
Frame 7



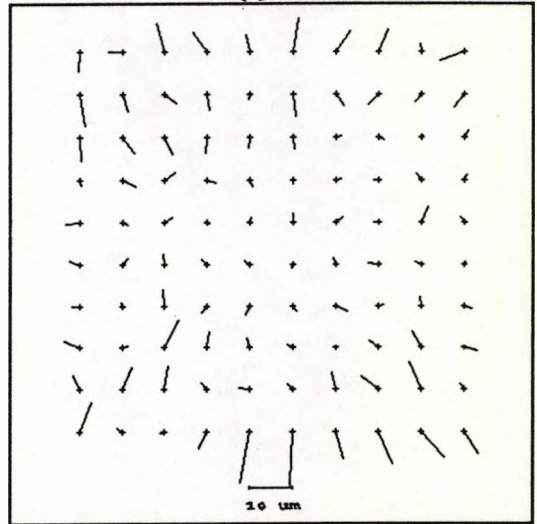
Frame 8



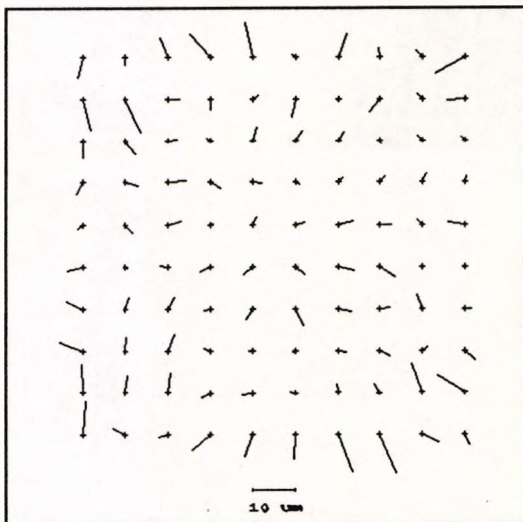
Frame 9



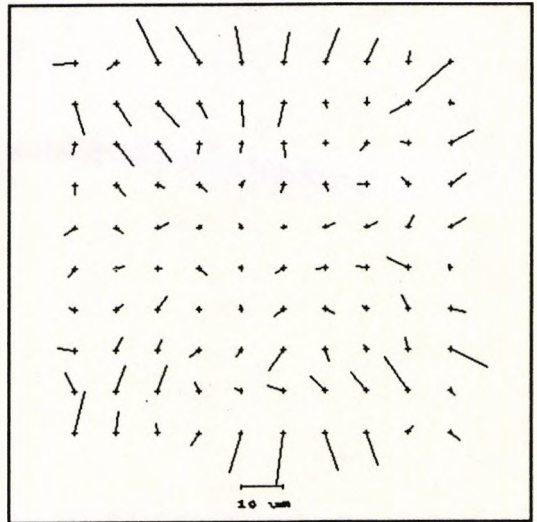
Frame 10



Frame 11

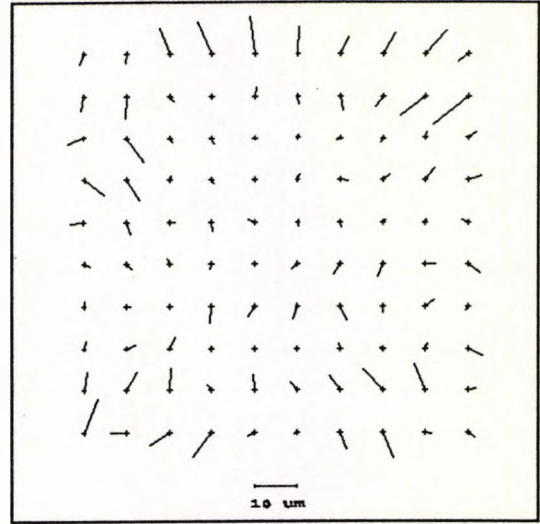


Frame 12

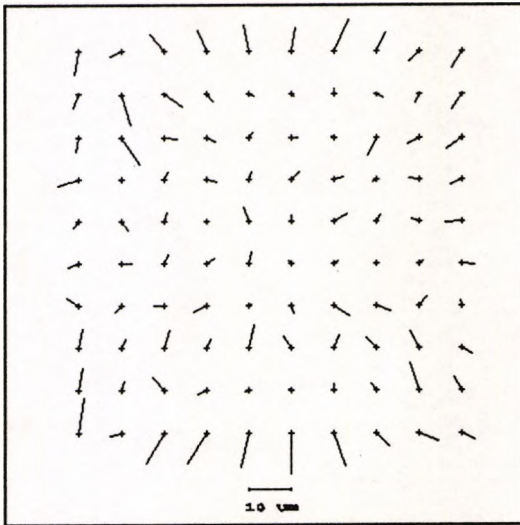


Exposures made using Modified Hasselblad SWC Camera (HS2)
onto Kodak Technical Pan 120 Film (Roll B, Camera Back A).

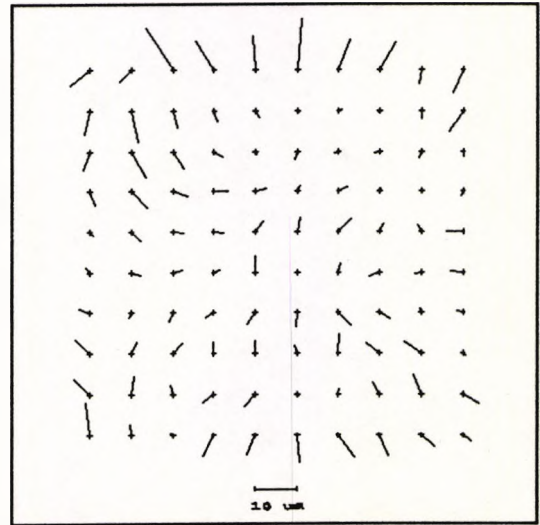
Frame 2



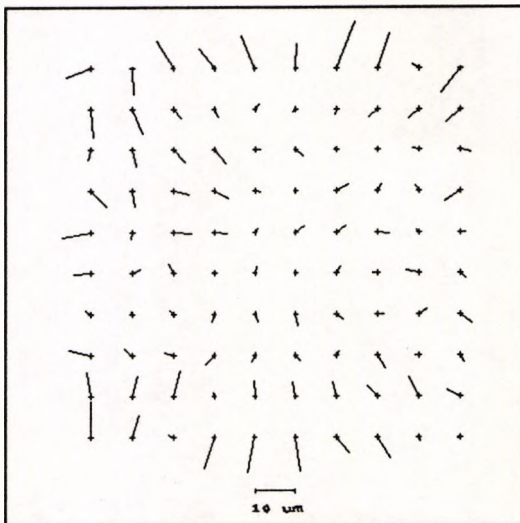
Frame 3



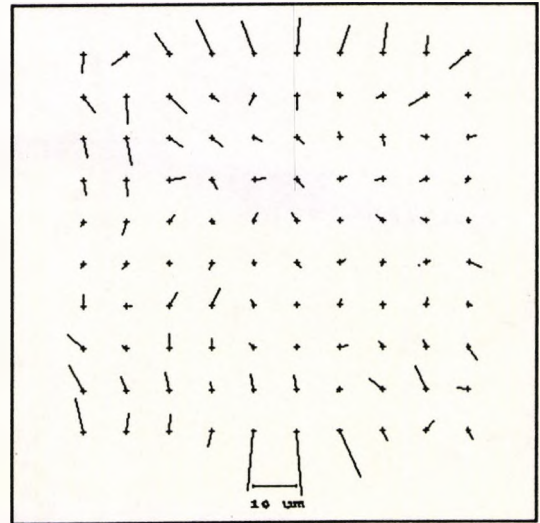
Frame 4



Frame 5

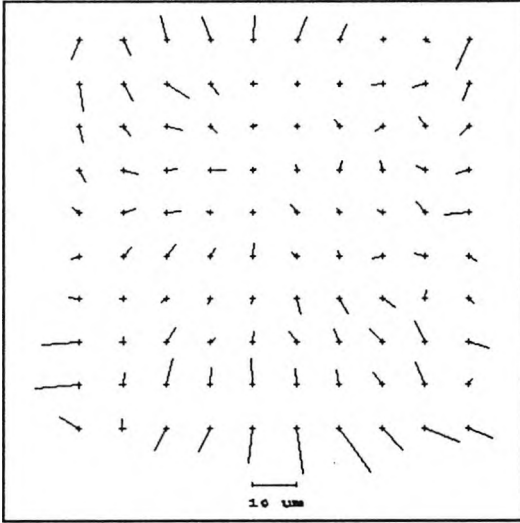


Frame 6

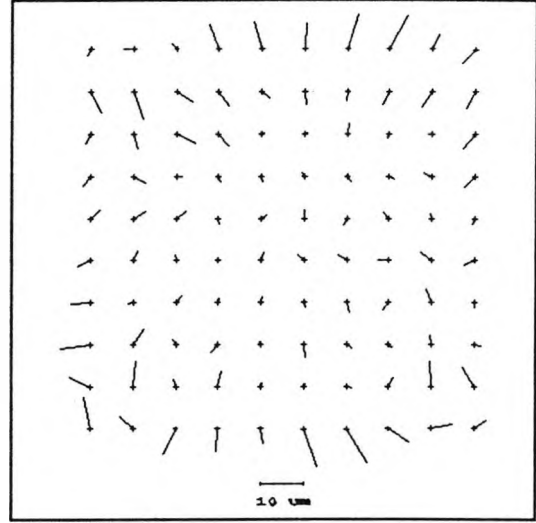


Exposures made using Modified Hasselblad SWC Camera (HS2)
onto Kodak Technical Pan 120 Film (Roll B, Camera Back A).

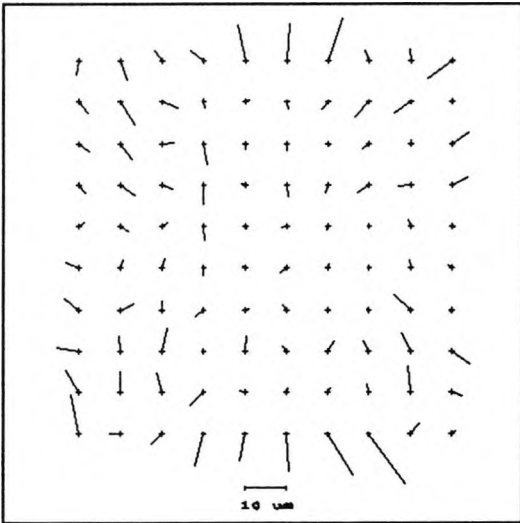
Frame 7



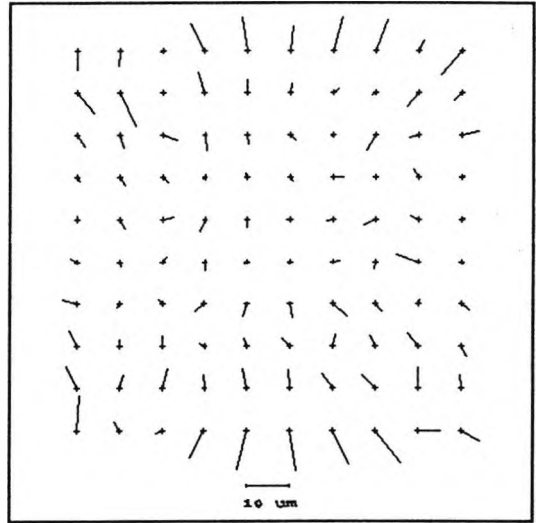
Frame 8



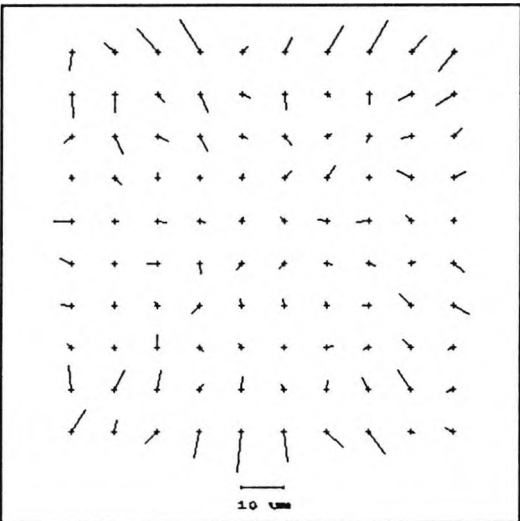
Frame 9



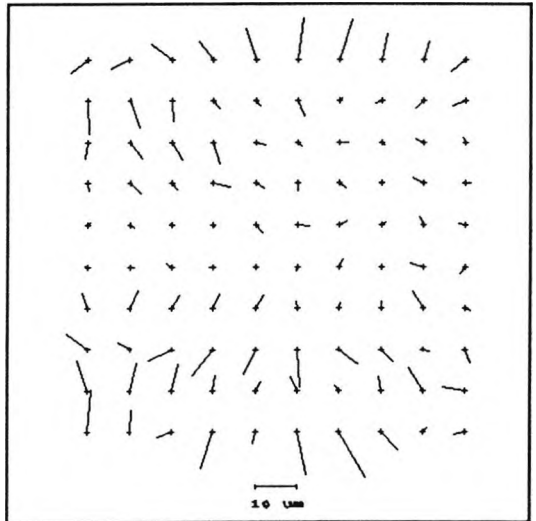
Frame 10



Frame 11

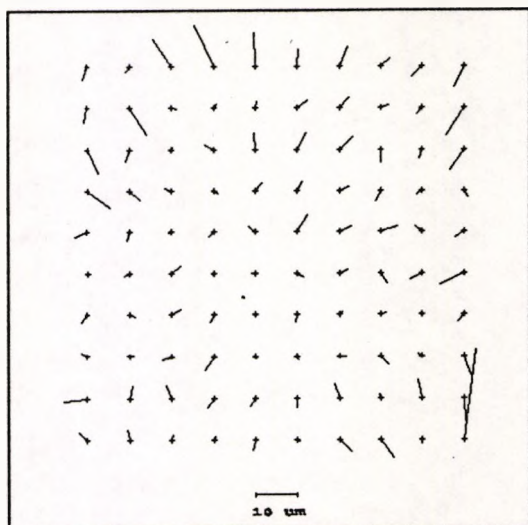


Frame 12

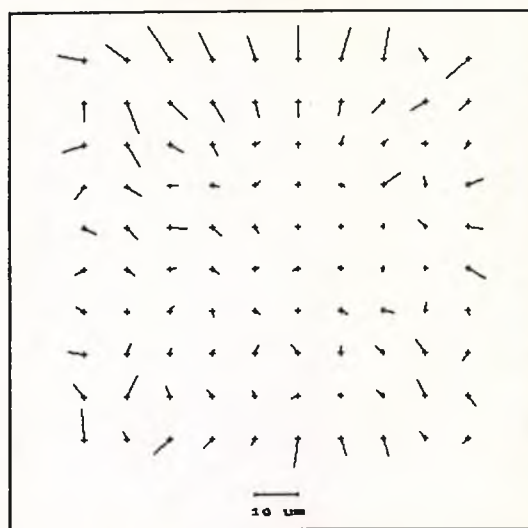


Exposures made using Modified Hasselblad SWC Camera (HS2)
onto Kodak Technical Pan 120 Film (Roll C, Camera Back A).

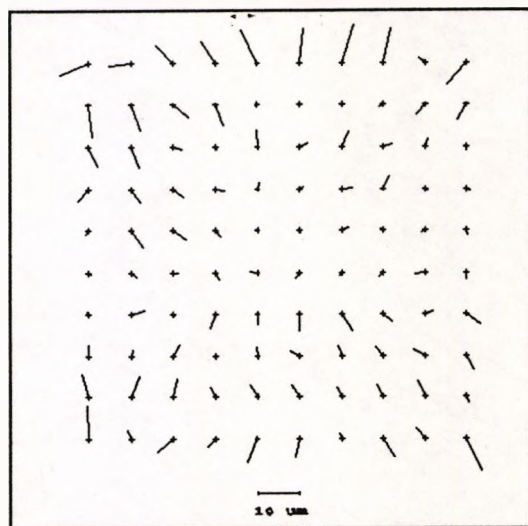
Frame 1



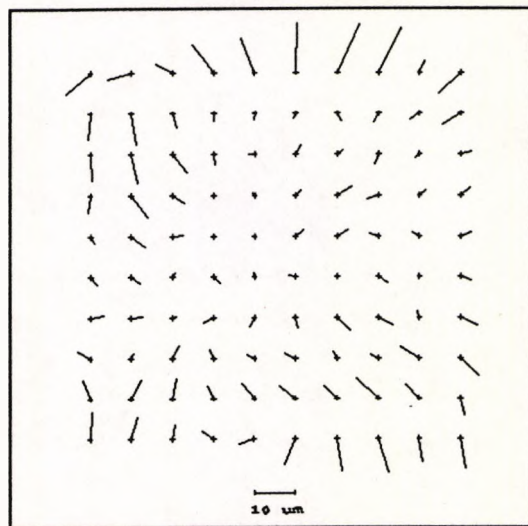
Frame 2, (Bundle 003).



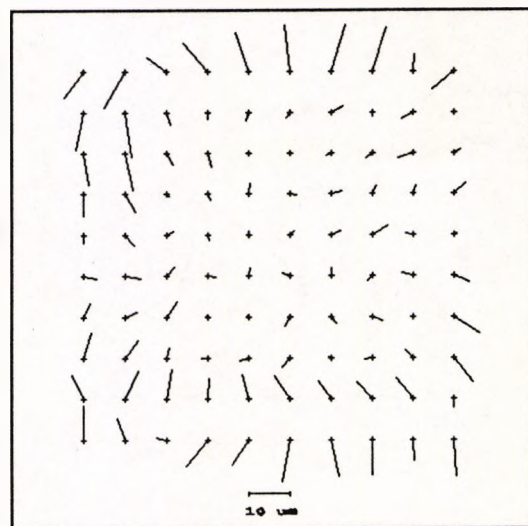
Frame 3, (Bundle 031).



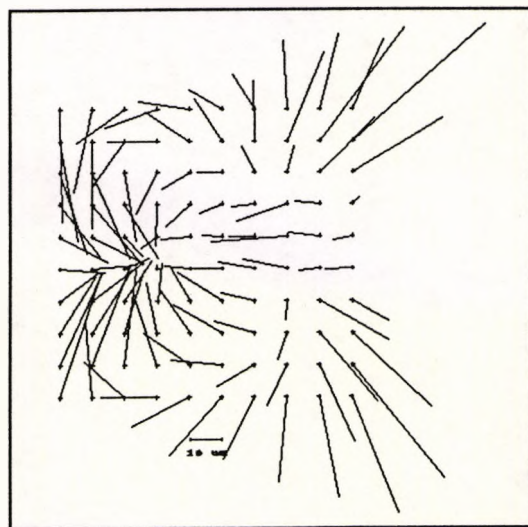
Frame 4, (Bundle 001).



Frame 5, (Bundle 011).

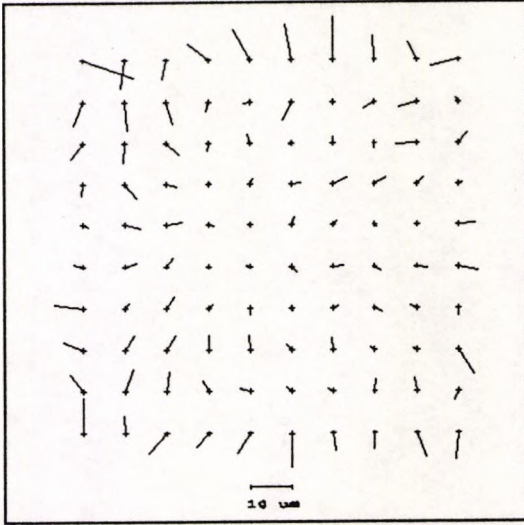


Frame 6, (Bundle 002).

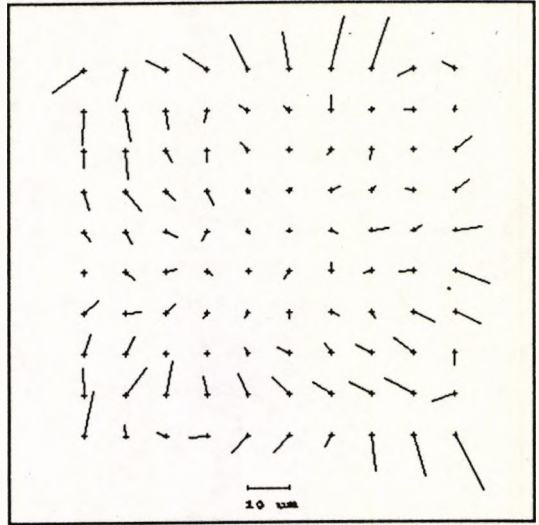


Exposures made using Modified Hasselblad SWC Camera (HS2)
onto Kodak Technical Pan 120 Film (Roll C, Camera Back A).

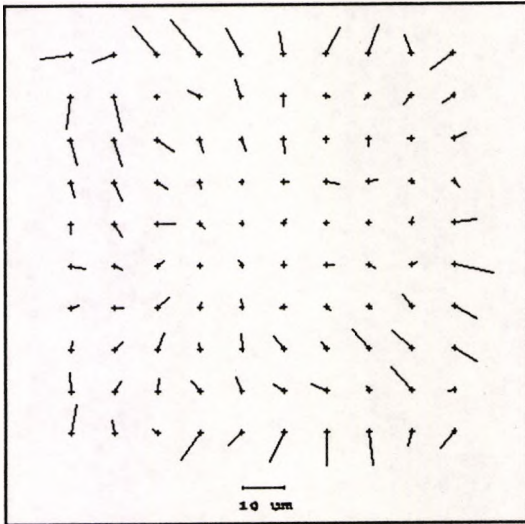
Frame 7, (Bundle 041).



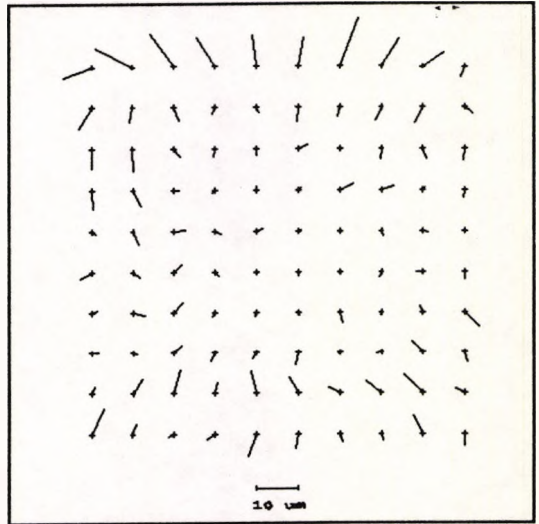
Frame 8, (Bundle 004).



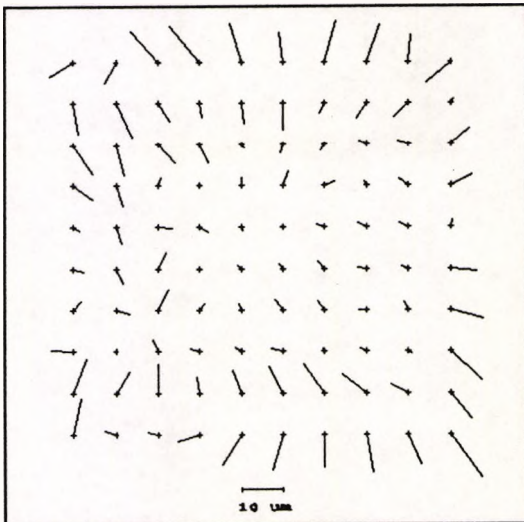
Frame 9, (Bundle 005).



Frame 10, (Bundle 051).

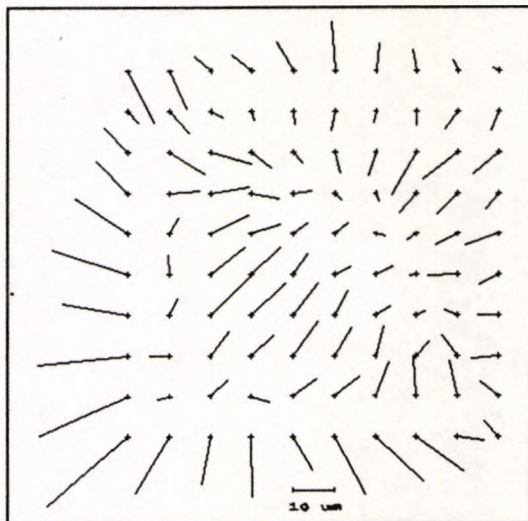


Frame 11

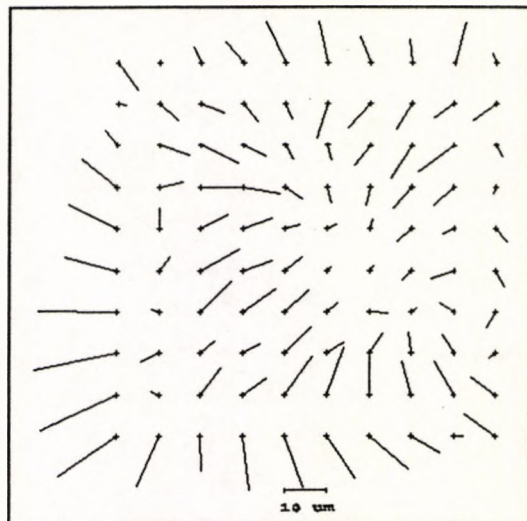


Exposures made using Modified Hasselblad SWC Camera (HS2)
onto Kodak Technical Pan 120 Film (Roll A, Camera Back B).

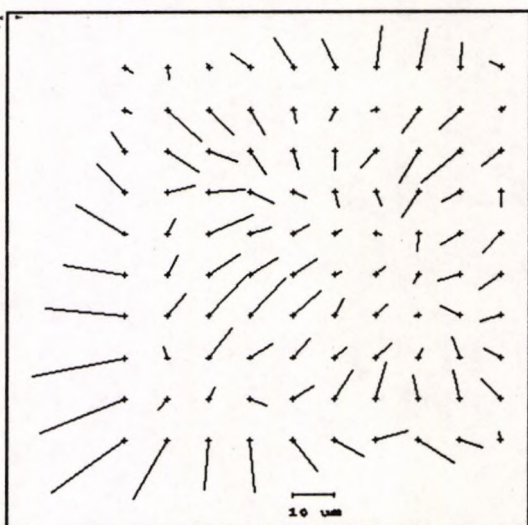
Frame 1



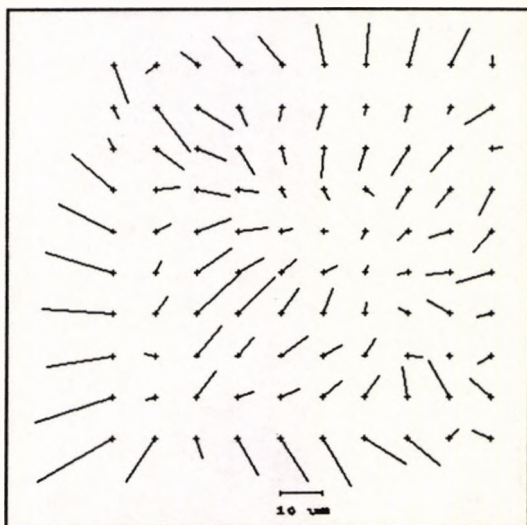
Frame 2



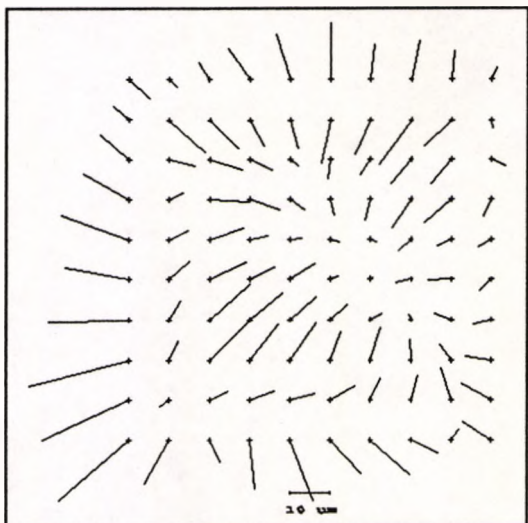
Frame 3



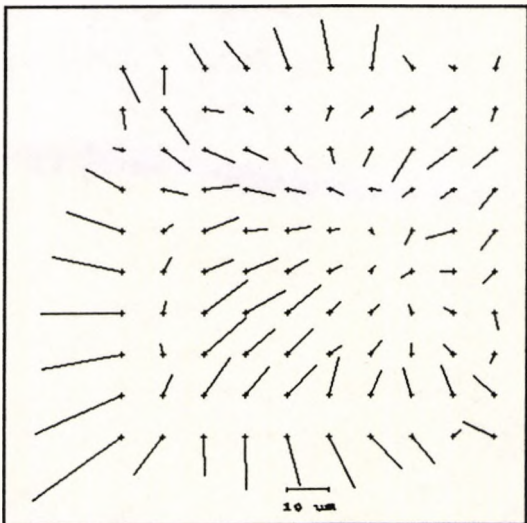
Frame 4



Frame 5

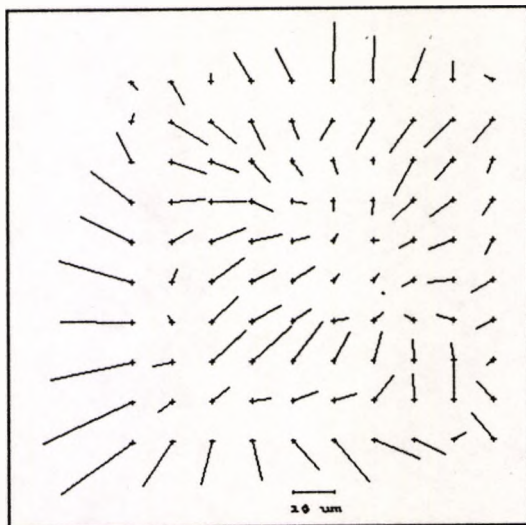


Frame 6

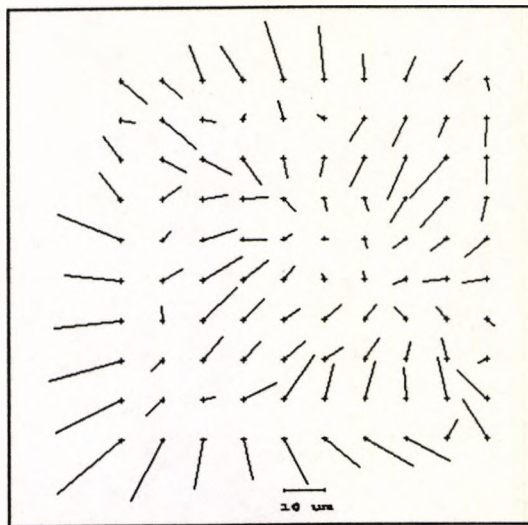


Exposures made using Modified Hasselblad SWC Camera (HS2)
onto Kodak Technical Pan 120 Film (Roll A, Camera Back B).

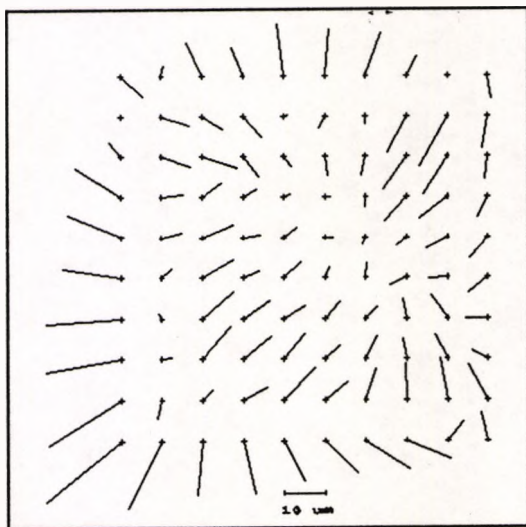
Frame 7



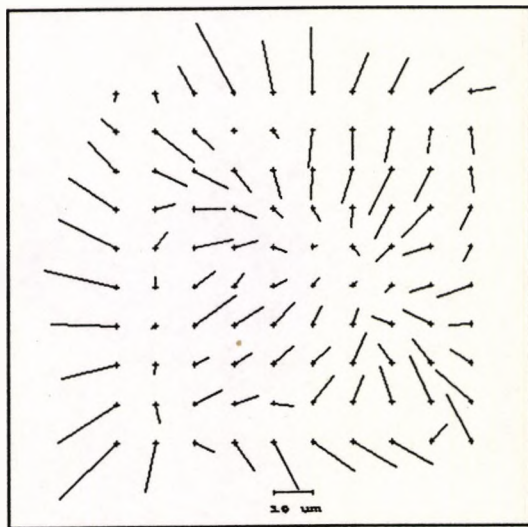
Frame 8



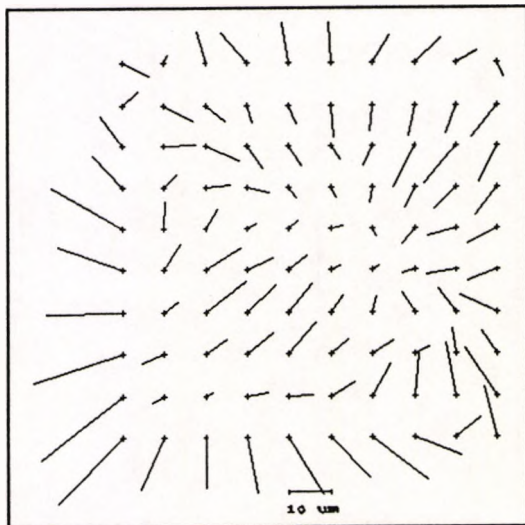
Frame 9



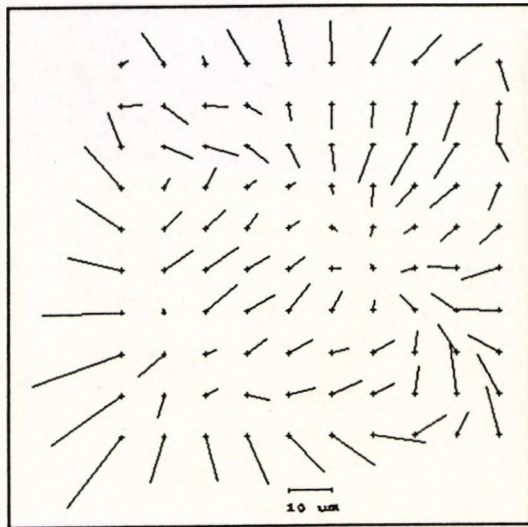
Frame 10



Frame 11

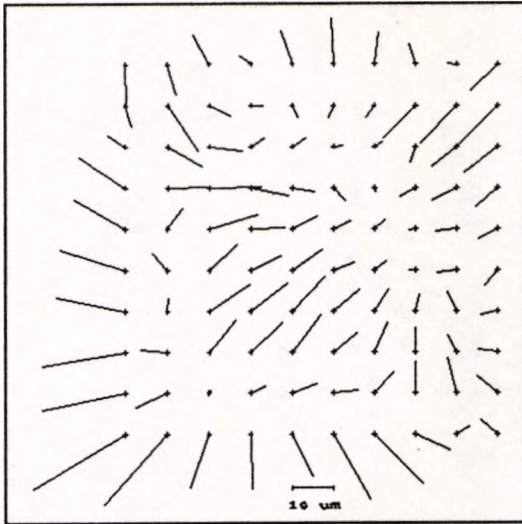


Frame 12

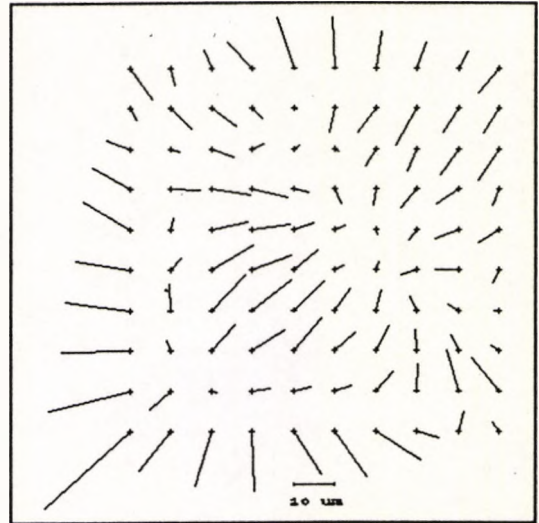


Exposures made using Modified Hasselblad SWC Camera (HS2)
onto Kodak Technical Pan 120 Film (Roll B, Camera Back B).

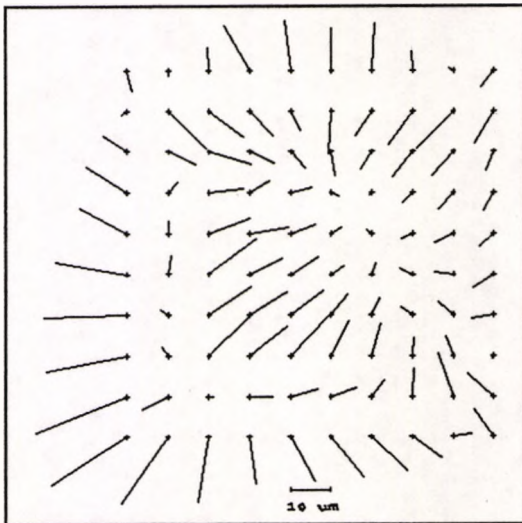
Frame 1



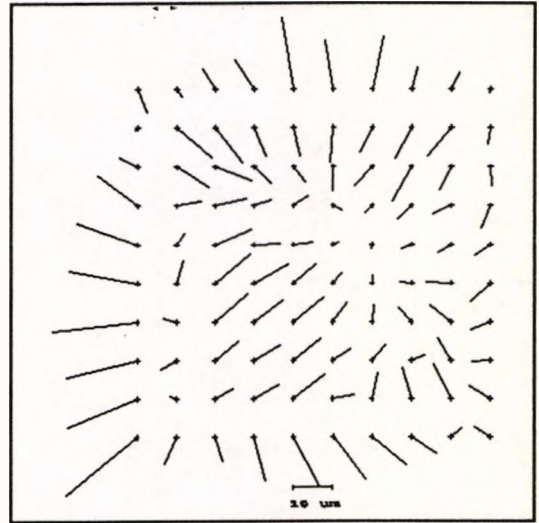
Frame 2



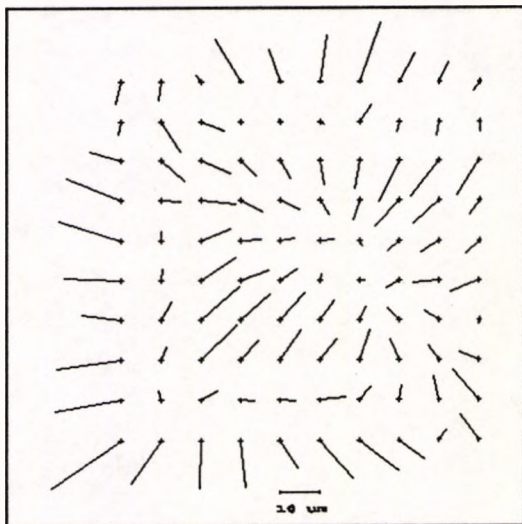
Frame 3



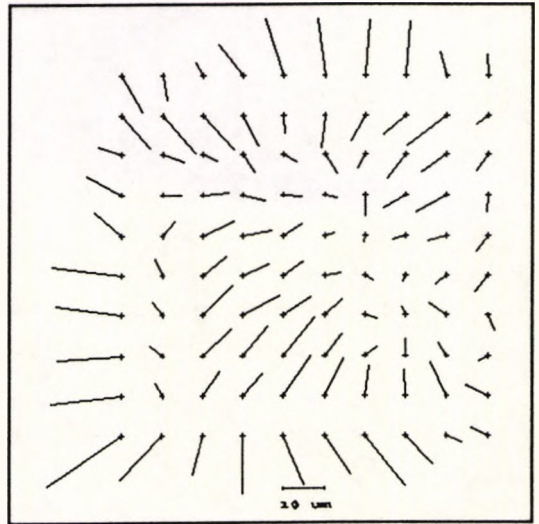
Frame 4



Frame 5

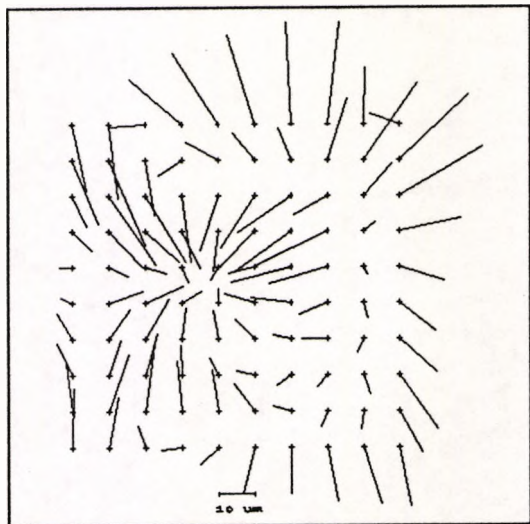


Frame 6

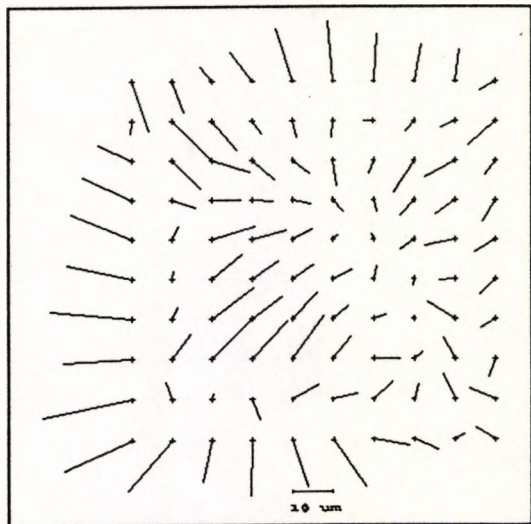


Exposures made using Modified Hasselblad SWC Camera (HS2)
onto Kodak Technical Pan 120 Film (Roll B, Camera Back B).

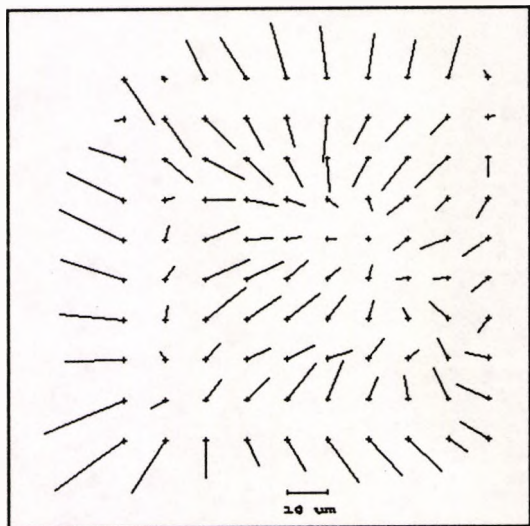
Frame 7



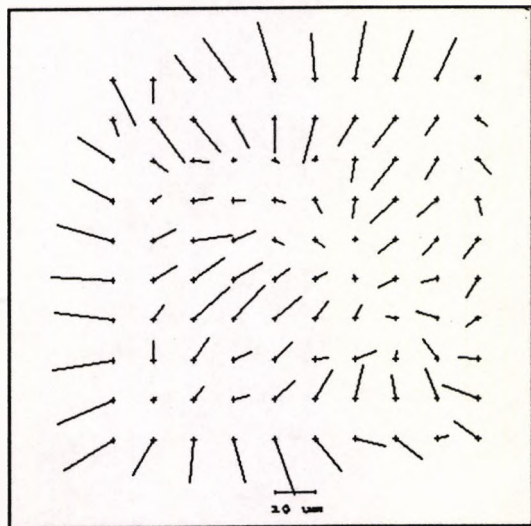
Frame 8



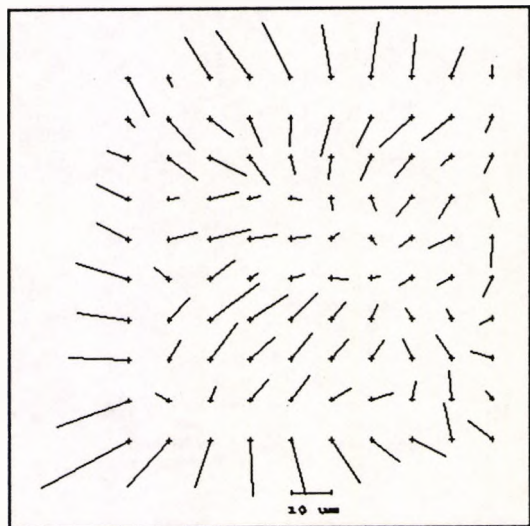
Frame 9



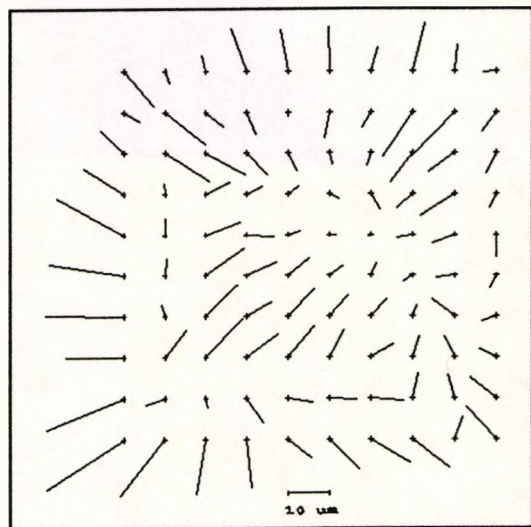
Frame 10



Frame 11

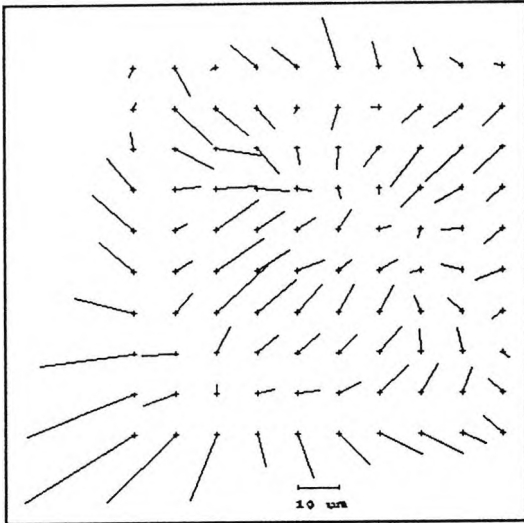


Frame 12

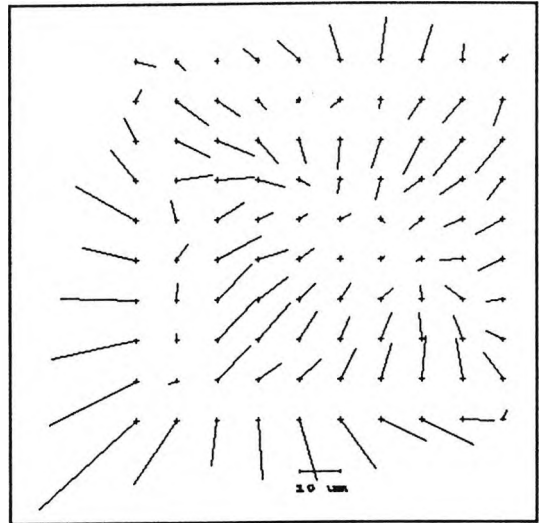


Exposures made using Modified Hasselblad SWC Camera (HS2)
onto Kodak Technical Pan 120 Film (Roll C, Camera Back B).

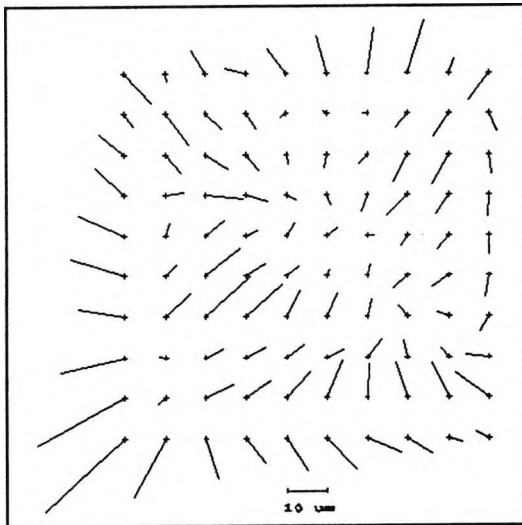
Frame 1



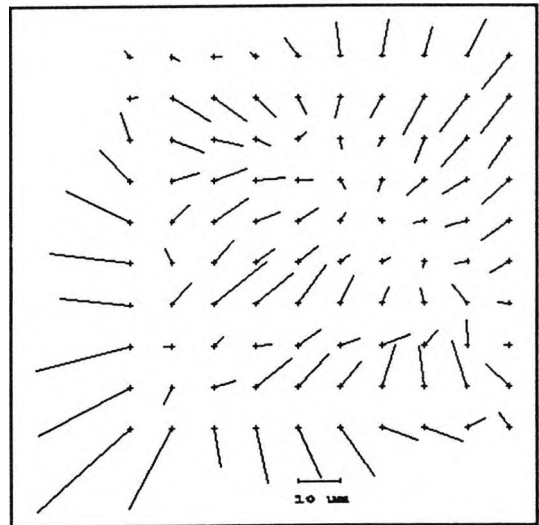
Frame 2, (Bundle 051).



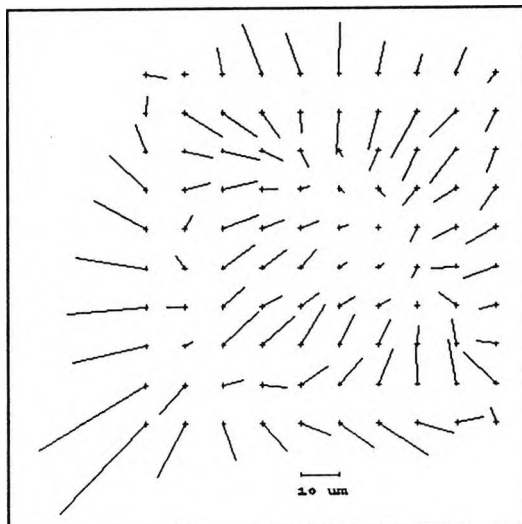
Frame 3, (Bundle 005).



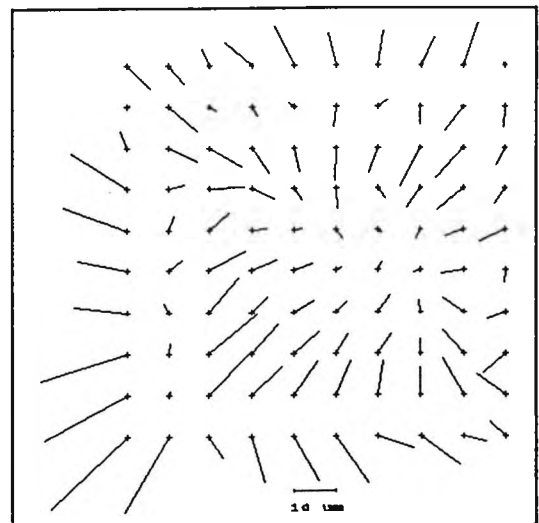
Frame 4, (Bundle 001).



Frame 5, (Bundle 011).

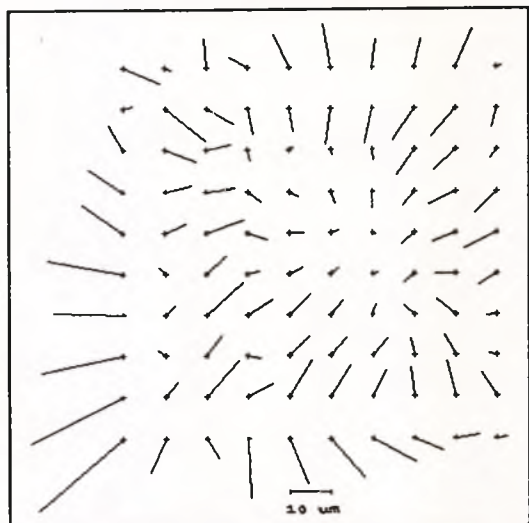


Frame 6, (Bundle 002).

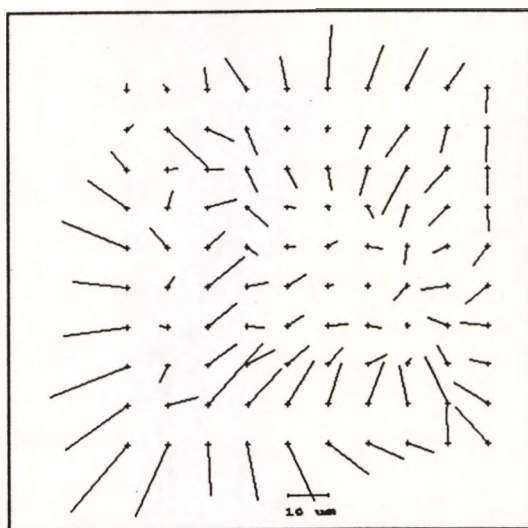


Exposures made using Modified Hasselblad SWC Camera (HS2)
onto Kodak Technical Pan 120 Film (Roll C, Camera Back B).

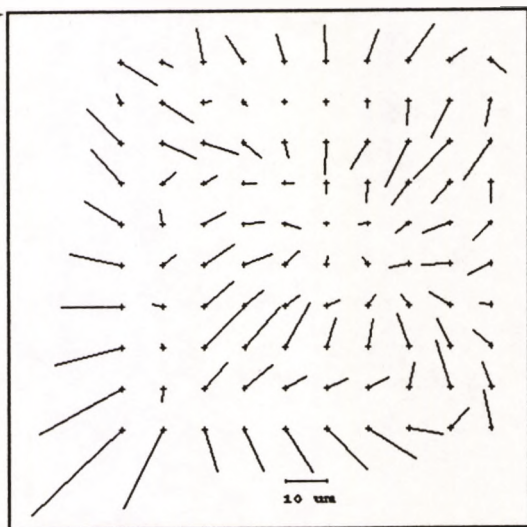
Frame 7, (Bundle 004).



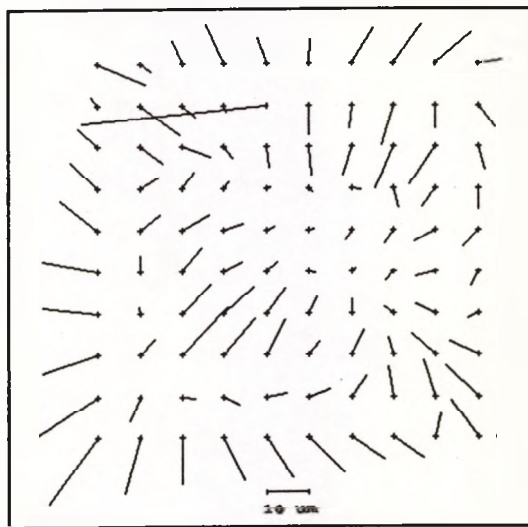
Frame 8



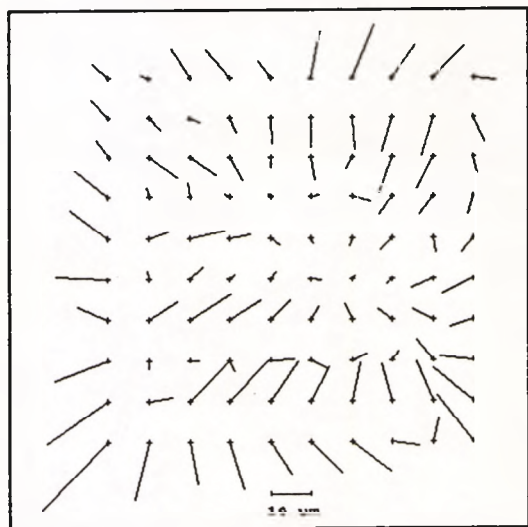
Frame 9, (Bundle 041).



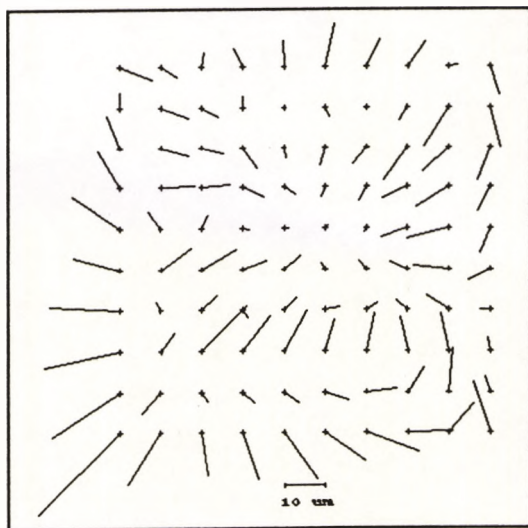
Frame 10, (Bundle 031).



Frame 11, (Bundle 003).

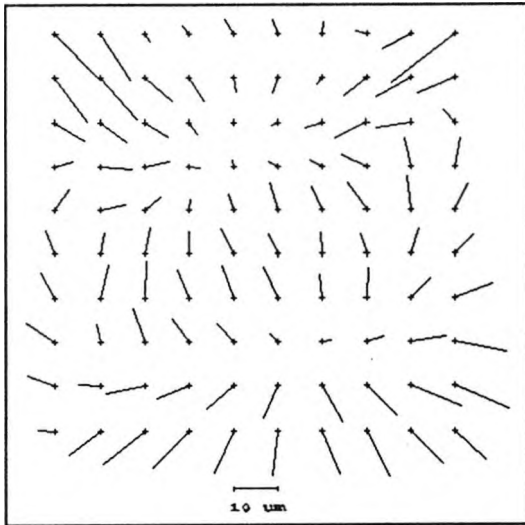


Frame 12

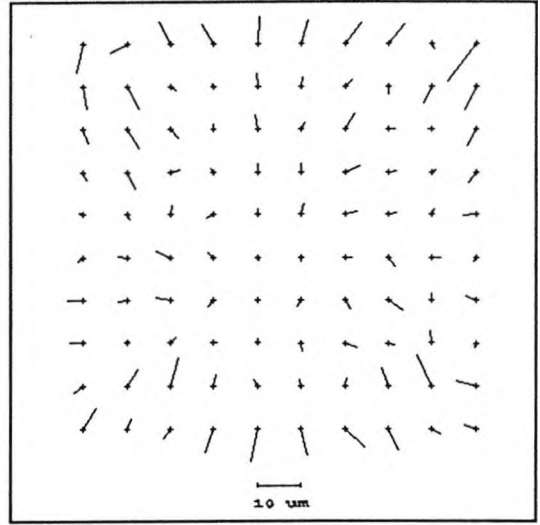


Exposures made using Modified Hasselblad SWC Camera (HS2)
onto Ilford FP4 120 Film (A).

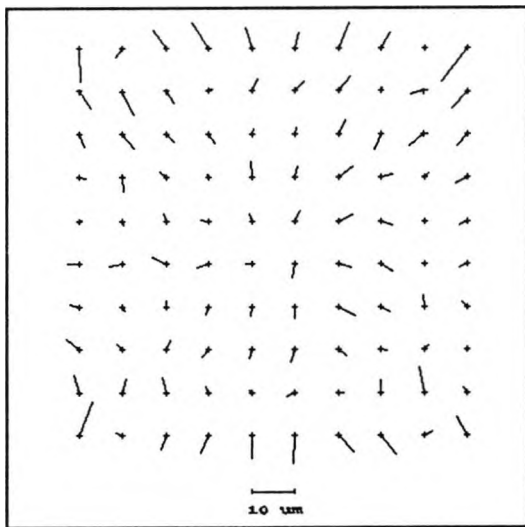
Frame 1



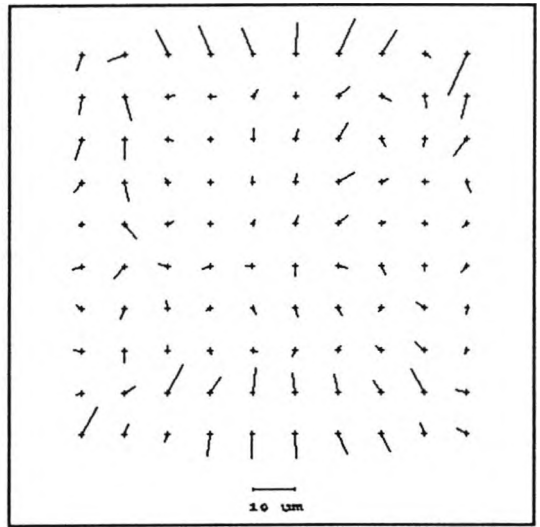
Frame 2



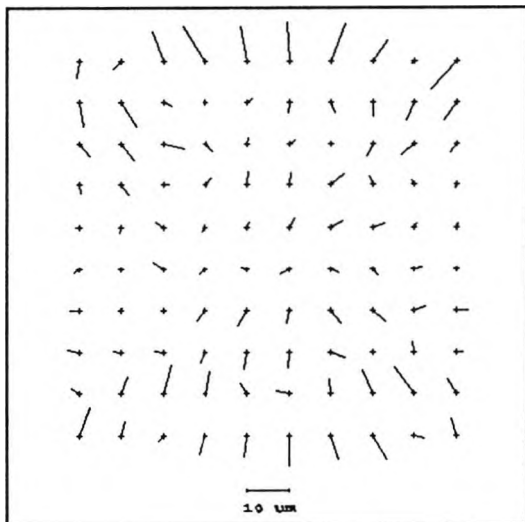
Frame 3



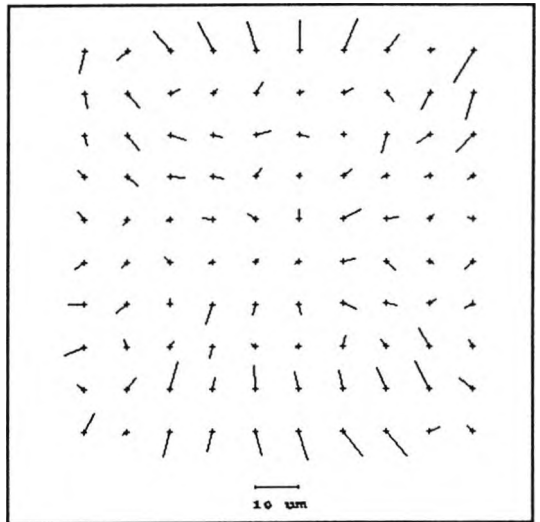
Frame 4



Frame 5

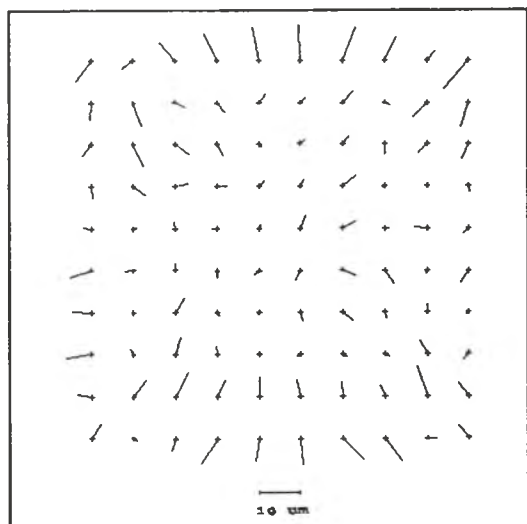


Frame 6

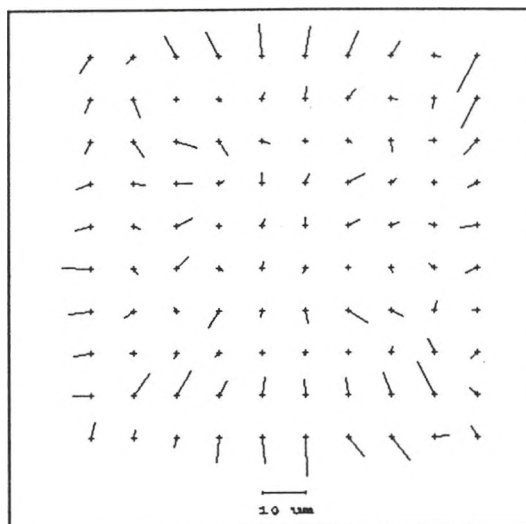


Exposures made using Modified Hasselblad SWC Camera (HS2)
onto Ilford FP4 120 Film (A).

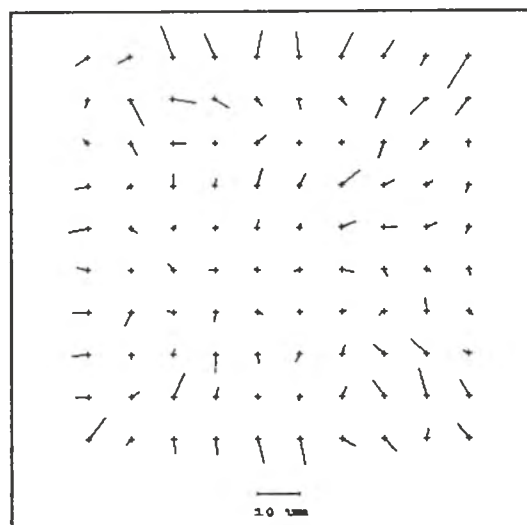
Frame 7



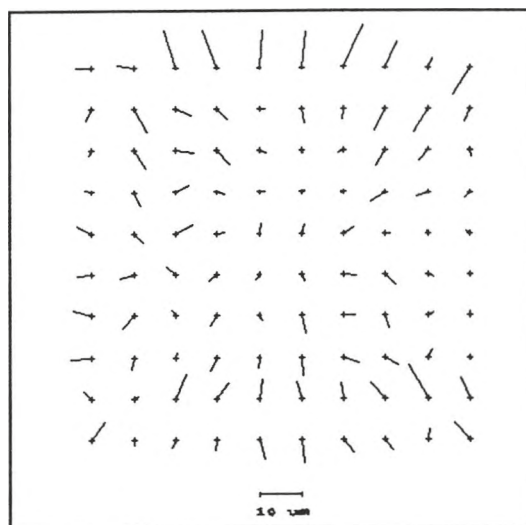
Frame 8



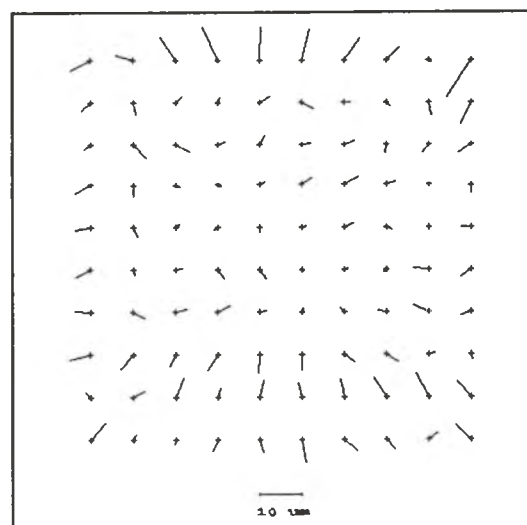
Frame 9



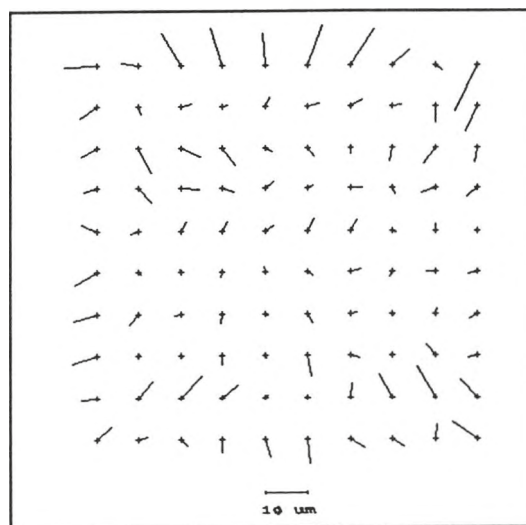
Frame 10



Frame 11

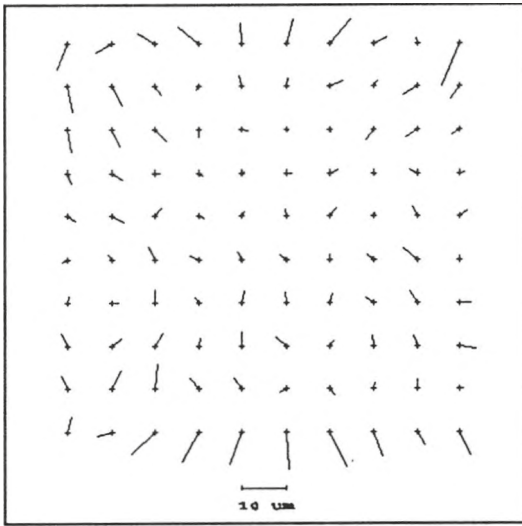


Frame 12

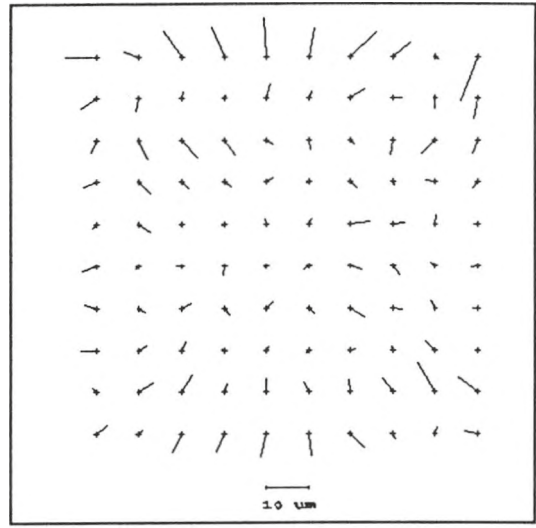


Exposures made using Modified Hasselblad SWC Camera (HS2)
onto Ilford FP4 120 Film (B).

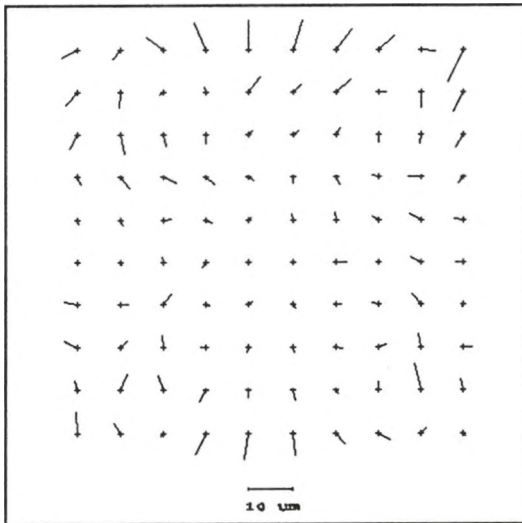
Frame 1



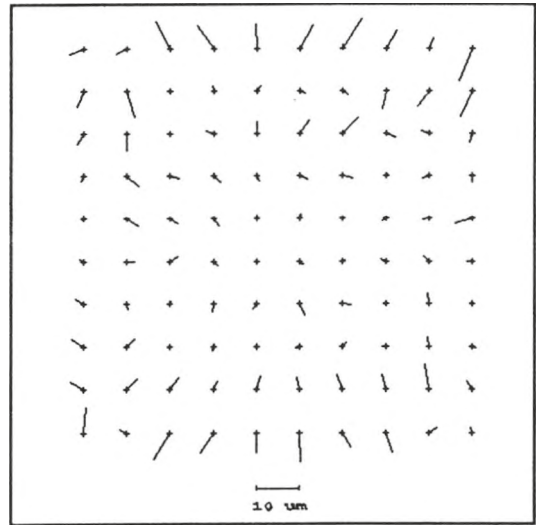
Frame 02, (Bundle 004).



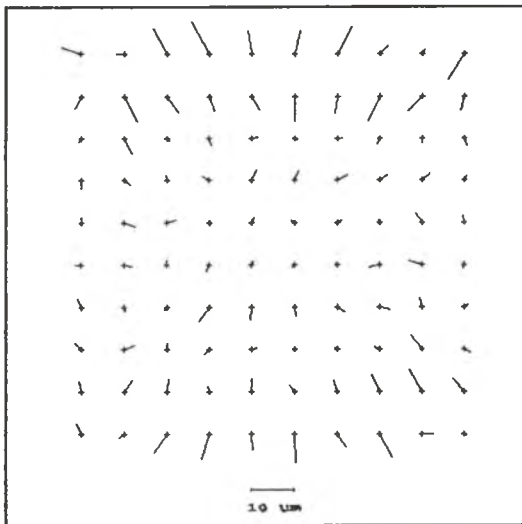
Frame 03, (Bundle 041).



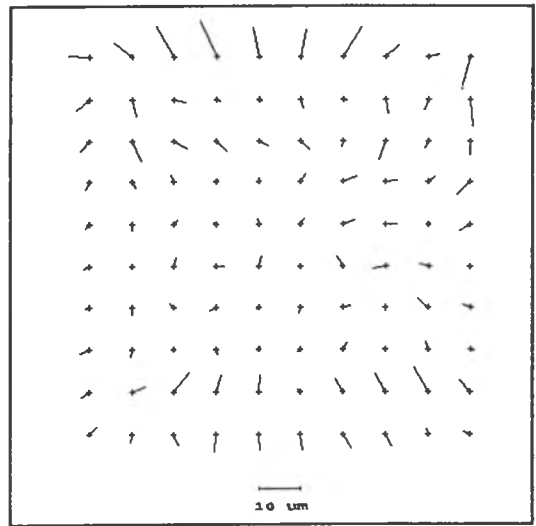
Frame 04, (Bundle 002).



Frame 05, (Bundle 001).

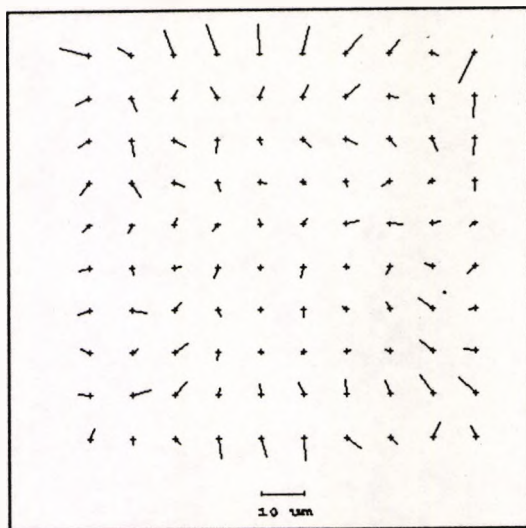


Frame 06, (Bundle 011).

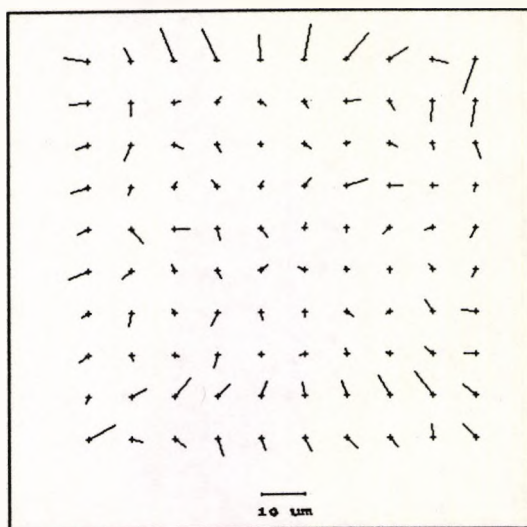


Exposures made using Modified Hasselblad SWC Camera (HS2)
onto Ilford FP4 120 Film (B).

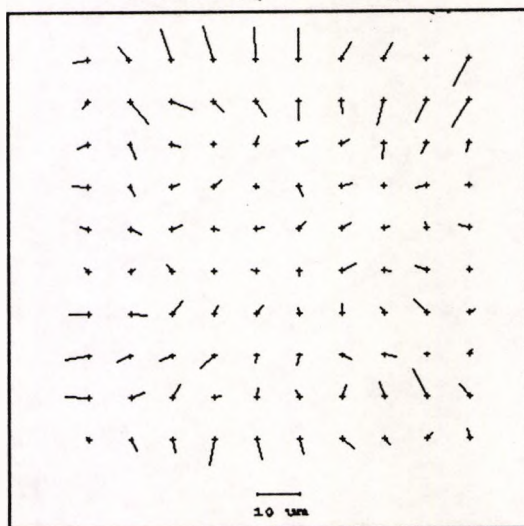
Frame 07, (Bundle 031).



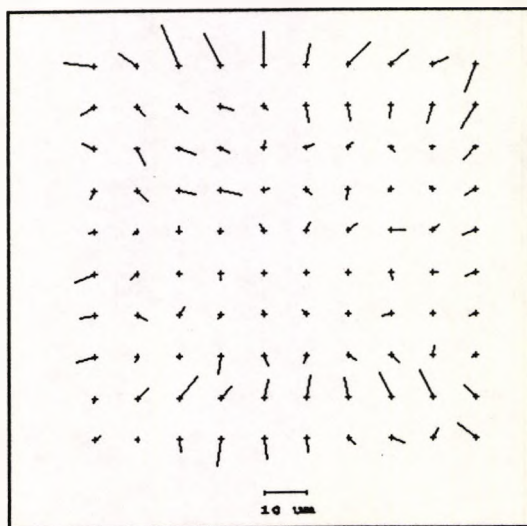
Frame 08, (Bundle 003).



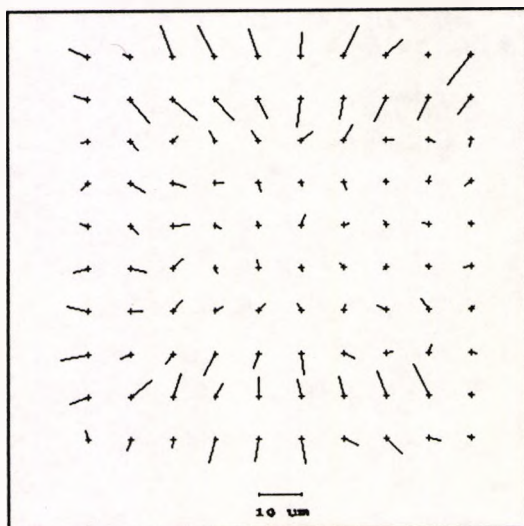
Frame 09, (Bundle 005).



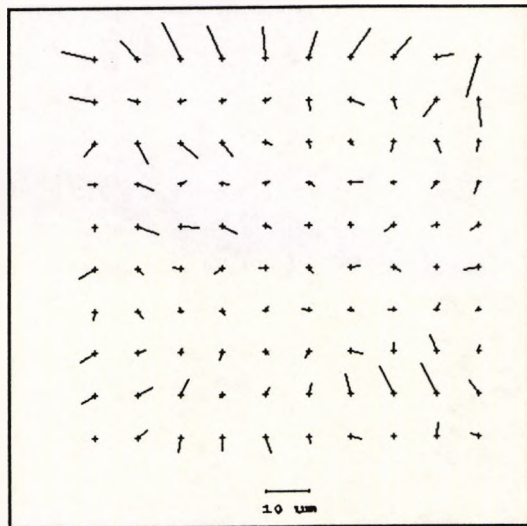
Frame 10.



Frame 11, (Bundle 051).

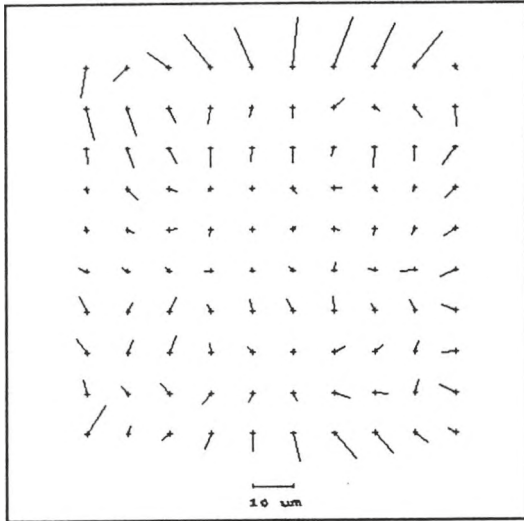


Frame 12.

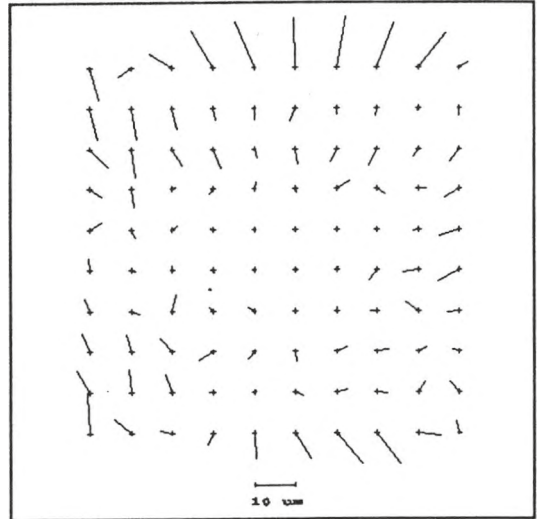


Some exposures made using the modified Hasselblad SWC Camera (HS2)
onto Ilford FP4 220 Film (A).

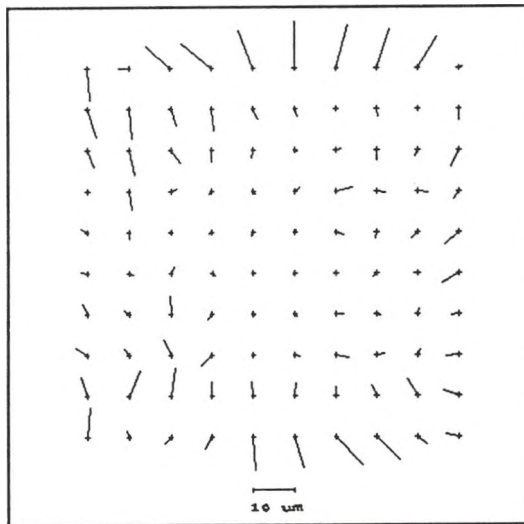
Frame 1



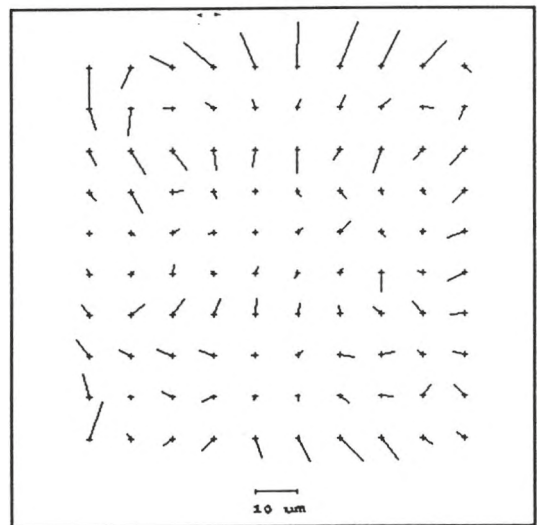
Frame 4



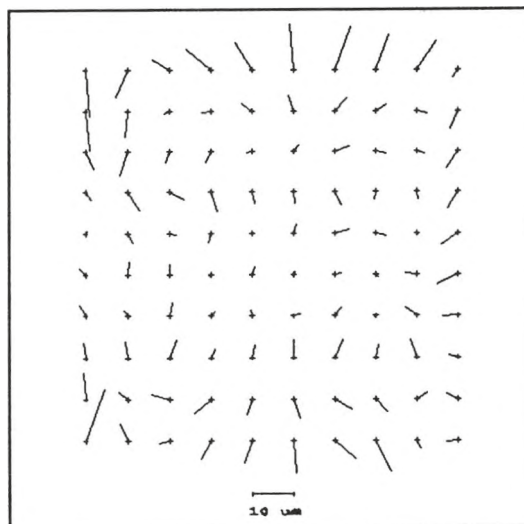
Frame 6



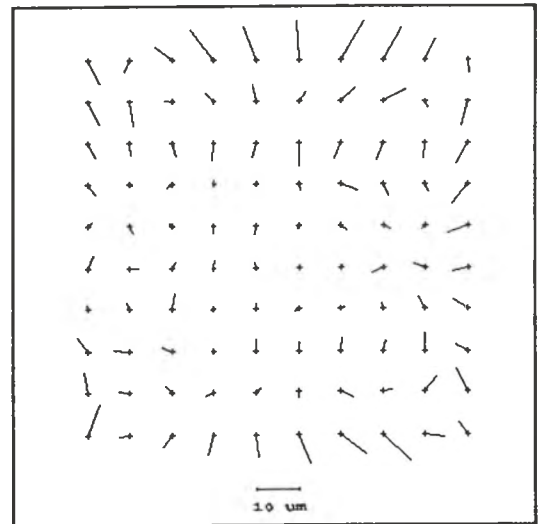
Frame 8



Frame 10

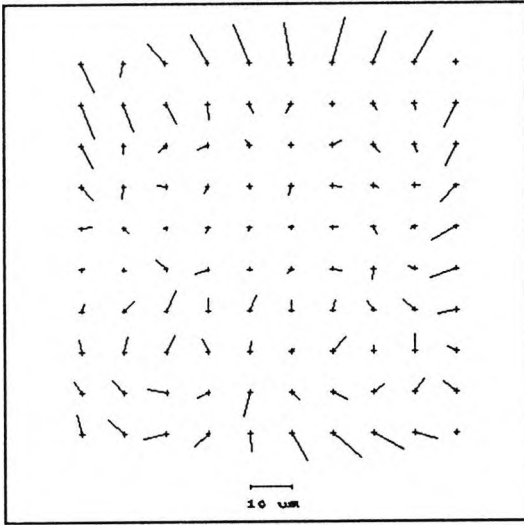


Frame 12

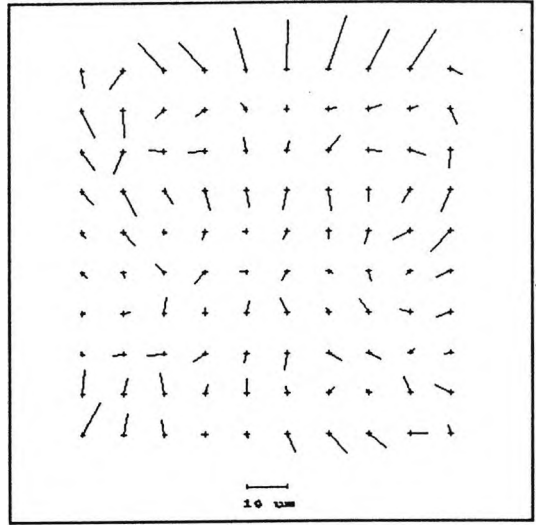


Some exposures made using the modified Hasselblad SWC Camera (HS2)
onto Ilford FP4 220 Film (A).

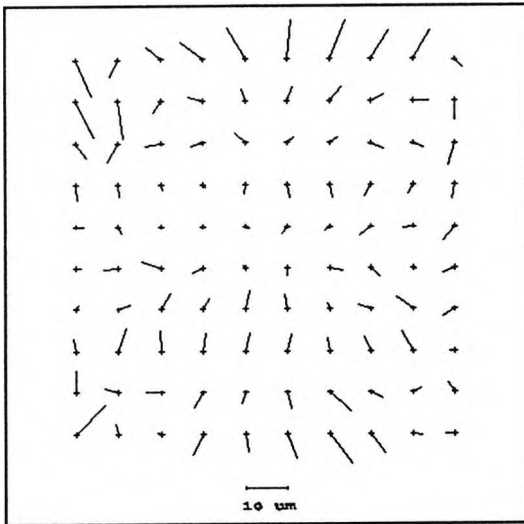
Frame 14



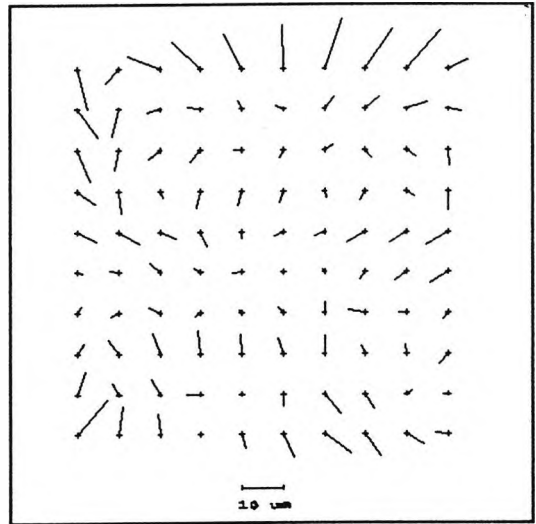
Frame 16



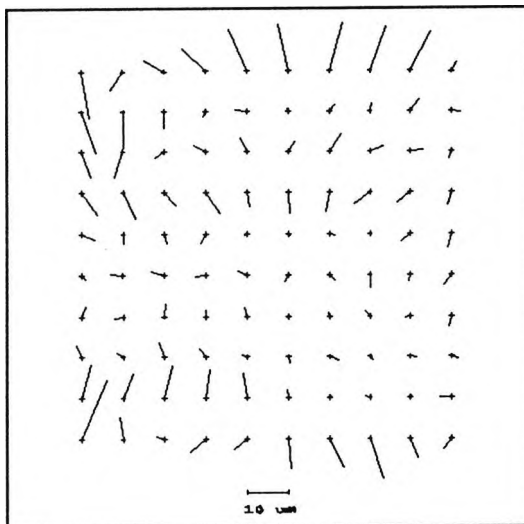
Frame 18



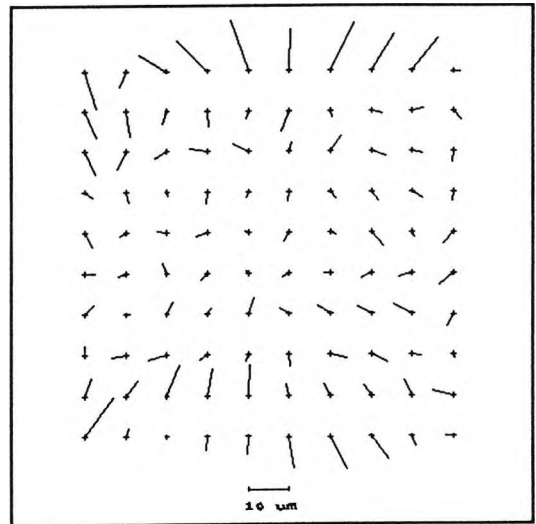
Frame 20



Frame 22

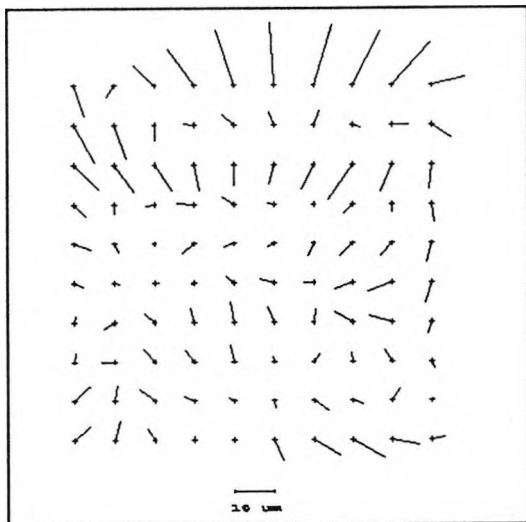


Frame 24

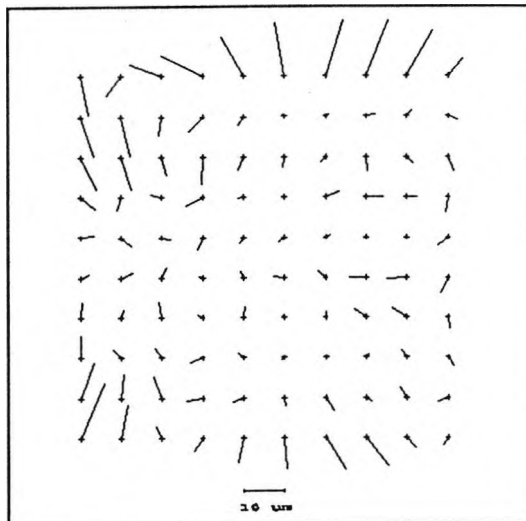


Some exposures made using the modified Hasselblad SWC Camera (HS2)
onto Ilford FP4 220 Film (B).

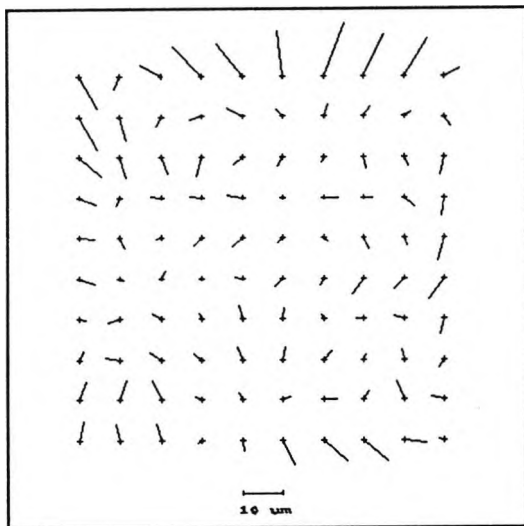
Frame 1



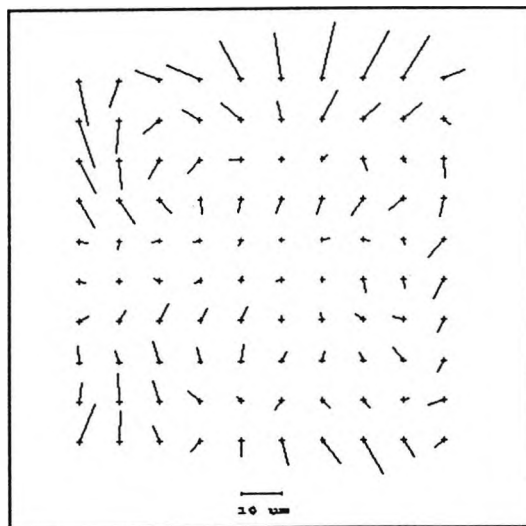
Frame 3



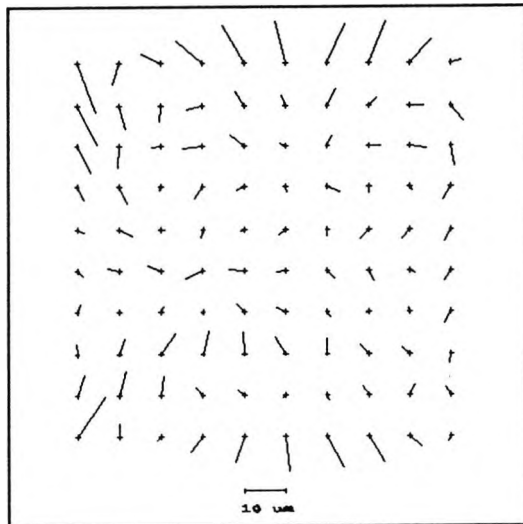
Frame 5



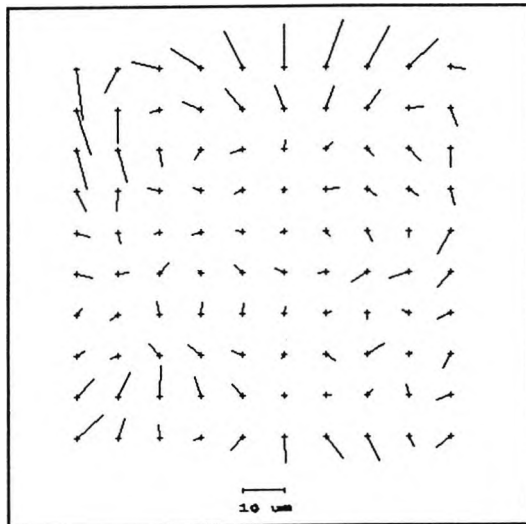
Frame 7



Frame 9

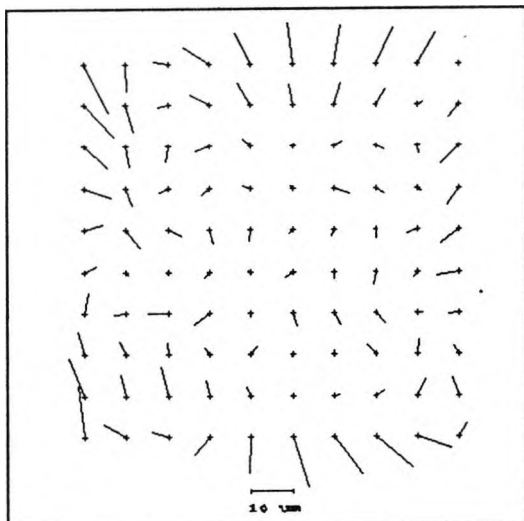


Frame 11

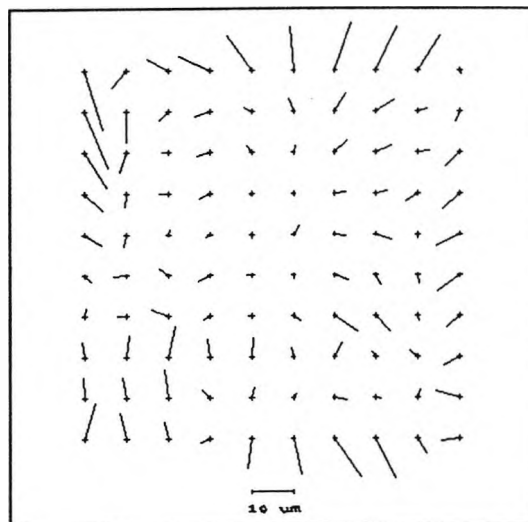


Some exposures made using the modified Hasselblad SWC camera (HS2)
onto Ilford FP4 220 Film (B).

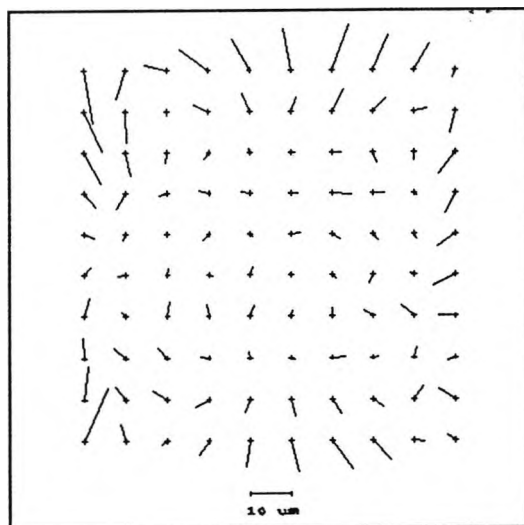
Frame 13



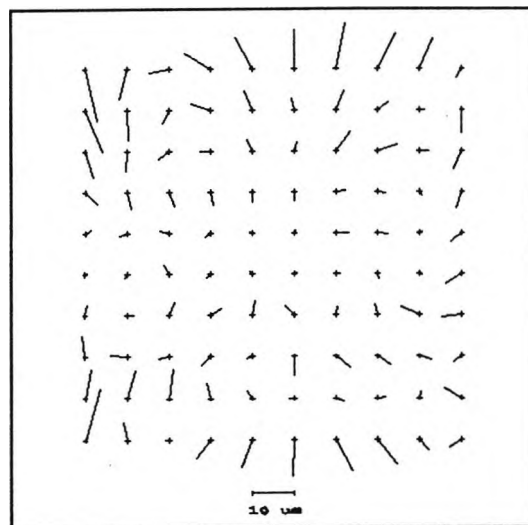
Frame 15



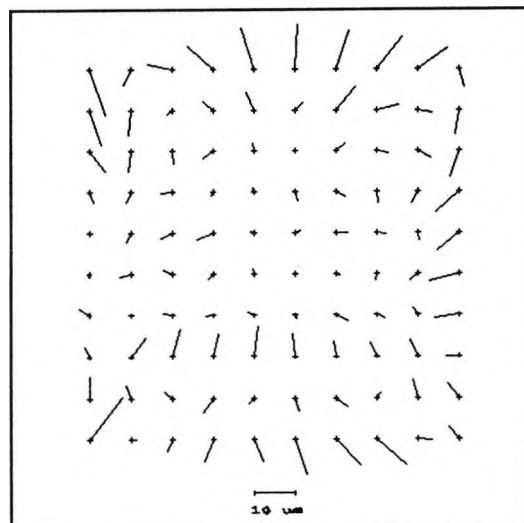
Frame 17



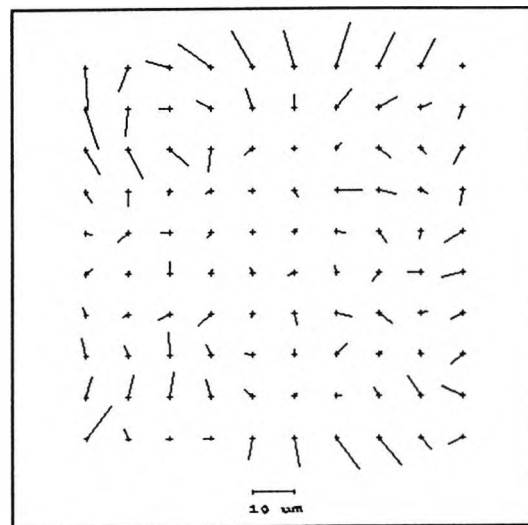
Frame 19



Frame 21

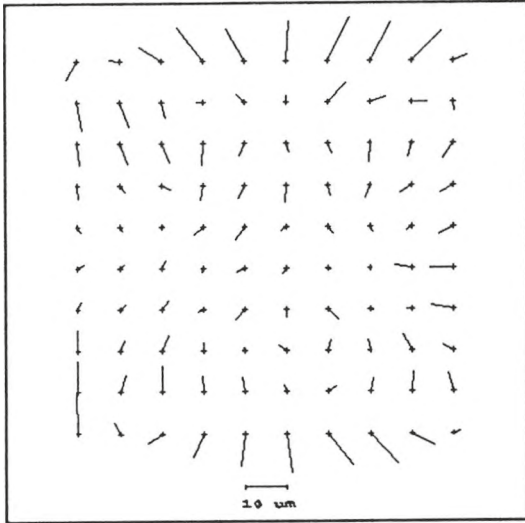


Frame 23

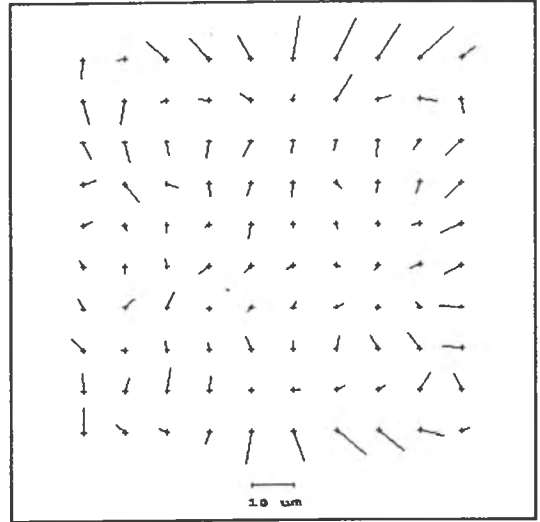


Exposures made using Modified Hasselblad SWC Camera (HS2)
onto Ilford FP4 220 Film (C).

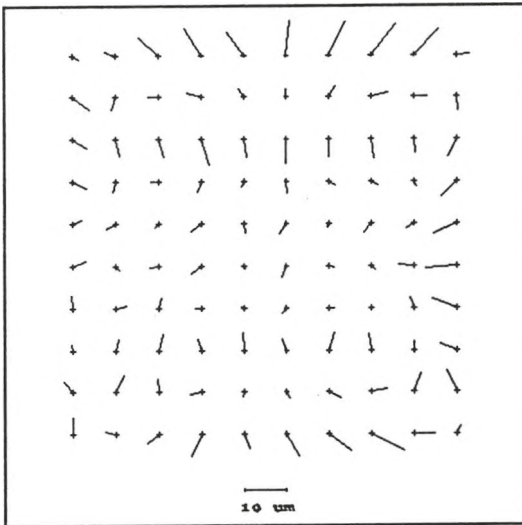
Frame 1



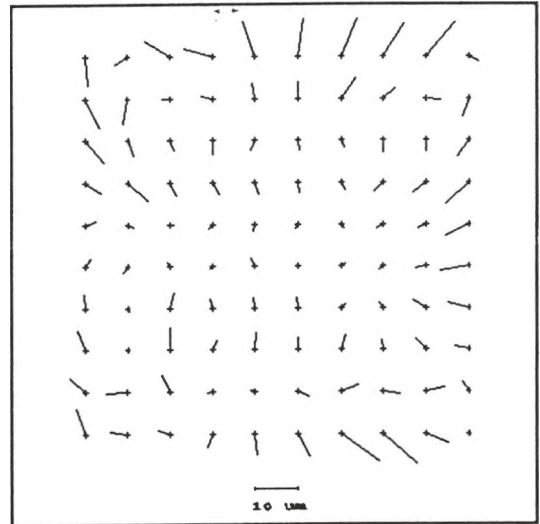
Frame 2



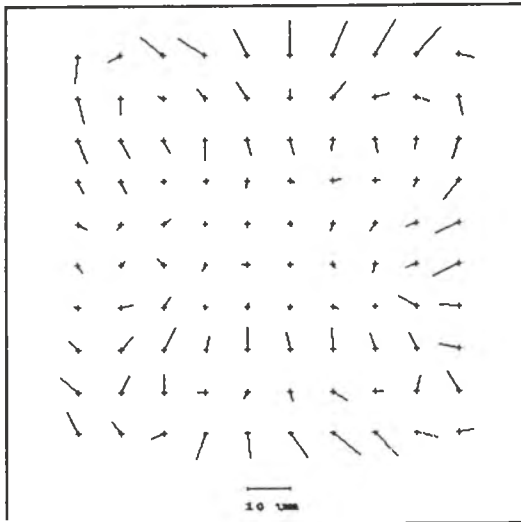
Frame 3



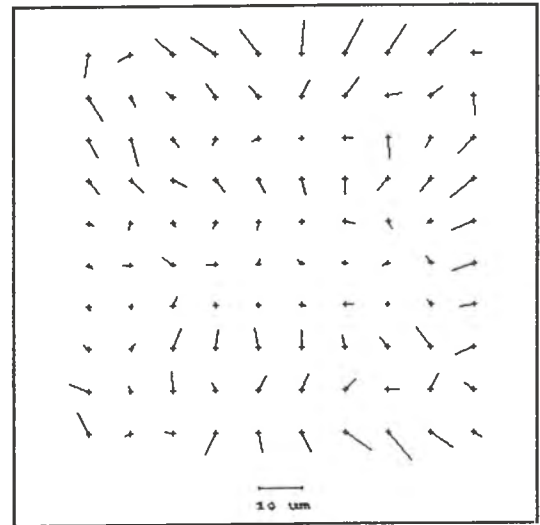
Frame 4



Frame 5, (Bundle 004).

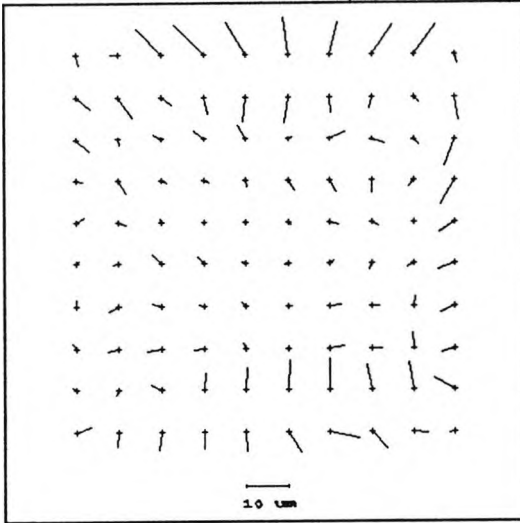


Frame 6

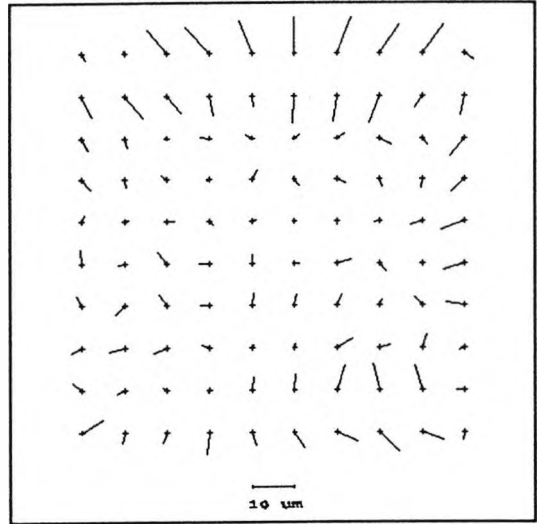


Exposures made using Modified Hasselblad SWC Camera (HS2)
onto Ilford FP4 220 Film (C).

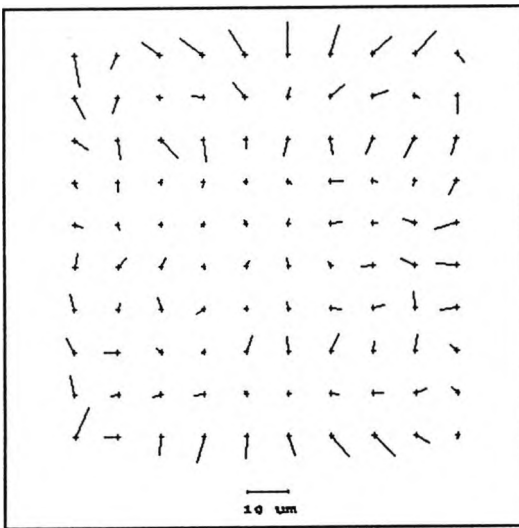
Frame 7, (Bundle 041).



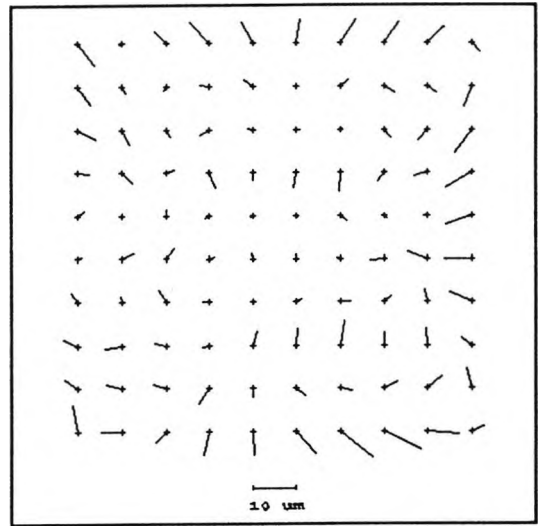
Frame 8, (Bundle 002).



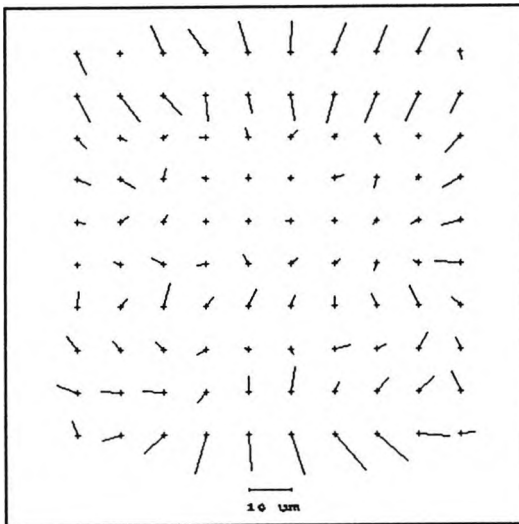
Frame 9



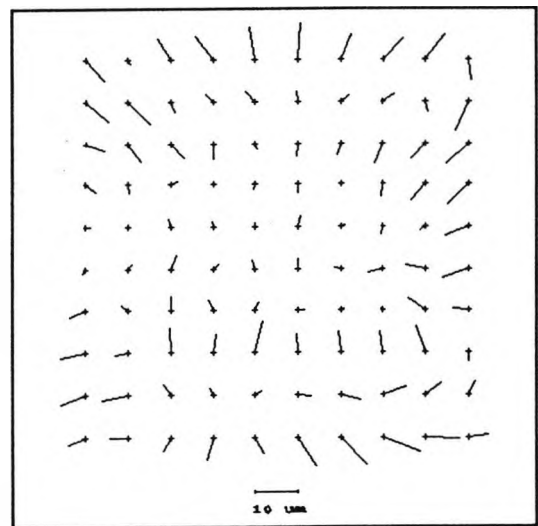
Frame 10, (Bundle 001).



Frame 11, (Bundle 051).

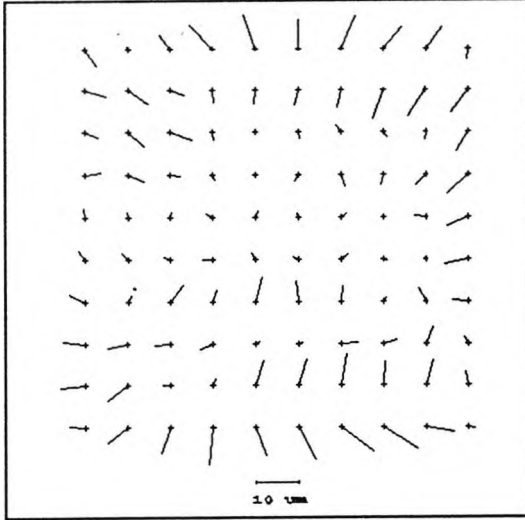


Frame 12

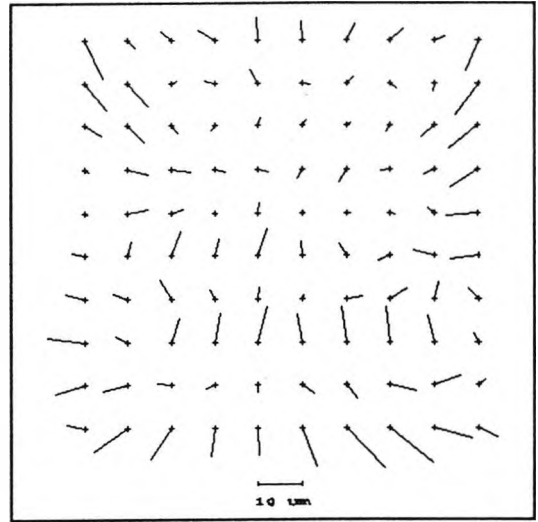


Exposures made using Modified Hasselblad SWC Camera (HS2)
onto Ilford FP4 220 Film (C).

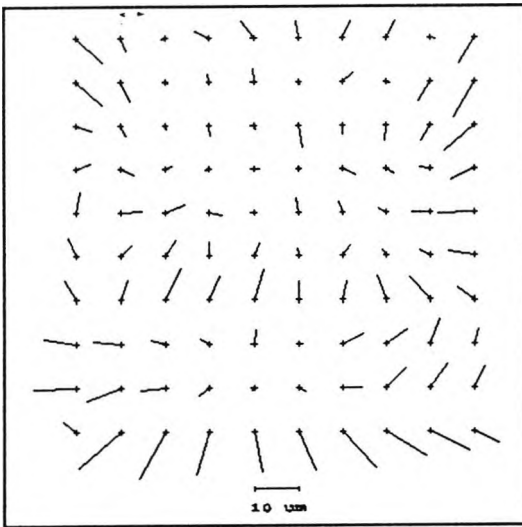
Frame 13, (Bubndle 005).



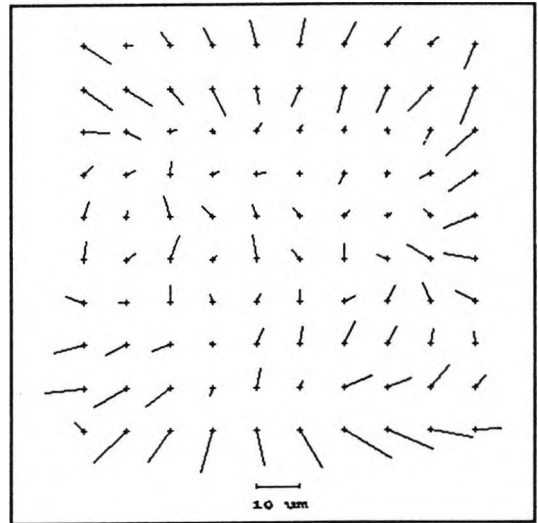
Frame 14



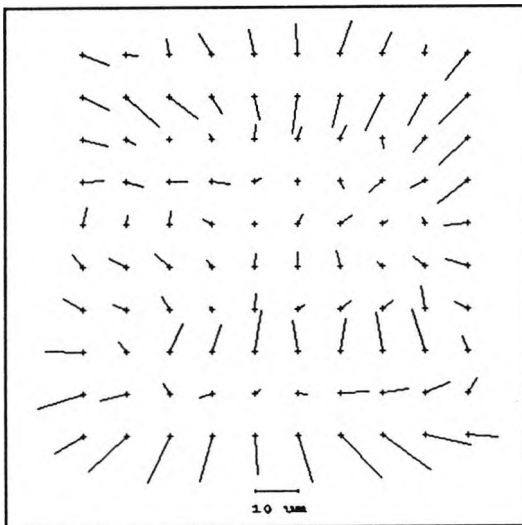
Frame 15



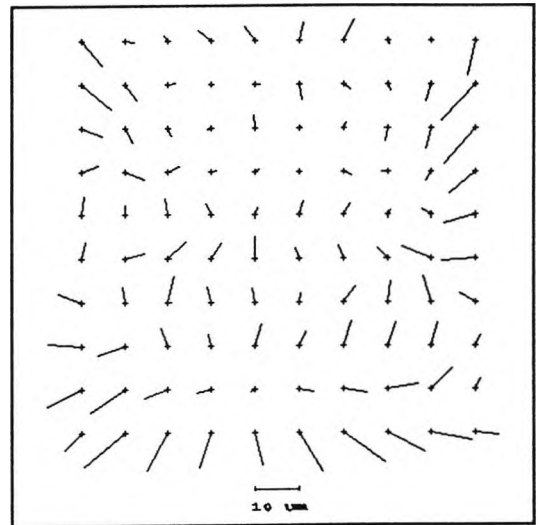
Frame 16



Frame 17

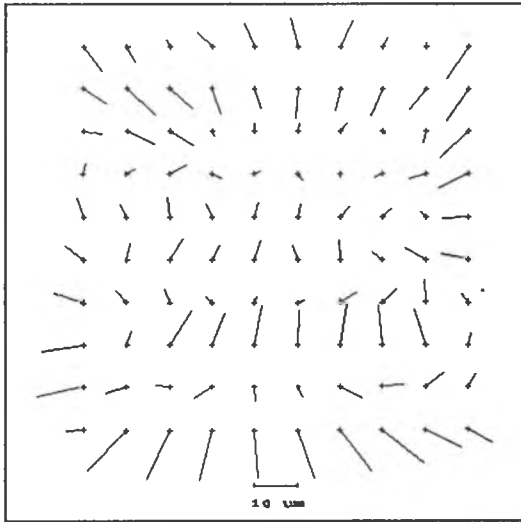


Frame 18

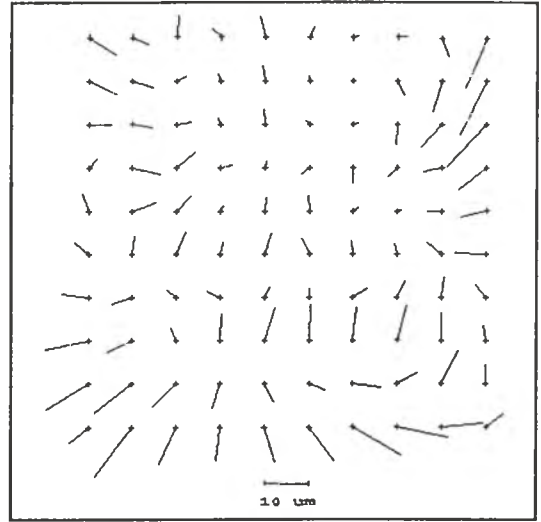


Exposures made using Modified Hasselblad SWC Camera (HS2)
onto Ilford FP4 220 Film (C).

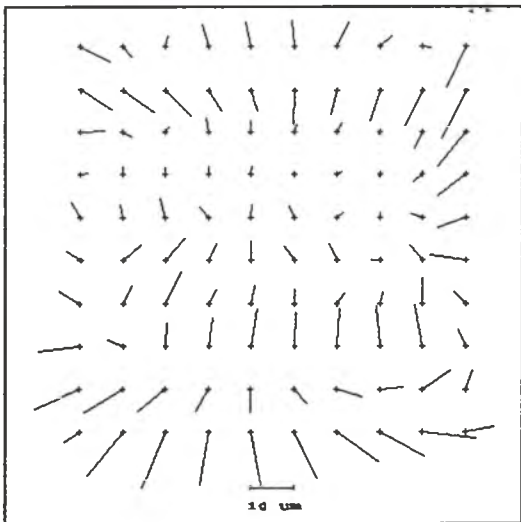
Frame 19, (Bundle 003).



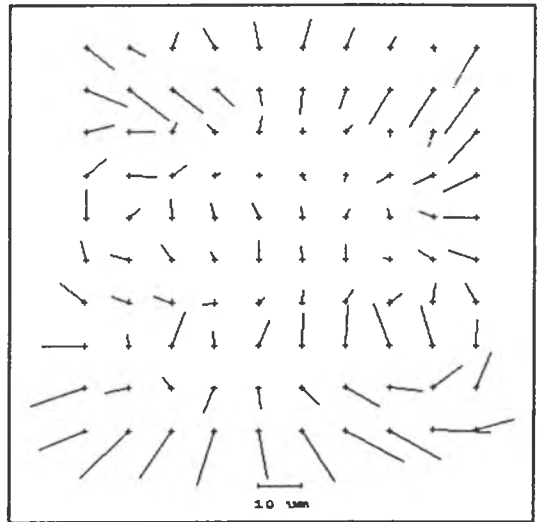
Frame 20



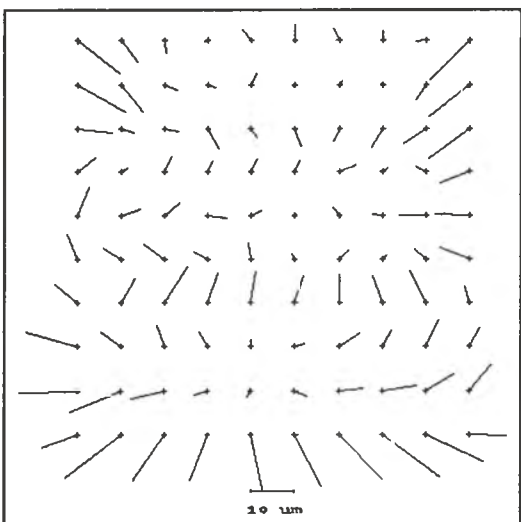
Frame 21, (Bundle 031).



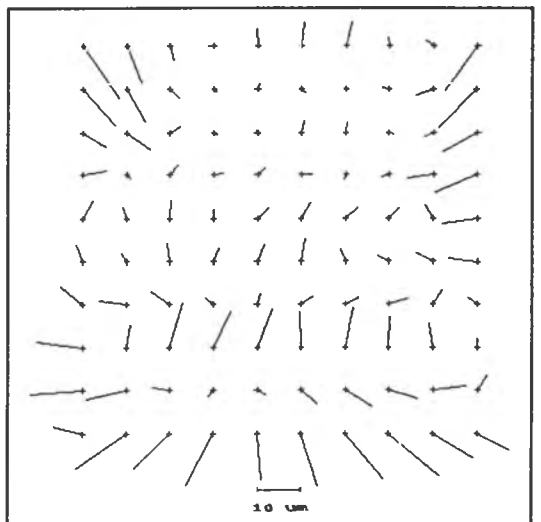
Frame 22



Frame 23



Frame 24



Object space coordinates and their associated standard deviations,
 Estimated from measurements carried out during a student project (Godfrey (1989))

Target	X(m)	Y(m)	Z(m)	σ_x (m)	σ_y (m)	σ_z (m)
11	99.7291	110.8822	6.0703	0.0009	0.0020	0.0009
102	99.7295	110.7295	6.0897	0.0006	0.0016	0.0010
12	99.3121	110.4720	6.0761	0.0009	0.0018	0.0009
13	100.7643	109.4569	6.0768	0.0004	0.0015	0.0009
14	101.7881	108.7360	6.0824	0.0008	0.0012	0.0009
15	102.8311	108.0006	6.0786	0.0008	0.0013	0.0009
21	99.3151	110.4761	5.3205	0.0006	0.0019	0.0009
22	100.1415	109.8909	5.3268	0.0006	0.0016	0.0010
23	101.3668	109.0326	5.2979	0.0005	0.0014	0.0017
24	102.2107	108.4453	5.2904	0.0007	0.0011	0.0009
31	98.7358	110.8802	4.8516	0.0008	0.0020	0.0009
32	99.7320	110.1762	4.8080	0.0006	0.0016	0.0009
33	100.7634	109.4556	4.7770	0.0003	0.0015	0.0009
34	101.7805	108.7397	4.8019	0.0004	0.0011	0.0009
35	102.8094	108.0127	4.7664	0.0008	0.0012	0.0009
41	99.3278	110.4625	4.3269	0.0006	0.0019	0.0009
42	100.1386	109.8905	4.3139	0.0004	0.0018	0.0009
43	101.3662	109.0306	4.2960	0.0003	0.0014	0.0010
44	102.1846	108.4505	4.2812	0.0006	0.0013	0.0009
51	98.7201	110.8854	3.6011	0.0008	0.0020	0.0011
52	99.7274	110.1771	3.5719	0.0006	0.0017	0.0009
53	100.7702	109.4514	3.5460	Fixed	Fixed	Fixed
54	101.7625	108.7313	3.5337	0.0004	0.0010	0.0009
55	102.8006	108.0211	3.5235	0.0005	0.0003	0.0010
61	99.3244	110.4655	2.8184	0.0006	0.0017	0.0009
62	100.1488	109.8824	2.8161	0.0004	0.0016	0.0016
63	101.3806	109.0182	2.7891	0.0003	0.0013	0.0014
64	102.1937	108.4465	2.7812	0.0006	0.0011	0.0009
71	98.7292	110.8849	2.3615	0.0008	0.0021	0.0009
72	99.7439	110.1726	2.3179	0.0005	0.0016	0.0009
73	100.7622	109.4596	2.3091	0.0003	0.0013	0.0009
74	101.7891	108.7360	2.2962	0.0004	0.0010	0.0009
75	102.8114	108.0193	2.2709	0.0007	0.0010	0.0009
81	99.3371	110.4567	1.8229	0.0006	0.0017	0.0008

Target	X(m)	Y(m)	Z(m)	$\sigma_x(m)$	$\sigma_y(m)$	$\sigma_z(m)$
82	100.1519	109.8831	1.8036	0.0004	0.0015	0.0010
83	101.3784	109.0213	1.8077	0.0002	0.0010	0.0009
84	102.1958	108.4501	1.7859	0.0005	0.0009	0.0009
91	98.7332	110.8818	1.1007	0.0008	0.0019	0.0009
92	99.7453	110.1742	1.0740	0.0005	0.0015	0.0015
93	100.7656	109.4569	1.0528	0.0003	0.0012	0.0009
94	101.7855	108.7398	1.0490	0.0004	0.0009	0.0009
95	102.8131	108.0230	1.0403	0.0007	0.0008	0.0009

$$\sigma_0^2 = 0.839.$$

References and Bibliography.

- ABDEL-AZIZ, Y.I. (1974). Expected Accuracy and Convergent Photographs, Photogrammetric Engineering and Remote Sensing 40(11): 1341-1346.
- ABDEL-AZIZ, Y.I. (1975). Film Distortion in Non Metric Cameras, Photogrammetric Engineering and Remote Sensing 41(5): 613-615.
- ABDEL-AZIZ, Y.I. (1979). An Application of Photogrammetric Techniques to Building Construction. Photogrammetric Engineering and Remote Sensing 45(4): 539-544.
- ABDEL-AZIZ, Y.I. (1980). The Use of Non-Metric Cameras in Short Range Photogrammetry, PHOTOGRAMMETRIA 36(2): 51-60.
- ABDEL-AZIZ, Y.I. (1982). Accuracy of the Normal Case of Close Range Photogrammetry, Photogrammetric Engineering and Remote Sensing 48(2): 207-213.
- ABDEL-AZIZ, Y.I. (1984). The Accuracy of Control Points for Close Range Photogrammetry. International Archives of Photogrammetry and Remote Sensing 24(5): 1-10.
- ADAMS, L.P. (1980). The Use of Non-Metric Cameras in Short Range Photogrammetry, International Archives of Photogrammetry and Remote Sensing 23(5): 1-8
- ADELSTEIN, P.Z. and LEISTER, D.A. (1963). Nonuniform Dimensional Changes in Topographic Aerial Films, Photogrammetric Engineering 29 (1): 149-161.
- ADELSTEIN, P.Z, JOSEPHSON, P.R. and LEISTER, D.A. (1966). Nonuniform Film Deformational Changes, Photogrammetric Engineering 32(9): 1028-1034.
- ADELSTEIN, P.Z. (1972). Dimensional Stability of Estar Based Films, Photogrammetric Engineering 18(1): 55-64.
- ADELSTEIN, P.Z. and McCREA, J.L. (1981). Stability of Processed Polyester Base Photographic Films, Applied Photographic Engineering 7(6): 160-167.
- ALBERTZ, J. and KREILING, J. (1975). Photogrammetric Guide. (Karlsruhe: Herbert Wichmann Verlag), 284pp.
- AGFA (1980). Agfa Aviphot Pan-200 PE film, Technical Information. Publication No. B2510. Morsel, Belgium.
- AGFA (1989). Agfa Holotest Materials, Agfa-Gevaert, Publication No. NDT1286/2012, Morsel, Belgium.
- ARJANOV, E.P. (1972). An Investigation of Film Flattening, International Archives of Photogrammetry and Remote Sensing 12(1): 12pp.
- ARNOLD, C.R., ROLLS, P.J. and STEWART, J.C.J. (1971). Applied Photography, (London: Focal Press), 510pp.
- BAARDA, W. (1976). Reliability and Precision of Networks, Presented paper to 7th International Course for Engineering Surveys of High Precision, Dorm Stadt.
- BAINES, H. and BOMBACK, E.S. (1976). The Science of Photography, 3rd Edition, England: Fountain Press), 246pp.
- BAUER, H. and MULLER, J. (1972). Height accuracy of blocks and bundle adjustment with additional parameters. Presented paper at the XIIIth Congress of the International Society for Photogrammetry, Ottawa.

- BENDER, L.U. (1972). Film Deformation Investigation, Photogrammetric Engineering 38 (3): 256-259.
- BOBERG, A. (1988). A Survey of Aerial Image Quality Assessment Methods, International Archives of Photogrammetry and Remote Sensing 27(1): 144-154.
- BOPP, H. and KRAUSS, H. (1978). An Orientation and Calibration Method for Non Topographic Applications, Photogrammetric Engineering and Remote Sensing 44(9): 1191-1196.
- BOYDJ, E. (1982). Digital Image Film Generation :- From the Photoscientists Perspective, Applied Photographic Engineering 8(1): 15-22.
- BRANCH, P.W, CLARK, E.R and MILTON, R.G. (1968). A Survey of Film Flatness in No. 126 Cartridges, Photographic Science and Engineering 12(6): 301-307.
- BROCK, G.C. (1968). The Limitations of Resolving Power as a Measure of Image Quality in Aerial Photography, Photogrammetric Record 31: 32-38.
- BROCK, G.C. (1970). Image Evaluation for Aerial Photography, Focal Press. 275pp.
- BROCK, R.H. (1972). Methods for Studying Film Deformation, Photogrammetric Engineering 38(4): 399-405.
- BROWN, D.C. (1958). A Solution to the Central Problem of Multiple Station Analytical Stereo-triangulation, RCS TR43, Patrick Airforce Base FLORIDA.
- BROWN, D.C. (1966). Decentring Distortion of Lenses, Photogrammetric Engineering 32(3): 444-462.
- BROWN, D.C. (1971). Close Range Camera Calibration, Photogrammetric Engineering and Remote Sensing 37(8): 855-866.
- BROWN, D.C. (1972). Calibration of Close Range Cameras, International Archives of Photogrammetry 19(5): 25pp.
- BROWN, D.C. (1974). Evolution, Application and Potential of the Bundle Method of Photogrammetric Triangulation, International Archives of Photogrammetry and Remote Sensing 20(3): 12pp.
- BROWN, D.C. (1976). The Bundle Adjustment- Progress and Prospects. International Archives of Photogrammetry 21 (3): 303-333.
- BROWN, D.C. (1980). Application of Close Range Photogrammetry to Measurements of Structures in Orbit, Geodetic Services Inc, Florida, 1: 31pp.
- BROWN, D.C. (1982). STARS a Turnkey System for Close Range Photogrammetry, International Archives of Photogrammetry and Remote Sensing 24 (1): 68-87.
- BROWN, D.C. (1984). A Large Format, Microprocessor Controlled Film Camera Optimised for Industrial Photogrammetry, International Archives of Photogrammetry and Remote Sensing 25(5) 29pp.
- BROWN, D.C. (1986). Unflatness of Plates as a Systematic Error in Close Range Photogrammetry, Photogrammetria 40(4): 343-363.
- BUJAKIEWICZ, A. (1976). The Correction of Lens Distortion with Polynomials, The Canadian Surveyor 30(2): 67-76.

- BURNHAM, J.M. and JOSEPHSON, P.R. (1969). Colour Plate Metric Stability, Photogrammetric Engineering 35(7): 679-685.
- BURCH, J.M. and FORNO, C. (1982). Preliminary Assessment of a New High Precision Camera, International Archives of Photogrammetry and Remote Sensing 24(5): 90-99.
- BURCH, J.M. and FORNO, C. (1982). High Resolution Moire Photography, Optical Engineering 21 (4): 602-614.
- BYER, R.J. (1983). Dimensional Stability Measurement of Photographic Film, Applied Photographic Engineering 9 (5): 135-138.
- CALHOUN, J.M, KELLER, L.E. and NEWELL, R.F. (1960). A method for studying possible local distortions in aerial films, Photogrammetric Engineering 26(4): 661-672.
- CARMAN, P.D. (1946). Dimensional Changes in Safety Topographic Base Aerial Films under Service Conditions, Canadian Journal of Research 24: 509-517.
- CARMAN, P.D. and MARTIN, J.F. (1969). Causes of Dimensional Changes in Estar Base Aerial Film under Simulated Service Conditions, The Canadian Surveyor 22(2): 238-246.
- CARMAN, P.D. and JOHNSON, S.F. (1980). Effects of Ambient Conditions on Film Sensitometry, The Canadian Surveyor 34(2): 131-138.
- CARMAN, P.D. (1982a). Sensitometry in Canadian Aerial Survey, Photogrammetric Engineering and Remote Sensing 48(5): 785-791.
- CARMAN, P.D. (1982b). Aerial Camera Vibration, Photogrammetric Engineering and Remote Sensing 48(12): 1845-1856.
- CARROLL, B.H. (1980). Iridium Sensitisation - A Literature Review, Photographic Science and Engineering 24: 10pp.
- CHANDLER, J.H. and COOPER, M.A.R. (1987). Analytical Photogrammetry applied to Nepalese Slope Morphology, Photogrammetric Record 12 (70): 443-459.
- CHANDLER, J.H. & COOPER, M.A.R. (1988). Monitoring the Development of Landslides using Archival Photography and Analytical Photogrammetry, Land and Minerals Surveying 6: 576-584.
- CHANDLER, J.H. & COOPER, M.A.R. (1989a). The Extraction of Positional Data from Historical Photographs and their Application in Geomorphology, Photogrammetric Record 13 (73): 69-78.
- CHANDLER, J.H., COOPER, M.A.R. & ROBSON, S. (1989b). Analytical Aspects of Small Format Surveys using Oblique Aerial Surveys, Journal of Photographic Science 37: 235-239.
- CHANDLER, J.H. (1989). The Extraction of Spatial Data from Archival Photographs and their Application to Geomorphology, PhD Thesis, City University, London.
- CHATFIELD, C. (1975). The Analysis of Time Series, Theory and Practice. Chapman and Hall, pp263.
- CHEFFINS, O.W. (1982). Further Photogrammetric Measurements of a Thin Base Aerial Film, Photogrammetric Record 10 (59): 587-589.
- CHEN, Y.Q., KAVOURAS, M. and CHRZANOWSKI, A. (1987). A Strategy for Detection of Outlying Observations in Measurements of High Precision, The Canadian Surveyor 41(4): 529-540.

- CLARK, E. R. (1968). Two Methods for Measuring Photographic Film Flatness, Photographic Science and Engineering 12 (6): 295-300.
- CLARK, J.M.T. (1972). Film Flatness in Survey Cameras, Photogrammetric Engineering 38(3): 277-284.
- COLTON, E.K. and WIEGAND, E.J. (1958). Moisture in Photographic Film and its Measurement, Photographic Science and Engineering 13: 170-176.
- CONRADY, A. (1919). Decentred Lens Systems, Monthly Notices of the Royal Astronomical Society 79: 380-390.
- CONTAX. (1990). Contax RTS III, the new professional standard in the non auto-focus SLR range. Press release, Photokina 90. 3pp.
- COOPER, M.A.R. (1980). An Introduction to Photogrammetry - Functional and stochastic modelling, Nelex 80 7 (8): 16pp.
- COOPER, M.A.R. (1984). Deformation Measurement by Photogrammetry. Photogrammetric Record 11 (63): 291-301.
- COOPER, M.A.R. (1987). Control surveys in civil engineering. (London: Collins), 381pp.
- COOPER, M.A.R. (1988). Degrees of freedom of Analytical Photogrammetry in Engineering, Paper presented at Institution of Civil Engineering Surveyors, Conference on Standards and Accuracies, University of Reading 28th to 29th March 1988.
- COOPER, M.A.R. and CROSS, P.A. (1988). Statistical Concepts and their Application in Photogrammetry and Surveying, Photogrammetric Record 12(71): 637-663.
- COOPER, M.A.R. and CROSS, P.A. (1990). Statistical Concepts and their Application in Photogrammetry and Surveying (continued), Photogrammetric Record 15(77): In Press.
- COOPER, M.A.R. and ROBSON, S. (1990). Methods for High Precision Photogrammetric Monitoring of the Deformation of a Steel Bridge, The Photogrammetric Record, 13:(76) 505-510.
- COX, R.J. (1977). Photographic Gelatin, Academic Press. 309pp.
- DAINTY, J.C. and SHAW, R. (1974). Image Science, Academic Press, London 401pp.
- DAUTRICH, D, GRANZER, F. and MOISER, E. (1973). Electron Microscope Investigation of the Effects of Dynamic Pressure on Photographic Emulsions, Photographic Science 21: 221.
- DOLD, J. (1990). A Large Format Film Camera for High Precision Object Recording, International Archives of Photogrammetry 28(5): 252-255.
- DUFFIN, G.F. (1966) Photographic Emulsion Chemistry, Focal Press London 62pp.
- DYSON, J. (1970) Interferometry as a Measuring Tool. The Machine Publishing Co Ltd. Brighton. 206pp.
- EBNER, H. (1976) Self-Calibrating Block Adjustment. Bildmessung und uftbildwesen 44(4): 128-139.
- EL-HAKIM, S.F. and FAIG, W. (1977). Compensation of Systematic Image Errors Using Spherical Harmonics, International Archives of Photogrammetry 28(3): 492-499.

- EL-HAKIM, S.F. and FAIG, W. (1979). Combined Geodetic and Photogrammetric Adjustment for Densification of Control Networks, Proceedings of American Society for Photogrammetry, 45th Annual Meeting, Washington, 582-590.
- EL-HAKIM, S.F. and ZIEMANN, H. (1984). A Step by Step Strategy for Gross Error Detection, Photogrammetric Engineering and Remote Sensing 50(6): 713-718.
- EL-HAKIM, S.F. (1985). Photogrammetric Measurement of Microwave Antennae, Photogrammetric Engineering and Remote Sensing 51(10): 1577-1587.
- EL-HAKIM, S.F. (1986). The Detection of Gross and Systematic Errors in the Combined Adjustment of Terrestrial and Photogrammetric Data, Photogrammetric Engineering and Remote Sensing 52(1): 59-66.
- EL-HAKIM, S. F. (1986). Real Time Image Metrology with CCD Cameras, Photogrammetric Engineering and Remote Sensing 52(11): 1757-1766.
- FAELENS, P.J. (1954). The Mechanism of the Photographic Pressure Effect and its Relation to Latent Image Formation, Photographic Science 2: 105.
- FALHBUSH, H. (1990) Verbal communication at AV distributors, Islington, London.
- FAIG, W. (1975). Calibration of Close Range Photogrammetric Systems. Photogrammetric Engineering and Remote Sensing 41(12): 1479-1486.
- FAIG, W. (1976): Photogrammetric Potentials of Non Metric Cameras, Photogrammetric Engineering and Remote Sensing 41 (12): 47-49.
- FAIG, W. and EL-HAKIM, S.F. (1982). The Use of Distances as Object Space Control in Close Range Photogrammetry, International Archives of Photogrammetry and Remote Sensing 24(1): 144-148.
- FAIG (1989) Non-Metric and Semi-Metric Cameras: Data Reduction. Chapter 6, The Handbook of Non-Topographic Photogrammetry. 2nd Edition, Pub. American Society of Photogrammetry and Remote Sensing. Falls Church USA.
- FARNELL, G.C. and CHANTER, J.B. (1968). The Quantum Sensitivity of Photographic Emulsion Grains, Photographic Science 9: 73-83.
- FARNELL, G.C., FLINT, R.B. and CODLING, A.J.B. (1982). Effects of Deformation on the Properties of Emulsion Grains, Photographic Science 30: 109-118.
- FORNO, C. (1980). Film Characteristics in High Resolution Moiré Photography, Optical Engineering 19(6): 908-910.
- FORNO, C. and KEARNEY, A. (1987). The Effects of Humidity on the Profile of Photographic Plates, Division of Mechanical and Optical Metrology, National Physical Laboratory, Teddington. 13pp.
- FORSTNER, W. (1980). The Theoretical Reliability of Photogrammetric Coordinates, International Archives of Photogrammetry and Remote Sensing 14(3): 223-235.
- FORSTNER, W. (1985). The Reliability of Block Triangulation, Photogrammetric Engineering and Remote Sensing 51(8): 1137-1149.
- FRASER, C.S. (1980). Multiple Focal Setting Self Calibration of Close Range Photogrammetric Cameras. 9 sept 1980, 1161.

- FRASER, C.S. (1982a). Film Unflatness Effects in Analytical Non-Metric Photogrammetry, International Archives of Photogrammetry and Remote Sensing 24(V/1): 156.
- FRASER, C.S. (1982b). On the use of Non-Metric Cameras in Close Range Photogrammetry. Canadian Surveyor 36(3): 259-279.
- FRASER, C.S. (1984a). Network Design for Close Range Photogrammetry, Photogrammetric Engineering and Remote Sensing 50(8): 1115-1126.
- FRASER, C.S. (1984b). Multiple Exposures in Non-Metric Camera Applications, International Archives of Photogrammetry and Remote Sensing 25(5): 232-239.
- FRASER, C.S. (1984c). The Analysis of Photogrammetric Deformation Measurements on Turtle Mountain, Photogrammetric Engineering and Remote Sensing 51(2): 207-216.
- FRASER, C.S. (1985). Photogrammetric Measurement of Thermal Deformation of a Large Process Compressor. Photogrammetric Engineering and Remote Sensing 51(10): 1569-1581.
- FRASER, C.S. (1986a). State of the Art in Industrial Photogrammetry, International Archives of Photogrammetry and Remote Sensing 27(5): 166-181.
- FRASER, C.S. (1986b). Microwave Antenna Measurement, Photogrammetric Engineering and Remote Sensing 52(10): 1627-1635.
- FRASER, C.S. (1989). Optimisation of Networks in Non-Topographic Photogrammetry, Chapter 8 in the Handbook of Non-Topographic Photogrammetry (ed Karara). Pub. American Society of Photogrammetry and Remote Sensing, Falls Church, USA.
- FRASER, C.S. (1990). Verbal communication at Close Range Photogrammetry meets Machine Vision, Zurich 1990.
- FRASER, C.S. and BROWN, D.C. (1986). Industrial Photogrammetry. New Developments and Recent Applications, Photogrammetric Record 12(68): 197-217.
- FRASER, C.S. and SHORTIS, M. (1990). A Correction Model for Variation of Distortion within the Photographic Field. International Archives of Photogrammetry and Remote Sensing 28(5): 244-251.
- FRYER, J. and BROWN, (1986). Lens Distortion for Close Range Photogrammetry, International Archives of Photogrammetry and Remote Sensing 26(5): 30-37.
- FRYER, J. (1987). Lens Distortion The Forgotten Component of Digital Photogrammetry, Presented at Department Civil Engineering, University of Newcastle Australia. 117-129.
- FRYER, J. (1988). Lens Distortion and Film Flattening: their Effect on Small Format Photogrammetry, International Archives of Photogrammetry and Remote Sensing 27(5): 194-202.
- GARAFAREND, E.W. and SCHRAFFRIN, B. (1974). Unbiased Free Net Adjustment, Survey Review 22(171): 200-218.
- GATES, J.W.C., OLDFIELD, S., FORNO, C., SCOTT, P.J. and KYLE, S.A. (1982). Factors Defining Precision in Close Range Photogrammetry, International Archives of Photogrammetry and Remote Sensing 24(5): 185-195.
- GERENCSEK, M.C. (1972). Microdensity and MTF. Comparative MTF test of the entire aerial Photogrammetric System in Black and White and Colour, Presented Paper International Society of Photogrammetry 19(1): 20pp.

- GHOSH, S.K. and MARTUCCI, L.M. (1972). Image Quality Effects on Image Geometry. International Archives of Photogrammetry 19(1): 11pp.
- GHOSH, S.K, RAHIMI, M. and SHI, Z. (1988). Calibration of an Amateur Camera for Various Object Distances, International Archives of Photogrammetry and Remote Sensing 27(5): 213-222.
- GODFREY, C. (1989). Construction of a Test Field for Investigating Camera Film Deformation. Final Year BSc Project. City University. 97pp.
- GRANSHAW, S.I. (1980). Bundle Adjustment Methods in Engineering Photogrammetry, Photogrammetric Record 10(56): 181-208.
- GRANSHAW, S.I. (1982). Precision and the Multistation Bundle Method, Concepts and Preconceptions, International Archives of Photogrammetry 24 (1): 235-244.
- GRÜN, A. (1978). Accuracy, Reliability and Statistics in Close Range Photogrammetry, International Archives of Photogrammetry and Remote Sensing Stockholm (V) unbound paper 24pp.
- GRÜN, A. (1982). The Accuracy Potential of the Modern Bundle Block Adjustment in Aerial Photogrammetry, Photogrammetric Engineering and Remote Sensing 48(1): 45-54.
- GRÜN, A. (1988). Digital photogrammetric processing systems - current status and prospects, International Archives of Photogrammetry and Remote Sensing 27(2): 342-351.
- GUSTAFSON, P.C. (1988). The Application of Real Time and Near Real-Time Photogrammetry in Industry: A Test of Accuracy. International Archives of Photogrammetry and Remote Sensing 27(5): 198-205.
- HALLERT, (1964). Determination of the Flatness of a Surface in Comparison with a Control Plane. 15 256.
- HALONEN, R.S. and SAVOLAINEN, A. (1968). On the Deformation of Polyester Film, Pub. Technical University of Helsinki, Otaniemi, Finland. 14pp.
- HAKKARAINEN, J. and SCHROEDER, M. (1988). The Effect of Forward Motion Compensation (FMC) on Resolving Power of Aerial Photographs, International Archives of Photogrammetry and Remote Sensing 27(1): 169-183.
- HARDY, R.L. (1977). Least squares prediction. Photogrammetric Engineering 43(4): 475-492.
- HARMAN, W.E.I. (1984). Negative Quality Required for Stereo Plotting Instruments, Photogrammetric Engineering and Remote Sensing 25(1): 365-371.
- HASSELBLAD (1989). Hasselblad Engineering Documentation, Gotenborg, Sweden.
- HAUG, G. (1976). Analysis and Reduction of Systematic Image and Model Deformations of the Aerial Triangulation Test "Oberschwaben" OEEPE, International Archives of Photogrammetry and Remote Sensing 21(3): 12pp.
- HERMANS, T. and VRIELYNK, M. (1982). Static Pressure Effects on Photographic Materials Part 1, Photographic Science 30: 13.
- HERMANS, T. and VRIELYNCK, H. (1983). Static Pressure Effects on Photographic Materials Part 2, Photographic Science 31: 238.
- HIGGINS, G.C. and PERRIN, F.H. (1959). Modulation Transfer Function. Photographic Science 2(2): 66-76.

- HORN, J.A. and TUGWOOD, J.M. (1984). Optimising Exposure and Processing for Aerial photography, ITC Journal 1984(3): 206-212.
- HOTTIER, P.H. (1976). Accuracy of Close Range Analytical Restitutions, Practical Experiments and Prediction, Photogrammetric Engineering 42(3): 345-375.
- ILFORD (1982). Ilford FP3 Aerial Film. Published by Ilford Ltd, London. 82.75.2.GB. 12pp.
- ILFORD (1991a). Ilford FP4 Plus. Ilford Ltd, London. 40101/4
- ILFORD (1991b). Ilford 400 Delta. Ilford Ltd, London. 39204/4.
- ILFORD (1991c). Ilford Product Information Catalogue, Ilford Ltd, London. 60pp.
- INTERGRAPH (1987). Intermap Analytic Photogrammetric Workstation, Intergraph Corp. Alabama USA. 7pp.
- ISO (1974). Speed of sensitised photographic emulsions, International Standards Organisation, 6.1974.
- JACOBSEN, K. (1982). Selection of Additional Parameters by Program, International Archives of Photogrammetry and Remote Sensing 24(5): 266-275.
- JACOBSON, K.I. and JACOBSON, R.E. (1980). Developing. 18th Edition, (New York: Focal Press). 422pp.
- JACOBSON, R.E. (1985). Photographic Science Lecture Notes, BSc Photographic Sciences Course, The Polytechnic of Central London.
- JACOBSON, R.E., AXFORD, N.R., JONES, I.A. and FORD, A. (1990). Image Quality and Extended Development of Tabular Grain and Conventional Photographic Emulsions, Photographic Science 38 Proceedings Issue: 140-142.
- JACOBSON, R.E., RAY, S.F., ATTRIDGE, G.G. and AXFORD, N.B. (1983). The Manual of Photography. 7th Edition, (London: Focal Press). 628pp.
- JAMES, T.H. (1966). The Theory of the Photographic Process, 4th Edition (N.York: Macmillan) 714pp.
- JAKSIC, Z. (1972). Deformations of Estar Based Aerial Films, Photogrammetric Engineering 38(3): 285-296.
- JI-YONG, W., and CHENGLIN, Z. (1988). Multi Plate, Multi Exposure and Multi Free Exterior Orientation Stellar Calibration for Metric Camera, International Archives of Photogrammetry 27(5): 181-189.
- JERIE, H.G. (1973). Development of a Computer Simulation System Concerning the Accuracy of Photogrammetric Operations, ITC Journal 1973(4): 73-90.
- KARARA, H.M. & ABDEL AZIZ, Y. (1974). Accuracy Aspects of Non-Metric Imageries. Photogrammetric Engineering and Remote Sensing 40(4): 1107-1117.
- KARARA, H.M. (1985). Close Range Photogrammetry, Where We are and Where We are Heading, Photogrammetric Engineering and Remote Sensing 51(5): 537-544.
- KARARA, H.M. (1989). The Handbook of Non Topographic Photogrammetry. 2nd Edition, American Society of Photogrammetry and Remote Sensing, Falls Church USA. 445pp.

- KARREN, R.J. (1968). Camera Calibration by the Multicollimator Method, Photogrammetric Engineering and Remote Sensing 34(7): 706-719.
- KEARNEY, A. and FORNO, C. (1987). The Mechanical Properties of Card Measured by Photographic Moiré, National Physical Laboratory Report ISSN 0309-3069.
- KENEFICK, J.F. (1971). Ultra Precise Analytics, Photogrammetric Engineering and Remote Sensing 37(11): 1167-1187.
- KENEFICK, J.F, GYER, M.S. & HARP, B.F., (1972) Analytical Self Calibration. Photogrammetric Engineering and Remote Sensing 38(11): 1117-1126.
- KILPELA, E. (1980) Compensation of Systematic Errors of Image and Model Coordinates, International Archives of Photogrammetry and Remote Sensing 13(9): 409-427.
- KING, R. and ASHLING, D. (1985) Mechanisms of Pressure Sensitivity Effects in a Model Halide Exchange, Journal of Photographic Science 33: 127.
- KODAK (1970a). Dimensional Stability of Kodak Acetate Films for the Graphic Arts, Eastman Kodak Publication Q33, Rochester N.York. 3pp.
- KODAK (1970b). Dimensional Stability of Kodak Estar Based Films for the Graphic Arts, Eastman Kodak Publication Q34, Rochester N.York. 15pp.
- KODAK (1972). Physical Properties of Kodak Aerial Films, Eastman Kodak Publication M62, Rochester N.York. 32pp.
- KODAK (1975). Physical Characteristics of Glass for Kodak Photographic Plates, Eastman Kodak Publication Q35, Rochester N.York.
- KODAK (1982). Characteristics of Kodak Plates for Scientific and Technical Applications, Eastman Kodak Publication, Rochester N.York.
- KODAK (1984). Kodak Professional Data Guide. Kodak Ltd, London. ISBN 0 901023 502.
- KODAK (1987a). Kodak T-MAX Professional Films, Kodak Ltd Publication F-25(H). 16pp.
- KODAK (1987b). Kodak Technical Pan Films, Kodak Ltd Publication P-255. 7-87-BX. 12pp.
- KODAK (1987c). Kodak TRI-X Film, Kodak Ltd Publication F916(H). 8pp.
- KODAK (1988a). Kodak HC110 Developer. Kodak Publication GH3(H). 4pp.
- KODAK (1988b). Videk Megaplus camera, Press release, Kodak Ltd, Hemmel Hempstead, England. 6pp.
- KODAK (1989). Storage and Care of Kodak Films and Papers before and after Processing. Eastman Kodak Publication E-30, Rochester N.York. 11pp.
- KODAK (1990). Kodak Product Catalogue, Kodak Ltd. Harrow.
- KONDO, H., IMAZEKI, H. and TSURUTA, T. (1983). Measurement of Image Blur due to Intrinsic Vibration of the Camera Body by Applying Speckle Photography, Applied Photographic Engineering 9: 138 to 142.
- KOPPERL, D.F, Goetting, R.R. and Huttemann, T.J. (1988). Use of Arrhenius testing to determine thiosulphate tolerance in silver halide black and white materials. Journal of Photographic Science 36(2): 40-42.

- KOWALISKI, P. (1960). Experiments on the Effects of Film Kinking, Photographic Science 14: 282-290.
- KRATKY, V. (1971). Image Transformations, Photogrammetric Engineering 38(5): 463-471.
- KRAKTY, V. (1976). Analytical On-line Systems in Close Range Photogrammetry. Photogrammetric Engineering and Remote Sensing 42(1):81-90.
- KRAUS, K. (1972). Film Deformation Correction with Least Squares Interpolation. Photogrammetric Engineering 38(5): 487-493.
- KRAUS, K. and MIKHAIL, E.M. (1972). Linear Least Squares Interpolation, Photogrammetric Engineering and Remote Sensing 38(10): 1016-1029.
- KUBIK, K. and BOTMAN, A.G. (1976). Interpolation Accuracy for Topographic and Geological Surfaces. International Society for Photogrammetry 21(3):36pp.
- KUPFER, G. (1976). Partial Calibration of Photogrammetric Systems Including Reseau Cameras, Using a flat test field area, International Archives of Photogrammetry 21(1): 21-.
- LAMBERTS, R.L. (1958). Modulation Transfer Function, Journal of Optical Society of America 49: 420-425.
- LAMPTON, B.F. and UMBACH, M.J. (1966). Film Distortion Compensation Effectiveness, Photogrammetric Engineering 32: 1035-1040.
- LANGFORD, M.J. (1982). Basic Photography. 4th Edition, (London: Focal Press) 397pp.
- LANGFORD, M.J. (1983). Advanced Photography. 4th Edition, (London: Focal Press) 355pp.
- LAIHO, A. and KILPELA, E. (1988). Stability Testing of Analytical Plotters, International Archives of Photogrammetry and Remote Sensing 27(2): 280-289.
- LAWRENCE, W.F. and SCHMID, H.H. (1974). Stellar Calibration of the Orbigon Lens, Photogrammetric Engineering and Remote Sensing 40(2): 101-115.
- LIGTERINK, G.H. (1972). Film-Glass Differences, Photogrammetric Engineering 38(2): 269-273.
- LEBERL, F. (1975). Photogrammetric Interpolation, Photogrammetric Engineering and Remote Sensing 41(5): 603-612.
- LUHMANN, T. and PEIPE, J. (1988). Reseau Scanner Rolleimetric RS1 - Close Range Applications, International Archives of Photogrammetry and Remote Sensing 27(5): 224-233.
- LUHMANN, T. and WESTER-EBBINGHAUS, W. (1986). Rolleimetric RS - a New Digital Image Processing System, International Archives of Photogrammetry and Remote Sensing 26(2): 110-119.
- MAGILL, (1955). Variation in Distortion with Magnification, Journal of Research of the National Bureau of Standards 54(3): 135-142.
- MASON, L.F.A. (1975). Photographic Processing Chemistry, (London: Focal Press) 326pp.
- MEIER, H.K. (1972). Film Flattening in Aerial Cameras, Photogrammetric Engineering 38(4): 367-372.
- MEIER, H.K. (1978). The Effects of Environmental Conditions on the Distortion, Calibrated Focal Length and Focus of Aerial Survey Cameras, International Archives of Photogrammetry and Remote Sensing 22(1): 9pp.

- MICHENER, B.C. (1972). Thickness Uniformity of Kodak Aerial Films, Photogrammetric Engineering 38(2): 192-196.
- MIKHAIL, E.M. (1970). Parameter Constraints in Least Squares, Photogrammetric Engineering and Remote Sensing 36(12): 1277-1291.
- MIKHAIL, E.M. (1976). Observations and Least Squares. (N.York: IEP-Dun-Donnelly) 497pp.
- MITCHELL, H.L. and PILGRIM, L.J. (1987). Selection of an Image Matching Algorithm, Department of Civil Engineering and Surveying, University of Newcastle New South Wales. 2308.
- MURAI, S, MATSUOKA, R. and OKUDA, T. (1984). A Study on Analytical Calibration for Non Metric Cameras and the Accuracy of 3D Measurement. International Archives of Photogrammetry and Remote Sensing 25(5): 570-579.
- MUNJY, R.A.H. (1986). Self Calibration using a Finite Element Approach, Photogrammetric Engineering and Remote Sensing 52(3): 411-418.
- NORTON, C.L. (1980). Image Properties with Environmental Factors (Report of Working Group I/3), International Archives of Photogrammetry and Remote Sensing 14(1): 71-87.
- NORTON, C.L. (1980b). Image Properties with Environmental Factors, Photogrammetric Engineering and Remote Sensing 46(6): 725-737.
- OLDFIELD, S. (1986). Photogrammetric Plate Measuring Facilities at NPL, International Archives of Photogrammetry and Remote Sensing 26(5): 541-545.
- OLDFIELD, S. (1990). Verbal communication at NPL, Teddington.
- PAPO, H.B. (1982). Free Net Analysis in Close Range Photogrammetry, Photogrammetric Engineering and Remote Sensing 48(4): 571-576.
- PAPO, H.B. (1985). Deformation Analysis by Close Range Photogrammetry, Photogrammetric Engineering and Remote Sensing 51(10): 1567-1575.
- PELZER, H. (1979). Criteria for the Reliability of Geodetic Networks, In Optimisation of the Design and Computation of Control Networks, (Ed. Halmos, F. and Somogyi, J.) Akademiai Kiado, Budapest. 553-562.
- PERSSON, C.G. (1981). On the Estimation of Variance Components in Linear Models and Related Problems, Thesis, Dept. of Geodesy, Royal Institute of Technology, Stockholm.
- PIEPE, J. (1990). Eine Neue 4" X 5" Aufnahmekammer Fur die Nahbereichsphotogrammat. International Archives of Photogrammetry and Remote Sensing 28(5) 256-263.
- RAIDH, A. and MUNJY, H. (1986a). Self Calibration using the Finite Element Approach, Photogrammetric Engineering and Remote Sensing 52(3): 411-418.
- RAIDH, A. and MUNJY, H. (1986b). Calibration of Non-metric Cameras using the Finite Element Method, Photogrammetric Engineering and Remote Sensing 50(11): 1201.
- ROBERTS, A. and GRISWOLD, L. (1986). Practical Photogrammetry from 35mm Aerial Photography, Photogrammetric Engineering and Remote Sensing 50(1): 6pp.
- ROBINSON, G.S. (1963). The Reseau as a means of Detecting Gross Lack of Flatness of Film at the Instant of Exposure, Photogrammetric Record 23: 283 to 286.
- ROBSON, S. (1990). A Future for Film in Close Range Photogrammetry. Photogrammetric Record 15(77): In press.

ROBSON S. (1990). The Physical Effects of Film Deformation in Small Format Camera Calibration. International Archives of Photogrammetry and Remote Sensing 28(5): 8pp.

ROLLEI (1986). Rollei Fototechnic, Camera Calibration Certificate. 005290011 29.6.86.

ROOS, M. (1975). The Automated Reseau Equipment ARME, Photogrammetric Engineering and Remote Sensing 41(9): 1109-1115.

ROSENBRUCH, K.J. (1976). Considerations regarding image geometry and Image Quality. International Archives of Photogrammetry and Remote Sensing 21(1): 26.

RUMSEY, A. (1988). Identification, Preservation and Storage of the Film, Paper presented at Photogrammetric Society Symposium on the Photogrammetric Archives in the United Kingdom, London, March 1988.

SALAMONOWICZ, P.H. (1982). USGS Aerial Photographic Resolution Targets, Photogrammetric Engineering and Remote Sensing 48(9): 1469-1473.

SCHLIENGER, R. (1972). Wild Cameras for Terrestrial and Close Range Photogrammetry International Archives of Photogrammetry and Remote Sensing 44(5): 18pp.

SCHROTH, R. (1982). On the Stochastic Properties of Image Coordinates, International Archives of Photogrammetry and Remote Sensing 24(3): 446-458.

SCHUT, G.H., (1974). Two Interpolation Methods. Photogrammetric Engineering 40(12): 1447-1453.

SCHUT, G.H., (1979). Selection of Additional Parameters for Bundle Adjustment, Photogrammetric Engineering and Remote Sensing 45(9): 1243-1252.

SCOTT, P.J. (1976). Close Range Camera Calibration, A New Method, Photogrammetric Record 8(48): 806-812.

SCOTT, P.J. (1977). The Pupil in Perspective, Photogrammetric Record 9(49): 83-92.

SCOTT, P.J. (1978). Structural Deformation Measurement of a Model Box Girder Bridge, Photogrammetric Record 9(51): 361-376.

SCOTT, P.J. and GEORGOPOUOS, A. (1979). Camera Calibration at Very Close Focal Settings, Photogrammetric Record 9(54): 853-855.

SELWYN, E.W.H. (1959). A theory of graininess, Journal of Photographic Science 7: 138.

SHEPPARD, S.E. and ELLIOT, F.A. (1921). Photometric Methods and Apparatus for the Study of Colloids, Journal of the American Chemical Society 43: 531-539.

SHEPPARD, S.E. and SWEET, S.S. (1921). The Elastic Properties of Gelatin Jellies, American Chemical Society 43: 539-547.

SHORTIS, M.R. (1986). Close Range Photogrammetric Measurements for Structural Monitoring, Deformation Surveys and Engineering Surveillance, Australian Journal of Geodesy Photogrammetry and Surveying 45: 55-64.

SHORTIS, M.R. (1987). The Feasibility of the Application of Digital Imagery to Precise Close Range Photogrammetric Metrology, Department of Surveying and Land Information, University of Melbourne

SLAMA, C.C. (1980). The Manual of Photogrammetry (4th Edition), (Falls Church: American Society of Photogrammetry), 1056pp.

- SMITH, A.G., (1981). Astronomical Photography at 1.1 Micrometers, Applied Photographic Engineering 7(6): 168-170.
- SPRACKLING, M.T. (1987). The Deformation of a Photographic Film, Journal of Photographic Science 35: 92-96.
- STEEL, W.H. (1983). Interferometry. 2nd Edition, Cambridge University Press. 308pp.
- STURGE (1977). Neblettes Handbook of Photography and Reprography, 7th Ed. Pub. Van Nostrad, N.York. 625pp.
- TAYMAN, W.P. (1984). User Guide for the USGS Aerial Camera Report of Calibration, Photogrammetric Engineering 50(5): 577-584.
- TAYMAN, W.P. and ZIEMANN, H. (1984). Photogrammetric Camera Calibration, Photogrammetria 39(2): 31-53.
- TEMPFLI, K. (1973). Film Flatness in Aerial Cameras, A Model for it's Computer Simulation, ITC Journal 1973(4): 562-582.
- TEMPFIL, K. (1974). Analysis and Simulation of Film Deformation, ITC Journal 1974(2): 111-137.
- TEMPFLI, K. and MAKOROVIC, B. (1978). Transfer Functions of Interpolation Methods, ITC Journal 1978(1): 50-80.
- THOMPSON, E.H. (1957). The Geometrical Theory of the Camera and it's Application to Photogrammetry, Photogrammetric Record 2(10): 241-263.
- THOMPSON, E.H. (1977). A Note on Distortion, Photogrammetric Record 9(49): 93-99.
- TORLEGÅRD, J. (1986). New Challenges of Close Range Photogrammetry, International Archives of Photogrammetry and Remote Sensing 27(5): 1-9.
- TORLEGÅRD, J. (1989). Theory of Image Coordinate Errors. Chapter 7 from the Handbook of Non-Topographic Photogrammetry (ed KARARA). 2nd Edition, American Society of Photogrammetry and Remote Sensing, Falls Church USA. 445pp.
- TRINDER, J.C. (1971). Pointing Accuracies to Blurred Signals, Photogrammetric Engineering and Remote Sensing 27(2): 207-216.
- TRINDER, J.C. (1982). The Effects of Photographic Noise on Pointing Precision, Detection and Recognition, Photogrammetric Engineering and Remote Sensing 48(10): 1563-1575.
- TRINDER, J.C. (1984). Pointing Precisions on Aerial Photogrammetry, Photogrammetric Engineering and Remote Sensing 50(10): 1449-1462.
- TRITCH, C.D., (1985). Is Your Contact Printer Really a 'Contact' Printer, Photogrammetric Engineering and Remote Sensing 51(10): 1639-1649.
- TSURUTA, T., ITOH, Y. and ANZAI, S. (1970). Moiré Topography for the Measurement of Film Flatness, Applied Optics 9(12): 2802-2804.
- VETTER, H.G., (1970). Perception of Quantum Limited Images, Photogrammetric Engineering and Remote Sensing 36(11): 1179-1188.
- VISSER, J., LEBERL, F. and KURE, J. (1974). Oberschwaben Reseau Investigations (OEEPE), ITC Journal 1974(2): 138-166.

VLECK, J. (1969). Systematic Errors of Image Coordinates, Photogrammetric Engineering 35(6): 585-593.

VOSS, G. (1980). 10 Years UMK/10/1318 Universal Measuring Camera, International Archives of Photogrammetry and Remote Sensing 24(1): 185-195.

WALLS, H.J. and ATTRIDGE, G.G. (1977). Basic Photo Science. (London: Focal Press) 418pp.

WEISS, D.A. and SHALIT, H. (1983). Characteristics of the Stress Desensitisation Phenomenon of the Silver Halide Emulsion, Photographic Science and Engineering 27: 231-235.

WELFORD, W.T. (1973). Bubble Chamber Photography. Film Flatness, Lens Distortion Illumination and Others, Photogrammetric Record 8(44): 167.

WELCH, R. (1971). Modulation Transfer Functions, Photogrammetric Engineering and Remote Sensing 37(3): 247-259.

WELCH, R. (1972). Quality and Applications of Aerospace Imagery, Photogrammetric Engineering and Remote Sensing 38(4): 379-398.

WELCH, R., SLATER, P.N., TIZIANI, H. and TRINDER, J.C. (1981). The ISP Image Quality Working Group 1976-1980, Photogrammetric Engineering and Remote Sensing 47(8): 1215-1222.

WESTER-EBBINGHAUS, W. (1983). Ein Photogrammetrisches System für Sonderanwendungen. Bildmessung und Luftbild Wesser 51(3): 118-128.

WESTER-EBBINGHAUS, W. (1986). Analytical Camera Calibration, International Archives of Photogrammetry and Remote Sensing 26(5): 77-84.

WESTER-EBBINGHAUS, W. (1988). Analytics in Non-Topographic Photogrammetry, International Archives of Photogrammetry and Remote Sensing 27(5): 380-392.

WIENER, H. (1949). Extrapolation, Interpolation and Smoothing of Stationary Time Series, (N.York: Wiley).

WILD (1984). Camera Calibration Certificate for a P32 Camera, Wild Heerbrugg Ltd.

WILD (1977) Wild P32 Terrestrial Camera, Wild Heerbrugg Ltd. Publication No. P1226a -X77.

WOLF, P.R. (1985). Elements of Photogrammetry. (London: McGraw Hill), 663pp.

WONG, K.W. (1975) Propagation of Variance and Covariance, Photogrammetric Engineering and Remote Sensing 41(1): 75-89.

WORTON, F.J. (1976) Aerial Film Processing by the Rewind Method, Photogrammetric Record 8(47): 652-660.

WORTON, F.J. and CHEFFINS, O.W. (1978) A Practical Photogrammetric Test of Thin Base Aerial Film, Photogrammetric Record 10(58): 493-496.

YAGLOM, A.M. (1962) An introduction to the theory of stationary random functions. (N.Jersey: Prentice Hall), 235pp.

YOUNG, M.E. and ZIEMANN, H. (1972) Film Diapositive Deformation, Photogrammetric Engineering and Remote Sensing 38(1): 65-69.

ZEISS (1985). ZKM 02-150D and ZKM 1-150D. Two Coordinate Measuring Microscopes. VEB Carl Zeiss (Jena). D.D.R. Publication No. Ag. 98/091/75. 17pp.

- ZEISS (1983). UMK 1318 and SMK 5,5108, VEB Carl Zeiss (Jena). D.D.R. Ag 29/114/83. 36pp.
- ZEISS (1985). Camera Calibration Certificate for the Zeiss (JENA) UMK 10/1318 camera
- ZIEMANN, H. (1971a). Is the request for Eight Fiducial Marks Justified?, Photogrammetric Engineering 37(1): 67-75.
- ZIEMANN, H. (1971b). Image Deformation and Methods for It's Correction, Canadian Surveyor 25(4): 367-377.
- ZIEMANN, H. (1971c). Sources of Image Deformation, Photogrammetric Engineering 37(12): 1259-1265.
- ZIEMANN, H. (1971d). Image Deformation - A Discussion of Several Contributing Sources, The Canadian Surveyor 25(5): 521-529. .
- ZIEMANN, H. (1972a). Economics of Image Deformation Correction, Photogrammetric Engineering 38(2): 155-162.
- ZIEMANN, H. (1972b). Image Geometry - Factors Contributing to it's change, International Archives of Photogrammetry and Remote Sensing 19(3): 60pp.
- ZIEMANN, H. and YOUNG, M.E.H. (1972c) Film Diapositive Deformation, Photogrammetric Engineering 38(4): 65-69.
- ZIEMANN, H. (1976) Remarks on Dr. A. Bujakiewicz Paper, "The Correction of Lens Distortion with Polynomials", The Canadian Surveyor 30 (2): 77-80.
- ZIEMANN, H. (1978) Repeated Photographic Laboratory Calibrations of Two Reseau Cameras, Photogrammetria 34(4): 167-178.
- ZIEMANN, H. (1980a) High Accuracy Photogrammetric Determination using Image Deformation Correction, The Canadian Surveyor 38(1): 65-74.
- ZIEMANN, H. (1980b) The Activities of the Working Group on Image Geometry between 1972 and 1980, International Archives of Photogrammetry and Remote Sensing 24(3): 215-232.
- ZIEMANN, H. and EL-HAKIM, S.F. (1983) On the Definition of Lens Distortion Reference Data With Odd Power Polynomials, The Canadian Surveyor 37(3): 135-143.
- ZIEMANN, H. and EL-HAKIM, S.F. (1986a) System Calibration Versus Self Calibration, Photogrammetric Engineering and Remote Sensing 52(10): 1617-1625.